

# **Breakdown Properties of Mineral Oil and Ester Based TiO<sub>2</sub> and BN Nanofluids**

Thesis presented for the degree of

**Doctor of Philosophy**

in the

**Department of Electronic & Electrical Engineering**

**University of Strathclyde**

**Yi Jing, BEng, MSc**

Department of Electronic & Electrical Engineering  
University of Strathclyde  
Glasgow, U.K.

**2016**

# **Declaration of Authenticity and Author's Rights**

This thesis is the result of the author's original research. It has been composed by the author and has not been previously submitted for examination which has led to the award of a degree.

The copyright of this thesis belongs to the author under the terms of the United Kingdom Copyright Acts as qualified by University of Strathclyde Regulation 3.50. Due acknowledgement must always be made of the use of any material contained in, or derived from, this thesis.

Signed:

Date:

# Acknowledgement

Firstly, most sincere gratitude to my supervisor: Dr Igor. V. Timoshkin. I appreciate him for giving me the opportunity for this study. When I feel anxious during the study, he gives me a lot of technically and mentally supports and helps me to finish this project. I learn not only the academic research skill but also the rigorous research attitude from him. I believe these experiences will be like a lighthouse to guide me in the future.

I would like to thanks to Prof. Scott. J. MacGregor, Dr Martin. J. Given, Dr Mark. P. Wilson, Dr Michelle Maclean, Dr Tao Wang for their help during my study.

I would like to thanks to all teammate in HVT research group and all my friends in who give me help in my study.

I would like to thanks my comrades during my study: Gongzhang Rui, Sirui Li, Yiming Gao; and best wishes to all of them.

There is also thanks to my parents and parents-in-law who always give me the sincere encouragement and best wish to support me to finish this study.

At last but not least, I want to thanks to my wife. I believe I meet her during my PhD study is my greatest luck in my life. Without her support, I will not be able to finish my study. This study experience contains a lot of meaning to me because of her presence. I think it will be the one of my most precious treasures in my whole life.

# Abstract

Dielectric liquids are widely used as electrical insulation industry area. Currently the insulating liquids which are typically employed in high-voltage (HV) systems are naphthenic mineral oils. However, stringent environmental protection regulations encourage operators of HV equipment to use more environmentally friendly liquids. There is also a strong demand for the development of industry which requires insulating liquids provide advanced dielectric properties.

Natural and synthetic esters are considered as potential substitutes for traditional mineral oils due to their environmental friendly properties. Meanwhile a new approach to the modification of dielectric properties of insulating liquids has been introduced which is based on the addition of ultra-fine particles (with sub-micrometre dimensions) to insulating liquids (nanofluids). There are a number of published papers reported that nanofluids provide better thermal and breakdown properties than those of base liquids. However the full understanding of the breakdown properties of nanofluids is not completed. The comprehensive study of breakdown properties of nanofluids is required.

In this thesis, the breakdown properties of mineral oil, ester, and nanofluids based on these liquids, developed using titanium dioxide ( $\text{TiO}_2$ ) and boron nitride (BN) nanoparticles have been investigated. Nanofluids were prepared with various concentrations. The experiments have been designed and preformed: AC breakdown voltage, lightning impulse breakdown voltage, lightning impulse pre-breakdown time, and DC pre-breakdown current.

The experimental results show that nanofluids with low concentration provide higher breakdown voltage as compare with those of base liquids. There is an 'optimal' concentration, nanofluids provide the highest AC, impulse breakdown voltage, and longest impulse pre-breakdown time as compare with those of other tested liquids.

The measurement of DC pre-breakdown current in base liquids allowed calculation of the field distribution in liquids. As the pavement for further investigations, several potential mechanisms of nanoparticle influence on breakdown properties of nanofluid have been compared and discussed.

## LIST OF ACRONYMS

|                  |                             |
|------------------|-----------------------------|
| HV               | High Voltage                |
| AC               | Alternating Current         |
| DC               | Direct Current              |
| PVC              | Polyvinyl chloride          |
| TiO <sub>2</sub> | Titanium dioxide            |
| BN               | Boron Nitride               |
| CI               | Confidence Interval         |
| HVDC             | High Voltage Direct Current |

# LIST OF SYMBOLS

|                          |  |
|--------------------------|--|
| $I_{pre-breakdown}$      | Pre-breakdown current (A)  |
| $V_{read}$               | Amplifier output voltage (V)   |
| $R_{viewing}$            | Current viewing resistor ( $\Omega$ )  |
| $G$                      | Gain of amplifier  |
| $\alpha$                 | Weibull scale parameter  |
| $\beta$                  | Weibull shape parameter  |
| $\gamma$                 | Weibull location parameter   |
| $s$                      | Standard deviation   |
| $SE_{diff}$              | Standard error between samples   |
| $t_{1-\frac{\alpha}{2}}$ | Degree of freedom taken from t-distribution table                                |
| $\epsilon_0$             | Vacuum permittivity  |
| $\epsilon_l$             | Relative permittivity  |
| $d$                      | Distance (cm)  |
| $\mu$                    | Mobility of charge carrier ( $\text{cm}^2\text{V}^{-1}\text{s}^{-1}$ )           |
| $a$                      | Distance between the tip radius center and the plane (m)                         |
| $x$                      | The distance between tip to the point of interest (m)                            |
| $r$                      | Tip radius ( $\mu\text{m}$ )   |
| $E$                      | Electrical field strength (V)  |
| $\nu$                    | The ratio of distance from the tip to the point of interest and the gap distance |
| $\tau$                   | Relaxation time constant of nanoparticle (s)                                     |
| $\sigma$                 | Conductivity (S)   |
| $\rho_p$                 | Densities of positive ion  |
| $\rho_n$                 | Densities of negative ion  |
| $\rho_e$                 | Densities of electron  |
| $\rho_{np}$              | Densities of nanoparticle  |
| $\rho_{np,sat}$          | Charging limitation of nanoparticle saturation                                   |

|            |  |
|------------|--|
| $\mu_p$    | Mobility of positive ion                         |
| $\mu_n$    | Mobility of negative ion                         |
| $\mu_e$    | Mobility of electron                             |
| $\mu_{np}$ | Mobility of nanoparticle                         |
| $R_{pn}$   | Langevin ion-ion recombination coefficients      |
| $R_{pe}$   | Langevin ion-electron recombination coefficients |
| $G_I$      | Field ionization charge density rate             |
| $\sigma_p$ | The dipole surface charge density                |

# CONTENTS

|   |    |
|---|----|
| CHAPTER 1 INTRODUCTION .....  | 12 |
| 1.1 Background .....  | 12 |
| 1.2 Main Objectives and Research Tasks .....  | 15 |
| 1.2.1 Analysis of the literature data on the dielectric performance of nanofluids .....                 | 15 |
| 1.2.2 Development of nanofluids .....   | 16 |
| 1.2.3 Investigation of AC breakdown strength .....  | 16 |
| 1.2.4 Investigation of impulse breakdown strength .....   | 17 |
| 1.2.5 Statistical analysis of pre-breakdown time .....  | 17 |
| 1.2.6 Investigation of mobility of charge carriers and space-charge-influenced field distribution ..... | 17 |
| 1.3 Outline of the Thesis .....   | 17 |
| 1.4. Publications During PhD Study .....  | 19 |
| CHAPTER 2 BACKGROUND INTRODUCTION AND LITERATURE REVIEW .....   | 20 |
| 2.1 Introduction .....  | 20 |
| 2.2 Breakdown Mechanisms in Dielectric Liquids .....  | 23 |
| 2.2.1 Electrostriction breakdown mechanism .....  | 23 |
| 2.2.2 Ionisation in liquid: Streamer mechanism .....  | 25 |
| 2.2.3 Suspended particles theory .....  | 28 |
| 2.3 Chemical Structure and Physical Properties of Dielectric Liquid .....                               | 28 |
| 2.3.1 Chemical structure of dielectric liquids .....  | 28 |
| 2.3.2 Pour point .....  | 31 |
| 2.3.3 Viscosity and thermal conductivity .....  | 31 |
| 2.3.4 Fire point and flash point .....  | 32 |
| 2.4 Dielectric Properties of Liquids .....  | 32 |
| 2.4.1 Streamer characteristics in dielectric liquids .....  | 32 |
| 2.4.2 AC breakdown strength of dielectric liquids .....   | 35 |
| 2.4.3 Lightning, step, and switching impulse breakdown strengths of dielectric liquids .....            | 38 |
| 2.4.4 Ageing of dielectric liquids .....  | 41 |
| 2.5 Fine and Ultra-fine particles in Dielectric Liquids .....   | 44 |
| 2.5.1 Preparation of nanofluids .....   | 48 |

|  |     |
|--|-----|
| 2.5.2 Physical properties of nanofluids.....   | 48  |
| 2.5.2.1 Viscosity .....  | 48  |
| 2.5.2.2 Pour point, fire point, and flash point .....  | 50  |
| 2.6 Dielectric Properties of Nanofluids .....  | 50  |
| 2.6.1 Resistivity and relative permittivity of nanofluids .....  | 50  |
| 2.6.2 AC dielectric strength.....  | 52  |
| 2.6.2.1 Influence of type of nanoparticles .....   | 52  |
| 2.6.2.2 Influence of surface treatment .....   | 54  |
| 2.6.2.3 Influence of concentration of nanoparticles .....  | 56  |
| 2.6.2.4 Influence of moisture content .....  | 60  |
| 2.6.3 Lightning and switching impulse dielectric strength .....  | 64  |
| 2.6.3.1 Influence of type of nanoparticles .....   | 64  |
| 2.6.3.2 Influence of concentration of nanoparticles .....  | 67  |
| 2.6.4 Ageing of nanofluids .....   | 71  |
| 2.6.5 Thermal conductivity of nanofluids .....   | 75  |
| 2.7 Summary .....  | 79  |
| CHAPTER 3 EXPERIMENTAL SETTING AND SAMPLE PREPARATION.....   | 81  |
| 3.1 Introduction .....   | 81  |
| 3.2 Insulating Liquids Used in This Study .....  | 82  |
| 3.3 Nanoparticles Used for Modification of Dielectric Liquid.....  | 85  |
| 3.3.1 Physical properties of nanoparticles.....  | 85  |
| 3.3.2 Concentration of nanoparticles in dielectric liquids .....   | 86  |
| 3.3.3 Nanoparticle surface modification and sample preparation procedure .....                                       | 86  |
| 3.3.4 Average size of nanoparticles in suspension sample investigation .....   | 90  |
| 3.4 Experimental System for AC Breakdown Voltage Measurement .....   | 96  |
| 3.4.1 Test cell design.....  | 96  |
| 3.4.2 Electrode topology.....  | 97  |
| 3.4.3 Measurement systems and devices.....   | 98  |
| 3.5 Experimental Setting for Fixed-peak Lightning Impulse and Minimum Impulse<br>Breakdown Voltage Measurement ..... | 101 |
| 3.5.1 Marx generator topology.....   | 102 |

|  |     |
|--|-----|
| 3.5.2 Test cell design.....  | 104 |
| 3.5.3 Diagnostic devices and pneumatic system .....  | 107 |
| 3.6 Charge Carrier Mobility in Insulating Liquids.....   | 111 |
| 3.6.1 Electrode topology and test cell design.....   | 112 |
| 3.6.2 Calibration of amplifier for I-V current measurements .....                                    | 115 |
| 3.6.3 I-V measurement system .....   | 116 |
| 3.7 Summary .....  | 119 |
| CHAPTER 4 AC BREAKDOWN CHARACTERISTIC OF BASE AND NANO-MODIFIED LIQUIDS                              | 121 |
| 4.1 Introduction .....   | 121 |
| 4.2 Experimental Procedures.....   | 122 |
| 4.3 Investigation of AC Breakdown Voltages.....  | 123 |
| 4.3.1 AC breakdown characteristics of TiO <sub>2</sub> nanofluids.....                               | 123 |
| 4.3.2 AC breakdown characteristics of BN nano-modified liquids .....                                 | 128 |
| 4.4 AC Breakdown Experimental Results: Weibull Analysis and Comparison .....                         | 134 |
| 4.4.1 Weibull analysis of breakdown voltage data of TiO <sub>2</sub> nano-modified liquids.....      | 135 |
| 4.4.2 Weibull analysis results for BN nano-modified samples.....                                     | 138 |
| 4.5 AC Breakdown: Confidence Analysis.....   | 141 |
| 4.5.1 Confidence interval .....  | 141 |
| 4.5.2 Calculation of confidence intervals.....   | 142 |
| 4.5.3 Confidence analysis: AC breakdown voltage of TiO <sub>2</sub> nano-modified liquids.....       | 143 |
| 4.5.4 Confidence analysis: AC breakdown voltage of BN nano-modified liquids.....                     | 145 |
| 4.6 Summary .....  | 147 |
| 4.6.1 Nano-modified insulating liquid theory.....  | 147 |
| 4.6.2 Experimental results comparison .....  | 148 |
| 4.6.3 Confidence statistical analysis results.....   | 152 |
| CHAPTER 5 STANDARD LIGHTNING IMPULSE BREAKDOWN VOLTAGE AND PRE-<br>BREAKDOWN TIME INVESTIGATION..... | 153 |
| 5.1 Introduction .....   | 153 |
| 5.2 Experimental Procedure .....   | 154 |
| 5.3 Standard Lightning Impulse Investigation .....   | 155 |
| 5.3.1 Standard lightning impulse test: TiO <sub>2</sub> nano-modified liquids .....                  | 155 |
| 5.3.2 Standard lightning impulse test: BN nano-modified liquids .....                                | 161 |
| 5.3.3 Streamer velocity in nano-modified liquids.....  | 167 |

|   |     |
|---|-----|
| 5.4 Weibull Analysis of Pre-breakdown Times for Standard Lightning Impulses .....                     | 172 |
| 5.4.1 Weibull analysis of pre-breakdown times in TiO <sub>2</sub> nano-modified liquids.....          | 173 |
| 5.4.2 Weibull analysis of the pre-breakdown times in BN nano-modified liquids .....                   | 181 |
| 5.5 Confidence Analysis of the Pre-breakdown Times for Standard Lightning Tests .....                 | 190 |
| 5.5.1 Confidence analysis of the pre-breakdown times for TiO <sub>2</sub> nano-modified liquids ..... | 190 |
| 5.5.2 Confidence analysis of the pre-breakdown times for BN nano-modified liquids.....                | 195 |
| 5.6 Summary .....   | 200 |
| 5.6.1 Discussion of pre-breakdown time measurement results.....                                       | 201 |
| 5.6.2 Streamer velocity of nano-modified samples discussion .....                                     | 201 |
| 5.6.3 Discussion of the Weibull distribution analysis .....   | 202 |
| 5.6.4 Discussion of confidence analysis .....   | 204 |
| CHAPTER 6 MINIMUM-LIGHTNING IMPULSE BREAKDOWN VOLTAGE INVESTIGATION ....                              | 205 |
| 6.1 Introduction .....  | 205 |
| 6.2 Experimental Procedure .....  | 206 |
| 6.3 Minimum-lightning Impulse Breakdown Voltage of Liquids.....                                       | 208 |
| 6.3.1 ASTM D3300-00 method test results.....  | 208 |
| 6.3.2 IEC 60897 method test results.....  | 217 |
| 6.4 Minimum-lightning Impulse Breakdown Voltage Confidence Analysis and Comparison .....              | 225 |
| 6.4.1 Confidence analysis results for the ASTM method .....   | 226 |
| 6.4.2 Confidence analysis of the breakdown results by IEC method.....                                 | 230 |
| 6.5 Summary .....   | 234 |
| 6.5.1 Discussion of minimum-lightning impulse breakdown voltage by ASTM method .....                  | 235 |
| 6.5.2 Discussion of minimum-lightning impulse breakdown voltage by IEC method ..                      | 236 |
| 6.5.3 Discussion of confidence analysis .....   | 237 |
| CHAPTER 7 MOBILITY OF CHARGE CARRIERS AND POTENTIAL MECHANISMS OF BREAKDOWN IN NANOFUIDS.....         | 239 |
| 7.1 Introduction .....  | 239 |
| 7.2 Mobility of Charge Carries .....  | 240 |
| 7.2.1 DC breakdown voltage .....  | 240 |
| 7.2.2 Pre-breakdown current measurement and mobility of charge carriers.....                          | 242 |
| 7.3 Space-charge Influenced Electrical Field.....   | 247 |

|  |     |
|--|-----|
| 7.3.1 Field distribution without space charge .....  | 247 |
| 7.3.2 Field distribution with space charge .....   | 248 |
| 7.4 Potential Mechanisms of Nanoparticles on the Breakdown Strength of the Liquid .                                    | 254 |
| 7.4.1 Polarisation of nanoparticles .....  | 254 |
| 7.4.2 Model of trapping potential.....   | 259 |
| 7.4.3 Model of the electron shallow trap .....   | 262 |
| 7.5 Summary .....  | 263 |
| CHAPTER 8 CONCLUSIONS AND FUTURE WORK.....   | 266 |
| 8.1 Brief review .....   | 266 |
| 8.2 Summary of results and major contributions .....   | 267 |
| 8.2.1 Conclusion of AC breakdown test .....  | 267 |
| 8.2.2 Conclusion of fixed-peak standard lightning impulse .....  | 268 |
| 8.2.3 Conclusion of the minimum-lightning impulse breakdown voltage test.....  | 269 |
| 8.2.4 Conclusion of DC pre-breakdown current measurement, liquid mobility<br>calculation, and further discussion ..... | 270 |
| 8.2.5 Summary of major findings.....   | 271 |
| 8.2.6 Summary of major achievements and contributions .....  | 272 |
| 8.3 Future Work .....  | 273 |
| REFERENCES .....   | 274 |
| APPENDIX: PUBLISHED JOURNAL PAPER .....  | 299 |

# CHAPTER 1

## INTRODUCTION

### 1.1 Background

The dielectric insulation of high-voltage (HV) systems, including power transformers, circuit breakers, power electronic devices, pulsed power transmission lines, and plasma closing switches is important for reliable operation of the components and systems used in the power and pulsed power industries. Coordination of electrical insulations could be conducted by an electrical engineer or a researcher by designing and building HV power and pulsed power systems to avoid electrical breakdown events in such systems. Failure of dielectric insulation in HV equipment may potentially lead to catastrophic results, such as explosion of oil-filled power transformers or oil-filled circuit breakers and destruction of the HV components of the pulsed power systems. Thus, it is important to select dielectric materials with sufficient breakdown strength that could withstand nominal HV and potential transient overvoltage events. Liquid insulation has another important role in power transformers – heat transfer from the winding to the metal transformer tank. Thus, transformer failure due to overheating could be avoided.

In the case of liquid insulation, mineral oil is the most common insulating liquid used in power equipment, such as power transformers. Statistical analysis of the transformer (the primary voltage over 34.5 kV and at least 10 MVA capability) failure events has indicated that the average transformer life is 17.8 years, which is much shorter than the design life of a modern transformer at 35 to 40 years [1]. The main factor that results in such a significant reduction of the lifetime of the power transformers is failure of their dielectric insulation. It was shown in [2] that 75% of transformer failures were caused by insulation failure due to HV overload, overheating, and ageing insulating material.

Mineral oil is the most commonly used insulating liquid for transformer applications. Mineral oils are produced by distillation of crude oil and are a hydrocarbon mixture, including alkanes, cyclic paraffins, and aromatic hydrocarbons. Depending on the distillation process, mineral oils can contain significant

quantities of n-paraffins (paraffinic oil) or low concentrations of these chemical species (naphthenic oils). Naphthenic oils have a naturally low pour point, better viscosity, and longer service life compared with paraffinic oils; thus, these types of oils are more widely used in power and pulsed power equipment as insulation liquids. Mineral oils are characterised by a relatively low manufacturing cost. Their dielectric properties have been intensively studied for many decades, leading to the accumulation of significant knowledge on their dielectric behaviour.

However, mineral oils are toxic, and these liquids are non-biodegradable. Therefore, in the event of an accident, oil leaks may cause significant environmental pollution, resulting in a complex clean-up process and financial losses. Mineral oils are flammable liquids (for example, the fire point of Nynas oil is 170°C [3]). Thus, it can result in fires or explosions of the electrical equipment with potentially catastrophic consequences.

Currently, stricter environmental regulations and environmental concerns have resulted in additional limitations and requirements for the use of mineral oils in HV systems. Thus, power utility companies and manufacturers of power equipment are constantly looking for potential substitution of mineral oils with more environmentally friendly fluids.

There is a high demand for new insulating liquids with a potential to replace the traditional mineral oils. These new liquids should have high dielectric strength, high thermal conductivity, low flammability, low toxicity, and should be biodegradable. There are a few potential candidates for such substitution, including synthetic and natural ester liquids. They are considered potential substitutes for traditional naphthenic mineral oils due to their low toxicity, biodegradability, high fire point, and good dielectric performance [4]–[8].

Synthetic ester liquids are composed of chemicals that are typically carboxylic acids, which are bonded to a polyol structure. Natural ester liquids are produced from vegetable oils and consist of glycerol and bonded fatty acid groups. Natural esters have good biodegradability, which make them a very attractive alternative to the traditional mineral oils.

Many researchers investigated the dielectric properties of ester liquids, and the results indicated that ester liquids provide a comparable dielectric performance with mineral oil, such as in alternating current (AC) [4]–[6], [9], [10] and regarding impulse withstand strength [4], [11], [12]. Furthermore,

it has been shown that the ester liquids provide better dielectric performance with ageing [4], [13], [14], they have lower flammability, and the reduction in the breakdown strength caused by increasing water content is less pronounced than for mineral oil [3]. However, the dielectric performance of synthetic and especially natural ester liquids is not fully known yet. Further studies are required to understand fully their dielectric properties, which will potentially result in wider application of these liquids in power and pulsed power HV equipment.

In recent years, a new approach to the modification of dielectric properties of insulating liquids has been introduced and actively explored. This approach is based on the addition of ultra-fine particles (with sub-micrometre dimensions) to solid dielectrics and later into insulating liquids. This conceptual idea was first introduced in the 1990s, in [15], which were focused on investigation of the effect of the addition of nanoparticles into solid insulating materials in order to improve their life and heat dissipation performance.

Moreover, the effect of nanoparticles on dielectric properties of mineral oils has been studied in [4]–[6], [9]–[12], in which particles of magnetite were added to mineral oil, and the dielectric performance of such nanofluid was investigated.

It has been shown that these (semi) conductive nanoparticles of magnetite have the potential to enhance the withstand voltage of mineral oils [17]–[19]. However in [20]–[27], it was shown that there is a problem with the stability of such nanofluids, as ultra-fine particles of magnetite tend to be redistributed in the nonuniform electrical fields that exist in the power equipment. Additionally, magnetite nanoparticles tend to agglomerate into larger clusters with time; thus, the stability of the suspension of magnetite ultra-fine particles will be disturbed.

Therefore, to investigate and potentially prevent such agglomeration, further research is needed. Moreover, it is interesting to investigate the potential dielectric behaviour of nanofluids with low conductive nanoparticles, such as ultra-fine particles of metal oxides (e.g., titanium dioxide [TiO<sub>2</sub>]) [28]–[31]. Recently, it has been shown that nanoparticles of boron nitride (BN) nano-flakes can increase the thermal conductivity of mineral oils and thus may improve heat dissipation if such nanofluids are used in power equipment [32]–[35].

Based on this motivation and the available literature data and results, this project is focused on the investigation of the dielectric performance of mineral oil, natural and synthetic ester liquids, and the nanofluids developed based on these liquids using low conductive, ultra-fine particles of TiO<sub>2</sub> and BN. Thus, the main aim of the study was to provide further information on the breakdown strengths of mineral oils, ester liquids, and their nano-modified derivatives (nanofluids) to expand the potential range of their practical applications in the HV systems used in power and pulsed power equipment (e.g., liquid-filled switches used in pulsed power). Thus, this study addresses an important issue in the search for environmentally friendly alternatives to mineral oils that will potentially have even better dielectric performance compared with the traditional insulating liquids.

## **1.2 Main Objectives and Research Tasks**

In this study, two types of semi-conductive nanoparticles, TiO<sub>2</sub> and BN, were selected and used to prepare three nanofluids based on insulating liquids (mineral oil, synthetic ester liquid, and natural ester liquid). The AC breakdown voltage, impulse breakdown voltage, and the pre-breakdown time under the impulse stress have been investigated. Simultaneously, to explore the potential mechanisms through which the nanoparticles can modify the dielectric properties of insulating, the electrical field distribution has been determined, and the charge carrier mobility in three types of insulating liquids has been studied to evaluate the space-charge effects, which may result in field redistribution.

### **1.2.1 Analysis of the literature data on the dielectric performance of nanofluids**

One of the tasks of this work was the comprehensive critical review of literature data on the dielectric behaviour of nanofluids. In recent years, several authors have reported on different aspects of the dielectric behaviour of insulating liquids doped with fine and ultra-fine particles with high and low conductivity. However, currently, no systematic analysis of the experimental and analytical data available in the literature has been conducted. This lack of analysis may result in restrictions in further studies; therefore, to identify the optimal path for further research and development in the field of insulating nanofluids, it was important to collect available information and to conduct a critical review of the available literature data. Based on this review, the type of nanoparticles, their surface treatment, and the range of concentrations have been identified for the present study.

### **1.2.2 Development of nanofluids**

The important aspect of this study was the development of suitable nanoparticle suspensions. It was shown in the literature review that there are several approaches to the production of a nanofluid; the simplest is just to add nanoparticles into the insulating fluids as they are, without any additional treatment of these nanoparticles. However, this approach may result in the agglomeration of nanoparticles and in the development of larger clusters, which may precipitate under gravity. Another approach is to conduct a specific surface treatment, which will help to develop a stable emulsion of nanoparticles in insulating liquids. Based on the literature review, the most suitable treatment procedure has been selected and used in this research. Stability and size distribution of nanoparticles of TiO<sub>2</sub> and BN in all the liquids have been investigated.

### **1.2.3 Investigation of AC breakdown strength**

The AC breakdown strength is an important dielectric characteristic of insulating liquids. The AC breakdown strength is measured under power-frequency HV stress. This parameter is one of the most important parameters that define the dielectric performance of dielectric liquid. The AC breakdown strength is highly sensitive to the chemical composition of the liquid under the test and to the contaminants in the liquid including particulate matter or moisture. As indicated in [36], AC breakdown strength can be used to indicate the presence of contaminants in the dielectric liquid. Thus, it is important to investigate how the addition of nanoparticles in the dielectric fluids may change this critical breakdown characteristic compared with the AC breakdown strength of base liquids.

The AC breakdown strengths of mineral oil (Shell Diala), synthetic ester (Midel 7131), and natural ester (vegetable oil) have been investigated. These base liquids have been used as the base liquids to develop nanofluids using the semi-conducting nanoparticles of TiO<sub>2</sub> and BN. The AC breakdown properties of these nanofluids have been investigated and compared with those of base liquids. Several different concentrations of nanoparticles have been used in the present study to identify the optimal concentration that can provide the best dielectric performance. This is one of the main tasks of this research project: investigation of the AC breakdown voltage of nanofluids as a function of concentration and type of nanoparticles. It was also important to compare the dielectric performance of different types of nanofluids (oil-based and ester-based nanofluids), as the use of ester-based nanofluids would potentially be preferred from an environmental perspective. The search for the

optimal concentration of nanoparticles in the base fluid (which provides the highest AC breakdown voltage) has been conducted.

#### **1.2.4 Investigation of impulse breakdown strength**

The impulse breakdown stress is another important characteristic of the dielectric behaviours of insulating liquids. In power and pulsed power systems, the dielectric liquids are subjected to transient electric stress (transient impulse over-voltages). Thus, in addition to a steady-state power-frequency AC energisation, it is important to characterise the dielectric behaviours of base liquids and nanofluids stressed with high-voltage (HV) impulses. The impulse breakdown voltages of TiO<sub>2</sub> and BN nanofluids based on mineral oil, synthetic ester, and natural ester under both positive and negative polarities have been investigated in this project. As in the case of AC energisation, the search for the optimal concentration of nanoparticles that provides the longest time to breakdown and the highest breakdown voltage has been conducted.

#### **1.2.5 Statistical analysis of pre-breakdown time**

The pre-breakdown times for TiO<sub>2</sub> and BN nanofluids based on mineral oil, synthetic ester, and natural ester under both positive and negative polarities have been obtained in this project. These experimental results were used to calculate the average propagation velocity of streamers. Additionally, statistical analysis of the pre-breakdown time intervals has been conducted to classify the dielectric liquids per their pre-breakdown time.

#### **1.2.6 Investigation of mobility of charge carriers and space-charge-influenced field distribution**

The charge carrier mobility can be obtained by measuring the DC pre-breakdown current and by fitting the analytical I-V curves calculated using the space-charge-distributed electrical field to the experimental data. The fitting parameter is the charge carrier's mobility. The charge carrier mobilities of three insulating liquids were presented in this project. Based on these results, the field distribution of three liquids has been calculated and simulated.

### **1.3 Outline of the Thesis**

A brief summary of each chapter in this thesis is presented below.

## **Chapter 1 (Introduction)**

Chapter 1 introduces the project and outlines the motivation and main objectives of this study.

## **Chapter 2 (Literature Review)**

In Chapter 2, a literature review of the main physical and dielectric properties of liquid insulators is presented. This chapter also provides a comprehensive literature review on the dielectric properties of nanofluids.

## **Chapter 3 (Experimental Setting and Sample Preparation)**

In this chapter, the details of experimental setup used in this study are presented and discussed. The experimental systems include HV diagnostic devices, AC breakdown voltage measurement system, impulse HV generator, and charge carrier mobility measurement system. The physical properties of nanoparticles and base liquids used in this study are given in this chapter. The process of the development of nanofluids is also discussed.

## **Chapter 4 (Investigation of AC Breakdown Characteristics)**

In this chapter, the experimental procedure and the results regarding the AC breakdown voltage are discussed. The Weibull distribution analysis was conducted to classify the breakdown voltages statistically.

## **Chapter 5 (Standard Lightning Impulse Breakdown Voltage and Pre-breakdown Time Investigation)**

In this chapter, the results of the measurements of the impulse breakdown voltage and pre-breakdown time under both positive and negative standard lightning impulses are presented and discussed. The Weibull distribution is used to analyse the pre-breakdown time distribution.

## **Chapter 6 (Minimum-lightning Impulse Breakdown Voltage Investigation)**

In Chapter 6, the measurement results of the minimum impulse breakdown voltage under both positive and negative polarities are presented and discussed. Various measurement methods are used, including the ASTM D3300 method and IEC 60897 method. The comprehensive analysis of the results is presented. Statistical analysis is used to confirm the effects of nanoparticles on the breakdown voltage.

## **Chapter 7 (Charge Carrier Mobility and Potential Mechanisms of Breakdown in Nanofluid)**

The pre-breakdown currents in three base liquids under positive and negative DC field stress were measured. The mobilities of charge carriers in three liquids were obtained. Based on these results, the space-charge-influenced field distribution has been obtained for mineral oil and ester liquids. Paving the way for future research, a review and discussion of several potential mechanisms of breakdown in nanofluids is presented.

## **Chapter 8 (Conclusion and Future Work)**

In this chapter, there is a summary of the project, which includes the review of this project and the major contribution of this project. Then, a short discussion about the future work and potential research direction is presented.

## **1.4. Publications During PhD Study**

### **Journal paper**

Yi Jing, Igor V. Timoshkin, Mark P. Wilson, Martin J. Given, Scott J. MacGregor, Tao Wang, and Jane M. Lehr. ‘Dielectric properties of natural ester, synthetic ester Midel 7131 and mineral oil Diala D’. *IEEE Transactions on Dielectrics and Electrical Insulation* 21.2 (2014): pp. 644–652.

### **Conference paper and poster presentation**

Yi Jing, Igor V. Timoshkin, Mark P. Wilson, Martin J. Given, Scott J. MacGregor, Tao Wang, and Jane M. Lehr. ‘Dielectric properties of natural ester, synthetic ester Midel 7131 and mineral oil Diala D’. *IEEE International Power Modulator and HV Conference (IPMHVC)*, 2012: pp. 63–66.

Yi Jing, Igor V. Timoshkin, Scott J. MacGregor. ‘Dielectric properties of insulating liquids’. Poster, *UHVnet Colloquium* 2013.

“<http://www.uhvnet.org.uk/downloads/Delegate%20Information%206th%20UHVnet%20Colloquium%20v3.pdf>” entered on 16/11/2016.

Yi Jing, Igor V. Timoshkin, Scott J. MacGregor. ‘Dielectric properties of insulating liquids’. Poster, *UHVnet Colloquium* 2014.

# CHAPTER 2

## BACKGROUND INTRODUCTION AND LITERATURE REVIEW

### 2.1 Introduction

Dielectric liquids are used in transformers to protect the HV elements of the transformers. These liquids also provide heat dissipation from the transformer winding; thus, it is important to use dielectric liquids with good thermal conduction properties. The insulating liquids that are typically employed in power and pulsed power systems are mineral oils. In [1] and [2], it is indicated that, with the developments in the power industry systems, the traditional liquid insulating material, mineral oils, may not be able to satisfy strict (technical and environmental) requirements.

Furthermore, the mineral oils have some significant disadvantages. Older oils are toxic, as they contain polychlorinated biphenyls (PCBs), and mineral oils are not biodegradable. The PCBs were widely used as additives in transformer oils due to their ability to improve the dielectric strength and performance stability of mineral oils. It was found that PCBs are carcinogenic. In the case of older oils containing PCBs, burning PCBs can form high toxicity products, such as chlorinated dibenzofurans and chlorinated dioxins. Due to these disadvantages, PCBs have been banned in many countries; however, multiple power and pulsed power HV systems still contain older style traditional mineral oils with PCBs, which were added in various proportions to improve the dielectric strength of these mineral oils. In the case of leakage or fire, these old-style oils can cause significant environmental damage; cleaning operations could be difficult and expensive.

However, even mineral oils without PCBs are toxic. They are non-biodegradable; therefore, in the case of spillage and leakages, they can cause serious land and water pollution problems. Moreover, in the case of fire, burning mineral oils can cause serious atmospheric pollution [37]. Because of these disadvantages of traditional mineral oils, researchers and industrialists have begun to look for new insulating liquids that could substitute for mineral oils.

Ester liquids have low toxicity. They are biodegradable liquids and provide higher flash points compared with mineral oils [3]. Due to their environmental properties (biodegradability and low/zero toxicity), ester liquids have attracted the attention of power utilities and insulating liquid manufacturers as potential substitutes for mineral oils in HV power systems [4]–[8].

The use of nano-materials, including nanoparticles, in practical industrial applications has provided multiple breakthrough developments in recent decades. One of the promising approaches is to combine nanoparticles and insulating liquids to control and improve the dielectric and thermal conductive properties of the dielectric liquids. A nano-modified insulating liquid called a ‘nanofluid’ was proposed to be used as a dielectric liquid for the first time by Choi et al. at Argonne National Laboratory in the USA in 1995 [38]. In [38], the authors dispersed metal powder nanoparticles into the traditional transformer oil and formed a uniform suspension with a mass concentration of nanoparticles in the range of a few per cent (% , b/w). This nanofluid was also intended to provide better thermal conductivity compared with the base transformer oil.

In 1998, Segal designed the experimental system that he used to investigate the dielectric properties of a new nanofluid, which was prepared by dispersing the magnetic nanoparticle into traditional mineral oil [17]. His experimental work provides a distinct finding, which attracted the attention of many researchers. Segal’s results showed that, through adding magnetic nanoparticles with a specific concentration into the traditional mineral oil, the nanofluid provides higher AC breakdown voltage than the base oil sample if the oil has a relatively high moisture content ( $> 30$  ppm). In contrast, the nanofluid showed similar AC breakdown voltage compared with the base oil if its moisture content was relatively low ( $< 5$  ppm). Under the impulse energisation, in the point-sphere electrode topology, the nanofluid provided an almost 50% increase in the positive breakdown voltage compared with the base oil. However, the negative breakdown voltage was similar to that of the base oil sample.

Nanofluids with conductive nanoparticles have attracted significant attention because of their unique dielectric properties. However, recently, new published research results showed that not only conductive nanoparticles but also semi-conductive and non-conductive nanoparticles can improve the dielectric strength of the oils. Nanofluids based on such semi/non-conductive particles also demonstrated an increase in their breakdown voltage [39], [40].

In [20]–[27], it was shown that nanofluids that contain conductive nanoparticles (magnetite) may have an obvious problem under high field stress applied over a long period. These results indicated that the conductive nanoparticles may be redistributed under the action of the external electrical field. They can start to aggregate, which will increase the particle size and precipitate, which will reduce the nanofluid stability, and hence will weaken the dielectric properties of the nanofluid.

As semi/non-conductive nanoparticles have lower conductivity compared with magnetite, which may prevent the aggregation from occurring in the nanofluid due to the external field effect, multiple researchers have started to focus on the investigation of the dielectric performance of nanofluids based on such nanoparticles [28]–[31]. Moreover, semi/non-conductive nanoparticles may provide better operational stability in the high electrical field conditions compared with magnetite nanoparticles, as the electrophoretic force that will act upon them will be substantially weaker due to their lower conductivity/dielectric permittivity.

Based on the above discussion, the demand to find new insulating liquids to replace the traditional mineral oils in the pulsed power and power HV systems is urgent. Ester liquids can be considered potential alternative insulating liquids due to their comparable dielectric properties and environmentally friendly properties compared with that of mineral oils. On the other hand, adding nanoparticles to insulating liquids to enhance their dielectric properties has been recognised as a viable approach. Thus, to expand practical applications of new insulating liquids with better environmentally friendly properties, investigation into the dielectric properties of ester-based nanofluids is necessary.

This project is focused on the comparative study of the dielectric characteristics of three insulating liquids, naphthenic mineral oil, synthetic ester liquid, and vegetable oil (natural ester liquid) and nanofluids developed on their basis. Nanofluids have been prepared using two types of semi-conductive nanoparticles ( $\text{TiO}_2$  and BN) in various mass concentrations.

In this chapter, the breakdown mechanisms in insulating liquids are discussed, and the comprehensive literature review on dielectric properties of base and nano-modified dielectric liquids is presented. First, the basic breakdown theory of liquids is discussed in Section 2.2, which involves the electrostriction breakdown theory, ionisation breakdown theory, and suspended particles theory. Then,

the results of the investigations of the dielectric properties of insulating liquids are presented in Sections 2.3–2.4. These sections include a brief discussion of the physical properties and chemical structure of the mineral oils, synthetic esters, and natural esters. The comparison of the dielectric properties of various liquids is also given. The investigations of the dielectric properties of nanofluids are presented in Sections 2.5–2.6, which include the methods of preparation of nanofluids, physical properties of nanofluids, and their dielectric properties. In Section 2.7, a summary of this review is presented.

## **2.2 Breakdown Mechanisms in Dielectric Liquids**

It is important to understand the breakdown mechanisms in dielectric liquids to optimise and utilise the dielectric liquid insulation in HV systems. Thus far, there has been no single theory that is unanimously accepted for the description of the breakdown mechanism in liquids and for the explanation of the breakdown behaviours of the liquids. The reason for the lack of this theory is that liquid, as an insulation material, has a complex nature compared to gas. The ideal base liquid can be treated as a high-density gas to simulate and analyse the breakdown behaviours. However, in practical situations, liquid contains a lot of impurities, such as fibre, water, carbide, and dust, which will significantly affect the breakdown behaviours in liquid. Furthermore, it is challenging to control the liquid purity in practical applications.

Several ideas have been put forward to try to investigate the potential mechanism of breakdown in liquid. There are three predominate theories that have been widely recognised as the main theories for breakdown in liquids. These theories, discussed in Section 2.2.1, are the electrostriction theory, electronic ionisation theory, and suspended particle theory [41]–[46].

### **2.2.1 Electrostriction breakdown mechanism**

In the cavity breakdown theory, the formation of a gas bubble (cavity) near the HV electrode surface is required. After the bubble is formed, the electron avalanche process begins in the bubble, which will produce an ionisation region. There are several processes that contribute to the formation of the pre-breakdown cavities in the liquid. For example, the local joule heating will produce the vapour bubble near the HV electrode. Another mechanism of bubble formation is based on the electrostriction effect. The force exerted by the external electrical field on the liquid may also produce the bubble.

In the case of electrostriction bubble formation, the primary mechanism to produce the bubble is the local electromechanical (electrostriction) process [46]–[52]. In [46], Lewis explained the bubble formation progress due to the electromechanical stresses in the liquid. When the external field is strong enough and close to its breakdown, there is a mechanical stress exerted on the liquid (electrostriction effect). This mechanical stress will produce a ‘crack’ in the liquid, which will propagate away from the HV electrode. Pre-existing micro-bubbles (density fluctuations) will help in propagation of the crack through the liquid. These micro-bubbles weaken the liquid molecular structure and lead the crack to form in the liquid near by the cathode electrode surface. These cracks are called ‘vacuoles’, which are low-density (gas/vapour) regions that allow electrons to inject. These vacuoles can form due to mechanical stress and do not require vaporisation of the liquid. In the vacuole, the electron avalanche can be triggered and developed. When the vacuole contains large numbers of electrons, this region can be treated as an extension of the cathode and can form a protrusion. The enhanced field will repeat this process. Once there is a vacuole form in the liquid, the liquid structure will continue breaking and will lead the vacuole to develop towards the other electrode. The illustration of the bubble formation and development progress has been shown in Figure 2-1.

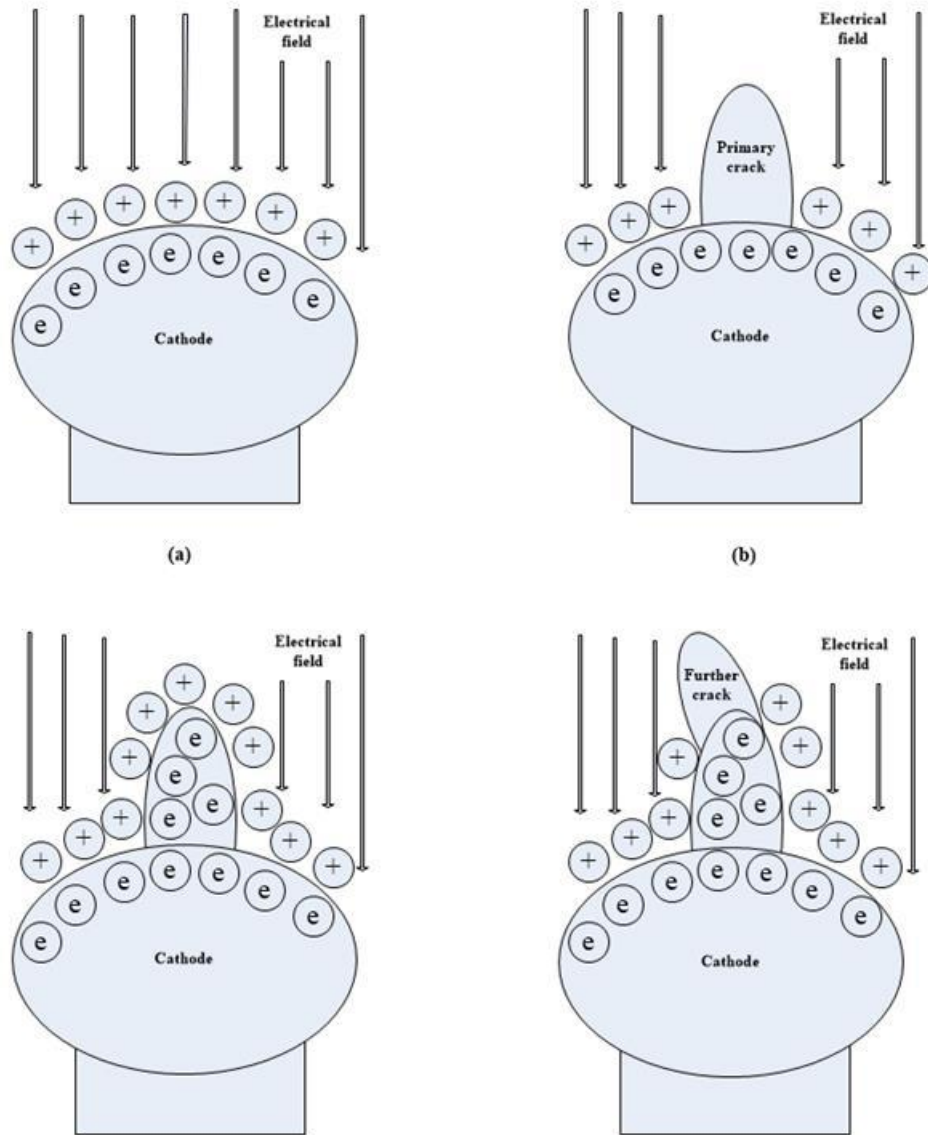


**Figure 2-1.** Illustration of bubble formation and development progress. (a) Before the bubble forms, the positive ions and electrons gather around the electrode surface. (b) Due to the electrical force effect, the primary crack in the liquid occurs near the electrode surface. (c) Electrons inject into the crack, and this crack can be treated as an electrode extension, which will distort the field severely. (d) Due to the electrical force effect, a new crack occurs near the primary crack.

### 2.2.2 Ionisation in liquid: Streamer mechanism

The research of breakdown in gas has indicated that the main reason leading to gas breakdown is the electron avalanches caused by continuous electron collision ionisation. A similar principle was introduced to explain the breakdown events in liquids. A review of this theory is discussed by Lewis in [46]. In the case of initiated ionisation, Lewis indicated that the ionisation progresses in the cases of the cathode and anode are different.

In the case of the cathode ionisation initiated process, the electrons will emit from the cathode surface into the liquid. While the external applied field injects the electrons into the liquid, the collisions between the electrons and the molecule particles take place. These collisions induce the neutral molecules to ionise, and the local temperature increases. This temperature rise leads to liquid evaporation and then the vapour cavities appear near the electrode surface [41]. These vapour cavities comprise a low-density region that allows more electrons to pass through and obtain more energy from the field before affecting the molecules. The ionisation effect of one neutral molecule will produce two electrons with low velocity. These slow electrons will stay at the front of the cavities and drift towards the anode due to the Coulombic forces and then form the negative charge cloud. With the slow electron drift, the cavities will develop and form a region of finger-shaped protrusions containing large numbers of charge ions and electrons, which is called a streamer. This negative streamer will expand and appear thick and bushy as it propagates through the gap between the electrodes. Once the streamer reaches the other electrodes, the charge ions in the streamer will form a conductivity channel between the anode and cathode. This conductivity channel has very low resistance and will produce a high energy current passing through the gap distance, which is called the breakdown [42], [53]–[57]. The illustration of cathode ionisation has been shown in Figure 2-2.

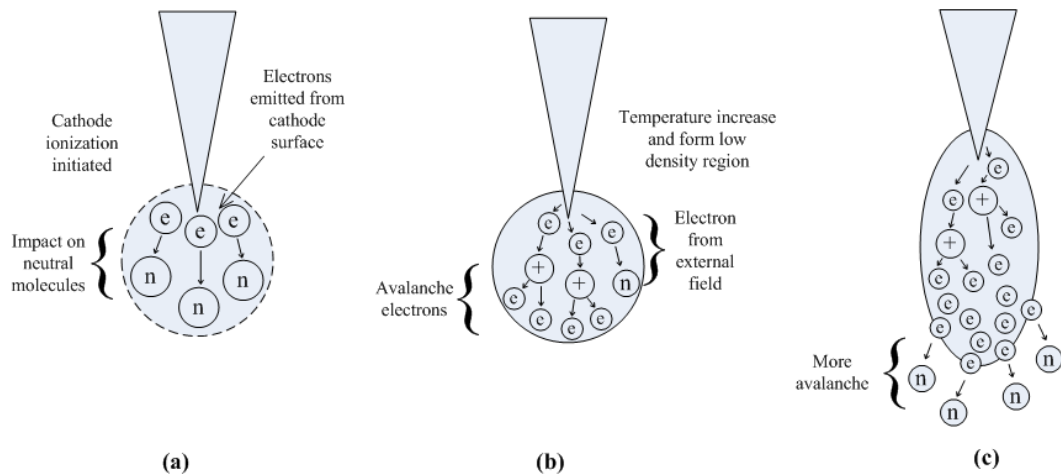


**Figure 2-2.** Illustration of the initiated cathode ionisation negative streamer formation and propagation. (a) In the case of the initiated cathode ionisation, the electrons are emitted from the cathode surface. These electrons impact neutral molecules and induce the molecules to ionise. (b) Due to the molecule ionisation, the local temperature rises and forms a low-density region, which allows more electron avalanches to occur. (c) The slow electrons stay at the front of the space-charge region and drift towards the anode due to the Coulombic forces. The negative streamer continues developing, repeating the above process.

In the case of the anode ionisation initiated process, the electrons near the electrode are attracted towards the anode. Because the electrons have high velocity compared with the positive ions that have low velocity, when the electrons reach the anode, the positive ions are 'left behind' and form a positive charging region, which is a positive streamer. These positive space-charge regions can be treated as an anode extension to attract more electrons. This phenomenon results in more avalanches forming at the front of the streamer; hence, the positive streamer will continue developing. As the positive ions have low velocity, the positive space-charge region will form in a wider area in the liquid compared with the cathode case. Thus, the positive streamer appears thin and filamentary as it propagates through the gap distance. The anode ionisation illustration is shown in Figure 2-3.

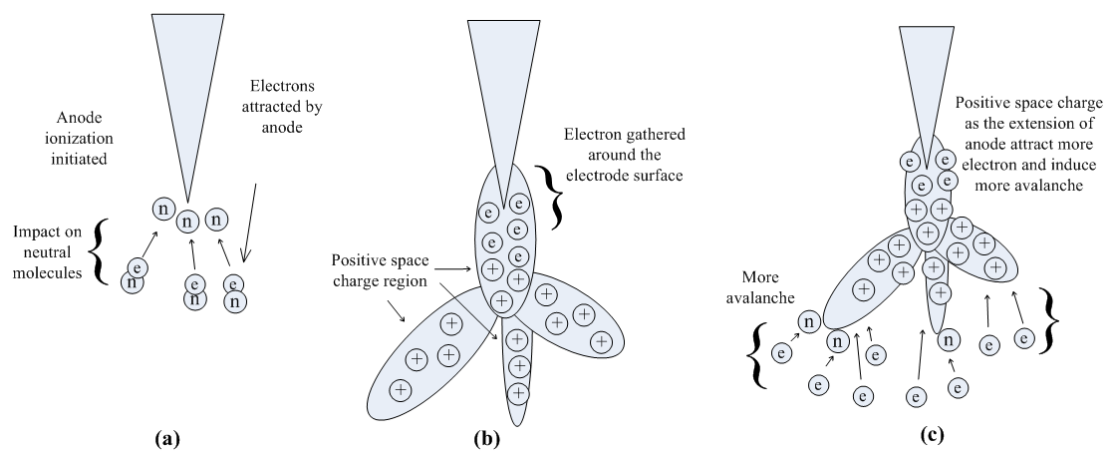


**Figure 2-3.** Illustration of the initiated anode ionisation, positive streamer formation, and propagation. (a) In the case of the initiated anode ionisation, the free electrons in liquid are attracted by the anode surface. These electrons impact neutral molecules and induce the molecules to ionise. (b) Due to the high velocity of the electrons compared with the low velocity positive ions, when the electrons reach the anode, the positive ions are 'left behind' and form the positive charging region, which is a positive streamer. (c) Positive space-charge regions can be treated as an anode extension to attract more electrons; hence, the positive streamer will continue developing.

The streamer formation and propagation is the result of several complex mechanisms. Streamers in dielectric liquid can be classified as fast, slow, subsonic, and supersonic streamers. However, this is inconvenient and may result in confusion when comparing between different streamer propagation modes [58], [59]. In order to compare the streamer characteristics using a uniform standard, in [60], Hebner classified the streamers into first, second, third, and fourth modes, depending on their propagation velocity. The typical velocity of the streamer modes in mineral oil is presented in Table 2-1.

**Table 2-1.** Typical velocity of streamer modes in mineral oil [60].

| <b>Streamer modes</b>       | <b>1<sup>st</sup> mode</b> | <b>2<sup>nd</sup> mode</b> | <b>3<sup>rd</sup> mode</b> | <b>4<sup>th</sup> mode</b> |
|-----------------------------|----------------------------|----------------------------|----------------------------|----------------------------|
| Propagation velocity (km/s) | 0.1                        | 1 ~ 2                      | 10                         | 100                        |

The velocity of streamers depends on the applied voltage and type of liquid. These velocities indicate the pre-breakdown time and different energisation requirements, which is important from a practical point of view in the development and coordination of the dielectric insulation of HV power and pulsed power systems. More details on the review of streamer characteristics that are relevant to the current project are given in Section 2.4.1.

### **2.2.3 Suspended particles theory**

In practical applications, it is hard to maintain the purity of the insulation liquid. In general, liquid contains a significant number of contaminants, such as fibre, water, and carbide, which will affect the liquid breakdown behaviours. The concentration and properties of suspended particles can explain the variation in the breakdown behaviour of liquids. The particles that are usually of observable size will be polarised and receive the electrical charge due to the external field; thus, the electrical force will be exerted on these particles. This force will result in particle movement on the liquid. If the polarised particles are concentrated near the electrode, they can be treated as a virtual extension of the electrode and enhance the local field distortion. The particles will drift towards the centre axis between the electrode and form a bridge, which may result in breakdown [61]–[67].

## **2.3 Chemical Structure and Physical Properties of Dielectric Liquid**

Three dielectric liquids have been used in the investigation in this project. These liquids are mineral oil (Diala S3 ZX-IG), synthetic ester (Midel 7131), and natural ester (food-grade rapeseed oil). The review of the chemical structure and physical properties of these liquids has been presented in this section.

### **2.3.1 Chemical structure of dielectric liquids**

Mineral oil is refined from crude oil, which primarily consists of hydrogen and carbon atoms in several different molecular structures. There are three main chemical structures of such liquids: aromatic, naphthenic, and paraffinic liquids, as shown in Figure 2-4. These molecular structures have

different electron trapping properties that affect the streamer properties in liquid under both positive and negative polarity conditions. Aromatic components influence the positive and negative streamer characteristics due to their low ionization potential and large electron-trapping sections respectively [57], [68], [69].

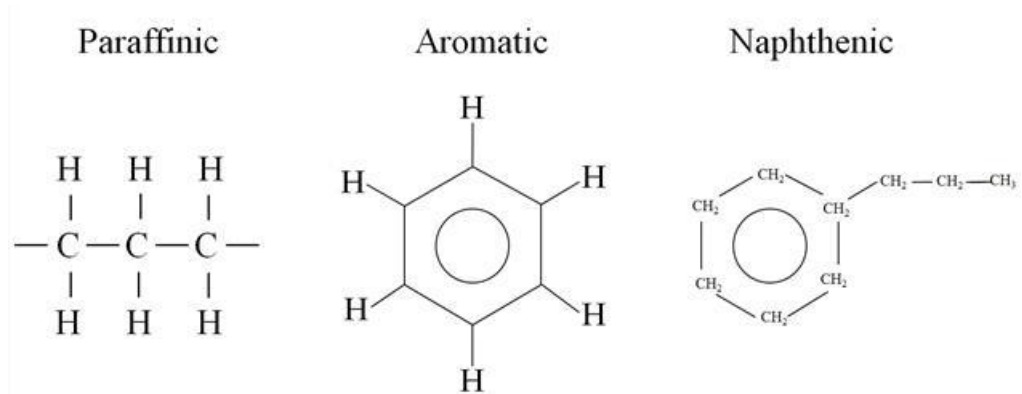
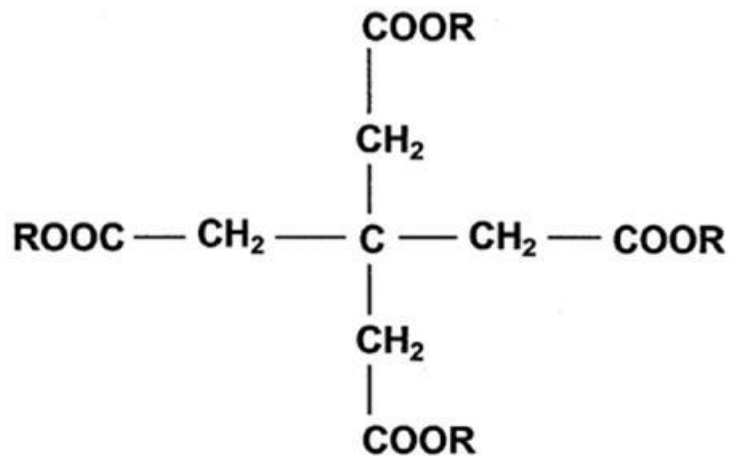


**Figure 2-4.** The main chemical structures of the mineral oils are paraffinic, naphthenic, and aromatic [68].

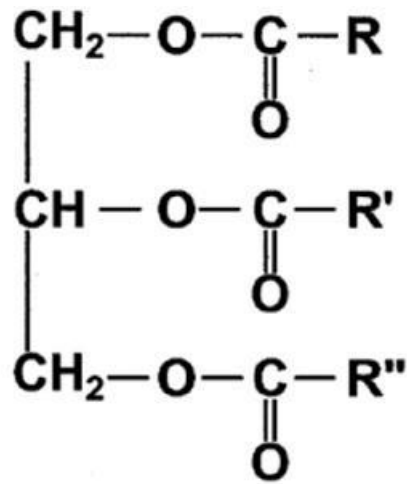
Midel 7131, a synthetic ester, is classified as a T1 insulating liquid, which is a halogen-free pentaerythritol ester [70]. The chemical composition of the molecules of this synthetic ester is shown in Figure 2-5. In this molecular structure, as Figure 2-5 shows, there are four groups of '-COOR' components at the end of the chain structure. In these components, the symbol 'R' indicates a multiple organic group, which could be the same or different in these four -COOR components. The -COOR components contain oxygen atoms, which have high electronegative performance, which makes synthetic ester (Midel 7131) more polar compared to the traditional mineral oil. Thus, the volume resistivity of Midel 7131 ( $> 5 \times 10^{12}$ ,  $\Omega\text{-cm}$  at  $25^\circ\text{C}$ ) is generally lower than the traditional mineral oil ( $\sim 2.5 \times 10^{13}$ ,  $\Omega\text{-cm}$  at  $25^\circ\text{C}$ ) [71] but the relative permittivity of Midel 7131 ( $\sim 3.2$ ) is higher than that of mineral oil ( $\sim 2.2$ ) [72].



Pentaerythritol ester

**Figure 2-5.** Pentaerythritol ester structure [45], [72], [73].

Food-grade natural oils can be refined from many agronomic crops, such as sunflower, soya, rapeseed, olive, coconut, cottonseed, and so on. In this thesis, rapeseed oil was chosen as the test liquid used in all experiments. As a food-grade oil, rapeseed oil consists of several chemical components. The main molecular component of rapeseed oil is triglyceride fatty acid. The chemical structure of the triglyceride fatty acid, which includes saturated and unsaturated fatty acids, contains 22 carbon length chains, which contain one to three double bands, as shown in Figure 2-6. The bond number of saturation could affect the ester dielectric properties. The anti-oxidation ability could increase with increased bond of saturation, but it also increases the viscosity of the liquid, which would lead to decreased cooling ability of the liquid. Similar to synthetic ester (Midel 7131), the volume resistivity of natural ester is lower than the resistivity of traditional mineral oil, and the relative permittivity of natural ester is higher than that of mineral oil [72], [73].



Triglyceride ester

Figure 2-6. Triglyceride ester structure [73].

### 2.3.2 Pour point

The pour point is defined as the lowest temperature that can maintain the liquid flow properties. It is a key parameter that is used to evaluate whether a material is suitable for a practical application, especially in low temperature conditions. The insulating liquids that have a high pour point will start to curdle, and their insulation function may become invalid. In [74] and [75], the experimental results indicated that the vegetable oil pour point is  $-30^{\circ}\text{C}$ . The pour point of synthetic ester (Midel 7131) was reported in [75] at  $-60^{\circ}\text{C}$ , which is lower than the typical mineral oil pour point of  $-50^{\circ}\text{C}$ .

### 2.3.3 Viscosity and thermal conductivity

The viscosity of insulating liquids will affect their thermal conductivity and their self-healing capability. In the transformer, various parts of the liquid receive uneven heating, which will make liquids flow in the tank. Low viscosity means liquids can flow quickly and smoothly, thus transferring thermal energy from the hot spot to the tank to protect the transformer.

At  $20^{\circ}\text{C}$ , the viscosity of mineral oil, synthetic ester, and refined natural ester was reported to be  $20 \text{ mm}^2/\text{s}$ ,  $70 \text{ mm}^2/\text{s}$ , and  $85 \text{ mm}^2/\text{s}$ , respectively [75]. The potential reason for ester liquids to present higher viscosity than mineral oil is the different chemical structure and components; furthermore, ester liquids may contain fibres, which will raise the viscosity. The thermal conductivity of ester liquids is higher than that of mineral oils. However, ester liquids have high viscosity, which could slow the liquid flow and reduce the thermal dissipation ability [75].

### 2.3.4 Fire point and flash point

The fire point and flash point are used to evaluate nanofluid flammability, which is crucial for the power industry insulation system. The fire point is defined as the lowest temperature to maintain at least 5 seconds of burning after the material ignition by open fire. Generally, the fire point is higher than the flash point. The flash point is the lowest temperature to ignite the mixture of the material vapour and air. Normally, the ignition will not continuously burn; however, it may lead to an unexpected accident and explosion at high temperatures. The flammability, fire point, and flash point are vital for insulating materials because the unexpected flame may induce explosions of HV devices and lead to devastating consequences. In [3], both the fire point and flash point of several insulating liquids have been determined. As Table 2-2 shows, the results indicated that ester liquids provide obvious higher flash points and fire points than mineral oil, which is a main advantage in the consideration of these as alternatives to mineral oil.

**Table 2-2.** The fire points and flash points of mineral oil, synthetic ester, and natural ester [3].

| Liquid Type     | Fire Point (°C) | Flash Point (°C) |
|-----------------|-----------------|------------------|
| Mineral oil     | 170-180         | 160-170          |
| Synthetic ester | >300            | >250             |
| Natural ester   | >350            | >300             |

## 2.4 Dielectric Properties of Liquids

In this section, a review of the dielectric properties of mineral oil, synthetic ester, and natural ester is presented. The review includes the 1) streamer characteristics of dielectric liquids relevant to the present work, 2) AC and lightning impulse breakdown voltages of the liquids, and 3) ageing of the liquids.

### 2.4.1 Streamer characteristics in dielectric liquids

In [76] Sitorus et al. investigated the streamer characteristics in mineral oil and jatropha curcas methyl ester oil (JMEO) stressed with positive and negative lightning impulses. The point-plane electrodes were used in Sitorus's experiments. The HV electrode was a tungsten needle with a 15- $\mu\text{m}$  tip radius. The ground electrode was a 40-mm diameter brass disc. The gap distances were 20, 25, and 30 mm. The images of the streamer in the case of the 30-mm gap distance are shown in Figure 2-7. The results

showed that negative streamers in mineral oil are highly filamentary and luminous compared to those in JMEO. There was no obvious difference between the shapes of positive streamers in both liquids. Based on the shape and the stopping length, the author concluded that JMEO could be considered a potential substitute for mineral and other synthetic oils for electric insulation, particularly in HV power transformers.

In [11], [76], and [77], Duy et al. measured the streamer characteristics in natural ester liquids using both positive and negative ‘step’ impulses. Streamer propagation was investigated in a point-plane electrode system, constituted by a steel needle with 1- to 100- $\mu\text{m}$  tip radius facing a grounded-plane disc with a 20 cm diameter. The gap distance was from 20 mm to 200 mm. The authors indicated that the standard lightning impulse (1.2/50  $\mu\text{s}$ ) has a relatively short rising and falling time, which may not inject enough energy (charge) into the liquid to affect the streamer formation and propagation. The switching impulse (250/2500  $\mu\text{s}$ ), which has a longer rising time would induce a large jitter on the streamer initiation. Thus, to minimise the jitter, the step impulse (0.5/1400  $\mu\text{s}$ ) was used in these experiments. The streamer charge, average propagation velocity, and stopping length in natural ester, stressed with both positive and negative impulses at a 100-mm gap distance, are shown in Figure 2-8.

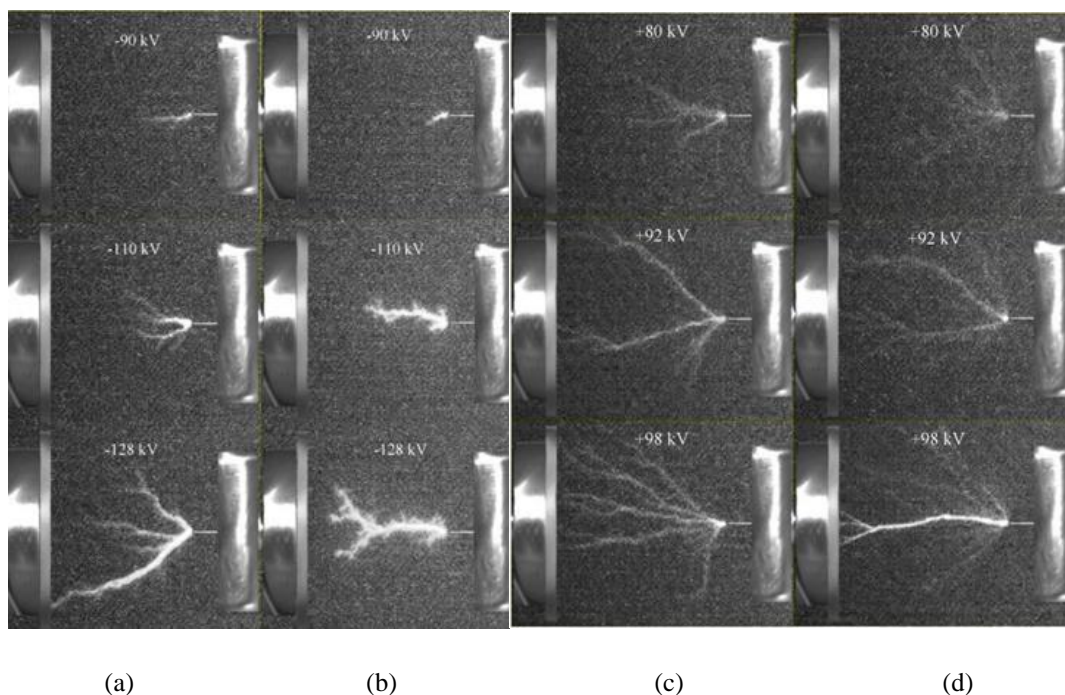


**Figure 2-7.** Streamer in JMEO (a) and mineral oil (b) stressed with the negative impulse. The streamer in JMEO (c) and mineral oil (d) stressed with the positive impulse. The HV electrode is a tungsten needle with 15- $\mu\text{m}$  tip radius. The ground electrode is a 40-mm diameter brass disc. The gap distance is 30 mm. These figures are from [76].

Under the positive impulse, the streamer stopping length in the natural ester has an increasing tendency and was close to that in mineral oil (dashed line). After breakdown, the streamer propagation velocity in natural ester increases much faster with an increase in the applied voltage compared with that in mineral oil. Under the negative impulse, the streamer stopping length in natural ester is significantly longer than that in mineral oil. After breakdown, the streamer propagation velocity in natural ester increases faster with an increase in applied voltage compared with that in mineral oil, but the difference did not provide as significant results as the positive streamer measurements.

The authors indicated that the streamers in natural esters propagate easier than that in mineral oil, which induces the step impulse breakdown voltages of natural ester, which are lower than that of mineral oil in both polarities. These results showed that, in the case of the liquid stress step impulse, the dielectric properties of mineral oil are better than the dielectric properties of base natural ester. For example, mineral oil provides a higher step impulse breakdown voltage and better streamer inhibition capability. The potential reason for this behaviour is that the mineral oil contains polyaromatic molecules, which can significantly enhance the dielectric strength. This polyaromatic compound is absent in natural ester; hence, the dielectric strength of natural ester is lower than that of mineral oil.

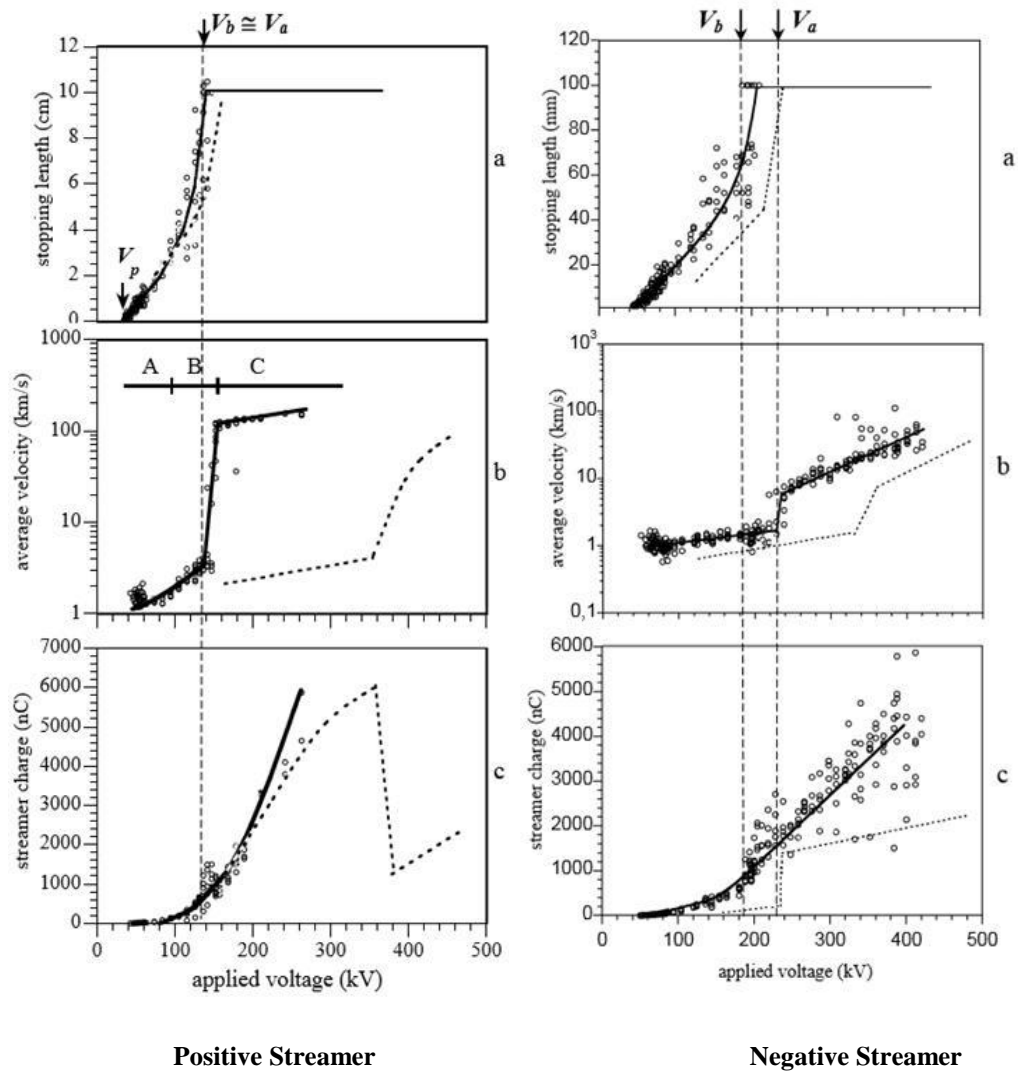


**Figure 2-8.** Characteristics of positive streamers (left column) and negative streamers (right column) in natural ester at a gap distance of 100 mm at a stress step impulse of 0.5/1400  $\mu$ s; (a) streamer stopping length, (b) streamer average velocity, (c) streamer charge – dashed line represents mineral oil; ( $V_a$ : acceleration voltage;  $V_b$ : 50% probability breakdown voltage). Figures taken from [11].

### 2.4.2 AC breakdown strength of dielectric liquids

In [9], Martin et al. measured the AC breakdown voltage of the mineral oil, synthetic ester, and natural ester using the method described in the international standard ASTM D1816. The mineral oil under the test was Nynas Nitro 10GBN. The synthetic ester was Midel 7131, and the natural ester was FR3. Spherically capped electrodes with 36-mm diameter were used. The gap distance was 1 mm gap.

The authors also calculated the breakdown voltage per the breakdown probability using the Weibull statistical analysis as shown in the Figure 2-9. The results indicated that the synthetic ester provides the highest breakdown voltage at all breakdown probabilities. In the case of relatively high breakdown probability (50% and 10%), natural ester provides a comparable breakdown voltage to the mineral oil.

In the case of low breakdown probability (5%, 2%, and 1%), the breakdown voltages of mineral oil were higher than that of natural ester.

The authors indicated that these results prove that the ester liquids provide a comparable AC withstand strength compared with that of mineral oil. Hence, ester liquids can be as capable as mineral oil in acting as transformer insulation materials.

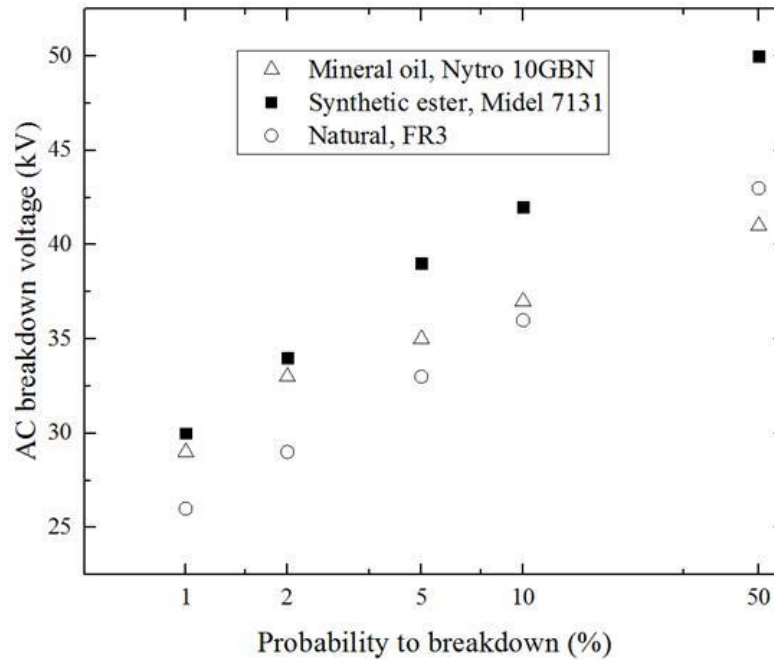


**Figure 2-9.** AC breakdown voltage of liquids as a function of the breakdown probability. Figure plotted using data from [9].

In [4], Martin et al. measured the AC breakdown voltage of the mineral oil, synthetic ester, and natural ester under two different moisture content conditions, concerning parts per million and relative humidity percentage, as Figure 2-10 shows. The test method followed the international standard ASTM D1816. The mineral oil under testing was Nynas Nitro 10GBN. The synthetic ester was Midel 7131, and the natural ester was FR3. The spherically capped electrodes with 36-mm diameter were used. The gap distance was 1 mm.

These results showed that the breakdown voltage of mineral oil decreases significantly with an increase in the moisture content. In contrast, the breakdown voltage of both ester liquids did not show a clear change with an increase in the moisture content.

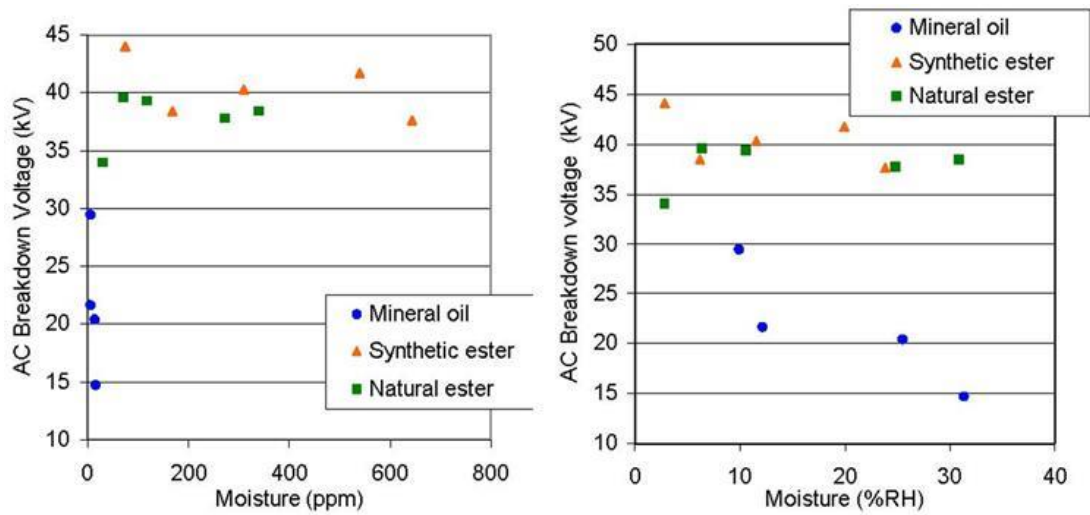


**Figure 2-10.** The AC breakdown strength of different types of insulating liquids with respect to (left side) moisture (ppm) and (right side) moisture (% RH). Figures taken from [4].

In [10], Wang et al. measured the AC breakdown voltage of mineral oil, synthetic ester, and natural ester under the ‘as received’ and ‘clean process’ conditions, as Figure 2-11 shows. The mineral oil under testing was 10 Gemini X. The synthetic ester was Midel 7131, and the natural ester was FR3. Measurement procedures followed the ASTM D1816 international standard. The spherically capped electrodes were used. The gap distance was 1 mm.

The results showed that, under the ‘as received’ condition, both ester liquids provide higher breakdown voltage than the mineral oil. However, under the clean process conditions, mineral oil shows a higher breakdown voltage. Considering practical application situations, insulating liquid will be used in the transformer tank in as received conditions, these results showed the ester liquid AC breakdown strength comparable to that of mineral oil.

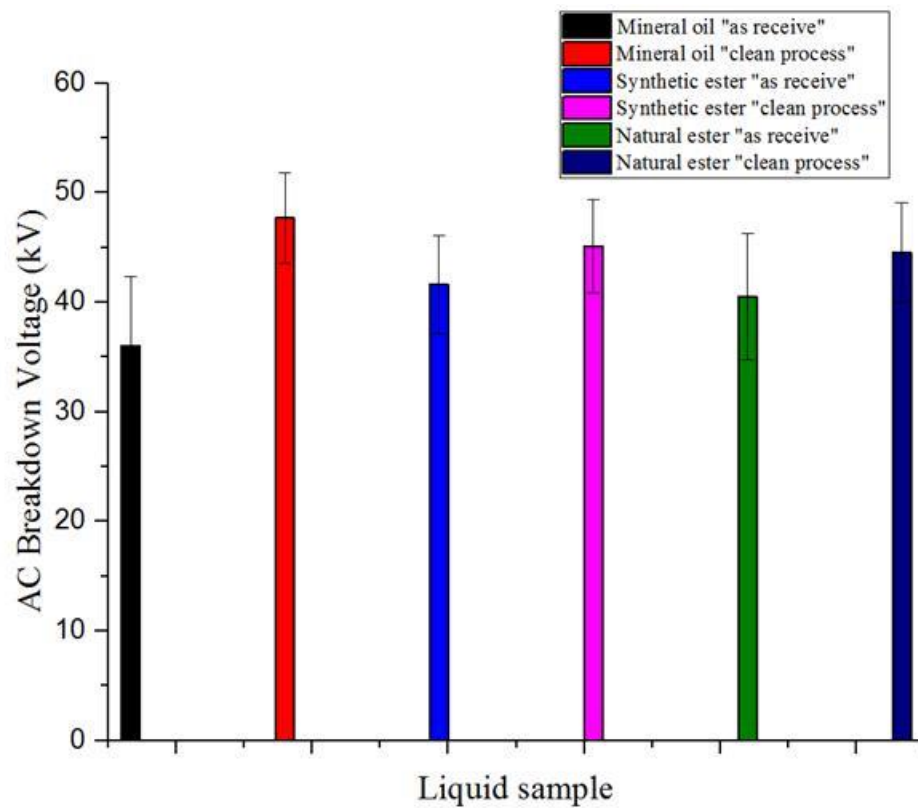


**Figure 2-11.** The AC breakdown voltage of mineral oil, synthetic ester, and natural ester under the ‘as received’ and ‘clean process’ conditions. Figure plotted using data from [10].

### 2.4.3 Lightning, step, and switching impulse breakdown strengths of dielectric liquids

Several research groups investigated the impulse breakdown strength of mineral oil and ester liquids. Unlike the AC breakdown experimental results, under the impulse field, mineral oils provide generally higher breakdown strengths than ester liquids [4], [11], [72].

In [4], Martin et al. measured the lightning impulse breakdown voltage of the mineral oil, synthetic ester, and natural ester under two different moisture content conditions, concerning the parts per million and relative humidity percentage, as Figure 2-12 shows. The measurement procedure follows the international standard ASTM D3300. The mineral oil under the test was Nynas Nitro 10GBN. The synthetic ester was Midel 7131, and the natural ester was FR3.

The results showed that, in the case of mineral oil, the breakdown strength is significantly affected by moisture content. In the case of ester liquids, the breakdown strength shows insensitivity to moisture content. These results are similar to the AC breakdown experiment results shown in Section 2.4.2. However, these results also indicate that mineral oil provides significantly higher breakdown strength

than that of the ester liquids in relatively low moisture content conditions (< 10 ppm). In relatively high moisture content conditions (> 10 ppm), the breakdown voltage of mineral oil is still comparable to the ester liquids, which is different with the AC breakdown experimental results show.

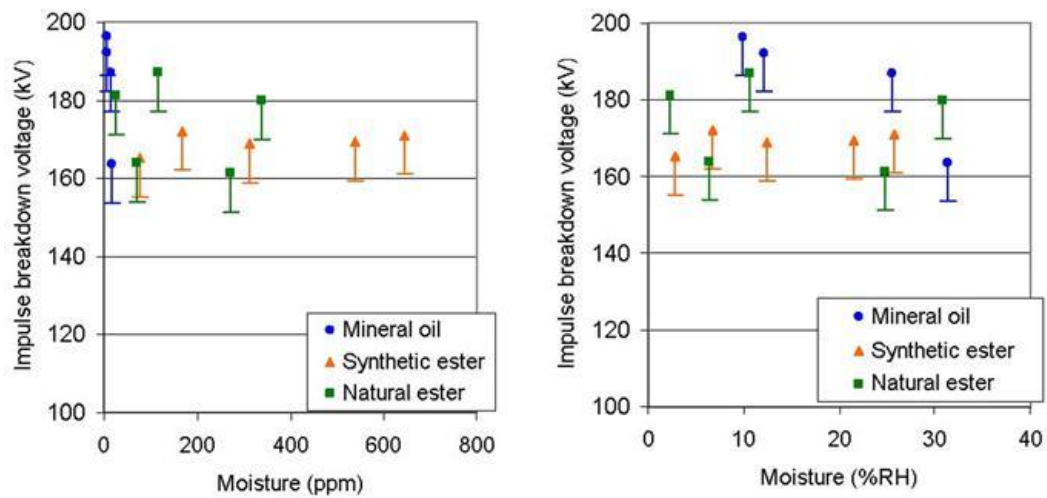


**Figure 2-12.** The lightning impulse breakdown strength of different types of insulating liquids with respect to (left side) moisture (ppm) and (right side) moisture (%RH). Figures taken from [4].

In [11], Duy et al. measured the step impulse (0.5/1400  $\mu$ s) breakdown voltage of natural ester (RS50, a special formulation of rapeseed oil with lower viscosity). Positive and negative impulses were used with various gap distances (2 cm to 20 cm). The breakdown voltages of esters were compared with the breakdown voltages of mineral transformer oil. The ratio plot of the breakdown voltage of natural ester divided by the breakdown voltage of mineral oil is shown in Figure 2-13.

The results showed that the breakdown voltages of natural ester are lower than those of mineral oil stress with both positive and negative impulses with various gap distances. The authors in [11] concluded that, under the impulse conditions, mineral oil provides higher breakdown strength, attributed to their polyaromatic molecules, which are absent in ester liquids.

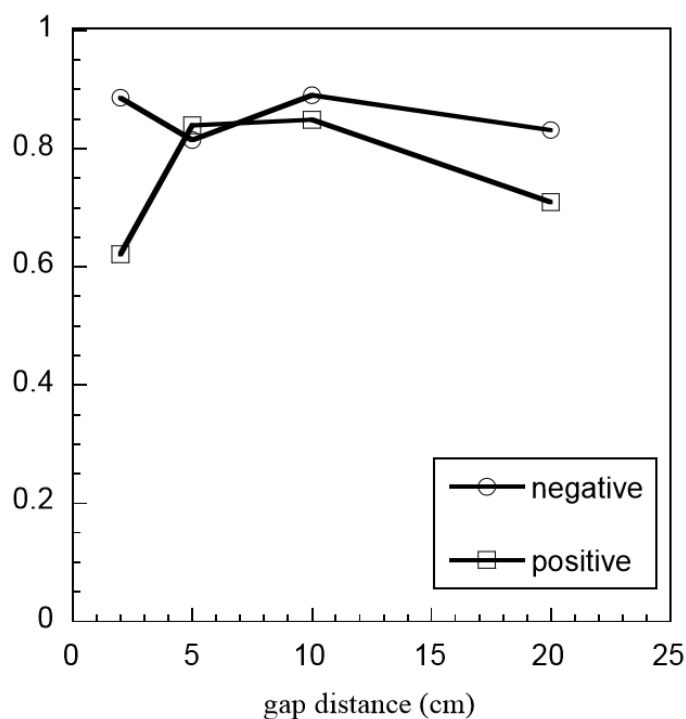


**Figure 2-13.** The ratio of breakdown voltage in natural ester divided by the breakdown voltage in mineral oil stress step impulse (0.5/1400  $\mu$ s) versus distance. The HV electrode is a steel needle with 1- to 100- $\mu$ m tip radius. The ground electrode is a 20-cm diameter plane. Figure taken from [11].

In [72], Liu et al. measured the impulse breakdown voltage of mineral oil (Gemini X), synthetic ester (Midel 7131), and natural ester (FR3) in a quasi-uniform field (sphere-sphere electrodes) using the lightning impulse and switching impulse. The gap distance was 3.8 mm. The measurement procedure followed the ASTM D3300 standard.

As Figure 2-14 shows, the lightning impulse breakdown voltages of all liquids were higher than the switching impulse breakdown voltages of all liquids. In the case of the liquid stress lightning impulse, the breakdown voltage of mineral oil was significantly higher than that of ester liquids. In the case of the liquid stress switching impulse, the breakdown voltage of mineral oil was just slightly higher than that of ester liquids.

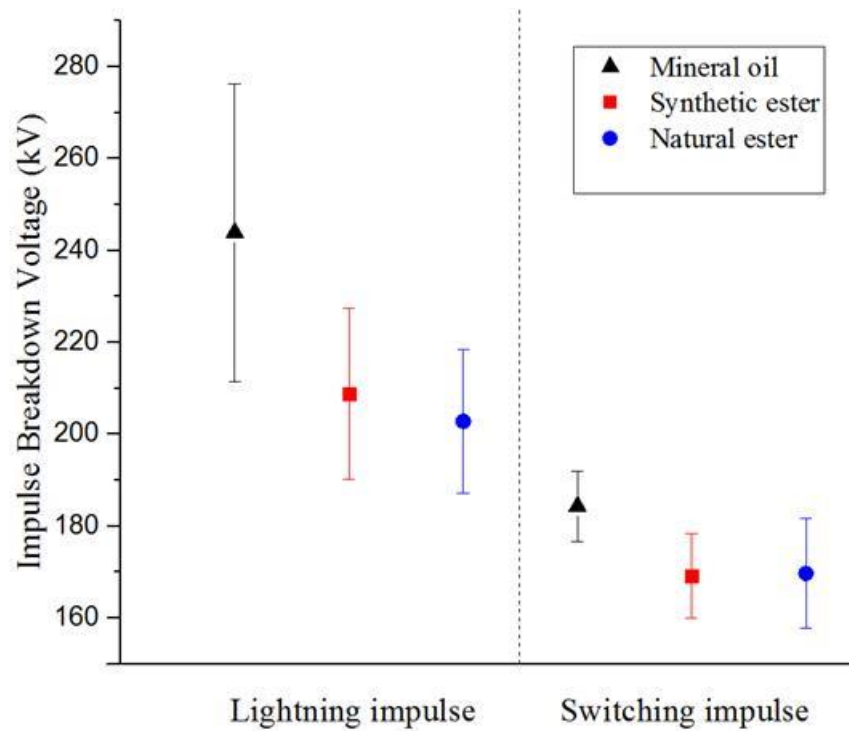


**Figure 2-14.** The impulse breakdown voltage of mineral oil (Gemini X), synthetic ester (Midel 7131), and natural ester (FR3) with lightning impulse (left column) and switching impulse (right column). Figure plotted using the data from [72].

#### 2.4.4 Ageing of dielectric liquids

In [13] and [14], the experimental results showed that, in the Kraft paper insulation system, the ester liquids present a lesser ageing degradation compared with mineral oil. Moreover, in [4], Martin et al. measured the AC breakdown voltage and lightning impulse breakdown voltage of mineral oil (Nynas Nitro 10GBN), synthetic ester (Midel 7131), and natural ester (FR3) under different ageing conditions following the ASTM D1816 [79] and ASTM D3300 [80] international standards. Samples of liquids were heated and kept at 115 °C for up to 28 days in an air circulating oven with a copper catalyst.

As Figure 2-15 shows, the AC breakdown voltage of mineral oil increased and then decreased with an increase in ageing time. The reason for this phenomenon is that the thermal ageing will reduce the sample water content; thus, the dielectric strength of the mineral oil increases. With long ageing, sample dielectric strengths start to drop because the thermal ageing degradation effect on the mineral oil dielectric properties becomes dominant [81].

Both ester liquids showed good stability and less ageing degradation under the AC voltage and lightning impulse voltage. The authors indicated that the reason for this phenomenon is that, under the thermal ageing effect, the mineral oil becomes a more viscous sludge, which would reduce the liquid

insulating performance. In contrast, the sludge did not occur in ester liquids because the chemical structure difference between the ester liquids and mineral oil induces the ageing interaction and the by-product of the ester was different [4].

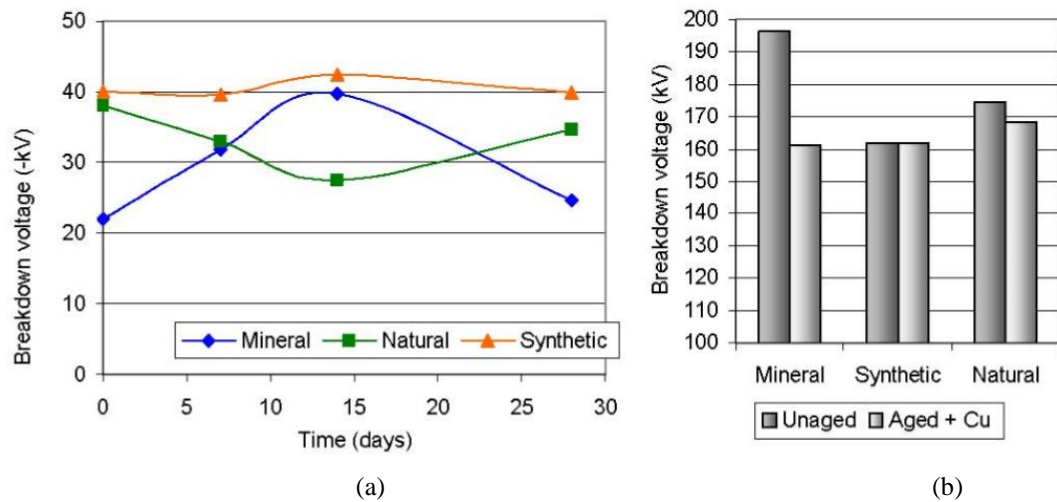


**Figure 2-15.** The AC breakdown voltage (a) and lightning impulse breakdown voltage (b) of different base liquids. Figures taken from [4].

In [5], Perrier et al. investigated the AC breakdown voltage of mineral oil, synthetic ester, and natural ester using a fresh and an ageing sample. The IEC 60156 method was used in this experiment. The gap distance was 2.5 mm. The electrode topology was sphere capped. The samples used in this investigation included vegetable oil 1 (blend of mono- and tri-ester without additive); vegetable oil 2, 3 (tri-ester); synthetic ester (tetra-ester); and mineral oil 1,2,3 (naphthenic, noninhibited), 4 (naphthenic, inhibited), 5 (paraffinic, noninhibited). The ageing procedure consisted of putting the liquids at 120°C in contact with the atmosphere and copper for 14 days. The measurement results are shown in Figure 2-16. The white bar is the AC breakdown voltage of fresh samples, and the blue bar is the AC breakdown voltage of ageing samples. The value in brackets is the lowest breakdown voltage of 30 breakdown events, which the authors consider a security coefficient (SC).

Figure 2-16 shows the average AC breakdown voltage (30 breakdown events). The results showed that, in the case of fresh samples, the breakdown voltage of all liquids were similar to each other. In the case of the ageing samples, the breakdown voltages of natural tri-ester samples (vegetable oil 2, 3) showed insensitivity to ageing. The breakdown voltage of mineral oil shows relatively higher degradation compared with natural ester. The vegetable oil 1 showed the lowest SC (15kV) due to this sample's lack additives.

In the case of the synthetic ester sample, the breakdown voltage was relatively low with respect to the other samples shown, but the standard deviation of the fresh sample and ageing sample is the same. These results indicated that the ester liquids provided less degradation of AC breakdown strength compared with mineral oil. A similar conclusion was also achieved by Martin in [4].

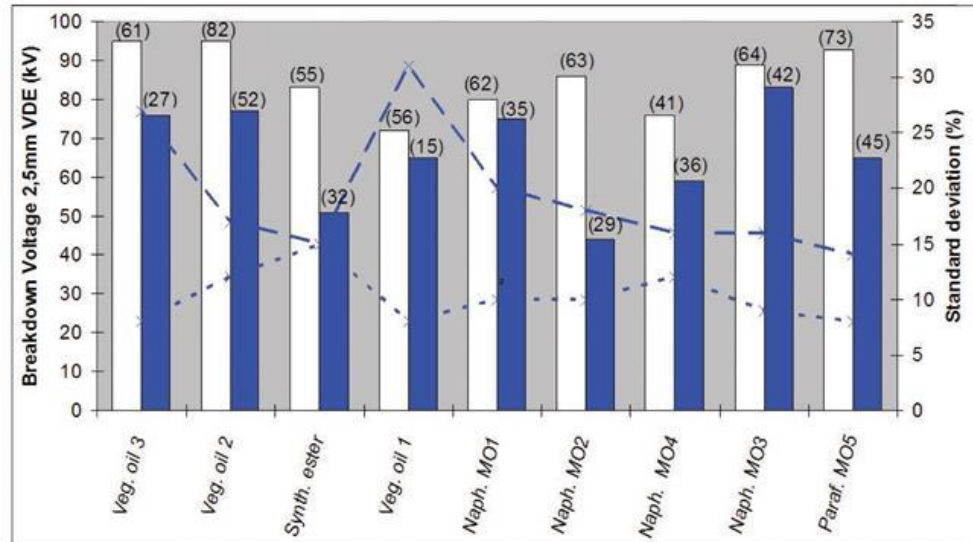


**Figure 2-16.** The average AC breakdown voltage (30 breakdown events) of mineral oil, synthetic ester, and natural ester using fresh and ageing samples. The IEC 60156 method was used in this measurement. The gap distance was 2.5 mm. The electrode topology was sphere capped. The white bar is the AC breakdown voltage of fresh samples; the blue bar is the AC breakdown voltage of ageing samples. The value in brackets is the lowest breakdown voltage of the 30 breakdown events, which the authors consider a security coefficient (SC). The dashed line represents the standard deviation of fresh samples; the dotted line represents the standard deviation of ageing samples. Figure taken from [5].

The results presented in this section indicate that, in the case of liquids stressed with AC and lightning impulses, the ageing degradation of the breakdown voltage of ester liquids was significantly less than the ageing degradation of the breakdown voltage of mineral oil. The potential reason for this phenomenon is the difference in chemical structures of mineral oil and ester liquids. The sludge occurs in mineral oil during the ageing progress, which reduces the mineral oil dielectric strength (in the case of AC breakdown voltage and lightning impulse breakdown voltage). Conversely, the sludge did not occur in ester liquids. Hence, the ageing influence on the breakdown strength of ester liquids was not obvious.

## 2.5 Fine and Ultra-fine particles in Dielectric Liquids

During the operation period of HV devices, the high electrical field will interact with the apparatus and produce heat. This extra heat induces additional stress on the equipment and insulating materials, resulting in ageing and may lead to unexpected accidents.

In order to solve this problem, previous action has been to add relatively large (micron level) particles into the insulating liquids to try to combine the properties of particles and insulating liquids [82]. The results showed that dispersing the micron-level particles into insulating liquids improved the thermal conductivity. However, these actions also decreased the insulating liquids' dielectric withstand strength because of the liquid breakdown theory [83]. Another disadvantage of the micron-level particle modified liquid is that these particles rapidly separated from the suspension and formed the precipitate because their densities were much larger than the densities of the base liquids.

In [65], Chen et al. investigated the pre-breakdown characteristics of contaminated transformer oil stressed with the DC field. Pressboard dust was used as the contaminant and was dispersed into the transformer oil at 0.0025%, 0.005%, and 0.0075% b/w. The applied voltages were 2, 7.5, and 15 kV DC voltage. The electrodes were two spherical electrodes with diameters of 10 mm. The gap was 10 mm. The experimental results are shown in Figure 2-17.

Figure 2-17 shows that the bridge formation in contaminated oil is significant with an increase in the contaminant concentration. Additionally, the pre-breakdown current rises rapidly with an increase in the contaminant concentration and stress voltage. Similar results were also reported in [62]–[64], [66] by Mahmud et al. These results showed that the large particles in liquid can be treated as contaminants, which will form the bridge between HV electrodes before breakdown is achieved. The pre-breakdown current will increase rapidly due to this bridging phenomenon. High pre-breakdown current will promote the streamer propagation, hence resulting in the reduction of the dielectric strength of the liquid. These results can be explained by the suspended particles theory, which has been discussed in Section 2.2.3 [61], [67].

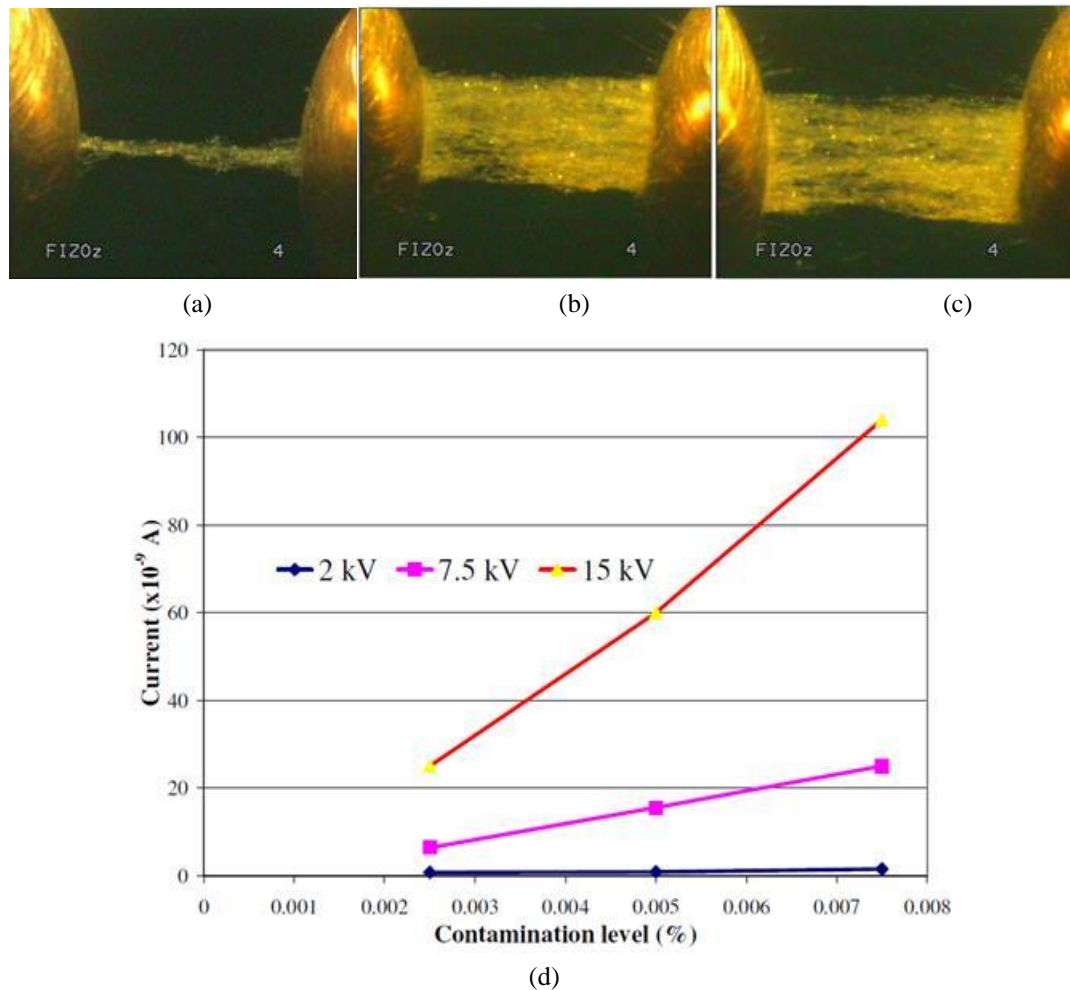


**Figure 2-17.** Bridge formation phenomenon (a) to (c) and pre-breakdown current (d) in contaminate oil. (a) Oil with 0.0025% (b/w) contaminants stressed with 15 kV DC voltage after 300 s. (b) Oil with 0.005% (b/w) contaminants stressed with 15 kV DC voltage after 300 s. (c) Oil with 0.0075% (b/w) contaminants stressed with 15 kV DC voltage after 300 s. (d) The pre-breakdown current with various contamination levels stressed with various DC voltage. This experiment was performed using two spherical electrodes with 10-mm diameters. The gap is 10 mm. Figures were taken from [65].

The use of nano-materials, including nanoparticles, in practical industrial applications provided multiple breakthrough developments in recent decades. Adding nanoparticles into an insulating liquid could form a stable suspension, called a ‘nanofluid’, which combines the characteristics of the particles and insulating liquids [38]. It was shown that such nanofluids can provide better thermal conductivity and long lifetime [38], [84]–[87]. Furthermore, it was shown that nanofluids may have better dielectric properties compared with the conventional insulating liquids [83].

The potential reason for nanofluids with better dielectric properties is that the nanoparticles with dimensions smaller than a few micrometres provide a large inter-facial area between the particles and the base liquid. The large inter-facial area between the particles and the base liquid acts as an electron

scavenger, which can trap the fast electrons and transform them to slow charge particles to inhibit streamer formation and propagation, hence enhancing the liquid dielectric strength. More details are discussed and presented in Chapter 7.

The stability and lifetime of insulation material should be considered before using these materials. In practical application, the stability and lifetime of nanofluids may be reduced due to the suspended nanoparticles that are affected by the electrical field and stressed with the electrical force to aggregate into a larger cluster. In this case, the cluster can be treated as a contaminant that acts in a similar function as discussed. This aggregation phenomenon will be obvious in the case of nanofluids stressed within the DC field because, under the DC field, the direction of the electric force is always the same and will promote the nanoparticle aggregation. Similar results are reported in [20]–[27].

In the case of nanofluids stressed with AC voltage (such as power transformers) and impulse voltage (such as pulsed power applications), the nanoparticle aggregation is not as significant as the DC case. This conclusion can be proved because there are many published results reporting that the nanofluid provides better dielectric strength (AC and impulse) compared with the base liquids. The potential reason for this phenomenon is that, in the case of liquids stressed with AC voltage, the direction of the electrical force will become the opposite in a short time (normally 50 Hz). Thus, the electrical force stress on the nanoparticle will reach a ‘balance’ condition, which will maintain the nanoparticle stably suspended in liquid. In the case of nanofluid stressed with impulse voltage, the rise and fall time of the impulse normally lasts microseconds, which means the time of electrical force stress on the nanoparticle is very short. Hence, the nanoparticle distribution will not be significantly affected by the electrical force in such a short time.

The distinct dielectric properties of nanofluids have resulted in considering them to be a new class of insulating liquids that can be used in AC, and impulse HV applications. Based on this background, a significant number of research projects have started to focus on the development of the nanofluids with specific dielectric properties to meet the demand of the ultra-HV power and pulsed power industry. As Figure 2-18 shows, in the last five years, 54 journals and conference papers have been published just on the IEEE platform with significant growth over the last few years [88].

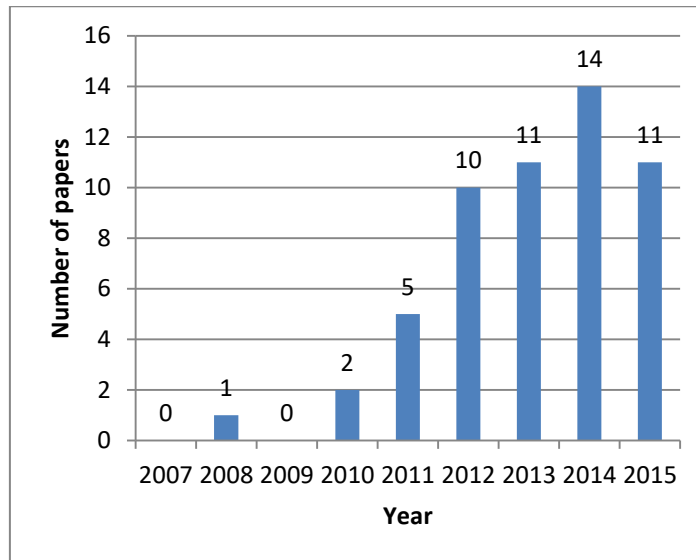


**Figure 2-18.** Number of papers published on IEEE, dealing with ‘nanofluids for application in transformers’ from 2007 to 2015. Figure plotted using data from [88].

**Table 2-3.** Electrical conductivity of various nanoparticles at room temperature.

| Nanoparticles                  | Electrical Conductivity<br>(S/cm)         |
|--------------------------------|---|
| Fe <sub>3</sub> O <sub>4</sub> | 10 <sup>-3</sup> ~10 <sup>-2</sup> [89]   |
| Fe <sub>2</sub> O <sub>3</sub> | ~10 <sup>-7</sup> [90]                    |
| SiC                            | 0.5~1000 [91]                             |
| ZnO                            | 7.26×10 <sup>-7</sup> [92]                |
| TiO <sub>2</sub>               | ~10 <sup>-12</sup> [93]                   |
| CuO                            | 1~100 [94]                                |
| Cu <sub>2</sub> O              | 10 <sup>-8</sup> ~10 <sup>-3</sup> [94]   |
| BN                             | 10 <sup>-15</sup> ~10 <sup>-14</sup> [95] |
| SiO <sub>2</sub>               | ~10 <sup>-15</sup> [96]                   |
| Al <sub>2</sub> O <sub>3</sub> | ~10 <sup>-14</sup> [97]                   |

An insulation liquid is called a nanofluid if the liquid contains a stable dispersion of nanoparticles. Different types of nanoparticles can be added into the insulating liquid to form nanofluids. Based on the conductivity and dielectric permittivity of nanoparticles, they can be classified into conductive nanoparticles, such as Fe<sub>3</sub>O<sub>4</sub> [17], [18], [98]–[100]; semi-conductive nanoparticles, such as Fe<sub>2</sub>O<sub>3</sub>

[101], SiC [20], ZnO [39], TiO<sub>2</sub> [29], [39], [101]–[110], CuO [101], Cu<sub>2</sub>O [101], and BN [32]–[35]; and insulated nanoparticles, such as SiO<sub>2</sub> [31], [39], [106], [111] and Al<sub>2</sub>O<sub>3</sub> [101], [106]. The base liquids for nanofluids are normally mineral oils or ester liquids. The electrical conductivity at room temperature of nanoparticles is shown in Table 2-3.

### **2.5.1 Preparation of nanofluids**

The preparation methods for nanofluids can be categorised into the single-step and two-step methods. In the case of the single-step method, nanoparticles are simultaneously formed and suspended in the liquids. During the preparation procedure, the nanoparticles are formed by the physical or chemical methods, while being dispersed into the base liquids. This method can prevent the potential problem and inconvenience of the conveyance, storage, and drying of the nanoparticles. Furthermore, because the nanofluids form in a single step, this method can reduce the agglomeration and precipitation to improve the stability of nanofluids. The disadvantages of this method are the need for expensive equipment, the high cost of starting materials, and the complex preparation conditions. Thus, this method may be a serious problem in the case of large-scale industry production [112], [113].

In the case of the two-step method, the nanoparticles in the form of powder are prepared using a chemical or physical method. Then, these powders are dispersed into the base liquid using magnetic stirring and/or ultrasonic treatment to form a stable suspension. This method can be used in a large-scale industry production because it requires less complex requirements for equipment, starting materials, and preparation environment conditions [17], [98], [99]. However this method may increase the chance of the agglomeration of nanoparticles in nanofluid [114]. In this project, the major objective is the investigation of the dielectric properties of nanofluids for practical applications. Thus, the two-step method is used to prepare the nanofluid samples in this study.

### **2.5.2 Physical properties of nanofluids**

#### **2.5.2.1 Viscosity**

As briefly discussed in Section 2.3.3, the viscosity of base liquids affects the nanofluid thermal conductivity and nanofluid dielectric performance. In [115]–[117], the results showed that the viscosity of nanofluids were significantly affected by the temperature. The viscosities of the tested samples decreased with an increase in temperature. Moreover, in [35], Jaime et al. investigated the

viscosity of the nanofluid formed by dispersion of BN nanoparticles into mineral oil. The results indicated that the viscosity of nanofluids was not significantly affected by the BN concentration.

In [118]–[120], experiments were performed to investigate the effect of various nanoparticle concentrations on nanofluid viscosity. Different nanoparticles (CuO [111], Al<sub>2</sub>O<sub>3</sub> [119], and multiwall carbon nanotubes (MWCNT) [113]) were used to prepare the nanofluids. The results indicated that the viscosity of nanofluids increased with an increase in nanoparticle concentration. The potential explanation for this phenomenon is that, with an increase in nanofluid concentration, the nanoparticles agglomerate into a larger cluster, which reduces the suspension stability and viscosity.

In [121]–[123], the effect of the size and shape of the nanoparticle (Al [121], SiO<sub>2</sub> [122], and CuO [123]) on the viscosity of nanofluid was investigated. The authors of these papers concluded that the shape of the nanoparticles influenced the nanofluid viscosity. With an increase in the size of the nanoparticles, the viscosity of the nanofluid increased.

The notable results presented in [124] showed that the method of preparation of the nanoparticles (Al<sub>2</sub>O<sub>3</sub>, and CuO) also affected the nanofluid viscosity. The potential reason for this phenomenon is that the different nanofluid preparation methods affect the nanoparticle aggregation and precipitation phenomenon and then affect the nanoparticle size and distribution in the nanofluid. Consequently, the viscosity can also be affected by the nanofluid preparation methods. For the one-step method, the nanoparticles form in the liquid directly and the average size of the suspension particles will be relatively small (<100 nm). Thus the viscosity of the nanofluid will not be significantly affected due to the small size of the particles. For the two-step method case, the nanoparticles are produced at first and then are dispersed into liquid to form nanofluids. This method may lead the nanoparticles aggregate during the produce and disperse process which induce the average size of the suspension particles is relatively large (100nm~several hundred nanometers). Thus the viscosity of nanofluids will decrease.

In summary, these experimental results indicated that, in the case of nano-modified samples with various nanoparticles (Al, Al<sub>2</sub>O<sub>3</sub>, CuO, SiO<sub>2</sub>, BN, and MWCNT), the viscosity of nanofluids increased with a decrease in the temperature, an increase in concentration, and an increase in nanoparticle size.

### **2.5.2.2 Pour point, fire point, and flash point**

The pour point, fire point, and flash point of nanofluids are very important physical properties that affect the transport, storage, and utilisation environment of nanofluids. Thus, their practical applications require comprehensive understanding of these parameters of nanofluids.

The pour point is defined as the lowest temperature at which the liquids retain their flow properties. In [125], Beheshti et al. measured the pour point of base transformer oil, 0.001% mass fraction MWCNT nanofluid, and 0.01% mass fraction MWCNT nanofluid. All tested samples showed pour points of less than  $-45^{\circ}\text{C}$ . There was no significant difference between the pour point of the base sample and the nanofluids. In [35], Jaime et al. investigated the pour point of the nanofluid with dispersed BN nanoparticles in mineral oil. The results indicated that the pour point decreased for the 0.01% (b/w) mass fraction samples.

The flash point means the lowest temperature required to ignite the mixture of the material vapour and air. This could lead to an accident, including explosion at high temperatures. In [125], the flash points of the base transformer oil and the 0.001% and 0.01% mass fraction MWCNT nanofluid samples were measured. The results showed that, for the 0.001% sample, the flash point provided 4.6% improvement compared with the base oil sample. However, in the case of the 0.01% (b/w) concentration sample, the flash point of the nanofluid was lower than that of the base oil sample.

These results prove that the fire point and flash point of mineral-oil-based nanofluid with different nanoparticles and various concentrations were higher than that of the base oil samples.

## **2.6 Dielectric Properties of Nanofluids**

### **2.6.1 Resistivity and relative permittivity of nanofluids**

In [21], Ramu et al. measured the resistivity and relative permittivity of base mineral oils and nanofluids (based on mineral oil) with  $\text{Fe}_3\text{O}_4$  and  $\text{SiO}_2$  nanoparticles under a 50 Hz AC field. The results showed that, compared with the resistivity and the relative permittivity of base mineral oil, the nanofluid with non-conductive nanoparticles ( $\text{SiO}_2$ ) provided 10 times higher resistivity and the same relative permittivity. The nanofluid with conductive nanoparticles ( $\text{Fe}_3\text{O}_4$ ) provided a million times

( $10^6$ ) lower resistivity and more than 15 times higher relative permittivity compared with those of the base mineral oil.

In [104], Du et al. measured the resistivity and relative permittivity of base mineral oil and the mineral-oil-based nanofluids with  $\text{TiO}_2$  nanoparticles under a DC field using A Jiantong Automatic Oil Tester JDC-1 according to IEC 60247-2004 method. The results showed the nanofluid with  $\text{TiO}_2$  nanoparticles provided more than 20 times lower resistivity and 1.5 times higher relative permittivity with respect to the base mineral oil.

The results of [21] and [104] showed that two of the most popular nanofluids,  $\text{Fe}_3\text{O}_4$  and  $\text{TiO}_2$  suspensions, provided lower resistivity but higher relative permittivity compared with the traditional mineral oil. Higher relative permittivity helps nanoparticles reduce the field distortion introduced by unfavourable factors.

**Table 2-4.** Dielectric properties of mineral oil and nanofluids [104], [21], [27].

| Oils and Nanofluids                                    | Resistivity                                   |  | Relative Permittivity |
|--|---|--|-----------------------|
| Mineral oil [21]                                       | $6.25 \times 10^{13} (\Omega \cdot \text{m})$ |  | 2.2                   |
| $\text{Fe}_3\text{O}_4$ /mineral oil [21]              | $3.63 \times 10^7 (\Omega \cdot \text{m})$    |  | 36.5                  |
| $\text{SiO}_2$ /mineral oil [21]                       | $7.14 \times 10^{14} (\Omega \cdot \text{m})$ |  | 2.2                   |
| Mineral oil [104]                                      | $1.82 \times 10^{12} (\Omega \cdot \text{m})$ |  | 2.26                  |
| $\text{TiO}_2$ /mineral oil [104]                      | $8.30 \times 10^{10} (\Omega \cdot \text{m})$ |  | 3.92                  |
| Mineral oil [27]                                       | $36.0 (\times 10^{10} \Omega)$<br>(RHO-)      | $19.7 (\times 10^{10} \Omega)$<br>(RHO+)   | 2.1                   |
| Magnetic nanoparticle/mineral oil<br>(0.8 vol%) [27]   | $0.0021 (\times 10^{10} \Omega)$<br>(RHO-)    | $0.0028 (\times 10^{10} \Omega)$<br>(RHO+) | 8.8                   |
| Magnetic nanoparticle/mineral oil<br>(0.016 vol%) [27] | $0.73 (\times 10^{10} \Omega)$<br>(RHO-)      | $0.63 (\times 10^{10} \Omega)$<br>(RHO+)   | 2.1                   |
| Magnetic nanoparticle/mineral oil<br>(0.008 vol%) [27] | $1.75 (\times 10^{10} \Omega)$<br>(RHO-)      | $0.95 (\times 10^{10} \Omega)$<br>(RHO+)   | 2.1                   |
| Magnetic nanoparticle/mineral oil<br>(0.004 vol%) [27] | $2.5 (\times 10^{10} \Omega)$<br>(RHO-)       | $11.3 (\times 10^{10} \Omega)$<br>(RHO+)   | 2.1                   |

The authors of [27] measured the resistivity and relative permittivity of mineral-oil-based magnetic nanofluid with concentrations of nanoparticles from 0 to 0.8 vol% using the IEC 60247 standard method. The results showed that, with an increase in concentration, the resistivity of nanofluid decreased, while the relative permittivity increased. More details are presented in Table 2-4.

Considering that there is a significant number of research results that have shown that mineral-oil-based  $\text{Fe}_3\text{O}_4$  and  $\text{TiO}_2$  suspensions can provide better dielectric performance compared with base liquids, it is important to conduct further study of the dielectric performance of such fluids.

## **2.6.2 AC dielectric strength**

The AC breakdown voltage of nanofluids is a key parameter that be used to evaluate the nanofluid dielectric performance, and this parameter has been investigated by many researchers [17], [18], [28]–[31], [39], [104], [106], [126]–[130]. Most experiments follow the international standard ASTM 1816 [79] or IEC 60156 [131], which require a pair of spherically capped electrodes to be immersed in tested liquid stressed with AC voltage. The applied voltage should start at a relatively low level to prevent breakdown in the initial stage and should rise with a specific rate until the breakdown occurs. To obtain accurate measurement results, several independent samples should be tested, and several breakdowns should be performed for each sample.

The published results indicated that the AC breakdown voltage of nanofluids was affected by many factors, such as the nanoparticle types, nanoparticle surface modification, nanoparticle concentrations, and sample moisture content. The published results of the AC breakdown voltages of nanofluids are separated into four classifications based on the above factors and are discussed in this section.

### **2.6.2.1 Influence of type of nanoparticles**

In [39] and [96], the investigation of the AC breakdown voltage of nanofluid with different nanoparticles and their different concentrations is described. The results indicated that there is an optimal concentration in which the correlative sample provides the best dielectric properties compared with the samples of other concentrations. Normally, the best dielectric properties mean the highest breakdown voltage or the longest pre-breakdown time. More details are shown in Section 2.6.2.3.

In [106], a mineral-oil-based nanofluid was prepared using  $\text{Al}_2\text{O}_3$ ,  $\text{TiO}_2$ , and  $\text{SiO}_2$ , with the concentration from 0 to 5% g/L. No surfactant was added during the preparation of the nanofluids. The measurement procedure followed the IEC 60156 standard. The results are shown in Figure 2-19. The results showed that the AC breakdown voltages of  $\text{Al}_2\text{O}_3$  and  $\text{SiO}_2$  nanofluids at all concentrations were lower than the breakdown voltage of base mineral oil. In the case of  $\text{TiO}_2$  nanofluids, the breakdown voltage of the nanofluid samples with the optimal concentration was 13% higher than the breakdown voltage of the base sample.

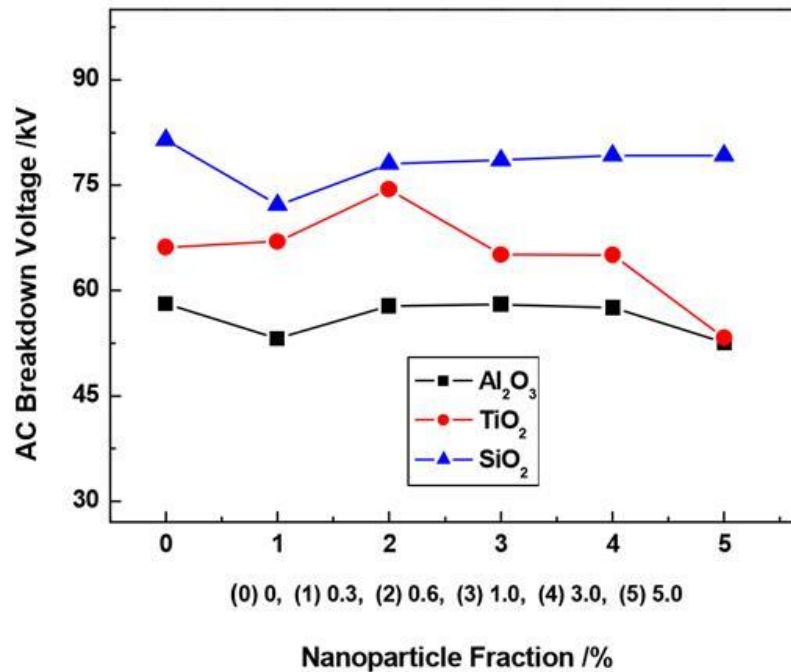


**Figure 2-19.** The AC breakdown voltage of nanofluids with different nanoparticles and various concentrations (% , g/L). Figure taken from [106].

In [39], Bakruthen et al. prepared transformer oil-based nanofluids with  $\text{TiO}_2$ ,  $\text{SiO}_2$ , and  $\text{ZnO}$  nanoparticles with 0.01% and 0.075% volume concentrations. The measurement procedure followed the IEC 60156 standard. The gap distance was 2.5 mm. To remove the moisture from the samples, the samples were heated to 100°C. Then, the breakdown voltage of the samples was measured after the temperature was reduced to the atmospheric temperature.

The results are shown in Figure 2-20. The results showed that the breakdown voltages of all nanofluids were higher than the breakdown voltage of base oil. The high concentration nanofluid samples (0.075 vol%) provided higher breakdown voltages compared with the low concentration nanofluid samples (0.01 vol%).

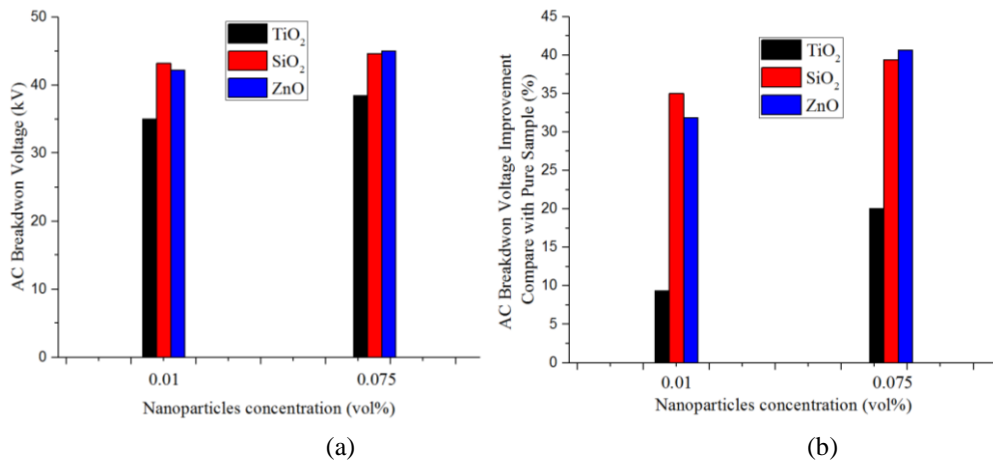


**Figure 2-20.** (a) The AC breakdown voltage of mineral-oil-based TiO<sub>2</sub>, SiO<sub>2</sub>, and ZnO nanofluids [39]. (b) The breakdown voltage improvement of mineral-oil-based TiO<sub>2</sub>, SiO<sub>2</sub>, and ZnO nanofluids compared with base mineral oil. The measurement procedure followed the IEC 60156 standard. The gap distance was 2.5 mm. Figure plotted using data from [39].

In [104], Du et al. measured the AC breakdown voltage of base mineral oil and mineral-oil-based TiO<sub>2</sub> nanofluid with low moisture content (~10 ppm). The measurement procedures followed the ASTM D1816 standard. Thirty breakdown events were recorded and the average value of AC breakdown voltage is given in Table 2-5. The results showed that the breakdown voltage of TiO<sub>2</sub> nanofluid demonstrated a ~19% increase compared with that of base oil. The standard deviation of base oil and nanofluid were almost the same.

**Table 2-5.** Comparison of AC breakdown voltage of base mineral oil and TiO<sub>2</sub> nanofluid [104].

| Samples                    | Mean Breakdown Voltage<br>(kV) | Standard Deviation<br>(kV) |
|----------------------------|--------------------------------|----------------------------|
| Mineral oil                | 67.9                           | 5.4                        |
| TiO <sub>2</sub> nanofluid | 80.9                           | 5.3                        |

### 2.6.2.2 Influence of surface treatment

In [28], the authors investigated the relation between the AC breakdown strength of TiO<sub>2</sub> nanofluid and the nanoparticle surface modification. The nanofluid samples were prepared with concentrations from 0.003 g/mL to 0.05 g/mL, and different surfactants, silicon oil and octadecanoic acid, were used

to treat nanoparticles before introducing them into a base fluid. The breakdown voltages of each type of sample with optimal concentration are shown in Table 2-6.

The results indicated that the surfactant can affect the breakdown strength of nanofluids, and the potential reason is that the different surface modifications may affect the surface electron trapping and releasing process of the nanoparticles and hence may affect the nanofluid breakdown strength.

**Table 2-6.** The AC breakdown voltage of base oil and nanofluid with different surfactants in the optimal concentration [28].

| <b>Oils and Nanofluids</b>                               | <b>Breakdown Voltage<br/>(kV)</b> | <b>Moisture Content<br/>(ppm)</b> |
|--|-----------------------------------|-----------------------------------|
| Base transformer oil                                     | 37.8                              | 16.56                             |
| Octadecanoic acid-treated TiO <sub>2</sub><br>suspension | 57.8                              | 16.43                             |
| Silicon oil-treated TiO <sub>2</sub> suspension          | 49                                | 16.62                             |
| Untreated TiO <sub>2</sub> suspension                    | 48.2                              | 17.48                             |

In [18], Du et al. measured the AC breakdown voltage of the transformer oil-based nanofluid prepared with Fe<sub>3</sub>O<sub>4</sub>. The magnetite nanoparticles were treated with the surfactant hexadecyl trimethyl ammonium bromide (CTAB). The measurement methods and the electrode design were in accordance with the IEC 156 standard.

Figure 2-21 shows the AC breakdown voltage of nanofluids with various concentrations of surfactant. The results showed that there was an optimal concentration of surfactant that provided the highest breakdown voltage. In the case of nanofluids that contain lower concentrations of surfactant than the optimal concentration, the breakdown voltage rose with an increase in surfactant concentration. In the case of nanofluids with higher surfactant concentrations, the breakdown voltage fell with an increase in surfactant content.

The authors concluded that the potential reason for these effects is that a specific amount of surfactant can improve the capability of nanoparticles to trap electrons and bind water molecules. However, the excess surfactant will not combine with nanoparticles, which means the nanofluid contains another

type of impurity. Thus, the breakdown voltages of such nanofluids with high surfactant content would decrease.

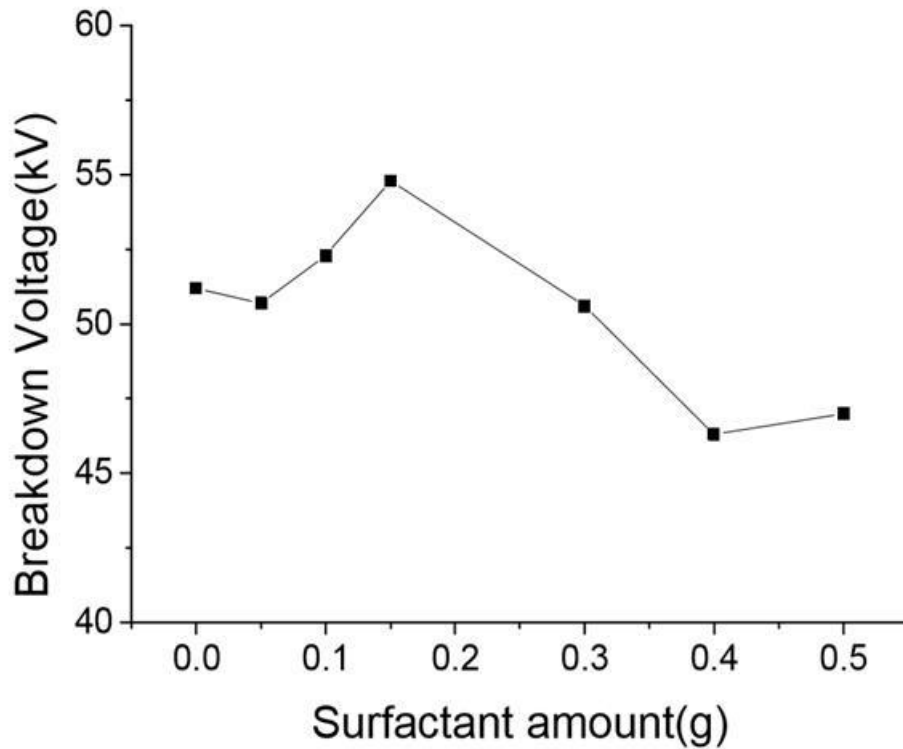


**Figure 2-21.** The AC breakdown voltages of nanofluids with Fe<sub>3</sub>O<sub>4</sub> nanoparticles with various surfactant content. The measurement methods and the electrode design followed the IEC 156 standard. Figure taken from [18].

### 2.6.2.3 Influence of concentration of nanoparticles

In [29], Du et al. prepared nanofluid samples with dispersed TiO<sub>2</sub> nanoparticles in transformer oil. The concentrations of these samples were from 0.003 g/L to 0.05 g/L. The breakdown voltage measurement procedure followed the IEC 60156 standard. A pair of brass spherical electrodes with 2.5-mm gap distance was used. Thirty breakdown events were recorded. The mean breakdown voltage and the standard deviation for various concentrations of nanoparticles are presented in Figure 2-22. The results showed that there was an ‘optimal’ concentration that provided the highest breakdown voltage. In the case of the samples with concentrations higher or lower than the optimal concentration, the breakdown voltage started to drop.

In the case of high concentrations, such as 0.05 g/L, the breakdown voltage of nanofluid was lower than that of base oil. The authors indicated that this phenomenon may be explained by the

nanoparticle agglomeration with an increase in concentration. The nanoparticles start to agglomerate to larger clusters, which reduces the breakdown voltage of the nanofluids with high concentrations of nanoparticles.

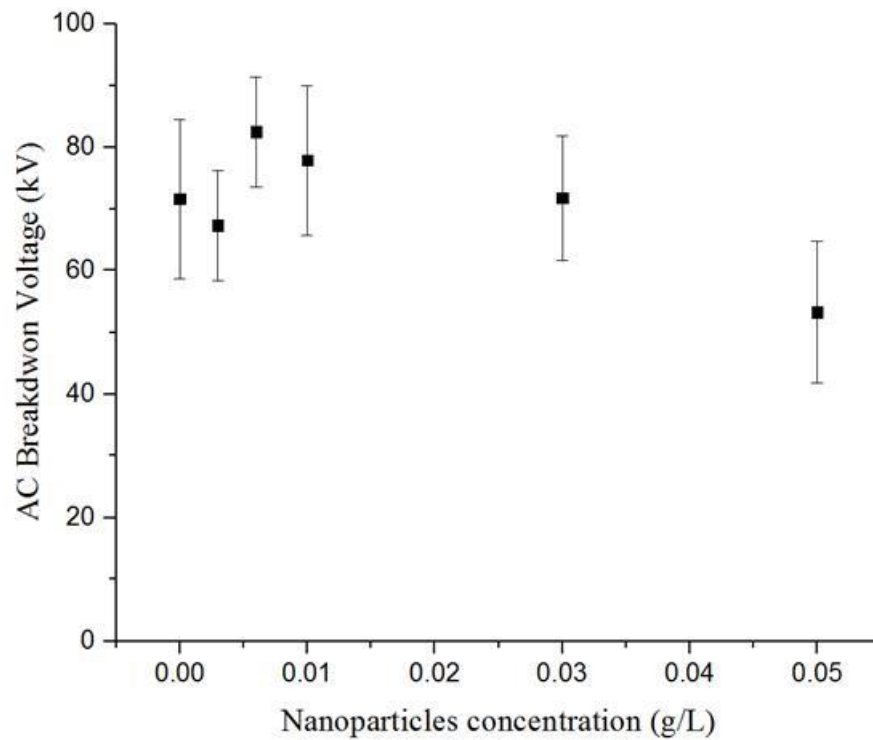


**Figure 2-22.** The mean AC breakdown voltage and the standard deviation of the base transformer oil and TiO<sub>2</sub> nano-modified samples with various concentrations. Figure plotted using data from [29].

Du et al. [18] investigated the AC breakdown voltage of the nano-modified samples of mineral oil with conductive nanoparticles (Fe<sub>3</sub>O<sub>4</sub>) with various concentrations. The concentrations of nanoparticles in the nanofluid samples were 0 to 300 ppm. As Figure 2-23 shows, the behaviour of the breakdown voltage of the nanofluid was similar to the results discussed in the previous section. In the case of low concentrations, the breakdown voltage increased with the concentration and reached the crest value at the optimal concentration. In the higher concentrations (higher than the optimal concentration), the breakdown voltage of the nanofluid started to decrease.

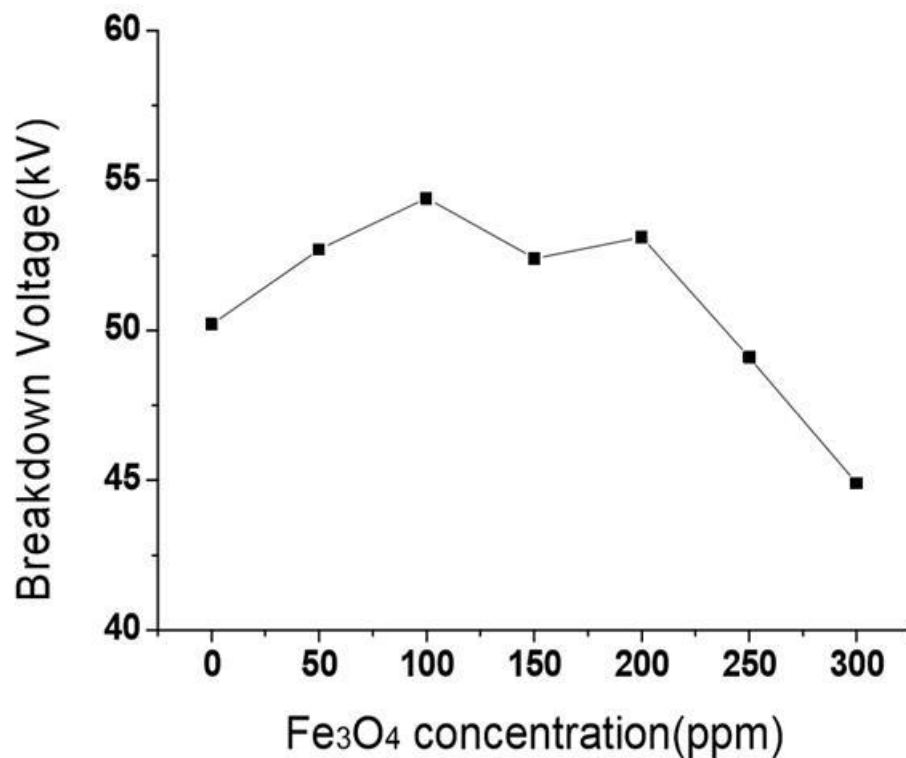


**Figure 2-23.** The AC breakdown voltage of the Fe<sub>3</sub>O<sub>4</sub> nanofluid sample with various concentrations. The measurement methods and the electrode design followed the standard IEC 60156. Figure taken from [18].

Jin et al. measured the AC breakdown voltage of transformer oil (OPG-100 A) and fullerene nanofluid samples with the 0.05% and 0.1% mass fraction concentration of fullerene nanoparticles following the IEC 60156 international standard [126]. The sample moisture was 24 ppm. The breakdown voltages with the probability to breakdown were evaluated using the Weibull distribution analysis, shown in Figure 2-24.

In the case of 63.2% breakdown probability, the breakdown voltages of nanofluids with 0.1% and 0.05% (b/w) concentrations were 33% and 20% higher than the breakdown voltage of base oil sample, respectively. The authors indicated that, based on the charger trap theory, the nanoparticle can provide the trap to capture the free electrons, which would inhibit the streamer formation and slow the streamer propagation in the insulating liquid. The fullerene nanoparticle can be treated as the charger trap in the liquid to enhance its dielectric strength. The nanofluids with high concentration provided a large number nanoparticle to provide more charger traps; hence, the breakdown strength was higher than in the other tested samples.

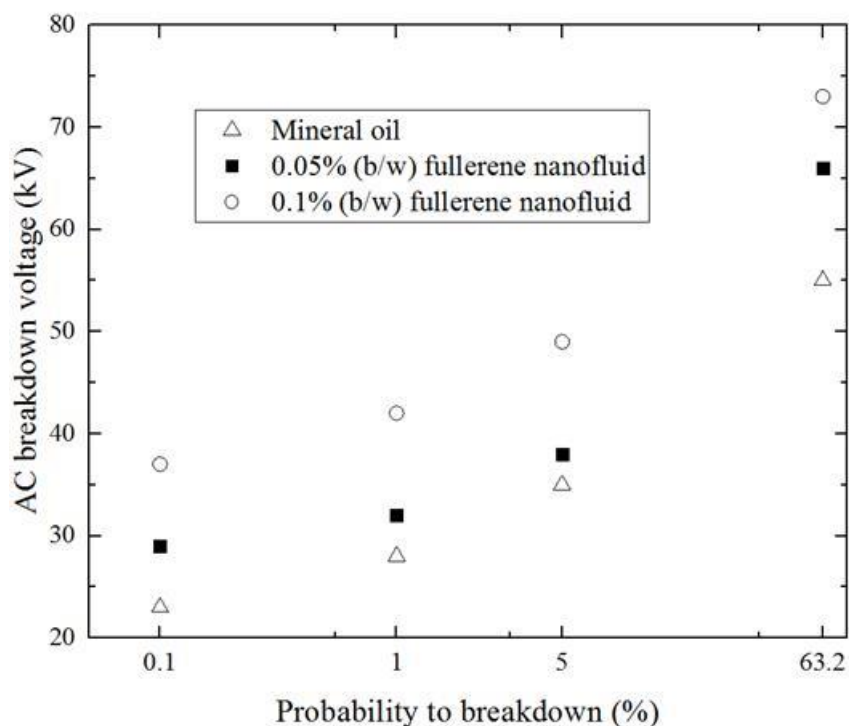


**Figure 2-24.** AC breakdown voltage of mineral oil and fullerene nanofluid at 0.05% and 0.1% (b/w). The sample moisture was at 24 ppm. Figure plotted using data from [126].

In summary, the results presented by [18] and [29] showed that the AC breakdown strength of the nanofluid was significantly affected by the nanoparticle concentration. In the case of samples, with low concentration, the breakdown voltages rose with an increase in concentration. There was an optimal concentration that provided the highest AC breakdown voltage. In the case of samples with concentrations higher than the optimal concentration, the breakdown voltage started to drop. The authors explained these results with the aggregation theory, which states that higher concentrations of nanoparticles lead to aggregation of these particles into larger clusters and to reduction in breakdown voltage.

In [126], the result show that, in the case of fullerene nanofluid, the high concentration (0.1% b/w) provided an obvious increase in breakdown voltage compared with the low concentration sample and the base oil. The authors indicated that, based on the charger trap theory, fullerene nanoparticles have a relaxation time constant that is much shorter than the streamer formation and propagation time. The nanoparticles acted as charger traps in the liquid and inhibited the streamer formation and slowed its propagation. Hence, a high concentration of nanoparticles means that there are more charge traps to inhibit the streamer and to enhance the dielectric performance. Due to the chemical structure

difference between fullerene and metal oxide nanoparticles, the aggregation phenomenon may not exist in the fullerene nanofluid with high concentrations. Thus, the breakdown voltage of the fullerene nanofluid did not drop with an increase in concentration.

The optimal concentrations for different nanoparticles may be different, and this optimal concentration may be affected by the inherent properties of the nanoparticle, such as the relaxation time constant; for example, fullerene particles have a time constant of 75 to 80 ns, while the time constant of TiO<sub>2</sub> is in tens of seconds. Furthermore, potentially, there is more than a single mechanism that defines the interaction between nanoparticles and electrons. Thus, more experiments and theoretical studies will be needed to investigate the nanoparticle concentration effect on the liquid insulating performance. Further discussion of the charger trap theory and nanoparticle relaxation time constant will be presented in Chapter 7.

#### **2.6.2.4 Influence of moisture content**

The moisture content in insulating liquids affects the breakdown voltage of both base insulating liquids and nanofluids. In [17], [30], and [31], experimental investigation of the effect of moisture content on the AC breakdown voltage of insulating liquids was conducted.

In [17], Segal et al. prepared nanofluids with Fe<sub>3</sub>O<sub>4</sub> conductive nanoparticles dispersed into mineral oil. The AC breakdown voltage was measured following the standard, ASTM D877. The effect of moisture content on the AC breakdown strength of mineral oil (Univlot 60 Exxon) and nanofluids was examined. The moisture content in the oil and nanofluid was from < 5 ppm to > 30 ppm. The results of this study are shown in Figure 2-25.

As Figure 2-25 shows, in the case of samples with low moisture content (< 5 ppm), the results indicated that the AC breakdown voltages of base mineral oil and nanofluids were almost the same. With an increase in the moisture content, the AC breakdown strength of both base mineral oil and nanofluids decreased. A notable phenomenon of these results is that, in the case of samples with high moisture content, the AC breakdown voltage of base mineral oil sample dropped significantly compared with the AC breakdown voltage of base oil with low moisture content. Conversely, with an increase in moisture content, the breakdown voltage of nanofluids dropped insignificantly. These

results indicated that nanofluids may have better performance to resist dielectric strength degradation with an increase in liquid moisture content.

The authors indicated that the potential reason for this phenomenon is that the nanoparticle surface may capture some water molecules. In [113] and [132], the authors concluded that the breakdown strength of insulating liquids may be weakened by the multi-molecular water clusters. Considering this theory and the results shown in [17], the potential explanation could be some multi-molecular water clusters were broken into single water molecules during the nanofluid preparation process and then were captured by the surface of the nanoparticles in the nanofluid. Thus, the breakdown strength of nanofluids may be enhanced by this mechanism.

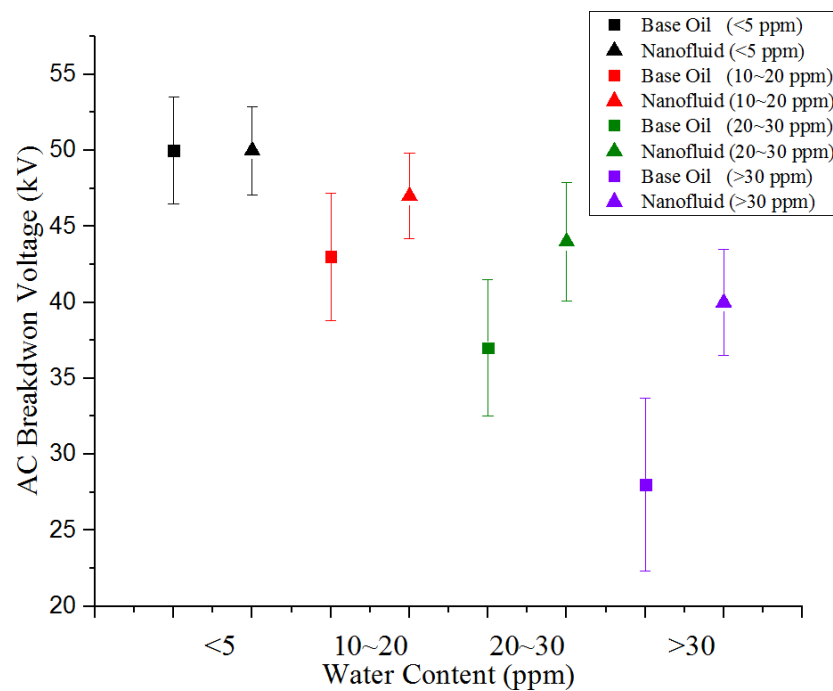


**Figure 2-25.** The AC breakdown voltage of base mineral oil (Univolt 60; square symbol) and nanofluid ( $\text{Fe}_3\text{O}_4$ ; triangle symbol) under different moisture content levels (different colours). Figure plotted using data from [17].

In [30], Du et al. prepared the transformer oil-based semi-conductive nanoparticle suspension samples with  $\text{TiO}_2$  nanoparticles. Then, the authors measured the AC breakdown voltages of the base oil and nanofluid. The concentration of  $\text{TiO}_2$  nanoparticles in the tested nanofluid was 0.075% (b/v), and the relative humidity of nanofluids was from 10% to 80%. The AC breakdown voltage was measured following the international standard ASTM D1816.

As Figure 2-26 shows, in the case of the sample with 10% relative humidity, the AC breakdown voltage of the base oil and the nanofluid were similar. With an increase in the relative humidity, the breakdown strength of the base oil sample fell rapidly. In contrast, the breakdown voltage of the nanofluid dropped more slowly with an increase in the relative humidity. In the case of samples with 80% relative humidity, the breakdown voltage of the nanofluid was twice the breakdown voltage of the base oil.

The authors concluded that the reason for the breakdown strength of the nanofluid showing less degradation at the high relative humidity is that the  $\text{TiO}_2$  nanoparticles can reduce the distortion effect of the electrical field induced by the water content. The higher relative humidity will produce a stronger field distortion; hence, the nanofluids provided resistance to the degradation of the breakdown voltage due to moisture in the liquid.

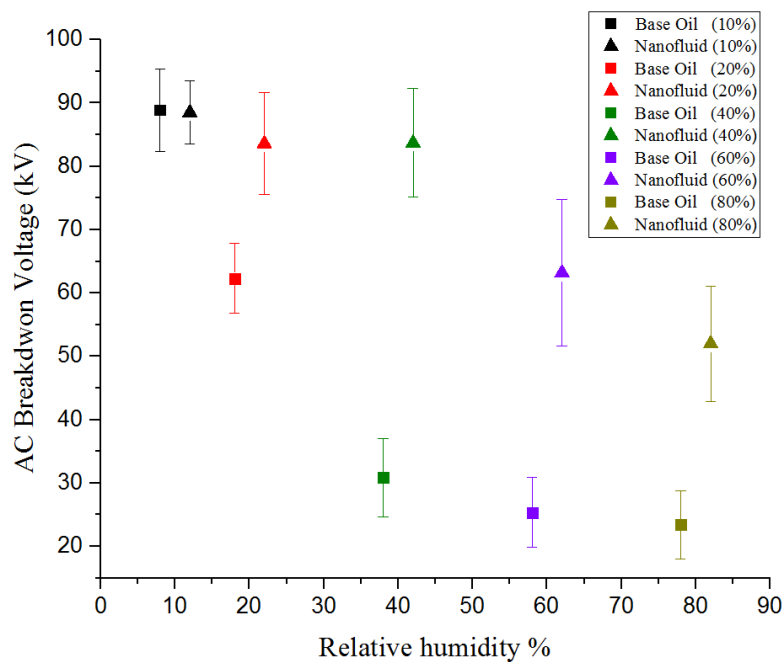


**Figure 2-26.** The AC breakdown voltage of base mineral oil (square symbol) and nanofluid (0.075 vol%,  $\text{TiO}_2$ ; triangle symbol) by relative humidity level (different colours). Figure plotted using data from [30].

In [31], Jin et al. measured the AC breakdown voltage of mineral oil (Diala S3ZXIG) and a nanofluid with non-conductive ( $\text{SiO}_2$ ) nanoparticles. The measurements were performed per the IEC standard 50156. The electrodes topology was sphere-sphere with a 2.5-mm gap. The concentrations of

nanoparticles were set to 0.01% and 0.02% (mass fraction). The moisture content of the samples was set to 15 ppm and 25 ppm. The measurement results are shown in Figure 2-27.

The results indicated that, in the case of samples with both 15 ppm and 25 ppm moisture content, the 0.02% (b/w) nanofluid provided the highest AC breakdown voltage compared with other concentrations. The base mineral oil has the lowest breakdown voltage for both 15 ppm and 25 ppm moisture content. Comparing the breakdown voltages of samples with 15 ppm and 25 ppm moisture content, the 25 ppm nanofluid provided 33%, 28%, and 27% lower breakdown voltages for the base oil, 0.01% concentration sample, and 0.02% concentration sample, respectively, compared with the 15 ppm nanofluid.

The authors indicated that the surface of the SiO<sub>2</sub> nanoparticles was hydrophilic; thus, it could capture free water and result in improvement in dielectric performance of the nanofluid with high water content.

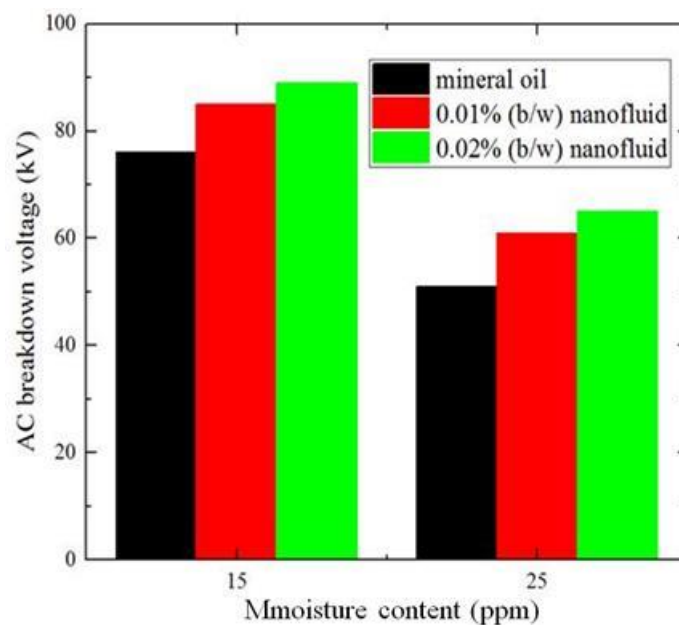


**Figure 2-27.** The AC breakdown voltage of base mineral oil and nanofluid (SiO<sub>2</sub>) with 15 ppm (left side) and 25 ppm (right side) moisture content. Figure plotted using data from [31].

In summary, the results provided by [17], [30], and [31] indicated that the AC breakdown voltage of nanofluids with different nanoparticles (Fe<sub>3</sub>O<sub>4</sub>, TiO<sub>2</sub>, and SiO<sub>2</sub>) showed a lesser degree of degradation with high moisture content with respect to base liquids. The potential reason for this phenomenon is that the water in the nanofluid or base oil can distort the electrical field distribution and reduce its

dielectric strength. Nanoparticles may capture free water molecules and thus may reduce the field distortion effect and enhance the dielectric strength [31].

However, there is no uniform agreement on how to explain the process of capturing water molecules by nanoparticles. Furthermore, in the process of capturing water molecules by nanoparticles, the difference in the capture mechanisms between various types of nanoparticles is unknown. Thus, the interaction mechanism between nanoparticles and water molecules, especially in the case of high water content, is a potential area that needs to be investigated further.

### **2.6.3 Lightning and switching impulse dielectric strength**

In addition to the AC breakdown voltage, the impulse breakdown voltage is another important parameter used to evaluate the material insulating performance. Most experiments were performed using 12/50  $\mu\text{s}$  lightning impulses, which means the impulse should reach 90% magnitude in 1.2  $\mu\text{s}$  on a rising slope and fall to 50% magnitude in 50  $\mu\text{s}$  on a falling slope. Generally, the experimental design followed the international standards IEC 60897 [133] or ASTM D3300 [80]. Many researchers designed the experiments to investigate the effect of the nanoparticle concentrations and the nanoparticle types on the impulse breakdown strength [17], [19], [21], [29], [109], [129], [134], [135]. The results showed that both parameters (the concentration and the type of nanoparticles) significantly affected the impulse withstand voltage strength.

#### **2.6.3.1 Influence of type of nanoparticles**

Different nanoparticles have a unique chemical structure and inherent properties, such as relative permittivity and conductivity, which may affect the dielectric properties of nanofluids. Many researchers investigated the impulse withstand voltage strength of nanofluids with various types of nanoparticles.

In [19], Sima et al. measured the lightning impulse (1.2/50  $\mu\text{s}$ ) breakdown strength of base mineral oil (Karamay 25) and mineral-oil-based nanofluid following the IEC 60897 standard method. The electrodes used were the point-plane electrodes with 5-mm gap. The nanofluids were prepared by dispersing  $\text{Fe}_3\text{O}_4$ ,  $\text{TiO}_2$ , and  $\text{Al}_2\text{O}_3$  nanoparticles into the mineral oil. The concentrations were 0.03 g/L, 0.01 g/L, and 0.02 g/L. The average diameter of the spherical nanoparticles which were used in this

study was 20 nm. Ten breakdown events were recorded, and the average breakdown voltage was obtained. The results of this study are presented in Figure 2-28.

The results indicated that the type of nanoparticles had a significant effect on the liquid lightning impulse breakdown strength. In the case in which the samples were stressed with positive lightning impulses, all breakdown voltages of nanofluids were higher than the breakdown voltage of the base oil. In the case in which the samples were stressed with negative lightning impulses, the breakdown voltage of the  $\text{Fe}_3\text{O}_4$  nanofluid was significantly lower than that of the base oil. In contrast, the breakdown voltage of the nanofluids with  $\text{TiO}_2$  and  $\text{Al}_2\text{O}_3$  were almost the same as that of the base oil.

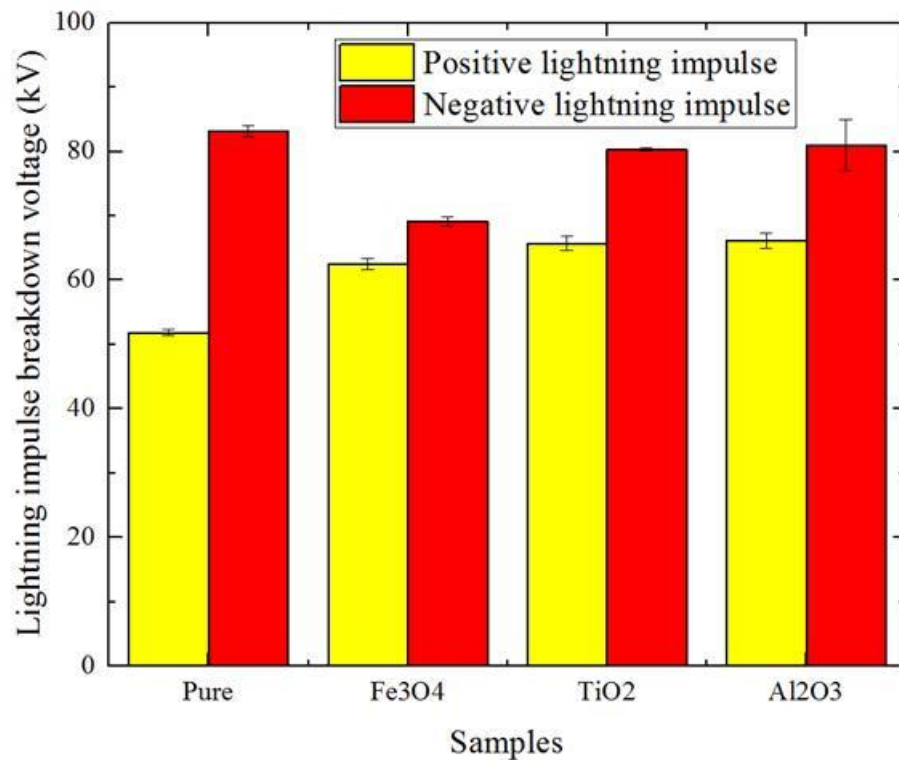


**Figure 2-28.** The positive and negative lightning impulse breakdown voltage of the base mineral oil (Karamay 25) and nanofluids. The nanofluid concentration is 0.03 g/L for  $\text{Fe}_3\text{O}_4$ , 0.01 g/L for  $\text{TiO}_2$ , and 0.02 g/L for  $\text{Al}_2\text{O}_3$ . The average breakdown voltage and the standard deviation calculated by 10 breakdown events. Figure plotted using data from [19].

In [109], Pugazhendhi investigated the negative lightning impulse (1.2/50  $\mu\text{s}$ ) breakdown voltage of mineral oil and nanofluids with dispersed  $\text{TiO}_2$  and  $\text{ZrO}_2$  nanoparticles. The measurement procedure followed the IS 11697:1986 Indian standard [136]. The electrodes used in these tests were sphere electrodes.

The results indicated that, in the case in which the liquid samples were stressed with negative lightning impulses, all nanofluid samples provided breakdown voltages higher than that of base oil. The samples with 0.005% mass fraction provided the maximum negative impulse breakdown. The enhancement compared with the base oil was 16.02% and 19.24% for  $ZrO_2$  and  $TiO_2$  nanofluids, respectively. The breakdown voltages are presented in Figure 2-29.

In [129], Li et al. measured the positive and negative lightning impulse (1.2/50  $\mu s$ ) breakdown voltage strength of  $Fe_3O_4$  nanofluid based on vegetable oil (RBD). The measurement procedure followed the IEC 60897 standard. The electrodes were a steel needle (HV electrode) and steel ball with 13-mm diameter (ground electrode). The gap distance was 15 mm. Five breakdown events were recorded. The average breakdown voltages and standard deviations are presented in Figure 2-29.

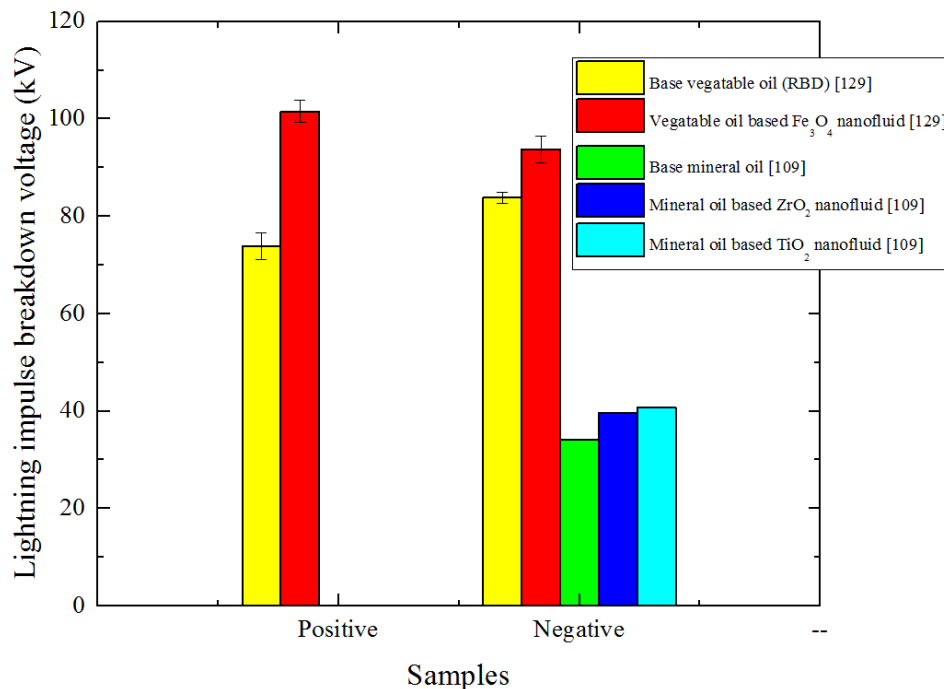


**Figure 2-29.** The positive and negative lightning impulse breakdown of base vegetable oil (RBD) and vegetable oil-based  $Fe_3O_4$  nanofluids [129]. The average breakdown voltages and standard deviations were calculated using five breakdown events [129]. The negative lightning impulse breakdown of the base mineral oil and mineral oil-based  $ZrO_2$ ,  $TiO_2$  nanofluids [109]. The measurement procedure followed the IS 11697:1986 Indian standard. The electrodes used needle-to-sphere topology [109]. Figure plotted using data from [109], [129].

The results indicated that, compared with the breakdown voltage of the base oil, the positive lightning impulse breakdown voltage of the nanofluid provided a 37.3% increase, and the negative lightning impulse breakdown voltage of the nanofluid provided an 11.8% increase.

In summary, the results shown in this section indicated that the type of nanoparticles will significantly affect the liquid lightning impulse dielectric strength. In the case of samples with stressed positive impulses, the breakdown voltage of all nanofluids with various nanoparticles was higher than that of the base liquids (mineral oil or ester liquid). In the case in which the samples were stressed with negative impulses, the breakdown voltage of nanofluids did not show a significant increase, as in the case of the positive impulse compared with that of the base liquid samples. Moreover, the negative lightning breakdown voltage of mineral-oil-based nanofluid with  $\text{Fe}_3\text{O}_4$  was found to be significantly lower than that of the base oil [19]. Similar results were also reported by Segal et al. [17], [135].

In the case of nanofluid with the optimal concentration of nanoparticles, the breakdown voltage was higher compared with that of the base liquid. When the concentration of nanoparticles was higher than the optimal value, the breakdown voltages started to decrease. Further details and discussions of this effect are presented in Section 2.6.2.2.

### **2.6.3.2 Influence of concentration of nanoparticles**

In [29], Du et al. prepared the transformer oil-based  $\text{TiO}_2$  nanofluid with concentrations from 0.003 g/L to 0.05 g/L and investigated the lightning impulse (1.2/50  $\mu\text{s}$ ) breakdown strength of the base mineral oil and mineral-oil-based nanofluid with  $\text{TiO}_2$ . The impulse breakdown voltage was measured using the IEC 60897 standard method. The electrodes were set as needle to sphere with a 25-mm gap. The water content of the samples was ~10 ppm. The mean breakdown voltage and its standard deviation were calculated using five breakdown events.

As Figure 2-30 shows, the results indicated that there was an optimal concentration of nanoparticles that provided the highest breakdown voltage compared with other concentrations. In this case, the optimal concentration was 0.03 g/L. When the concentration of nanoparticles was higher than the optimal value, the breakdown voltage started to decrease. The nanofluid with 0.03 g/L concentration provided a breakdown voltage that was 16.7% higher than that of the base mineral oil.

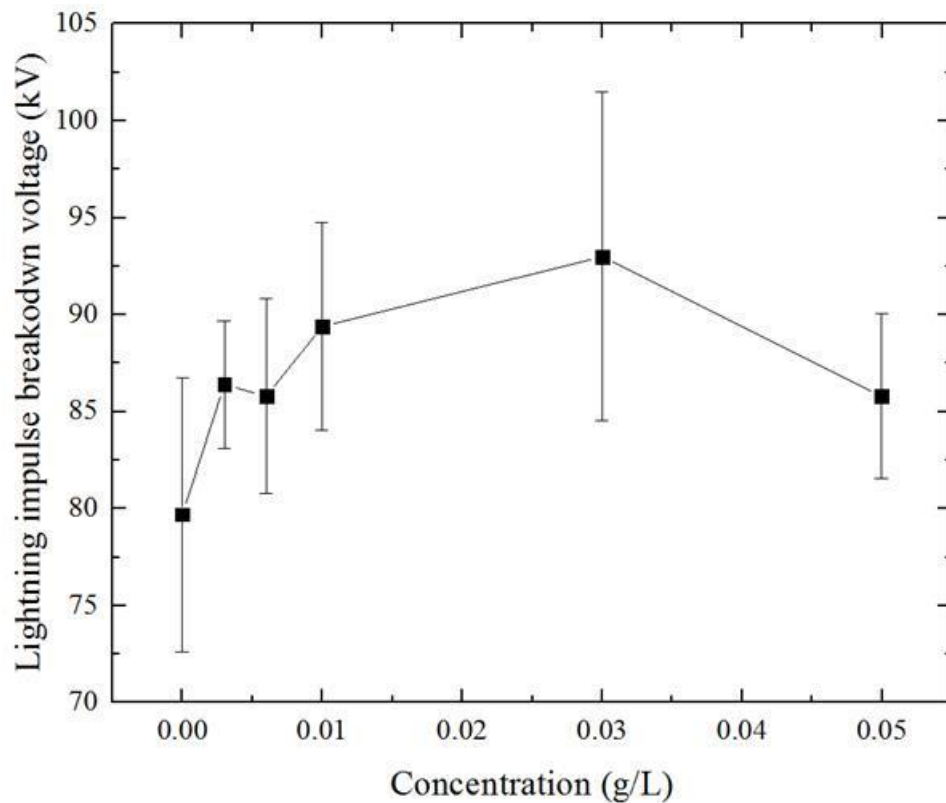


**Figure 2-30.** Lightning impulse breakdown voltage of base liquid and nanofluids as a function of the  $\text{TiO}_2$  nanoparticle concentration. The mean breakdown voltages and standard deviations of the samples are calculated using the five breakdown events. Figure plotted using data from [29].

In [19], Sima et al. measured the positive and negative switching impulse (250/2500  $\mu\text{s}$ ) breakdown strength of base mineral oil (Karamay 25) and mineral-oil-based nanofluid following the IEC 60897 standard method. The electrodes used in these tests were the point-plane with 5-mm gap. The nanofluids were prepared for dispersing  $\text{Fe}_3\text{O}_4$ ,  $\text{TiO}_2$ , and  $\text{Al}_2\text{O}_3$  nanoparticles into the mineral oil with concentrations from 0 g/L to 0.1 g/L. The mean breakdown voltages were calculated based on 10 breakdown events.

The switching impulse breakdown voltage results are shown in Figure 2-31. These results indicated that there was an optimal concentration at which the correlative samples provided the highest breakdown voltage compared with other samples. In the case of the samples stressed with positive switching impulses, the breakdown voltages of all nanofluids were significantly higher than the breakdown voltages of the base oil samples. The optimal concentrations for nanofluid with  $\text{Fe}_3\text{O}_4$ ,  $\text{TiO}_2$ , and  $\text{Al}_2\text{O}_3$  nanoparticles were 0.03 g/L, 0.01 g/L, and 0.02 g/L, respectively. These

concentrations provided breakdown voltages of 44.1%, 33.3%, and 35.5% higher than the breakdown voltages of the base oil samples.

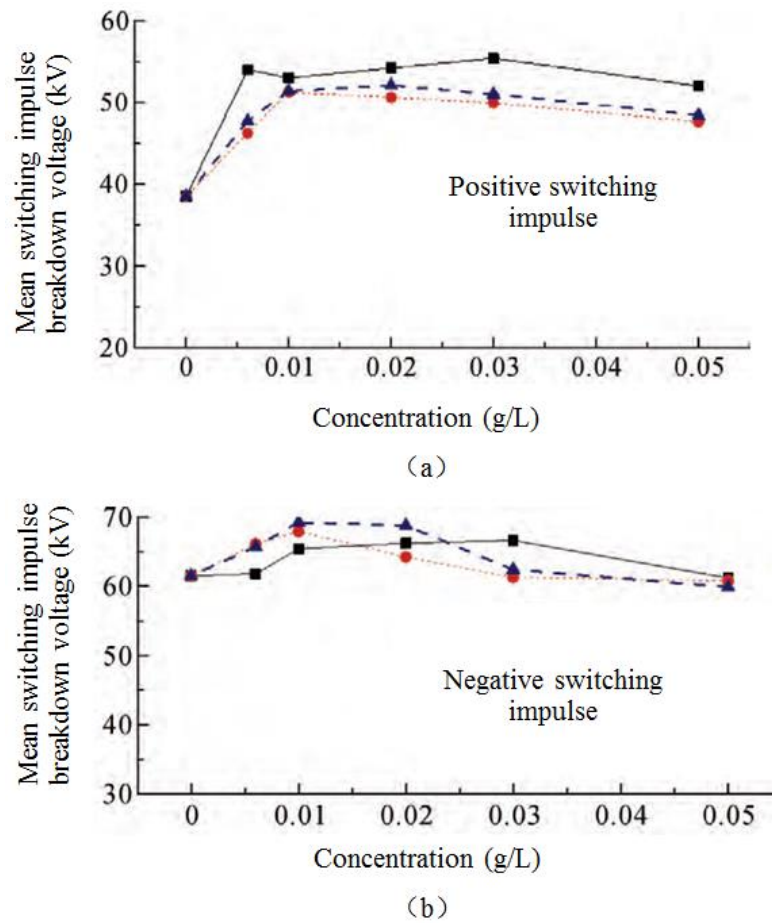


**Figure 2-31.** The positive (a) and negative (b) switching impulse (250/2500  $\mu$ s) breakdown voltages of base mineral oil and nanofluids. The electrode used the point-plane topology with 5-mm gap distance. Square symbols are Fe<sub>3</sub>O<sub>4</sub> nanofluids. Circular symbols are TiO<sub>2</sub> nanofluids. Triangle symbols are Al<sub>2</sub>O<sub>3</sub> nanofluids. Figures taken from [19].

In [109], Pugazhendhi investigated the negative lightning impulse (1.2/50  $\mu$ s) breakdown voltage of mineral oil and nanofluid disperse with TiO<sub>2</sub> and ZrO<sub>2</sub> nanoparticles. The concentration of nanoparticles in nanofluid was from 0% to 0.05% mass fraction. The measurement procedure followed the IS 11697:1986 Indian standard [136]. The electrodes used were needle-to-sphere electrodes. The results are shown in Figure 2-32.

These results indicated that, in the case of samples stressed with negative lightning impulses, all nanofluids provided breakdown voltages higher than that of base oil. Again, there was an optimal concentration that provided the highest breakdown voltage compared with other samples. In this case,

the optimal concentration was 0.005% (b/w). When the concentration of nanoparticles was higher than the optimal value, the breakdown voltage started to decrease.

Compared with the base liquid, the samples with 0.005% mass fraction of nanoparticles provided the maximum negative impulse breakdown enhancements, which were 16.02% and 19.24% for  $ZrO_2$  and  $TiO_2$  nanofluids, respectively.

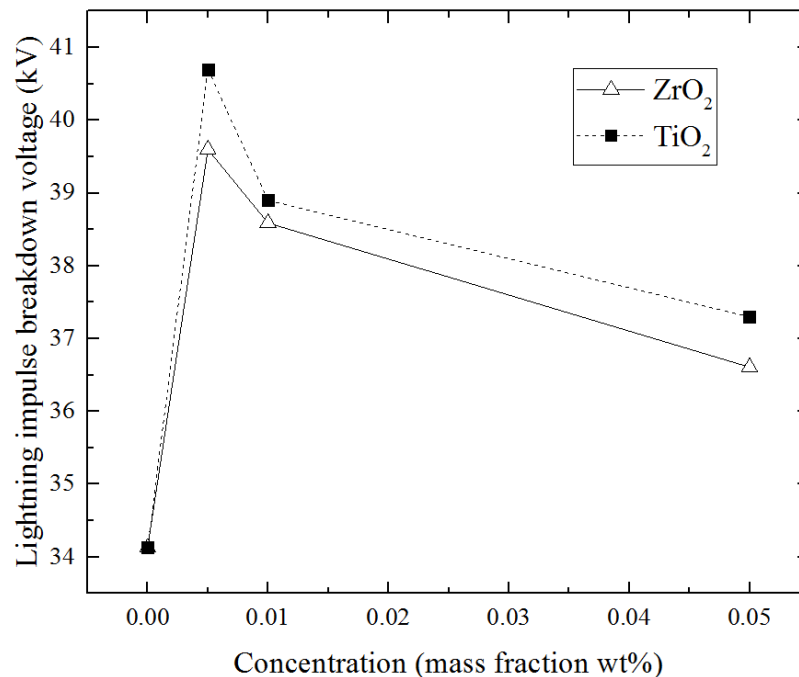


**Figure 2-32.** The negative lightning impulse breakdown voltages of base mineral oil and nanofluids with  $ZrO_2$  and  $TiO_2$  nanoparticles. Figure plotted using data from [109].

In summary, the presented results demonstrated that there was an optimal concentration of nanoparticles in nanofluids, which provided the highest dielectric strength compared with that of other concentrations and base oils. In the case in which the concentration of nanoparticles was higher than the optimal value, the breakdown voltage decreased with an increase in the concentration.

The potential reason for these results, in the case of low concentration of nanoparticles in nanofluid, is that the nanoparticles can 1) act as scavengers in the liquid and trap free electrons produced by the ionisation, 2) bind the water molecules, and 3) reduce the distortion of the electrical field to enhance the nanofluid dielectric performance. The excess nanoparticles start to agglomerate into larger clusters when the concentrations in the test liquid reach a high level. These larger clusters can be treated as a traditional impurity to weaken the fluid dielectric performance.

#### **2.6.4 Ageing of nanofluids**

In [99], Segal et al. investigated the AC and lightning impulse breakdown voltage of the aged mineral oil and nanofluid. The transformer oil-based  $\text{Fe}_3\text{O}_4$  nanofluid samples were aged at  $185^\circ\text{C}$  for 12 weeks. The AC breakdown voltage was measured using the ASTM D877 standard method; the lightning impulse breakdown voltage was measured using the ASTM D3300 standard method. The results are shown in Figure 2-33.

These results showed that nanofluid provided a higher AC and positive lightning impulse breakdown voltages than those of base oil. In addition, they showed slightly lower negative impulse breakdown voltages than that of base oil. Another notable result is the AC breakdown voltages of nanofluids provided less ageing degradation compared with the base oil.

In the case of samples stressed with AC voltage, the breakdown strength of aged nanofluid was 9.3% lower than the breakdown voltage of fresh nanofluid. The breakdown voltage of aged base oil was 34.6% lower than that of fresh base oil. Moreover, in the case of samples stressed with impulse voltage, the impulse breakdown voltage of the nanofluid showed slightly less degradation with ageing compared with the base oil. The impulse breakdown voltage of nanofluid was 12.4% (for positive impulse) and 16.8% (for negative impulse) lower than the breakdown voltage of fresh nanofluids. The impulse breakdown voltage of base oil was 12.9% (for positive impulse) and 17.8% (for negative impulse) lower than that of fresh base oil.

In [137], Lv et al. investigated the AC and lightning impulse breakdown voltages of ageing samples of base mineral oil and nanofluids with  $\text{TiO}_2$  nanoparticles. The aged samples were prepared at  $130^\circ\text{C}$  for 36 days. The AC breakdown voltage was measured using the IEC 60156 standard method; the lightning impulse breakdown voltage was measured using the IEC 60897 standard method. The results in Figure 2-33 show that the AC breakdown voltage and impulse breakdown voltage of aged nanofluid increase of 2.21 and 1.33 times, respectively, compared with those of the aged base oil.

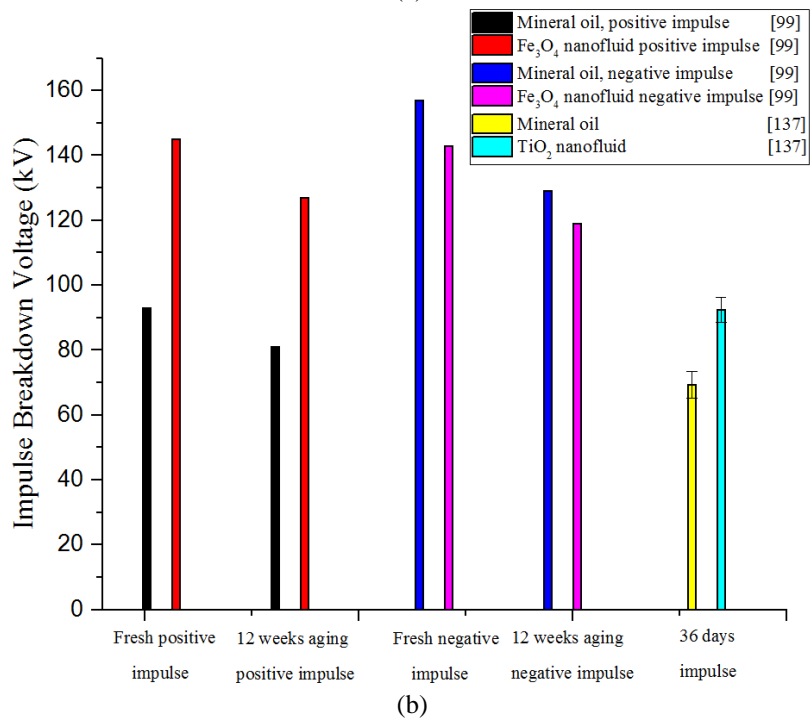
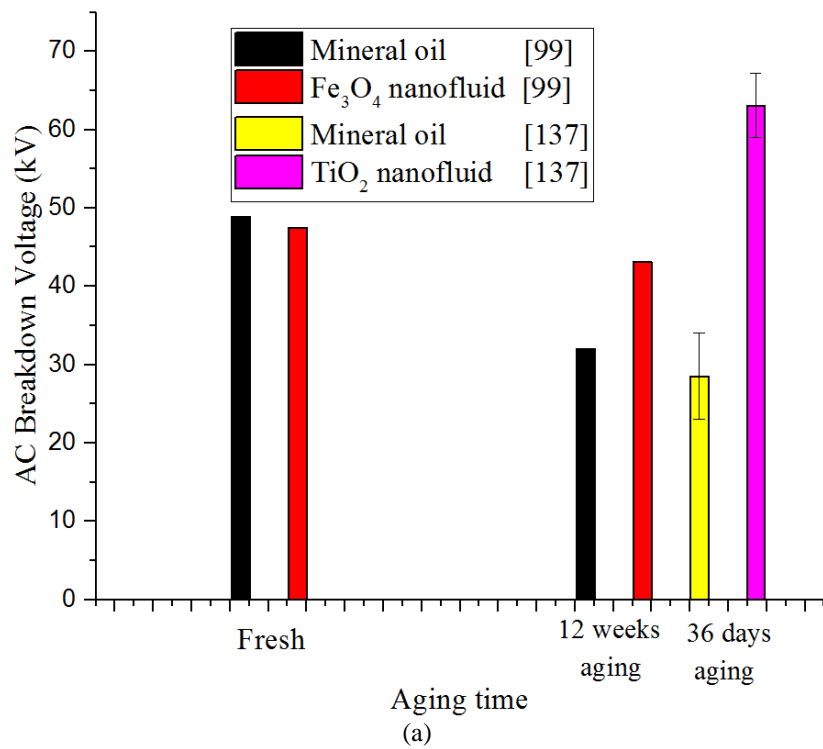
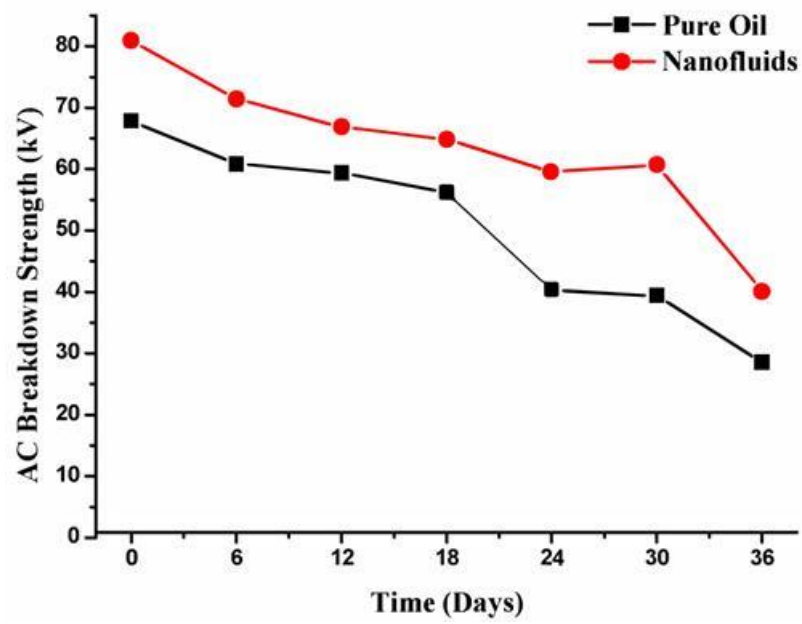
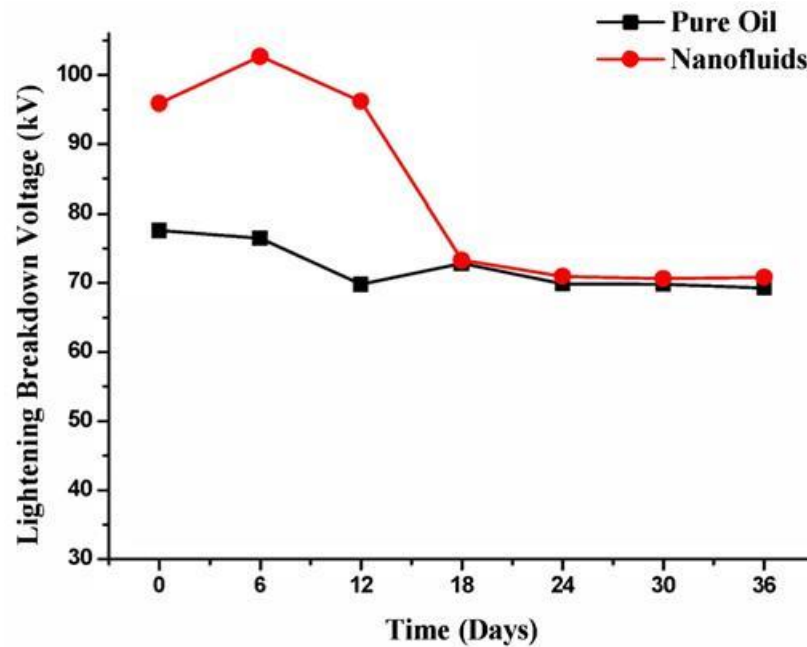


**Figure 2-33.** (a) AC and (b) impulse breakdown strength of the fresh and ageing samples of base oil and nanofluids (Fe<sub>3</sub>O<sub>4</sub> [99] and TiO<sub>2</sub> [137]). Figures plotted using data from [99] and [137].



(a)



(b)

**Figure 2-34.** The AC breakdown voltage (a) and positive lightning impulse breakdown strength (b) of the fresh and various ageing time samples of base oil and TiO<sub>2</sub> nanofluid. Figures taken from [138].

In [138], the transformer oil-based TiO<sub>2</sub> (Karamay 25) nanofluid aged samples were prepared at 130°C for 36 days, and the dielectric properties of the aged samples were investigated by Hu et al. The AC breakdown voltage was measured using the IEC 60156 standard. The brass sphere-sphere electrodes with 2-mm gap were used. Thirty breakdown events were recorded. The positive lightning

impulse breakdown voltage was measured using the IEC 60897 standard. The 50- $\mu\text{m}$  tip radius needle-sphere electrodes with 25-mm gap were used. Six breakdown events were recorded.

As Figure 2-34 shows, in the case of samples stressed with AC voltage, the breakdown voltages of aged nanofluids provided higher results than that of the aged base oil. After 36 days of ageing, the AC breakdown voltage of aged nanofluids was 1.4 times higher than that of the aged base oil.

In the case of samples stressed with positive lightning impulses, the breakdown voltage of nanofluid (fresh, 6 days aged, and 12 days aged) were significantly higher than that of base oil (fresh, 6 days aged, and 12 days aged). When the ageing time was longer than 12 days, the breakdown voltage of the aged nanofluid showed significant degradation and was just slightly higher than that of the aged base oil. After 36 days of ageing, the positive lightning breakdown voltage of aged nanofluid was 1.03 times higher than that of the aged base oil.

In [139], the transformer oil-based  $\text{TiO}_2$  (Karamay 25) nanofluid aged samples with concentrations of nanoparticles from 0 to 0.125 vol% were prepared at 130  $^{\circ}\text{C}$  for 36 days. The dielectric properties of aged samples with 5-ppm and 15-ppm moisture content were investigated by Lv et al. The AC breakdown voltage was measured using the IEC 60156 standard. Six breakdown events were recorded for each sample. The positive lightning impulse breakdown voltage was measured using the IEC 60897 standard. Six breakdown events were recorded for each of these samples as well.

As Figure 2-35 shows, the results indicated both AC and positive lightning impulse breakdown voltages of aged nanofluids were higher than those of the aged base oil. In the case of the 5-ppm moisture content samples stressed with AC voltage, the aged nanofluid with 0.075 vol% concentration of nanoparticles had the highest breakdown voltage, which was 7.7% higher than that of the aged base sample. In the case of samples with 15-ppm moisture content stressed with AC voltage, the aged nanofluid with 0.05 vol% concentration of nanoparticles had the highest breakdown voltage, which was 17.5% higher than that of the aged base sample.

In the case of the 5-ppm moisture content samples stressed with positive lightning impulses, the aged nanofluid with the 0.025 vol% concentration of nanoparticles had the highest breakdown voltage, which was 49.4% higher than that of the aged base sample.

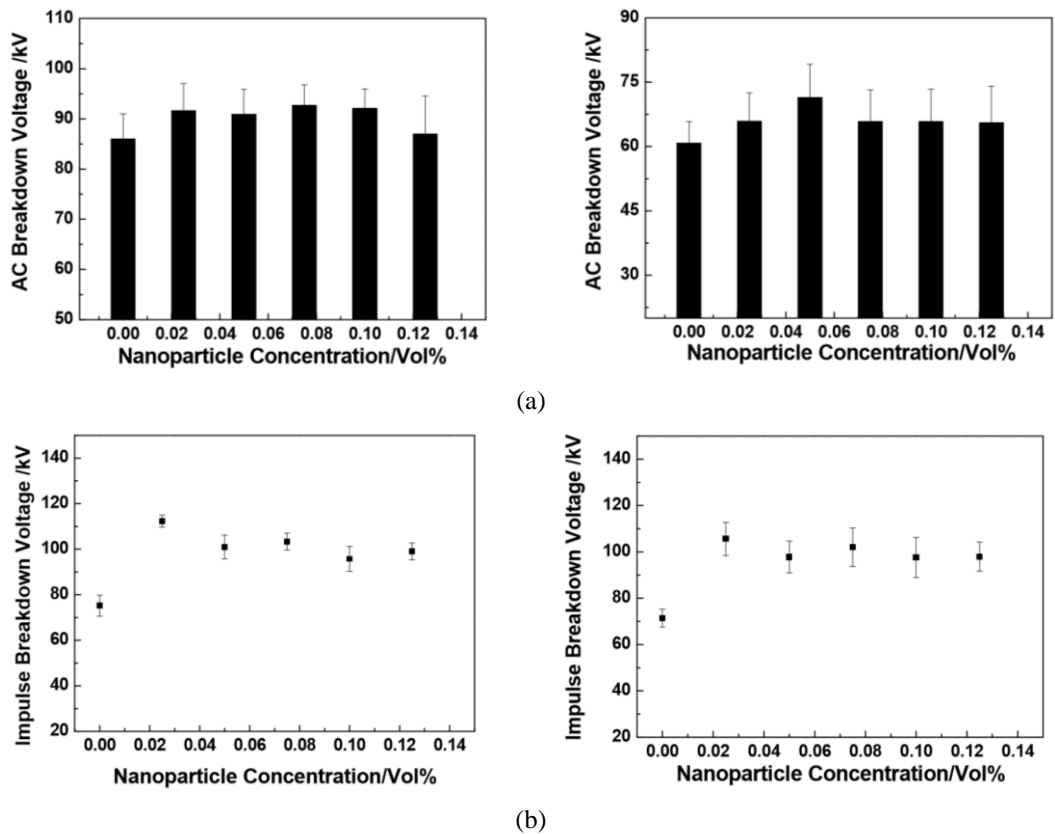


**Figure 2-35.** (a) AC breakdown voltage and (b) positive lightning impulse breakdown strength of the ageing samples of base oil and TiO<sub>2</sub> nanofluid with various concentrations under the 5-ppm (left column) and 15-ppm (right column) moisture content. Figures taken from [139].

In summary, the above results indicated that the dielectric strength of nanofluids shows less degradation with ageing compared with that of the base oil. The aged nanofluids had a higher breakdown threshold, and the modification of the nanoparticles can improve the AC and impulse breakdown strength and moisture resistance of the aged mineral oils.

### 2.6.5 Thermal conductivity of nanofluids

To protect the HV power system and devices, the insulating liquids must perform two key functions: insulation and cooling. During the operation period of HV devices, the copper and iron core produce heat. This extra heat will induce additional stress on the equipment and insulating material, resulting in ageing and may lead to unexpected accidents. To avoid this problem, the insulating liquid must act as a cooling material to transfer heat from the hot spot to the shield of the device, such as transferring heat from the transformer core to the metal shield. Thus, liquid thermal conductivity is an important parameter that is used to evaluate the quality of the insulating liquids.

Several types nanoparticles were dispersed into insulating liquids with an aim to enhance their thermal conductivity. Thus far, there are several published results that indicated that adding nanoparticles can enhance the nanofluid thermal conductivity. It was found that the mineral-oil-based nanofluid with Cu [140], SiO<sub>2</sub> [141], and Al<sub>2</sub>O<sub>3</sub> [142] nanoparticles provided positive results for thermal conductivity enhancement.

Many factors may affect the nanofluid thermal conductivity. These factors include the based fluid, nanoparticle type, concentration, and environment temperature. In the following section, the experimental results and discussion of nanofluid thermal conductivity studies are presented.

### ***Base fluid***

The base liquid would affect the thermal conductivity of the nanofluid because the base liquid's inherent viscosity will affect the Brownian motion of the nanoparticles and will affect the liquid circulation in the case of nonuniform heating [121]. In [143], Gobin et al. investigated the thermal conductivity of nanofluids using the electric double layer model. The results showed that the double layer formation and the thermal conductivity were dependent on the base liquid of the nanofluid. Thus, for the mineral oil and for the ester liquids (mostly vegetable oil and synthetic ester), the nanoparticle's effects on the thermal conductivity of the nanofluid were different. To date, there is no uniform theory to explain both the results of the mineral oil and ester liquids. More experiments and research will be needed to investigate the base liquid effects on the nanofluid thermal conductivity.

### ***Nanoparticle types***

Among many factors that affect the thermal conductivity of the nanofluid, the type of nanoparticles is one of the key factors. In [144], Choi et al. investigated the thermal conductivity of oil-based nanofluids, which were prepared by dispersing multiwalled carbon nanotubes (MWCNT) at room temperature. The results indicated that the thermal conductivity of nanofluids (0.2317 W/mK) was 1.6 times higher than that of base oil samples (0.1448 W/mK).

Boron nitride (BN) is a new type of semi-conductive material that has a high thermal conductivity due to its unique two-dimensional chemical structure [35]. In [35], Jaime et al. investigated the thermal conductivity of the nanofluid mineral oil with dispersed BN nanoparticles. The results indicated that

the thermal conductivity of the BN nanofluid has been increased with 76% enhancement, from 0.115 W/mK to 0.202 W/mK, in the case of nanofluid with a 0.1% mass fraction concentration.

In [32] and [34], Bu et al. investigated the thermal conductivity of nanofluids prepared by dispersing BN nanoparticles into mineral oil [34] and vegetable oil [32]. The results showed that, with an increase in concentration of BN nanoparticles, the thermal conductivity of the nanofluids increases. These research results showed that the nanofluids prepared with new types of nano-material (MWCNT and BN) provided significant enhancement in thermal conductivity.

#### *Concentration of nanoparticles*

Jin et al. investigated the thermal conductivity of mineral-oil-based SiO<sub>2</sub> and fullerene nanofluids in [145]. The nanofluids with concentrations of nanoparticles were 0.01% and 0.1% (b/v). The thermal conductivity measurements were performed at 10°C to 80°C. The results indicated that the concentration of nanoparticles did not affect the thermal conductivity. Compared with other researchers' published results, the potential reason for this phenomenon is that the concentrations of nanoparticles in these nanofluids were too small to produce a noticeable effect on their thermal conductivity.

In [118], Fontes et al. investigated the thermal conductivity of transformer oil-based nanofluid with diamond and multiwalled nanotubes (MWCNT). The concentrations of nanoparticles in oil were 0.005, 0.01, and 0.05% (b/v). The results indicated that the thermal conductivity rises with an increase in concentration. Compared with the base oil, the maximum increase in the thermal conductivity was 23% and 27% for diamond and MWCNT nanotubes, respectively. In this paper, the authors also used the effective medium theory by Maxwell [146] to predict the changes in thermal conductivity. The experimental results were much higher than the calculated values of thermal conductivity.

In [140], the nanofluid samples were prepared with Cu nanoparticles dispersed in kerosene with 0 to 0.01% mass fraction. The thermal conductivity of nanofluid increased linearly with an increase in concentration of nanoparticles. In [142], the nanofluid samples were prepared with Al<sub>2</sub>O<sub>3</sub> nanoparticles dispersed into mineral oil with concentrations of 0.1 to 1.0 vol%. The thermal conductivity of the samples was measured at temperatures of 20°C to 50°C. The results showed the thermal conductivity increased nonlinearly with an increase in concentration. Compared with base

liquid, the maximum improvement of thermal conductivity was 4% in the nanofluids with 0.1 to 0.3 vol% concentrations.

In [147], Zeng et al. investigated the thermal conductivity of nanofluids by adding a lipophilic nanoparticle, MoS<sub>2</sub>, with mass fraction from 0.25 to 1.0%. The thermal conductivity of samples was measured at temperatures from 40°C to 200°C. The results showed that the thermal conductivity raised with an increase in concentration. Furthermore, the thermal conductivity raised with an increase in temperature. Compared with base liquid, the maximum improvement of thermal conductivity was a 38.7% increase, which occurred in the nanofluids with 1.0% concentration at 180°C.

There are several published results that discuss the behaviour of nanofluid thermal conductivity with the change of nanoparticle concentration. Thus far, the nanofluid thermal conductivity behaviours with the nanoparticle concentration still cannot be explained by a single theory. Thus, further experiments and investigation will be needed.

### ***Temperature***

Another important parameter that may affect the thermal conductivity of nanofluids is their temperature. The potential reason for this effect is that temperature affects the viscosity of the liquid and the Brownian motion of the nanoparticles and hence will affect the nanofluid thermal conductivity.

Patel et al. [148] investigated the temperature effect on the thermal conductivity of nanofluids using different base liquids (water, transformer oil, and ethylene glycol) and different nanoparticles, CuO, Cu, Al<sub>2</sub>O<sub>3</sub>, and Al. The concentrations of nanoparticles were to 0.5 to 3.0% b/v, and the measurements were performed at the temperatures of 20°C to 50°C. The results showed that the thermal conductivity of all tested samples rose nonlinearly with an increase in temperature and an increase in concentration. The maximum thermal conductivity enhancements for all nanofluid samples occurred in the highest concentrations of nanoparticles, 3 vol%, and the highest temperature, 50°C. Compared with the base liquid, the maximum thermal conductivity enhancement for nanofluid samples was 26% for CuO, 38% for Cu, 24% for Al, and 17% for Al<sub>2</sub>O<sub>3</sub>.

In [149], Xuan et al. investigated the thermal conductivity of mineral oil-based Cu nanofluid, and the experimental results showed a similar phenomenon as presented in [148]. The experiments were

performed with 1.0%, 2.0%, and 3.0% volume fraction of nanoparticles at temperatures from 20°C to 60°C. Compared with base liquid, the maximum thermal conductivity enhancement was 45%, which was achieved for 3.0 vol% concentration at 60°C.

In [35], Jaime et al. investigated the thermal conductivity of the nanofluid prepared by dispersing BN nanoparticles into mineral oil. The results indicated that the thermal conductivity of the nanofluid nonlinearly increased with an increase in the temperature. Therefore, these published results indicated that nanofluids could potentially provide better thermal conduction performance compared with that of the base liquid.

## **2.7 Summary**

This chapter started with a brief review of the liquid breakdown theory, the chemical and physical properties of dielectric liquids, and a comprehensive discussion of the dielectric performance of different nanofluids reported in the literature. As discussed in Section 2.1, traditional naphthenic mineral oils, in many cases, are not able to meet current strict environmental requirements. Additionally, it is difficult to satisfy advanced requirements of the modern pulsed power and power industry in terms of insulation performance and compactness of the advanced HV systems using these traditional liquids. Thus, there are two potential research directions to solve this problem. One is to improve the dielectric performance of the traditional insulating liquids, and the other one is to find new environmentally friendly dielectric liquids that can be used as substitutions for mineral oils.

To understand the basic principles of the dielectric breakdown and to form a basis for explanation of the dielectric properties of potential new nano-modified dielectric liquids, a review of breakdown mechanisms in liquids has been provided in Section 2.2 based on [42], [46]–[57], [61]. The streamer formation and the streamer development in dielectric liquids also have been discussed in Section 2.2 [58]–[60]. This information will help in understanding the breakdown mechanisms in base and nano-modified dielectric liquids. Thus, dielectric performance of the dielectric liquids, including their breakdown and pre-breakdown characteristics, can be analysed.

In Sections 2.3 and 2.4, the dielectric performance of the ester liquids has been revised and found to be comparable with that of mineral oil [3]–[6], [9]–[14]. Thus, a conclusion can be made that ester

liquids can be considered an alternative to traditional mineral oils, as these insulating liquids provide attractive properties including comparable dielectric performance and low environmental effects [4]–[8].

The results of the investigations of dielectric properties of nanofluids have been presented in Sections 2.5 to 2.6. It was shown that multiple research groups studied dielectric properties of nano-modified liquids and found that nanoparticles can result in substantial changes in the dielectric performance of such liquids [29], [39], [40], [102]–[110], [150]–[152]. The conductive nanoparticles (magnetite) have been used to provide enhancement in the withstand breakdown voltage of nano-modified liquids, and it was found that these particles can substantially increase their dielectric strength [17]–[19]. However, in [20]–[27], it was shown that nanofluids based on magnetite nanoparticles may experience particle agglomeration and sedimentation if such nanofluids are stressed with high electrical stress over a long period. These results indicated that nanofluids based on conductive nanoparticles may not be suitable for continuous operations in HV equipment used in the power industry. To minimise this problem and to increase the stability of nano-modified liquids, semi-conductive and non-conductive nanoparticles can be used [28]–[31].

Based on this review, three different types of insulating liquids (mineral oil, synthetic ester, and natural ester) and two types of semi-conductive nanoparticles ( $\text{TiO}_2$  and BN) have been selected for investigation in the present research project. The following chapters of this thesis will report on the AC breakdown voltage (Chapter 4), standard lightning impulse breakdown voltage (Chapter 5), and the lightning impulse breakdown voltage (Chapter 6) of base and nano-modified liquids. In Chapter 7, the pre-breakdown currents in these three types of liquids have been measured under DC stress, and the mobility of charge carriers and space-charge-influenced electrical field distribution has been obtained. These results help to understand the dielectric behaviour of the insulating liquids stressed with a high electrical field. The review and discussion of the potential mechanisms of dielectric performance enhancement by nanoparticles are also presented in Chapter 7.

# CHAPTER 3

## EXPERIMENTAL SETTING AND SAMPLE PREPARATION

### 3.1 Introduction

This chapter introduces all experimental settings and systems, which include the experimental description, experimental environment conditions, and procedure of sample preparation and test cell cleaning. The experimental procedure is discussed later in a related chapter.

In the present work, three experimental procedures have been used to test AC breakdown voltage, lightning impulse fixed-peak breakdown voltage, and lightning impulse minimum-peak breakdown voltage DC pre-breakdown current. The design of the AC breakdown voltage testing system is based on the international standard ASTM D1816-04 [79]. Both fixed-peak standard lightning impulse breakdown voltage test facilities and minimum-lightning impulse breakdown voltage test facilities have been designed based on the international standard ASTM D3300-00 [80]. All experiments were conducted at atmospheric pressure and room temperature. From the data presented in [153], the expected increase in the breakdown voltage of mineral oil is ~5% when the ambient pressure is increased from 0 atm to 1 atm. It is known that temperature affects the conduction and breakdown properties of the insulating liquids [154], [155]. However, a change in temperature from 20 °C to 80 °C only resulted in a ~7% decrease in the AC breakdown voltage for mineral oil, [156]. From data in [157] changes of  $\pm 5$  °C at a temperature of 20 °C led to a ~5% change in measured conductivity. Therefore, it is assumed that the small shifts in ambient temperature and pressure that occurred during the measurements will have had negligible effects on the results.

The oil samples were used as received with no pre-treatment before measurements. It is known that contaminants and moisture in dielectric fluids affect their breakdown properties [154]. For example, a ~34% decrease in the AC breakdown strength for mineral oil with 43% relative humidity compared with dry oil has been reported in [158]. Many different pre-treatment protocols have been described in

the literature aimed at reducing moisture, dissolved gases, and contaminants from liquid samples. Samples have been degassed and dried but not filtered [9], filtered using a relatively large filter (10-16  $\mu\text{m}$ ) but not degassed or dried [159], or only filtered using a 5- $\mu\text{m}$  filter [160]. The results of dielectric studies in which ‘as received’ insulating fluids were used without any additional filtration, degassing, or de-humidification were reported in the literature [161], [162]. In the work reported on aged biodegradable oils [163], no details of pre-treatment of the liquids before or post-ageing was reported. Given this wide range of possible pre-treatments, the authors felt that using the oils as received provided the starting point for assessing the relative properties of the three liquids. This approach has the advantage that the results help to understand the dielectric behaviour of commercially available insulating liquids used in practical engineering applications without additional processing. The results in the present work were compared with the studies in which pre-treated dielectric liquids have been used.

The relative water content of the liquids used in the present study has been examined using an ‘Omniport 20’ moisture in oil probe (E+E Elektronik GmbH). The examined results can be converted into absolute water content using the linear relationship between these two values [164]. The water solubility values for Diala S3 (~77 ppm), Midel 7131 (~2600 ppm), and rapeseed (~772 ppm) oils required for this analysis have been taken from [165] and [6], respectively. The evaluated absolute water content for Diala S3 is ~39 ppm, while Midel 7131 is ~1352 ppm, and rapeseed oil is ~417 ppm. These values were not exact and are given here for evaluation purposes only. Such high values of absolute water content can be explained by the fact that the liquid samples were kept in ambient laboratory conditions [158].

The remains of liquids and nanoparticles after each test may affect the next test results. To avoid this effect, the test cell and electrodes were cleaned with ethanol and then washed with distilled water to remove the previous experiment remnants. After that, the test cell was dried in the oven at a temperature 40°C for 2 hours to remove the remaining water.

### **3.2 Insulating Liquids Used in This Study**

The base samples of Diala S3, Midel 7131, and rapeseed oil (samples of ‘as received’ oils) are shown in Figure 3-1. The mineral oil (Diala S3) is colourless and transparent. The synthetic ester (Midel

7131) has a light-yellow colour, and the rapeseed oil has a deep yellow colour. The general physical properties of Diala S3, Midel 7131, and natural ester have been obtained using the manufacturer's datasheets (if available) and the literature data. These properties are shown in Table 3-1, which includes physical, chemical, and electrical parameters that have been published in technical data sheets [75], [166]. In this thesis, the rapeseed oil is a food-grade natural ester in which the basic general properties have not been investigated. In Table 3-1, the parameters of natural ester from [75] were treated as a reference to compare with those of Diala S3 and Midel 7131.

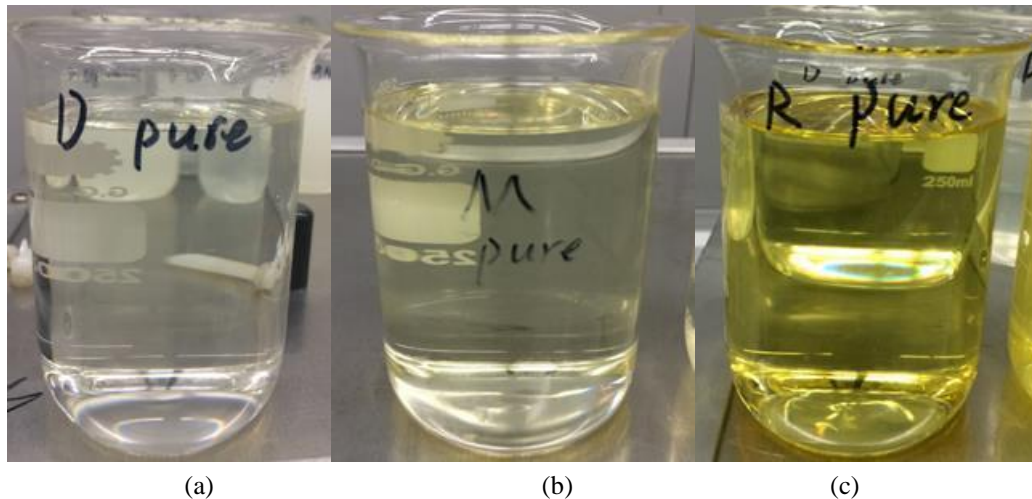


**Figure 3-1.** Picture of base samples of (a) Diala S3, (b) Midel 7131, and (c) rapeseed oil.

Comparing the general properties of mineral oil, synthetic ester, and natural ester, several specific features of ester liquids can be identified. Ester liquids, specifically natural ester, is biodegradable. Moreover, ester liquids are non-toxic and do not contaminate water. These features make ester liquids suitable for the engineering needs of modern society with advanced environmental protection, safety, and health requirements.

Ester liquids have almost twice or even higher flash points than mineral oil, and they are more hygroscopic than mineral oil. A high flash point means ester liquids mostly have good resistance to ignition; thus, it helps to reduce the risk of fire and explosion hazards in the HV power systems. The strong hygroscopic ability means ester liquids could absorb more moisture than traditional mineral oils from cellulose insulation and slow the hydrolysis ageing process of cellulose material. The thermal conductivities of ester liquids are higher than that of mineral oil, but ester liquids have a high viscosity, which could slow the liquid flow and reduce the thermal dissipation ability [75].

**Table 3-1.** General properties of mineral oil, Midel 7131, and natural ester. Data from [71], [72], [75], [166].

| Properties   | Units              | Midel 7131          | Mineral Oil         | Natural Ester       |
|--|--------------------|---------------------|---------------------|---------------------|
| <b>General Properties</b>                          |                    |                     |                     |                     |
| Density at 20 °C                                   | kg/dm <sup>3</sup> | 0.97                | 0.88                | 0.92                |
| Specific Heat at 20 °C                             | J/kg K             | 1880                | 1860                | 1848                |
| Thermal Conductivity at 20 °C                      | W/m K              | 0.144               | 0.126               | 0.177               |
| Kinematic Viscosity at -30 °C                      | mm <sup>2</sup> /s | 1400                | 1100                | N/A                 |
| Kinematic Viscosity at 20 °C                       | mm <sup>2</sup> /s | 70                  | 22                  | 84.8                |
| Kinematic Viscosity at 40 °C                       | mm <sup>2</sup> /s | 28                  | 8                   | N/A                 |
| Kinematic Viscosity at 100 °C                      | mm <sup>2</sup> /s | 5.25                | 2.6                 | 9.3                 |
| Pour Point   | °C                 | -60                 | -57                 | -31                 |
| Expansion Coefficient                              | / °C               | 0.00075             | 0.00075             | 0.00074             |
| Flash Point to ISO 2719                            | °C                 | 260                 | 136                 | 327                 |
| Fire Point to ISO 2592                             | °C                 | 316                 | 170                 | 360                 |
| Biodegradability at 28 Days                        |                    |                     |                     |                     |
| - OECD 301 F                                       | %                  | 89                  | N/A                 | 97                  |
| - OECD 301 D                                       | %                  | N/A                 | <10                 | N/A                 |
| <b>Chemical Properties</b>                         |                    |                     |                     |                     |
| Neutralisation Value                               | mg KOH/g           | <0.03               | <0.01               | <0.05               |
| Net Calorific Value                                | MJ/kg              | 31.6                | 46                  | 37.5                |
| <b>Dielectric Properties</b>                       |                    |                     |                     |                     |
| Dielectric Dissipation Factor<br>Tan δ at 90°C     |                    | <0.008              | 0.002               | <0.005              |
| Breakdown Voltage                                  | kV                 | >75                 | >70                 | >75                 |
| Volume resistivity at 25 °C                        | Ω-cm               | >5×10 <sup>12</sup> | 25×10 <sup>12</sup> | 20×10 <sup>12</sup> |
| Fire Hazard Classification to IEC 61100/ IEC 61039 |                    | K3                  | O                   | K2                  |
| Permittivity at 20 °C                              |                    | 3.2                 | 2.2                 | 2.5                 |

Compared with mineral oil, the relatively low volume resistance of ester liquids reduces the insulation electrical resistance of ester liquids. The high polarity of ester liquids could result in the initial space charge, and streamers were easier to form than in mineral oil [11].

For natural ester, there are a significant number of original materials that can be refined as natural ester liquids. Moreover, components of these natural ester liquids are complex and different from each other. Thus, the performance of these ester liquids is difficult to evaluate. A substantial number of experimental studies have been conducted as discussed in Chapter 2. However, there is still a significant gap in knowledge of the dielectric properties of ester liquids. The relatively low pour point of natural ester liquids may affect their application in cold areas. In Table 3-1, natural ester was a type of industry product that would be expected to have better parameters than the food-grade natural ester used in this study.

### 3.3 Nanoparticles Used for Modification of Dielectric Liquid

#### 3.3.1 Physical properties of nanoparticles

Recently a large number of researchers have focused on ester liquids, which can be used to replace traditional mineral insulating oils [5], [8], [12], [159], [161], [167]–[181]. Several researchers described the use of nanoparticles as additives to improve dielectric and thermal conductivity performance of traditional mineral oil dielectrics [100], [105], [135], [182], [183]. In [17], it was shown that a mineral oil that is modified by the conductive nanoparticle,  $\text{Fe}_3\text{O}_4$ , provides an improvement in dielectric and thermal conductive behaviour. Because of the high conductivity of magnetite nanoparticles with polarisation, there were many nanoparticle agglomeration phenomena that were observed under long-term electrical stress. Another shortcoming of the magnetite nanoparticle is that, in a high temperature environment, the  $\text{Fe}_3\text{O}_4$  nanoparticle in a nano-modified liquid may oxidise and become  $\text{Fe}_2\text{O}_3$  particles. Additionally, the agglomeration and separation phenomena were observed [25], [184], [185].

**Table 3-2.** Main properties of nanoparticles used in this project [93], [95], [186]–[189].

| Properties                                      | $\text{TiO}_2$ (anatase)        | h-BN                                 |
|---|---------------------------------|--------------------------------------|
| Average particle size (nm)                      | 25 [187]                        | 70 [189]                             |
| Relative permittivity                           | 50 [186]                        | 4 [188]                              |
| Surface area ( $\text{m}^2/\text{g}$ )          | 35-65 [187]                     | 45 [189]                             |
| Thermal conductivity                            | 11.7 ( $\text{WmK}^{-1}$ ) [93] | 0.08 ( $\text{cal/cm.sec.K}$ ) [189] |
| Dielectric strength (kV/mm)                     | 4 [93]                          | 35 [189]                             |
| Resistivity at 25 °C ( $\Omega\cdot\text{cm}$ ) | $10^{12}$ [93]                  | $10^{14}$ [95]                       |

Several published works reported that not only conductive nanoparticles but also non-conductive nanoparticles could improve the insulating behaviour of liquid dielectrics and their thermal conductivity properties [190]–[192]. It was shown that both semi-conductive and non-conductive nanoparticles, such as  $\text{TiO}_2$  and  $\text{Al}_2\text{O}_3$ , could improve insulating properties of the liquid dielectric withstand property. Some nanoparticles, for example, BN nanoparticles, could significantly improve/increase the thermal conductivity of insulating liquids [34], [35].

In the present work, two types of semi-conductive nanoparticles, TiO<sub>2</sub>, which was purchased from Aeroxide, and BN, which was purchased from Lower Friction Ltd, were chosen as additives to prepare the nano-modified suspensions of insulating liquids. The physical properties of these two types of nanoparticles are shown in Table 3-2.

### **3.3.2 Concentration of nanoparticles in dielectric liquids**

There are several published research works that were focused on finding the optimal nanoparticle concentration for providing maximum improvement in the withstand voltage. These published results also indicated that, based on the nanoparticle concentration in insulating liquids, the dielectric properties of these liquids could be deteriorated when the nanoparticle concentration is higher than a critical level TiO<sub>2</sub> used in [29], [105], [106]; barium strontium titanate (BST) used in [193]. As [193] showed, the withstand voltage of nanoparticle suspension decreased from 0.1% (b/w) nanoparticle concentration. The nanoparticle concentrations in these studies were on a relatively large-scale (from 0.1% to a few dozens of per cent). Based on these published results, in the present study, the range of concentration of nanoparticles was selected from 0.0006% to 0.1% (b/w), not to enter higher concentrations, which will result in a decrease of the breakdown voltage.

### **3.3.3 Nanoparticle surface modification and sample preparation procedure**

There are many experimental studies that indicated that adding nanoparticles into insulating liquids directly and using ultrasonic technology to help nanoparticles disseminate uniformly in insulating liquids to form a stable nano-modified suspension may improve the insulating liquid dielectric property strength.

However, some published works also indicated that, under high temperature and high external applied electrical field conditions, the nano-suspension nano-modified insulating liquid nanoparticles may agglomerate and separate from the suspension, which means the operating life of these suspensions may be affected. These published works also indicated that using nanoparticle surface-modified technology would help the nano-suspension to approach a longer operating life. The generally theory of nanoparticle surface modification is that, when adding nanoparticles and surface-modified reagents into an organic solution, such as n-hexane or ethanol, with a specific ratio, the surface-modified reagent would fully cover the nanoparticle. Mostly surface-modified reagents have a lipophilic

chemical structure, which would help nanoparticles suspend in the insulating liquids stably and prevent agglomeration or precipitation [194]–[196].



(a)

(b)



(c)

(d)



(e)

(f)

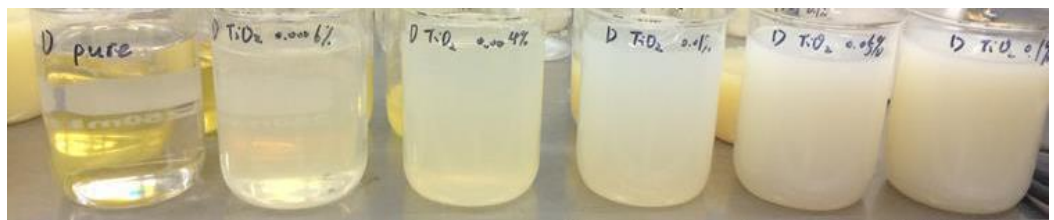
(g)

**Figure 3-2.** Device pictures for nanoparticle surface modification: (a) Ethanol and oleic acid, (b) Water bath, (c) Magnetic stirring, (d) Ultrasonic bath, (e) Centrifuge, (f) Oven, and (g) Vacuum pump.

To make a stable suspension of nanoparticles in insulating liquids, the surface of the nanoparticles was modified. The following procedure of surface modification was used. One gram of  $\text{TiO}_2$  nanoparticles was added to 100 ml of ethanol and then placed into  $60^\circ\text{C}$  Grant water baths for 1 hour. After the water bath, 0.25 g of oleic acid was added to the nanoparticle-ethanol mixture using a pipette. This liquid was mechanically agitated for 15 minutes using IKA Yellowline MSH B basic magnetic stirring and then was placed in an Ultrawave ultrasonic bath for 2 hours. The nanoparticles were then separated from the mixture using a Thermo Scientific Heraeus Labofuge 400R centrifuge, washed three times with ethanol, and dried in an oven at  $60^\circ\text{C}$  for 24 hours. Then, using glass mortar and pestle, the nanoparticle agglomeration was ground to obtain a powder. Figure 3-2 shows pictures of the materials and equipment used for the nanoparticle surface modification.

Titanium dioxide ( $\text{TiO}_2$ ) and Boron Nitride (BN) were used to prepare the nano-modified samples of the insulating liquids. The weight ratio of nanoparticles to liquid was set to 0.0006%, 0.004%, 0.01%, 0.05%, and 0.1% in accordance with the concentration of magnetite nanoparticles. The nano-modified samples of liquids were prepared using the following protocol.

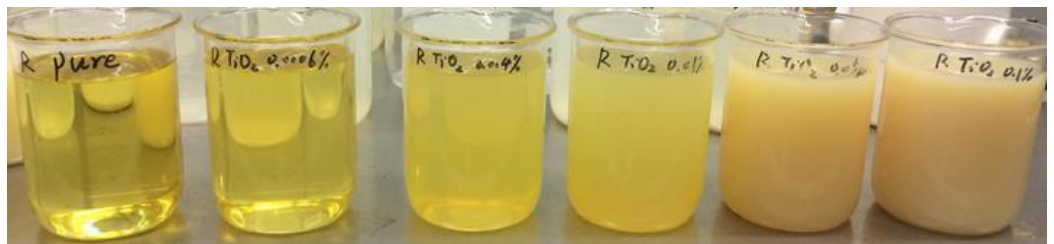
First, the surface treated nanoparticles were weighted, and specific amounts of these nanoparticles were added to the base insulating liquids to achieve desirable concentrations. Then, the beaker was put in an ultrasonic bath for 1 hour to obtain a well-mixed suspension. To avoid a temperature increase due to the long ultrasonic treatment, the ultrasonic treatment was separated into four intervals. Each ultrasonic treatment interval lasted 15 minutes with 5 minutes of rest. Nanoparticle suspension was added to the test cell and placed in the Edwards 12E3/1395 vacuum pump (shown in Figure 3-2 (g)) for 1.5 hours to remove the small gas bubbles from the test cell and electrode surfaces. The photos of the  $\text{TiO}_2$  and BN nanoparticle suspensions based on mineral oil, synthetic ester, and natural ester are shown in Figures 3-3 and 3-4.



(a)



(b)



(c)

**Figure 3-3.** TiO<sub>2</sub> nanoparticle suspension based on (a) mineral oil, (b) synthetic ester, and (c) natural ester.



(a)



(b)



(c)

**Figure 3-4.** BN nanoparticle suspension based on (a) mineral oil, (b) synthetic ester, and (c) natural ester.

### 3.3.4 Average size of nanoparticles in suspension sample investigation

To confirm that nanoparticles indeed disperse into the liquid sample and form a uniform stable nanofluid and to determine the size distribution of the nanoparticles in these suspensions, the average size of the nanoparticles in the nanofluids have been measured using a laser analyser, the Malvern Zetasizer Nano ZSP. Some published results indicated that adding the surfactant during the nanofluid preparation can reduce and even prevent the aggregation of nanoparticles [194]–[196]. By adding the surfactant, the nanoparticle surface chemical performance could be modified from oleophobic to lipophilic, which could improve the stability of nanoparticles in the insulating liquids [197]. The Malvern Zetasizer Nano ZSP laser analyser was used to measure the average size of the nanoparticles.

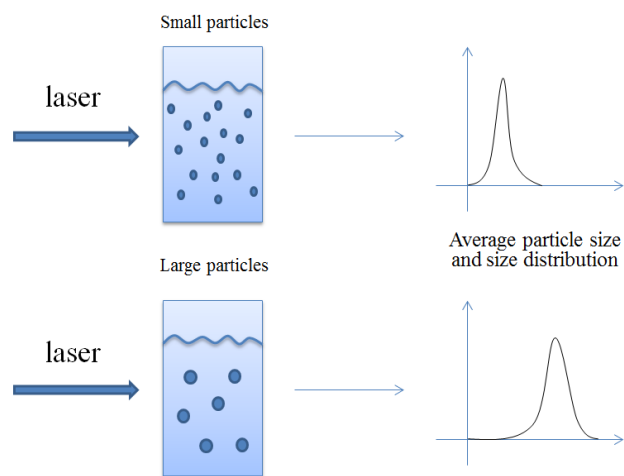


**Figure 3-5.** Laser analyser operation principle.

The particles in the liquids will have a constant random thermal motion, called Brownian motion. The motion speed of the particles depends on their size and temperature. The smaller particles at higher temperatures will move faster. The operation principle of this laser analyser is to use dynamic light scattering to measure the particles' Brownian motion to calculate the particle size and size distribution. For the purpose of measuring the particle motion speed, the speckle pattern produced by illuminating the particles with a laser is observed. The light scattering intensity at a specific angle will fluctuate with time, and this is detected using a sensitive avalanche photodiode detector. The light scattering intensity changes are analysed with a digital auto correlator, which generates a correlation function. This curve can be analysed to give the size and the size distribution [198]. The relative parameters for the nanoparticles average size measurement are shown in Tables 3-3 and 3-4.



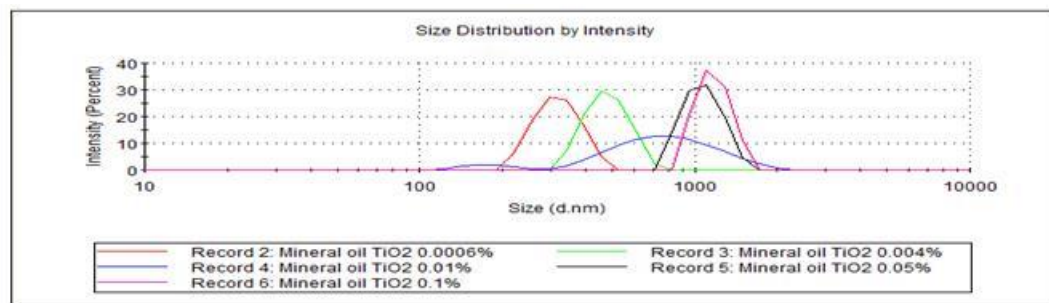
**Figure 3-6.** Malvern Zetasizer ZSP laser analyser.

**Table 3-3.** Relative parameters of the insulating liquid for the average size measurement of nanoparticles [75], [81], [199].

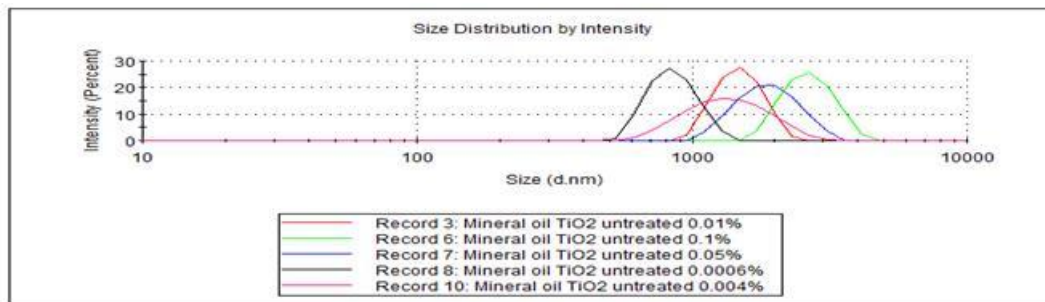
| Parameters                        | Mineral Oil | Synthetic Ester | Nature Ester |
|-----------------------------------|-------------|-----------------|--------------|
| Refractive Index at 20 °C         | 1.48        | 1.455           | 1.475        |
| Dynamic Viscosity at 20°C (mPa*s) | 19.36       | 67.9            | 78.02        |

**Table 3-4.** Nano-powder relative parameters for the average size measurement of nanoparticles [200]–[205].

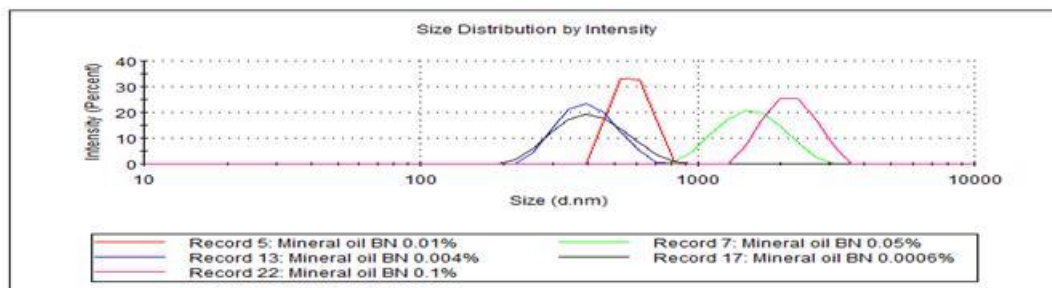
| Parameters             | TiO <sub>2</sub> | BN     |
|------------------------|------------------|--------|
| Refractive Index       | 2.42             | 1.65   |
| Absorption Coefficient | 0.0006           | 0.0006 |



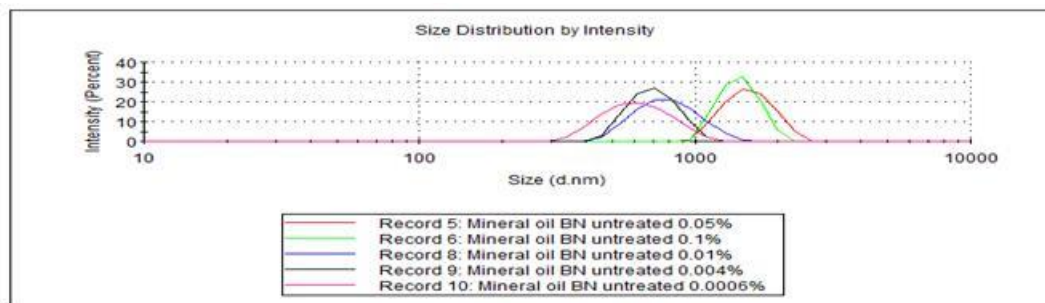
(a)



(b)

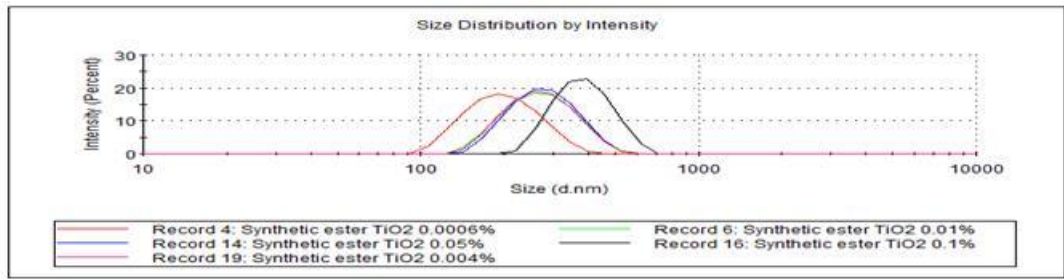


(c)

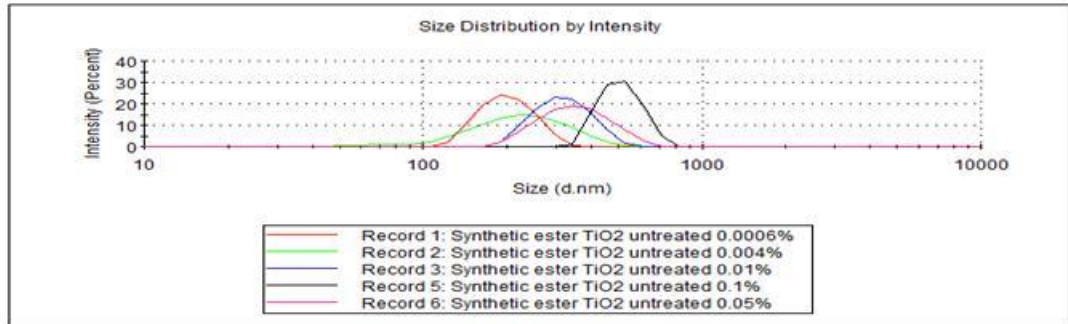


(d)

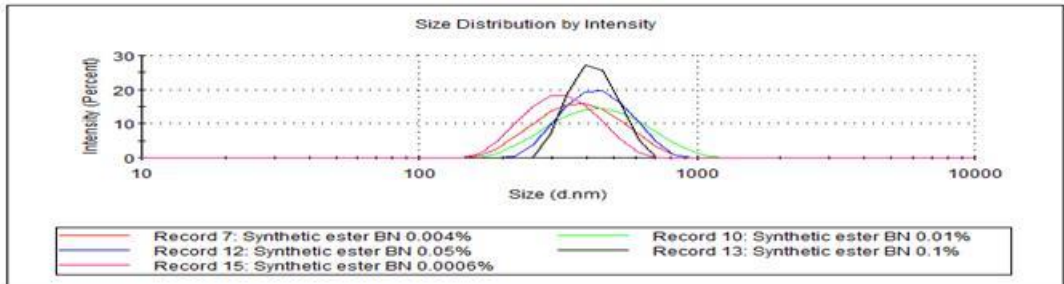
**Figure 3-7.** Average size of nanoparticles for TiO<sub>2</sub> and BN series weight concentration mineral oil samples: (a) TiO<sub>2</sub> with surfactant treatment; (b) TiO<sub>2</sub> without surfactant treatment; (c) BN with surfactant treatment; and (d) BN without surfactant treatment.



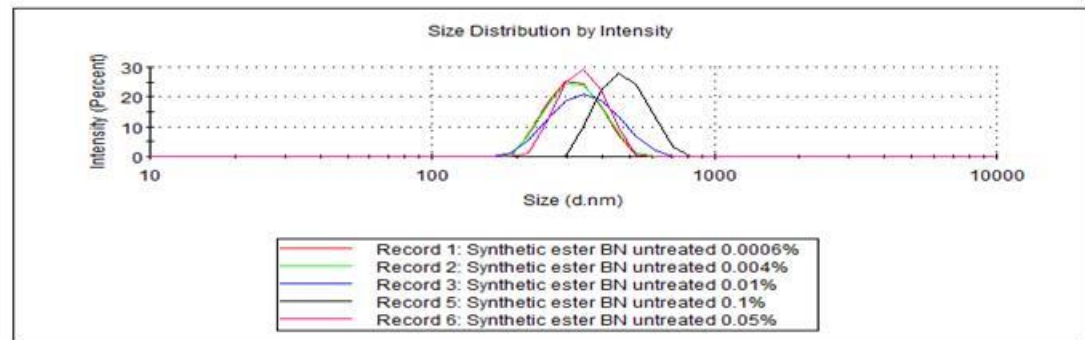
(a)



(b)

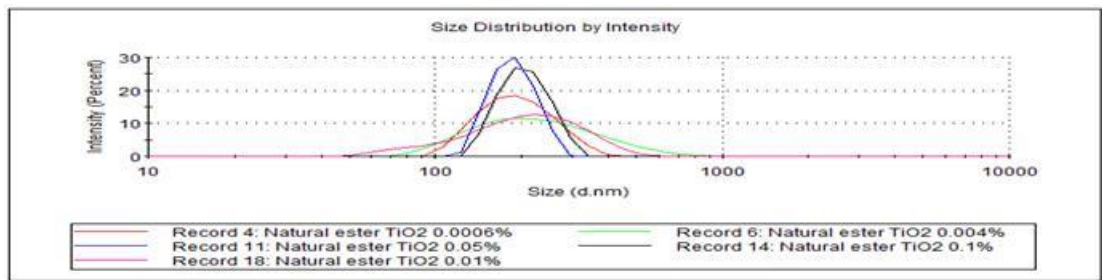


(c)

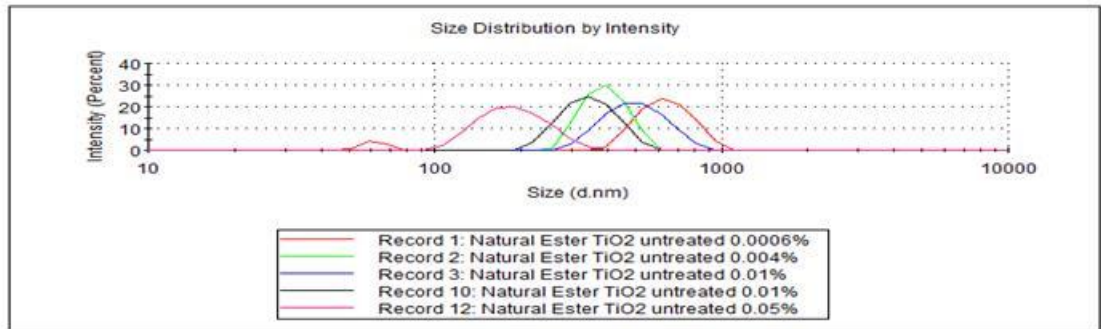


(d)

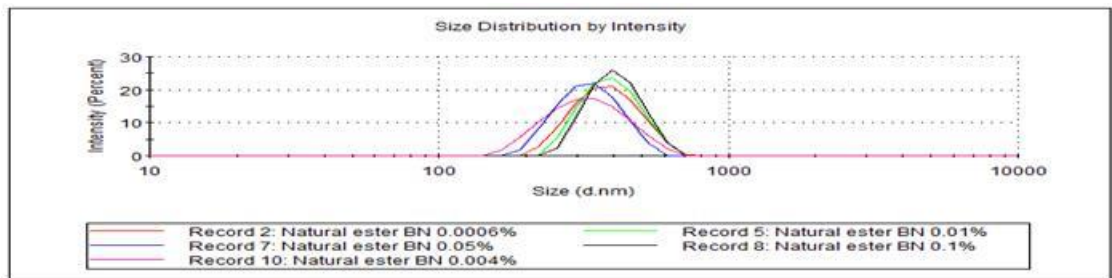
**Figure 3-8.** Average size of nanoparticle for TiO<sub>2</sub> and BN series weight concentration of synthetic ester samples: (a) TiO<sub>2</sub> with surfactant treatment; (b) TiO<sub>2</sub> without surfactant treatment; (c) BN with surfactant treatment; and (d) BN without surfactant treatment.



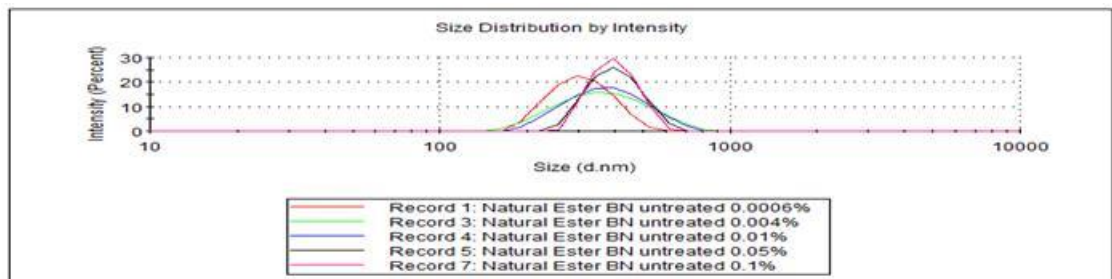
(a)



(b)



(c)



(d)

**Figure 3-9.** Average size of nanoparticles for TiO<sub>2</sub> and BN series weight concentration of natural ester samples: (a) TiO<sub>2</sub> with surfactant treatment; (b) TiO<sub>2</sub> without surfactant treatment; (c) BN with surfactant treatment; and (d) BN without surfactant treatment.

Figures 3-7 to 3-9 show the average size distribution of nanoparticles in the nanofluid samples. The results showed that, for the mineral oil samples, the nanoparticle average size was from 300 nm to > 1000 nm, which was several times greater than both ester samples. For both ester samples, the average size of the nanoparticles was from 180 nm to ~500 nm. Comparing the series of nano-

modified samples with and without surface treatment, it was shown that the surfactant significantly reduced the average nanoparticle size for mineral oil samples, especially for high concentration samples. For both ester samples, the effect of the surfactant was not well pronounced. The average size of the nanoparticle samples that have surfactants was just slightly smaller than or equivalent to the average size of the nanoparticle samples that were without surface treatment. More detailed results of these measurements are shown in Table 3-5.

**Table 3-5.** Nanoparticle average size measurement results.

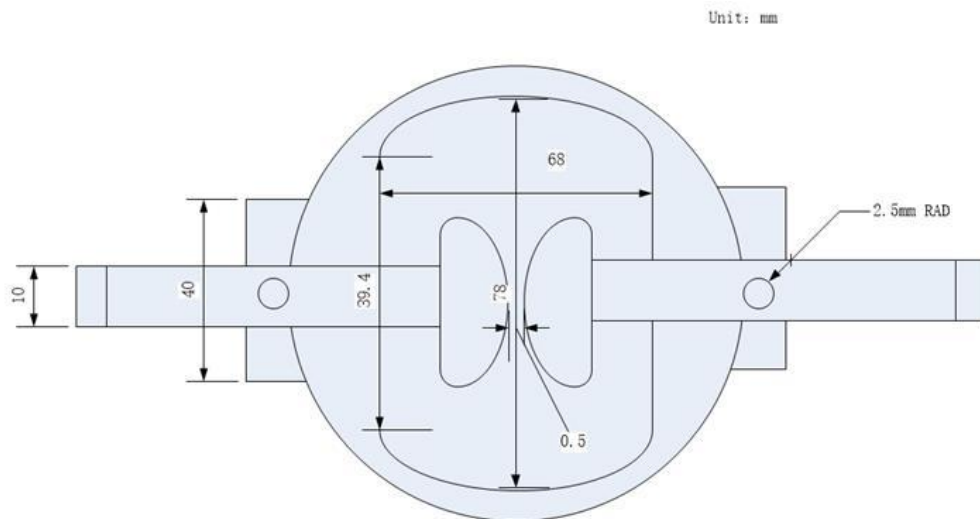
| <b>Nanoparticle Average Size (nm)</b> |                                   |                                  |                      |                     |
|---------------------------------------|-----------------------------------|----------------------------------|----------------------|---------------------|
| <b>Concentration by Weight (%)</b>    | <b>TiO<sub>2</sub> Oleic Acid</b> | <b>TiO<sub>2</sub> Untreated</b> | <b>BN Oleic Acid</b> | <b>BN Untreated</b> |
|                                       | <b>Mineral Oil</b>                |                                  |                      |                     |
| 0.0006                                | 302                               | 824                              | 389                  | 596                 |
| 0.004                                 | 481                               | 1259                             | 407                  | 760                 |
| 0.01                                  | 630                               | 1437                             | 545                  | 773                 |
| 0.05                                  | 1039                              | 1541                             | 1416                 | 1626                |
| 0.1                                   | 1678                              | 2509                             | 2193                 | 2200                |
|                                       | <b>Synthetic Ester</b>            |                                  |                      |                     |
| 0.0006                                | 188                               | 187                              | 296                  | 315                 |
| 0.004                                 | 257                               | 200                              | 318                  | 321                 |
| 0.01                                  | 230                               | 307                              | 396                  | 345                 |
| 0.05                                  | 267                               | 334                              | 371                  | 345                 |
| 0.1                                   | 368                               | 537                              | 441                  | 490                 |
|                                       | <b>Natural Ester</b>              |                                  |                      |                     |
| 0.0006                                | 185                               | 466                              | 359                  | 303                 |
| 0.004                                 | 195                               | 407                              | 307                  | 302                 |
| 0.01                                  | 177                               | 475                              | 399                  | 332                 |
| 0.05                                  | 195                               | 178                              | 323                  | 402                 |
| 0.1                                   | 206                               | 339                              | 411                  | 399                 |

### 3.4 Experimental System for AC Breakdown Voltage Measurement

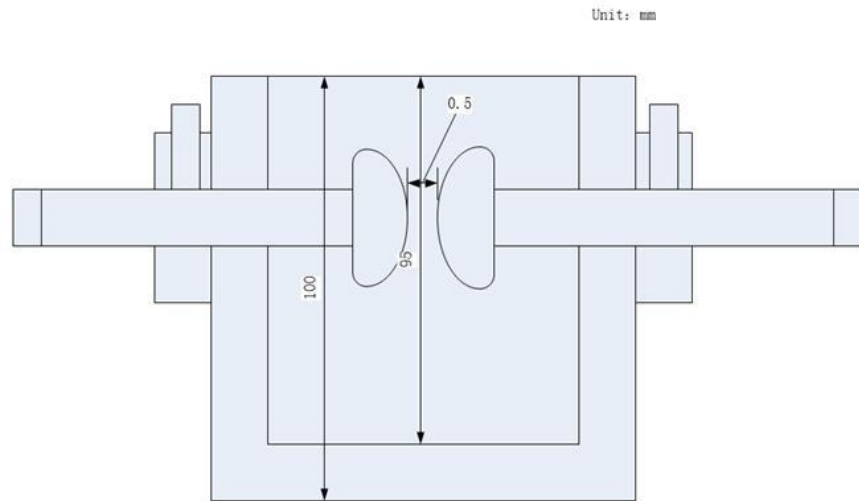
For insulating materials, the dielectric strength under AC stress is a key parameter that defines the insulating performance and should be evaluated. These experiments focus on investigating the breakdown voltages of three different insulating liquids with two types of nanoparticles with several different concentrations under AC stress. The AC breakdown voltages of the liquids under investigation were measured in an electrode configuration that satisfies the ASTM D1816-04 standard [79].

#### 3.4.1 Test cell design

Figure 3-10 shows the test cell details. This test cell has a ceramic body and open top. This vessel has two adjustable brass bars that can be used to adjust an inter-electrode gap. The screw nuts on the socket of the bar were used to fix the metal bar. On the bottom of these bars, screw nuts fix the power cable from the AC Foster transformer and HV probe. The electrodes were removable; hence, this test cell is also suitable for the experiment that investigates the insulating liquid performance under different electrical fields (different geometry electrode topologies).



(a) Top view of the test cell.



(b) Profile of the test cell.

**Figure 3-10.** Schematic view of the test cell: (a) top view, (b) profile of the test cell.

### 3.4.2 Electrode topology

Figure 3-11 shows the electrode topology used in the present tests; the details were according to the ASTM D1816-04 standard [79]. A pair of spherically capped, polished, brass electrodes was incorporated into a ceramic container. The electrode profile is shown in Figure 3-12. The gap between the two electrodes is 0.5 mm.

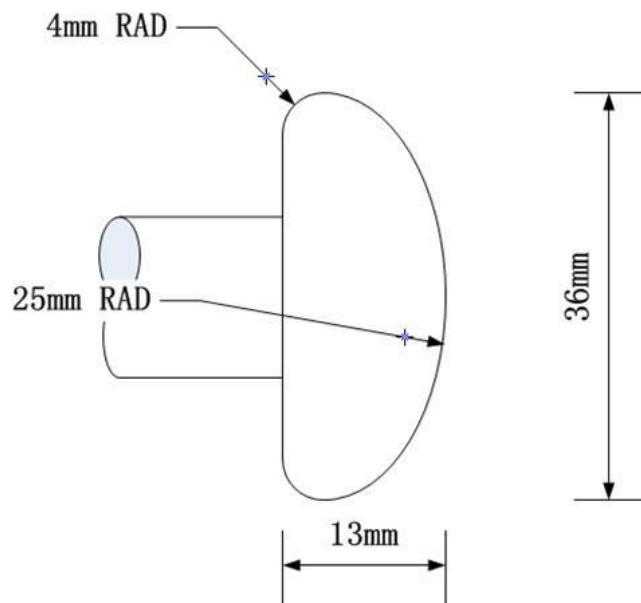


**Figure 3-11.** Cross section of the spherically capped electrode.



**Figure 3-12.** Practical spherically capped electrode.

### **3.4.3 Measurement systems and devices**

Figures 3-13 to 3-15 show the devices used in the measurement system. Figures 3-16 and 3-17 show the AC breakdown voltage measurement circuit. An AC Foster breakdown test apparatus was connected in parallel with the test cell. This apparatus produces a 50 Hz AC voltage across the test cell filled with a dielectric liquid. The AC breakdown voltages were measured using a Tektronix P6015A HV probe (Maximum 20 kV DC; 40 kV peak impulse voltage; 100 ms) with a division ratio of 1:1000 and Tektronix digitising oscilloscope.



(a): AC Foster breakdown test apparatus.



(b): Apparatus control panel.

**Figure 3-13.** AC Foster breakdown test apparatus: (a) AC Foster breakdown test apparatus, (b) apparatus control panel.



**Figure 3-14.** Tektronix P6015A HV probe.



**Figure 3-15.** Tektronix digitising oscilloscope.

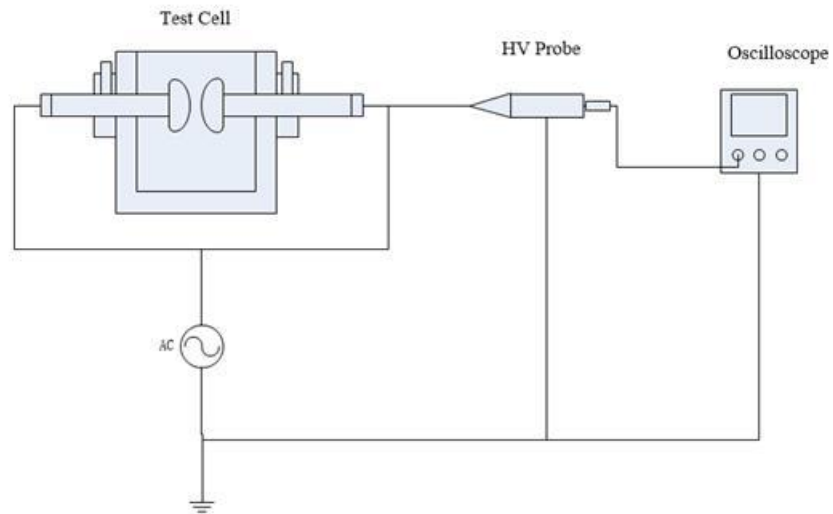


**Figure 3-16.** AC breakdown voltage measurement circuit.

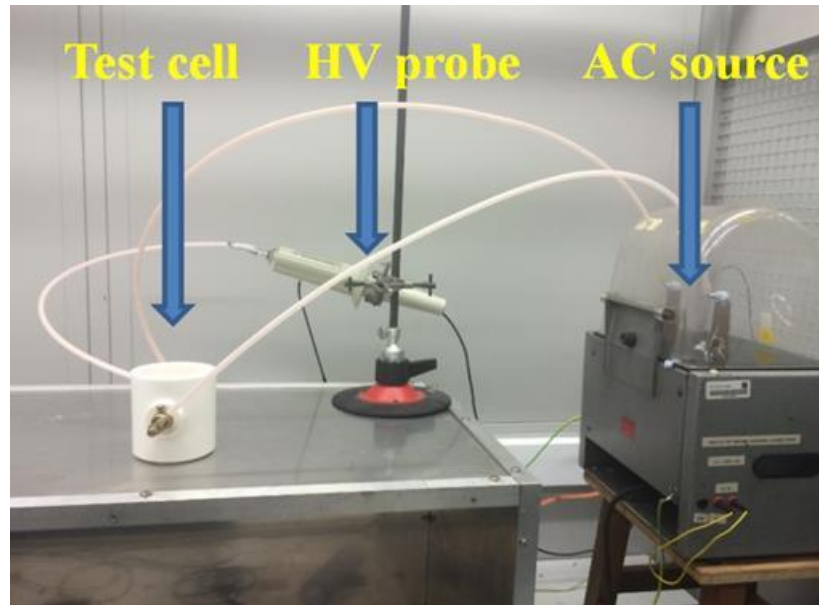


**Figure 3-17.** Practical AC breakdown voltage measurement circuit.

### **3.5 Experimental Setting for Fixed-peak Lightning Impulse and Minimum Impulse Breakdown Voltage Measurement**

The fixed-peak lightning impulse breakdown voltage was measured using an electrode configuration that satisfies the ASTM D3300-00 standard [80]. The breakdown tests were conducted under ambient conditions (room temperature, pressure, and humidity) as described in Section 3.1. The same HV impulse generation circuit and measurement system was used throughout all impulse tests, which include the impulse pre-breakdown time tests, and minimum impulse breakdown voltage tests.

The gap between the electrodes was set to 3 mm. The electrode type was a gramophone needle-sphere, and more details will be presented in Section 3.5.3. The wave-shape of the applied positive and negative HV impulse was 1.2/50  $\mu$ s, generated with a three-stage Marx generator. For impulse overvoltage breakdown tests, three samples of each type of liquid of each nanoparticle weight concentration were prepared and stressed with identical 1.2/50  $\mu$ s impulses, resulting in breakdown. Thirty breakdown events were registered for each liquid sample. Average breakdown voltages and pre-breakdown times were calculated based on three independent tests (fresh samples were used for each test) for each type of liquid.

For the purposes of measuring the minimum-lightning impulse breakdown voltage, the initial charging voltage was set such that the output voltage was well below the expected breakdown voltage. The gap between the electrodes was set to 2 mm. The charging voltage was then increased in steps of 2 kV. If no breakdown occurred (3 shots for ASTM method; 1 shot for IEC method), then this procedure was repeated until breakdown occurred, and the peak voltage of the 1.2/50  $\mu$ s wave-shape was registered as the breakdown voltage. Three independent samples were prepared for each type liquids, nanoparticles and concentrations. For ASTM method, five breakdown events were record for each sample; for IEC method ten breakdown events were record or each sample.

Before the impulse tests, the samples were kept under vacuum for 1.5 hours at room temperature to remove gas bubbles. A new gramophone needle was used for each series of tests for each sample, and the ground-sphere electrode was polished after each series of tests. The electrodes were cleaned with alcohol and then washed with distilled water. The test cell and electrodes were then dried in an oven for 2 hours at 40  $^{\circ}$ C to remove water before the next test.

### 3.5.1 Marx generator topology

A Marx generator was used throughout all impulse experiments. This generator is a three-stage, air-insulated, inverting, single-shot Marx generator, which is shown in Figures 3-18 and 3-19. A DC power supply (Glassman Inc. USA) was used to charge the capacitor. There is a  $1\text{ M}\Omega$  charging resistor, which is made up of 100 Meggitt (UK)  $10\text{ k}\Omega$  ceramic-cased wire wound resistor series connected between the DC power supply and the Marx generator.

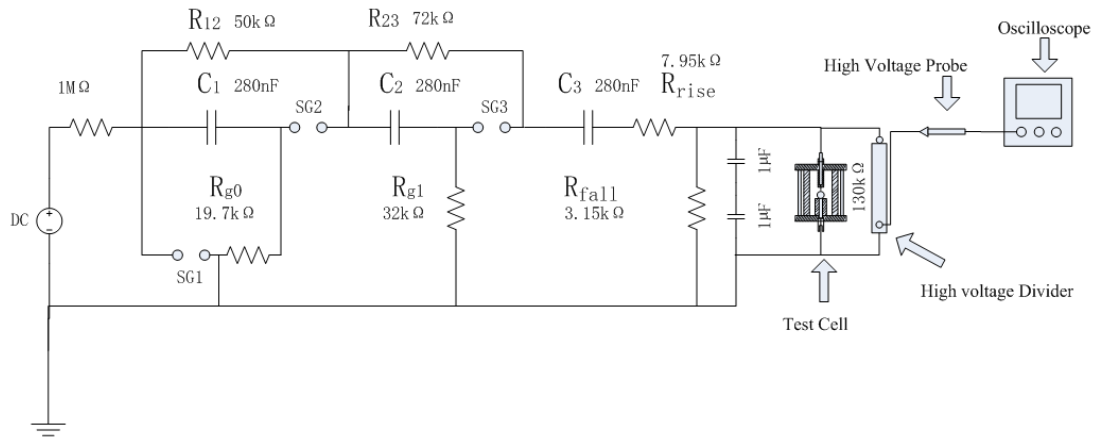


Figure 3-18. Marx generator circuit.

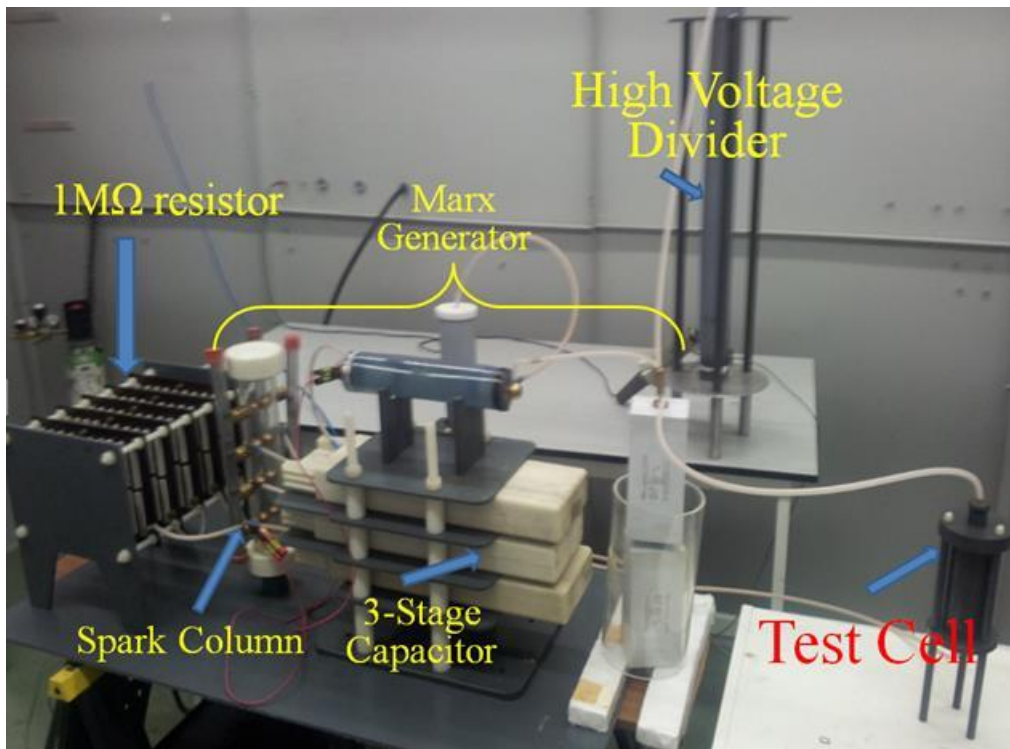


Figure 3-19. Marx generator circuit.

The trigger components and spark column comprise a vertical transparent Perspex cylinder and three pairs of bronze-phosphor electrodes. Inside the cylinder, these electrodes are 25-mm diameter spheres. These electrodes are connected through the wall of the Perspex cylinder to external electrodes, to allow connection to the energy-storage capacitors, and charging and wave-shaping resistors. These three pairs of electrodes were affixed on the Perspex cylinder and placed in horizontal axis symmetry with a 10-mm gap distance. The sphere side electrodes were used as spark gap triggers, which were immersed in compressed air during the experiment. The cylinder side electrodes were series connected to the capacitor. There is a 6-mm nylon tube connecting the Perspex cylinder bottom and gas control system, which was used to inject the compressed gas and for depressurisation. The energy storage components in this system were three 280 nF capacitors. These capacitors were series connected with the cylinder electrodes on the Perspex cylinder and placed vertically stacked on a polyvinyl chloride (PVC) plate. There is a PVC plate that is slightly longer than the capacitor placed between each capacitor. On the top of these capacitors, there is a 3.15 k $\Omega$  inter-stage charging resistor that makes up a PVC tube filled with aqueous copper sulphate (CuSO<sub>4</sub>) solution and a bronze-phosphor electrode. A similar 7.95 k $\Omega$  CuSO<sub>4</sub> discharge resistor was vertically placed beside the energy storage component and connected between alternate pipes.

In this Marx generator system, the maximum charge is limited by the trigger system maximum withstand voltage. Although the capacitor-rated voltage was 70 kV and the spark gap electrodes were immersed in compressed air, it could withstand even higher voltage. The distance between the external side electrodes of the spark gaps limited the charging voltage. To prevent an arc occurrence between these external electrodes, the DC charging voltage was fixed below 30 kV. In the practical experiment, the DC charging voltage of the standard breakdown voltage test was fixed at 20 to 21 kV (considering fluctuations of the voltage); the maximum DC charging voltage of the minimum impulse breakdown voltage test and the D3300-00 test was lower than 30 kV.

The operation of this Marx generator can be explained based on the circuit topology shown in Figure 3-18. After being fully charged, voltage potential across all capacitors reached the charging potential, +V. Then, the air pressure in the spark column was decreased by the gas control system to trigger the spark gap. According to the conventional theory, the lowest spark gap (SG1) would break first. The capacitor (C1) was connected to the ground due to the SG1 short circuit. For SG2, the potential of side



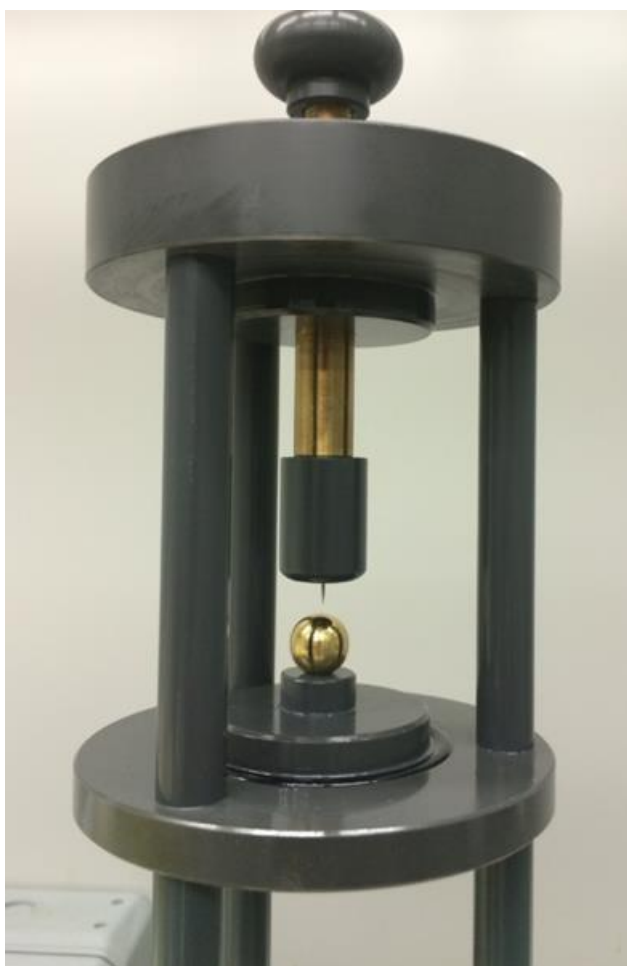


**Figure 3-21.** Picture of the practical test cell.

The main material of this test cell was PVC, which can provide good insulating and anticorrosion performance. The main body of this test cell included two PVC discs and one PVC cylinder. The electrode holder was a pair of brass rods, which penetrated through the top of the PVC discs into the test cell. There was a socket on both electrode holders, which was used to connect the HV and earth cables. The length of the earth electrode holder was fixed. A screw thread on the HV electrode holder body was used to adjust the gap distance between electrodes. Considering that the breakdown event is highly sensitive to gap distance in small gap scale, a PVC screw nut on the HV electrode holder bottom was used to affix the holder to prevent the holder from being moved by the breakdown acting force to change the electrode gap distance. There are two PVC shells surrounding both electrode holders to prevent corona discharge, which may affect the breakdown event. Three PVC rods penetrated through both top and bottom PVC disc outside the test cell body. There is a screw nut on both the top and bottom of these rods to affix and press the whole test cell together. Additionally, to

prevent liquid leakage, there were two rubber rings clamped between the cylinder and bottom dish and between the earth electrode holder and bottom disc.

As Figure 3-22 shows, the 13-mm diameter earth (sphere) electrode was made of polished brass. Figure 3-23 presents the HV (point) electrode, which was a standard soft tone gramophone needle with a tip radius of  $\sim 14 \mu\text{m}$ .



**Figure 3-22.** Ground brass sphere electrode.

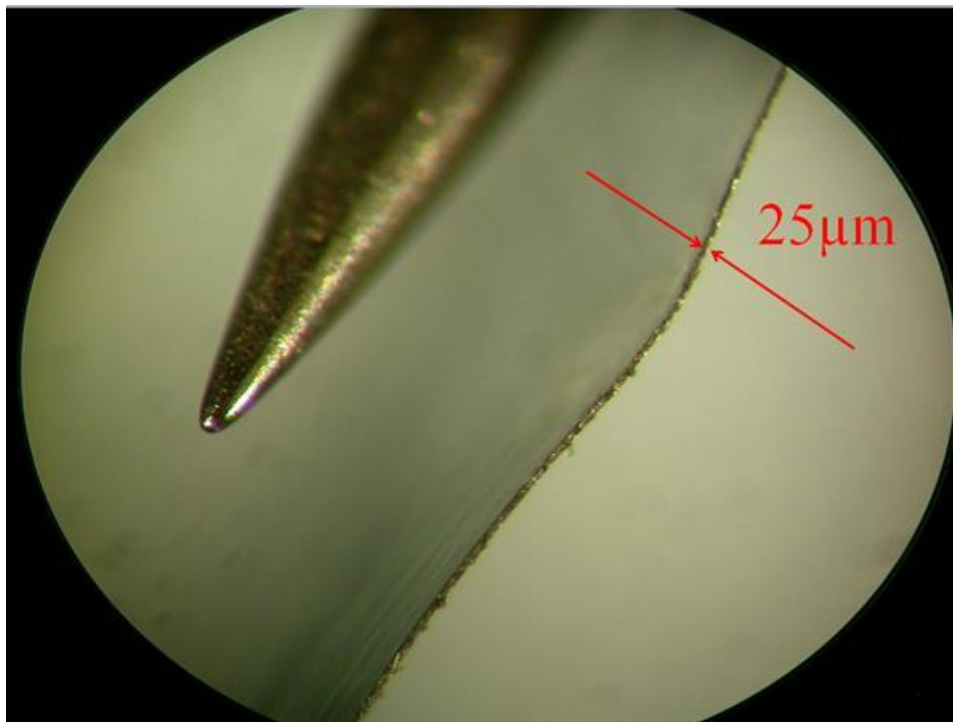


**Figure 3-23.** HV point electrode – gramophone needle tip.

### 3.5.3 Diagnostic devices and pneumatic system

The impulse breakdown voltage was measured using a combination of a custom-built liquid-based HV divider and a commercial 1:1000 high-voltage probe (Tektronix P6015A); a TDS2024 digital oscilloscope was used to record the voltage wave shapes.

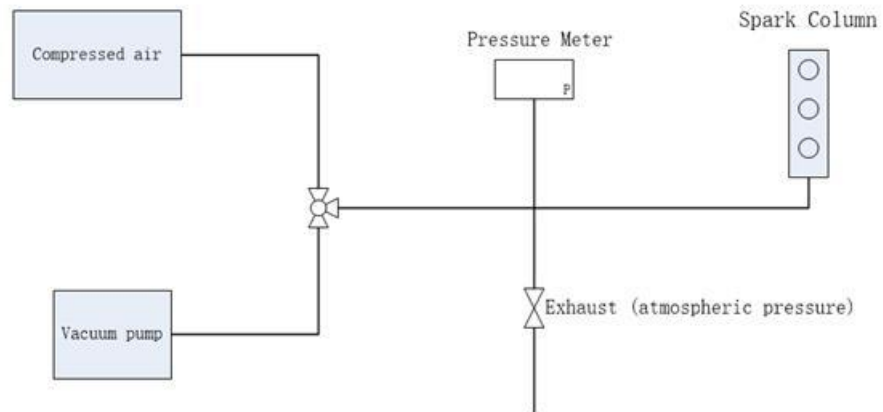


**Figure 3-24.** Gas control topology.



**Figure 3-25.** Gas control devices.

The spark column was control by a gas pressure control system, consisting of a FICA air compressor compressed air pump, an Edwards E2M2 two-stage high-vacuum rotary vane pump, and a double-

acting valve incorporating a gas pressure meter. Figures 3-24 and 3-25 show the topology of this gas control system and practical device.

There were four tubing junctions on the valve that were connected to the compressed air pump, vacuum pump, spark column of the Marx generator, and exhaust tube. The exhaust tube junction was designed for the possibility that the experiment would inject specific gases as spark column insulating gases. These specific gases may potentially harm people, devices, and the environment and cannot be exhausted into the atmosphere directly. In this project, the insulating gas used in the Marx generator was basic compressed air. Thus, this gas is safe for people and the environment and was vented to the atmosphere directly.

Based on the measurement results from [206], as Figure 3-26 shows, the minimum gas pressure of the spark column was set to 5 bar to prevent the breakdown from occurring before fully charging. Before charging the Marx generator, the valve on the gas port would be switched on to inject the compressed gas into the spark column until the gas pressure of the spark column reached 5 bar. After the capacitors of the Marx generator were fully charging, the gas valve would switch on the vacuum port to reduce the internal gas pressure of the spark column until the spark gaps reached self-breakdown. The vacuum port would be switched off, and the gas port would be switched on to inject the compressed gas until the pressure reached 5 bar again to wait for the next trigger. When all experiments were finished, the valve exhaust port would switch on to vent the spark column compressed gas as the final step of the experiment.

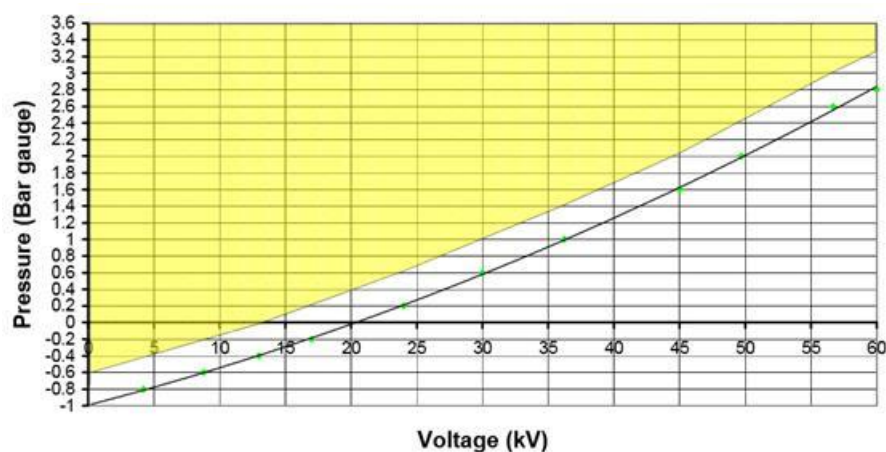


**Figure 3-26.** Gauge pressure versus self-breakdown voltage for the spark column. The yellow-shaded region represents the initial gas pressure before charging the impulse generator stages, bounded by a region at least 0.4 bar above the self-breakdown pressure [206].

There was an HV divider parallel connection to the test cell to protect the devices and measure tens of kilovolts of HV impulses. A Samtech Ltd. (UK) DE (LRP)-02 liquid resistive voltage divider is shown in Figure 3-27. The main body of this divider was a 50-mm vertical PVC tube filled with aqueous  $\text{CuSO}_4$  solution of appropriate rate to provide a specific resistor. The length of this PVC tube was 700 mm. There was a tap electrode incorporated on the PVC tube, and the length between this tap electrode and the earth electrode was 70 mm. This length was one-tenth of the whole PVC tube; thus, the theory voltage of this tap electrode would be divided 10:1 compared with the total voltage across the divider. The tap electrode consisted of an internal electrode and an external electrode. Both internal and external electrodes were 10-mm diameter bronze-phosphor spheres, connected to each other with an M3 screwed rod passed through the PVC tube wall.

The HV electrode of this divider was a 25-mm diameter bronze-phosphor sphere. This HV electrode was immersed in an aqueous  $\text{CuSO}_4$  solution and was connected to an external circuit with an M6 screwed rod on the top of the PVC tube. An external 19-mm diameter bronze-phosphor sphere was connected to the screwed rod on another side and covered the sharp threaded edge. The PVC tube bottom side earth electrode was a 40 mm length and 50 mm diameter brass rod connected to a 250 mm diameter, 3-mm-thick aluminium plate.

There were three 130 mm length and 25 mm diameter cylindrical aluminium legs below the earth aluminium plate to support the whole divider. A 250 mm diameter PVC plate with a central hole passing through the PVC tube was fixed to it. There were three 650 mm length and 20 mm diameter PVC rods between the PVC plate and earth plate to affix the divider upper structure.

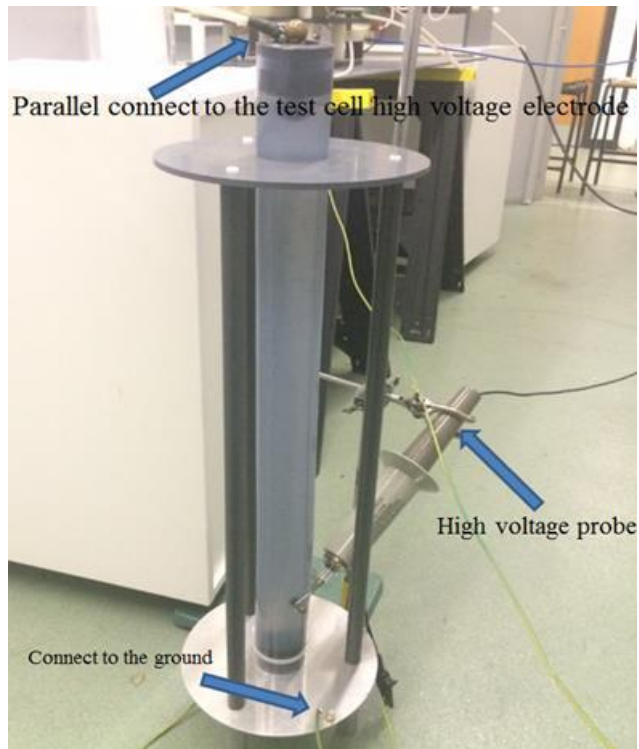


**Figure 3-27.** HV divider structure.

A Tektronix (USA) P6015A HV probe (1000:1 division ration) was connected between the tap electrode and the earth electrode to measure the voltage. Counting the voltage divider, the total division ratio of measurement was 10000:1. The maximum voltage the probe can measure was 40 kV; thus, the maximum voltage of this measurement system was 400 kV. The nominal bandwidth of this probe was 75 MHz. A Tektronix (USA) TDS2024 digital oscilloscope with a bandwidth of 200 MHz and sampling rate of 2GS/s was used to view and record the impulse waveforms.

The typical impulse voltage waveforms are shown in Figures 3-28 and 3-29. In both these figures, the rise time was 1.2  $\mu\text{s}$  according to the international standard IEC 60060-1, defined as ‘front time’, and the fall time was 50  $\mu\text{s}$  according to the international standard IEC 60060-1, defined as ‘time to half value’ [207].

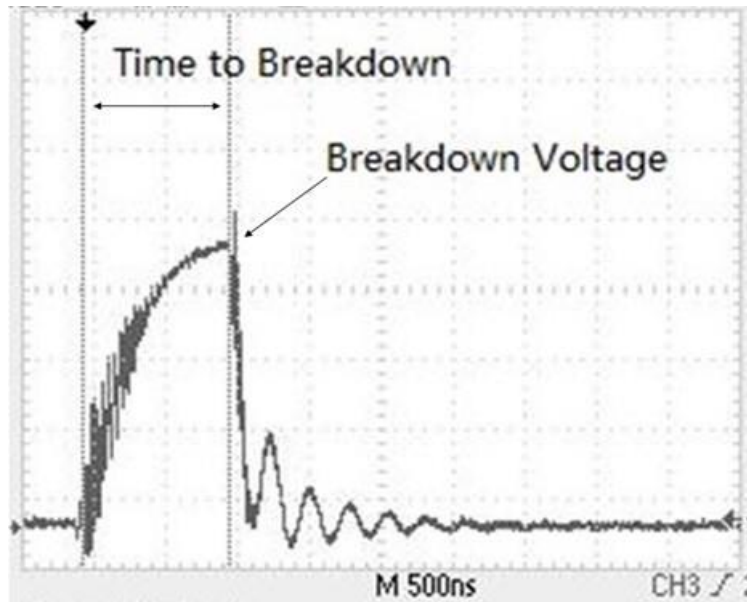


Figure 3-28. Positive impulse breakdown waveform.

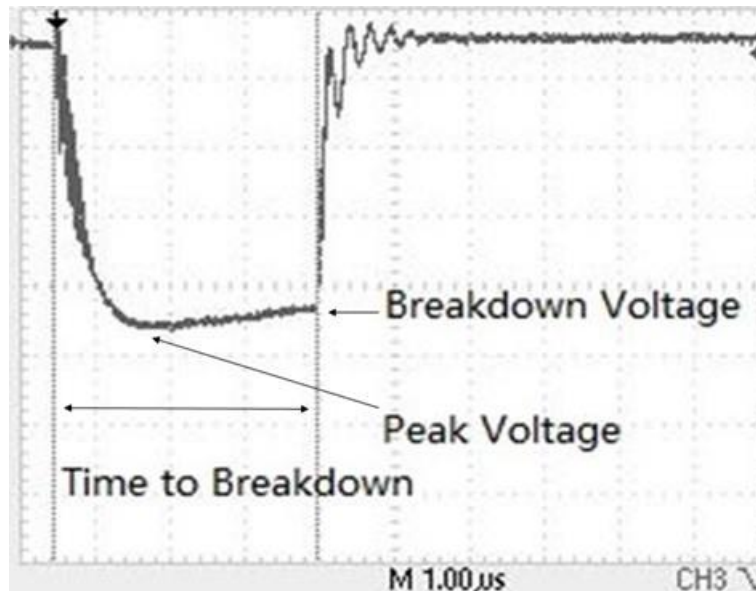


Figure 3-29. Negative impulse breakdown waveform.

### 3.6 Charge Carrier Mobility in Insulating Liquids

Natural organic oils and synthetic esters are considered potential substitutes for traditional naphthenic mineral oils. However, their dielectric properties are not yet fully known, especially in the case of DC energisation. Recent advances and investment in HVDC systems require detailed information about the dielectric behaviour of insulating fluids under AC and DC electrical stresses [208].

The HVDC techniques are suitable for transmission of electrical power over long distances, and with the development of renewable sources, this approach has attracted the attention of the power industry

for transmission of electrical power generated by offshore wind farms. In HVDC systems, such as HVDC converter transformers, the insulation is stressed with both AC and DC voltages. Therefore, it is important to investigate the dielectric properties of insulating liquids and to understand their behaviour under both types of energisation. As indicated in a report by National Grid [208], ‘DC transformers cost in the region of £5M per phase and failures have significant outage cost’. Additionally, it is known that the HVDC transformer failure rate exceeds the failure rate of conventional transmission-based units by 5-10 times [208]. Information on the DC dielectric behaviour of insulating liquids will influence the design of HVDC systems and will help manage this liquid in the power systems. The DC conductivity may significantly affect the design and management of HVDC systems. Moreover, oil producers, HV equipment manufacturers, and power utilities are interested in information on the DC conductivity of insulating liquids. As stated in [208], however, ‘the measurement of the DC conductivity of oil is not routine’ and repeatable methods are required.

In this section, the experimental details for measurements of the DC pre-breakdown volt-current characteristics and mobility of the charge carriers of mineral oil (Diala S3), synthetic ester fluid (Midel 7131), and food-grade rapeseed oil have been discussed.

### **3.6.1 Electrode topology and test cell design**

The I-V curves were measured in the point-plane electrode topology. The point electrode was a needle with the tip radius of 8  $\mu\text{m}$ ; the plane electrode was a stainless-steel disc of 30 mm in diameter. The gap between the electrodes was 5 mm.

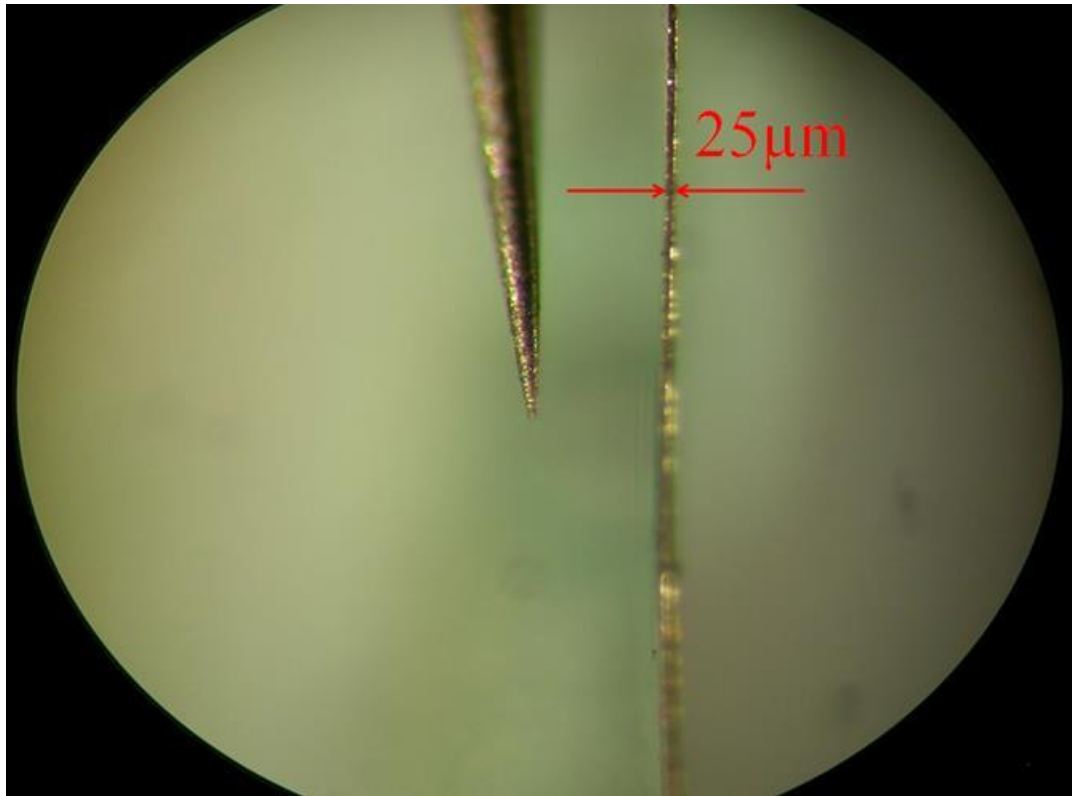


**Figure 3-30.** The standard steel needle.

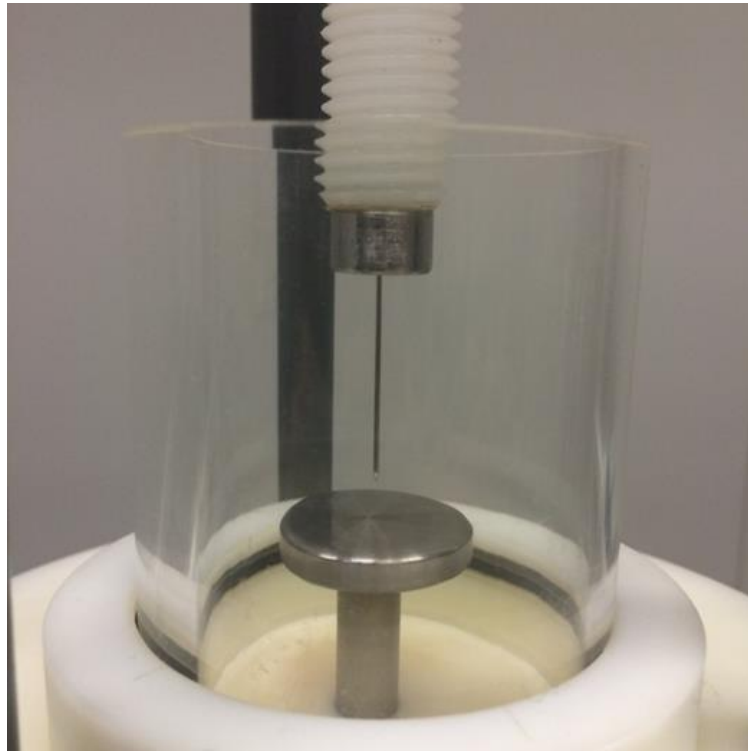


**Figure 3-31.** The electrode topology of DC pre-breakdown current experiment.

The test cell shown in Figures 3-32 and 3-33 was used in DC pre-breakdown current measurements. The ground electrode was made of stainless steel, and the point electrode was made of a swing needle, which was sharpened in the mechanical workshop. The top and bottom flanges of the test cell were made of PVC. The cylinder body was made of Perspex. A rubber O-ring was placed between the cylindrical body and the bottom PVC flange to avoid an oil leak. The PVC sleeves were wrapped around the metal electrode holders to prevent partial discharges.

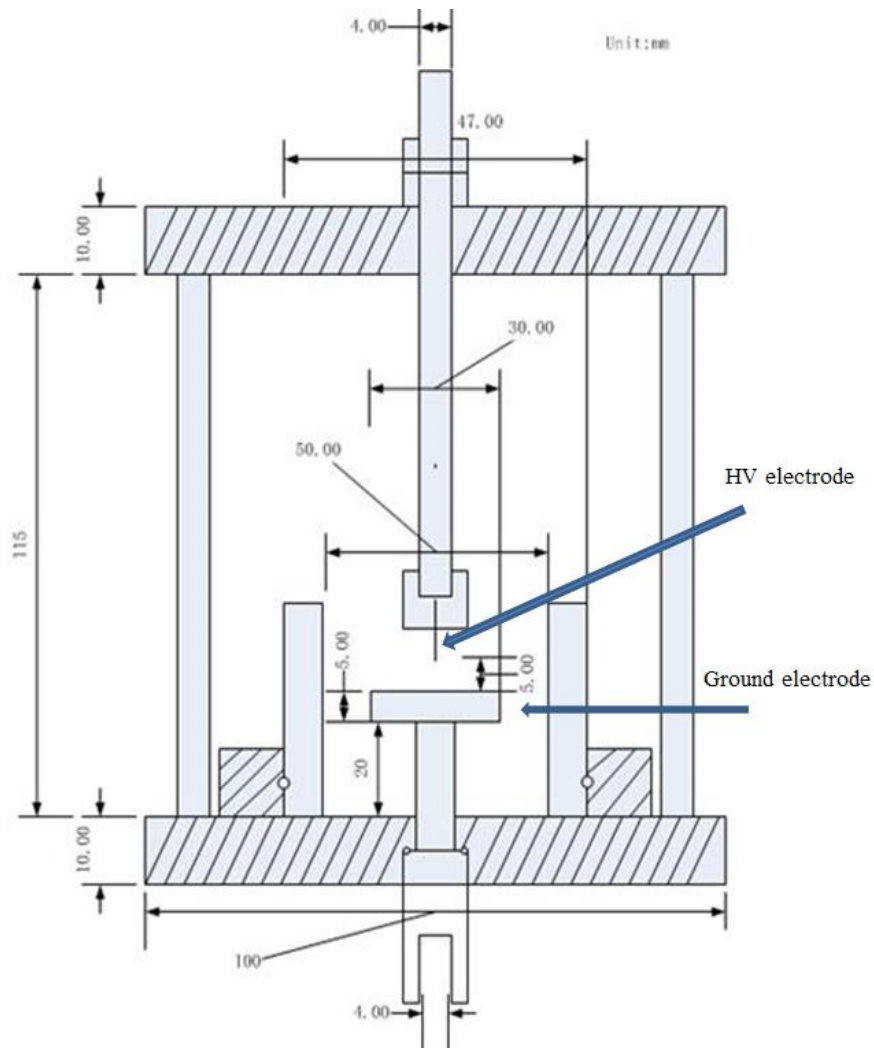
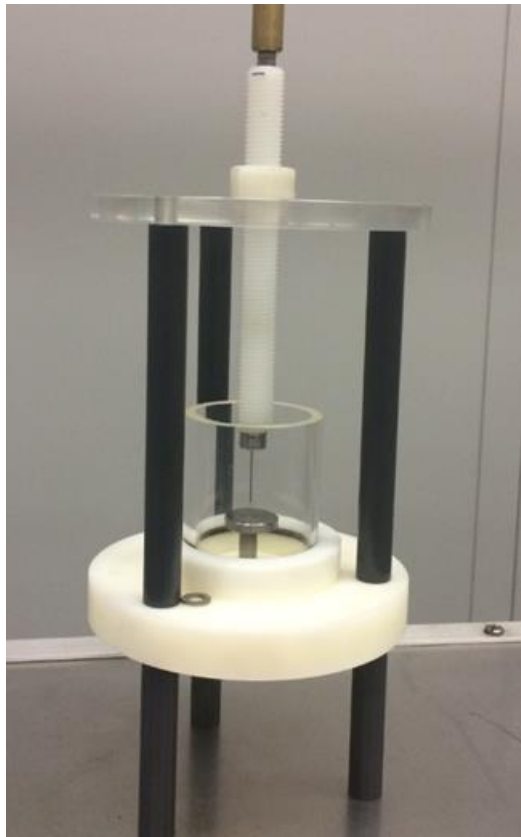


Figure 3-32. DC pre-breakdown current test cell.



**Figure 3-33.** Assembled DC pre-breakdown current measurement test cell.

### **3.6.2 Calibration of amplifier for I-V current measurements**

The custom-built current-sensing amplifier has been developed and should be calibrated. The gain of this amplifier is set to 1000. An accurate, sensitive voltage source (515 A portable calibration, John Fluke MFC CO. INC. USA) was connected to the amplifier. The voltage output from the amplifier was monitored using a TDS 2024 digitising oscilloscope. The applied voltage was increased from 0 V to 1 mV with 50- $\mu$ V steps. The relative output voltages from the amplifier were recorded. The output voltage divided by the applied voltage provided the actual voltage gain of this amplifier.

The calibration procedure was repeated three times. The actual voltage gain was obtained using the average values of three calibrations.

$$Gain = 956.9 \pm 12.4$$

This result showed that the deviation between the ideal and actual gain was smaller than 5%.

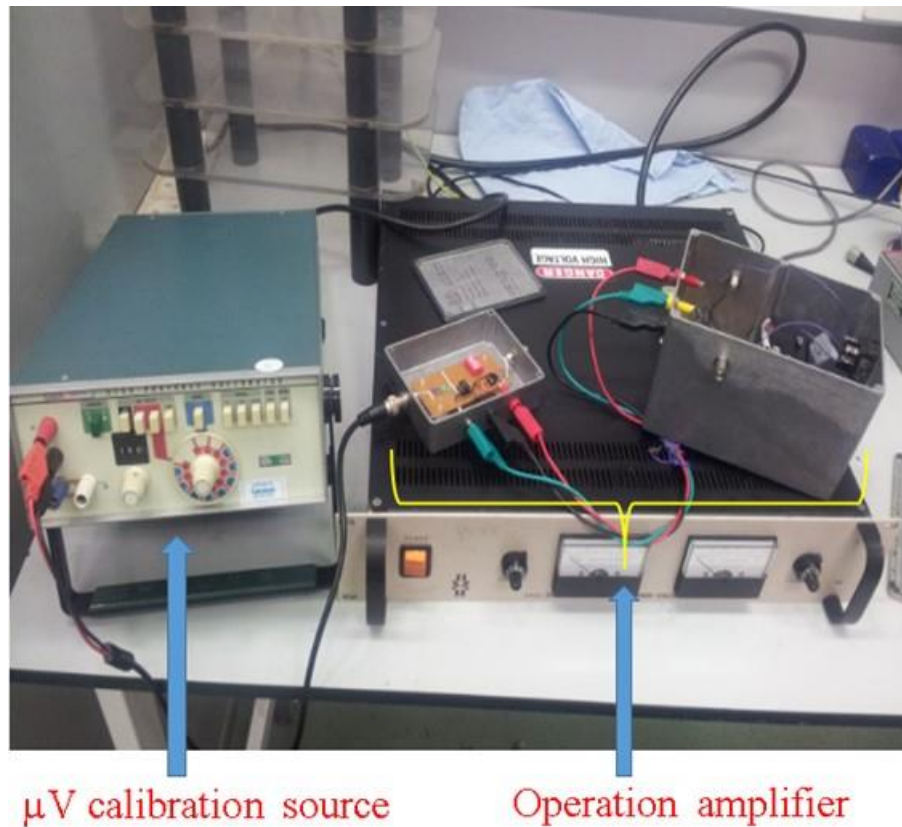


**Figure 3-34.** Calibration circuit.

### 3.6.3 I-V measurement system

Positive and negative DC voltage was applied to the point electrode. The conduction current in the oil samples was measured using a custom-built current-sensing amplifier with a 1 k $\Omega$  current-viewing resistor. The voltage output from the amplifier was monitored using a TDS 2024 digitising oscilloscope, and the applied voltage was monitored using a TES&TEC HVP-40 HV probe.

Before measuring the DC pre-breakdown currents in insulating liquids, the DC breakdown strength of these liquids must be evaluated. An unexpected breakdown may damage the measurement devices. The maximum applied voltage in these DC pre-breakdown current measurement experiments must be lower than the measured breakdown voltage to avoid undesirable breakdowns in the liquid.

Figure 3-35 shows the schematic diagram of the DC breakdown strength evaluating circuit. The DC voltage has been applied across the point-plane electrode, which was immersed in dielectric liquid. The applied voltage was increased from 0 V to breakdown at a rate of 0.5 kV/s. Furthermore, a 1 M $\Omega$  protection resistor was used to minimise the energy delivered into the breakdown spark, and its value

is significantly lower than the resistance of the oil between electrodes. The breakdown voltage was monitored using digital multimeter and TES&TEC HVP-40 HV probe. All devices were connected to the same ground point.

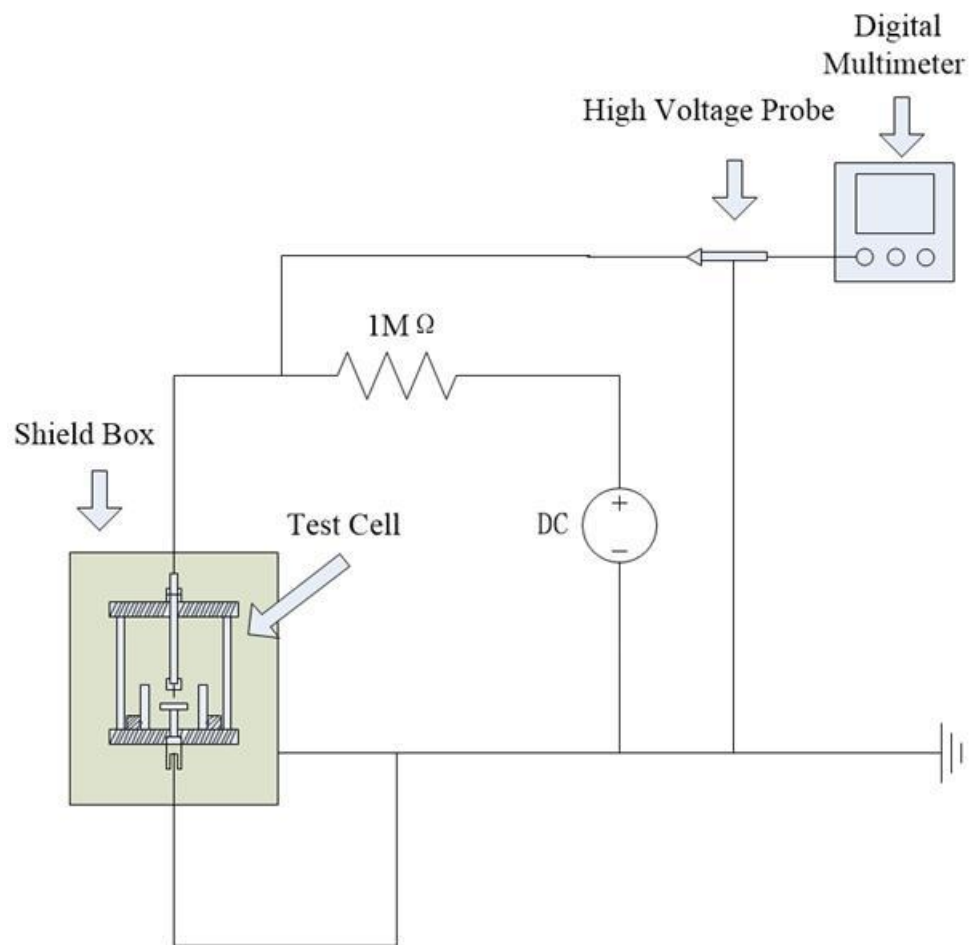


**Figure 3-35.** DC breakdown voltage measurement circuit.

In these DC pre-breakdown current experiments, the maximum applied voltage was set to several thousand volts lower than the lowest DC breakdown voltage. Since the pre-breakdown current is very small (nano amp range), any unexpected noise can have a significant effect on the measurement results. The test cell must be put into a metal box that connects to the ground to shield the electromagnetic wave from other HV devices in the lab. Figure 3-36 shows the schematic diagram of the DC pre-breakdown current measurement circuit.

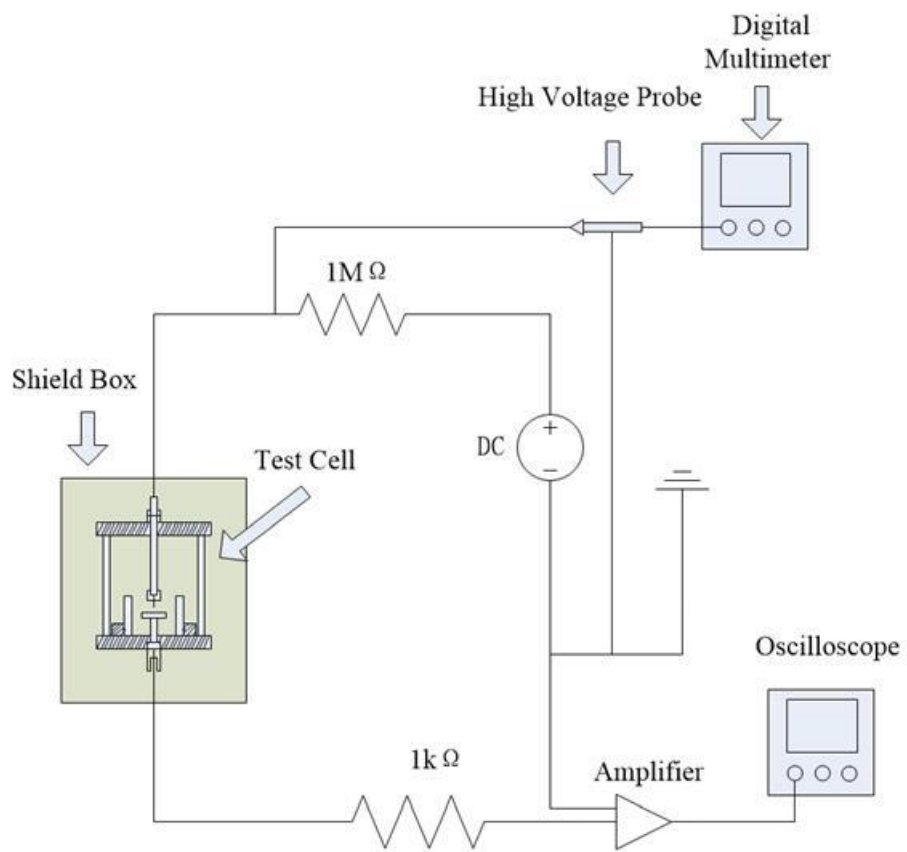


**Figure 3-36.** DC pre-breakdown current measurement circuit.

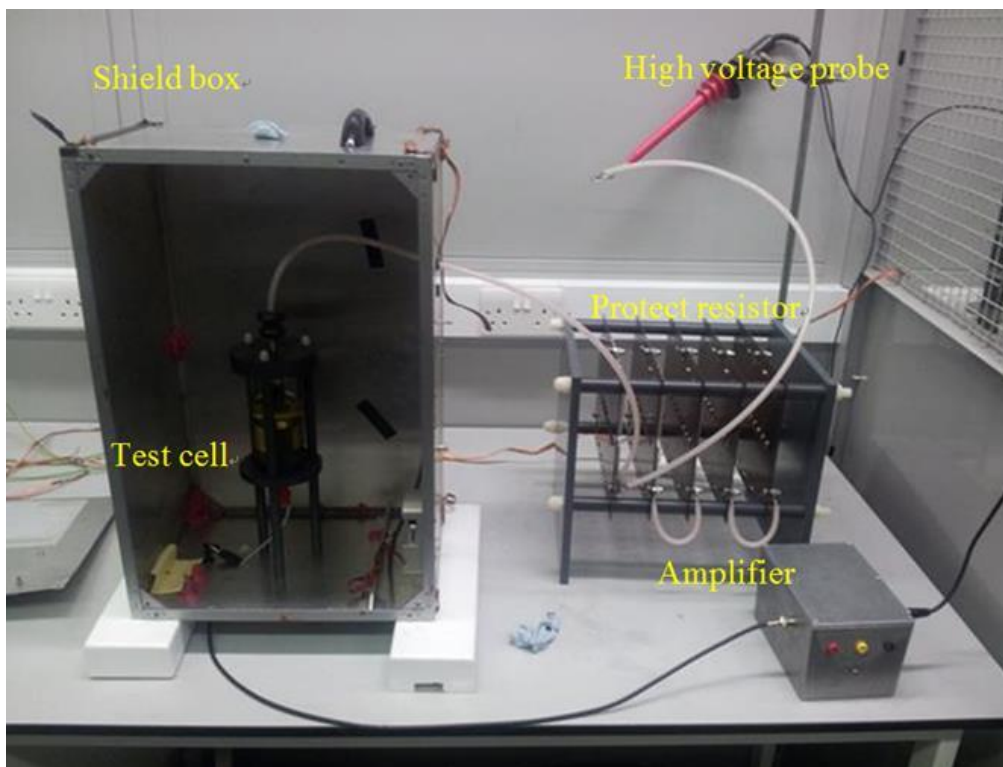


**Figure 3-37.** Practical DC pre-breakdown current measurement circuit.

The TES&TEC HVP-40 HV probe and digital multimeter were connected to the test cell as described above. They were used to monitor the applied voltage across the test cell. The DC voltage was monitored using a TDS 2024 digitising oscilloscope and TES&TEC HVP-40 HV probe. A 1 k $\Omega$  current-viewing resistor was connected to the plane electrode, and a custom-built current-sensing amplifier (with a gain of 1000) was used to increase the voltage signal across this resistor. This voltage signal was monitored using a TDS 2024 digitising oscilloscope. The pre-breakdown current was calculated according to the following equation:

$$I_{pre-breakdown} = \frac{V_{read}}{G * R_{viewing}}, \quad (3.1)$$

where  $I_{pre-breakdown}$  is the pre-breakdown current,  $V_{read}$  is amplifier output voltage,  $G$  is the gain of the amplifier, and  $R_{viewing}$  is the current-viewing resistor.

### 3.7 Summary

In this chapter, the physical and chemical properties of insulating liquids and nanoparticles that affect the material dielectric strength have been discussed. The nano-modified sample preparation procedure has been laid out, which includes the nanoparticle surface modification, nanofluid sample concentration selection, and sample preparation. To confirm the nanoparticle dispersion in the liquid, to form a uniform distribution, and to investigate the effects of the surfactant on the size range of the particles, the average size of the nanoparticles that were dispersed in the nanofluid samples was obtained.

The results showed that the average size of the TiO<sub>2</sub> nanoparticles in the samples were slightly smaller than the BN nanoparticles in the samples, which indicated that different nanoparticles present different dispersion and aggregation abilities. More experiments are necessary to investigate this performance. With the increase in concentration, the average size of the nanoparticles rose, as expected. Compared with the mineral-oil-based and ester-based samples, the average size of the nanoparticles of the mineral oil was several times larger than that of the ester. Especially in the case of high concentrations, the average size of nanoparticles in mineral oil was greater than ~1000 nm. On the other hand, the effect of the nanoparticle surface treatment for the mineral oil sample was obvious. The average size of nanoparticles of the samples with the surfactant was twice or three times smaller than the samples

without the surfactant. For both ester samples, the average size of the nanoparticle for all concentrations stayed relatively small, 180 nm to 550 nm, compared with the mineral oil sample. The difference between the average size of the nanoparticles of the samples with or without surface treatment was not clear.

All experimental details in this project have been presented, including the AC breakdown voltage measurement, impulse breakdown voltage and pre-breakdown time measurement, and the measurement of the DC pre-breakdown current. More details of the experiment are presented in the related chapters.

# CHAPTER 4

## AC BREAKDOWN CHARACTERISTIC OF BASE AND NANO-MODIFIED LIQUIDS

### 4.1 Introduction

Because most of the power equipment designs use AC power, the AC breakdown voltage becomes one of the key parameters used to characterise the dielectric properties of insulating material. In engineering practice, it is important to evaluate not only the actual breakdown voltage but also different percentiles that indicate the probability to breakdown: lower,  $V_{bd\ 10\%}$  and others, and higher,  $V_{bd\ 90\%}$  and others. Percentiles are used for classification of the dielectric properties of insulating oils. Power and HV system engineers can use these breakdown voltage percentiles for insulation coordination in the power/HV systems to prevent catastrophic breakdown events. It is important to note that, for practical applications involving dielectric liquids, it is important to know the lower percentiles as well as the higher percentiles of the breakdown voltage or the average breakdown voltage.

Two types of nanoparticles ( $TiO_2$  and BN) were used to produce nanofluid samples with six concentrations: three types of insulating liquids (mineral oil, Diala S3; synthetic ester liquid, Midel 7131; and natural ester liquid, food-grade vegetable oil) have been used as the base liquids for production of these nano-modified liquids. All tests have been conducted at ambient temperature and humidity, and oil samples of 'as received' grade was used. The test cell used to measure the AC breakdown voltage, the experimental system, and the experimental preparation procedures have been discussed in Sections 3.3 and 3.4.

The Weibull distribution is one of the main statistical methods for analysis of the reliability of dielectric materials, including dielectric liquids, stressed with HV stress. In [9] and [209], Liu and Martin et al. analysed the AC breakdown voltage of insulating liquids using Weibull, and Gaussian distributions. Based on the analysis results, the authors indicated that the Weibull analysis could

accurately evaluate the average probability breakdown voltage and the low probability breakdown voltage for the AC experiment.

The statistical analysis is used to estimate the mean value of a normally distributed population where the sample size is small and the population standard deviation is unknown. In [210] and [211], the statistical difference between two samples and the confidence interval (CI) has been calculated, considering the effects of the sample number and standard deviation.

In the present chapter, the Weibull analysis was applied to the experimentally obtained breakdown AC data for all nanofluids to obtain the breakdown percentiles. The statistical difference analysis was used to find the breakdown voltage statistical difference and the CI between the base sample and nano-modified samples to identify the dielectric property improvements of the liquid samples due to the nano-modification.

## **4.2 Experimental Procedures**

The AC voltage was applied across the electrodes of the test cell described in Section 3.4 (AC breakdown test cell manufactured according to ASTM 1816 standard [79]) with a voltage rate-of-rise of  $\sim 1\text{kV/s}$ . The applied voltage manually increased until breakdown occurred between the test cell electrodes. An automatic overvoltage protection system of the Foster breakdown test apparatus cuts off the applied voltage as soon breakdown occurs, limiting the duration of the arc and the current passing through the liquid sample during the fault event. A Tektronix HV probe P6015A was used to measure the breakdown voltage. This breakdown voltage was recorded using a digitising oscilloscope, Tektronix TDS 2024, 200 MHz 2GS/s. There are three independent samples are prepared for each concentration. In total, 70 breakdown events were registered for each liquid sample. Average breakdown voltages were calculated using these breakdown data obtained in three independent tests (fresh samples were used for each test) for each type of liquid.

Before AC tests, the liquid samples were kept under vacuum for  $\sim 1.5$  hours at room temperature to remove gas bubbles introduced into the liquid during the pouring procedure. The electrodes used in the test cell were polished after each series of tests to remove damage produced by the breakdowns. After that, the test cell and the electrodes were cleaned with alcohol and then washed with distilled

water. The test cell and electrodes were then dried in an oven for 2 hours at 40 °C to evaporate water before the next series of tests.

### **4.3 Investigation of AC Breakdown Voltages**

#### **4.3.1 AC breakdown characteristics of TiO<sub>2</sub> nanofluids**

In this section, the AC breakdown characteristics of the TiO<sub>2</sub> nano-modified liquids based on mineral oil, synthetic ester, and natural ester were obtained and analysed. The concentrations of nanoparticles in the base liquids were 0.0006%, 0.004%, 0.01%, 0.05%, and 0.1%. (b/w). This section presents the results of this investigation.

Figure 4-1 shows AC breakdown voltages for the mineral oil sample, Diala S3, as a function of TiO<sub>2</sub> nanoparticle concentration (b/w). These results showed that all tested nano-modified samples of mineral oil demonstrated higher AC breakdown voltages compared with the base (as received) oil. This figure also shows that there was a peak in the breakdown voltage as a function of the TiO<sub>2</sub> nanoparticle concentration in mineral oil. The maximum AC average breakdown voltage was registered for oil samples with a 0.0006% (b/w) concentration of TiO<sub>2</sub> nanoparticles. Figure 4.1 show that AC breakdown voltage increased from  $21.81 \pm 2.43$  kV (base sample) to  $31.81 \pm 3.78$  kV (0.0006% (b/w) concentration of TiO<sub>2</sub> nanoparticles), which is a ~46% increase in the average AC breakdown voltage. With further increases in concentration of nanoparticles in the mineral oil from 0.0006% to 0.1% (b/w), the average AC breakdown voltage started to decrease. When the TiO<sub>2</sub> nanoparticle concentration reached 0.1%, which is the highest concentration of nanoparticles used in this study, the AC breakdown voltage ( $22.38 \pm 2.33$  kV) became just slightly higher than the breakdown voltage of the base oil ( $21.81 \pm 2.43$  kV).

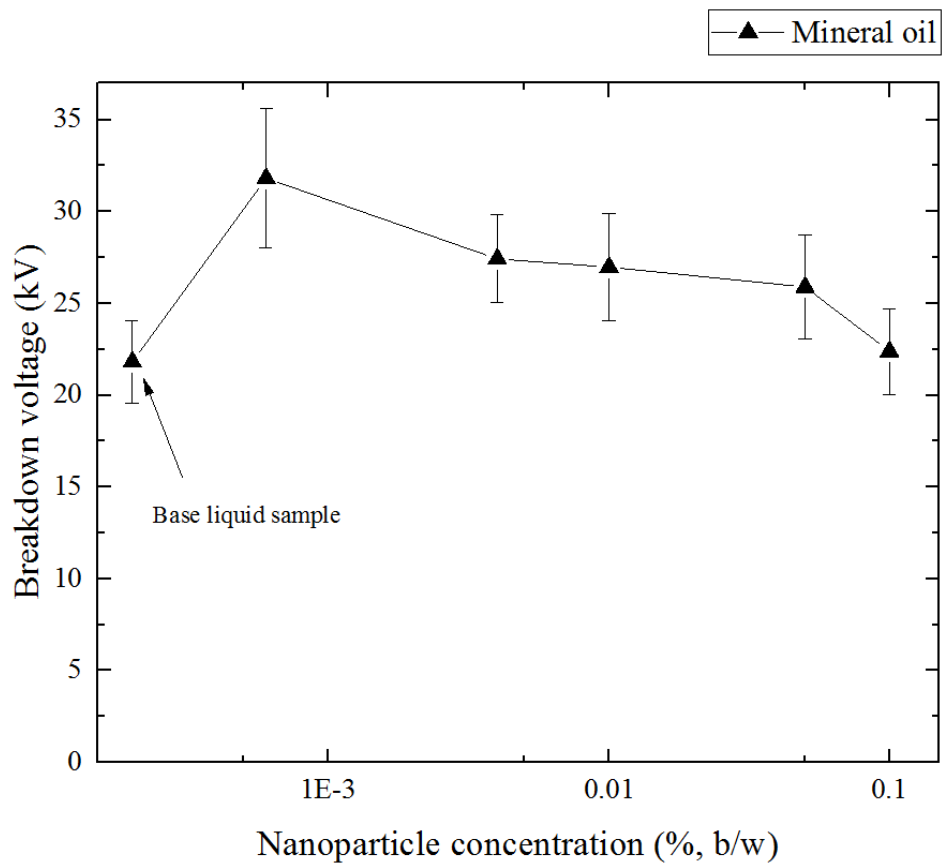


**Figure 4-1.** AC breakdown voltage of mineral oil TiO<sub>2</sub> samples as a function of nanoparticle concentration. Each data point is an average of breakdown measurements conducted using three fresh samples; each sample has been tested 70 times. The error bars show the standard deviation.

A similar tendency was observed in nano-modified samples of Midel 7131, synthetic ester. Figure 4-2 shows the AC breakdown voltage of nano-modified synthetic ester, as a function of the concentration of TiO<sub>2</sub> nanoparticles. As in the case of the AC breakdown voltage for mineral oil, a similar tendency was observed for synthetic ester fluid. The AC breakdown voltage is a nonlinear function of the TiO<sub>2</sub> particle concentration, and the maximum AC breakdown voltage was demonstrated by samples with a 0.0006% (b/w) concentration of TiO<sub>2</sub> particles.

The AC breakdown voltage of synthetic ester samples with the concentration of nanoparticles at 0.0006% (b/w) was higher than an average breakdown voltage for base synthetic ester (no nanoparticles). The AC breakdown voltage increased from 21.45 ± 4.13 kV for base ester liquid to 31.47 ± 2.67 kV, for the nano-modified fluid, which is a ~ 47% (b/w) magnitude increase. In the synthetic ester fluid, with further increases in the nanoparticle concentration, for particle concentrations above 0.0006%, the average breakdown voltage showed a decreasing tendency. When

the concentration of nanoparticles reached 0.1% (b/w), which is the highest concentration used in this study, the sample AC breakdown voltage ( $23.19 \pm 3.33$  kV) became just slightly higher than that for the base sample ( $21.45 \pm 4.13$  kV).

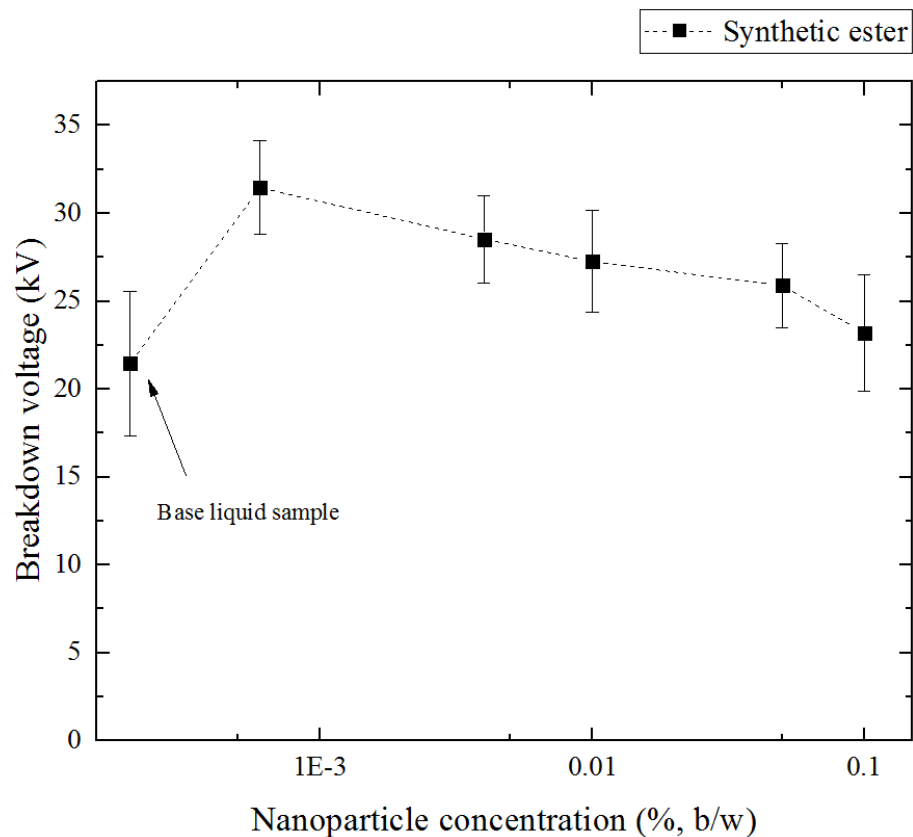


**Figure 4-2.** AC breakdown voltage of synthetic ester  $\text{TiO}_2$  samples as a function of nanoparticle concentration. Each data point is an average of breakdown measurements conducted using three fresh samples; each sample has been tested 70 times. The error bars show the standard deviation.

Figure 4-3 shows the natural ester sample (rapeseed oil) AC breakdown results as a function of  $\text{TiO}_2$  nanoparticle concentration by weight. These results showed that all nano-modified samples provided higher AC breakdown voltages than the base sample. The changing breakdown voltage behaviour with nanoparticle concentration increases was similar to the mineral oil and synthetic ester samples. The optimal concentration that provided the highest AC breakdown voltage was 0.0006%. The breakdown voltage increased from  $21.17 \pm 2.66$  kV (base sample) to  $29.23 \pm 4.44$  kV, which is a 38% magnitude increase. With nanoparticle concentrations increasing higher than 0.0006%, the voltage magnitudes started to decrease. When the concentration reached 0.1%, which is the highest concentration in this study, the sample AC breakdown voltage ( $22.76 \pm 4.04$  kV) became just slightly higher than the base sample ( $21.17 \pm 2.66$  kV).

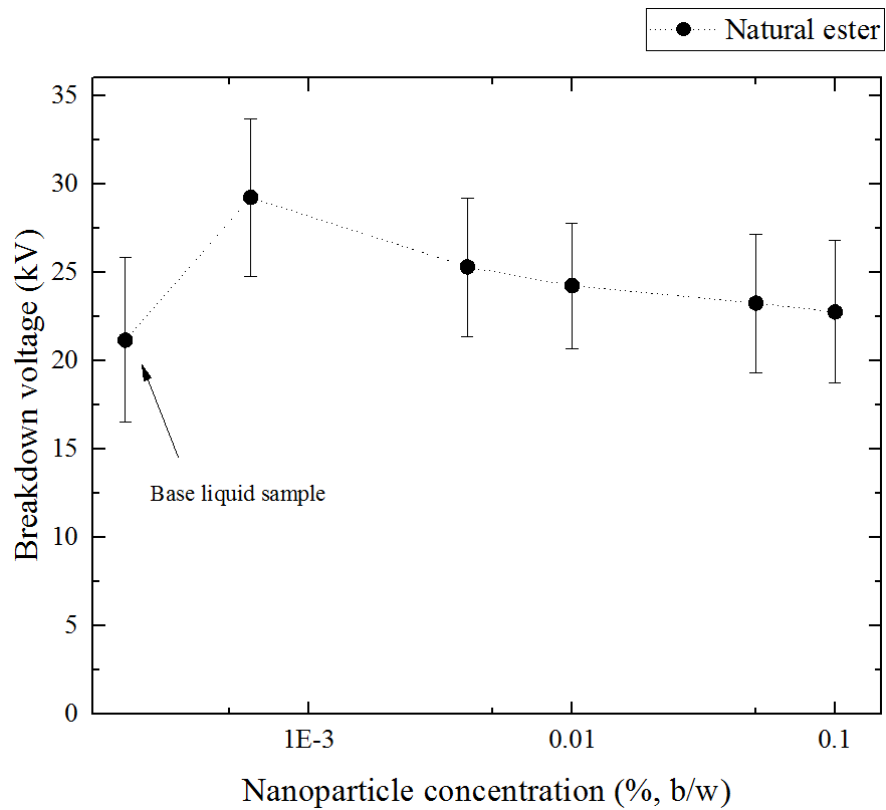


**Figure 4-3.** AC breakdown voltage of natural ester TiO<sub>2</sub> samples as a function of nanoparticle concentration. Each data point is an average of breakdown measurements conducted using three fresh samples; each sample has been tested 70 times. The error bars show the standard deviation.

Figure 4-4 illustrates the comparison of the AC breakdown voltages for all three types of insulating liquid samples as functions of the TiO<sub>2</sub> nanoparticle concentration. The AC breakdown voltages of all three liquids demonstrated a similar tendency. In the case of base liquids, their AC breakdown voltages were almost the same. The potential reason for the food-grade natural ester sample having an AC breakdown voltage similar to that for the industry grade dielectric liquids is the use of the ‘as received’ liquids in the AC breakdown tests (i.e., no filtration, degassing, or de-humidification procedures were applied to any of these liquids). Therefore, all liquids had similar relative humidity, as they were kept and tested in an open ambient laboratory environment and potentially had a similar degree of contamination particles/micro-bubbles or other impurities, which may have affected their breakdown voltage strength.

However, for the nano-modified liquids, the difference between AC breakdown voltages for the industry grade liquids and a food-grade natural ester liquid became clear. Two types of commercially produced liquids, mineral oil Diala S3 and synthetic ester Midel 7131, demonstrated similar AC

breakdown voltages. The food-grade natural ester, rapeseed oil, provided a clearly lower AC breakdown voltage than the other two commercially available liquids, as expected. For the samples with 0.1% concentration (b/w), the AC breakdown voltages for all three liquids became similar.

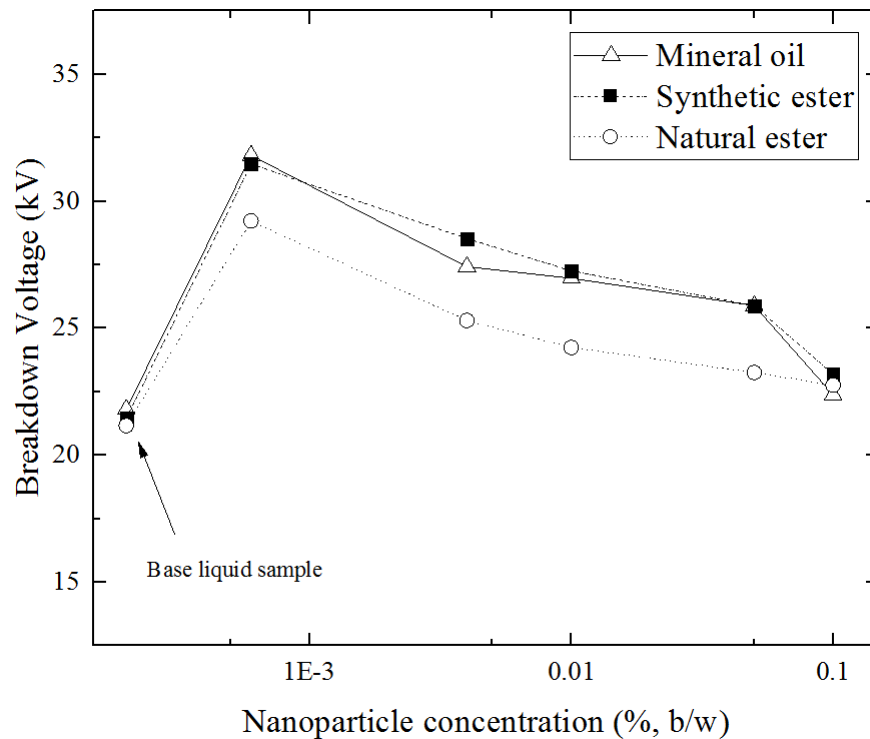


**Figure 4-4.** Cumulative plots of AC breakdown voltages for all three insulating liquids with  $\text{TiO}_2$  nanoparticles as a function of the nanoparticle concentration. Each data point is an average of the breakdown measurements conducted using three fresh samples; each sample has been tested 70 times.

Table 4-1 provides the average breakdown voltage, standard deviation, and changing voltage magnitude for all  $\text{TiO}_2$  samples. The mineral oil sample, Diala S3 0.0006%, showed the highest breakdown voltage ( $31.81 \pm 3.78$  kV). Furthermore, the mineral oil sample also provided the smallest standard deviation compared with other liquid samples.

The standard deviation of the AC breakdown voltage of the natural ester stayed at a relatively high level for all concentrations of  $\text{TiO}_2$  nanoparticles. The potential reason for this performance is that the natural ester liquid contains a significant amount of fibre and unknown particles, which would lead the breakdown to occur at a relatively low voltage level and lead to an increase in the standard deviation.

**Table 4-1.** AC breakdown test results of three insulating liquid TiO<sub>2</sub> samples as a function of nanoparticle concentration.

| Concentration | Mineral Oil  | Synthetic Ester      | Natural Ester        |
|---------------|--|----------------------|----------------------|
| (%)           | V <sub>ave</sub> ± STD (kV); V <sub>change</sub> (%) |                      |                      |
| 0.00%         | 21.81 ± 2.43; 0.00%                                  | 21.45 ± 4.13; 0.00%  | 21.17 ± 2.66; 0.00%  |
| 0.0006%       | 31.81 ± 3.78; 45.85%                                 | 31.47 ± 2.67; 46.71% | 29.23 ± 4.44; 38.07% |
| 0.004%        | 27.43 ± 2.38; 25.77%                                 | 28.54 ± 2.49; 33.05% | 25.31 ± 3.92; 19.56% |
| 0.01%         | 26.97 ± 2.89; 23.66%                                 | 27.26 ± 2.91; 27.09% | 24.25 ± 3.54; 14.55% |
| 0.05%         | 25.89 ± 2.85; 18.71%                                 | 25.89 ± 2.39; 20.7%  | 23.25 ± 3.92; 9.83%  |
| 0.10%         | 22.38 ± 2.33; 2.61%                                  | 23.19 ± 3.33; 8.11%  | 22.76 ± 4.04; 7.51%  |

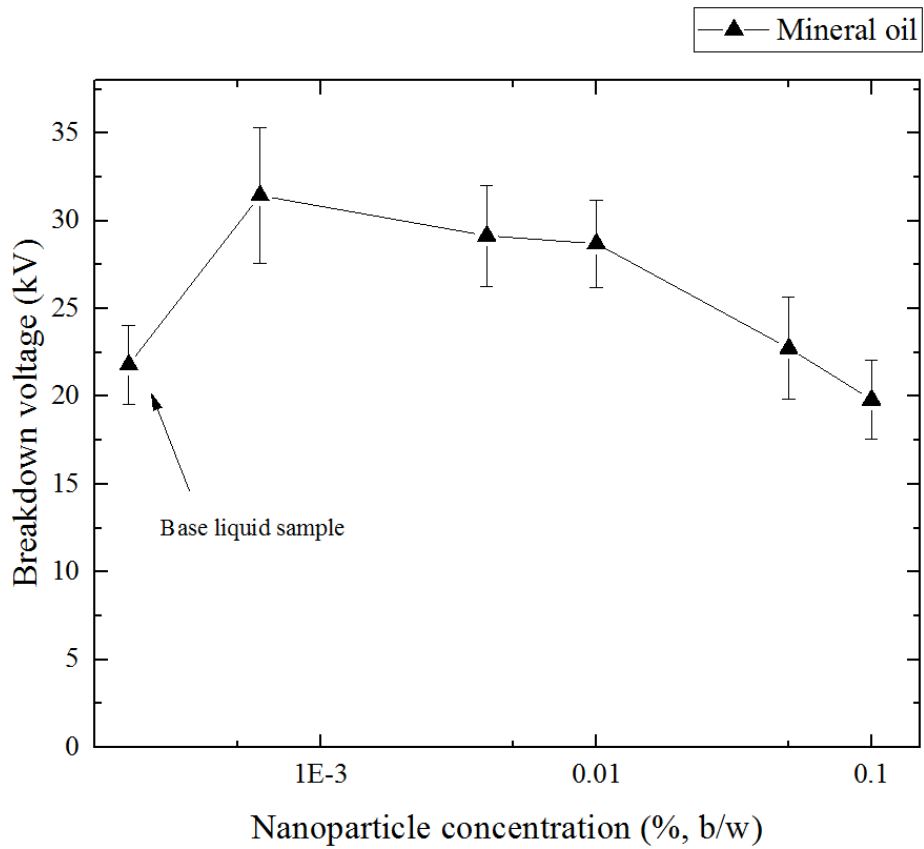
For the synthetic ester sample, Midel 7131 0.0006%, provided the highest breakdown voltage improvement (~47%). With increasing nanoparticle concentration, the AC breakdown voltage of the sample started to decrease. Furthermore, the standard deviation of the sample became small. This phenomenon may show that the nanoparticles not only increase the dielectric strength of insulating liquid but also may help make the breakdown occur in a relatively narrow voltage range.

### 4.3.2 AC breakdown characteristics of BN nano-modified liquids

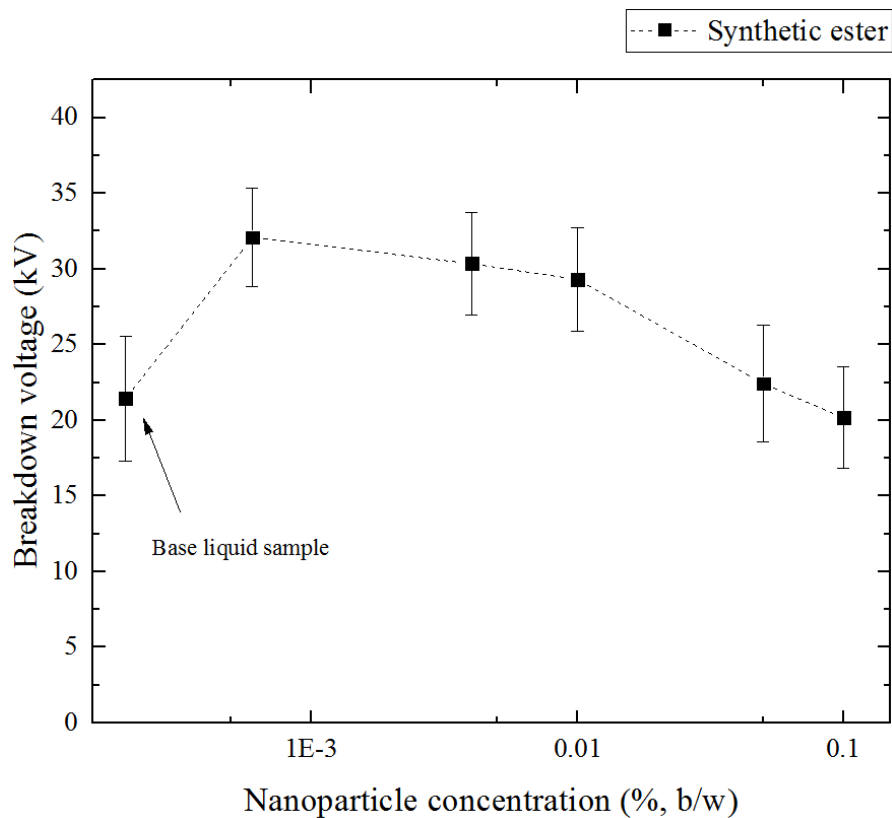
In this section, the AC breakdown characteristics of the BN nano-modified samples based on mineral oil, synthetic ester, and natural ester were provided and discussed. The concentrations were base liquids, 0.0006%, 0.004%, 0.01%, 0.05%, and 0.1% (b/w). The concentration selection is the same as the TiO<sub>2</sub> nano-modified samples, which facilitates the result comparison.

Figure 4-5 shows the AC breakdown results of the mineral oil sample, Diala S3, as a function of the BN nanoparticle concentration by weight. These results showed that 0.0006%, 0.004%, 0.01%, and 0.05% (b/w) concentration samples provided higher AC breakdown voltages than the base sample. However, for the 0.1% concentration (b/w) of BN nanoparticles, the breakdown voltage became lower than that for the base sample. The breakdown voltage behaviour corresponding to concentration was similar to the behaviour of the breakdown voltages of fluids with TiO<sub>2</sub> nanoparticles. It was found that the optimal concentration that provided the highest AC breakdown voltage is 0.0006% (b/w). For this concentration, the breakdown voltage increased from 21.81 ± 2.43 kV (base sample) to 31.46 ± 3.85 kV (0.0006%, b/w), which was a ~44 % increase. With increasing nanoparticle concentration, for concentrations higher than 0.0006% (b/w), the breakdown voltage started to decrease. When the concentration reached 0.05% (b/w), the AC breakdown voltage (22.75 ± 2.93 kV) became just slightly

higher than that for the base sample ( $21.81 \pm 2.43$  kV). When the concentration reached 0.1% (b/w), the AC breakdown voltage was  $19.81 \pm 2.24$  kV, which was ~9% lower than that for the base sample.

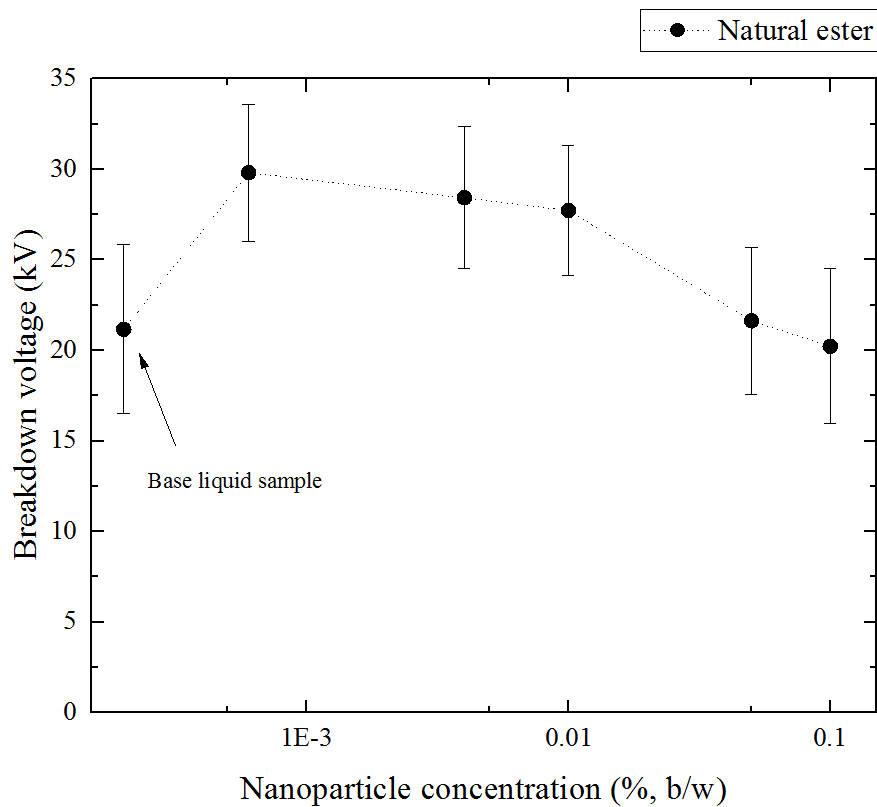


**Figure 4-5.** AC breakdown voltage of mineral oil BN samples as a function of nanoparticle concentration. Each data point is an average of breakdown measurements conducted using three fresh samples; each sample has been tested 70 times. The error bars show the standard deviation.



**Figure 4-6.** AC breakdown voltage of synthetic ester BN samples as a function of nanoparticle concentration. Each data point is an average of breakdown measurements conducted using three fresh samples; each sample has been tested 70 times. The error bars show the standard deviation.

Figure 4-6 shows the AC breakdown results of the synthetic ester sample, Midel 7131, as a function of BN nanoparticle concentration by weight. These results showed that 0.0006%, 0.004%, 0.01%, and 0.05% (b/w) concentration samples provided a higher AC breakdown voltage than the base sample. For the 0.1% (b/w) concentration sample, the breakdown voltage became lower than the base sample. The changing breakdown voltage behaviour with increasing nanoparticle concentration was similar to the Diala S3 samples. The optimal concentration that provided the highest AC breakdown voltage was at 0.0006% (b/w). The breakdown voltage increased from  $21.45 \pm 4.13$  kV (base sample) to  $32.09 \pm 3.25$  kV, which was a ~50% increase in magnitude. With increasing sample nanoparticle concentration, at higher than 0.0006%, the voltage increasing magnitudes started to decrease. When the sample nanoparticle concentration reached 0.05% (b/w), the AC breakdown voltage ( $22.42 \pm 3.84$  kV) became just slightly higher than that for the base sample ( $21.45 \pm 4.13$  kV). When the sample nanoparticle concentration reached 0.1%, the sample AC breakdown voltage was  $20.17 \pm 3.36$  kV, which was ~6% lower than the breakdown voltage for the base sample.



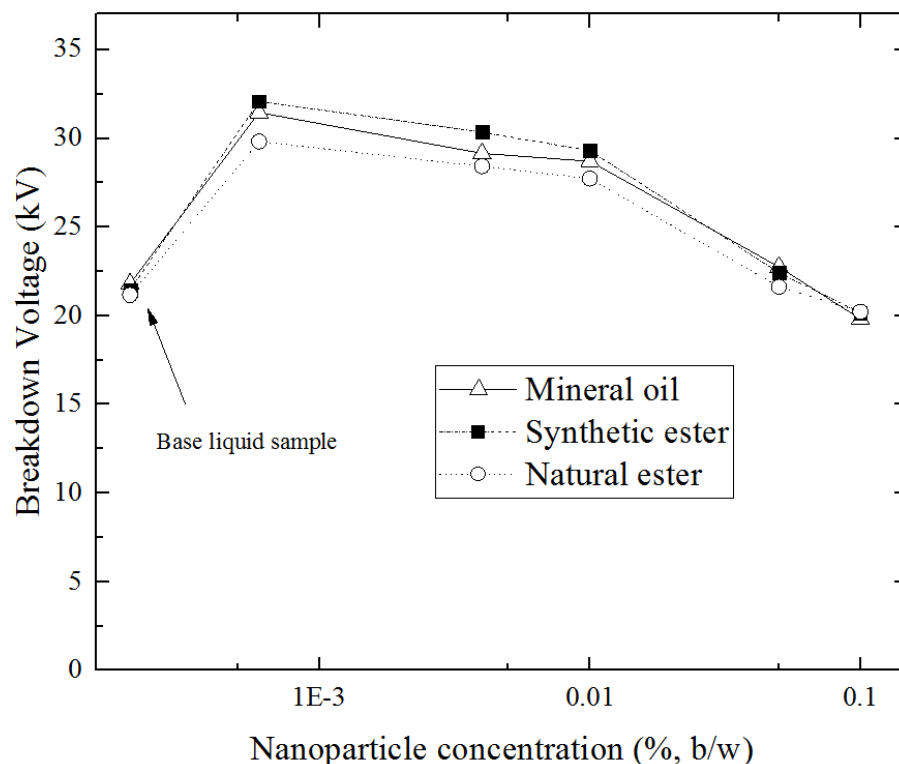
**Figure 4-7.** AC breakdown voltage of natural ester BN samples as a function of nanoparticle concentration. Each data point is an average of breakdown measurements conducted using three fresh samples; each sample has been tested 70 times. The error bars show the standard deviation.

Figure 4-7 shows the AC breakdown voltage for the natural ester (rapeseed oil) with BN nanoparticles. These results showed that 0.0006%, 0.004%, 0.01%, and 0.05% (b/w) concentrations provided higher AC breakdown voltages than that for the base sample. For the 0.1% (b/w) concentration, the breakdown voltage became lower than that for the base sample. The behaviour of the breakdown voltage with an increase of nanoparticle concentration was similar to that for the Diala S3 and Midel 7131 samples. The optimal concentration that provided the highest AC breakdown voltage was 0.0006% (b/w). The breakdown voltage of this nano-modified sample increased from  $21.17 \pm 2.66$  kV (base sample) to  $29.81 \pm 3.78$  kV (0.0006% b/w, sample), which was a ~41% magnitude increase. With increasing nanoparticle concentration to higher than 0.0006% (b/w), the breakdown voltage enhancement started to decrease. When the concentration reached 0.05% (b/w), the sample AC breakdown voltage ( $21.63 \pm 4.06$  kV) became just slightly lower than that for the base sample ( $21.17 \pm 2.66$  kV). When the concentration reached 0.1% (b/w), the sample AC breakdown voltage is  $20.22 \pm 4.27$  kV, which was ~4% lower than the breakdown voltage of the base sample.

Figure 4-8 depicts the comparison of the AC breakdown voltages for all three types of insulating liquid samples as functions of the BN nanoparticle concentration. The AC breakdown voltages of all three liquids demonstrated a similar tendency.

For the nano-modified liquids, the difference between AC breakdown voltages for the industry grade liquids and a food-grade natural ester liquid became clear but not as obviously as the TiO<sub>2</sub> sample results. Two types commercially produced liquids, mineral oil (Diala S3) and synthetic ester (Midel 7131), demonstrated similar breakdown voltages. The food-grade natural ester (rapeseed oil) provided a lower breakdown voltage than the other two industry productions, as expected.

For the samples with 0.05% concentration of BN nanoparticles, the breakdown voltages for all three types of liquids became close to that for the base sample. Compared with the TiO<sub>2</sub> samples, a similar performance was demonstrated for the 0.1% concentration sample. For the 0.1% concentration BN samples, the breakdown voltages of the three liquid-based samples were lower than the base samples, which were different from the TiO<sub>2</sub> samples.



**Figure 4-8.** AC breakdown voltage of three insulating liquid BN samples as a function of nanoparticle concentration. Each data point is an average of breakdown measurements conducted using three fresh samples; each sample has been tested 70 times.

Table 4-2 provides the average breakdown voltage, its standard deviation, and the magnitude of voltage changes for all samples of tested nano-modified liquids seeded with BN particles. Synthetic ester with a BN nanoparticle concentration of 0.0006% (b/w) showed the highest breakdown voltage ( $32.09 \pm 3.25$  kV). In addition, this concentration of nanoparticles provided the highest relative increase in the breakdown voltage compared with the base liquid, a ~50 % increase.

Mineral oil samples also provided the smallest standard deviation compared with the other liquid samples. The standard deviation of the natural ester samples stayed at a relatively high level for all concentrations. The potential reason for this performance is that the natural ester liquid contains a large amount of fibre and other contaminants (unknown particles), which would lead to the breakdown event at relatively low voltages and to an increase in the standard deviation.

**Table 4-2.** AC breakdown test results of three insulating liquid BN samples as a function of nanoparticle concentration.

| Concentration | Mineral Oil                            | Synthetic Ester          | Natural Ester            |
|---------------|--|--------------------------|--------------------------|
| (%)           | $V_{ave} \pm STD(kV); V_{change} (\%)$ |                          |                          |
| 0.00%         | 21.81 $\pm$ 2.43; 0.00%                | 21.45 $\pm$ 4.13; 0.00%  | 21.17 $\pm$ 2.66; 0.00%  |
| 0.0006%       | 31.46 $\pm$ 3.85; 44.25%               | 32.09 $\pm$ 3.25; 49.61% | 29.81 $\pm$ 3.78; 40.81% |
| 0.004%        | 29.15 $\pm$ 2.88; 33.65%               | 30.34 $\pm$ 3.41; 41.45% | 28.43 $\pm$ 3.91; 34.29% |
| 0.01%         | 28.71 $\pm$ 2.49; 31.64%               | 29.31 $\pm$ 3.45; 36.64% | 27.73 $\pm$ 3.58; 30.98% |
| 0.05%         | 22.75 $\pm$ 2.93; 4.31%                | 22.42 $\pm$ 3.84; 4.52%  | 21.63 $\pm$ 4.06; 2.17%  |
| 0.10%         | 19.81 $\pm$ 2.24; -9.17%               | 20.17 $\pm$ 3.36; -5.97% | 20.22 $\pm$ 4.27; -4.49% |

For synthetic ester samples, the base liquid had the largest standard deviation in the breakdown voltage compared with standard deviations for other liquids. With an increase in the concentration of nanoparticles in liquids, the breakdown voltage started to rise. Moreover, the standard deviation of the breakdown voltage started to decrease. Similar tendencies in the breakdown voltage and its standard deviation behaviour were observed in liquids seeded with TiO<sub>2</sub> nanoparticles.

Comparing both types of nanoparticles used for production of nano-modified liquids, TiO<sub>2</sub> and BN, it is possible to conclude that, in most cases, nano-modified liquids demonstrated higher breakdown voltages compared with base liquids without nanoparticles (for concentrations used in the present study). It was established that the optimal concentration of nanoparticles in mineral oil and ester fluids was 0.0006 % (b/w). For the liquid samples, at concentrations of nanoparticles higher than 0.0006 %,

(b/w), the average AC breakdown voltage presented a decreasing tendency. For the 0.1% (b/w) concentration of BN nanoparticles in liquid, the breakdown voltages were lower than the base sample.

#### **4.4 AC Breakdown Experimental Results: Weibull Analysis and Comparison**

The Weibull distribution is a statistical method named after Professor Waloddi Weibull whose papers were published in 1951 [212]. He demonstrated that this analysis method fit many different datasets well and gave good results, even for small samples. The Weibull distribution has been used to analyse the reliability in the engineering field, for example, to analyse equipment maintenance and lifetime distributions, depending on the failure event occurrence.

Reliability analysis is the study of the distribution of object lifetimes in the engineering field. That is the study of the duration time (or other factor of interest) from the initiating event, such as the start of treatment or start of operation, to the terminal event, such as the breakdown or machine failure. The data values of this analysis are a mixture of the complete (terminal event occurred) and censored (terminal event has not occurred) observations. Through analysis of these data, the distribution of the object lifetime (or other factor of interest, such as withstand voltage) depends on the obtainability of the failure event occurrence. This distribution also brings a lot of useful information about the object, such as the expected lifetime, mean time to failure, and survivability [213], [214].

In [9], Martin et al. used the Gaussian distribution and Weibull distribution to analyse the AC breakdown voltages of mineral oil, synthetic ester, and natural ester. The authors indicated that the Gaussian distribution makes the assumptions that the skewness is zero and the kurtosis is 3 of the probability density function, whereas the Weibull distribution does not make these assumptions. The actual distribution of all breakdown voltage measurements obtained in this paper demonstrated non-zero skewness. Thus, the Gaussian distribution is not appropriate for the evaluation of the breakdown voltage distribution, especially for calculating the withstand voltages at low probabilities. Therefore, the Weibull distribution could be used for this task. Considering that the experimental methods and samples in this study are similar to [9], the Weibull distribution is used in the present work to analyse the breakdown voltage results.

The Weibull statistical analysis has been used in previous published papers, and it has been proved that it could be used for the analysis of the AC breakdown voltages in order to obtain the probability to breakdown [29], [31], [40], [104], [126], [212], [215]–[217]. By performing the Weibull analysis, the AC breakdown voltage, corresponding to the probability to breakdown, could be evaluated. Considering the practical design requirements for power transformers and power grids, it is important to coordinate the dielectric insulation to maximise the AC breakdown voltage for low breakdown probability. The experimental data on breakdown voltage is found to be best described by the three-parameter Weibull distribution, where the cumulative probability to failure  $F(V)$ , is defined in the below equation [212]:

$$F(V) = 1 - e^{-\left(\frac{V-\gamma}{\alpha}\right)^\beta} \quad (4.1)$$

In this equation,  $F(V)$  is the cumulative probability distribution function of breakdown events, where  $V$  is the AC breakdown voltage,  $\alpha$  is the scale parameter,  $\beta$  is the shape parameter, and  $\gamma$  is the location parameter. The location parameter  $\gamma$  is the minimum voltage, which provides the non-zero breakdown probability, while  $\alpha$  is the scale parameter of the Weibull distribution. In the case in which  $\gamma$  is zero (two-parameter Weibull distribution),  $\alpha$  is where the voltage has 63.2% probability to breakdown, which is equivalent to the mean of the normal distribution. The shape parameter  $\beta$  indicates how sensitive the probability to breakdown of the insulating liquid is to an increase in voltage. All Weibull analyses were performed using Microsoft Excel and Origin Pro 2015.

#### 4.4.1 Weibull analysis of breakdown voltage data of TiO<sub>2</sub> nano-modified liquids

Figures 4-9 to 4-11 show the Weibull plots of the breakdown events in mineral oil, synthetic ester, and natural ester liquids seeded with TiO<sub>2</sub> nanoparticles with  $n$  different concentrations (b/w). Scale, shape, and location parameter and 5%, 10%, 50%, and 90% probabilities to breakdown (percentiles) for mineral oil, synthetic ester, and natural ester liquids modified with TiO<sub>2</sub> nanoparticles are shown in Table 4-3. These results showed that, for all three insulating liquids, in the cases of 5%, 10%, 50%, and 90% probabilities to breakdown, the optimal nanoparticle concentration was at 0.0006% concentration (b/w).

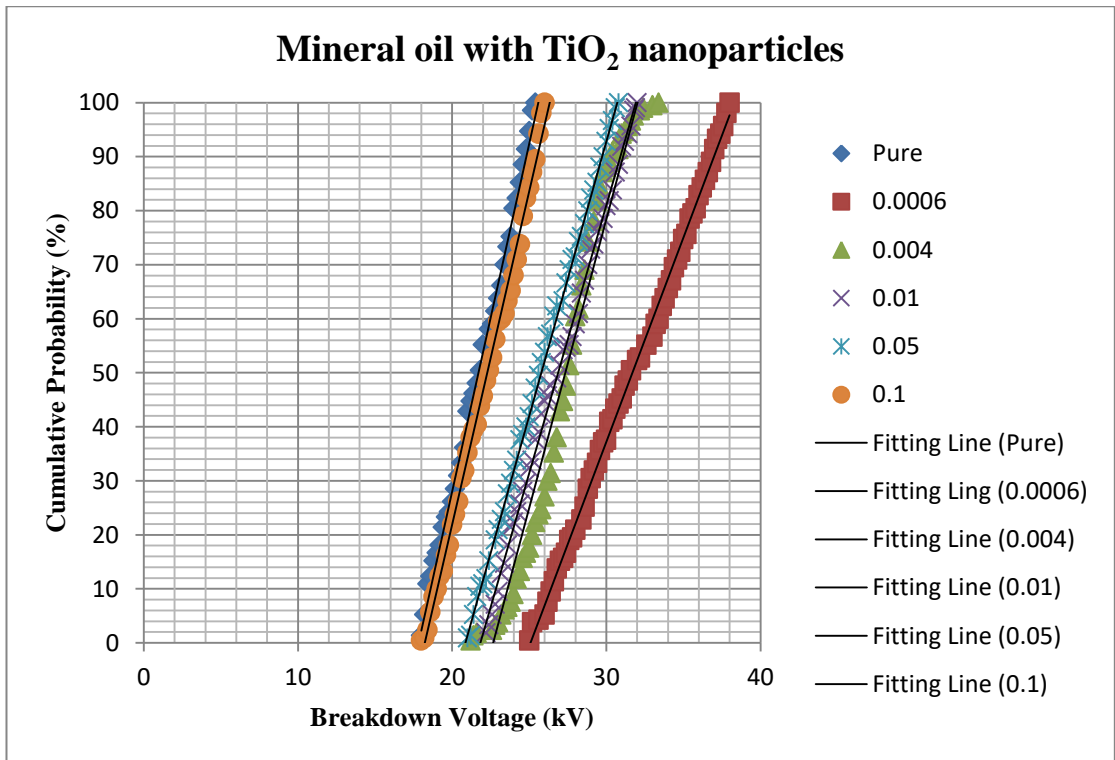


**Figure 4-9.** Cumulative probability plots of mineral oil with TiO<sub>2</sub> nanoparticles.

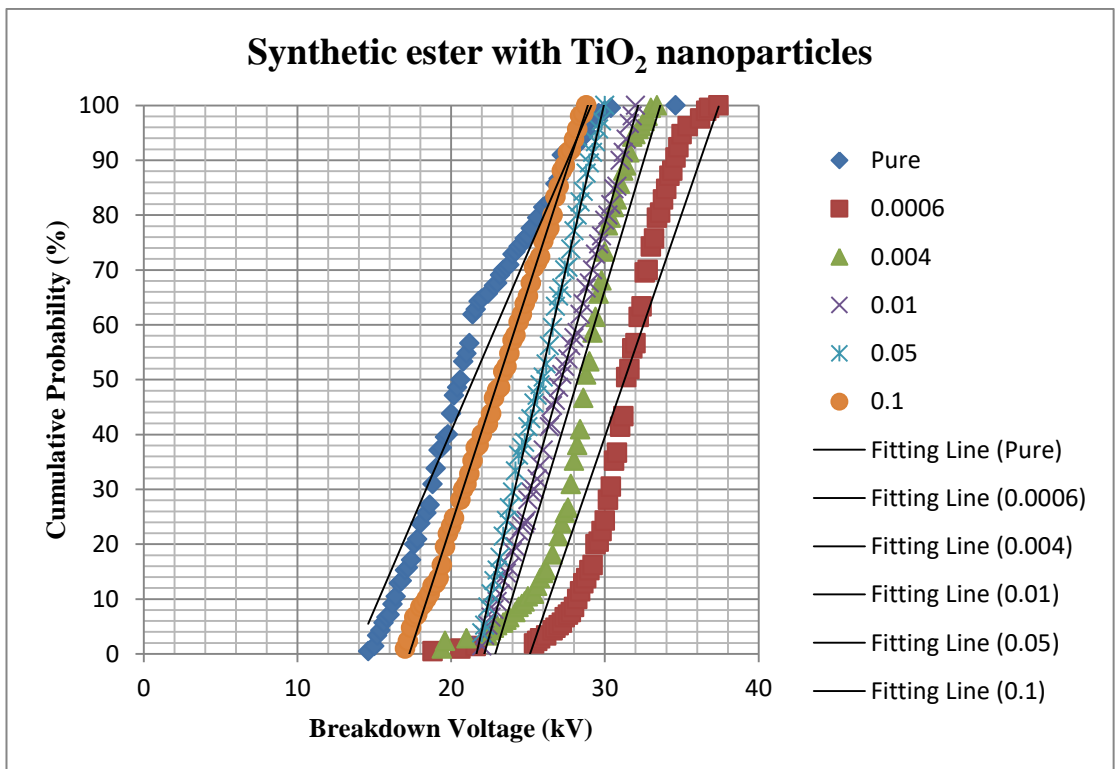


**Figure 4-10.** Cumulative probability plots of synthetic ester with TiO<sub>2</sub> nanoparticles.

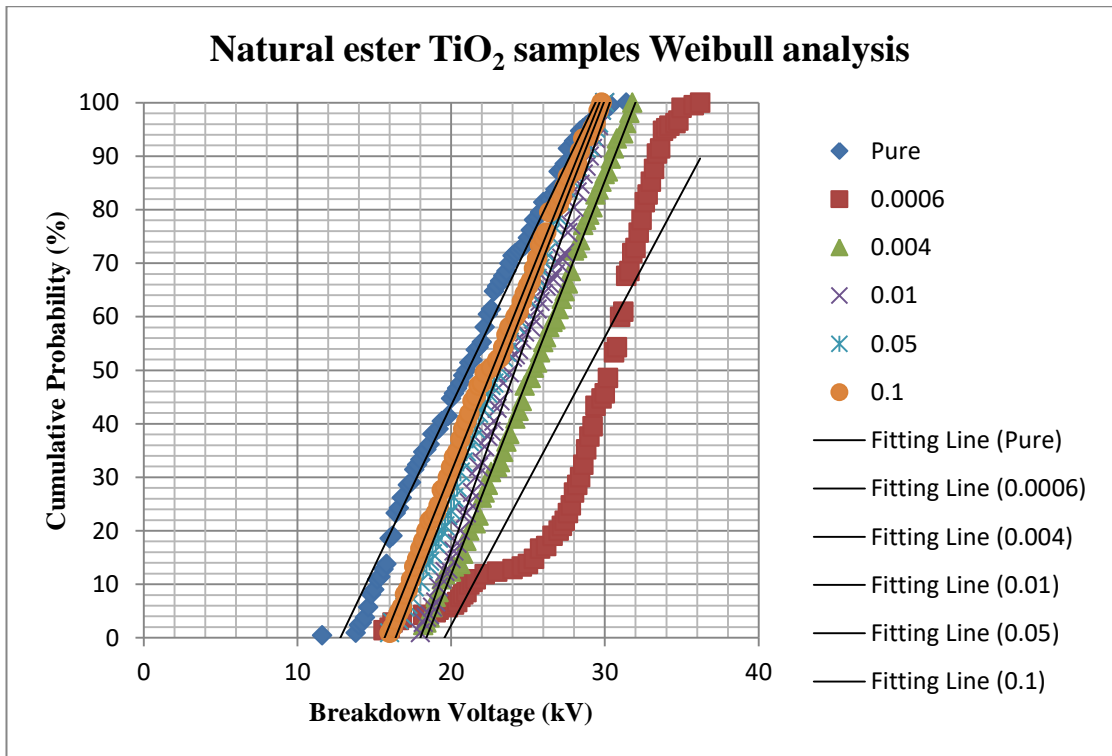


Figure 4-11. Cumulative probability plots of natural ester with TiO<sub>2</sub> nanoparticles.

Table 4-3. Weibull analysis parameter of mineral oil, synthetic ester, and natural ester with TiO<sub>2</sub> nanoparticles.

| TiO <sub>2</sub> |      |      |      |      |                          |                       |               |
|------------------|------|------|------|------|--------------------------|-----------------------|---------------|
| Mineral Oil      |      |      |      |      |                          |                       |               |
| Concentration    | V5%  | V10% | V50% | V90% | Location $\gamma$ , (kV) | Scale $\alpha$ , (kV) | Shape $\beta$ |
| 0.00             | 18.2 | 18.4 | 21.8 | 24.8 | 3.1276                   | 22.8182               | 11.2902       |
| 0.0006           | 26   | 26.4 | 31.6 | 36.8 | 3.5118                   | 33.507                | 9.591         |
| 0.004            | 23.2 | 24   | 27.6 | 30.4 | 3.3504                   | 28.515                | 12.643        |
| 0.01             | 22.6 | 23   | 26.8 | 30.8 | 3.3424                   | 28.2876               | 10.4465       |
| 0.05             | 21.4 | 21.8 | 25.6 | 29.8 | 3.3021                   | 27.1699               | 10.2686       |
| 0.1              | 18.6 | 19   | 22.4 | 25.4 | 3.1538                   | 23.4256               | 11.2034       |
| Synthetic Ester  |      |      |      |      |                          |                       |               |
| Concentration    | V5%  | V10% | V50% | V90% | Location $\gamma$ , (kV) | Scale $\alpha$ , (kV) | Shape $\beta$ |
| 0.00             | 15.6 | 16.4 | 20.6 | 27.2 | 3.1436                   | 23.1863               | 5.447         |
| 0.0006           | 27   | 28.2 | 31.4 | 34.6 | 3.4851                   | 32.6268               | 13.9124       |
| 0.004            | 23   | 25   | 28.8 | 31.4 | 3.3894                   | 29.6479               | 13.81         |
| 0.01             | 22.4 | 23   | 27.2 | 31   | 3.3518                   | 28.5548               | 10.885        |
| 0.05             | 22.2 | 22.6 | 26   | 29   | 3.2952                   | 26.9819               | 12.2301       |
| 0.1              | 17.4 | 18.4 | 23.4 | 27.4 | 3.2042                   | 24.6365               | 8.0775        |
| Natural Ester    |      |      |      |      |                          |                       |               |
| Concentration    | V5%  | V10% | V50% | V90% | Location $\gamma$ , (kV) | Scale $\alpha$ , (kV) | Shape $\beta$ |
| 0.00             | 14.6 | 15.2 | 21   | 27.6 | 3.1376                   | 23.0487               | 5.0681        |
| 0.0006           | 19.2 | 21.2 | 30.2 | 33.4 | 3.432                    | 30.9395               | 9.2971        |
| 0.004            | 18.8 | 19.4 | 25.4 | 30.4 | 3.2951                   | 26.9802               | 7.5079        |
| 0.01             | 18.6 | 19.2 | 23.8 | 29   | 3.2501                   | 25.7941               | 7.7905        |
| 0.05             | 17   | 18   | 23.2 | 28.4 | 3.2155                   | 24.9155               | 6.7825        |
| 0.1              | 16.6 | 17.4 | 22.6 | 28.4 | 3.1972                   | 24.4631               | 6.378         |

For samples with concentrations of nanoparticles higher than 0.0006% (b/w), their breakdown voltages started to decrease. The changing breakdown voltage behaviours were similar to each other for all insulating liquid samples and concentration samples. The location parameter also demonstrated a similar behaviour to the behaviour of the breakdown voltage. The 0.0006% (b/w) concentration sample had the highest location and scale parameters of the samples. The high location parameter means that the breakdown voltage of the 0.0006% (b/w) sample was higher than the other samples. The high scale parameter means that, for the 0.0006% (b/w) sample, the breakdown voltage had a higher degree of spread than for the other samples, which also means a high standard deviation. The large shape parameter means the failure rate increased with an increase in the voltage. For mineral oil samples, the 0.0006% concentration sample showed the smallest shape parameter, indicating this sample provided more stable breakdown behaviour than the other samples under the high electrical field. For both ester liquids, the 0.0006% (b/w) concentration of nanoparticles showed the highest shape parameter; therefore, although they could provide the highest breakdown voltage, this breakdown behaviour was not very stable compared with the samples with other concentrations of nanoparticles. This behaviour is a disadvantage compared with mineral oil samples.

#### **4.4.2 Weibull analysis results for BN nano-modified samples**

Figures 4-12 to 4-14 show the Weibull analysis plots of BN nanoparticle modified mineral oil, synthetic ester, and natural ester samples. The scale, shape, and location parameters for the breakdown events in the three types of liquids modified with BN nanoparticles at 5%, 10%, 50%, and 90% probabilities to breakdown in these liquids are shown in Table 4-4. These tables demonstrate that, for all three insulating liquids, in the case of 5%, 10%, 50%, and 90% probabilities to breakdown, the optimal concentration that provided the best dielectric performance was the 0.0006% concentration, which was similar to the case of the TiO<sub>2</sub> seeded liquids.

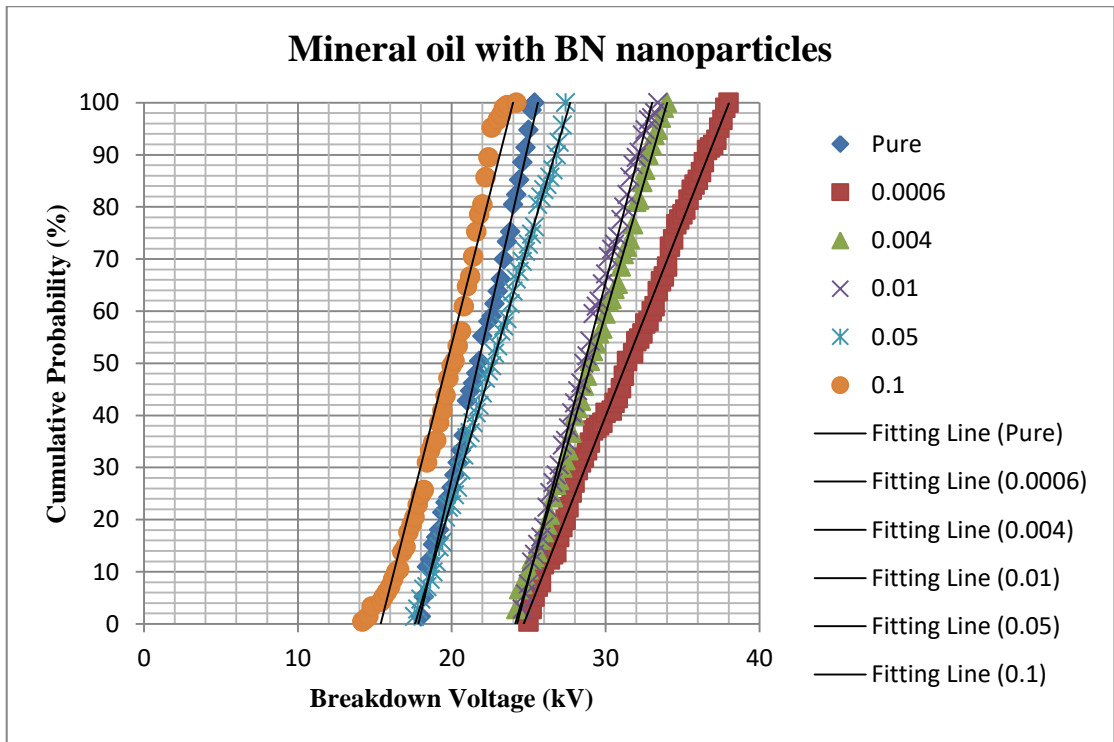


**Figure 4-12.** Cumulative probability plots of mineral oil with BN nanoparticles.

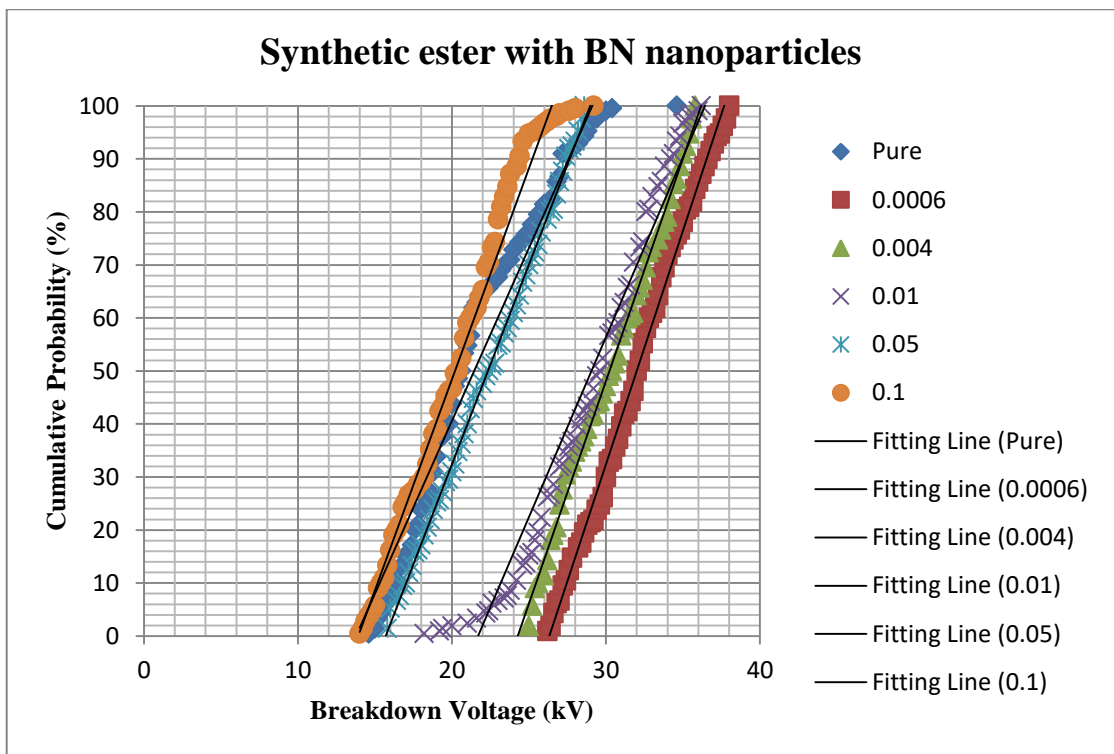


**Figure 4-13.** Cumulative probability plots of synthetic ester with BN nanoparticles.

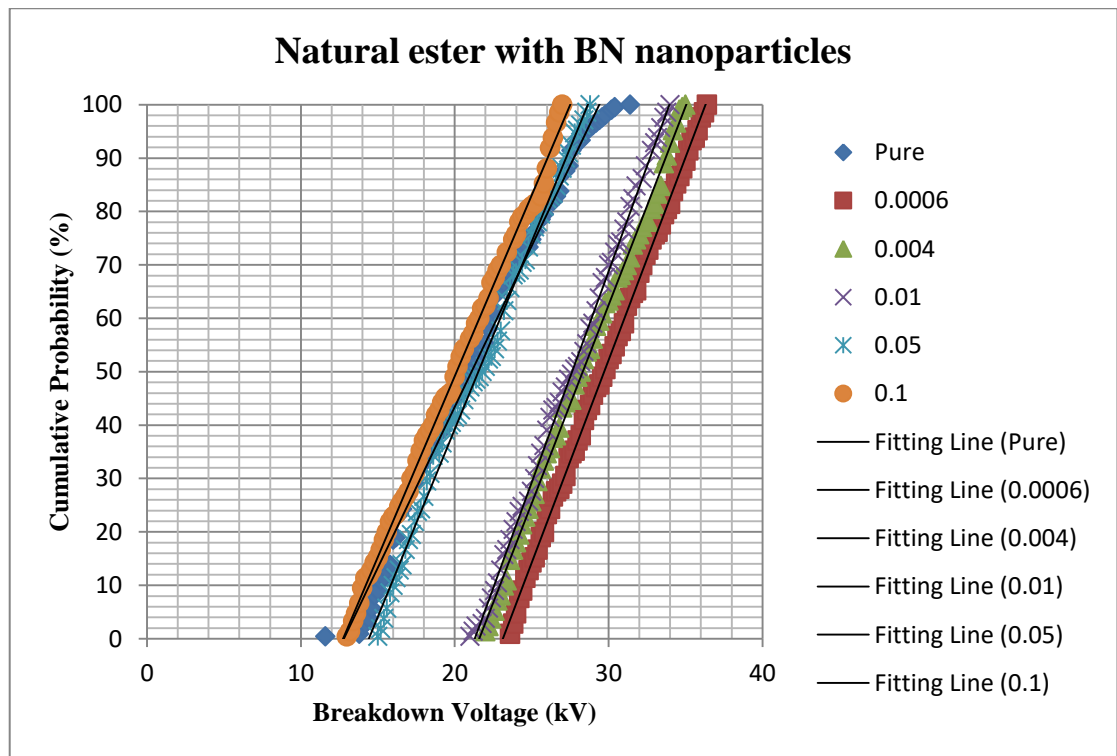


Figure 4-14. Cumulative probability plots of mineral oil with BN nanoparticles.

Table 4-4. Weibull analysis parameter of mineral oil, synthetic ester, and natural ester with BN nanoparticles.

| BN              |      |      |      |      |                          |                       |               |
|-----------------|------|------|------|------|--------------------------|-----------------------|---------------|
| Mineral Oil     |      |      |      |      |                          |                       |               |
| Concentration   | V5%  | V10% | V50% | V90% | Location $\gamma$ , (kV) | Scale $\alpha$ , (kV) | Shape $\beta$ |
| 0.00            | 18.2 | 18.4 | 21.8 | 24.8 | 3.1276                   | 22.8182               | 11.2902       |
| 0.0006          | 25.4 | 25.8 | 31.4 | 36.6 | 3.5015                   | 33.1648               | 9.3223        |
| 0.004           | 24.4 | 25   | 29   | 32.8 | 3.416                    | 30.446                | 11.7454       |
| 0.01            | 24.8 | 25.2 | 28.6 | 32.2 | 3.397                    | 29.8739               | 12.7421       |
| 0.05            | 18   | 18.8 | 22.6 | 26.8 | 3.1795                   | 24.0338               | 8.8833        |
| 0.1             | 15.6 | 16.4 | 20.2 | 22.4 | 3.0353                   | 20.8073               | 10.5886       |
| Synthetic Ester |      |      |      |      |                          |                       |               |
| Concentration   | V5%  | V10% | V50% | V90% | Location $\gamma$ , (kV) | Scale $\alpha$ , (kV) | Shape $\beta$ |
| 0.00            | 15.6 | 16.4 | 20.6 | 27.2 | 3.1436                   | 23.1863               | 5.447         |
| 0.0006          | 26.6 | 27.4 | 32   | 36.6 | 3.5137                   | 33.5717               | 10.9688       |
| 0.004           | 25.2 | 25.6 | 30.4 | 35   | 3.4619                   | 31.8783               | 10.1379       |
| 0.01            | 22.4 | 24.2 | 29.6 | 34.2 | 3.4331                   | 30.9724               | 8.9981        |
| 0.05            | 16   | 17   | 22.4 | 27.4 | 3.1801                   | 24.0484               | 6.7587        |
| 0.1             | 14.8 | 15.4 | 20.4 | 24.4 | 3.0732                   | 21.6099               | 6.6113        |
| Natural Ester   |      |      |      |      |                          |                       |               |
| Concentration   | V5%  | V10% | V50% | V90% | Location $\gamma$ , (kV) | Scale $\alpha$ , (kV) | Shape $\beta$ |
| 0.00            | 14.6 | 15.2 | 21   | 27.6 | 3.1376                   | 23.0487               | 5.0681        |
| 0.0006          | 24   | 24.4 | 29.8 | 35   | 3.4499                   | 31.4982               | 8.8599        |
| 0.004           | 22.6 | 23.2 | 28.2 | 33.8 | 3.4056                   | 30.1332               | 8.2586        |
| 0.01            | 22.2 | 22.8 | 27.8 | 32.8 | 3.3788                   | 29.3343               | 8.6705        |
| 0.05            | 15.6 | 16   | 21.8 | 27.2 | 3.1498                   | 23.3324               | 5.9844        |
| 0.1             | 13.6 | 14   | 20   | 26.2 | 3.0892                   | 21.9597               | 5.4315        |

For samples with concentrations of nanoparticles higher than 0.0006% (b/w), their breakdown voltages started to decrease. The changing breakdown voltage behaviours were similar to each other for all insulating liquid samples and concentration samples. The location parameter also demonstrated a similar behaviour of the breakdown voltage. The 0.0006% (b/w) concentration sample had the highest location and scale parameters of the samples. The high location parameter means that the breakdown voltage of the 0.0006% (b/w) sample was higher than the other samples. The high scale parameter means that, for the 0.0006% (b/w) sample, the breakdown voltage had a higher degree of spread than the other samples, which also means a high standard deviation. The large shape parameter indicated the failure rate increased with an increase in the voltage. For mineral oil samples, the 0.0006% (b/w) concentration of nanoparticles showed the smallest shape parameter, which means this sample provided more stable breakdown behaviour than the other samples under a high electrical field. For both ester liquids, the 0.0006% (b/w) concentration sample showed the highest shape parameter, which means that, although they could provide the highest breakdown voltage, they were not very stable compared with samples with other concentrations of nanoparticles. This behaviour is a disadvantage compared with mineral oil samples.

## **4.5 AC Breakdown: Confidence Analysis**

In this section, the CIs for the difference between the average values of breakdown voltages of base and nano-modified liquids were calculated. The calculation results of the CIs proved that the statistical difference between average values of breakdown voltages,  $\Delta V$ , of the base and nano-modified liquids exist, confirming the nanoparticle enhancement of the dielectric liquid behaviours. More details about the CIs and the statistical difference analysis have been presented below.

### **4.5.1 Confidence interval**

In statistics, the CI of a probabilistic sample is an estimated interval of a population parameter for the sample. The CI shows that the true value of the population parameter has a certain probability of falling within a certain interval related to the measurement result. The CI gives the degree of confidence that the true value of the population parameter is within the range of the measured value, that is, the 'certain probability'. This probability is called the confidence level. Based on the standard error approach, the CI was used to describe the statistical difference between the tested samples.

In this situation, the CI is a convenient method to present the range of the statistical difference between two samples, which is affected by the sample size and standard deviation. The width of a CI is based on a sample statistic and depends partly on its standard error and hence on both the standard deviation and sample size. It also depends on the degree of ‘confidence’ that we want to associate with the resulting interval. In the present work, the typical confidence level, 95%, is used, which means the statistical difference between the tested samples has a 95% chance to be located within the CI. The CI was used to investigate the breakdown voltage accuracy in many published results [16], [105], [107], [108], [211], [217]–[219].

#### 4.5.2 Calculation of confidence intervals

In [210] and [211], the statistical difference analysis was used to calculate the CI based on the standard error to investigate the statistical difference between the samples, considering the number of samples and the standard deviation effect. The mathematical procedure of applying the statistical difference analysis to the raw data is given below.

To calculate the CI, first the ‘pooled’ standard deviation of the two samples must be calculated:

$$s = \sqrt{\frac{(n_1 - 1) \times s_1^2 + (n_2 - 1) \times s_2^2}{n_1 + n_2 - 2}} \quad (4.3)$$

In this function  $n_1$  and  $n_2$  denote the sample sizes of the two samples;  $s_1$  and  $s_2$  denote the standard deviations of the two samples, while  $s$  indicates the pooled standard deviation.

$$SE_{diff} = s \sqrt{\frac{1}{n_1} + \frac{1}{n_2}} \quad (4.4)$$

In this function  $n_1$  and  $n_2$  denote the sample sizes of the two samples;  $s$  indicates the pooled standard deviation, and  $SE_{diff}$  denotes the standard error between the two samples.

The CI is presented below:

$$\bar{x}_1 - \bar{x}_2 - (t_{1-\frac{\alpha}{2}} \times SE_{diff}) \text{ to } \bar{x}_1 - \bar{x}_2 + (t_{1-\frac{\alpha}{2}} \times SE_{diff}), \quad (4.5)$$

where  $\bar{x}_1$  and  $\bar{x}_2$  denote the mean values of the two samples, and  $t_{1-\frac{\alpha}{2}}$  is taken from the  $t$ -distribution with  $n_1 + n_2 - 2$  degrees of freedom.

In the present work, the objective was to investigate the statistical difference of the average breakdown voltages,  $\Delta V$ , of the base and nano-modified samples of three dielectric liquids and to confirm that nano-modified samples have statistically different breakdown voltages compared with base liquids. If the  $\Delta V$  value is a positive number, there is a statistical difference between the two investigated samples. In contrast, if the statistical error equals zero, the statistical difference may not exist between two investigated samples.

The 95% upper and lower bounds of the CI indicate that the true value of the measurement data has a 95% probability of falling in this range. As the figure in Sections 4.5.3 and 4.5.4 presents, if the lower bound of the CI is higher than zero, the  $\Delta V$  is a positive number in the 95% CI, and indicates that the statistical difference of the average breakdown voltages between two samples exists. In contrast, if the lower bound of the CI is equal to or lower than zero, the  $\Delta V$  may equal zero in the 95% CI; hence, the statistical difference of the average breakdown voltage may not exist between the two samples.

Investigating whether the statistical difference indicates that the value of the breakdown voltage of the base and nano-modified liquids exists is important because it can confirm the nanoparticle enhancement phenomenon of the dielectric liquid behaviour.

### **4.5.3 Confidence analysis: AC breakdown voltage of TiO<sub>2</sub> nano-modified liquids**

The confidence analysis results are shown in Figures 4-15 to 4-17. In these figures, the AC breakdown voltages shown in Figures 4-1 to 4-4 were used to verify the statistical significance in the difference between the breakdown voltages of base and nano-modified samples.

For all TiO<sub>2</sub> nano-modified liquid samples, it was found that the optimal concentration was 0.0006% b/w, which is the concentration of nanoparticles that provided the highest breakdown voltage. By these results, the 0.0006% (b/w) concentration samples provided the largest  $\Delta V$  compared with that of the base samples. With an increase in the concentration of nanoparticles, the AC breakdown voltages of the nano-modified samples started to decrease. For the highest concentration sample, 0.1% (b/w), the breakdown voltages were close to the base sample. The lower bounds of the CI of these samples

were very close to zero, which indicated that the statistical difference of the average breakdown voltage between the base and nano-modified liquids became very small.

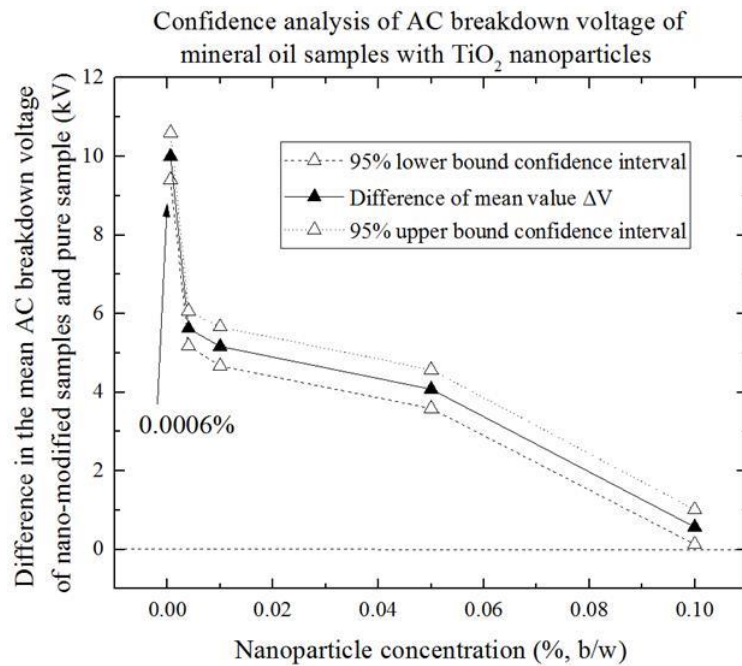


**Figure 4-15.** Confidence analysis,  $\Delta V$  of mineral oil with TiO<sub>2</sub> nanoparticles. Each data point denotes the  $\Delta V$  between the mean value of the breakdown voltages of the base and nano-modified samples. The dotted line represents the upper 95% confidence bound; the dashed line represents the lower 95% confidence bound.

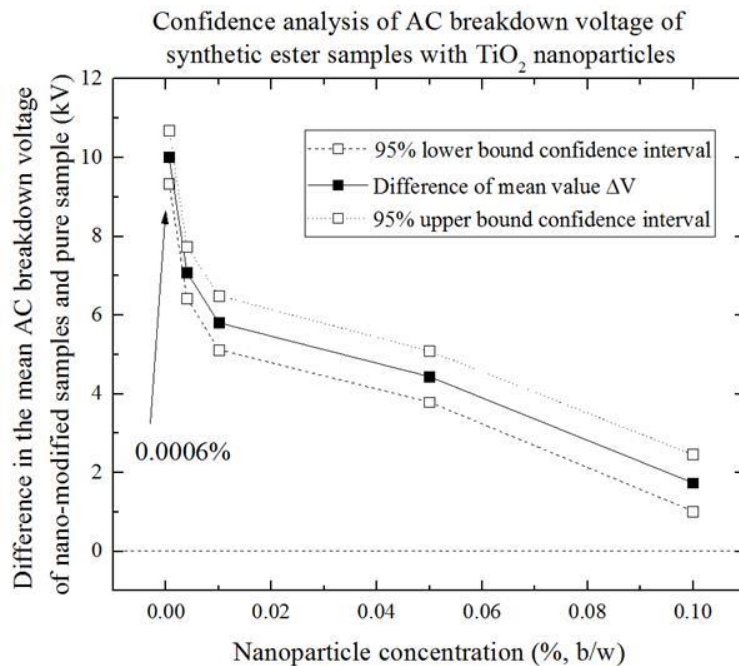


**Figure 4-16.** Confidence analysis,  $\Delta V$  of synthetic ester with TiO<sub>2</sub> nanoparticles. Each data point denotes the  $\Delta V$  between the mean value of the breakdown voltages of the base and nano-modified samples. The dotted line represents the upper 95% confidence bound; the dashed line represents the lower 95% confidence bound.

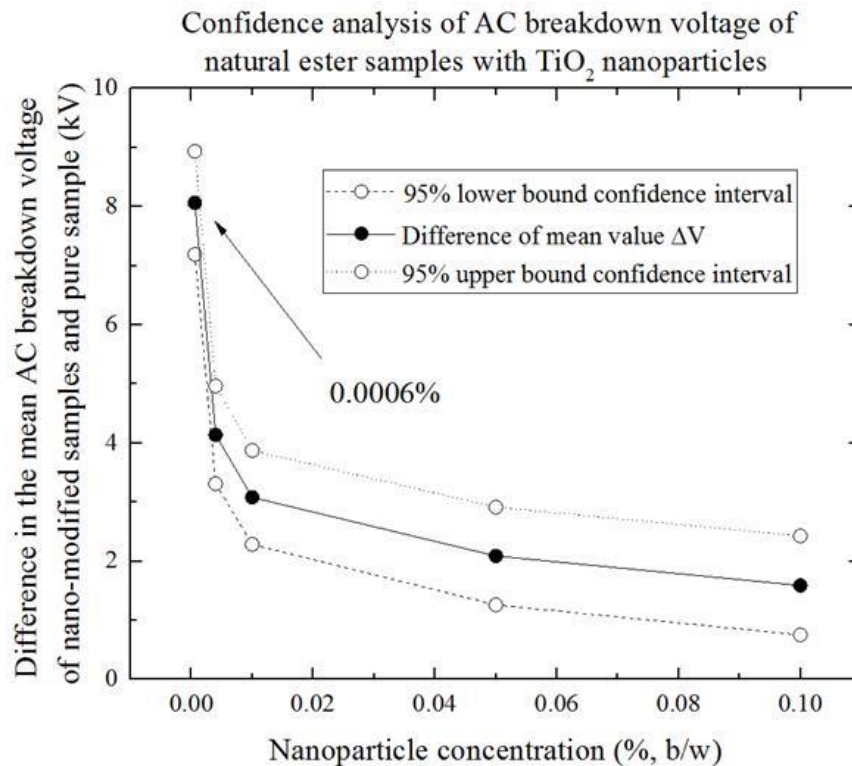


**Figure 4-17.** Confidence analysis,  $\Delta V$  of natural ester with  $\text{TiO}_2$  nanoparticles. Each data point denotes the  $\Delta V$  between the mean value of the breakdown voltages of the base and nano-modified samples. The dotted line represents the upper 95% confidence bound; the dashed line represents the lower 95% confidence bound.

#### 4.5.4 Confidence analysis: AC breakdown voltage of BN nano-modified liquids

The confidence analysis results are shown in Figures 4-18 to 4-20. In these figures, the AC breakdown voltages shown in Figures 4-5 to 4-8 were used to verify the statistical significance in difference between breakdown voltages of base and nano-modified samples.

For all BN nano-modified liquid samples, it was found that the optimal concentration is 0.0006% (b/w) at which the concentration of nanoparticles provided the highest breakdown voltages, similar to the  $\text{TiO}_2$  nano-modified sample results. The 0.0006% (b/w) concentration sample provided the largest  $\Delta V$  compared with the base sample. With an increase in the concentration of nanoparticles, the AC breakdown voltages of the nano-modified samples started to decrease. The experimental results showed that the AC breakdown voltages of BN nano-modified samples decreased much faster than those of the  $\text{TiO}_2$  nano-modified samples with an increase in the concentration of nanoparticles.

The breakdown voltage of the 0.5% (b/w) concentration of BN samples was almost equal to the breakdown voltage of the base samples. Thus, these samples provided the lowest lower bound of the CI in all samples. For the three liquid samples with the highest concentration, 0.1% (b/w), the nano-

modified samples exhibit breakdown voltages that are lower than the base sample, which means the  $\Delta V$  between the base and nano-modified was greater than that for the 0.5% (b/w) nano-modified sample. Thus, the lower bounds of the CI of these samples were higher than those of the 0.5% (b/w) concentration samples.

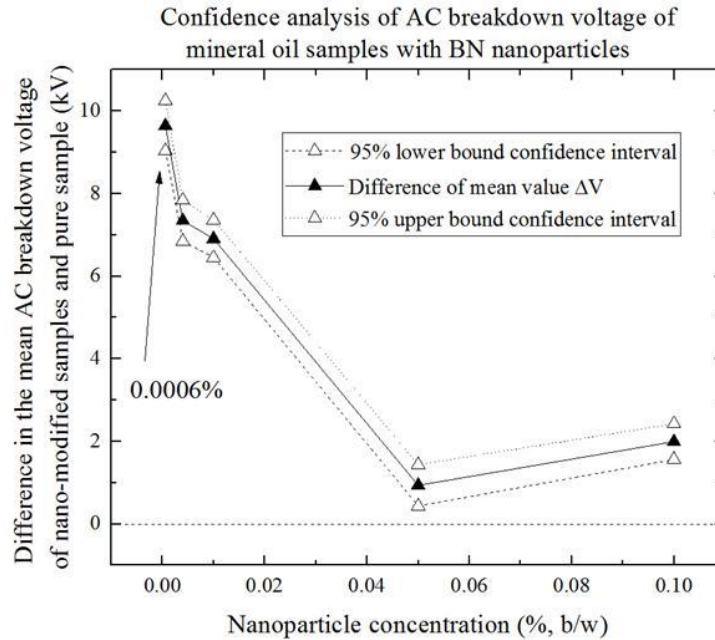


**Figure 4-18.** Confidence analysis,  $\Delta V$  of mineral oil with BN nanoparticles. Each data point denotes the  $\Delta V$  between the mean value of the breakdown voltages of the base and nano-modified samples. The dotted line represents the upper 95% confidence bound; the dashed line represents the lower 95% confidence bound.

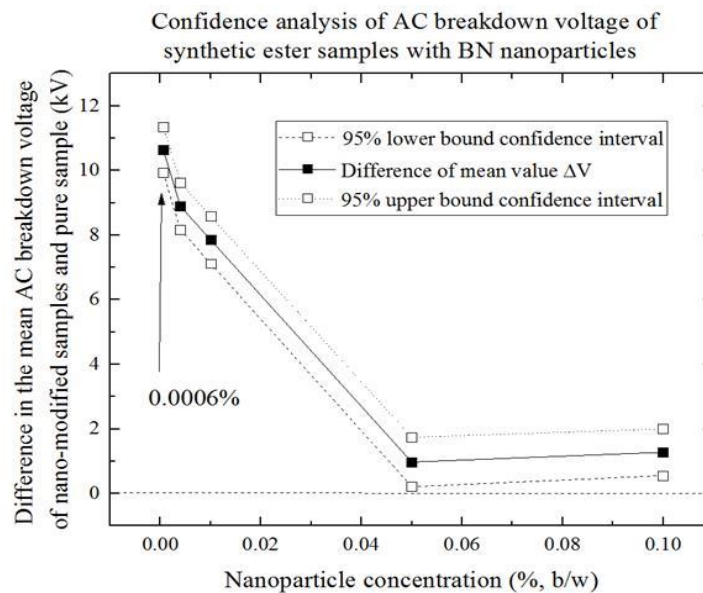


**Figure 4-19.** Confidence analysis,  $\Delta V$  of synthetic ester with BN nanoparticles. Each data point denotes the  $\Delta V$  between the mean value of the breakdown voltages of the base and nano-modified samples. The dotted line represents the upper 95% confidence bound; the dashed line represents the lower 95% confidence bound.

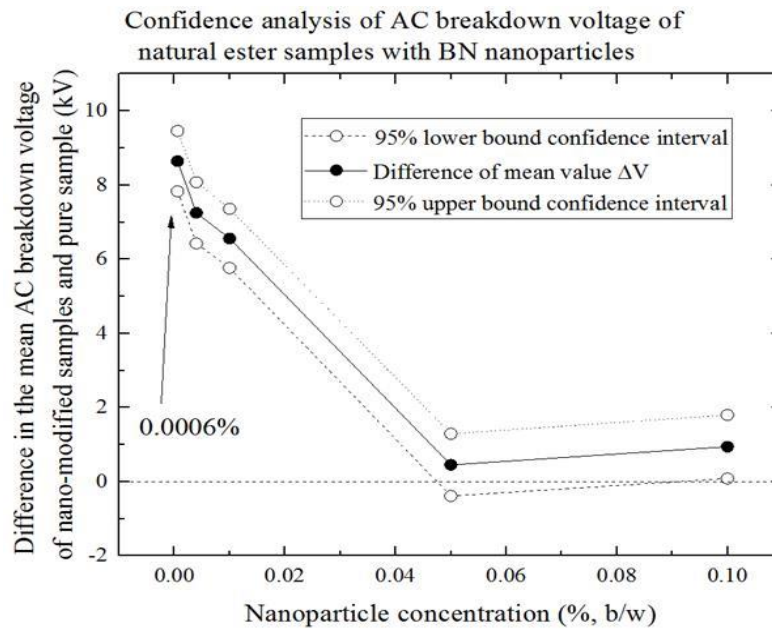


**Figure 4-20.** Confidence analysis,  $\Delta V$  of natural ester with BN nanoparticles. Each data point denotes the  $\Delta V$  between the mean value of the breakdown voltages of the base and nano-modified samples. The dotted line represents the upper 95% confidence bound; the dashed line represents the lower 95% confidence bound.

## 4.6 Summary

### 4.6.1 Nano-modified insulating liquid theory

In the framework of traditional liquid breakdown theory, the particles (including micrometre-sized particles and fibres) would be treated as contaminants because the particles would cause polarisation under a high electrical field. These polarisation particles would strongly distort the electrical field and form a ‘conductive bridge’ between two electrodes following the electrical field direction. This conductive bridge is a conductive channel that contains many electrons and charge carriers. Once this channel forms and connects to the electrodes, the breakdown happens [45], [220], [221].

However, in [17], Segal’s experimental results showed that adding the magnetite nanoparticle into the insulating liquid may help to increase the withstand voltage strength of the insulating material. If the particle size is on a nanometre scale, traditional theory can no longer explain these experimental results. The potential reason for this phenomenon is that, compared with the large particles, the nanoparticles are much smaller, and they would be distributed in the liquids more uniformly. Under the electrical field, these nanoparticles would polarise. These nanoparticles would catch and slow the electrons, which produces ionisation to reduce the electron kinetic energy. Because the number of electrons decreases and the electron kinetic energy reduces, the streamer formation is inhibited. On the

other hand, compared with the large particles, the nanoparticles are distributed more uniformly in the liquids and thus do not form an easily conductive bridge. Furthermore, this uniform distribution would help them inhibit the electrical field distortion caused by ionisation.

#### **4.6.2 Experimental results comparison**

Both TiO<sub>2</sub> and BN nano-modified sample test results showed that the nano-modified sample would provide a higher breakdown voltage than the base sample in a specific scale of nanoparticle concentration. For both TiO<sub>2</sub> and BN, the optimal concentration is 0.0006% (b/w), which provides the highest breakdown voltage compared with other liquid samples with different concentrations. With increasing concentrations, the breakdown voltage would reach a crest and start to decrease. All the TiO<sub>2</sub> nano-modified samples provided higher breakdown voltages than the base sample. In the BN sample test, the 0.1% sample showed a slightly lower breakdown voltage than the base sample. The changing voltage tendency was similar for the three insulating liquids and both TiO<sub>2</sub> and BN nano-modified samples. Thus, with the increasing nanoparticle concentration, the nano-modified sample breakdown voltage would be lower than the base sample, as expected.

In the Weibull analysis, the results indicate that the nanofluids with optimal concentration generally provide higher breakdown voltage at low breakdown probability than the base liquid. These results show that nanofluids with optimal concentration provide better reliability than the base liquids. In some case, such as in Figures 4-10 and 4-11, the data do not fit the Weibull fitting line (straight line), which indicates that there may be several competing breakdown processes.

Similar behaviour has been reported in [29], [95], [96] and [193]. In [29], [95], and [96], the TiO<sub>2</sub> nano-modified samples were tested, and it was found that the optimal concentration of nanoparticles was 0.006 g/L, which is almost equal to 0.0006% b/w.

In [93] and [95], the AC breakdown voltages of the three types of TiO<sub>2</sub> nano-modified samples with different surfactants (untreated, octadecanoic acid, stearic acid, and silicon oil) have been presented. The results [105] demonstrated that the nano-modified sample with octadecanoic acid treatment presented the highest breakdown voltage strength. With the increasing concentration, the changing withstand voltage tendency was similar to that of this experiment. The breakdown voltage improvement magnitudes were different, and the optimal concentrations were different. The optimal

concentration was at 0.01 g/L, which is between 0.0006% and 0.004% b/w. The nano-modified samples with untreated TiO<sub>2</sub> and silicon oil-treated TiO<sub>2</sub> also showed breakdown voltage improvement. However, the breakdown voltage of both samples did not show a clear tendency with increasing concentration. Furthermore, with increasing concentrations, the magnitude of the improvement of the drop speed of the breakdown voltages was different for different nanoparticles or surface modifications. Comparing these results, the potential reasons that the inherent properties and surface modification methods (including different additives and productions) of the nanoparticles were decide the optimal concentration of nanofluids. The influence of the insulating liquid selection on the optimal concentration was not clear.

The results [103] showed that the nano-modified sample with stearic acid treatment presented the highest breakdown voltage strength (34% increase). With the increasing concentration, the changing withstand voltage tendency was similar to this experiment. The optimal concentration was 0.01 g/L, which is between 0.0006% and 0.004% b/w. The optimal concentration of the untreated TiO<sub>2</sub> nano-modified sample was at 0.006 g/L and presented a 13% withstand voltage increase. The breakdown voltage of the silicon oil-treated TiO<sub>2</sub> nano-modified samples did not show a clear improvement for all concentrations. These results indicated that the surfactant may have affected the withstand voltage strength of the insulating liquid.

In [106], the voltage change tendencies of the different nanoparticle (Al<sub>2</sub>O<sub>3</sub>, TiO<sub>2</sub>, and SiO<sub>2</sub>) samples were laid out. For the TiO<sub>2</sub> nano-modified samples, the optimal concentrations occurred at 0.006 g/L, which is almost equal to 0.0006% b/w. This sample showed a 13% breakdown voltage increase compared with the base sample. All breakdown voltages of the Al<sub>2</sub>O<sub>3</sub> and SiO<sub>2</sub> nano-modified samples were lower than those of the base sample.

In [222], the AC breakdown voltages of mineral-oil-based nano-modified samples with insulating metal oxide nanoparticles (INPS), semi-conductive metal oxide nanoparticles (SNPS), and the conductive metal oxide nanoparticles (CNPS) with 0.05 g/L concentration were presented. The results showed the breakdown voltages of all nano-modified samples increased compared with the base sample, which was 23% for the CNPS sample, 43% for the INPS samples, and 14% for the SNPS

samples. These results showed that the conductivity of the nanoparticles may affect the strength of the withstand voltage enhancement.

The comparison [102] of the AC breakdown voltages of the semi-conductive nanoparticles with the modified transformer oil samples and the base oil sample showed that all nano-modified samples provided higher breakdown voltages than the base sample. With the increasing concentration, the breakdown voltages of nano-modified samples reached a crest and then dropped.

Researchers in [31] and [217] investigated the relation between the breakdown voltages of the mineral-oil-based  $\text{SiO}_2$  nano-modified samples regarding the humidity level. Two specific concentrations were selected in [31], 0.01% and 0.02% b/w. The results showed that, under both 15-ppm and 25-ppm humidity levels, the 0.02%  $\text{SiO}_2$  nano-modified sample provided a higher breakdown voltage than the other samples. These results are different than those shown in [106]. Regarding the experimental conditions and the humidity level effects, more experiments are needed to investigate these results.

The results in [109] compared the mineral-oil-based  $\text{ZrO}_2$  and  $\text{TiO}_2$  nano-modified samples. The concentration was selected from 0.005% to 0.05% b/w. The optimal concentration for the  $\text{TiO}_2$  nano-modified samples was found to be 0.005%, which provided a breakdown voltage improvement of 31.3%. The optimal concentration for the  $\text{ZrO}_2$  nano-modified samples was 0.01%, which provided a breakdown voltage improvement of 22.94%.

In [223], the authors investigated the mineral-oil-based  $\text{TiO}_2$  nano-modified samples for fresh oil and ageing oil (4 and 15 years). The results showed the optimal concentration occurred in 0.003 g/L. All nano-modified samples provided higher breakdown voltages than the base sample. These demonstrated that the nano-modified technique can enhance the dielectric strength of the insulating liquids and have a positive effect for the anti-ageing process.

In [126], the authors investigated the AC breakdown voltage and viscosity of mineral-oil-based fullerene nanofluids. Samples with 0.05% and 0.1% b/w concentrations were tested. The results showed that the 0.1% sample provided a higher breakdown voltage. The concentration was much higher than other published results. A potential reason is that, for other published results, the nanoparticles were metal oxide particles, such as  $\text{Al}_2\text{O}_3$ ,  $\text{TiO}_2$ ,  $\text{SiO}_2$ , and  $\text{ZrO}_2$ . Fullerene (also called

C60) is a type of particle consisting of carbon atoms. Thus, the chemistry structure difference may have affected the optimal concentration of the nano-modified sample.

In this study and in [29], [92], [95], [96], [99], [222] and [223], it has been shown that, with the increase in concentration of nanoparticles, the enhancement of the breakdown voltage started to decrease. The potential reason for these results is that, with an increase in concentration, the nanoparticles in the liquid started to agglomerate and precipitate [194], [195]. This phenomenon will reduce the nanoparticle surface area, which is in touch with the surrounding liquid. A lower nanoparticle surface area will reduce the probability of electron attachment to nanoparticles. Thus, the magnitude of breakdown voltage started to decrease. Agglomeration also will increase the particle size. For relatively high concentrations, large agglomerations can occur and would be treated as a 'large particle'. The nano-modified sample would become a particle contamination sample, and the breakdown voltage would be lower than the base sample. The experimental results of this study and those of [29], [102], [105], [106], [109], [222], [223] coincide with this assumption.

In [81] and [135], the authors developed a model to explain a potential mechanism of the inhibition of the streamer formation and propagation by magnetite nanoparticles. They also indicated that the inherent physical properties of the nanoparticle may affect their capability to catch free electrons, inhibiting the streamer formation and propagation. Based on the theory provided in [81] and [135], the different nano-modified samples provided different dielectric behaviour, which could potentially be explained by the different capabilities to catch the electrons, which means their capability to inhibit the streamer growth and formation is different. With an increase in concentration of nanoparticles, the breakdown voltages of samples with nanoparticles that have a weak inhibition capability would decrease faster than the others, which is another potential reason some nanoparticles were easier to agglomerate than other nanoparticles. Thus, with increasing concentration, these nanoparticles may form a large agglomeration more easily than other nanoparticles, which may also lead the improvement magnitudes of the breakdown voltage to decrease faster than the other samples. The mechanism of the optimal concentration in the insulating liquids is not clearly and fully understood. More experimental and theoretical investigation is needed in further work.

### **4.6.3 Confidence statistical analysis results**

Considering the effects of the number of tested samples on the standard deviation of the breakdown voltage, the accuracy of the improvement of the dielectric withstand voltage strength of the nano-modified samples compared with the base liquid samples must be investigated and confirmed. In this chapter, the statistical analysis was used to calculate the  $\Delta V$  and the 95% CI to describe the statistical difference of the average voltage between the base and nano-modified samples. The optimal concentration of the nano-modified samples, which provided the highest AC breakdown voltage, also provided a significant statistical difference from the base samples. With an increase in nanoparticle concentration (% b/w), the AC breakdown voltages of the nano-modified samples started to drop and became close to the AC breakdown voltage of the base sample. Thus, the  $\Delta V$  of these samples decreased with an increase in the concentration of nanoparticles. In some cases, the AC breakdown voltages of nano-modified samples are higher than those of the base samples, such as in the case of the natural ester sample with 0.5% b/w BN nanoparticles. The lower bound of the CI is lower than zero, which means that the statistical difference between the base and nano-modified samples may not exist; therefore, the improvements of the withstand voltage strength of the tested samples cannot be confirmed.

The results of the confidence analysis showed that the enhancement of the AC breakdown voltage of the nano-modified samples with the optimal concentration of nanoparticles was statistically significant.

# CHAPTER 5

## STANDARD LIGHTNING IMPULSE BREAKDOWN VOLTAGE AND PRE- BREAKDOWN TIME INVESTIGATION

### 5.1 Introduction

Dielectric materials in HV power and pulsed power systems can be stressed not only with AC voltages but also with short HV impulses; therefore, it is important to investigate not only AC breakdown characteristics of the insulating fluids but also their dielectric behaviour under lightning impulse stress. The lightning impulse is an impulse with a rise time of 1.2  $\mu\text{s}$  and a 50  $\mu\text{s}$  fall time (50% from the peak maximum voltage). The pre-breakdown time for both  $\text{TiO}_2$  and BN nano-modified liquids stressed with 1.2/50  $\mu\text{s}$  lightning HV impulses has been measured, and the results and their analysis are presented and discussed in this chapter. In the lightning test experiment, the peak impulse voltage generated by the Marx generator described in Section 3.5 was set to 63 kV. In these series of tests, the pre-breakdown time, breakdown voltage, and streamer velocity of base and nano-modified liquids were obtained and analysed. The Weibull distribution analysis was used in the statistical analysis of the results, which allows the classification of the liquid in accordance with their dielectric behaviour.

All tests were conducted in accordance with the ASTM D3300-00 standard [80]. The peak voltage was fixed to 63 kV. The HV impulses had a standard 1.2/50  $\mu\text{s}$  wave-shape, and the gap between the HV needle and spherical grounded electrode was set to 3 mm. The impulse voltage was measured using an in-house built copper sulphate HV divider and a commercial Tektronix P6015A HV probe. A detailed description of the liquid sample preparation procedure, test cell design, and waveform measurement methodology has been discussed in Chapter 3.

## 5.2 Experimental Procedure

Before starting a serial standard lightning impulse breakdown test, the measurement system should be calibrated to prevent measurement error due to the measurement device setting. To perform this calibration, two P6015A HV probes are connected to the top sphere electrode of the HV divider and the tap electrode of the HV divider, which is close to the bottom and divides the applied voltage to 1/10, respectively.

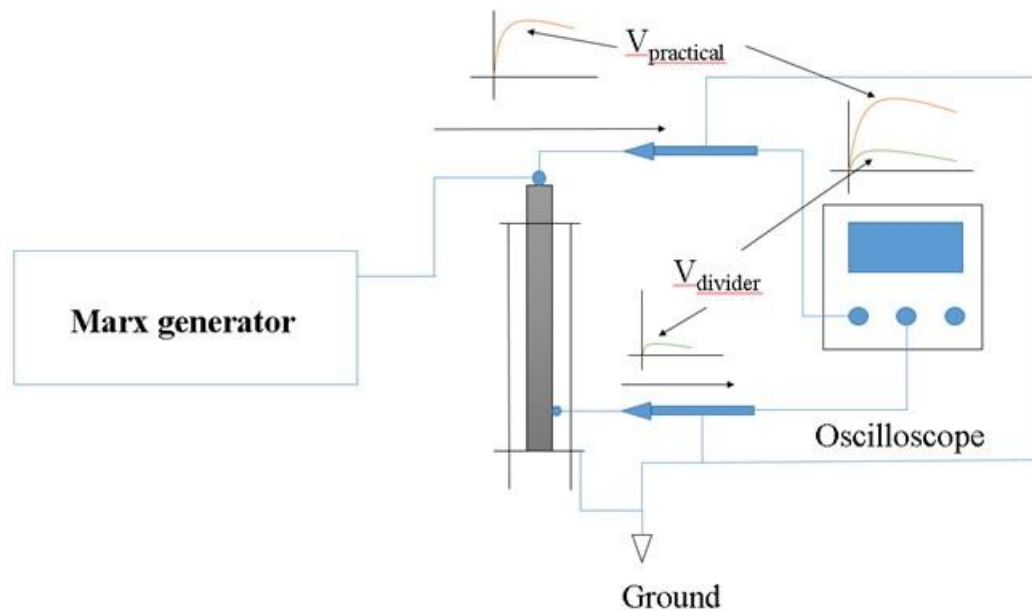


**Figure 5-1.** Calibration system schematic diagram.

A series of measurement impulse voltages were applied on the measurement system. Two probes recorded the practical voltage,  $V_{\text{practical}}$ , and the divider voltage,  $V_{\text{divider}}$ , respectively. The peak voltages of these impulse voltages were lower than the maximum impulse voltage of the HV probe (lower than 40 kV). In practice, the gain value of the applied voltage divided by the record voltage differed slightly depending on the applied voltage level. Thus, it was necessary to calculate the calibration factor. In this study, 10 kV, 12 kV, 14 kV, 16 kV, 18 kV, and 20 kV were used to calibrate the measurement system. The calibration factor of each impulse voltage was calculated using the practical voltages divided by the divider voltages. The final calibration factor was the average value of all calibration factors of each impulse voltage. The calculation equation of the calibration factor is shown below:

$$Factor_{Calibration} = \frac{\frac{V_{practical-1}}{V_{divider-1}} + \frac{V_{practical-2}}{V_{divider-2}} + \frac{V_{practical-3}}{V_{divider-3}} + \dots + \frac{V_{practical-n}}{V_{divider-n}}}{n}, \quad (5.1)$$

where the  $V_{practical-n}$  and  $V_{divider-n}$  are the practical voltage and divider voltage, respectively, for  $n$  case measurement impulses (in this study,  $n$  is six).

The final calibration factor is used to transfer the results recorded by the oscilloscope to the practical voltage, produced by the Marx generator across the test cell.

To compare the sample dielectric properties under the lightning impulse condition, the experimental setting and the applied procedure were the same. The test cell was parallel connected with a load resistor and then connected to the custom-built Marx generator. There is a metal connection ball near the resistor bottom sides. An HV probe connects this metal ball and the oscilloscope. When the breakdown occurs, the waveform details are automatically recorded on the oscilloscope.

Once all devices have been connected properly, the DC power supply starts to charge the Marx generator, and the peak voltage was set to 63 kV, which is a relatively HV to ensure the breakdown could be achieved. There were 30 breakdowns registered for each sample. There were three independent samples tested for each concentration, each nanoparticle, each base insulating liquid, and each polarity. Each point in the figure is an average value of the average pre-breakdown times of the three samples (total 90 breakdown events).

## 5.3 Standard Lightning Impulse Investigation

### 5.3.1 Standard lightning impulse test: TiO<sub>2</sub> nano-modified liquids

In this section, the results of the lightning impulse pre-breakdown tests are provided and discussed. The concentrations of TiO<sub>2</sub> nanoparticles in all three liquids were 0.0006%, 0.004%, 0.01%, 0.05%, and 0.1%. Moreover, base liquids with no nanoparticles were stressed with the lightning impulses, and these results were used as control (baseline) data. The liquids were stressed with 1.2/50  $\mu$ s impulses of both polarities, positive and negative. The typical waveform of the positive and negative impulse breakdown measurements has been shown in Section 3.5.3.

Figures 5-2 and 5-3 show the pre-breakdown times for the three types of liquid as a function of the concentration of  $\text{TiO}_2$  nanoparticles in both positive and negative impulse tests. The results showed that the pre-breakdown time behaved nonlinearly as a function of the nanoparticle concentration. The pre-breakdown time can be regarded as the key parameter in the evaluation of the insulating capability of dielectric liquids stressed with HV impulses. Longer pre-breakdown time means that the insulating liquids have a higher capability to inhibit the initiation and propagation of plasma streamers in such liquids. The optimal concentration of nanoparticles in liquids that provides the longest time until breakdown was obtained and correlated with the breakdown voltages.

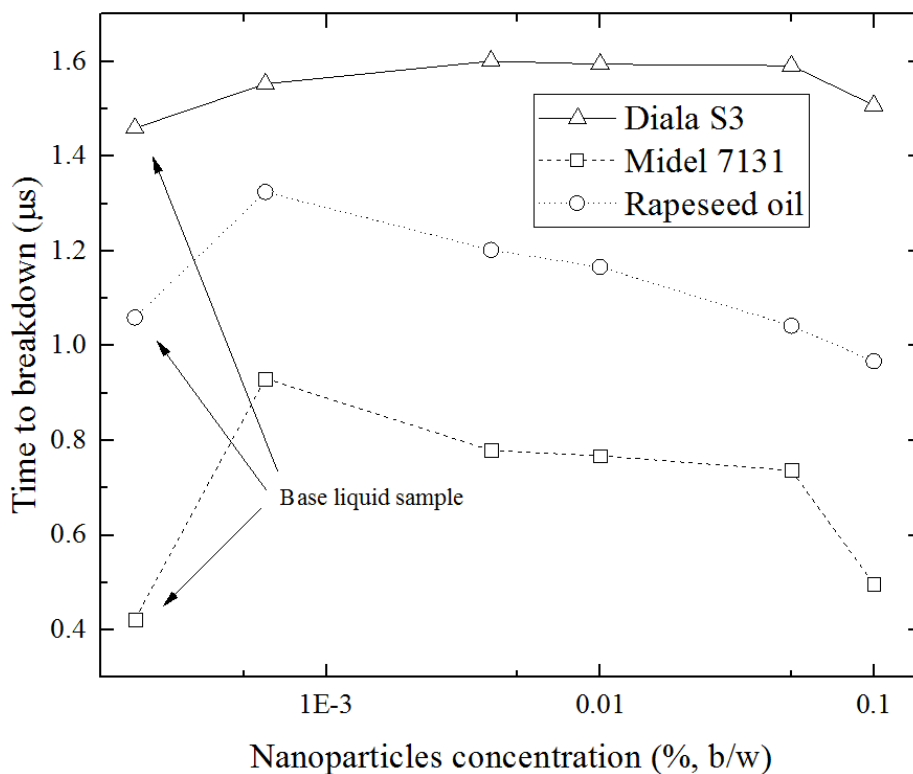


**Figure 5-2.** Pre-breakdown time as a function of the  $\text{TiO}_2$  nanoparticle concentration of different insulating liquids for positive lightning impulses. The lines in this graph are given for visual guidance only.

Figure 5-2 shows the pre-breakdown time as a function of the  $\text{TiO}_2$  nanoparticle concentration in the liquids stressed with positive lightning impulses. As shown in the figure, the optimal concentrations of  $\text{TiO}_2$  nanoparticles for the Midel 7131 ester fluid and the rapeseed natural oil was 0.0006% (b/w). For the Diala S3 mineral oil, the optimal concentration of  $\text{TiO}_2$  nanoparticles was found to be 0.004% (b/w). In the case of 1.2/50  $\mu\text{s}$  impulses with positive polarity, different insulating liquids behaved differently when stressed with the lightning impulses. Diala S3 demonstrated the highest pre-

breakdown time compared with the other liquids. The Midel 7131 synthetic ester liquid had the shortest pre-breakdown time among all tested liquids.

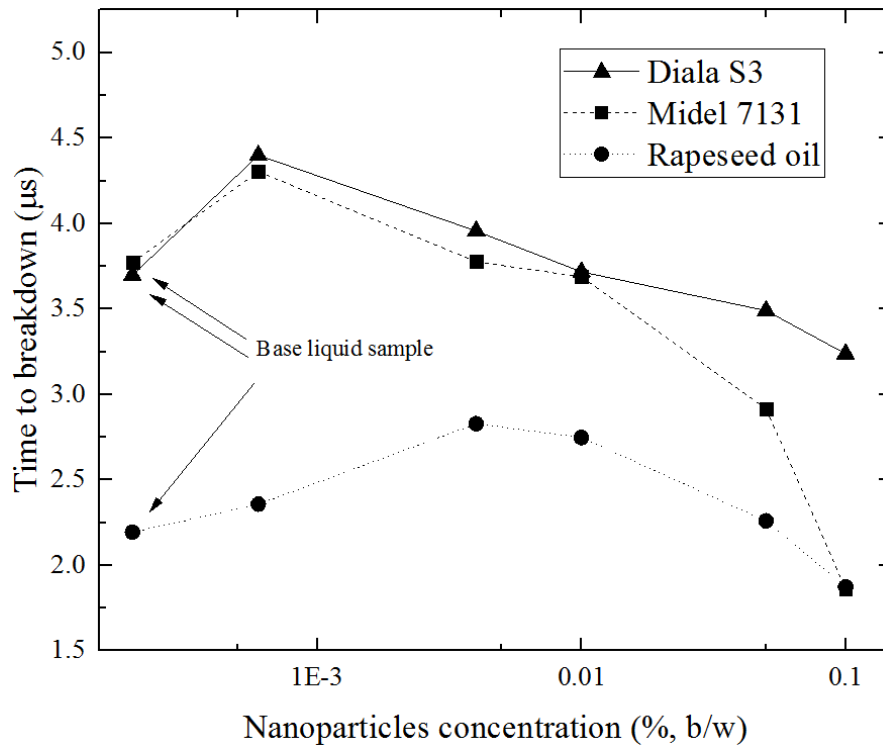


**Figure 5-3.** Pre-breakdown time as a function of the TiO<sub>2</sub> nanoparticle concentration of different insulating liquids for negative lightning impulses. The lines in this graph are given for visual guidance only.

Figure 5-3 shows the pre-breakdown time as a function of the TiO<sub>2</sub> nanoparticle concentration in the liquids stressed with negative lightning impulses. As shown in the figure, the optimal concentration of the TiO<sub>2</sub> nanoparticles for the mineral oil, Diala S3, and synthetic ester, Midel 7131, was 0.0006% (b/w). For the natural ester, rapeseed oil, the optimal concentration of TiO<sub>2</sub> nanoparticles was 0.004% (b/w). In the case of the samples stressed with a negative impulse, two commercial products, Diala S3 and Midel 7131, demonstrated longer pre-breakdown times compared with the rapeseed oil. With an increase in the nanoparticle concentration, the pre-breakdown time of Midel 7131 rapidly became short compared with the other liquids.

Figures 5-4 and 5-5 show the practical breakdown voltages for all tested TiO<sub>2</sub> nanoparticle samples as a function of nanoparticle concentration under both positive and negative 1.2/50 µs impulses with the fixed-peak magnitude of 63 kV.

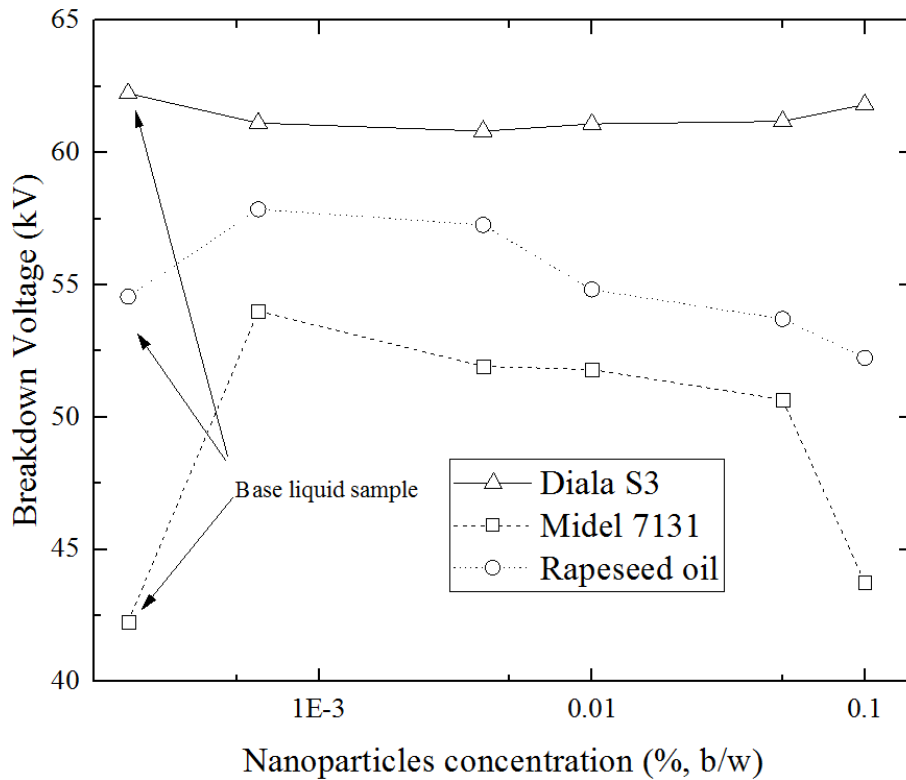


**Figure 5-4.** Breakdown voltage as a function of the TiO<sub>2</sub> nanoparticle concentration for different insulating liquids stressed with positive lightning impulses. The lines in this graph are given for visual guidance only.

In the case of positive impulses, breakdown events for the Diala S3 mineral oil took place at the crest voltage or on a falling slope of the voltage waveform; thus, with increasing pre-breakdown time, the breakdown voltage decreased. For both Midel 7131 ester liquid and rapeseed oil, all breakdowns took place on the rising slope of the voltage waveform; thus, the breakdown voltage increased with an increase in the pre-breakdown time. Figure 5-4 shows the results for positive impulses with the breakdown voltage as a function of the nanoparticle concentration. This figure shows that the breakdown voltage for Diala S3 was almost the same, regardless of the concentration of nanoparticles (although base oil and oil with 0.1% nanoparticles demonstrated a slight increase in the breakdown voltages). For both the Midel 7131 and the rapeseed oil sample, the highest breakdown voltage was observed for samples with a concentration of nanoparticles of 0.0006% (b/w). These results showed a correlation with the results presented in Figure 5-2; the longer pre-breakdown time corresponds to a higher breakdown voltage. As in the case with the positive stress, all breakdown events occurred on the rising slope of the voltage waveform or at the peak voltage.

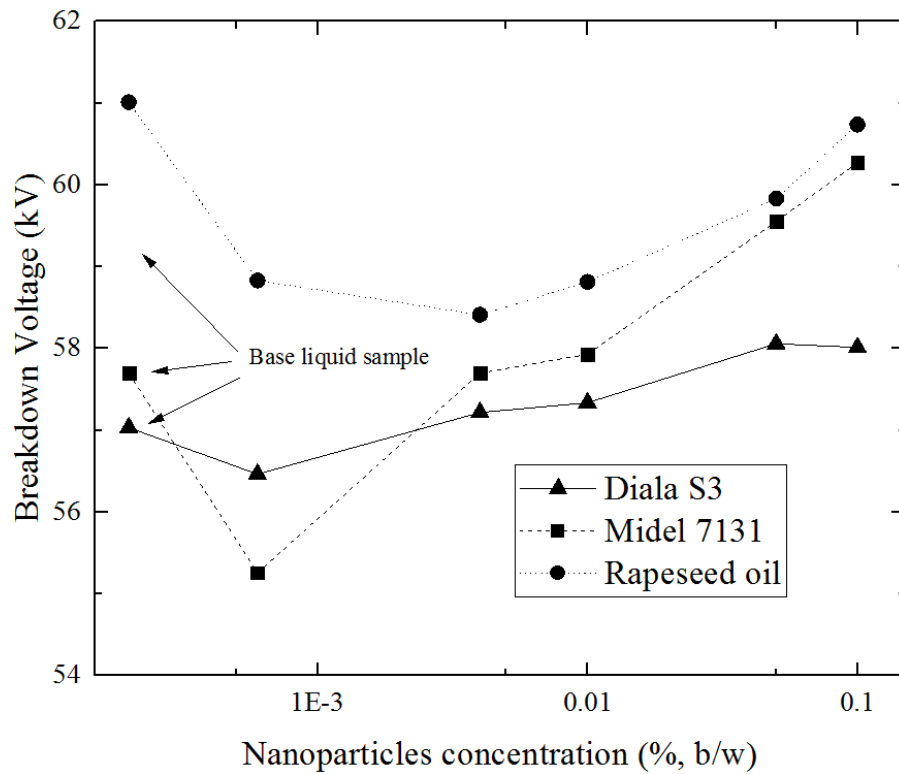


**Figure 5-5.** Breakdown voltage as a function of the TiO<sub>2</sub> nanoparticle concentration of different insulating liquids for negative lightning impulses. The lines in this graph are given for visual guidance only.

The negative impulsive breakdown voltages for the three liquids, as functions of the TiO<sub>2</sub> nanoparticle concentration, are shown in Figure 5-5. In the case of the negative 1.2/50  $\mu$ s voltage waveforms, all breakdown events took place on the falling slope of the impulse; thus, the breakdown voltage decreased with an increase in the pre-breakdown time. As shown in Figure 5-5, the lowest breakdown voltages were observed for the 0.0006% (b/w) concentration of nanoparticles for Diala S3 and Midel 7131 liquids. For rapeseed oil, the lowest voltage was observed for the 0.004% (b/w) concentration. As a correlation with the results presented in Figure 5-3, the pre-breakdown times of the natural ester samples stressed with the negative impulse demonstrated significantly shorter times than the other liquids. This phenomenon demonstrated that the breakdown event of the natural ester mostly took place at a range on the falling slope, close to the crest voltage. Hence, the negative impulse breakdown voltages of natural ester were higher than the negative impulse breakdown voltage of other liquids.

Tables 5-1 and 5-2 show the breakdown voltage and time to breakdown for Diala S3, Midel 7131, and rapeseed oil samples with different TiO<sub>2</sub> nanoparticle concentrations for both positive and negative lightning impulses. The breakdown events during the positive stress took place on the rising slope or

near the crest of the voltage waveform, while the negative breakdowns took place on its peak area or on a falling slope. In these tables, the results are shown in ‘Average pre-breakdown time or average breakdown voltage  $\pm$  its standard deviation’ format.

**Table 5-1.** Breakdown times of three insulating liquids at different concentrations of TiO<sub>2</sub> nanoparticles.

| Concentration by Weight | Positive Time to Breakdown and Its Standard Deviation ( $\mu s$ ) |                 |                 | Negative Time to Breakdown and Its Standard Deviation ( $\mu s$ ) |                 |                 |
|-------------------------|---|-----------------|-----------------|---|-----------------|-----------------|
|                         | Diala S3  | Midel 7131      | Rapeseed Oil    | Diala S3  | Midel 7131      | Rapeseed Oil    |
| 0.00%                   | 1.46 $\pm$ 0.16   | 0.42 $\pm$ 0.1  | 1.06 $\pm$ 0.5  | 3.7 $\pm$ 1.5   | 3.77 $\pm$ 0.64 | 2.19 $\pm$ 0.74 |
| 0.0006%                 | 1.55 $\pm$ 0.17   | 0.93 $\pm$ 0.48 | 1.32 $\pm$ 0.6  | 4.4 $\pm$ 2.18  | 4.3 $\pm$ 1.37  | 2.36 $\pm$ 0.69 |
| 0.004%                  | 1.6 $\pm$ 0.23  | 0.78 $\pm$ 0.43 | 1.2 $\pm$ 0.55  | 3.96 $\pm$ 2.23   | 3.78 $\pm$ 0.71 | 2.83 $\pm$ 0.58 |
| 0.01%                   | 1.59 $\pm$ 0.17   | 0.77 $\pm$ 0.38 | 1.17 $\pm$ 0.62 | 3.72 $\pm$ 1.05   | 3.69 $\pm$ 1.22 | 2.75 $\pm$ 0.48 |
| 0.05%                   | 1.59 $\pm$ 0.17   | 0.74 $\pm$ 0.49 | 1.04 $\pm$ 0.61 | 3.49 $\pm$ 1.81   | 2.92 $\pm$ 1.18 | 2.26 $\pm$ 0.71 |
| 0.1%                    | 1.51 $\pm$ 0.11   | 0.49 $\pm$ 0.22 | 0.96 $\pm$ 0.64 | 3.24 $\pm$ 1.16   | 1.86 $\pm$ 1.12 | 1.87 $\pm$ 0.82 |

**Table 5-2.** Breakdown voltages of three insulating liquids at different concentrations of TiO<sub>2</sub> nanoparticles.

| Concentration by Weight | Positive Breakdown Voltage and Its Standard Deviation (kV) |                  |                  | Negative Breakdown Voltage and Its Standard Deviation (kV) |                  |                  |
|-------------------------|--|------------------|------------------|--|------------------|------------------|
|                         | Diala S3   | Midel 7131       | Rapeseed Oil     | Diala S3   | Midel 7131       | Rapeseed Oil     |
| 0.00%                   | 62.24 $\pm$ 0.28   | 42.25 $\pm$ 5.15 | 54.56 $\pm$ 6.01 | 57.03 $\pm$ 2.69   | 57.7 $\pm$ 1.21  | 61.01 $\pm$ 1.33 |
| 0.0006%                 | 61.12 $\pm$ 0.32   | 54.02 $\pm$ 4.58 | 57.86 $\pm$ 3.52 | 56.46 $\pm$ 3.83   | 55.26 $\pm$ 2.42 | 58.83 $\pm$ 1.28 |
| 0.004%                  | 60.82 $\pm$ 0.33   | 51.29 $\pm$ 7.69 | 57.27 $\pm$ 5.15 | 57.22 $\pm$ 4.09   | 57.7 $\pm$ 1.46  | 58.41 $\pm$ 0.96 |
| 0.01%                   | 61.09 $\pm$ 0.52   | 51.8 $\pm$ 6.65  | 54.82 $\pm$ 6.14 | 57.34 $\pm$ 2.08   | 57.93 $\pm$ 2.53 | 58.82 $\pm$ 1.12 |
| 0.05%                   | 61.18 $\pm$ 0.36   | 50.67 $\pm$ 7.71 | 53.71 $\pm$ 6.89 | 58.06 $\pm$ 2.79   | 59.56 $\pm$ 1.41 | 59.83 $\pm$ 1.19 |
| 0.1%                    | 61.82 $\pm$ 0.4  | 43.74 $\pm$ 8.64 | 52.24 $\pm$ 7.81 | 58.01 $\pm$ 1.91   | 60.27 $\pm$ 1.95 | 60.74 $\pm$ 1.15 |

During the positive lightning impulse, most breakdown events occurred on the rising slope of the impulse where the change in voltage with time has a larger magnitude. For negative energisation, the pre-breakdown time for all liquids was several times longer than the pre-breakdown time for the positive impulse stress. In this case, the breakdown events typically occurred on the falling slope of the lightning impulse where the change in voltage with time was minimal. This difference in the breakdown behaviour of the insulating fluids when stressed with positive and negative impulses can explain the difference in the standard deviations of the time to breakdown for stresses with different polarities.

For positive impulses, pre-breakdown times for all Diala S3-based nanofluid samples had smaller standard deviations compared with the Midel 7131 and vegetable oil-based nanofluids. Additionally,

the pre-breakdown time was almost the same for all Diala S3-based nanofluid samples. The breakdown events primarily took place on the crest of the impulse, and they were almost the same. Thus, the standard deviations of the positive breakdown voltages were smaller than other ester liquids. In the case of negative impulses, the pre-breakdown times for Diala S3 samples were the longest compared with the pre-breakdown times for the other two ester liquids. In some cases, the pre-breakdown times of the Diala S3 sample were significantly longer than the other ester samples. Consequently, the standard deviations of the pre-breakdown times and the breakdown voltages of the Diala S3 samples were larger than the other ester liquids.

In the case of the Midel 7131 and rapeseed oil samples stressed with positive impulses, the pre-breakdown times for samples with all concentrations were shorter than those for mineral oil. The breakdown events took place on the initial or middle period of the impulse rise slope. Thus, the pre-breakdown times and breakdown voltages of the Midel 7131 and rapeseed oil samples had larger standard deviations compared with the mineral oil samples.

For the Midel 7131 and rapeseed oil samples stressed with negative impulse, the breakdown events took place in a small range on the falling slope of the impulse waveform. Hence, the pre-breakdown times and breakdown voltages of Midel 7131 and rapeseed oil samples had smaller standard deviations compared with the mineral oil samples.

### **5.3.2 Standard lightning impulse test: BN nano-modified liquids**

Figures 5-6 and 5-7 show the pre-breakdown times for three types of liquids as a function of the concentration of BN nanoparticles in both positive and negative impulse tests. The results showed that the pre-breakdown time behaved nonlinearly as a function of the nanoparticle concentration, which was similar to that of the TiO<sub>2</sub> samples. The optimal concentration of nanoparticles in liquids that provided the longest time until breakdown was obtained and correlated with the breakdown voltages. In the case of the samples with higher concentrations than the optimal concentration, the pre-breakdown time became short with an increase in concentration.

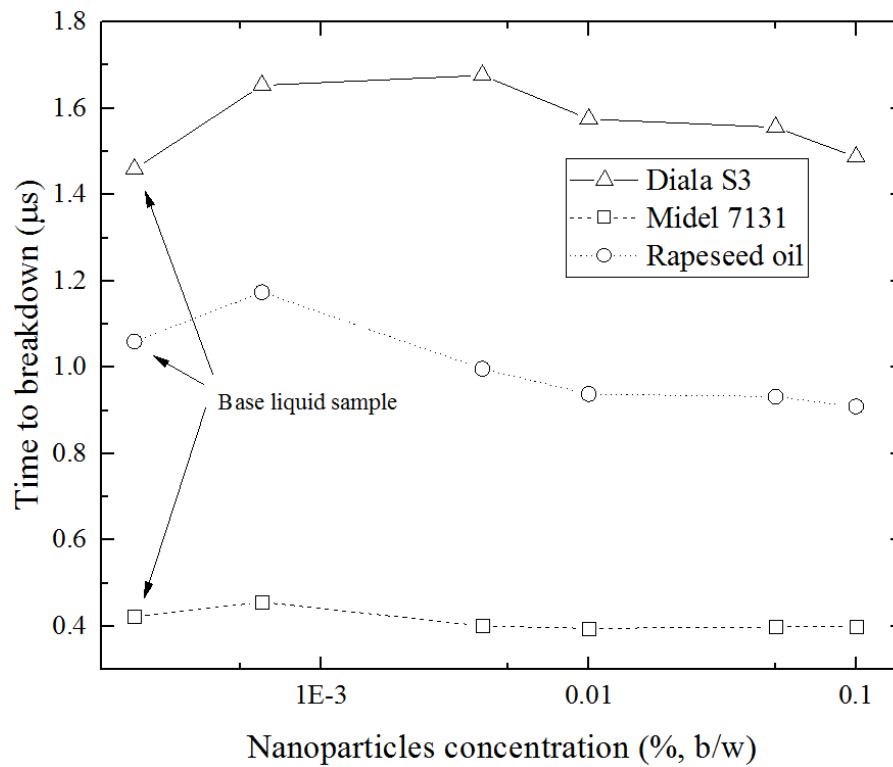


**Figure 5-6.** Pre-breakdown time as a function of the BN nanoparticle concentration of different insulating liquids for positive lightning impulses. The lines in this graph are given for visual guidance only.

Figure 5-6 shows the pre-breakdown time as a function of the BN nanoparticle concentration in the liquids stressed with positive lightning impulses. As shown in the figure, the optimal concentrations of BN nanoparticles for the Midel 7131 ester fluid and the rapeseed natural oil was 0.0006% (b/w). For Diala S3 mineral oil, the optimal concentration of BN nanoparticles was found to be 0.004% (b/w). In the case of the 1.2/50  $\mu$ s impulses with positive polarity, different insulating liquids behaved differently when stressed with the lightning impulses. The Diala S3 demonstrated the highest pre-breakdown time compared with the other liquids. The Midel 7131 synthetic ester liquid had the shortest pre-breakdown time among all tested liquids.

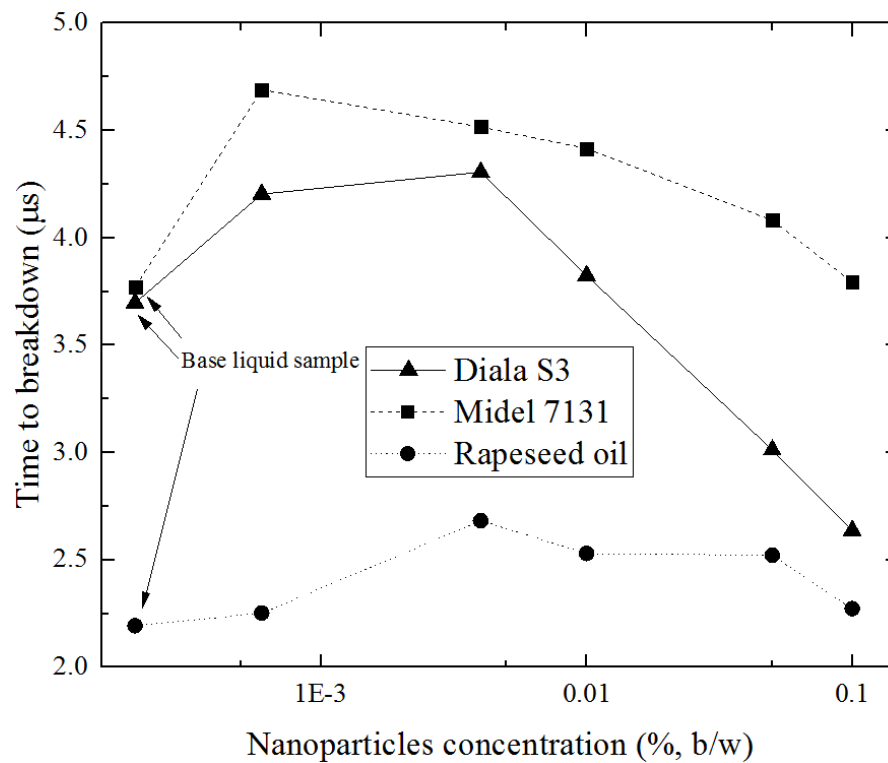


**Figure 5-7.** Pre-breakdown time as a function of the BN nanoparticle concentration of different insulating liquids for negative lightning impulses. The lines in this graph are given for visual guidance only.

Figure 5-7 shows the negative pre-breakdown time of the three liquids as a function of the BN nanoparticle concentration. The optimal concentration of BN nanoparticles for the Midel 7131 ester fluid was 0.0006% (b/w). For Diala S3 mineral oil and the rapeseed natural oil, the optimal concentration of BN nanoparticles was found to be 0.004% (b/w). In the case of the samples stressed with the negative impulse, two commercial products, Diala S3 and Midel 7131, demonstrated longer pre-breakdown times compared with the rapeseed oil. With an increase with the nanoparticle concentration, the pre-breakdown time of the mineral oil rapidly became short compared with the other liquids.

Figures 5-8 and 5-9 show the practical breakdown voltages for all tested BN nanoparticle samples as a function of the nanoparticle concentration under both positive and negative 1.2/50  $\mu$ s impulses with the fixed-peak magnitude of 63 kV.

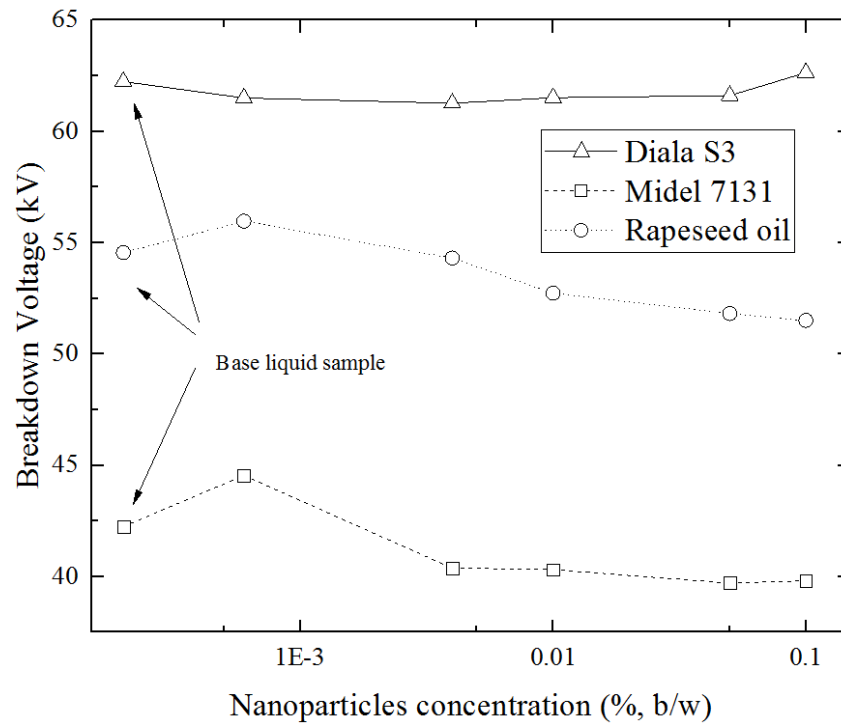


**Figure 5-8.** Breakdown voltage as a function of the BN nanoparticle concentration of different insulating liquids for positive lightning impulses. The lines in this graph are given for visual guidance only.

In the case of positive impulses, the breakdown events for the Diala S3 mineral oil took place at the crest voltage or on a falling slope of the voltage waveform; thus, with increasing pre-breakdown time, the breakdown voltage decreased. For both Midel 7131 ester liquid and the rapeseed oil, all breakdowns took place on the rising slope of the voltage waveform; thus, the breakdown voltage increased with an increase in the pre-breakdown time. Figure 5-8 shows the results for the positive impulses with the breakdown voltage as a function of the nanoparticle concentration. This figure shows that the breakdown voltage for Diala S3 was almost the same regardless of the concentration of nanoparticles (although base oil and oil with 0.1% nanoparticles demonstrated a slight increase in the breakdown voltages). For both the Midel 7131 and rapeseed oil samples, the highest breakdown voltage was observed for samples with a concentration of nanoparticles at 0.0006% (b/w). These results showed a correlation with the results presented in Figure 5-6; the longer pre-breakdown time corresponds to a higher breakdown voltage. As in the case of the positive stress, all breakdown events occurred on the rising slope of the voltage waveform or at the peak voltage.

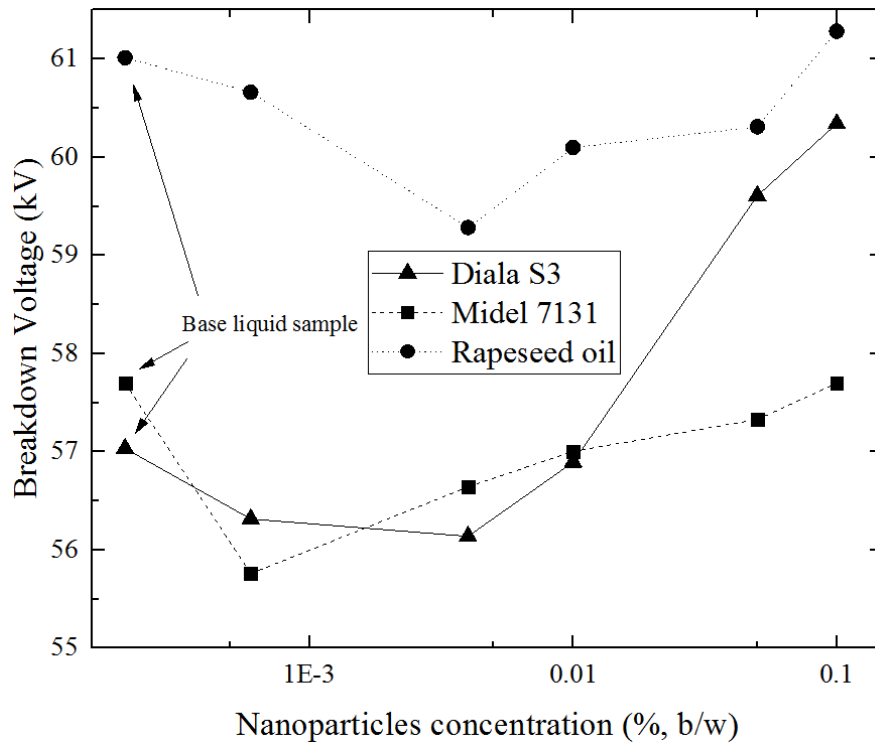


**Figure 5-9.** Breakdown voltage as a function of the BN nanoparticle concentration of different insulating liquids for negative lightning impulses. The lines in this graph are given for visual guidance only.

The negative impulse breakdown voltages for the three liquids, as functions of the BN nanoparticle concentration, are shown in Figure 5-9. For the negative 1.2/50  $\mu$ s voltage waveforms, all breakdown events took place on the falling slope of the impulse; thus, the breakdown voltage decreased with an increase in the pre-breakdown time. As shown in Figure 5-9, the lowest breakdown voltages were observed for the 0.0006% b/w concentration of nanoparticles for Diala S3 and Midel 7131 liquids. For rapeseed oil, the lowest voltage was observed for 0.004% b/w concentration. As a correlation with the results presented in Figure 5-7, the pre-breakdown times of natural ester samples stressed with the negative impulse were significantly shorter than those of the other liquids. This phenomenon indicates that the breakdown event of the natural ester tended to take place at a range on the falling slope, close to the crest voltage. Hence, the negative impulse breakdown voltages of natural ester were higher than the other liquids.

Tables 5-3 and 5-4 show the time to breakdown and the breakdown voltage for Diala S3, Midel 7131, and rapeseed oil samples with different BN nanoparticle concentrations for both positive and negative lightning impulses. Typically, the positive breakdowns took place on the rising slope or near the crest

of the voltage waveform, while the negative breakdowns took place on its peak area or falling slope.

In these tables, the results were shown as ‘average value  $\pm$  standard deviation’.

**Table 5-3.** Breakdown time of three insulating liquids with different concentrations of BN nanoparticles.

| Concentration<br>by Weight | Positive Time to Breakdown Its Standard Deviation ( $\mu s$ ) |                 |                 | Negative Time to Breakdown Its Standard Deviation ( $\mu s$ ) |                 |                 |
|----------------------------|---|-----------------|-----------------|---|-----------------|-----------------|
|                            | Diala S3  | Midel 7131      | Rapeseed Oil    | Diala S3  | Midel 7131      | Rapeseed Oil    |
| 0.00%                      | 1.46 $\pm$ 0.16   | 0.42 $\pm$ 0.1  | 1.06 $\pm$ 0.5  | 3.7 $\pm$ 1.51  | 3.77 $\pm$ 0.64 | 2.19 $\pm$ 0.74 |
| 0.0006%                    | 1.65 $\pm$ 0.11   | 0.46 $\pm$ 0.12 | 1.17 $\pm$ 0.73 | 4.2 $\pm$ 1.45  | 4.69 $\pm$ 0.85 | 2.25 $\pm$ 0.66 |
| 0.004%                     | 1.68 $\pm$ 0.15   | 0.4 $\pm$ 0.11  | 1 $\pm$ 0.63    | 4.31 $\pm$ 1.45   | 4.52 $\pm$ 0.84 | 2.68 $\pm$ 0.63 |
| 0.01%                      | 1.58 $\pm$ 0.11   | 0.39 $\pm$ 0.12 | 0.94 $\pm$ 0.67 | 3.82 $\pm$ 1.5  | 4.42 $\pm$ 0.66 | 2.53 $\pm$ 0.79 |
| 0.05%                      | 1.56 $\pm$ 0.08   | 0.4 $\pm$ 0.13  | 0.93 $\pm$ 0.73 | 3.01 $\pm$ 0.61   | 4.08 $\pm$ 0.93 | 2.52 $\pm$ 0.71 |
| 0.1%                       | 1.49 $\pm$ 0.12   | 0.4 $\pm$ 0.1   | 0.91 $\pm$ 0.68 | 2.64 $\pm$ 0.57   | 3.79 $\pm$ 0.9  | 2.27 $\pm$ 0.72 |

**Table 5-4.** Breakdown voltage of three insulating liquids with different concentrations of BN nanoparticles.

| Concentration<br>by Weight | Positive Breakdown Voltage Its Standard Deviation (kV) |                  |                  | Negative Breakdown Voltage Its Standard Deviation (kV) |                  |                  |
|----------------------------|--|------------------|------------------|--|------------------|------------------|
|                            | Diala S3   | Midel 7131       | Rapeseed Oil     | Diala S3   | Midel 7131       | Rapeseed Oil     |
| 0.00%                      | 62.24 $\pm$ 0.28                                       | 42.25 $\pm$ 5.15 | 54.56 $\pm$ 6.01 | 57.03 $\pm$ 2.69                                       | 57.7 $\pm$ 1.21  | 61.01 $\pm$ 1.33 |
| 0.0006%                    | 61.5 $\pm$ 0.29  | 44.55 $\pm$ 6.97 | 55.97 $\pm$ 9.6  | 56.32 $\pm$ 2.37                                       | 55.76 $\pm$ 1.35 | 60.66 $\pm$ 1    |
| 0.004%                     | 61.27 $\pm$ 0.24                                       | 40.38 $\pm$ 8.55 | 54.31 $\pm$ 6.32 | 56.14 $\pm$ 2.37                                       | 56.64 $\pm$ 1.5  | 59.28 $\pm$ 3.86 |
| 0.01%                      | 61.52 $\pm$ 0.28                                       | 40.31 $\pm$ 7.08 | 52.73 $\pm$ 6.82 | 56.89 $\pm$ 2.41                                       | 57 $\pm$ 1.5     | 60.1 $\pm$ 1.15  |
| 0.05%                      | 61.62 $\pm$ 0.22                                       | 39.71 $\pm$ 7.03 | 51.82 $\pm$ 7.42 | 59.61 $\pm$ 1.04                                       | 57.33 $\pm$ 1.62 | 60.31 $\pm$ 1.11 |
| 0.1%                       | 62.64 $\pm$ 0.18                                       | 39.81 $\pm$ 7.39 | 51.51 $\pm$ 6.31 | 60.34 $\pm$ 1.2  | 57.7 $\pm$ 1.46  | 61.28 $\pm$ 1.87 |

In the case of the positive lightning impulse, most breakdown events occurred on the rising slope of the impulse where the change in voltage with time was at a large magnitude. For negative energisation, the pre-breakdown time for all liquids was several times longer than the pre-breakdown time for the positive impulse stress. In this case, the breakdown events typically occurred on the falling slope of the lightning impulse where the change in voltage with time was minimal. This difference in the breakdown behaviour of the insulating fluids when stressed with positive and negative impulses can explain the difference in the standard deviations of the time to breakdown for stresses with different polarities.

For positive impulses, pre-breakdown times for all Diala S3-based nanofluid samples had smaller standard deviations compared with the Midel 7131 and vegetable oil-based nanofluids. Additionally, the pre-breakdown time was almost the same for all Diala S3-based nanofluid samples. The breakdown events primarily took place on the crest of the impulse and were almost the same. Thus,

the standard deviations of the positive breakdown voltages were smaller than those of the other ester liquids.

In the case of negative impulses, pre-breakdown times for Diala S3 samples were the longest compared with the pre-breakdown times for other two ester liquids. In some cases, the pre-breakdown times of the Diala S3 samples were significantly longer than those of the other ester samples. Consequently, the standard deviations of the pre-breakdown times and the breakdown voltages of the Diala S3 samples were larger than those of other ester liquids.

In the case of the Midel 7131 and rapeseed oil samples stressed with the positive impulse, the pre-breakdown times for samples with all concentrations were shorter than those for mineral oil. The breakdown events took place on the initial or middle period of the impulse rise slope. Thus, the pre-breakdown times and breakdown voltages of the Midel 7131 and rapeseed oil samples have larger standard deviations compared with those of the mineral oil samples.

For the Midel 7131 and rapeseed oil samples stressed with the negative impulse, the breakdown events took place in a small range on the falling slope of the impulse waveform. Hence, the pre-breakdown times and breakdown voltages of the Midel 7131 and rapeseed oil samples had smaller standard deviations compared with the mineral oil samples.

### **5.3.3 Streamer velocity in nano-modified liquids**

Average velocities of pre-breakdown streamers in insulating liquids can be calculated by dividing the inter-electrode distance by the pre-breakdown time (5.1):

$$v = \frac{d}{t}, \quad (5.1)$$

where  $d$  is the gap distance between electrodes, and  $t$  is the pre-breakdown time recorded during the test.

These average velocities were calculated using the pre-breakdown times given in Tables 5-5 and 5-6 for TiO<sub>2</sub> and BN nano-modified liquids and shown in Figures 5-10 to 5-13 as functions of the nanoparticle concentrations. In the case of the positive impulsive breakdown voltage, the streamers were “positive” streamers and vice versa.

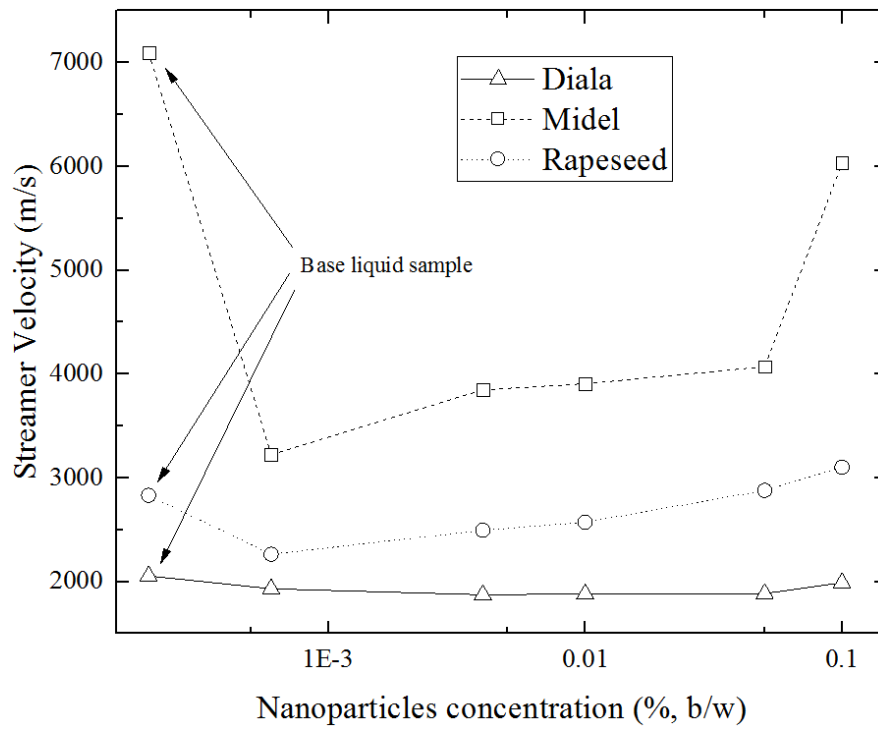


**Figure 5-10.** Average positive streamer velocities in TiO<sub>2</sub> nano-modified liquids as a function of the particle concentration. The lines in this graph are given for visual guidance only.

Figure 5-10 shows the average velocity of the positive streamers in the TiO<sub>2</sub> nano-modified liquids. This graph shows that the streamer velocities were different in different liquids and were nonlinear functions of the particle concentration. In the case of the Midel 7131 and rapeseed oil, the slowest velocity was observed for the concentration at 0.0006% (b/w). In the case of the Diala S3 samples, the slowest positive streamer velocity was observed for samples with a concentration of 0.004% b/w.

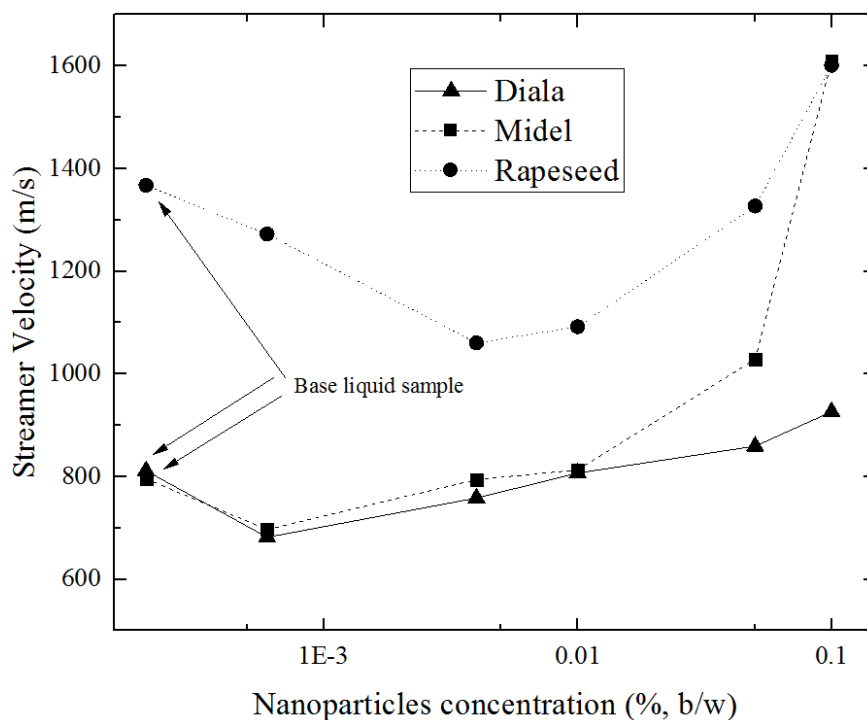


**Figure 5-11.** Average negative streamer velocities in TiO<sub>2</sub> nano-modified liquids as a function of the particle concentration. The lines in this graph are given for visual guidance only.

Figure 5-11 shows the average velocity of the negative streamers in the TiO<sub>2</sub> nano-modified liquids. This graph shows that the streamer velocities were different in different liquids and were nonlinear functions of the particle concentration. In the case of the Diala S3 and Midel 7131 samples, the slowest velocity was observed for the concentration of 0.0006% (b/w). In the case of the rapeseed oil, the slowest positive streamer velocity was observed for samples with a concentration of 0.004% b/w.

**Table 5-5.** Positive and negative streamer velocity of the samples with TiO<sub>2</sub> nanoparticles.

| TiO <sub>2</sub> Sample Streamer Velocity (m/s) |          |            |              |
|---|----------|------------|--------------|
| Positive  |          |            |              |
| Concentration                                   | Diala S3 | Midel 7131 | Rapeseed Oil |
| 0.00%   | 2055     | 7098       | 2831         |
| 0.0006%   | 1931     | 3223       | 2264         |
| 0.004%  | 1874     | 3848       | 2494         |
| 0.01%   | 1881     | 3906       | 2572         |
| 0.05%   | 1885     | 4071       | 2879         |
| 0.1%  | 1989     | 6033       | 3102         |
| Negative  |          |            |              |
| Concentration                                   | Diala S3 | Midel7131  | Rapeseed Oil |
| 0.00%   | 811      | 795        | 1367         |
| 0.0006%   | 681      | 696        | 1272         |
| 0.004%  | 758      | 794        | 1060         |
| 0.01%   | 806      | 813        | 1092         |
| 0.05%   | 859      | 1028       | 1327         |
| 0.1%  | 926      | 1610       | 1601         |

Midel 7131 provided the fastest positive streamer velocity, while the positive streamers in Diala S3 had the slowest velocity. The positive streamer velocities for all Diala S3-based nano-modified liquids were close to ~2 km/s. The positive streamer velocities for all rapeseed samples were in the range

from 2 km/s to 3 km/s. For Midel 7131, the positive streamer in the base liquid had the highest average velocity at more than 7 km/s; the streamer velocity in liquids with the nanoparticle concentration of 0.1% was higher than 6 km/s. For liquids with other concentrations of nanoparticles (0.0006%, 0.004%, 0.01%, and 0.05%), the streamer velocities were in the range between 3 km/s and 4 km/s. This phenomenon means the TiO<sub>2</sub> nanoparticle showed an enhancement effect on the inhibition of the positive streamer propagation.

For all test liquids, the average velocities of the negative streamers were typically several times lower than the average velocities of the positive streamers. The reason for this difference in the velocities of the positive and negative streamers is the negative space charge that results in the field screening in front of the negatively energised HV point electrode and the streamer itself, which also can explain the difference in the breakdown voltages for the positive and negative energisation. The negative breakdown voltage is higher than the positive breakdown voltage.

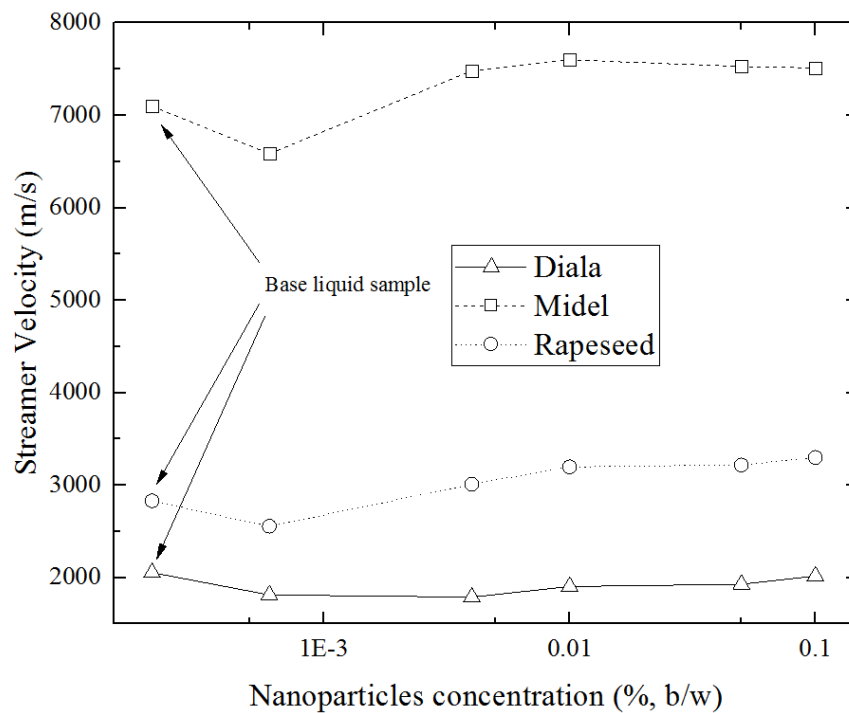


**Figure 5-12.** Average positive streamer velocities in the BN nano-modified liquids as a function of the particle concentration. The lines in this graph are given for visual guidance only.

Figure 5-12 shows the average velocity of the positive streamers in the BN nano-modified liquids. This graph shows that the streamer velocities were different in the different liquids and were nonlinear functions of the particle concentration. In the case of the Midel 7131 and rapeseed oil samples, the

slowest velocity was observed for the concentration of 0.0006% (b/w). In the case of the Diala S3 samples, the slowest positive streamer velocity was observed for samples with a concentration of 0.004% b/w.

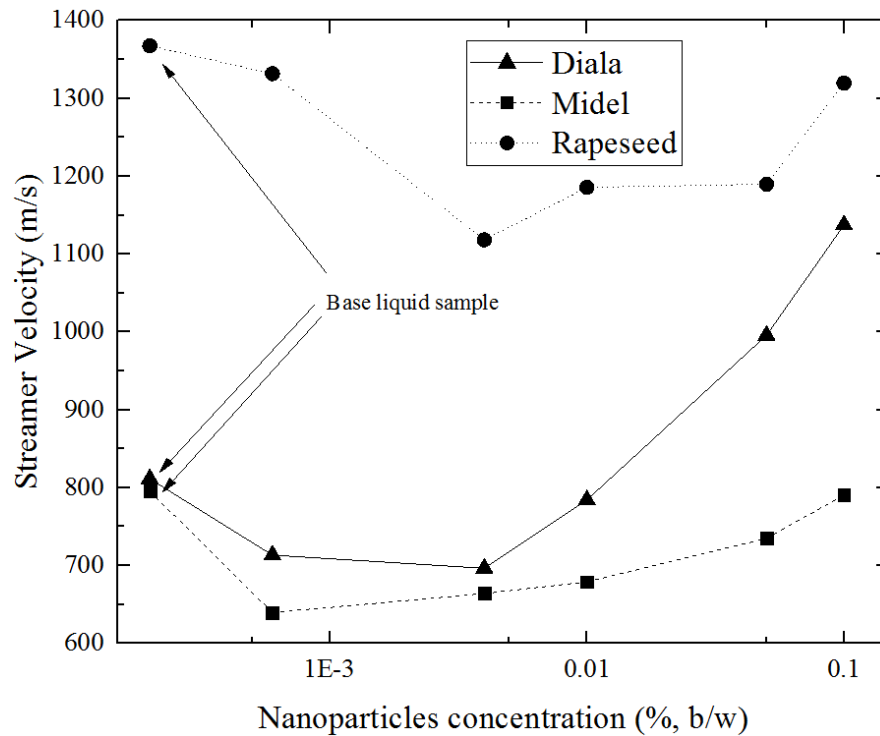


**Figure 5-13.** Average positive streamer velocities in the BN nano-modified liquids as a function of the particle concentration. The lines in this graph are given for visual guidance only.

Figure 5-13 shows the average velocity of the negative streamers in the BN nano-modified liquids. This graph shows that the streamer velocities were different in the different liquids and were nonlinear functions of the particle concentration. In the case of the Midel 7131 samples, the slowest velocity was observed for the concentration of 0.0006% (b/w). In the case of the Diala S3 and rapeseed oil samples, the slowest positive streamer velocity was observed for samples with a concentration of 0.004% b/w.

Midel 7131 provided the fastest positive streamer velocity, while the positive streamers in Diala S3 had the slowest velocities. The positive streamer velocities for all Diala S3-based nano-modified liquids were close to ~2 km/s. The positive streamer velocities for all rapeseed samples were in the range between 2.5 km/s and 3.5 km/s. For Midel 7131, the positive streamers in the base liquid had the highest average velocity of more than 7.5 km/s. The streamer velocity in liquids with all concentrations was higher than 6.5 km/s, which was significantly different from Midel 7131 samples

with TiO<sub>2</sub> nanoparticles. This phenomenon demonstrated that the BN nanoparticles did not show an obvious enhancement effect on the inhibition of the positive streamer propagation.

Similar to the samples with the TiO<sub>2</sub> nanoparticles, the average velocities of the negative streamers in the samples with BN nanoparticles were typically several times lower than the average velocities of the positive streamers. The potential reason was discussed above.

**Table 5-6.** Positive and negative streamer velocity of the samples with BN nanoparticles.

| <b>BN Sample Streamer Velocity (m/s)</b> |                 |                   |                     |
|--|-----------------|-------------------|---------------------|
| <b>Positive</b>                          |                 |                   |                     |
| <b>Concentration</b>                     | <b>Diala S3</b> | <b>Midel 7131</b> | <b>Rapeseed Oil</b> |
| 0.00%                                    | 2055            | 7098              | 2831                |
| 0.0006%                                  | 1814            | 6585              | 2555                |
| 0.004%                                   | 1789            | 7481              | 3010                |
| 0.01%                                    | 1904            | 7601              | 3199                |
| 0.05%                                    | 1928            | 7529              | 3218                |
| 0.1%                                     | 2017            | 7512              | 3299                |
| <b>Negative</b>                          |                 |                   |                     |
| <b>Concentration</b>                     | <b>Diala S3</b> | <b>Midel 7131</b> | <b>Rapeseed Oil</b> |
| 0.00%                                    | 811             | 795               | 1367                |
| 0.0006%                                  | 713             | 639               | 1331                |
| 0.004%                                   | 696             | 664               | 1118                |
| 0.01%                                    | 784             | 679               | 1185                |
| 0.05%                                    | 995             | 734               | 1189                |
| 0.1%                                     | 1137            | 790               | 1319                |

## **5.4 Weibull Analysis of Pre-breakdown Times for Standard Lightning Impulses**

In this chapter, the Weibull statistical analysis was used to analyse the failure time of the liquid samples. This statistic was used in the analysis of the pre-breakdown times for the nano-modified liquids obtained in the standard lightning tests. This approach to the statistical analysis of the impulse pre-breakdown time was used in [29], [31], [40], [94], [126], [212], and [215]–[217]. By performing the Weibull analysis, the time to breakdown according to the probability to breakdown can be evaluated. Considering the practical design requirements for power transformers and the power grid, it is important to coordinate the dielectric insulation to maximise the time to breakdown for a low breakdown probability. The details of the Weibull distribution were discussed in Section 2.5.

$$F(t) = 1 - e^{-\left(\frac{t-\gamma}{\alpha}\right)^\beta} \quad (5.1)$$

In this equation,  $F(t)$  is the cumulative probability distribution function of the failure time events, where  $t$  is the pre-breakdown time in this section. As usual,  $\alpha$  is the scale parameter, while  $\beta$  is the shape parameter, and  $\gamma$  is the location parameter.

In this section, the location parameter  $\gamma$  is the minimum pre-breakdown time which provides the non-zero breakdown probability while  $\alpha$  is the scale parameter of the Weibull distribution. In the case in which  $\gamma$  is zero (two-parameter Weibull distribution),  $\alpha$  is where the pre-breakdown time has a 63.2% probability to breakdown. The shape parameter  $\beta$  indicates that how sensitive the probability to breakdown of the insulating liquid is to an increase in pre-breakdown time. All Weibull analyses were performed using Microsoft Excel and Origin Pro 2015.

#### **5.4.1 Weibull analysis of pre-breakdown times in TiO<sub>2</sub> nano-modified liquids**

Figures 5-14 to 5-16 show the Weibull analysis results of mineral oil, synthetic ester, and natural ester with TiO<sub>2</sub> nanoparticle stressed with a positive impulse. The scale, shape, and location parameters and the 5%, 10%, 50%, and 90% probabilities of the time to breakdown the TiO<sub>2</sub> nanoparticle modified mineral oil, synthetic ester, and natural ester samples under a positive polarity impulse are shown in Table 5-7.

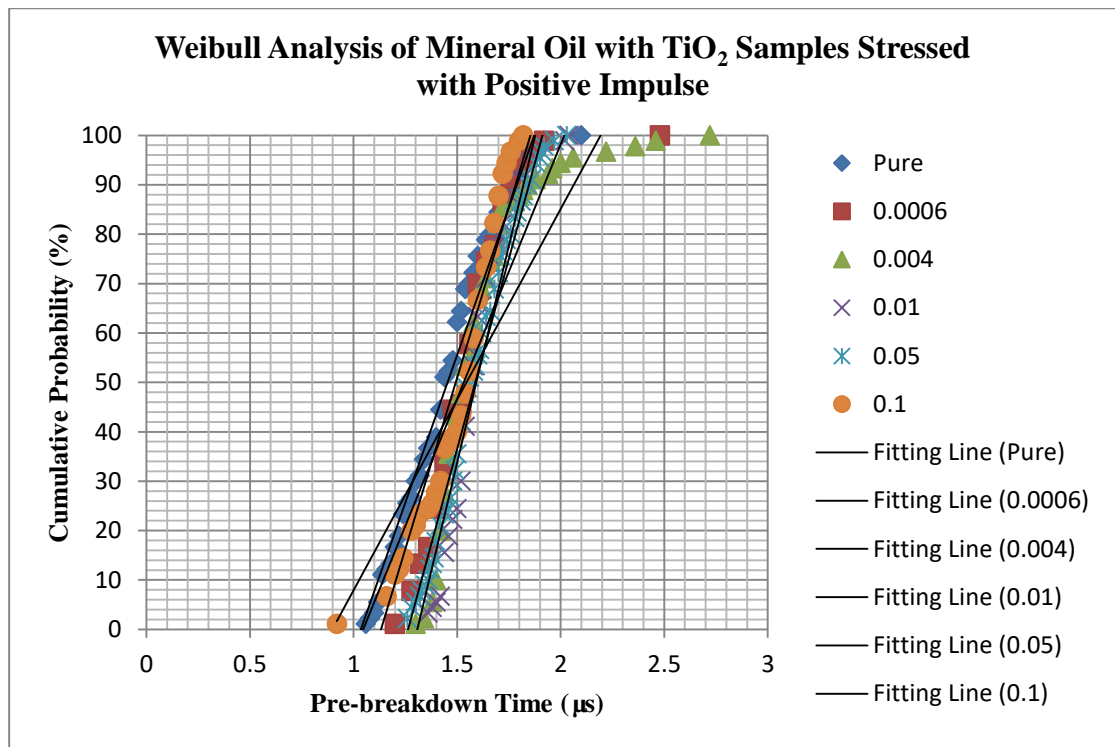


**Figure 5-14.** Weibull analysis of mineral oil with TiO<sub>2</sub> nanoparticles stressed with a positive impulse.

For the mineral-oil-based nano-modified samples, the longest 5% pre-breakdown time was obtained in the case of the 0.004% and 0.01% (b/w) concentrations. The longest 10% and 50% pre-breakdown times were obtained for the sample with a nanoparticle concentration of 0.01% (b/w). The longest 90% pre-breakdown time was obtained in the 0.004% concentration. It was found that, in the case of positive energisation, the 0.004% (b/w) concentration of TiO<sub>2</sub> nanoparticles provided the highest location parameter, the highest scale parameter, and the lowest shape parameter. The largest location parameter means that the minimum pre-breakdown time was the longest compared with nanofluids of other concentrations. The highest scale parameter means the pre-breakdown time had a wider spread than other samples, which can explain the high standard deviation shown in Section 5.3.1. The lowest shape parameter indicated that the mineral oil sample with 0.004% (b/w) concentration provided a better stability and low failure rate with an increase in pre-breakdown time compared with other samples.

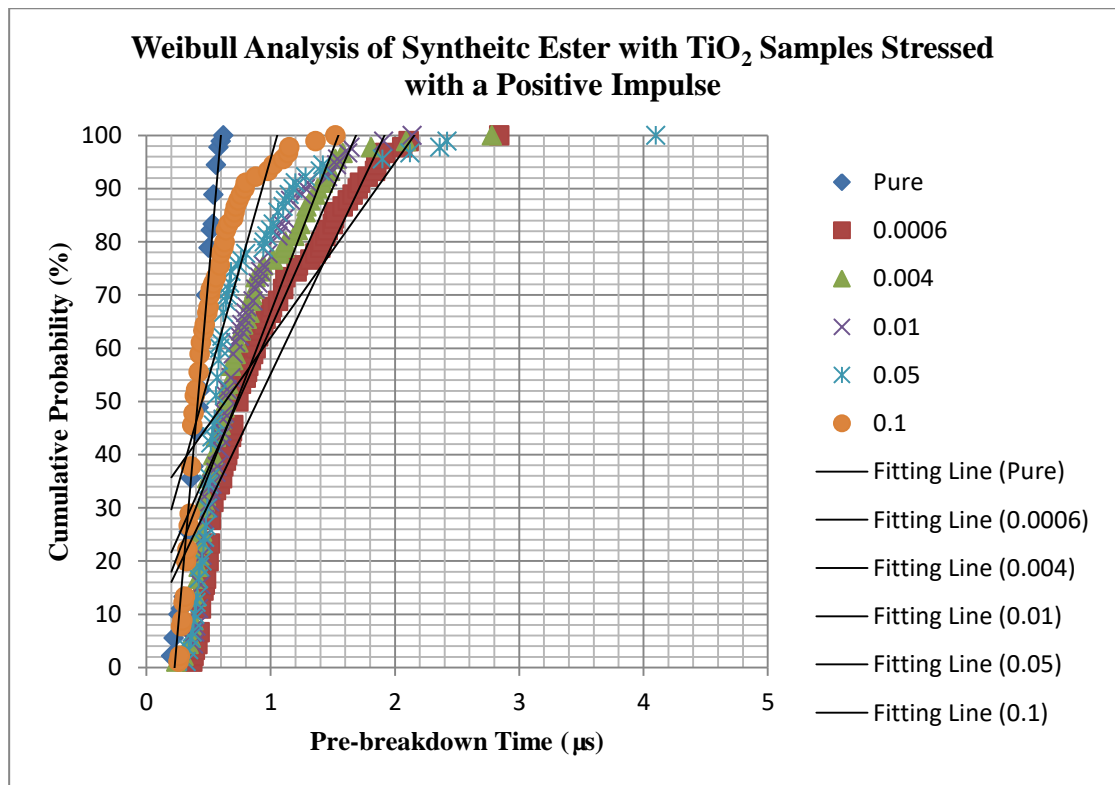


**Figure 5-15.** Weibull analysis of synthetic ester with TiO<sub>2</sub> nanoparticles stressed with a positive impulse.

For the synthetic ester nano-modified samples, the longest pre-breakdown times corresponding to all the breakdown probabilities were obtained in the case of the 0.0006% (b/w) concentration. The sample with the 0.0006% (b/w) concentration of TiO<sub>2</sub> nanoparticles provided the largest location parameter and the highest scale parameter. The largest location parameter indicated that the minimum pre-breakdown time was the longest compared with the nanofluids with other particle concentrations. The highest scale parameter indicated that the pre-breakdown time had a wider spread than in the other samples. The shape parameter of the sample with 0.0006% (b/w) concentration TiO<sub>2</sub> of nanoparticles was at the middle level of all synthetic ester tested samples.

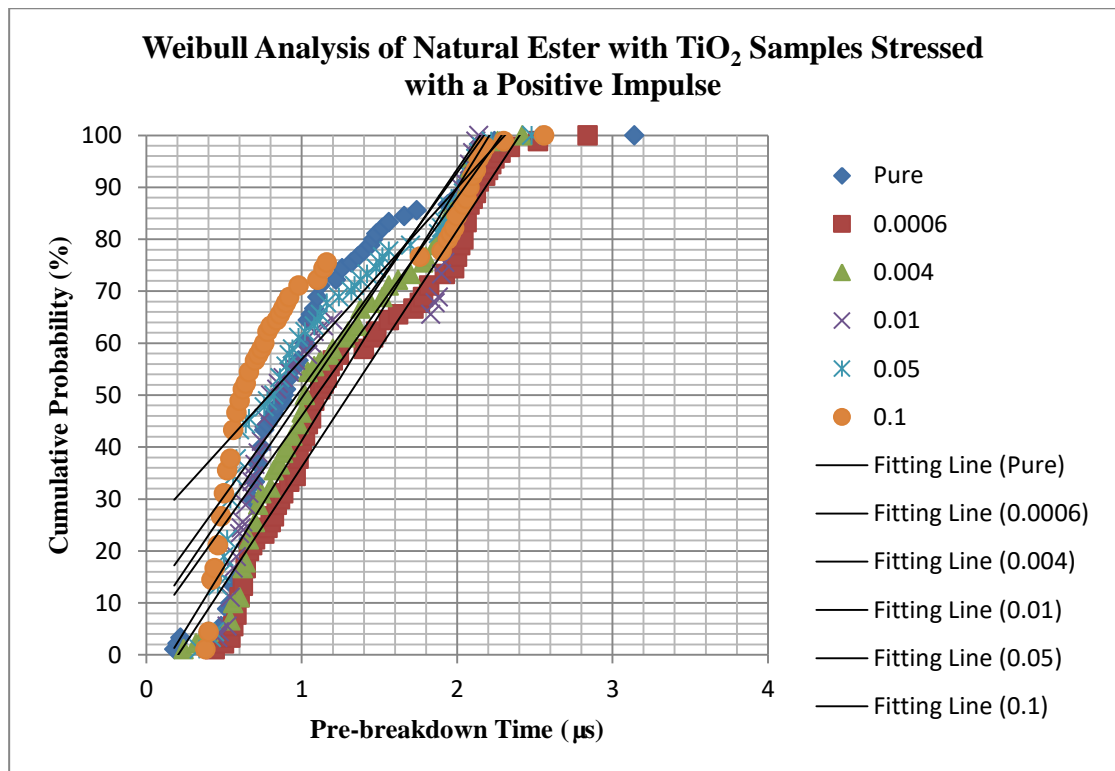


**Figure 5-16.** Weibull analysis of natural samples with TiO<sub>2</sub> nanoparticles stressed with positive impulses.

For the natural ester nano-modified samples, the longest pre-breakdown times corresponding to all the breakdown probabilities were obtained in the case of the 0.0006% (b/w) concentration. It was found that, in the case of positive energisation, the 0.0006% (b/w) concentration of TiO<sub>2</sub> nanoparticles provided the highest location parameter, the highest scale parameter, and the highest shape parameter. As discussed above, the highest location parameter and scale parameter means the sample with 0.0006% (b/w) nanoparticles provided the longest minimum pre-breakdown time, and these pre-breakdown times had a wider spread compared with other samples. The high shape parameter indicated that, for the sample with 0.0006% (b/w) nanoparticles, the failure probability (in this case, the breakdown probability) will rapidly increase with an increase in the pre-breakdown time. Hence, these results showed, in the case of positive energisation, that the natural ester with 0.0006% (b/w) concentration of TiO<sub>2</sub> nanoparticles provided the longest initial pre-breakdown time, but poor stability with an increase in the pre-breakdown time.

**Table 5-7.** All three Weibull parameters for all TiO<sub>2</sub> nano-modified samples stressed with positive impulses.

| TiO <sub>2</sub> Positive Polarity |      |      |      |      |                              |                           |               |
|------------------------------------|------|------|------|------|------------------------------|---------------------------|---------------|
| Diala S3                           |      |      |      |      |                              |                           |               |
| Concentration                      | t5%  | t10% | t50% | t90% | Location $\gamma$ ( $\mu$ s) | Scale $\alpha$ ( $\mu$ s) | Shape $\beta$ |
| 0.00%                              | 1.12 | 1.14 | 1.44 | 1.76 | 0.4433                       | 1.5579                    | 6.7799        |
| 0.0006%                            | 1.28 | 1.32 | 1.52 | 1.76 | 0.4944                       | 1.6395                    | 6.8901        |
| 0.004%                             | 1.38 | 1.4  | 1.54 | 1.84 | 0.5362                       | 1.7095                    | 5.4973        |
| 0.01%                              | 1.38 | 1.42 | 1.56 | 1.76 | 0.506                        | 1.6586                    | 10.9499       |
| 0.05%                              | 1.3  | 1.36 | 1.55 | 1.84 | 0.5148                       | 1.6734                    | 9.3303        |
| 0.1%                               | 1.16 | 1.2  | 1.54 | 1.72 | 0.4629                       | 1.5887                    | 9.9348        |
| Midel 7131                         |      |      |      |      |                              |                           |               |
| Concentration                      | t5%  | t10% | t50% | t90% | Location $\gamma$ ( $\mu$ s) | Scale $\alpha$ ( $\mu$ s) | Shape $\beta$ |
| 0.00%                              | 0.22 | 0.26 | 0.44 | 0.54 | -0.7717                      | 0.4622                    | 4.827         |
| 0.0006%                            | 0.41 | 0.44 | 0.74 | 1.7  | 0.0559                       | 1.0575                    | 1.9759        |
| 0.004%                             | 0.36 | 0.38 | 0.64 | 1.38 | -0.1225                      | 0.8847                    | 1.9052        |
| 0.01%                              | 0.38 | 0.42 | 0.64 | 1.28 | -0.1376                      | 0.8714                    | 2.1853        |
| 0.05%                              | 0.36 | 0.39 | 0.56 | 1.18 | -0.1838                      | 0.8321                    | 1.5945        |
| 0.1%                               | 0.28 | 0.3  | 0.39 | 0.79 | -0.5724                      | 0.5642                    | 2.1293        |
| Rapeseed Oil                       |      |      |      |      |                              |                           |               |
| Concentration                      | t5%  | t10% | t50% | t90% | Location $\gamma$ ( $\mu$ s) | Scale $\alpha$ ( $\mu$ s) | Shape $\beta$ |
| 0.00%                              | 0.4  | 0.54 | 0.88 | 2.04 | 0.1835                       | 1.2014                    | 2.0047        |
| 0.0006%                            | 0.56 | 0.6  | 1.12 | 2.14 | 0.4071                       | 1.5024                    | 2.3471        |
| 0.004%                             | 0.4  | 0.56 | 1.02 | 2.06 | 0.31                         | 1.3634                    | 2.2735        |
| 0.01%                              | 0.47 | 0.54 | 0.8  | 2.02 | 0.2823                       | 1.3262                    | 2.0183        |
| 0.05%                              | 0.44 | 0.46 | 0.82 | 2.04 | 0.1676                       | 1.1823                    | 1.8449        |
| 0.1%                               | 0.4  | 0.42 | 0.62 | 2.08 | 0.0872                       | 1.0912                    | 1.6119        |

Figures 5-17 to 5-19 show the Weibull analysis results of the mineral oil, synthetic ester, and natural ester with TiO<sub>2</sub> nanoparticles stressed with a negative impulse. The values of the scale, shape, and location parameters and the 5%, 10%, 50%, and 90% probabilities of time to negative breakdown for the TiO<sub>2</sub> nano-modified liquids based on mineral oil, synthetic ester, and natural ester with different concentrations of nanoparticles are shown in Table 5-8.

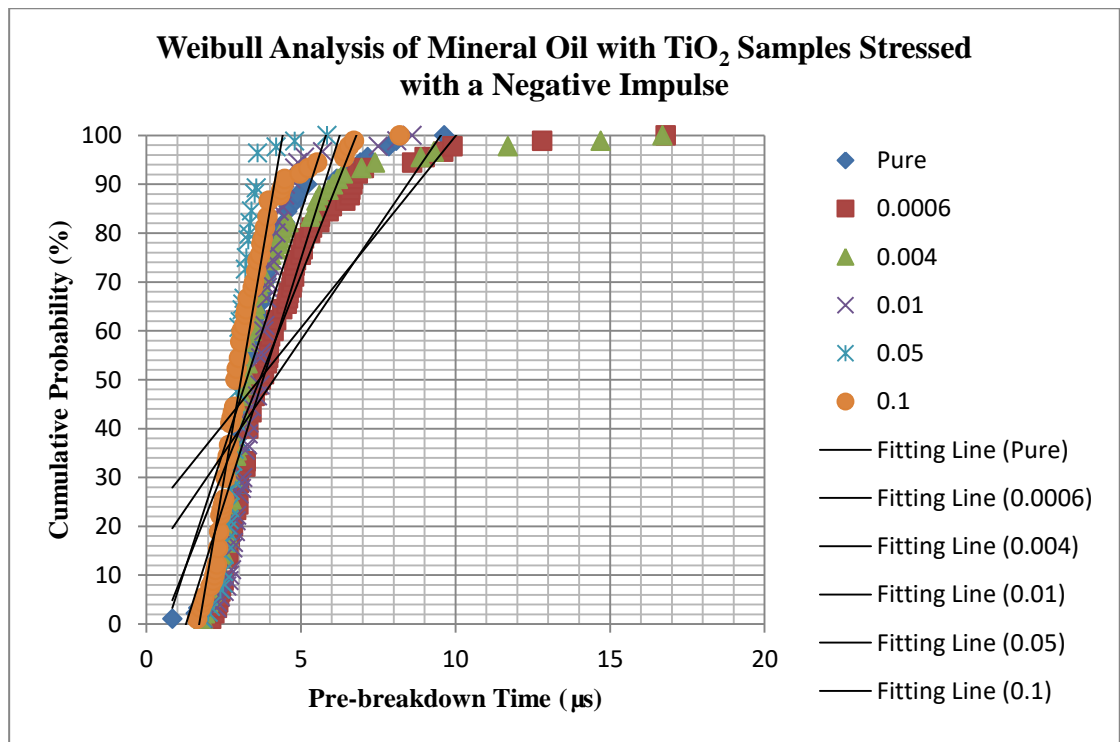


**Figure 5-17.** Weibull analysis of mineral oil with TiO<sub>2</sub> nanoparticles stressed with negative impulses.

For the mineral oil-based nano-modified samples, the longest 5%, 50%, and 90% pre-breakdown times were obtained in the case of the 0.0006% (b/w) concentration. However, the longest 10% pre-breakdown time was obtained for the sample with nanoparticle concentration of 0.01% (b/w). It was found that, in the case of negative energisation, the 0.0006% (b/w) concentration of TiO<sub>2</sub> nanoparticles provided the highest location parameter, the highest scale parameter, and the second-lowest shape parameter. The largest location parameter means that the minimum pre-breakdown time was the longest compared with nanofluids at other concentrations. The highest scale parameter indicated the pre-breakdown time had a wider spread than in other samples, which can explain the standard deviation shown in Section 5.3.1. The small shape parameter indicated that the mineral oil sample with 0.0006% (b/w) concentration provided a better stability and low failure rate with an increase in pre-breakdown time compared with other samples.

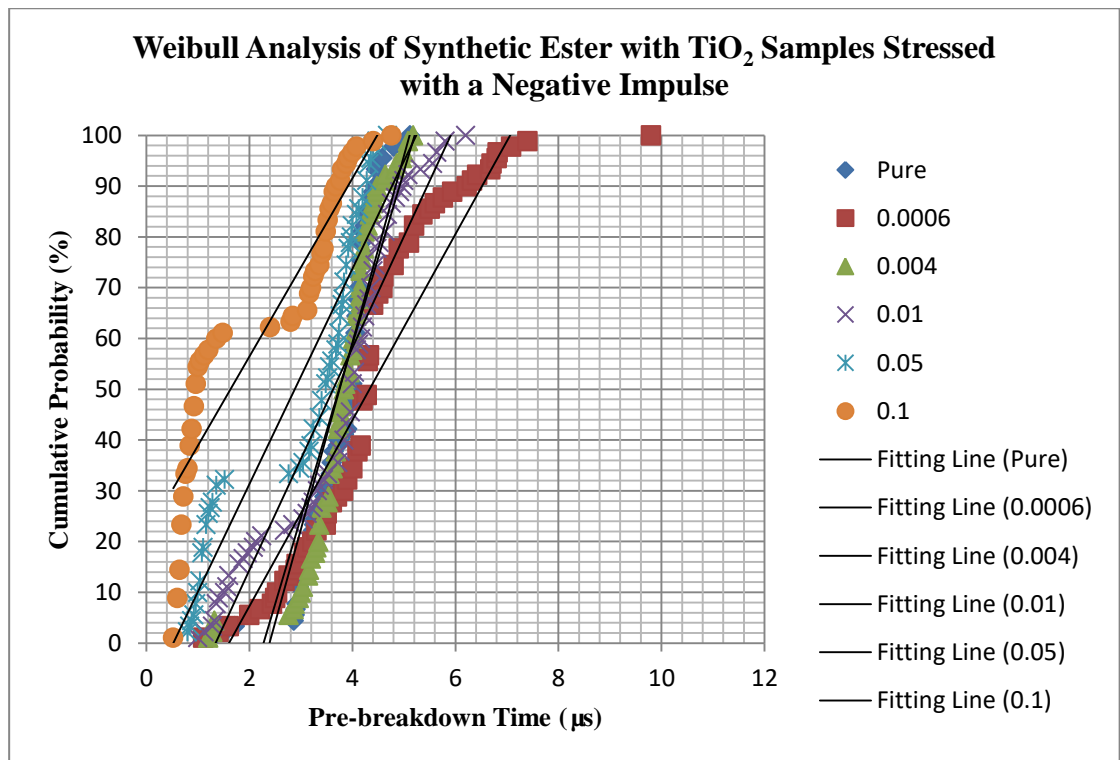


**Figure 5-18.** Weibull analysis of synthetic ester with TiO<sub>2</sub> nanoparticles stressed with negative impulses.

For the nano-modified samples of synthetic ester, the longest 50% and 90% pre-breakdown times were obtained in the case of the 0.0006% (b/w) concentration, and the longest 5% and 10% pre-breakdown times were obtained for the base sample. It was found that, in the case of the negative energisation, the 0.0006% (b/w) concentration of TiO<sub>2</sub> nanoparticles provided the highest location parameter and scale parameter. The largest location parameter means that the minimum pre-breakdown time was the longest compared with nanofluids at other concentrations. The highest scale parameter means the pre-breakdown time had a wider spread than in the other samples. The shape parameter of the sample with the 0.0006% (b/w) concentration of TiO<sub>2</sub> nanoparticles was at the middle level of all synthetic ester tested samples.

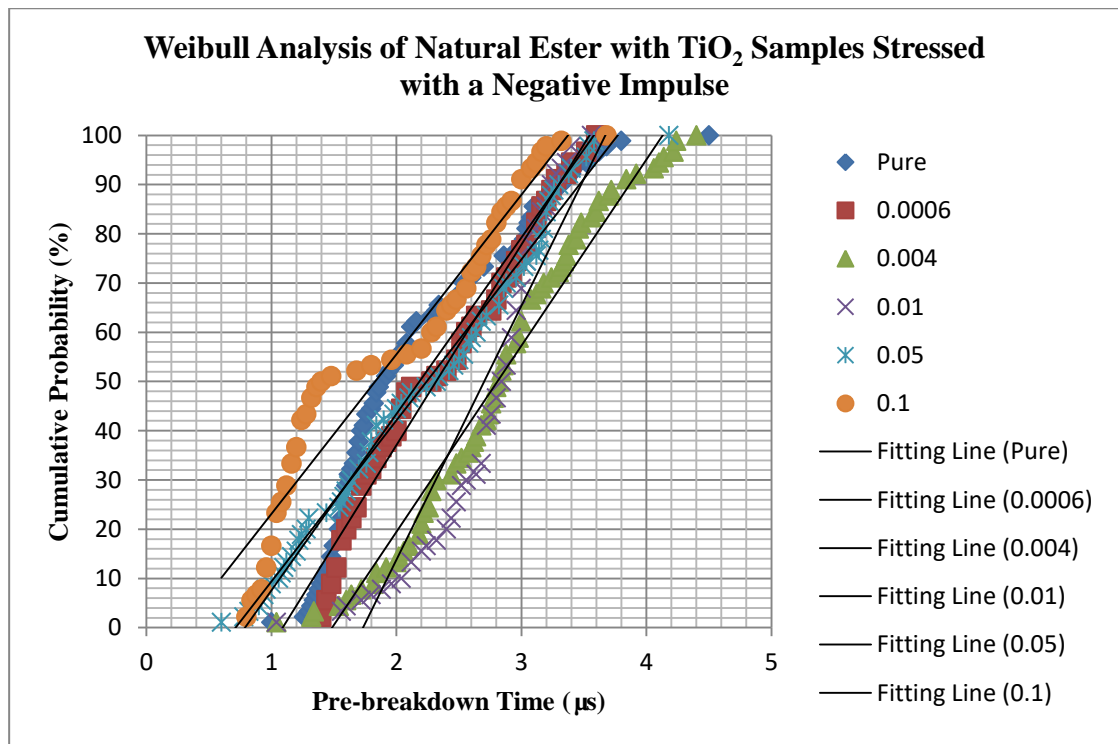


**Figure 5-19.** Weibull analysis of natural ester with TiO<sub>2</sub> nanoparticles stressed with negative impulses.

For the nano-modified samples of natural ester, the longest 5%, 10%, and 50% pre-breakdown times were obtained in the case of the 0.001% (b/w) concentration, while the longest 90% pre-breakdown time was obtained for the sample with the nanoparticle concentration of 0.004% (b/w). As Figure 5-3 shows, the average pre-breakdown time of the samples with 0.004% (b/w) and 0.01% (b/w) concentrations were similar. The 5%, 10%, and 50% pre-breakdown times of the sample with the 0.004% (b/w) concentration were slightly lower than the sample with the 0.01% (b/w) concentration but were significantly higher than other samples. It was found that, in the case of the negative energisation, the 0.004% (b/w) concentration of the TiO<sub>2</sub> nanoparticles provided the highest location parameter and the highest scale parameter. The largest location parameter means that the minimum pre-breakdown time was the longest compared with nanofluids at other concentrations. The highest scale parameter means the pre-breakdown times had a wider spread than in other samples. The shape parameter of the sample with the 0.004% (b/w) concentration of TiO<sub>2</sub> nanoparticles was at the middle level of all synthetic ester tested samples. The shape parameter of the sample with the 0.01% (b/w) concentration was significantly higher than the other samples, which means the failure rate of this sample will rapidly rise with an increase in pre-breakdown time. Considering the shape parameter

effect, in the case of the negative energisation, the 0.004% (b/w) concentration of TiO<sub>2</sub> nanoparticles was treated as the optimal concentration.

**Table 5-8.** All three Weibull parameters for all TiO<sub>2</sub> samples stressed with a negative impulse.

| <b>TiO<sub>2</sub> Negative Polarity</b> |            |             |             |             |   |  |                                 |
|--|------------|-------------|-------------|-------------|---|--|---------------------------------|
| <b>Diala S3</b>                          |            |             |             |             |   |  |                                 |
| <b>Concentration</b>                     | <b>t5%</b> | <b>t10%</b> | <b>t50%</b> | <b>t90%</b> | <b>Location <math>\gamma</math><br/>(<math>\mu</math>s)</b> | <b>Scale <math>\alpha</math><br/>(<math>\mu</math>s)</b> | <b>Shape <math>\beta</math></b> |
| 0.00%                                    | 2.12       | 2.3         | 3.36        | 5.2         | 1.4261  | 4.1626   | 2.5314                          |
| 0.0006%                                  | 2.36       | 2.5         | 3.7         | 6.66        | 1.6065  | 4.9855   | 2.0368                          |
| 0.004%                                   | 2.1        | 2.28        | 3.24        | 6.04        | 1.5011  | 4.4864   | 1.8132                          |
| 0.01%                                    | 2.3        | 2.7         | 3.68        | 4.5         | 1.4136  | 4.1109   | 3.2306                          |
| 0.05%                                    | 2.08       | 2.5         | 2.96        | 3.56        | 1.1802  | 3.2549   | 4.7195                          |
| 0.1%                                     | 1.84       | 2.2         | 2.88        | 4.44        | 1.2886  | 3.6279   | 2.7641                          |
| <b>Midel 7131</b>                        |            |             |             |             |   |  |                                 |
| <b>Concentration</b>                     | <b>t5%</b> | <b>t10%</b> | <b>t50%</b> | <b>t90%</b> | <b>Location <math>\gamma</math><br/>(<math>\mu</math>s)</b> | <b>Scale <math>\alpha</math><br/>(<math>\mu</math>s)</b> | <b>Shape <math>\beta</math></b> |
| 0.00%                                    | 2.88       | 2.96        | 4           | 4.44        | 1.3935  | 4.0288   | 7.0775                          |
| 0.0006%                                  | 2          | 2.54        | 4.28        | 6.22        | 1.5656  | 4.7856   | 3.2162                          |
| 0.004%                                   | 1.32       | 3           | 3.84        | 4.48        | 1.3999  | 4.0549   | 6.2346                          |
| 0.01%                                    | 1.32       | 1.52        | 4           | 4.96        | 1.4131  | 4.1086   | 3.4335                          |
| 0.05%                                    | 0.92       | 1           | 3.48        | 4.28        | 1.1909  | 3.29   | 2.4864                          |
| 0.1%                                     | 0.52       | 0.6         | 0.96        | 3.68        | 0.7262  | 2.0671   | 1.4397                          |
| <b>Rapeseed Oil</b>                      |            |             |             |             |   |  |                                 |
| <b>Concentration</b>                     | <b>t5%</b> | <b>t10%</b> | <b>t50%</b> | <b>t90%</b> | <b>Location <math>\gamma</math><br/>(<math>\mu</math>s)</b> | <b>Scale <math>\alpha</math><br/>(<math>\mu</math>s)</b> | <b>Shape <math>\beta</math></b> |
| 0.00%                                    | 1.32       | 1.42        | 1.86        | 3.32        | 0.8993  | 2.458  | 3.0703                          |
| 0.0006%                                  | 1.44       | 1.52        | 2.28        | 3.28        | 0.9614  | 2.6152   | 3.8193                          |
| 0.004%                                   | 1.6        | 1.84        | 2.82        | 3.84        | 1.1345  | 3.1095   | 4.2922                          |
| 0.01%                                    | 1.72       | 2.04        | 2.84        | 3.24        | 1.0773  | 2.9367   | 7.3215                          |
| 0.05%                                    | 0.92       | 1.06        | 2.32        | 3.3         | 0.9335  | 2.5435   | 2.8885                          |
| 0.1%                                     | 0.84       | 0.92        | 1.4         | 3           | 0.7538  | 2.125  | 2.436                           |

#### 5.4.2 Weibull analysis of the pre-breakdown times in BN nano-modified liquids

Figures 5-20 to 5-22 show the Weibull analysis results of the mineral oil, synthetic ester, and natural ester with BN nanoparticles stressed with a positive impulse. The scale, shape, and location parameters and the 5%, 10%, 50%, and 90% probabilities of time to breakdown of the BN nanoparticle modified mineral oil, synthetic ester, and natural ester samples under a positive polarity impulse are shown in Table 5-9.

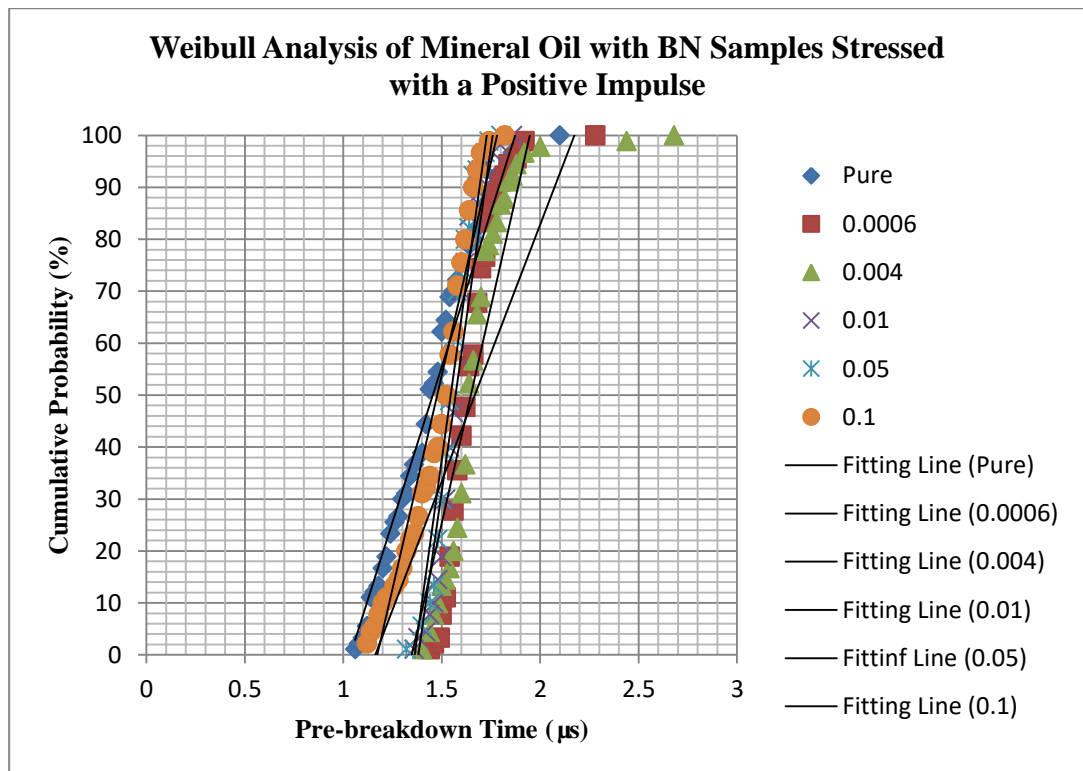


**Figure 5-20.** Weibull analysis of mineral oil samples with BN nanoparticles stressed with positive impulses.

For the nano-modified samples of mineral oil, the longest 5% and 10% pre-breakdown times were obtained in the case of the 0.0006% (b/w) concentration, and the longest 50% and 90% pre-breakdown times were obtained for the sample with nanoparticle concentration of 0.004% (b/w). It was found that, in the case of the positive energisation, the 0.004% (b/w) concentration of BN nanoparticles provided the highest location parameter, the highest scale parameter, and the second-lowest shape parameter. The largest location parameter means that the minimum pre-breakdown time was the longest compared with the nanofluids at other concentrations. The highest scale parameter means the pre-breakdown time had a wider spread than in the other samples. The second-lowest shape parameter indicated that the mineral oil sample with 0.004% (b/w) concentration provided a better stability and low failure rate with an increase in pre-breakdown time compared with the other samples (0.01%, 0.05%, and 0.1% b/w).

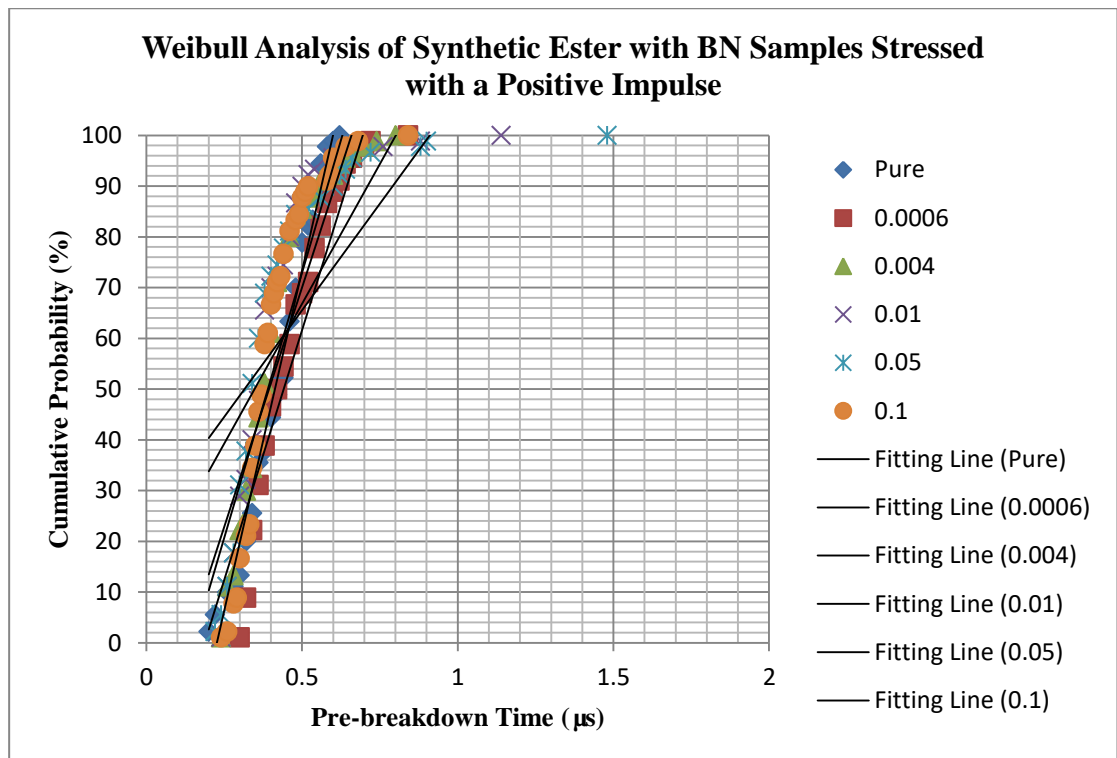


**Figure 5-21.** Weibull analysis of synthetic ester with BN nanoparticles stressed with positive impulses.

For the nano-modified samples of synthetic ester, the longest 5%, 10%, and 90% pre-breakdown times were obtained with the 0.0006% (b/w) concentration. The longest 50% pre-breakdown time was obtained for the base sample (0.44  $\mu\text{s}$ ), which was just slightly higher than the sample with the 0.0006% (b/w) BN nanoparticle concentration (0.42  $\mu\text{s}$ ). The sample with the 0.0006% (b/w) concentration of BN nanoparticles provided the largest location parameter and the highest scale parameter. The largest location parameter means that the minimum pre-breakdown time was the longest compared with nanofluids at other concentrations. The highest scale parameter means the pre-breakdown time had a wider spread than in the other samples. The sample with the 0.0006% (b/w) concentration of BN nanoparticles provided the second-highest shape parameter, which indicated that the failure rate will rise rapidly with an increase in the pre-breakdown time.

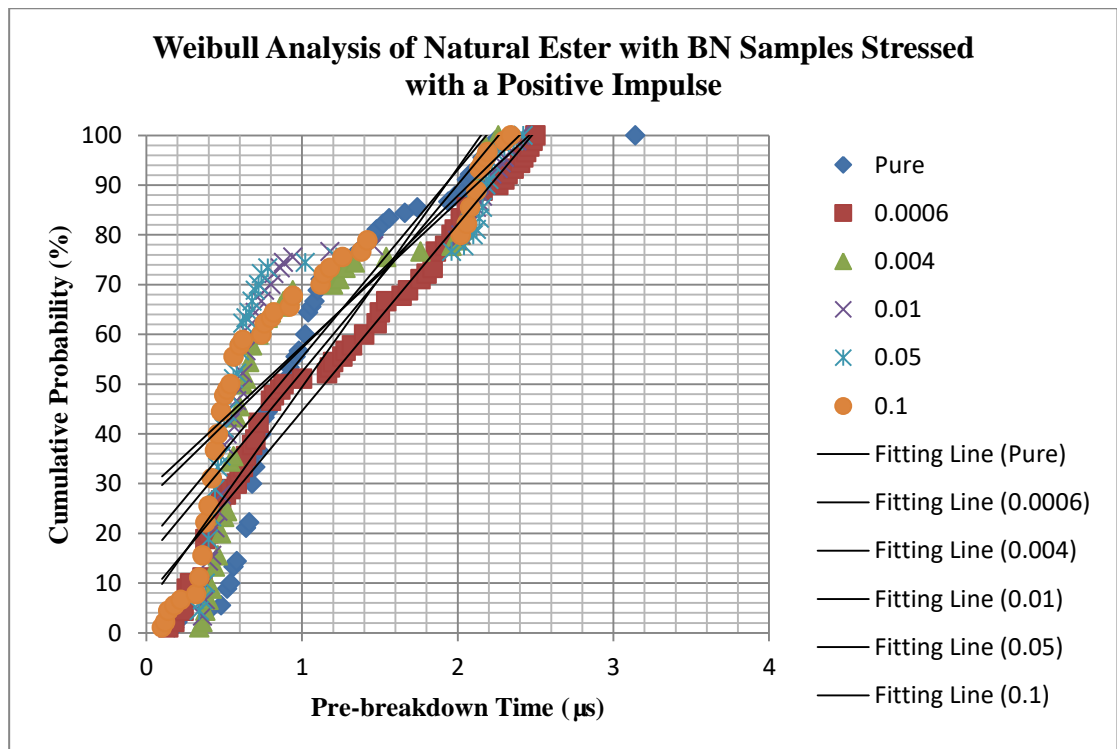


**Figure 5-22.** Weibull analysis of mineral oil samples with BN nanoparticles stressed with positive impulses.

For the natural ester, the longest 5%, 10%, and 50% pre-breakdown times were obtained in the base sample. The longest 50% and 90% pre-breakdown times were obtained for the sample with a nanoparticle concentration of 0.0006% (b/w). The natural ester sample with 0.0006% (b/w) BN nanoparticle concentration provided the largest location parameter and the highest scale parameter. The largest location parameter means that the minimum pre-breakdown time was the longest compared with nanofluids at other concentrations. The highest scale parameter means the pre-breakdown time had a wider spread than in other samples. The shape parameter of the sample with the 0.0006% (b/w) concentration of BN nanoparticles was at the middle level of all natural ester samples.

**Table 5-9.** All three Weibull parameters for all BN nano-modified samples stressed with positive impulses.

| <b>BN Positive Polarity</b> |            |             |             |             |   |  |                                 |
|-----------------------------|------------|-------------|-------------|-------------|---|--|---------------------------------|
| <b>Diala S3</b>             |            |             |             |             |   |  |                                 |
| <b>Concentration</b>        | <b>t5%</b> | <b>t10%</b> | <b>t50%</b> | <b>t90%</b> | <b>Location <math>\gamma</math><br/>(<math>\mu</math>s)</b> | <b>Scale <math>\alpha</math><br/>(<math>\mu</math>s)</b> | <b>Shape <math>\beta</math></b> |
| 0.00%                       | 1.12       | 1.14        | 1.44        | 1.76        | 0.4433  | 1.5579   | 6.7799                          |
| 0.0006%                     | 1.49       | 1.52        | 1.62        | 1.8         | 0.5396  | 1.7154   | 10.1722                         |
| 0.004%                      | 1.44       | 1.48        | 1.64        | 1.84        | 0.5675  | 1.7638   | 6.7915                          |
| 0.01%                       | 1.42       | 1.46        | 1.56        | 1.68        | 0.4816  | 1.6186   | 16.8155                         |
| 0.05%                       | 1.4        | 1.44        | 1.54        | 1.66        | 0.4685  | 1.5976   | 17.9656                         |
| 0.1%                        | 1.16       | 1.2         | 1.52        | 1.66        | 0.4432  | 1.5578   | 11.2144                         |
| <b>Midel 7131</b>           |            |             |             |             |   |  |                                 |
| <b>Concentration</b>        | <b>t5%</b> | <b>t10%</b> | <b>t50%</b> | <b>t90%</b> | <b>Location <math>\gamma</math><br/>(<math>\mu</math>s)</b> | <b>Scale <math>\alpha</math><br/>(<math>\mu</math>s)</b> | <b>Shape <math>\beta</math></b> |
| 0.00%                       | 0.22       | 0.26        | 0.44        | 0.54        | -0.7717   | 0.4622   | 4.827                           |
| 0.0006%                     | 0.3        | 0.32        | 0.42        | 0.62        | -0.6917   | 0.5007   | 4.0601                          |
| 0.004%                      | 0.24       | 0.26        | 0.38        | 0.56        | -0.8125   | 0.4438   | 3.5162                          |
| 0.01%                       | 0.24       | 0.26        | 0.36        | 0.5         | -0.8198   | 0.4405   | 2.7471                          |
| 0.05%                       | 0.24       | 0.26        | 0.34        | 0.6         | -0.8013   | 0.4487   | 2.2828                          |
| 0.1%                        | 0.26       | 0.29        | 0.37        | 0.52        | -0.8222   | 0.4395   | 3.6929                          |
| <b>Rapeseed Oil</b>         |            |             |             |             |   |  |                                 |
| <b>Concentration</b>        | <b>t5%</b> | <b>t10%</b> | <b>t50%</b> | <b>t90%</b> | <b>Location <math>\gamma</math><br/>(<math>\mu</math>s)</b> | <b>Scale <math>\alpha</math><br/>(<math>\mu</math>s)</b> | <b>Shape <math>\beta</math></b> |
| 0.00%                       | 0.4        | 0.54        | 0.88        | 2.04        | 0.1835  | 1.2014   | 2.0047                          |
| 0.0006%                     | 0.24       | 0.28        | 0.88        | 2.26        | 0.2725  | 1.3132   | 1.6174                          |
| 0.004%                      | 0.38       | 0.42        | 0.62        | 2.12        | 0.1178  | 1.125  | 1.6329                          |
| 0.01%                       | 0.38       | 0.4         | 0.6         | 2.18        | 0.0501  | 1.0513   | 1.4981                          |
| 0.05%                       | 0.36       | 0.38        | 0.56        | 2.18        | 0.0363  | 1.037  | 1.4191                          |
| 0.1%                        | 0.14       | 0.34        | 0.54        | 2.12        | 0.0023  | 1.0023   | 1.3767                          |

Figures 5-23 to 5-25 show the Weibull analysis results of the mineral oil, synthetic ester, and natural ester with BN nanoparticles stressed with a negative impulse. The scale, shape, and location parameter and the 5%, 10%, 50%, and 90% probabilities of the time to breakdown of the mineral oil, synthetic ester, and natural ester samples modified with BN nanoparticles under the negative polarity impulse are shown in Table 5-10.

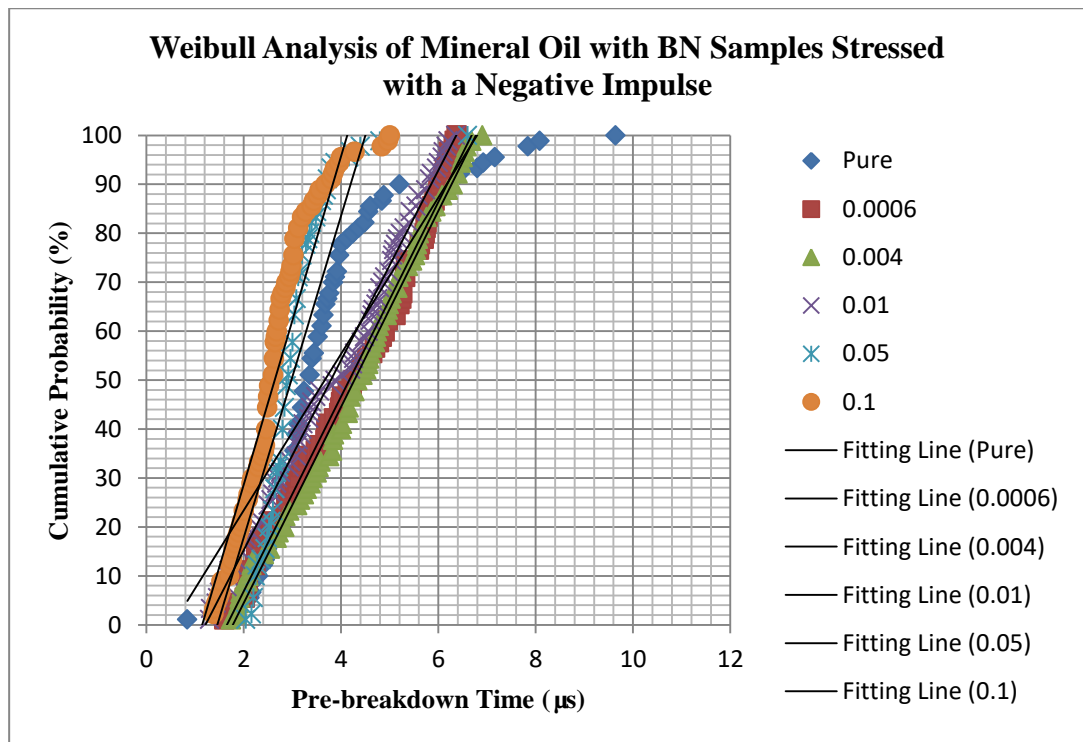


**Figure 5-23.** Weibull analysis of mineral oil samples with BN nanoparticles stressed with negative impulses.

For the mineral oil samples, the longest 5% pre-breakdown time was obtained in the case of the 0.05% (b/w) concentration, and the longest 10% pre-breakdown time was obtained for the base sample. The longest 50% and 90% pre-breakdown times were obtained in the case of the 0.004% (b/w) concentration. It was found that, in the case of positive energisation, the 0.004% (b/w) concentration of BN nanoparticles provided the highest location parameter, the highest scale parameter, and the second-lowest shape parameter. The largest location parameter means that the minimum pre-breakdown time was the longest compared with nanofluids at other concentrations. The highest scale parameter means the pre-breakdown time has a wider spread than in the other samples. The shape parameter of the sample with the 0.004% (b/w) concentration of BN nanoparticles was at the middle level of all mineral oil samples.

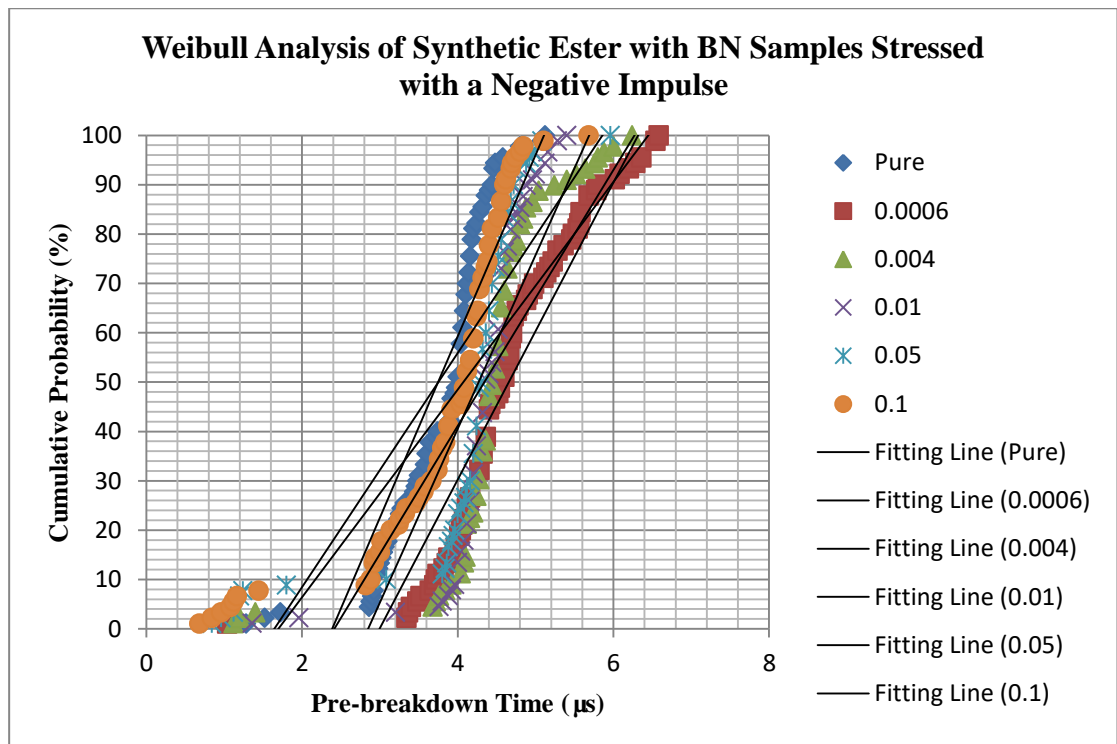


**Figure 5-24.** Weibull analysis of synthetic ester with BN nanoparticles stressed with negative impulses.

For the nano-modified samples of synthetic ester, the longest 5% and 10% pre-breakdown times were obtained for the sample with nanoparticle concentration of 0.01% (b/w), and the longest 50%, and 90% pre-breakdown times were obtained in the case of the 0.0006% (b/w) concentration. It was found that, in the case of negative energisation, the 0.0006% (b/w) concentration of BN nanoparticles provided the highest location parameter, the highest scale parameter, and the second-lowest shape parameter. The largest location parameter means that the minimum pre-breakdown time was the longest compared with the nanofluids at other concentrations. The highest scale parameter means the pre-breakdown time had a wider spread than in other samples. The second-lowest shape parameter indicated that the mineral oil sample with 0.0006% (b/w) concentration provided a better stability and lower failure rate with an increase in the pre-breakdown time compared with other samples (0.00%, 0.004%, 0.01%, and 0.05% b/w).

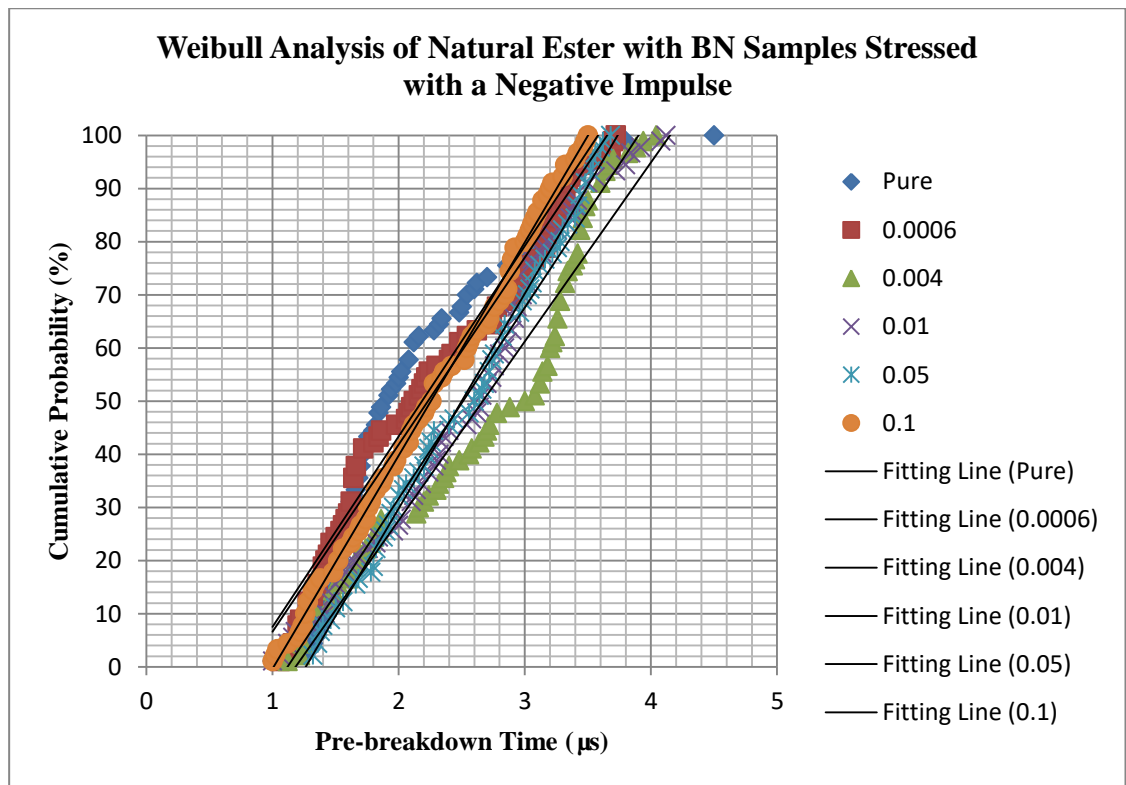


**Figure 5-25.** Weibull analysis of natural ester with BN nanoparticles stressed with negative impulses.

For the nano-modified samples of natural ester, the longest 5% and 10% pre-breakdown times were obtained for the sample with a nanoparticle concentration of 0.05% (b/w), and the longest 50% and 90% pre-breakdown times were obtained in the case of the 0.004% (b/w) concentration. The natural ester sample with the 0.004% (b/w) BN nanoparticle concentration provided the largest location parameter, the highest scale parameter, and the second-highest shape parameter. The largest location parameter means that the minimum pre-breakdown time was the longest compared with nanofluids at other concentrations. The highest scale parameter means the pre-breakdown time had a wider spread than in the other samples. The largest location parameter means that the minimum pre-breakdown time was the longest compared with nanofluids at other concentrations. The highest scale parameter means the pre-breakdown time had a wider spread than in the other samples. The second-highest shape parameter means the failure rate of the 0.004% (b/w) nano-modified natural ester sample will rise rapidly with an increase in the pre-breakdown time.

**Table 5-10.** All three Weibull parameters for all BN nano-modified samples stressed with negative impulses.

| <b>BN Negative Polarity</b> |            |             |             |             |   |  |                                 |
|-----------------------------|------------|-------------|-------------|-------------|---|--|---------------------------------|
| <b>Diala S3</b>             |            |             |             |             |   |  |                                 |
| <b>Concentration</b>        | <b>t5%</b> | <b>t10%</b> | <b>t50%</b> | <b>t90%</b> | <b>Location <math>\gamma</math><br/>(<math>\mu</math>s)</b> | <b>Scale <math>\alpha</math><br/>(<math>\mu</math>s)</b> | <b>Shape <math>\beta</math></b> |
| 0.00%                       | 2.12       | 2.3         | 3.36        | 5.2         | 1.4261  | 4.1626   | 2.5314                          |
| 0.0006%                     | 2.02       | 2.1         | 4.26        | 6.04        | 1.5483  | 4.7036   | 3.3337                          |
| 0.004%                      | 1.92       | 2.1         | 4.34        | 6.3         | 1.5697  | 4.8053   | 3.4298                          |
| 0.01%                       | 1.46       | 1.68        | 3.88        | 5.82        | 1.4595  | 4.3039   | 2.8987                          |
| 0.05%                       | 2.2        | 2.24        | 2.92        | 3.72        | 1.1862  | 3.2746   | 4.022                           |
| 0.1%                        | 1.48       | 1.7         | 2.6         | 3.68        | 1.073   | 2.924  | 3.4866                          |
| <b>Midel 7131</b>           |            |             |             |             |   |  |                                 |
| <b>Concentration</b>        | <b>t5%</b> | <b>t10%</b> | <b>t50%</b> | <b>t90%</b> | <b>Location <math>\gamma</math><br/>(<math>\mu</math>s)</b> | <b>Scale <math>\alpha</math><br/>(<math>\mu</math>s)</b> | <b>Shape <math>\beta</math></b> |
| 0.00%                       | 2.88       | 2.96        | 4           | 4.44        | 1.3935  | 4.0288   | 7.0775                          |
| 0.0006%                     | 3.48       | 3.72        | 4.6         | 5.8         | 1.6189  | 5.0473   | 5.7193                          |
| 0.004%                      | 3.68       | 3.92        | 4.44        | 5.24        | 1.5582  | 4.7501   | 6.5949                          |
| 0.01%                       | 3.76       | 3.96        | 4.36        | 4.88        | 1.5209  | 4.5761   | 10.4588                         |
| 0.05%                       | 1.2        | 3.08        | 4.3         | 4.72        | 1.4769  | 4.3792   | 6.0818                          |
| 0.1%                        | 1.08       | 2.88        | 4.08        | 4.6         | 1.4148  | 4.1158   | 5.0923                          |
| <b>Rapeseed Oil</b>         |            |             |             |             |   |  |                                 |
| <b>Concentration</b>        | <b>t5%</b> | <b>t10%</b> | <b>t50%</b> | <b>t90%</b> | <b>Location <math>\gamma</math><br/>(<math>\mu</math>s)</b> | <b>Scale <math>\alpha</math><br/>(<math>\mu</math>s)</b> | <b>Shape <math>\beta</math></b> |
| 0.00%                       | 1.32       | 1.42        | 1.86        | 3.32        | 0.8993  | 2.458  | 3.0703                          |
| 0.0006%                     | 1.16       | 1.22        | 2.12        | 3.34        | 0.9283  | 2.5303   | 3.0798                          |
| 0.004%                      | 1.24       | 1.28        | 3           | 3.6         | 1.0927  | 2.9823   | 3.8021                          |
| 0.01%                       | 1.12       | 1.42        | 2.66        | 3.5         | 1.0342  | 2.8128   | 3.6451                          |
| 0.05%                       | 1.36       | 1.46        | 2.6         | 3.44        | 1.0253  | 2.788  | 4.091                           |
| 0.1%                        | 1.12       | 1.26        | 2.26        | 3.2         | 0.9288  | 2.5314   | 3.6082                          |

## **5.5 Confidence Analysis of the Pre-breakdown Times for Standard Lightning Tests**

### **5.5.1 Confidence analysis of the pre-breakdown times for TiO<sub>2</sub> nano-modified liquids**

In this section, the CIs for the differences between the average values of the pre-breakdown times of the base and nano-modified liquids were calculated. The calculation results of the CIs prove that the statistical difference between the average values of the pre-breakdown time,  $\Delta t$ , of the base and nano-modified liquids exist and hence confirm the nanoparticle enhancement of the dielectric liquid behaviours. More details about the CI and the statistical difference analysis have been presented in Section 4.5. It is necessary to conduct this analysis to prove (or disprove) that the changes in the time to breakdown observed for nano-modified samples are statically different from the pre-breakdown time obtained for base liquids. This could be done with the statistical difference analysis, which is used for the calculation of the CIs for population means. The degree of confidence used in the present analysis is 95%. This is a typical degree of confidence used in the statistical difference analysis of experimental data in engineering, medicine, and other sectors [16], [105], [107], [108], [210], [217]–[219]. The 95% upper and lower bound CIs indicate that the true value of the measurement data has a 95% probability of falling into the range between the upper and lower bound CIs. In the case in which the CI lower bound is higher than zero in the 95% confidence level, the  $\Delta t$  is a positive number, indicating that the statistical difference of the average pre-breakdown times between two samples exists. In contrast, if the CI lower bound is equal to or lower than zero in a 95% confidence level, the  $\Delta t$  may equal zero; hence, the statistic difference of the average pre-breakdown time may not exist between two samples. The confidence analysis was performed using Microsoft Excel and Origin Pro 2015.

In the case of nano-modified samples with TiO<sub>2</sub> nanoparticles stressed with positive and negative impulses, the confidence analysis results of pre-breakdown times are shown in Figures 5-26 to 5-28. In these figures, the pre-breakdown times shown in Figures 5-2 and 5-3 were used to verify the statistical significance in the difference between the pre-breakdown times of base and nano-modified samples.

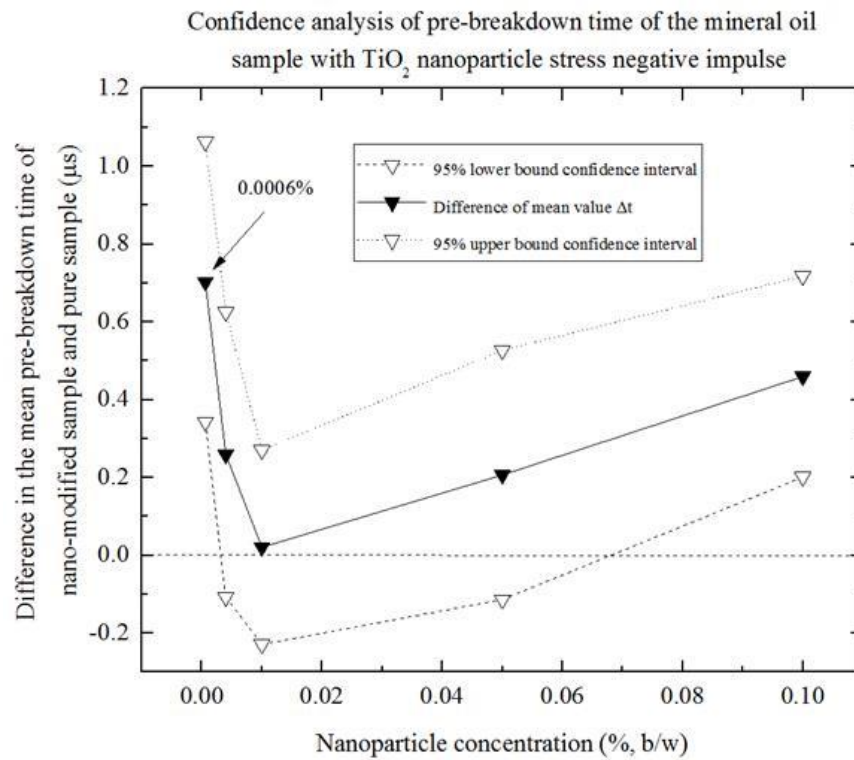
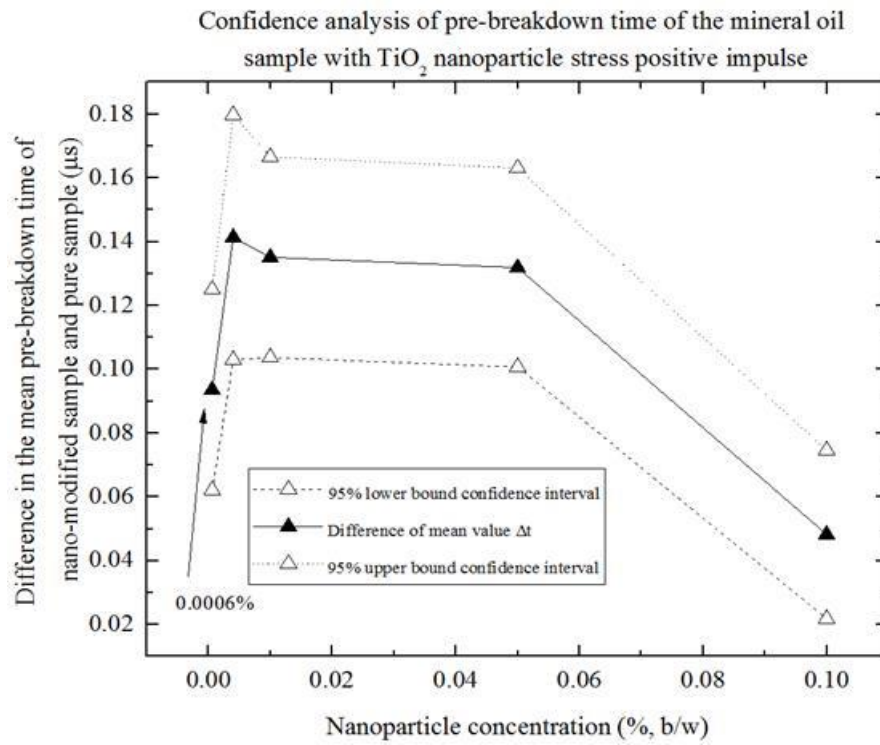


**Figure 5-26.** Confidence analysis results,  $\Delta t$ , of mineral oil with TiO<sub>2</sub> nanoparticles stressed with a positive impulse (a) and a negative impulse (b). Each data point denotes the  $\Delta t$  between the mean value of the breakdown voltages of the base and nano-modified samples. The dotted line represents the upper 95% confidence bound; the dashed line represents the lower 95% confidence bound.

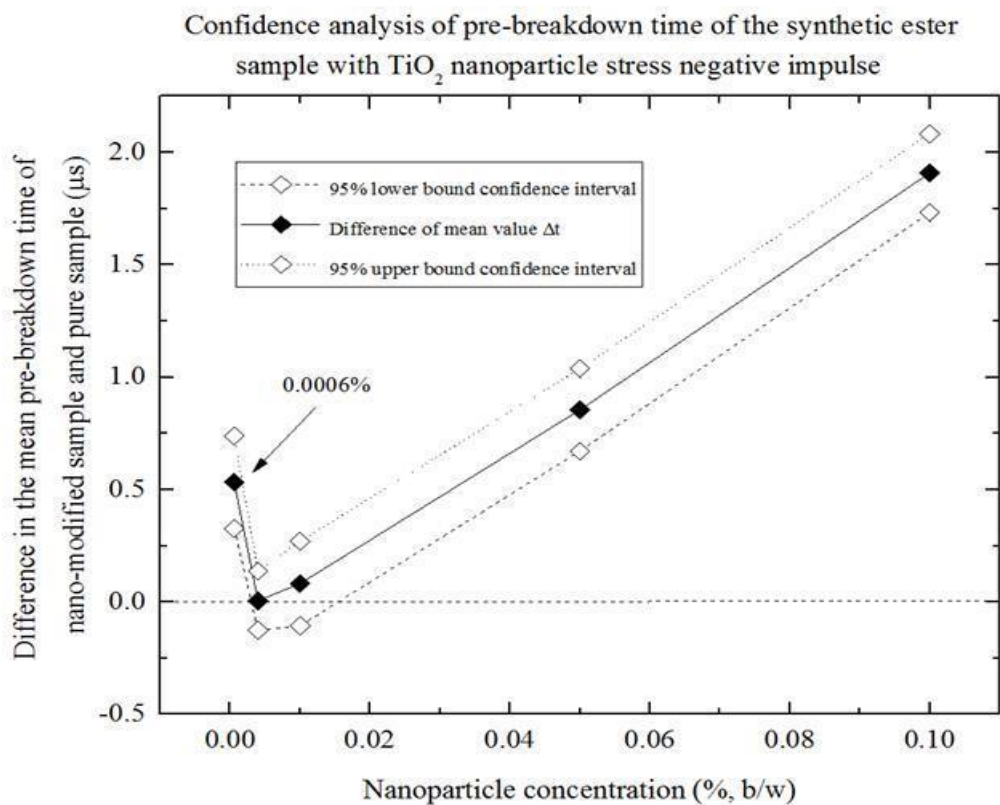
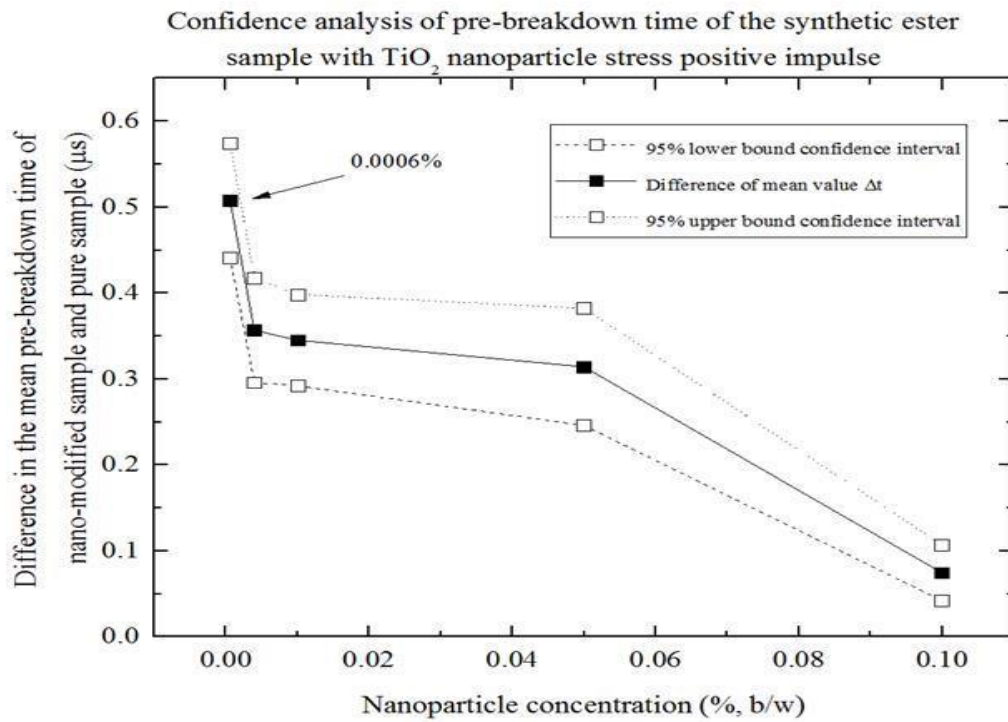
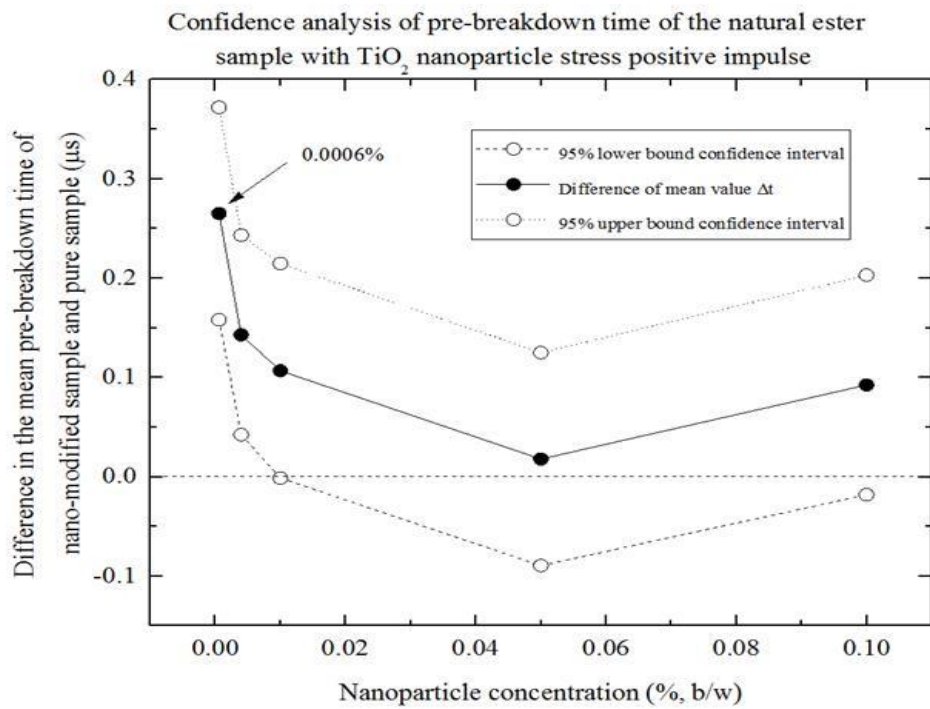
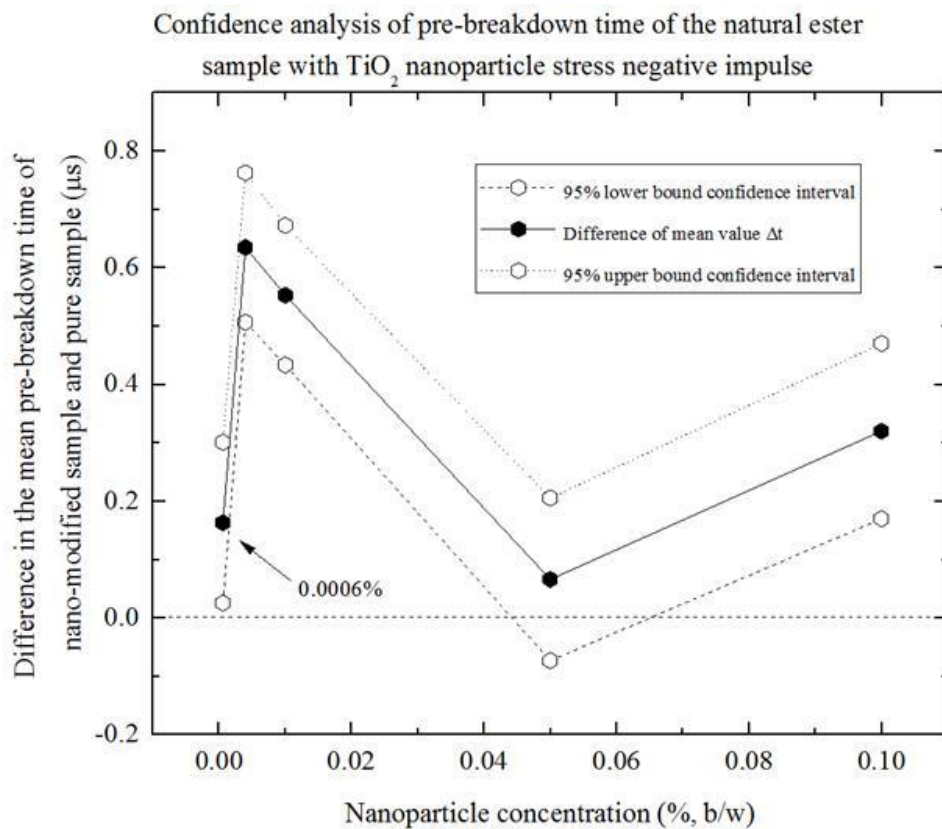


**Figure 5-27.** Confidence analysis results,  $\Delta t$ , of the synthetic ester with TiO<sub>2</sub> nanoparticles stressed with a positive impulse (a) and a negative impulse (b). Each data point denotes the  $\Delta t$  between the mean value of the breakdown voltages of the base and nano-modified samples. The dotted line represents the upper 95% confidence bound; the dashed line represents the lower 95% confidence bound.



(a)



(b)

**Figure 5-28.** Confidence analysis results,  $\Delta t$ , of the natural ester with TiO<sub>2</sub> nanoparticles stressed with a positive impulse (a) and a negative impulse (b). Each data point denotes the  $\Delta t$  between the mean value of the breakdown voltages of the base and nano-modified samples. The dotted line represents the upper 95% confidence bound; the dashed line represents the lower 95% confidence bound.

As Figures 5-26 to 5-28 show, the confidence analysis of the positive and negative impulses for the pre-breakdown time of the TiO<sub>2</sub> nano-modified liquids showed that the difference in the population decreased with an increase in the concentration of the nanoparticles. These graphs confirm that the small concentration of nanoparticles used in the present study (0.0006% or 0.004% (b/w) of TiO<sub>2</sub> nanoparticles) provided the largest improvement (increase) in the pre-breakdown time of the nano-modified liquids. Additionally, the lower 95% CI for  $\Delta t$  related to these concentrations stayed positive for all three liquids with TiO<sub>2</sub> nanoparticles, thus confirming that this increase in the pre-breakdown time compared with the base liquids (positive  $\Delta t$ ) was statistically significant for all tested nano-modified samples. With an increase in the concentration of nanoparticles, the difference in the pre-breakdown time of the base liquids and nano-modified liquids,  $\Delta t$ , started to decrease. In some cases, the optimal concentration of nanoparticles produced the largest  $\Delta t$  at 0.004% (b/w), for example, for the nano-modified mineral oil stressed with positive impulses and for the natural ester stressed with negative impulses. Again, as in the case of 0.004% optimal concentration,  $\Delta t$  started to decrease when the particle concentration increased above 0.004%.

The results showed that the lower 95% CI crosses the zero line for the nano-modified samples, which means, in the correlated concentration, this difference between the mean pre-breakdown time for the base oil and the mean pre-breakdown time of the nano-modified samples was not statistically significant. In the following cases, the pre-breakdown times of the samples with the correlating concentration were almost the same as the pre-breakdown time of the base sample:

- The nano-modified samples of the mineral oil with 0.004%, 0.01%, and 0.05% concentrations of nanoparticles stressed with a negative impulse;
- The synthetic ester nano-modified samples with 0.004% and 0.01% concentration of nanoparticles stressed with a negative impulse;
- The natural ester nano-modified samples with 0.01%, 0.05%, and 0.1% concentrations of nanoparticles stressed with a positive impulse and with the 0.05% concentration of nanoparticles stressed with a negative impulse.

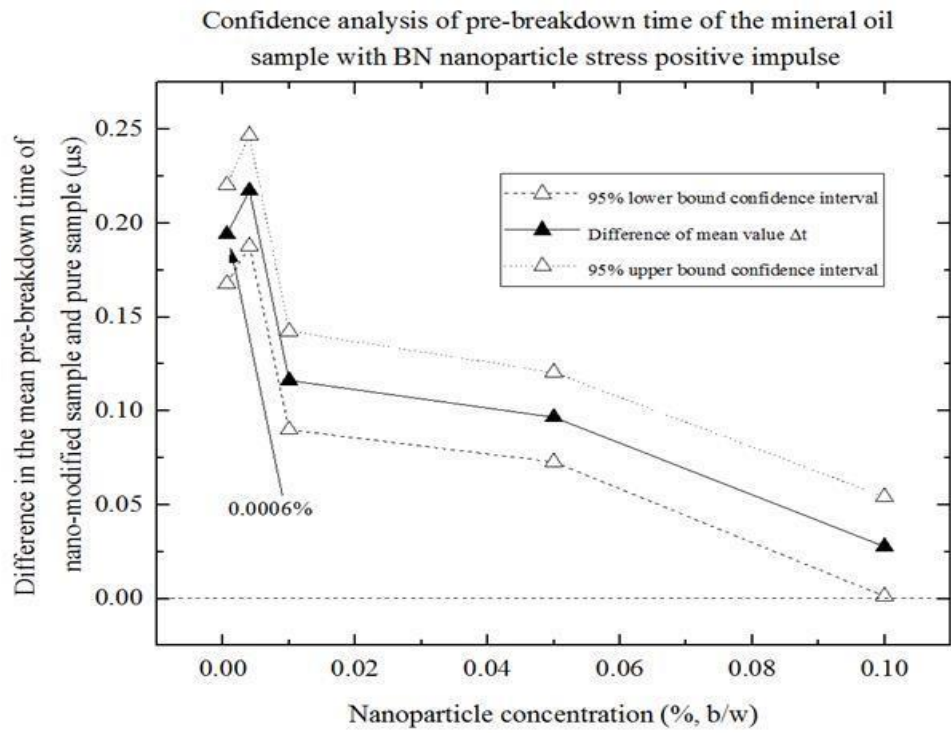
With an increase in concentration, the pre-breakdown time of the nano-modified samples was lower than the pre-breakdown time of the base sample. Hence, the difference between the mean pre-

breakdown time for the base oil and the mean pre-breakdown times of the nano-modified samples,  $\Delta t$ , were increased.

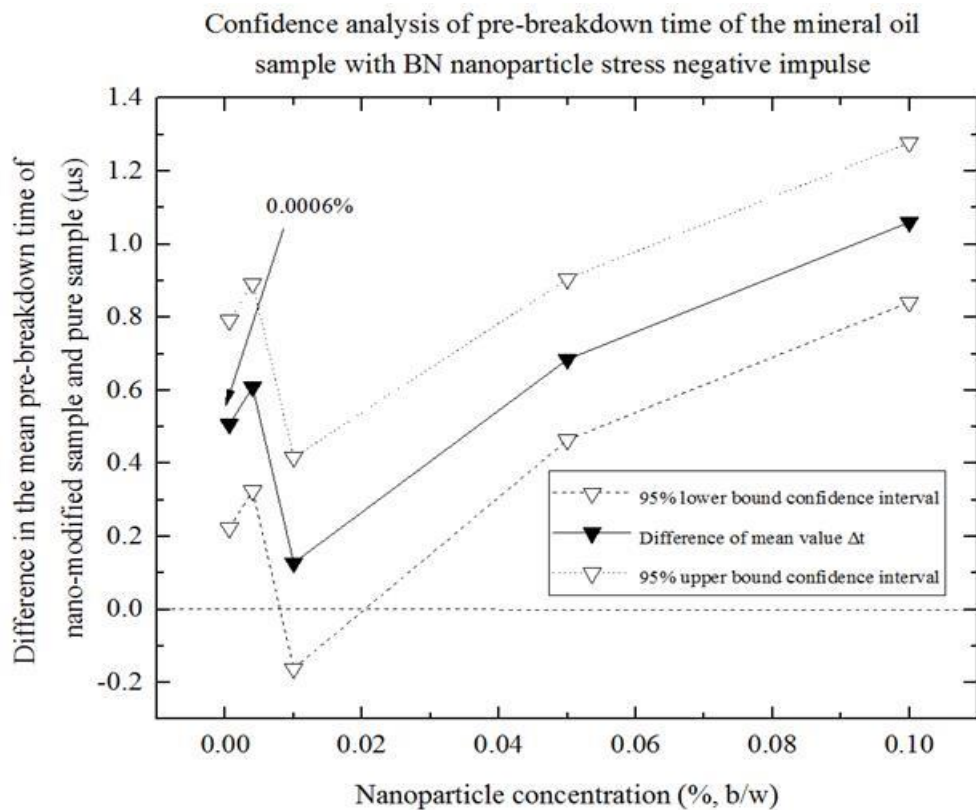
### **5.5.2 Confidence analysis of the pre-breakdown times for BN nano-modified liquids**

In the case of nano-modified samples with BN nanoparticles stressed with positive and negative impulses, the confidence analysis results of the pre-breakdown times are shown in Figures 5-29 to 5-31. In these figures, the pre-breakdown times shown in Figures 5-6 and 5-7 were used to verify the statistical significance of the difference between the pre-breakdown times of the base and nano-modified samples.

As Figures 5-29 to 5-31 show, the confidence analysis of the positive and negative impulse pre-breakdown times of BN nano-modified liquids showed that the difference in population means decreased with an increase in the concentration of nanoparticles. These graphs confirm that the small concentration of nanoparticles used in the present study (0.0006% or 0.004% (b/w) of BN nanoparticles) provided the largest improvement (increase) in the pre-breakdown time of the nano-modified liquids. Additionally, the lower 95% CI for  $\Delta t$  related to these concentrations stayed positive for all three liquids with BN nanoparticles (besides the case of the nano-modified sample of natural ester stressed with a positive impulse), thus confirming that this increase in the pre-breakdown time compared with the base liquids (positive  $\Delta t$ ) is statistically significant for all tested nano-modified samples. With an increase in concentration of nanoparticles, the difference in the pre-breakdown time of base liquids and nano-modified liquids,  $\Delta t$ , decreased. In some cases, the optimal concentration of nanoparticles producing the largest  $\Delta t$  was 0.004% (b/w), for example, for the nano-modified mineral oil stressed with positive and negative impulses and for the natural ester stressed with the negative impulses. Again, as in the case of the 0.004% optimal concentration,  $\Delta t$  decreased when the particle concentration increased above 0.004%.

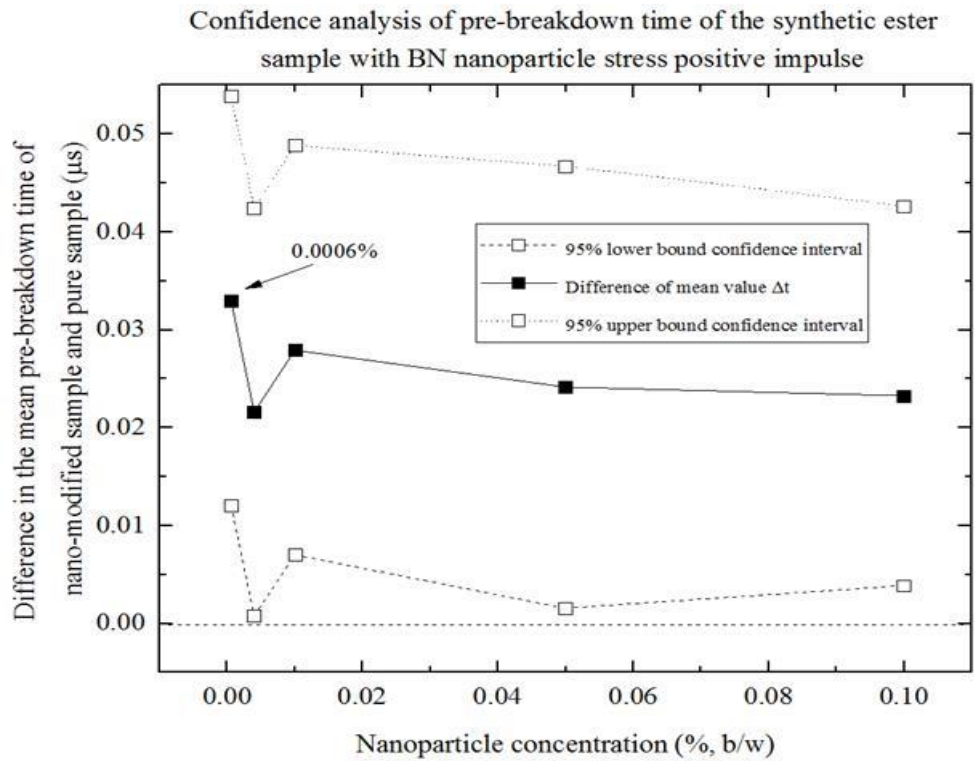


(a)

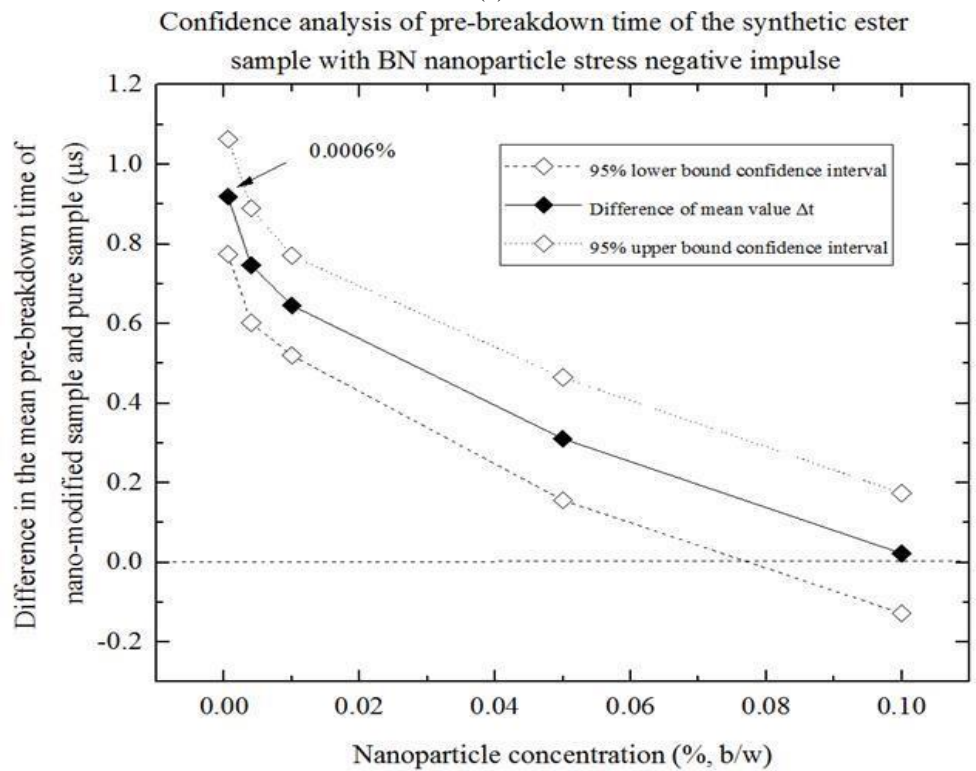


(b)

**Figure 5-29.** Confidence analysis results,  $\Delta t$ , of mineral oil with BN nanoparticles stressed with a positive impulse (a) and a negative impulse (b). Each data point denotes the  $\Delta t$  between the mean value of the breakdown voltages of the base and nano-modified samples. The dotted line represents the upper 95% confidence bound; the dashed line represents the lower 95% confidence bound.

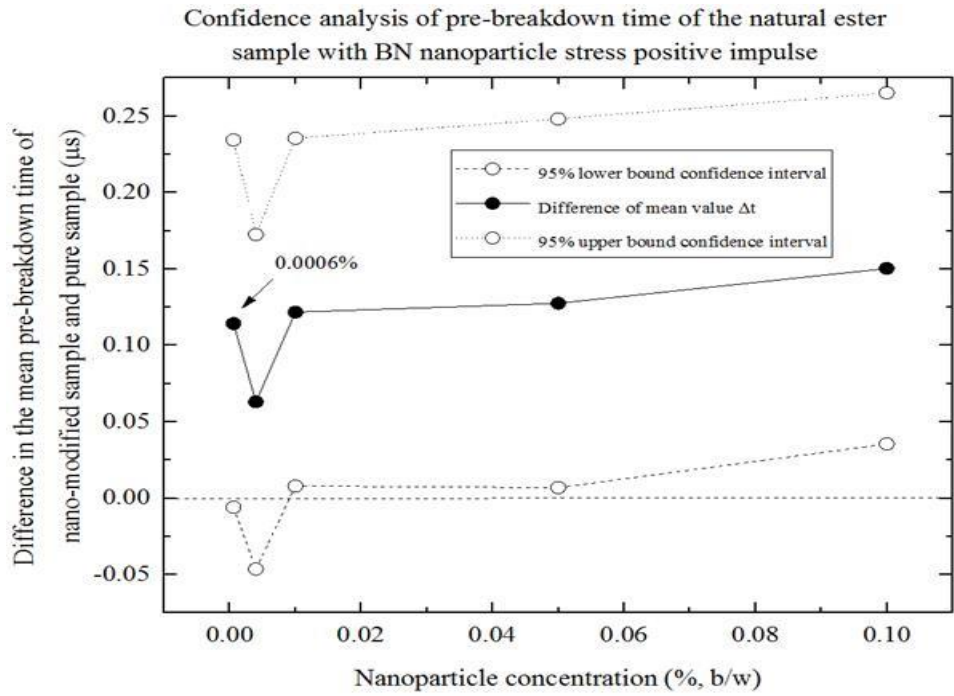


(a)

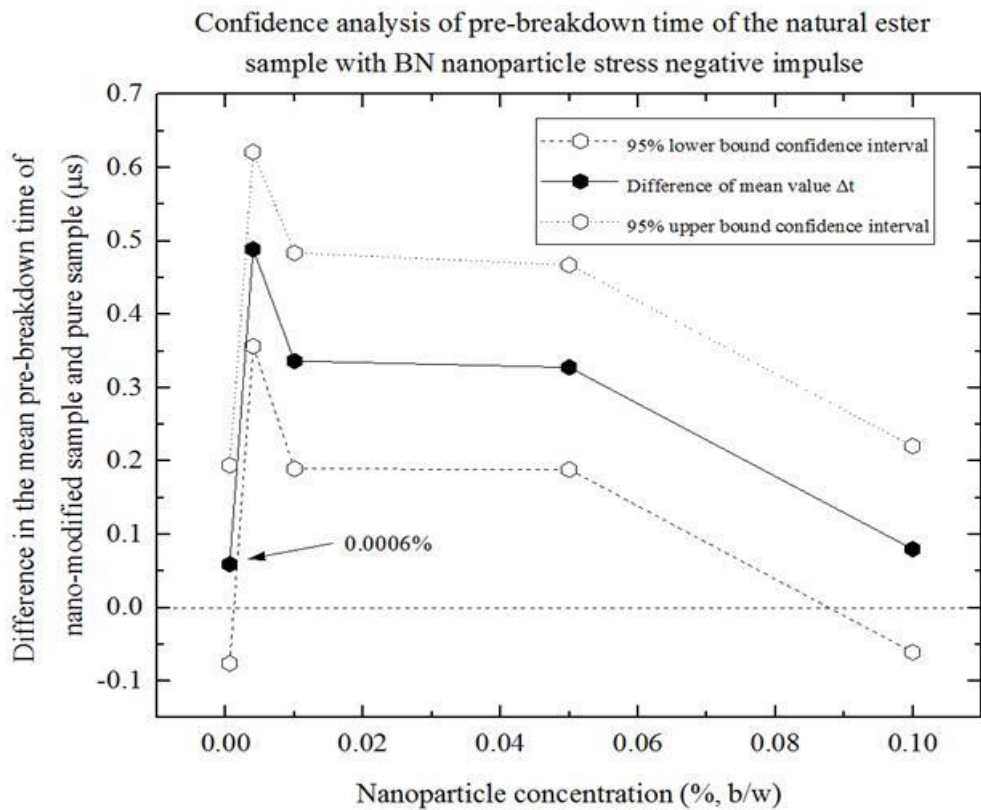


(b)

**Figure 5-30.** Confidence analysis results,  $\Delta t$ , of synthetic ester with BN nanoparticles stressed with a positive impulse (a) and a negative impulse (b). Each data point denotes the  $\Delta t$  between the mean value of the breakdown voltages of the base and nano-modified samples. The dotted line represents the upper 95% confidence bound; the dashed line represents the lower 95% confidence bound.



(a)



(b)

**Figure 5-31.** Confidence analysis results,  $\Delta t$ , of natural ester with BN nanoparticles stressed with a positive impulse (a) and a negative impulse (b). Each data point denotes the  $\Delta t$  between the mean value of the breakdown voltages of the base and nano-modified samples. The dotted line represents the upper 95% confidence bound; the dashed line represents the lower 95% confidence bound.

The results showed that the lower 95% CI crossed the zero line for the nano-modified samples, which means, in the correlated concentration, this difference between the mean pre-breakdown time for the base oil and the mean pre-breakdown time of the nano-modified samples was not statistically significant. In the following cases, the pre-breakdown times of the samples with correlated concentrations were almost the same as the pre-breakdown time of the base sample:

- The nano-modified samples of the mineral oil with a 0.1% concentration of nanoparticles stressed with a positive impulse and the samples with a 0.01% concentration of nanoparticles stressed with a negative impulse;
- The synthetic ester nano-modified samples with 0.1% concentration of nanoparticles stressed with a negative impulse;
- The natural ester nano-modified samples with 0.0006% and 0.004% concentrations of nanoparticles stressed with a positive impulse and with 0.0006% and 0.1% concentrations of nanoparticles stressed with a negative impulse.

With an increase in concentration, the pre-breakdown time of nano-modified samples was lower than the pre-breakdown time of the base sample. Hence, the difference between the mean pre-breakdown time for the base oil and the mean pre-breakdown times of the nano-modified samples,  $\Delta t$ , increased.

Figure 5-6 shows, in the case of natural ester, the nano-modified samples with 0.0006% (b/w) BN nanoparticles stressed with a positive impulse provided the highest pre-breakdown time compared with the other samples. The Weibull analysis results of this sample showed, in this case, the longest 50% and 90% pre-breakdown times and the highest location parameters. These results can confirm that the 0.0006% (b/w) concentration can be treated as the optimal concentration for the nano-modified samples of the natural ester with BN nanoparticles. However, the confidence analysis results showed that the 95% lower bound of the nano-modified samples with 0.0006% (b/w) concentration BN nanoparticles crossed the zero line, which means the difference between the mean pre-breakdown time for the base oil and the mean pre-breakdown time of the nano-modified samples were not statistically significant.

## 5.6 Summary

In the present section, the standard lightning impulse breakdown tests were conducted using TiO<sub>2</sub> and BN nano-modified samples of all three liquids. Based on the breakdown waveforms, the pre-breakdown times, breakdown voltages, and streamer velocities were obtained, and the statistical analysis of the results was conducted. The statistical analysis included the Weibull distribution analysis, which was applied to the pre-breakdown times in the nano-modified liquids. To investigate the statistical significance of the variation of the breakdown voltages and pre-breakdown times on the concentration of nanoparticles, the confidence analysis was applied on all tested samples, and the statistical difference analysis was used to calculate the statistical difference and the 95% CI between the average values of the pre-breakdown time,  $\Delta t$ , of the base and nano-modified liquids.

The pre-breakdown time can be a key factor in the dielectric performance evaluation of nano-modified dielectric fluids; this time indicates the ability of the dielectric liquid to withstand HV stress. A longer pre-breakdown time means that the insulating liquids have a higher capability to inhibit the initial streamer formation and propagation.

For both TiO<sub>2</sub> and BN nano-modified fluids, it was established that different concentrations of nanoparticles changed the pre-breakdown times in the case of positive and negative impulse stresses. It was found that the longest pre-breakdown time was demonstrated by the nano-modified samples with nanoparticle optimal concentrations of 0.0006% (or in some cases of 0.004%). For the liquid samples in which the mass concentration of the nanoparticles exceeded the optimal concentrations, the dielectric properties started to deteriorate. The pre-breakdown time started to be shorter, and the breakdown voltages also changed. The results mean that, by adding a small volume of nanoparticles into the insulating liquid sample, it can improve the insulating properties of the dielectric liquids. However, if the concentration of nanoparticles exceeded the optimal value, the dielectric strength of the nano-modified liquids deteriorated. It was shown that, in some cases, for the highest concentration of nanoparticles (0.1% b/w), the pre-breakdown time was even shorter than that for the base liquid. This performance was consistent with that of the published results [193].

### **5.6.1 Discussion of pre-breakdown time measurement results**

The pre-breakdown time measurement results showed that adding both TiO<sub>2</sub> and BN nanoparticles at a particular concentration into insulating liquid samples can improve the dielectric properties of these samples. In the case of the nano-modified samples with TiO<sub>2</sub> nanoparticles stressed with a positive impulse test, the pre-breakdown time of the mineral oil sample showed insensitivity to the concentration of the nanoparticles. Both ester samples provided significant pre-breakdown time changes with an increase in nanoparticle concentration. In the case of nano-modified samples stressed with a negative impulse, the pre-breakdown time of the nano-modified samples of mineral oil with TiO<sub>2</sub> nanoparticles showed insensitivity to the concentration of nanoparticles. Both ester samples provided pre-breakdown time significant changes with an increase in nanoparticle concentration. These results were similar to the case of the positive impulse measurement results.

In the case of the nano-modified sample with BN nanoparticles stressed with a positive impulse, the pre-breakdown time of the mineral oil sample showed high sensitivity to the concentration of nanoparticles compared with the nano-modified samples of mineral oil with TiO<sub>2</sub> nanoparticles. In contrast, the pre-breakdown time of the synthetic and natural nano-modified samples showed insensitivity to the concentration of nanoparticles. In the case of the nano-modified samples stressed with a negative impulse, the pre-breakdown time of the mineral oil and synthetic ester samples provided high sensitivity to the concentration of nanoparticles. The nano-modified samples of the natural ester showed that the pre-breakdown time was insensitive to the concentration of nanoparticles.

### **5.6.2 Streamer velocity of nano-modified samples discussion**

The streamer velocity was calculated based on the pre-breakdown time. For most cases of the three liquid-based nano-modified samples with TiO<sub>2</sub> nanoparticles stressed with positive and negative impulses, the streamer velocities were slower than 3 km/s, which belong to the ‘slow’ streamer, ‘second mode’ streamer [11], [82], [224]–[227]. In some cases (synthetic ester base samples and nano-modified samples with 0.1% (b/w) TiO<sub>2</sub> nanoparticles stressed with a positive impulse), the streamer velocities would reach faster than 7 km/s, which started to transfer into the ‘third mode’ streamer.

In the case of the nano-modified samples with BN nanoparticles stressed with a positive impulse, the streamer velocities of the mineral oil and natural ester were slower than 3.5 km/s, which belong to the aforementioned slow streamer. For all synthetic ester tested samples, the streamer velocities were higher than 6.5 km/s, which means it started to transfer into the third mode streamer. In the case of the synthetic ester sample with 0.0006% (b/w) BN nanoparticles stressed with a positive impulse, the streamer velocities (6.5 km/s) were slightly slower than the base sample (7 km/s). In the case of the synthetic ester sample with other concentrations, the streamer velocities were higher than 7 km/s. These results showed that, in the case of the synthetic ester sample with BN nanoparticles stressed with a positive impulse, the BN nanoparticle did not result in an obvious slow phenomenon on the streamer velocities.

In the case of the three liquid-based nano-modified samples with BN nanoparticles stressed with a negative impulse, the streamer velocities of all tested samples were slower than 1.4 km/s, which belonged to the slow streamer.

The streamer calculation results showed that adding nanoparticles into the insulating liquid can inhibit the streamer formation and propagation in some degree. In [193], the published results indicated that the insulating capability would decrease with the nanoparticle concentration increase by a relatively large amount. In the present work, the results showed that there was a relatively optimal concentration in the small concentration range (between base to 0.1%) that could improve the liquid insulating capability.

### **5.6.3 Discussion of the Weibull distribution analysis**

The Weibull distribution was applied to analyse the pre-breakdown time measurement results in the case of the nano-modified samples with TiO<sub>2</sub> and BN nanoparticles. The pre-breakdown times corresponding to the 5%, 10%, 50%, and 90% probabilities to breakdown were shown in Section 5.4. The location, scale, and shape parameters of the Weibull distribution were also presented in Section 5.4.

Compared with the experimental results shown in Section 5.3, the nano-modified samples with the optimal concentration provided the longest pre-breakdown times and the largest location parameters. In most cases, the scale parameters of these samples with the optimal concentration were higher than

the samples with other concentrations. The potential reason is that, for these samples with the optimal concentration, the maximum pre-breakdown time was longer than the samples with other concentrations and the pre-breakdown time showed a wider spread with respect to the samples with other concentrations. The shape parameters of the samples with the optimal concentration showed an average level compared with the samples with other concentrations, which means these samples with the optimal concentration provided longer pre-breakdown times, but the failure rate did not rise with an increase in time with respect to the other samples.

In the case of the mineral oil, the Weibull analysis results of the nano-modified samples with TiO<sub>2</sub> and BN nanoparticles stressed with positive and negative impulses were similar. Moreover, in the case of the synthetic ester, the samples with optimal concentration TiO<sub>2</sub> nanoparticles provided longer pre-breakdown times corresponding to the breakdown probability and larger location parameters compared with the samples with the optimal concentration of BN nanoparticles. The scale and shape parameters of the samples with the optimal concentration of TiO<sub>2</sub> nanoparticles were also smaller than the samples with the optimal concentration of BN nanoparticles, which indicates that the samples with the optimal concentration of TiO<sub>2</sub> nanoparticles provided better stability with an increase in pre-breakdown time compared with the samples with BN nanoparticles.

In the case of natural ester, the samples with the optimal concentration of TiO<sub>2</sub> nanoparticles provided longer pre-breakdown times corresponding to the breakdown probability and larger location parameters compared with the samples with the optimal concentration of BN nanoparticles. The scale and shape parameters of the samples with the optimal concentration of TiO<sub>2</sub> nanoparticles were higher than those of the samples with the optimal concentration of BN nanoparticles, which indicates that the mean samples with the optimal concentration of TiO<sub>2</sub> nanoparticles provided a longer HV withstand time but worse stability with an increase in pre-breakdown time compared with the samples with the BN nanoparticles.

In some cases, the data did not fit the Weibull fitting line (straight line) very well. The potential reason for this phenomenon is that there may be several different breakdown mechanisms occurring. In some cases, the pre-breakdown time with high cumulative probability is much longer than those of other cases. The reason for these results is that some breakdown events occurred on the impulse tail, which leads to longer pre-breakdown times. In future experiments, if the prospective peak applied voltage

were higher, such that all breakdown events occurred on the impulse front, the Weibull fitting line may provide a better fit to the data.

This phenomenon generally occurred for the nanofluids with optimal concentration of nanoparticles, thus the nanofluids with optimal concentration can be expected to provide comparatively longer pre-breakdown times than those of the other samples, even if the breakdown events all occurred on the impulse front.

#### **5.6.4 Discussion of confidence analysis**

In the confidence analysis, *t*-statistics were used to analyse the pre-breakdown time obtained for base and nano-modified liquids to find the statistical significance in the increase in the pre-breakdown time. The difference between the average pre-breakdown time of nano-modified samples and base samples,  $\Delta t$ , and the 95% CI were calculated and discussed in Section 5.5. The results of the confidence analysis showed that, in most cases of the nano-modified samples with the optimal concentration of nanoparticles (TiO<sub>2</sub> or BN), the lower bound of the 95% CI for  $\Delta t$  related to this concentration stayed positive, thus confirming that this increase in the pre-breakdown time compared with the base liquids (positive  $\Delta t$ ) was statistically significant. The lower bound of the 95% CI for  $\Delta t$  crossed the zero line only for the natural ester with BN nanoparticles stressed with a positive impulse, which indicates that the difference between the mean pre-breakdown time for the base oil and the mean pre-breakdown time of the nano-modified samples was not statistically significant.

# CHAPTER 6

## MINIMUM-LIGHTNING IMPULSE

### BREAKDOWN VOLTAGE INVESTIGATION

#### 6.1 Introduction

The insulation systems employed in modern power and pulsed power industries are complex systems. There are many factors that should be considered in the design and coordination of insulating systems. These factors include the 1) ability to inhibit the formation and propagation of the pre-breakdown streamers, 2) good thermal conductivity of insulating liquids, and 3) potential degradation of their dielectric properties during ageing (ageing processes). One of the main dielectric performance characteristics that should be considered in the insulation coordination is the minimum withstand voltage of the insulating material.

In addition to typical over-voltages, power systems can be subjected to transient nonlinear high voltages that can be generated by atmospheric events, such as lightning strikes. Such fast transient voltages are induced by direct attachment of the lightning strike to the power equipment or by strong transient electromagnetic fields generated by the lightning strike. Therefore, the electrical equipment and power systems should be tested to ensure that their insulation will withstand such high transient voltages. These tests are conducted in accordance with the minimum withstand voltage procedure, which requires the application of the impulse withstand voltage with a standard waveform of 1.2/50  $\mu$ s.

A large amount of experimental work has been conducted by multiple research groups who have investigated the minimum withstand voltage of traditional mineral oils under a various experimental conditions, including different inter-electrode gap distances [11] [12], different levels of humidity of oils [4], and different types of applied impulses [72].

The major objective of this project is to obtain the minimum withstand voltage of both synthetic and natural ester liquids (base and nano-modified) and to compare it with the minimum withstand voltage

of the traditional mineral oil (also base and nano-modified). The experiments on the minimum withstand voltage were designed in accordance with the international standards, ASTM D3300-00, [80] and IEC 60897 [133]. The electrode topology was set to the point-sphere type. The gap distance was set to 2 mm. Further details of the experimental setting and methodology were discussed in Section 3.5.

## 6.2 Experimental Procedure

Per the international standards ASTM D3300-00 and IEC 60897, to measure the minimum-lightning impulse breakdown voltage, the initial charging voltage of the Marx generator should be set to a value such that the output voltage from the Marx generator applied across the test cell is well below the expected breakdown voltage of the insulating liquid.

Per the ASTM standards, the point-sphere electrode topology was used. The gap between the HV point electrode and the grounded spherical electrode was set to 2 mm. The charging voltage of the Marx generator was then increased in steps of 2 kV until the breakdown occurred, and the peak voltage of the 1.2/50  $\mu$ s wave-shape was recorded as the breakdown voltage.

A new gramophone needle was used for each series of tests for each sample, and the brass spherical ground electrode was polished after each series of tests. The electrodes were cleaned with alcohol and then washed with distilled water. The test cell and electrodes were then dried in an oven for 2 hours at 40 °C to remove water prior to the next test. Before the impulse tests, the samples of dielectric liquids were kept under vacuum for 1.5 hours at room temperature to remove gas bubbles.

The main difference between the ASTM D3300-00 and IEC 60897 procedures is as follows: the ASTM standard requires performing three shots per voltage step, while the IEC standard requires only a single shot per each voltage step. The voltage was increased in steps until breakdown occurred, and after each breakdown, a new series of voltage steps started with the initial minimum safe voltage level. These procedures for both tests are shown schematically in Figures 6-1 and 6-2. In these Figures,  $\Delta T_1$  is the time interval between two consecutive shots without breakdown;  $\Delta T_2$  is the time interval between each test in the case of a breakdown event, and  $\Delta V_1$  is an increase in voltage per each step.

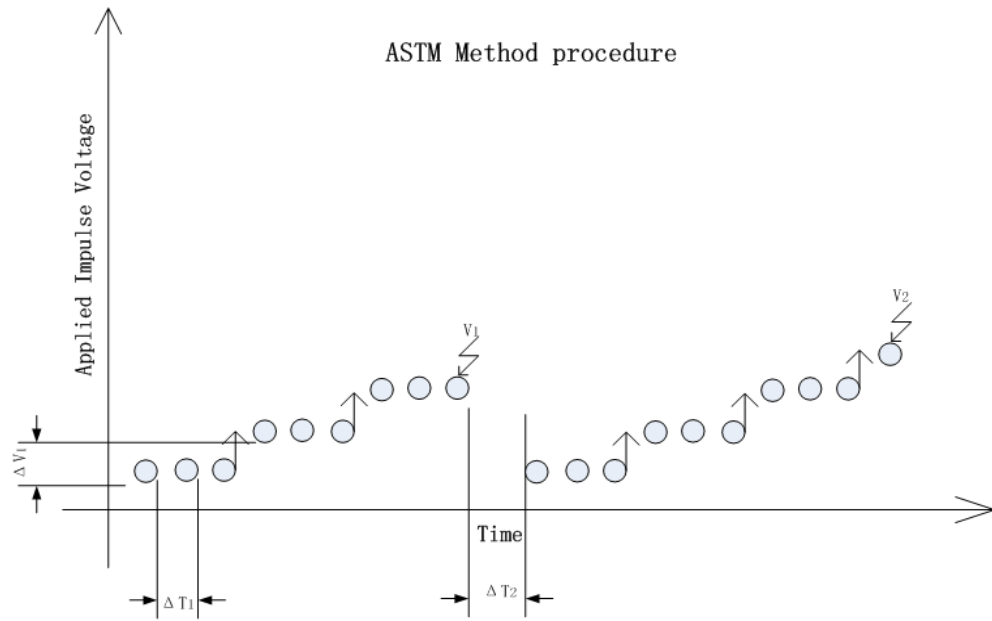


**Figure 6-1.** Measurement procedure of the ASTM standard.

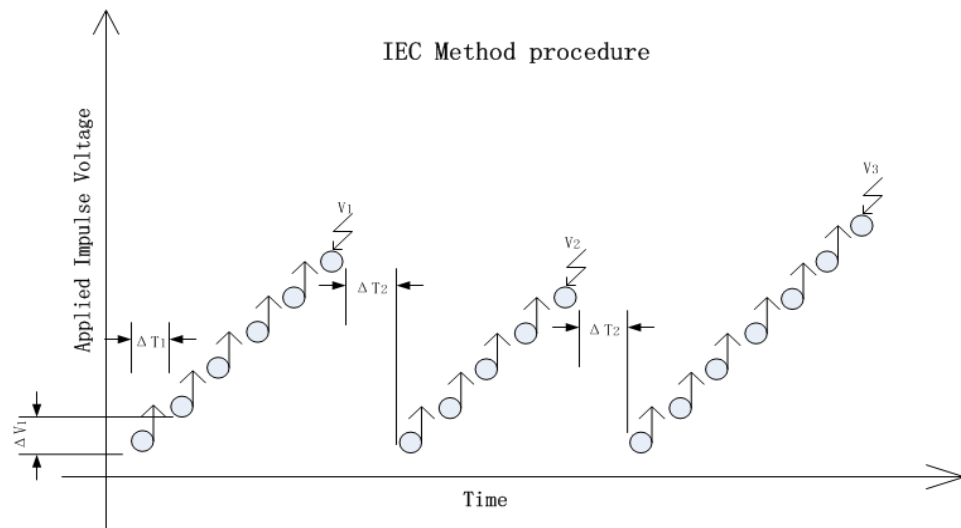


**Figure 6-2.** Measurement procedure of the IEC standard.

For the first test of a serial experiment, the test liquid was slowly filled in a test cell to avoid air bubbles. Moreover,  $\Delta T_2$  is the sample undisturbed time prior to starting the test to allow the potential micro-bubbles to dissipate. During the test, the impulse voltage applied on the electrodes will inject a lot of energy into the test liquid instantly. This large amount of energy will decompose the liquid molecularly and produce an arc near the electrode. The by-products of this phenomenon (such as carbon) will form between the electrodes, which may deteriorate the withstand voltage of the liquid. To avoid these by-products affecting the test results, the time interval  $\Delta T_1$  is necessary to allow these

substances to dissipate. As the international standard required,  $\Delta T_1$  is 30 seconds and  $\Delta T_2$  is 2 minutes in both the ASTM and IEC tests.

### **6.3 Minimum-lightning Impulse Breakdown Voltage of Liquids**

In this section, the results of the minimum withstand breakdown tests that have been performed following both ASTM D3300-00 and IEC 60897 procedures are presented. Three types of liquids – mineral oil, synthetic ester, and natural ester (base and nano-modified) – were used in these tests. The concentration of BN and TiO<sub>2</sub> nanoparticles in these liquids were the same as in the cases of the AC breakdown voltage tests and the standard lightning impulse tests: 0.0006%, 0.004%, 0.01%, 0.05%, and 0.1% (b/w). For the ASTM method, five independent samples were prepared and tested for each type of liquid and each nanoparticle concentration. For the IEC method, 10 independent samples of each liquid and each concentration of nanoparticles were prepared and tested.

#### **6.3.1 ASTM D3300-00 method test results**

Figures 6-3 and 6-4 show the minimum-lightning impulse breakdown voltage of base and TiO<sub>2</sub> nano-modified liquids measured in accordance with the ASTM standard. In these two figures, open data points show the breakdown voltages for positive lightning waveforms; the closed data points show the breakdown voltages for negative lightning waveforms. To identify the difference between breakdown voltages for different liquid samples with the same concentration of nanoparticles, all data points that belong to different concentrations of the same nano-modified liquid are shown using the same symbols. The measurement results of the three liquids with TiO<sub>2</sub> nanoparticles of a series of concentrations (base, 0.0006%, 0.004%, 0.01%, 0.05%, 0.1%, b/w) under both positive and negative impulse polarities are shown in Table 6-1.

### ASTM TiO<sub>2</sub> Positive Minimum Withstand Voltage

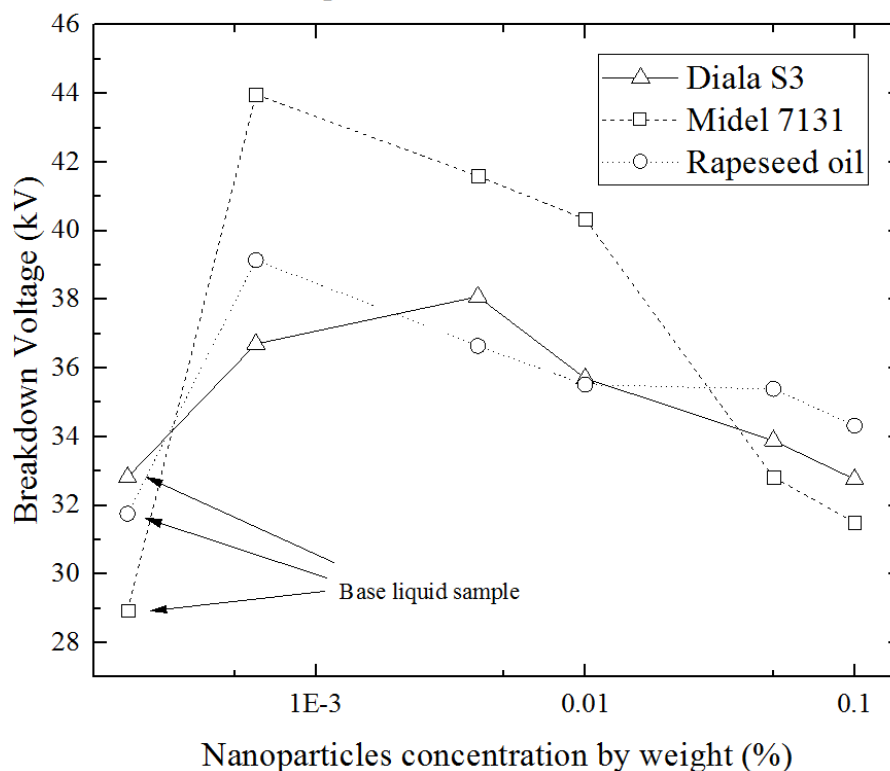


**Figure 6-3.** Positive minimum withstand voltage for base and nano-modified liquids obtained in accordance with the ASTM standard as a function of TiO<sub>2</sub> nanoparticle concentration. The lines in this graph are given for visual guidance only.

As Figure 6-3 shows, in the case of the mineral oil samples, the sample with the TiO<sub>2</sub> nanoparticle concentration of 0.004% (b/w) provided the highest breakdown voltage ( $38.09 \pm 5.45$  kV) and the largest improvement (increase) in the breakdown voltage (16.03% increase) compared with the lowest breakdown voltage (0.1% sample). For the samples with nanoparticle concentrations higher than 0.004%, the breakdown voltage started to drop. The nano-modified liquid with 0.1% concentration (b/w) provided the lowest breakdown voltage ( $32.76 \pm 5.11$  kV), this was the only concentration of nanoparticles that resulted in a breakdown voltage lower than the breakdown voltage of the base sample (0.19% decrease). The highest breakdown voltage (0.004% sample) provided a 16.06% increase with respect to the breakdown voltage of the base sample.

In the case of the synthetic ester, the sample with 0.0006% (b/w) concentration of TiO<sub>2</sub> nanoparticles provided the highest breakdown voltage ( $43.97 \pm 3.41$  kV) and the largest improvement (increase) in the breakdown voltage (51.95% increase) with respect to the lowest breakdown voltage (base sample). For the nano-modified samples with concentrations of TiO<sub>2</sub> nanoparticles higher than 0.0006%, the

breakdown voltage started to decrease. All nano-modified samples of Midel 7131 provided higher breakdown voltages than that for the base ester liquid. The sample with 0.1% concentration of nanoparticles provided the lowest breakdown voltage ( $31.51 \pm 3.75$  kV) among all tested nano-modified samples. The maximum voltage improvement in the breakdown voltage was more than 50% (i.e., the breakdown voltage of the sample with 0.0006% concentration of nanoparticles had a breakdown voltage 50% higher than the breakdown voltage of the base liquid).

In the case of the natural ester, the  $\text{TiO}_2$  nano-modified samples with 0.0006% concentration of nanoparticles (b/w) demonstrated the highest breakdown voltage ( $39.15 \pm 2.63$  kV) and the largest improvement in the voltage (23.27% increase compared with the breakdown voltage of the base liquid). For concentrations of nanoparticles higher than 0.0006%, the breakdown voltage started to drop. All nano-modified samples of the vegetable oil demonstrated higher breakdown voltage compared with the base oil. A concentration of 0.1% provided the lowest breakdown voltage ( $34.33 \pm 4.43$  kV) among all tested nano-modified samples of the vegetable oil. The maximum voltage improvement was more than 23% (i.e., the breakdown voltage of the samples with 0.0006% concentration of nanoparticles (b/w) was higher than the breakdown voltage of base vegetable oil by more than 23%).

As Figure 6-4 shows, for mineral oil samples, the sample with a  $\text{TiO}_2$  nanoparticle concentration of 0.0006% (b/w) provided the highest breakdown voltage ( $53.18 \pm 3.46$  kV), and the largest voltage increase in the breakdown voltage was 8% with respect to the lowest breakdown voltage (base sample). For the samples with nanoparticle concentrations higher than 0.0006%, the breakdown voltages started to drop. The nano-modified sample with 0.1% (b/w) concentration provided the lowest breakdown voltage compared with other nano-modified mineral oil samples,  $49.74 \pm 0.34$  kV, and a slight voltage improvement (1.02% increase) with respect to the breakdown voltage of the base sample.

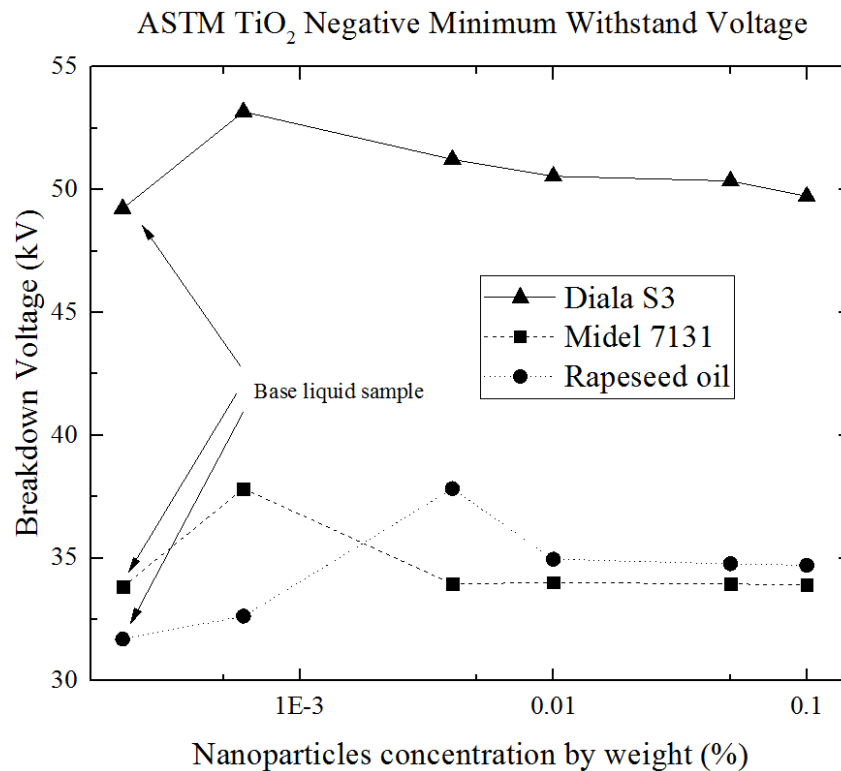


**Figure 6-4.** ASTM standard TiO<sub>2</sub> negative minimum withstand voltage for the samples with different nanoparticle concentrations. The lines in this graph are given for visual guidance only.

In the case of the synthetic ester, the 0.0006% (b/w) sample with TiO<sub>2</sub> nanoparticles provided the highest breakdown voltage ( $37.83 \pm 5.75$  kV) and the largest voltage increase (11.82% increase) with respect to the lowest breakdown voltage (base sample). For concentrations of nanoparticles higher than 0.0006%, the breakdown voltages started to drop. All nano-modified samples of synthetic ester demonstrated higher breakdown voltage compared with the base sample. A concentration of 0.1% provided the lowest breakdown voltage ( $33.91 \pm 0.17$  kV) among all tested nano-modified synthetic ester, which was slightly higher than the breakdown voltage of the base sample (0.24% increase). The maximum voltage improvement was 11.82% (i.e., the breakdown voltage of the samples with 0.0006% concentration of nanoparticles (b/w) was higher than the breakdown voltage of base synthetic ester by more than 11.82%).

In the case of the natural ester, the TiO<sub>2</sub> nano-modified samples with 0.004% concentration of nanoparticles (b/w) demonstrated the highest breakdown voltage ( $37.83 \pm 5.39$  kV) and the largest improvement in the breakdown voltage (19.38% increases) compared with the lowest breakdown voltage (base sample). For concentrations of nanoparticles higher than 0.004%, breakdown voltages

started to drop. All nano-modified samples of vegetable oil demonstrated higher breakdown voltage compared with the base sample. A concentration of 0.1% provided the lowest breakdown voltage ( $34.71 \pm 1.12\text{kV}$ ) among all tested nano-modified samples. The maximum voltage improvement was more than 19% (i.e., the breakdown voltage of the samples with 0.004% concentration of nanoparticles (b/w) was higher than the breakdown voltage of base vegetable oil by more than 19%).

**Table 6-1.** ASTM standard TiO<sub>2</sub> sample minimum withstand voltage test results.

| Concentration<br>by Weight | ASTM Method TiO <sub>2</sub> Sample Breakdown Voltage (kV) |            |                 |                  |            |                 |
|----------------------------|--|------------|-----------------|------------------|------------|-----------------|
|                            | Positive Impulse   |            |                 | Negative Impulse |            |                 |
|                            | Diala S3   | Midel 7131 | Rapeseed<br>Oil | Diala S3         | Midel 7131 | Rapeseed<br>Oil |
| 0.00%                      | 32.82±5.23   | 28.94±2.77 | 31.76±3.69      | 49.24±3.38       | 33.83±0    | 31.69±3.51      |
| 0.0006%                    | 36.71±5.05   | 43.97±3.41 | 39.15±2.63      | 53.18±3.46       | 37.83±5.75 | 32.64±1.79      |
| 0.004%                     | 38.09±5.45   | 41.59±4.89 | 36.64±5.34      | 51.24±2.56       | 33.95±0.17 | 37.83±5.39      |
| 0.01%                      | 35.71±2.64   | 40.34±0.34 | 35.52±8.02      | 50.55±3.01       | 34.01±0.28 | 34.95±3.49      |
| 0.05%                      | 33.89±4.21   | 32.82±6.93 | 35.39±5.15      | 50.36±2.21       | 33.95±0.17 | 34.77±1.53      |
| 0.1%                       | 32.76±5.11   | 31.51±3.75 | 34.33±4.43      | 49.74±0.34       | 33.91±0.17 | 34.71±1.12      |

Figures 6-5 and 6-6 show the minimum-lightning impulse breakdown voltages of base and BN nano-modified liquids measured in accordance with the ASTM standard. In these two figures, open data points show the breakdown voltages for positive lightning waveforms; the closed data points show the breakdown voltages for negative lightning waveforms. To identify the difference between breakdown voltages for different liquid samples with the same concentration of nanoparticles, all data points that belong to different concentrations of the same nano-modified liquid are shown using the same symbols. The measurement results of the three liquids with BN nanoparticles of a series of concentrations (base, 0.0006%, 0.004%, 0.01%, 0.05%, 0.1%, b/w) under both positive and negative impulse polarities are shown in Table 6-2.

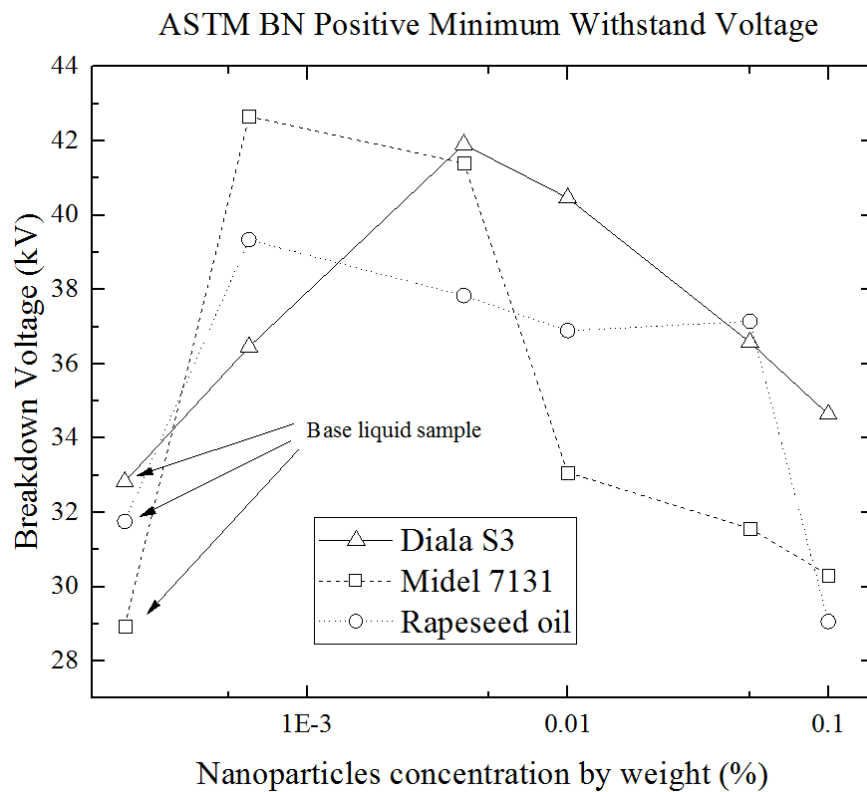


**Figure 6-5.** ASTM standard BN positive minimum withstand voltage for the samples with different nanoparticle concentrations. The lines in this graph are given for visual guidance only.

As Figure 6-5 shows, for mineral oil stressed with a positive impulse, the sample with the BN nanoparticle concentration of 0.004% (b/w) provided the highest breakdown voltage ( $41.91 \pm 6.98$  kV) and the largest improvement (increase) in the breakdown voltage (27.7% increase) compared with the lowest breakdown voltage (base sample). For the samples with nanoparticle concentrations higher than 0.004%, the breakdown voltage started to drop. The nano-modified liquid with the 0.1% concentration (b/w) provided the lowest breakdown voltage ( $34.64 \pm 0.36$  kV) among all tested nano-modified samples of the mineral oil. All nano-modified samples of Diala S3 provided higher breakdown voltages than those for all three base fluids.

In the case of the synthetic ester, the sample with 0.0006% (b/w) concentration of the BN nanoparticles provided the highest breakdown voltage ( $42.66 \pm 7.25$  kV) and the largest improvement (increase) in the breakdown voltage (47.41% increase) with respect to the lowest breakdown voltage (base sample). For the nano-modified samples with concentrations of BN nanoparticles higher than 0.0006%, the breakdown voltage started to decrease. The sample with the 0.1% concentration of nanoparticles provided the lowest breakdown voltage ( $30.32 \pm 7.24$  kV) among all tested nano-

modified samples of synthetic ester. All nano-modified samples of Midel 7131 provided higher breakdown voltages than that for the base ester liquid.

In the case of the natural ester, the BN nano-modified samples with 0.0006% concentration of nanoparticles (b/w) demonstrated the highest breakdown voltage ( $39.34 \pm 2.58$  kV) and the largest improvement in the voltage (35.38% increase compared with the breakdown voltage of the 0.1% sample). For concentrations of nanoparticles higher than 0.0006%, the breakdown voltage started to drop. A concentration of 0.1% provided the lowest breakdown voltage ( $29.06 \pm 3.19$  kV) among all tested nano-modified samples of the vegetable oil. This is the only concentration of nanoparticles that resulted in a breakdown voltage lower than the breakdown voltage of the base sample (8.5% decrease). The highest breakdown voltage (0.0006% sample) provided a 23.87% increase with respect to the breakdown voltage base sample.

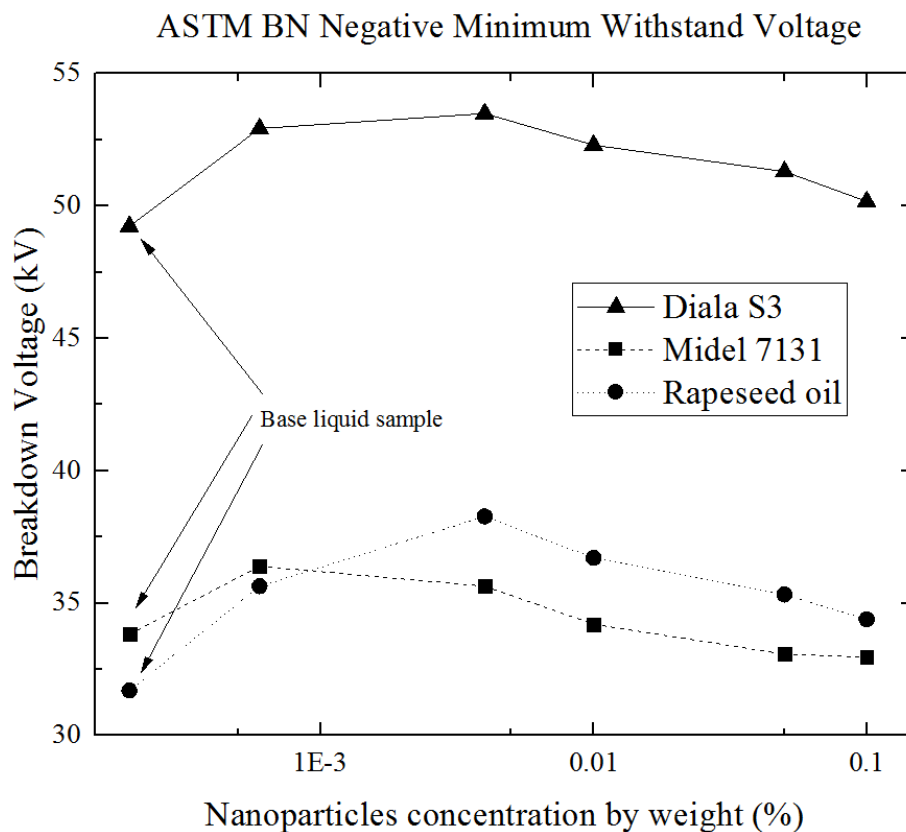


**Figure 6-6.** ASTM standard BN negative minimum withstand voltage for the samples with different nanoparticle concentrations. The lines in this graph are given for visual guidance only.

As Figure 6-6 shows, for mineral oil stressed with a negative impulse, the sample with a BN nanoparticle concentration of 0.004% (b/w) provided the highest breakdown voltage ( $53.49 \pm 2.33$  kV)

and the largest voltage increase in the breakdown voltage was an 8.63% increase with respect to the lowest breakdown voltage of the tested sample (base mineral oil sample). For the samples with nanoparticle concentrations higher than 0.004%, the breakdown voltages started to drop. The nano-modified sample with 0.1% (b/w) concentration provided the lowest breakdown voltage compared with the other nano-modified mineral oil samples,  $50.17 \pm 3.36$  kV, and a slight voltage improvement (1.89% increases) with respect to the breakdown voltage of the base sample.

In the case of the synthetic ester, the 0.0006% (b/w) sample with BN nanoparticles provided the highest breakdown voltage ( $36.39 \pm 3.24$  kV) and the largest voltage increase (10.41% increase) with respect to the lowest breakdown voltage of the tested sample (0.1% sample). For concentrations of nanoparticles higher than 0.0006%, the breakdown voltages started to drop. A concentration of 0.1% provided the lowest breakdown voltage ( $32.96 \pm 2.79$  kV) among all tested nano-modified synthetic ester, which was lower than the breakdown voltage of the base sample (2.57% decrease). The highest breakdown voltage (0.004% sample) provided a 7.57% increase with respect to the breakdown voltage of the base sample.

**Table 6-2.** ASTM standard BN sample minimum withstand voltage test results.

| Concentration<br>by Weight | ASTM Method BN Sample Breakdown Voltage (kV) |            |              |                  |            |              |
|----------------------------|--|------------|--------------|------------------|------------|--------------|
|                            | Positive Impulse                             |            |              | Negative Impulse |            |              |
|                            | Diala S3                                     | Midel 7131 | Rapeseed Oil | Diala S3         | Midel 7131 | Rapeseed Oil |
| 0.00%                      | 32.82±5.23                                   | 28.94±2.77 | 31.76±3.69   | 49.24±3.38       | 33.83±0    | 31.7±3.5     |
| 0.0006%                    | 36.46±6.95                                   | 42.66±7.25 | 39.34±2.58   | 52.93±6.03       | 36.39±3.24 | 35.64±2.68   |
| 0.004%                     | 41.91±6.98                                   | 41.41±8.1  | 37.83±3.3    | 53.49±2.33       | 35.64±2.67 | 38.27±3.66   |
| 0.01%                      | 40.47±8.64                                   | 33.07±8.04 | 36.89±5.82   | 52.3±0.38        | 34.2±0.26  | 36.71±3.24   |
| 0.05%                      | 36.58±3.49                                   | 31.57±7.18 | 37.14±5.73   | 51.3±2.59        | 33.07±5.02 | 35.33±2.67   |
| 0.1%                       | 34.64±0.36                                   | 30.32±7.24 | 29.06±3.19   | 50.17±3.36       | 32.96±2.79 | 34.39±0.14   |

In the case of the natural ester, the BN nano-modified samples with 0.004% concentration of nanoparticles (b/w) demonstrated the highest breakdown voltage ( $38.27 \pm 3.66$  kV) and the largest improvement in the breakdown voltage (20.73% increase) compared with the lowest breakdown voltage of the tested sample (base sample). For concentrations of nanoparticles higher than 0.004%, breakdown voltages started to drop. A concentration of 0.1% provided the lowest breakdown voltage ( $34.39 \pm 0.14$  kV) among all tested nano-modified samples. All nano-modified samples of vegetable

oil demonstrated higher breakdown voltages compared with the base sample. The highest breakdown voltage (0.0006% sample) provided a 20.73% increase with respect to the breakdown voltage of the base sample.

In the summary, the tested results of the sample with TiO<sub>2</sub> and BN nanoparticles were measured in accordance with the ASTM standard. In the case of the TiO<sub>2</sub> samples stressed with a positive impulse, synthetic ester samples provided both the highest and lowest breakdown voltages compared with all tested samples of the three liquids. The breakdown voltages of both synthetic and natural esters exhibited sensitivity to changing the nanoparticle concentration. The largest breakdown voltage improvements of the synthetic and natural ester were 51.95% and 23.27% increases with respect to the lowest breakdown voltage (base sample for both synthetic and natural ester). All nano-modified samples of the synthetic ester and natural ester provided higher breakdown voltages than that for the base sample. For the mineral oil, the sample with the 0.1% (b/w) concentration of TiO<sub>2</sub> nanoparticles provided the only breakdown voltage that was slightly lower than that for base sample (~0.19%).

In the case of the TiO<sub>2</sub> samples stressed with the negative impulse, the mineral oil samples showed significantly higher breakdown voltages than the other two ester samples. Similar to the positive impulse case, the breakdown voltage of the mineral oil demonstrated insensitivity to changing the concentration (the highest breakdown voltage provided an ~8% increase with respect to the lowest breakdown voltage). Compared with the dielectric behaviours of the mineral oil and synthetic ester liquids, the breakdown voltage of natural ester showed sensitivity to changing the concentration, and the highest breakdown voltage of the natural ester (0.004% sample) provided a ~19% increase with respect to the lowest breakdown voltage (base sample).

For the sample with the BN, the nanoparticles were measured in accordance with the ASTM standard. In the case of the samples stressed with the positive impulse, the highest breakdown voltages of the mineral oil ( $41.91 \pm 6.98$  kV) and the synthetic ester ( $42.66 \pm 7.25$  kV) were close and were higher than the highest breakdown voltage of the natural ester ( $39.34 \pm 2.58$  kV). Compared with the dielectric behaviours of the mineral oil and synthetic ester liquids, the breakdown voltages of both synthetic and natural ester liquid samples showed sensitivity to changing the concentration; the highest breakdown voltage (0.0006% sample for both ester liquids) provided 47.41% and 35.38%,

respectively, for the synthetic and natural ester with respect to the lowest breakdown voltage (base sample for synthetic ester, 0.1% sample for natural ester).

In the case of the BN samples stressed with the negative impulse, mineral oil samples showed significantly higher breakdown voltages than the other two ester samples. Compared with the breakdown voltage of the mineral oil and synthetic ester, the breakdown voltage of the natural ester showed sensitivity to changing the concentration. With respect to the lowest breakdown voltage, the highest breakdown voltage provided an ~8.63% increase for mineral oil, ~10.41% increase for synthetic ester, and ~20.7% for natural ester.

### **6.3.2 IEC 60897 method test results**

Figures 6-7 and 6-8 show the minimum-lightning impulse breakdown voltage of base and TiO<sub>2</sub> nano-modified liquids measured in accordance with the IEC standard. In these two figures, open data points show the breakdown voltages for positive lightning waveforms; the closed data points show the breakdown voltages for negative lightning waveforms. To identify the difference between breakdown voltages for different liquid samples with the same concentration of nanoparticles, all data points that belong to different concentrations of the same nano-modified liquid are shown using the same symbols. The measurement results of the three liquids of a series of concentrations (base, 0.0006%, 0.004%, 0.01%, 0.05%, 0.1%, b/w) under both positive and negative impulse polarities are shown in Table 6-3.

As Figure 6-7 shows, in the case of mineral oil stressed with positive impulses, the samples with a TiO<sub>2</sub> nanoparticle concentration of 0.004% (b/w) provided the highest breakdown voltage ( $45.96 \pm 5.33$  kV) and largest improvement (increase) in breakdown voltage (24.25% increase) compared with the lowest breakdown voltage (0.1% sample). For the samples with nanoparticle concentrations higher than 0.004%, the breakdown voltage started to drop. The nano-modified liquid with the 0.1% concentration (b/w) provided the lowest breakdown voltage ( $36.99 \pm 4.51$  kV), which was lower than the breakdown voltage of the base sample (5.66% decrease). The highest breakdown voltage (0.004% sample) provided a 17.21% increase with respect to the breakdown voltage of the base sample.

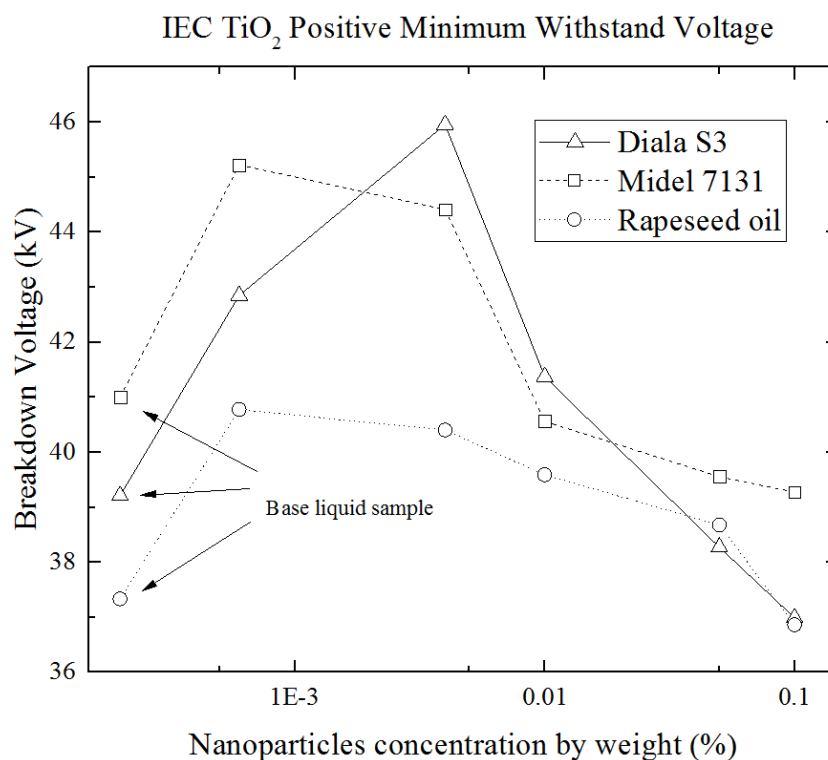


**Figure 6-7.** IEC standard TiO<sub>2</sub> positive minimum withstand voltage for the samples with different nanoparticle concentrations. The lines in this graph are given for visual guidance only.

In the case of the synthetic ester, the sample with the 0.0006% (b/w) concentration of TiO<sub>2</sub> nanoparticles provided the highest breakdown voltage ( $45.23 \pm 7.81$  kV) and the largest improvement (increase) in the breakdown voltage (15.15% increase) with respect to the lowest breakdown voltage (0.1% sample). For the nano-modified samples with concentrations of TiO<sub>2</sub> nanoparticles higher than 0.0006%, the breakdown voltage started to decrease. The sample with the 0.1% concentration of nanoparticles provided the lowest breakdown voltage ( $39.28 \pm 4.51$  kV) among all tested samples, which was lower than the breakdown voltage of the base sample (2.09% decrease). The highest breakdown voltage (0.0006% sample) provided a 12.79% increase with respect to the breakdown voltage of the base sample.

In the case of the natural ester, the TiO<sub>2</sub> nano-modified samples with the 0.0006% concentration of nanoparticles (b/w) demonstrated the highest breakdown voltage ( $40.78 \pm 6.23$  kV) and largest improvement (increase) in the breakdown voltage (10.63% increase) with respect to the lowest breakdown voltage (0.1% sample). For concentrations of nanoparticles higher than 0.0006%, the breakdown voltage started to drop. The sample with the 0.1% concentration of nanoparticles provided the lowest breakdown voltage ( $36.86 \pm 5.89$  kV) among all tested samples, which was lower than the

breakdown voltage of the base sample (1.26% decrease). The highest breakdown voltage (0.0006% sample) provided a 9.24% increase with respect to the breakdown voltage of the base sample.

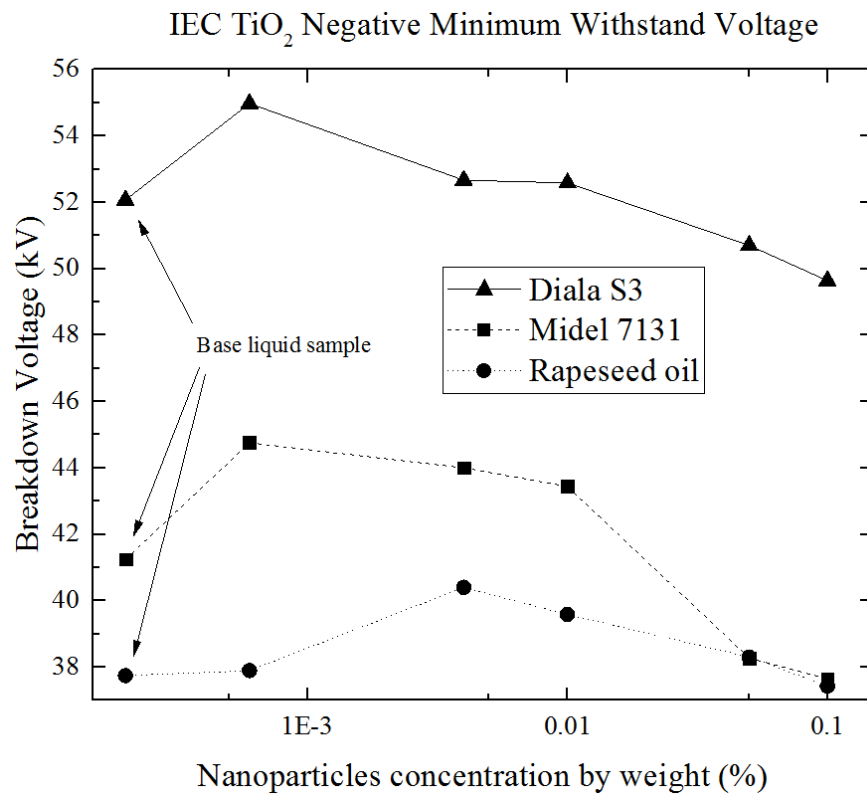


**Figure 6-8.** IEC standard TiO<sub>2</sub> negative minimum withstand voltage for the samples with different nanoparticle concentrations. The lines in this graph are given for visual guidance only.

As Figure 6-8 shows, in the case of mineral oil stressed with negative impulses, the samples with a TiO<sub>2</sub> nanoparticle concentration of 0.0006% (b/w) provided the highest breakdown voltage ( $54.98 \pm 2.88$  kV) and largest improvement (increase) in breakdown voltage (10.76% increase) compared with the lowest breakdown voltage (0.1% sample). For the samples with nanoparticle concentrations higher than 0.0006%, the breakdown voltage started to drop. The nano-modified liquid with the 0.1% concentration (b/w) provided the lowest breakdown voltage ( $49.64 \pm 3.27$  kV), which was lower than the breakdown voltage of the base sample (4.67% decrease). The highest breakdown voltage (0.0006% sample) provided a 5.59% increase with respect to the breakdown voltage of the base sample.

In the case of the synthetic ester, the sample with the 0.0006% (b/w) concentration of TiO<sub>2</sub> nanoparticles provided the highest breakdown voltage ( $44.76 \pm 11.27$  kV) and the largest improvement (increase) in the breakdown voltage (18.88% increase) with respect to the lowest breakdown voltage (0.1% sample). For the nano-modified samples with concentrations of the TiO<sub>2</sub>

nanoparticles higher than 0.0006%, the breakdown voltage started to decrease. The sample with the 0.1% concentration of nanoparticles provided the lowest breakdown voltage ( $37.65 \pm 4.32$  kV) among all tested samples, which was lower than the breakdown voltage of the base sample (8.73% decrease). The highest breakdown voltage (0.004% sample) provided an 8.51% increase with respect to the breakdown voltage of the base sample.

**Table 6-3.** IEC standard TiO<sub>2</sub> sample minimum withstand voltage test results.

| Concentration<br>by Weight | IEC Method TiO <sub>2</sub> Sample Breakdown Voltage (kV) |               |                 |                  |               |                 |
|----------------------------|---|---------------|-----------------|------------------|---------------|-----------------|
|                            | Positive Impulse  |               |                 | Negative Impulse |               |                 |
|                            | Diala S3  | Midel 7131    | Rapeseed<br>Oil | Diala S3         | Midel 7131    | Rapeseed<br>Oil |
| 0.00%                      | 39.21 ± 8.39  | 40.1 ± 7.59   | 37.33 ± 6.12    | 52.07 ± 3.87     | 41.25 ± 4.51  | 37.74 ± 4.33    |
| 0.0006%                    | 42.85 ± 5.89  | 45.23 ± 7.81  | 40.78 ± 6.23    | 54.98 ± 2.88     | 44.76 ± 11.27 | 37.9 ± 4.38     |
| 0.004%                     | 45.96 ± 5.33  | 44.41 ± 7.52  | 40.41 ± 4.58    | 52.67 ± 4.8      | 44.01 ± 9.19  | 40.41 ± 5.87    |
| 0.01%                      | 41.37 ± 5.56  | 40.56 ± 7.91  | 39.59 ± 4.29    | 52.59 ± 0.27     | 43.444 ± 5.79 | 39.59 ± 5.47    |
| 0.05%                      | 38.27 ± 5.18  | 39.56 ± 10.45 | 38.68 ± 7.68    | 50.71 ± 3.01     | 38.27 ± 5.11  | 38.31 ± 5.2     |
| 0.1%                       | 36.99 ± 4.51  | 39.28 ± 4.51  | 36.86 ± 5.89    | 49.64 ± 3.27     | 37.65 ± 4.32  | 37.43 ± 4.28    |

In the case of the natural ester, the TiO<sub>2</sub> nano-modified samples with 0.004% concentration of nanoparticles (b/w) demonstrated the highest breakdown voltage ( $40.41 \pm 5.87$  kV) and the largest improvement (increase) in the breakdown voltage (7.96% increase) with respect to the lowest breakdown voltage (0.1% sample). For concentrations of nanoparticles higher than 0.004%, the breakdown voltage started to drop. The sample with the 0.1% concentration of nanoparticles provided the lowest breakdown voltage ( $37.43 \pm 4.28$  kV) among all tested samples, which was lower than the breakdown voltage of the base sample (0.82% decrease). The highest breakdown voltage (0.004% sample) provided a 7.07% increase with respect to the breakdown voltage of the base sample.

Figures 6-9 and 6-10 show the minimum-lightning impulse breakdown voltage of base and BN nano-modified liquids measured in accordance with the IEC standard. In these two figures, open data points show the breakdown voltages for positive lightning waveforms; the closed data points show the breakdown voltages for negative lightning waveforms. To identify the difference between breakdown voltages for different liquid samples with the same concentration of nanoparticles, all data points that

belong to different concentrations of the same nano-modified liquid are shown using the same symbols. The measurement results of the three liquids of a series of concentrations (base, 0.0006%, 0.004%, 0.01%, 0.05%, 0.1%, b/w) under both positive and negative impulse polarities are shown in Table 6-4.

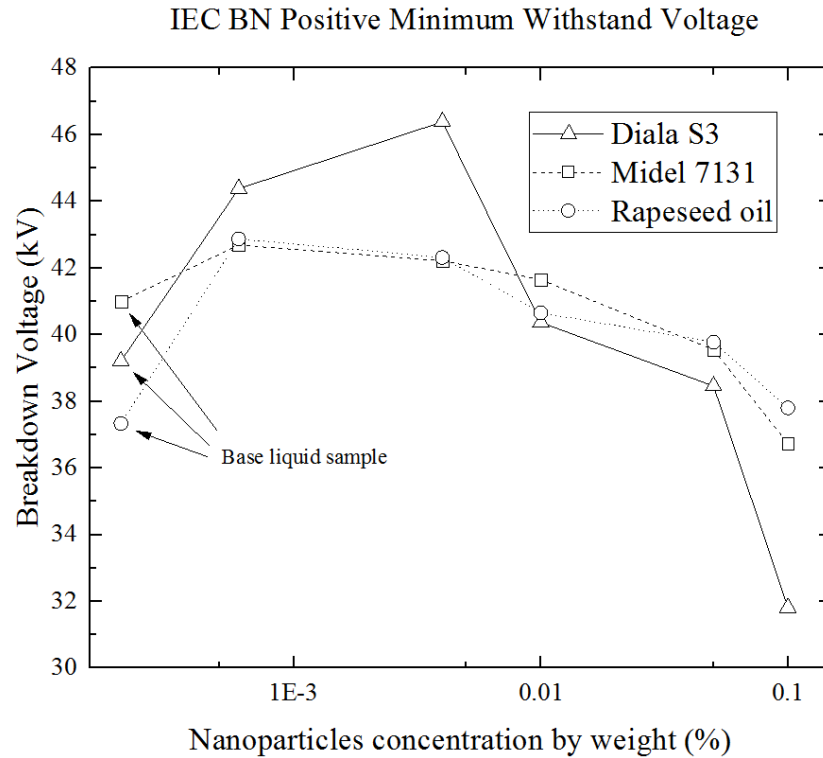


**Figure 6-9.** IEC standard BN positive minimum withstand voltage for the samples with different nanoparticle concentrations. The lines in this graph are given for visual guidance only.

As Figure 6-9 shows, in the case of mineral oil stressed with positive impulses, the samples with BN nanoparticle concentration of 0.004% (b/w) provided the highest breakdown voltage ( $46.38 \pm 5.21$  kV) and largest improvement (increase) in breakdown voltage (45.76% increase) compared with the lowest breakdown voltage (0.1% sample). For the samples with nanoparticle concentrations higher than 0.004%, the breakdown voltage started to drop. The nano-modified liquid with the 0.1% concentration (b/w) provided the lowest breakdown voltage ( $31.82 \pm 4.72$  kV), which was lower than the breakdown voltage of the base sample (18.85% decrease). The highest breakdown voltage (0.004% sample) provided an 18.29% increase with respect to the breakdown voltage of the base sample.

In the case of the synthetic ester, the sample with the 0.0006% (b/w) concentration of BN nanoparticles provided the highest breakdown voltage ( $42.69 \pm 3.03$  kV) and the largest improvement (increase) in the breakdown voltage (16.19% increase) with respect to the lowest breakdown voltage

(0.1% sample). For the nano-modified samples with concentrations of BN nanoparticles higher than 0.0006%, the breakdown voltage started to decrease. The sample with the 0.1% concentration of nanoparticles provided the lowest breakdown voltage ( $36.74 \pm 7.02$  kV) among all tested samples, which was lower than the breakdown voltage of the base sample (11.57% decrease). The highest breakdown voltage (0.0006% sample) provided a 4.15% increase with respect to the breakdown voltage of the base sample.

In the case of the natural ester, the BN nano-modified samples with the 0.0006% concentration of nanoparticles (b/w) demonstrated the highest breakdown voltage ( $42.88 \pm 5.49$  kV) and the largest improvement in the voltage (14.87% increase compared with the breakdown voltage of the base liquid). For concentrations of nanoparticles higher than 0.0006%, the breakdown voltage started to drop. All nano-modified samples of the vegetable oil demonstrated higher breakdown voltages compared with the base oil.

As Figure 6-8 shows, in the case of mineral oil stressed with negative impulses, the samples with the BN nanoparticle concentration of 0.004% (b/w) provided the highest breakdown voltage ( $55.46 \pm 2.69$  kV) and largest improvement (increase) in breakdown voltage (7% increase) compared with the lowest breakdown voltage (0.1% sample). For the samples with nanoparticle concentrations higher than 0.004%, the breakdown voltage started to drop. The nano-modified liquid with the 0.1% concentration (b/w) provided the lowest breakdown voltage ( $51.83 \pm 2.56$  kV), which was lower than the breakdown voltage of the base sample (0.46% decrease). The highest breakdown voltage (0.004% sample) provided a 6.51% increase with respect to the breakdown voltage of the base sample.

### IEC BN Negative Minimum Withstand Voltage

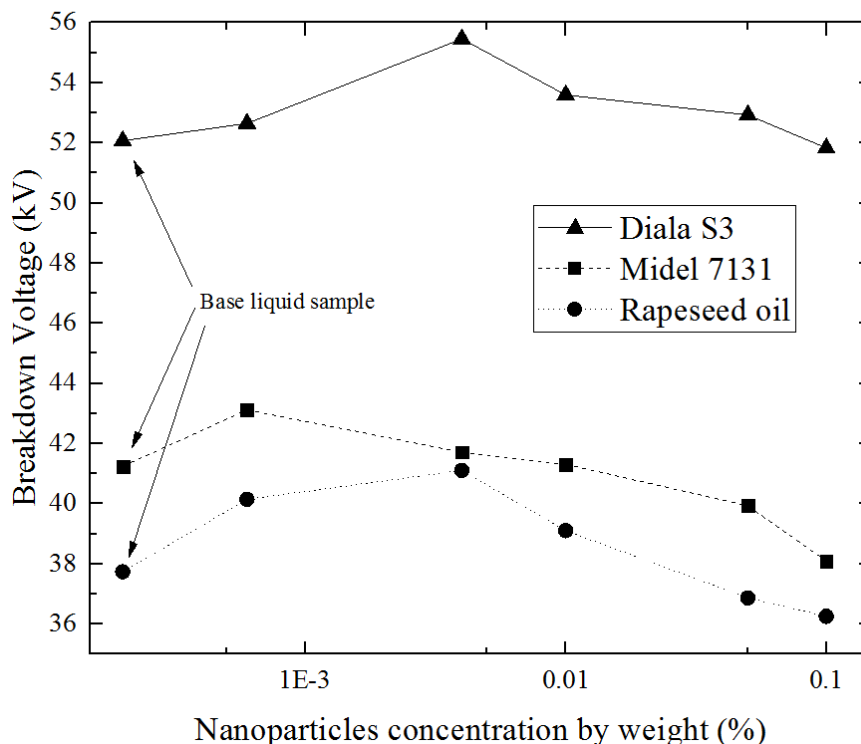


**Figure 6-10.** IEC standard BN negative minimum withstand voltage for the samples with different nanoparticle concentrations. The lines in this graph are given for visual guidance only.

In the case of the synthetic ester, the sample with the 0.0006% (b/w) concentration of BN nanoparticles provided the highest breakdown voltage ( $43.13 \pm 9.42$  kV) and the largest improvement (increase) in the breakdown voltage (13.23% increase) with respect to the lowest breakdown voltage (0.1% sample). For the nano-modified samples with concentrations of BN nanoparticles higher than 0.0006%, the breakdown voltage started to decrease. The sample with the 0.1% concentration of nanoparticles provided the lowest breakdown voltage ( $38.09 \pm 4.25$  kV) among all tested samples, which was lower than the breakdown voltage of the base sample (7.66% decrease). The highest breakdown voltage (0.0006% sample) provided a 4.56% increase with respect to the breakdown voltage of the base sample.

In the case of the natural ester, the BN nano-modified samples with the 0.004% concentration of nanoparticles (b/w) demonstrated the highest breakdown voltage ( $41.11 \pm 5.52$  kV) and the largest improvement (increase) in the breakdown voltage (13.38% increase) with respect to the lowest breakdown voltage (0.1% sample). For concentrations of nanoparticles higher than 0.004%, the breakdown voltage started to drop. The sample with the 0.1% concentration of nanoparticles provided

the lowest breakdown voltage ( $36.26 \pm 3.09$  kV) among all tested samples, which was lower than the breakdown voltage of the base sample (3.92% decrease). The highest breakdown voltage (0.004% sample) provided an 8.93% increase with respect to the breakdown voltage of the base sample.

**Table 6-4.** IEC standard BN sample minimum withstand voltage test results.

| Concentration by Weight | IEC Method BN Sample Breakdown Voltage (kV) |                  |                  |                  |                  |                  |
|-------------------------|---|------------------|------------------|------------------|------------------|------------------|
|                         | Positive Impulse                            |                  |                  | Negative Impulse |                  |                  |
|                         | Diala S3                                    | Midel 7131       | Rapeseed Oil     | Diala S3         | Midel 7131       | Rapeseed Oil     |
| 0.00%                   | 39.21 $\pm$ 8.39                            | 40.99 $\pm$ 7.59 | 37.33 $\pm$ 6.12 | 52.07 $\pm$ 3.87 | 41.25 $\pm$ 4.51 | 37.74 $\pm$ 4.33 |
| 0.0006%                 | 44.38 $\pm$ 3.55                            | 42.69 $\pm$ 3.03 | 42.88 $\pm$ 5.49 | 52.65 $\pm$ 3.98 | 43.13 $\pm$ 9.42 | 40.15 $\pm$ 5.91 |
| 0.004%                  | 46.38 $\pm$ 5.21                            | 42.22 $\pm$ 5.31 | 42.31 $\pm$ 4.17 | 55.46 $\pm$ 2.69 | 41.72 $\pm$ 5.75 | 41.11 $\pm$ 5.52 |
| 0.01%                   | 40.36 $\pm$ 3.76                            | 41.65 $\pm$ 6.15 | 40.65 $\pm$ 5.81 | 53.59 $\pm$ 4.05 | 41.31 $\pm$ 2.94 | 39.11 $\pm$ 5.48 |
| 0.05%                   | 38.46 $\pm$ 6.65                            | 39.55 $\pm$ 5.47 | 39.78 $\pm$ 5.33 | 52.93 $\pm$ 0.29 | 39.93 $\pm$ 6.15 | 36.87 $\pm$ 4.29 |
| 0.1%                    | 31.82 $\pm$ 4.72                            | 36.74 $\pm$ 7.02 | 37.81 $\pm$ 4.42 | 51.83 $\pm$ 2.56 | 38.09 $\pm$ 4.25 | 36.26 $\pm$ 3.09 |

In the summary of the tested results of the samples with the TiO<sub>2</sub> and BN, the nanoparticles were measured in accordance with the IEC standard. In the case of the TiO<sub>2</sub> samples stressed with positive impulses, the mineral oil sample provided the largest breakdown voltage improvement (17.21% increase) with respect to the breakdown voltage of the base sample. The breakdown voltage of the mineral oil with the TiO<sub>2</sub> nanoparticles showed sensitivity to changing the concentration. The highest breakdown voltage (0.004% sample) showed a 24.25% voltage increase compared with the lowest breakdown voltage (0.1% sample). The breakdown voltage of both the synthetic and natural esters did not show as much sensitivity as the mineral oil presented to changing the nanoparticle concentration. The largest breakdown voltage improvements of the synthetic and natural ester were 15.15% and 10.63% increases with respect to the lowest breakdown voltage (0.1% sample for both synthetic and natural ester).

In the case of the TiO<sub>2</sub> samples stressed with negative impulses, the mineral oil, synthetic ester, and natural ester samples provided the largest breakdown voltage improvement (5.59% for mineral oil, 5.51% for synthetic ester, and 7.07% for natural ester) with respect to the breakdown voltage of the base sample. The breakdown voltage of the synthetic ester with the TiO<sub>2</sub> nanoparticles showed sensitivity to changing the concentration. The highest breakdown voltage (0.0006% sample) showed an 18.88% voltage increase compared with the lowest breakdown voltage (0.1%).

For the sample with the BN nanoparticles stressed with positive impulses, the highest breakdown voltage of the mineral oil sample provided an 18.29% voltage increase compared with the breakdown voltage of the base sample. The breakdown voltage of the mineral oil with the BN nanoparticles showed sensitivity to changing the concentration. The highest breakdown voltage (0.004% sample) showed a 45.76% voltage increase compared with the lowest breakdown voltage (0.1% sample). The breakdown voltage of the ester liquid did not show as much sensitivity as the mineral oil presented to changing the nanoparticle concentration. The largest breakdown voltages of the synthetic and natural ester provided a 16.19% (for synthetic ester) and 14.87% (for natural ester) increase with respect to the breakdown voltage of the lowest breakdown voltage (0.1% sample for synthetic ester, base sample for natural ester). All nano-modified samples of the natural ester with the BN nanoparticles demonstrated higher breakdown voltages than the base sample.

In the case of the BN samples stressed with negative impulses, the mineral oil samples showed significantly higher breakdown voltages than the other two ester samples. Compared with the breakdown voltage of the mineral oil, the breakdown voltage of the synthetic ester and natural ester showed sensitivity to changing the concentration. With respect to the lowest breakdown voltage, the highest breakdown voltage provided a ~7% increase for mineral oil, ~13.23% increase for synthetic ester, and ~13.38% for natural ester.

#### **6.4 Minimum-lightning Impulse Breakdown Voltage Confidence Analysis and Comparison**

To investigate the statistical significance of the differences between breakdown voltages of base and nano-modified liquids, two-sample *t*-statistics were used. The detailed description of this method, based on the identification of the CIs for both samples, was given in Section 4.5. The value of the CIs used in the present analysis is 95% [16], [105], [107], [108], [210], [217]–[219]. The statistical difference analyses were performed using Origin Pro 2015.

In the statistical difference analysis, the population means of the two samples are calculated and then their difference,  $\Delta$ , is calculated and plotted as a function of the concentration of the nanoparticles. Additionally, the 95% upper and lower bounds of the CI were obtained for all concentrations of nanoparticles. If population means are the same,  $\Delta V = 0$ , and if there is a numerical difference in the

population means,  $\Delta V > 0$ . However, to state that this difference is statistically significant, the lower 95% interval of the difference between the population means also should be above the zero line [210]. Thus, in this case, the population means of two samples are statistically different (i.e., in the case of the change/increase in the breakdown voltage, it is possible to say that this increase satisfies the criteria of statistical significance compared with the breakdown voltage of base liquids).

#### 6.4.1 Confidence analysis results for the ASTM method

The *t*-statistics were used to analyse the minimum withstand breakdown voltages obtained for the base and nano-modified liquids to determine the statistical significance in the increase in the breakdown voltage. Figures 6-11 to 6-16 show the difference between the population means of the base liquid and nano-modified liquids for both types of nanoparticles: TiO<sub>2</sub> and BN. All three types of liquids (mineral oil, synthetic ester, and natural ester) and their nano samples were stressed using positive and negative impulse polarities, following the ASTM test procedure. Additionally, upper and lower bounds of the 95% CI are shown in these figures.

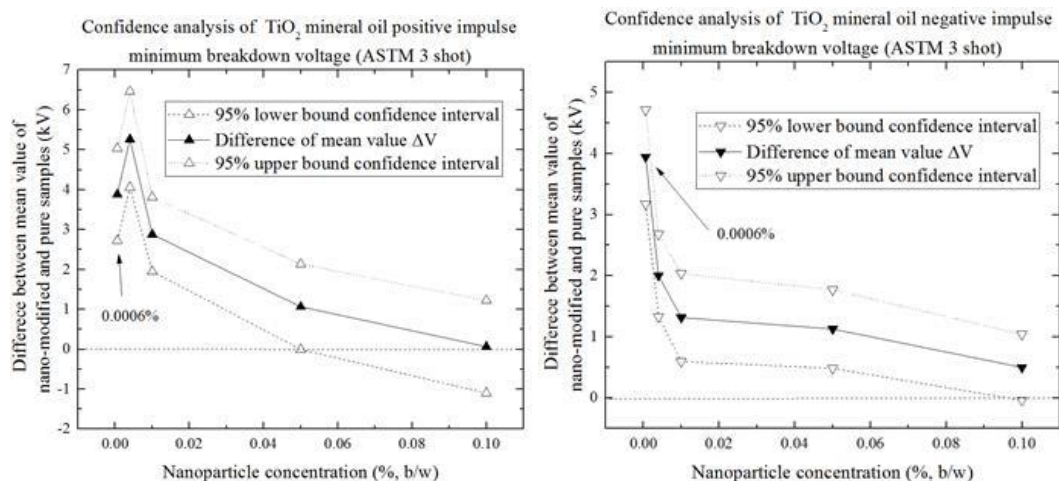


**Figure 6-11.** Confidence analysis results,  $\Delta V$ , of mineral oil with TiO<sub>2</sub> nanoparticles following the ASTM test procedure. (Left: positive impulse measurement results; right: negative impulse measurement results). Each data point denotes  $\Delta V$  between the mean value of the breakdown voltages of the base and nano-modified samples. The dotted line represents the upper 95% confidence bound; the dashed line represents the lower 95% confidence bound.

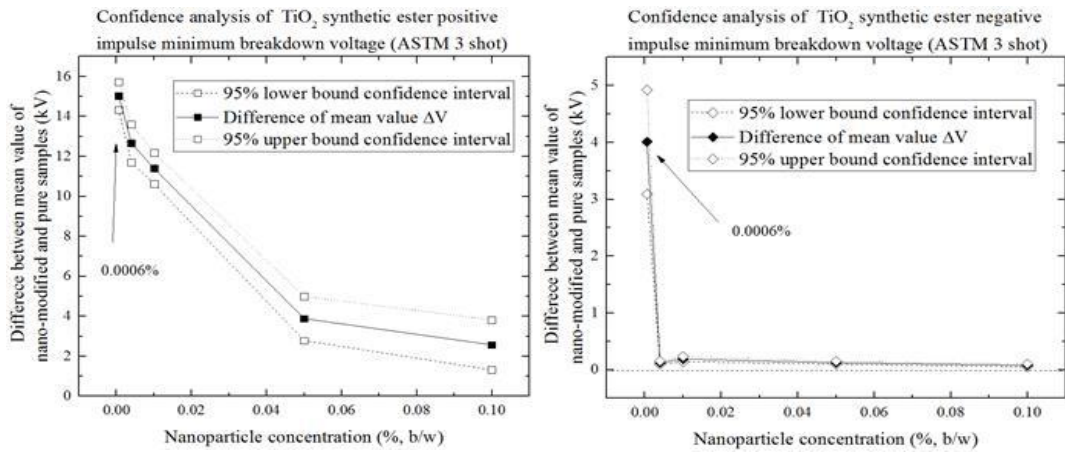


**Figure 6-12.** Confidence analysis results,  $\Delta V$ , of synthetic ester with  $\text{TiO}_2$  nanoparticles following the ASTM test procedure. (Left: positive impulse measurement results; right: negative impulse measurement results). Each data point denotes  $\Delta V$  between the mean value of the breakdown voltages of the base and nano-modified samples. The dotted line represents the upper 95% confidence bound; the dashed line represents the lower 95% confidence bound.

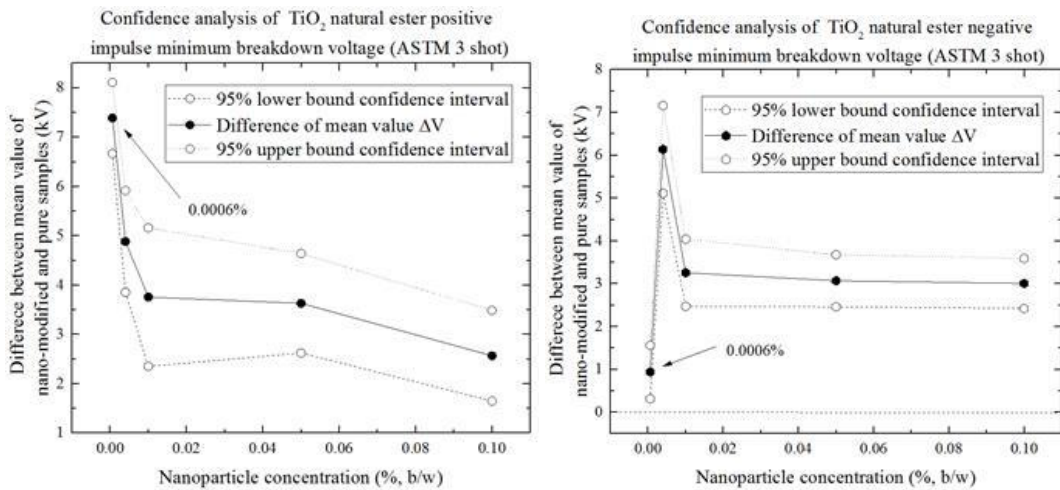


**Figure 6-13.** Confidence analysis results,  $\Delta V$ , of natural ester with  $\text{TiO}_2$  nanoparticles following the ASTM test procedure. (Left: positive impulse measurement results; right: negative impulse measurement results). Each data point denotes  $\Delta V$  between the mean value of the breakdown voltages of the base and nano-modified samples. The dotted line represents the upper 95% confidence bound; the dashed line represents the lower 95% confidence bound.

As Figures 6-11 to 6-13 show, the confidence analysis of the positive and negative impulse breakdown voltages of the  $\text{TiO}_2$  nano-modified liquids showed that the difference in population means decreased with an increase in the concentration of nanoparticles. These graphs confirm that the small concentration of nanoparticles used in the present study (0.0006% or 0.004% in the case of  $\text{TiO}_2$  nanoparticles) provided the largest improvement (increase) in the breakdown of the nano-modified liquids. Additionally, the lower 95% CI for  $\Delta V$  related to these concentrations stayed positive for all three liquids with  $\text{TiO}_2$  nanoparticles, thus confirming that this increase in the breakdown voltage compared with the base liquids (positive  $\Delta V$ ) was statistically significant for all tested nano-modified

samples. With an increase in concentration of nanoparticles, the difference in the breakdown voltage of base liquids and nano-modified liquids,  $\Delta V$ , started to decrease. In some cases, the optimal concentration of nanoparticles producing the largest  $\Delta V$  was 0.004% (b/w), for example, for the nano-modified mineral oil stressed with positive impulses and for the natural ester stressed with the negative impulses. Again, as in the case of the 0.004% optimal concentration,  $\Delta V$  started to decrease when the particle concentration increased above 0.004%. The results also showed that the lower 95% CI crossed the zero line for the mineral oil nano-modified samples with the 0.1% nanoparticle concentration under positive and negative impulse stress, which means that this difference between the mean breakdown voltage for the base oil and the mean breakdown voltage of the nano-modified samples was not statistically significant.

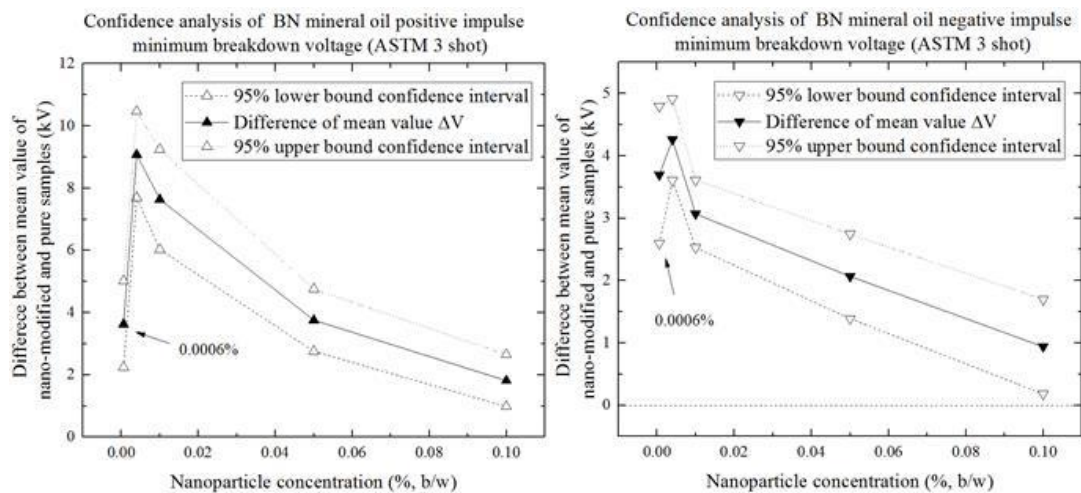


**Figure 6-14.** Confidence analysis results,  $\Delta V$ , of mineral oil with BN nanoparticles following the ASTM test procedure. (Left: positive impulse measurement results; right: negative impulse measurement results). Each data point denotes  $\Delta V$  between the mean value of the breakdown voltages of the base and nano-modified samples. The dotted line represents the upper 95% confidence bound; the dashed line represents the lower 95% confidence bound.

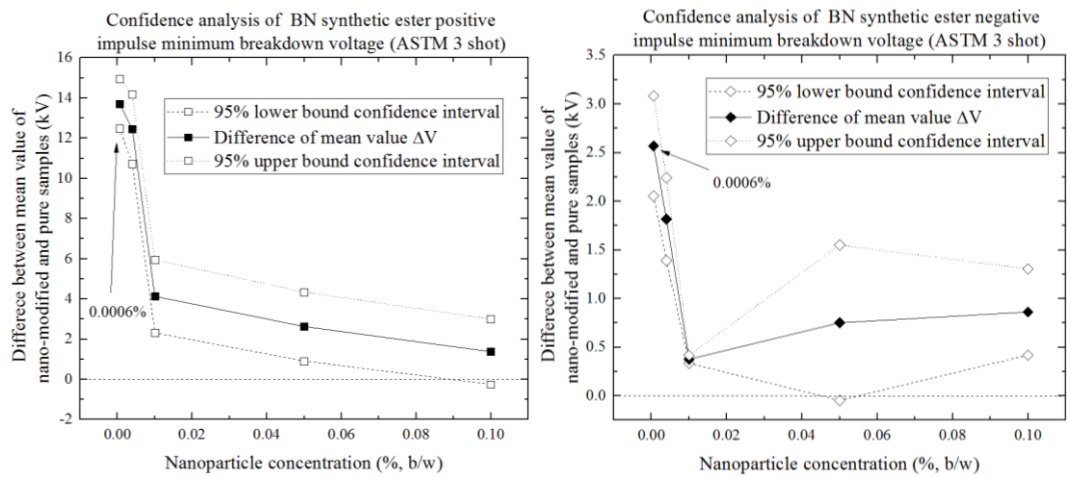


**Figure 6-15.** Confidence analysis results,  $\Delta V$ , of synthetic ester with BN nanoparticles following the ASTM test procedure (Left: positive impulse measurement results; right: negative impulse measurement results). Each data point denotes  $\Delta V$  between the mean value of the breakdown voltages of the base and nano-modified samples. The dotted line represents the upper 95% confidence bound; the dashed line represents the lower 95% confidence bound.

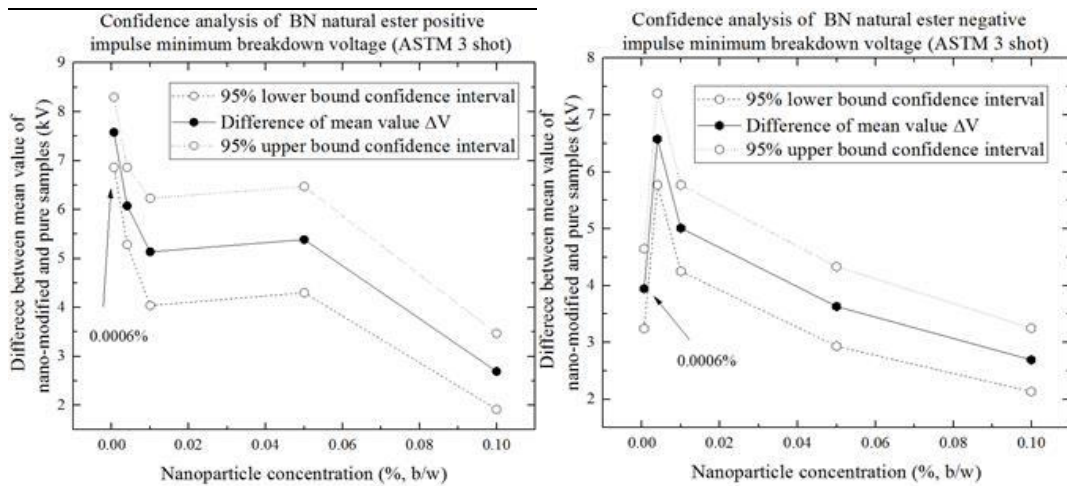


**Figure 6-16.** Confidence analysis results,  $\Delta V$ , of natural ester with BN nanoparticles following the ASTM test procedure. (Left: positive impulse measurement results; right: negative impulse measurement results). Each data point denotes  $\Delta V$  between the mean value of the breakdown voltages of the base and nano-modified samples. The dotted line represents the upper 95% confidence bound; the dashed line represents the lower 95% confidence bound.

The confidence analysis of the positive and negative impulse breakdown voltages of the BN nano-modified liquids showed that the difference in population means decreased with an increase in the concentration of nanoparticles. Similar to the case of the  $\text{TiO}_2$  nanoparticles, the small concentration of nanoparticles used in the present study (0.0006% or 0.004% b/w) provided the largest improvement (increase) in the breakdown of the nano-modified liquids. Additionally, the lower 95% CI for  $\Delta V$  related to this concentration stayed positive for all three liquids with the BN nanoparticles, thus

confirming that this increase in the breakdown voltage compared with the base liquids (positive  $\Delta V$ ) was statistically significant for all tested nano-modified samples. With an increase in concentration of nanoparticles, the difference in the breakdown voltage of base liquids and nano-modified liquids,  $\Delta V$ , started to decrease. In some cases, the optimal concentration of nanoparticles producing the largest  $\Delta V$  was 0.004% (b/w), for example, for the nano-modified mineral oil stressed with both positive and negative impulses and for the natural ester stressed with the negative impulses. In the case of the 0.004% optimal concentration,  $\Delta V$  started to decrease when the particle concentration increased above 0.004%. In the case in which the lower 95% CI crossed the zero line for the nano-modified samples of synthetic ester with the 0.1% nanoparticle concentration under positive impulse stress and the nano-modified samples of synthetic ester with the 0.5% nanoparticle concentration under negative impulse stress, this difference between the mean breakdown voltages for the base oil and the mean breakdown voltages of the nano-modified samples was not statistically significant.

#### 6.4.2 Confidence analysis of the breakdown results by IEC method

Figures 6-17 to 6-22 show the difference in the population means,  $\Delta V$ , for the minimum breakdown voltage of the TiO<sub>2</sub> and BN nano-modified samples of mineral oil and the synthetic and natural esters stressed with the positive impulses following the IEC procedure.

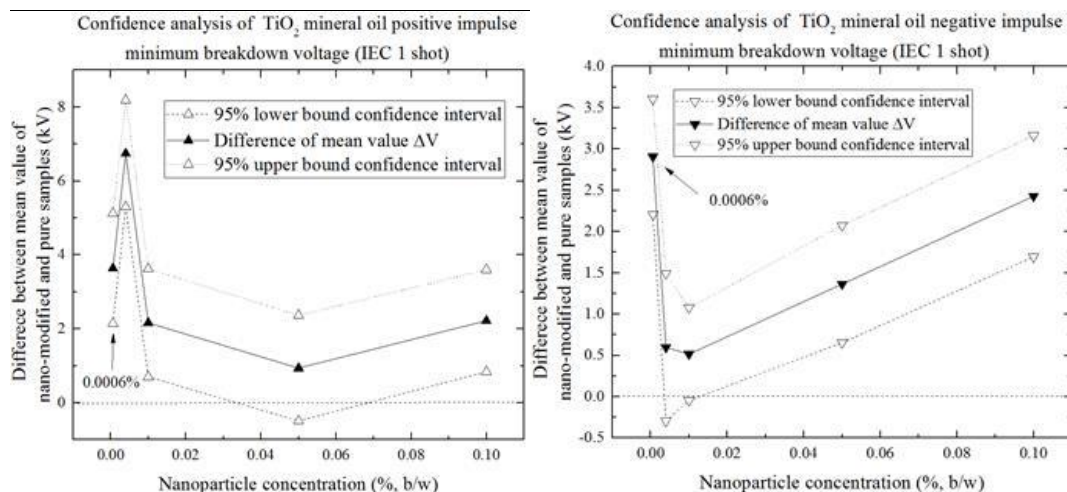


**Figure 6-17.** Confidence analysis results,  $\Delta V$ , of mineral oil with TiO<sub>2</sub> nanoparticles following the IEC test procedure. (Left: positive impulse measurement results; right: negative impulse measurement results). Each data point denotes  $\Delta V$  between the mean value of the breakdown voltages of the base and nano-modified samples. The dotted line represents the upper 95% confidence bound; the dashed line represents the lower 95% confidence bound.

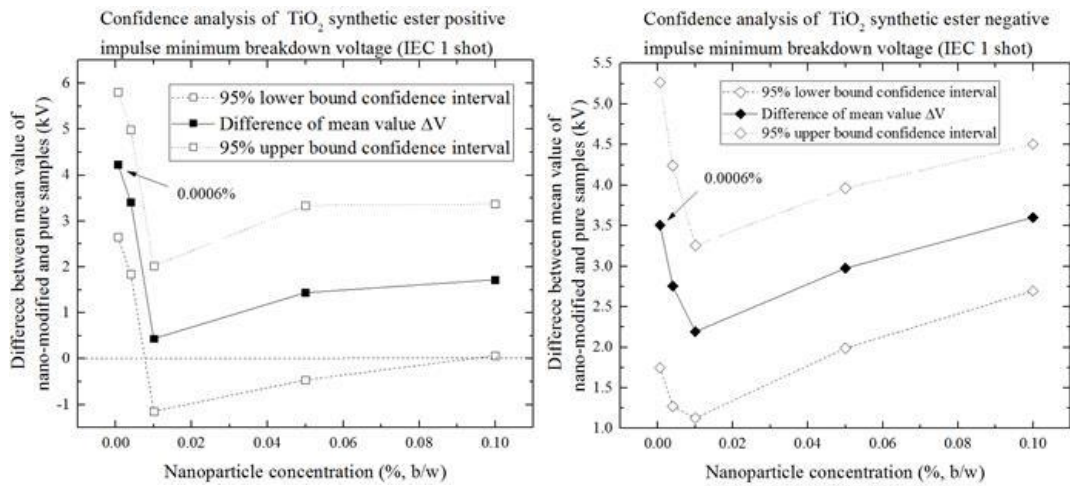


**Figure 6-18.** Confidence analysis results,  $\Delta V$ , of synthetic ester with  $\text{TiO}_2$  nanoparticles following the IEC test procedure. (Left: positive impulse measurement results; right: negative impulse measurement results). Each data point denotes  $\Delta V$  between the mean value of the breakdown voltages of the base and nano-modified samples. The dotted line represents the upper 95% confidence bound; the dashed line represents the lower 95% confidence bound.

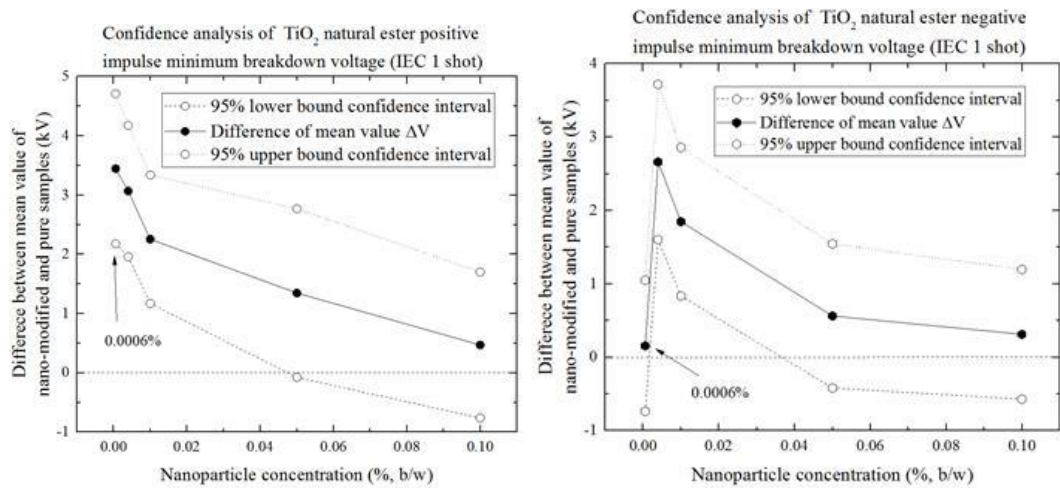


**Figure 6-19.** Confidence analysis results,  $\Delta V$ , of natural ester with  $\text{TiO}_2$  nanoparticles following the IEC test procedure. (Left: positive impulse measurement results; right: negative impulse measurement results). Each data point denotes  $\Delta V$  between the mean value of the breakdown voltages of the base and nano-modified samples. The dotted line represents the upper 95% confidence bound; the dashed line represents the lower 95% confidence bound.

In the case of the IEC standard measurement results, the confidence analysis of the positive and negative impulse breakdown voltages of the  $\text{TiO}_2$  nano-modified liquids showed that the difference in population means decreased with an increase in the concentration of nanoparticles. These graphs confirm that the small concentration of nanoparticles used in the present study (0.0006% or 0.004% in the case of the  $\text{TiO}_2$  nanoparticles) provided the largest improvement (increase) in the breakdown of the nano-modified liquids. Additionally, the lower 95% CI for  $\Delta V$  related to this concentration stayed positive for all three liquids with  $\text{TiO}_2$  nanoparticles, thus confirming that this increase in the

breakdown voltage compared with the base liquids (positive  $\Delta V$ ) was statistically significant for all tested nano-modified samples.

With an increase in concentration of nanoparticles, the difference in the breakdown voltage of base liquids and nano-modified liquids,  $\Delta V$ , started to decrease. In some cases, the optimal concentration of nanoparticles producing the largest  $\Delta V$  was 0.004% (b/w), for example, for the nano-modified mineral oil stressed with positive impulses and for the natural ester stressed with negative impulses. Again, as in the case of the 0.004% optimal concentration,  $\Delta V$  started to decrease when the particle concentration increased above 0.004%.

In case of the nano-modified samples, large concentrations of nanoparticles provided an increase in  $\Delta V$  with an increase in concentration, for example, for the nano-modified mineral oil stressed with positive and negative impulses and for the nano-modified synthetic ester stressed with positive and negative impulses. This phenomenon showed the breakdown voltages of the sample with large concentrations used in the present study (0.05% or 0.1%) was lower than the breakdown voltage of the base sample. With an increase in the concentration, the difference between the mean breakdown voltages of the nano-modified sample and base sample became large; hence, the  $\Delta V$  started to increase.

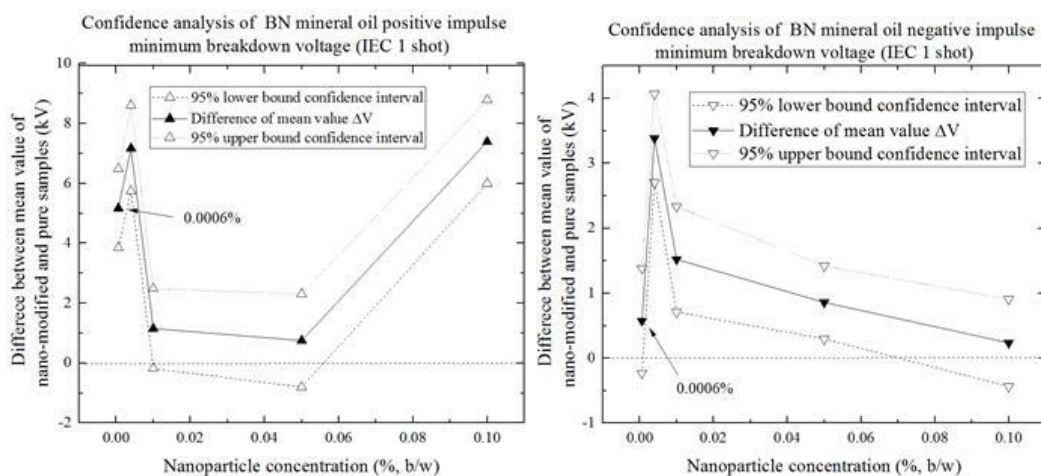


**Figure 6-20.** Confidence analysis results,  $\Delta V$ , of mineral oil with BN nanoparticles following the IEC test procedure. (Left: positive impulse measurement results; right: negative impulse measurement results). Each data point denotes  $\Delta V$  between the mean value of the breakdown voltages of the base and nano-modified samples. The dotted line represents the upper 95% confidence bound; the dashed line represents the lower 95% confidence bound.

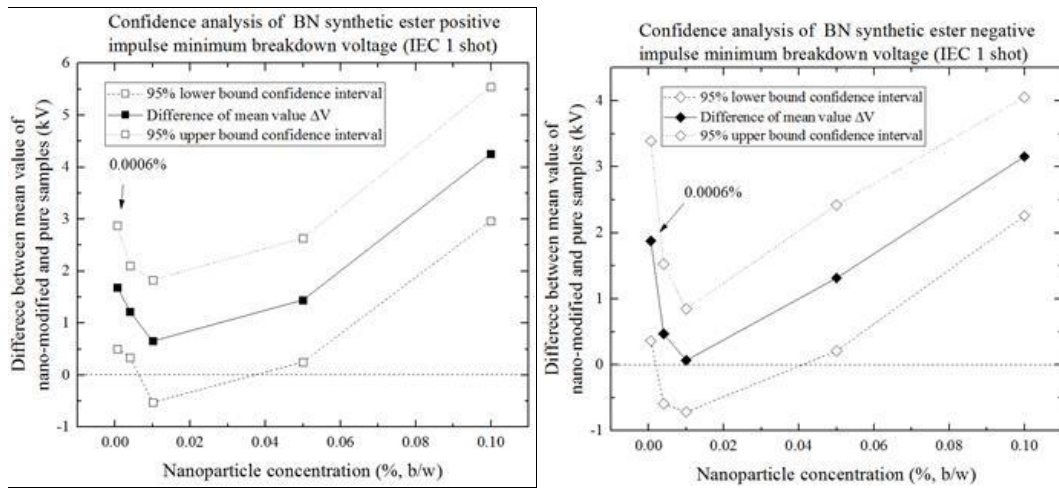


**Figure 6-21.** Confidence analysis results,  $\Delta V$ , of synthetic ester with BN nanoparticles following the IEC test procedure. (Left: positive impulse measurement results; right: negative impulse measurement results). Each data point denotes  $\Delta V$  between the mean value of the breakdown voltages of the base and nano-modified samples. The dotted line represents the upper 95% confidence bound; the dashed line represents the lower 95% confidence bound.

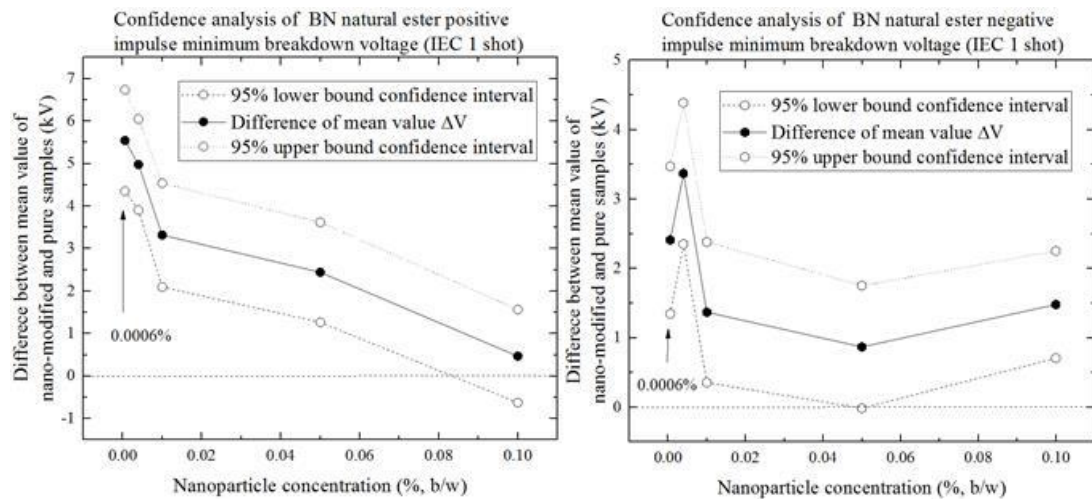


**Figure 6-22.** Confidence analysis results,  $\Delta V$ , of natural ester with BN nanoparticles following the IEC test procedure. (Left: positive impulse measurement results; right: negative impulse measurement results). Each data point denotes  $\Delta V$  between the mean value of the breakdown voltages of the base and nano-modified samples. The dotted line represents the upper 95% confidence bound; the dashed line represents the lower 95% confidence bound.

In the case of IEC standard measurement results, the confidence analysis of the positive and negative impulse breakdown voltages of BN nano-modified liquids showed that the difference in population means decreased with an increase in the concentration of nanoparticles. These graphs confirm that the small concentration of nanoparticles used in the present study (0.0006% or 0.004% in the case of the BN nanoparticles) provided the largest improvement (increase) in the breakdown of the nano-modified liquids. Additionally, the lower 95% CI for  $\Delta V$  related to this concentration stayed positive for all

three liquids with the BN nanoparticles, thus confirming that this increase in the breakdown voltage compared with the base liquids (positive  $\Delta V$ ) was statistically significant for all tested nano-modified samples. With an increase in concentration of nanoparticles, the difference in the breakdown voltage of base liquids and nano-modified liquids,  $\Delta V$ , started to decrease. In some cases, the optimal concentration of nanoparticles producing the largest  $\Delta V$  was 0.004% (b/w), for example, for the nano-modified mineral oil stressed with positive and negative impulses and for the natural ester stressed with the negative impulses. Again, as in the case of the 0.004% optimal concentration,  $\Delta V$  started to decrease when the particle concentration increased above 0.004%. The samples with large concentrations of nanoparticles provided an increase in  $\Delta V$  with an increase in concentration, for example, for the nano-modified mineral oil stressed with positive impulses, for nano-modified synthetic ester stressed with positive and negative impulses, and for nano-modified natural ester stressed with negative impulses. This phenomenon showed that the breakdown voltages of the sample with the large concentrations used in the present study (0.05% or 0.1%) was lower than the breakdown voltage of the base sample. With an increase in the concentration, the difference between the mean breakdown voltages of the nano-modified samples and base sample became large; hence, the  $\Delta V$  started to increase.

## 6.5 Summary

In this chapter, the results of the measurements of the minimum withstand voltages of the nano-modified liquids were presented and discussed. The liquids that have been used as base liquids to produce nano-modified samples were the mineral oils (Shell Diala S3), the synthetic ester (Midel 7131), and the natural ester (food-grade rapeseed oil). The  $\text{TiO}_2$  and BN nanoparticles were used as fillers for these nano-modified samples. The test procedure and methodology was based on the ASTM D3300-00 and IEC 60897 international standards. Statistical difference analysis was conducted for the results; this analysis investigated the statistical significance of the change in the breakdown voltages between the nano-modified samples and the base liquids.

### **6.5.1 Discussion of minimum-lightning impulse breakdown voltage by ASTM method**

In the case of the minimum withstand voltage tests that have been performed in accordance with the ASTM method, the results showed that, under the positive polarity impulses, both TiO<sub>2</sub> and BN nano-modified synthetic ester samples showed a relatively high sensitivity to the concentration of nanoparticles. For example, in the case of the synthetic ester, the sample with the 0.0006% (b/w) concentration of TiO<sub>2</sub> nanoparticles provided the highest breakdown voltage (43.97 ± 3.41 kV) and the largest improvement (increase) in the breakdown voltage (51.95% increase) with respect to the lowest breakdown voltage (base sample). Moreover, in the case of the synthetic ester, the sample with the 0.0006% (b/w) concentration of BN nanoparticles provided the highest breakdown voltage (42.66 ± 7.25 kV) and the largest improvement (increase) in the breakdown voltage (47.41% increases) with respect to the lowest breakdown voltage (base sample).

Almost all nano-modified samples (all three liquids) demonstrated higher breakdown voltages than the base liquids except for the 0.1% TiO<sub>2</sub> nano-modified sample of the mineral oil and the 0.1% BN nano-modified sample of the natural ester, which showed a breakdown voltage lower than that for the base liquids (reduction by 0.19% for the TiO<sub>2</sub> 0.1% mineral oil sample and reduction by 8.48% for the BN 0.1% natural ester sample). Both synthetic and natural ester nano-modified liquids provided a clear improvement/increase in the minimum withstand voltage. The mineral oil was relatively insensitive to the concentration of nanoparticles in the range of concentrations tested within this research project.

The results on the breakdown voltage obtained using the ASTM methodology showed that, under the negative polarity impulses, the mineral oil samples were relatively insensitive to the change in concentration of nanoparticles of both types (TiO<sub>2</sub> and BN) as in the case of the positive polarity impulses. The breakdown voltages of the natural ester (base liquid and nano-modified liquids) demonstrated higher sensitivity to the change in concentration of nanoparticles. All TiO<sub>2</sub> nano-modified samples provided higher breakdown voltages compared with the base liquids. Almost all BN nano-modified samples demonstrated higher breakdown voltages than the base liquids except for the 0.05% and 0.1% nano-modified synthetic ester samples.

In the case of mineral oil and natural ester, the sample with the BN nanoparticles provided the largest breakdown voltage improvements with respect to the lowest breakdown voltage and were higher than the sample with the TiO<sub>2</sub> providing the largest breakdown voltage improvements with respect to the lowest breakdown voltage. For example, for mineral oil with the BN nanoparticles, the samples provided the largest breakdown voltage at 27.7% (positive impulse) and 8.36% (negative impulse) higher than with the lowest breakdown voltage. For the mineral oil with the TiO<sub>2</sub> nanoparticles, the samples provided the largest breakdown voltage at 16.03% (positive impulse) and 8% (negative impulse) higher than the lowest breakdown voltage. For natural ester with the BN nanoparticles, the samples provided the largest breakdown voltage at 35.38% (positive impulse) and 20.73% (negative impulse) higher than the lowest breakdown voltage. For natural ester with TiO<sub>2</sub> nanoparticles, the samples provided the largest breakdown voltage at 23.27% (positive impulse) and 19.38% (negative impulse) higher than the lowest breakdown voltage.

The TiO<sub>2</sub> nano-modified synthetic ester samples demonstrated a larger improvement/increase in the minimum withstand voltage: an increase of 51.95% for positive impulses and 11.85% for negative impulses compared with base liquids for nano samples with concentration of 0.0006% (b/w). For the BN nano-modified liquids (0.0006% (b/w) sample), the increase in the breakdown voltage was also notable: 47.4% for positive impulses and 10.14% for negative impulses compared with the breakdown voltages of base liquids.

### **6.5.2 Discussion of minimum-lightning impulse breakdown voltage by IEC method**

In the case of the minimum withstand voltage tests that have been performed in accordance with the IEC method, the results showed that, under the positive polarity impulses, the breakdown voltage of the BN nano-modified samples showed higher sensitivity to changing the concentration compared with the breakdown voltage of the TiO<sub>2</sub> nano-modified samples. For example, in the case of the BN nano-modified sample, the largest breakdown voltages showed a 45.76% (for mineral oil), 16.19% (for synthetic ester), and 14.87% (for natural ester) increase compared with the lowest breakdown voltage. In the case of the TiO<sub>2</sub> nano-modified sample, the largest breakdown voltages showed a 24.25% (for mineral oil), 15.15% (for synthetic ester), and 10.63% (for natural ester) increase compared with the lowest breakdown voltage.

For the samples stressed with negative impulses, the breakdown voltage of the mineral oil showed significantly higher breakdown voltages than those of the ester liquids. There is no clear difference between the sensitivity of the breakdown voltage of the TiO<sub>2</sub> and BN nano-modified samples.

In summary, the breakdown voltage behaviours of two types of nanoparticle modification samples based on three types of liquids were measured following the ASTM and IEC methods. The breakdown voltages of nano-modified samples stressed with the positive and negative impulses were close. In the case of the mineral oil, the breakdown voltage of the sample stressed with negative impulses was significantly higher than the breakdown voltage of the sample stressed with positive impulses.

The dielectric behaviours of the breakdown voltage of nano-modified samples were similar with an increase in concentration. The nano-modified sample with the optimal concentration provided the highest breakdown voltage compared with other nano-modified samples. For the samples with concentrations of nanoparticles higher than the optimal concentration, the breakdown voltages started to drop.

In most cases, the breakdown voltage measurements performed following the ASTM method were lower than the measurements performed following the IEC method. The reason for this phenomenon is that, in the voltage raising procedure, the ASTM standard requires applying the same voltage three times before raising the voltage to the next step. In the case of the IEC method, the measurement procedure requires applying the voltage only one time before raising the voltage to the next step. Thus, for the ASTM method test, there is a higher possibility to achieve the breakdown at the same voltage since there are more impulses applied at the same voltage than in the IEC method. Hence, the breakdown voltages measured using the ASTM method can be expected to be lower than the IEC method results.

### **6.5.3 Discussion of confidence analysis**

In the confidence analysis, the *t*-statistics were used to analyse the minimum withstand breakdown voltages obtained for the base and nano-modified liquids to determine the statistical significance of the increase in the breakdown voltage. The difference between the average breakdown voltages of the nano-modified samples and base sample,  $\Delta V$ , and the 95% CIs were previously calculated and discussed. The confidence analysis results showed that, in the case of the nano-modified samples with

the optimal concentration of nanoparticles (TiO<sub>2</sub> or BN), the low bound of the 95% CI for  $\Delta V$  related to this concentration stayed positive, thus confirming that this increase in the breakdown voltage compared with the base liquids (positive  $\Delta V$ ) was statistically significant.

# CHAPTER 7

## MOBILITY OF CHARGE CARRIERS AND POTENTIAL MECHANISMS OF BREAKDOWN IN NANOFUIDS

### 7.1 Introduction

Recent advances and investments in HVDC systems require detailed information about the dielectric behaviour of insulating fluids under AC and DC electrical stresses [208]. The HVDC techniques are suitable for transmission of electrical power over long distances. With the development of renewable sources, this approach has attracted the attention of the power industry for transmission of electrical power generated by offshore wind farms. In HVDC systems, for example, in HVDC convertor transformers, the insulation is stressed with DC voltages. Therefore, it is important to investigate the dielectric properties of insulating liquids and to understand their behaviour under both types of energisation. As indicated in a report by National Grid [208], ‘DC transformers cost in the region of £5M per phase and failures have significant outage cost’. Additionally, it is known that the HVDC transformer failure rate exceeds the failure rate of conventional transmission-based units by 5 to 10 times [208].

Under DC conditions, it has been shown that, in solid insulation systems, the conductivity and resulting space charge (rather than the permittivity) dominates the resulting field distribution [228]. For a liquid, due to the higher mobility of charge carriers, it is likely that the effect of space-charge distributions will be more significant. The presence of this space charge implies that field calculations based on solutions to the Laplace equation will be inadequate and approaches based on the Poisson and current continuity equations are required [229]. To perform such analyses of the field distributions, information on the apparent mobility of the charge carriers in the liquids is required. At present, measurement of the DC conductivity of oil is not routine [208], and it is not possible to derive the

apparent mobility for the charge carriers from the data sheets provided by the manufacturers. Information on the DC dielectric behaviour of insulating liquids will potentially influence the design of HVDC systems and will help manage these liquids.

In this chapter, the values of the apparent mobility of the charge carriers in the liquids were obtained from the pre-breakdown I-V characteristics, measured in a point-plane electrode topology, following the procedure reported in [44]. The field distribution between electrodes was calculated using the charge carrier mobility following the Laplacian equation and the equation involving the mobility, which is presented in [230]. The field distribution calculation results presented the difference between the positive and negative fields and may explain why the breakdown voltage under the positive polarity was lower than that under the negative polarity. In the final section, a brief review about the potential mechanisms of enhancing the dielectric properties of liquids was presented and discussed.

## **7.2 Mobility of Charge Carriers**

The breakdown voltage and pre-breakdown current measurement system that is used for obtaining the mobility of the charge carriers was described in Section 3.6. The system consists of a point-plane topology immersed in dielectric liquid; the gap distance between the HV point electrode and plane-grounded electrode was set to 5 mm. For the breakdown voltage measurements, the applied voltage was increased from 0 V until breakdown occurred. The digitising oscilloscope was used to record the breakdown waveform. Ten independent breakdown events under both positive and negative DC fields were registered for each liquid. For the pre-breakdown current measurements, the voltage was increased from zero to the maximum value that could be applied without inducing breakdown (positive: +18 kV; negative: -30 kV) in 1 kV steps. The conduction-current values were recorded for each voltage step. Three independent current measurements were conducted per fluid, using a fresh liquid sample for each test.

### **7.2.1 DC breakdown voltage**

In this section, the results of the measurements of the DC breakdown voltages of three base insulating liquids are presented and discussed. The results were used to identify the maximum voltage that can be applied without breakdown in the liquid to prevent this breakdown event from occurring in the pre-breakdown current tests, which may damage the current amplifier.

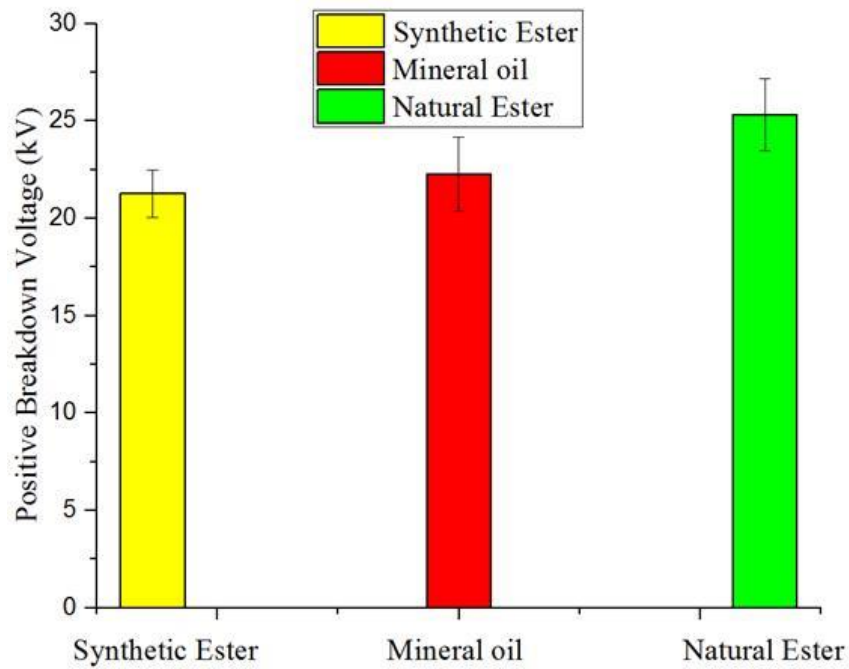


**Figure 7-1.** The positive DC breakdown voltage of mineral oil, synthetic ester, and natural ester. The mean value and standard deviation (error bars) were calculated using 10 independent breakdown events.

As Figure 7-1 shows, the positive DC breakdown voltage of mineral oil ( $22.3 \pm 1.9$  kV) and natural ester liquids ( $23.7 \pm 1.1$  kV) were close to each other and were slightly higher than that of the synthetic ester ( $21.3 \pm 1.2$  kV).

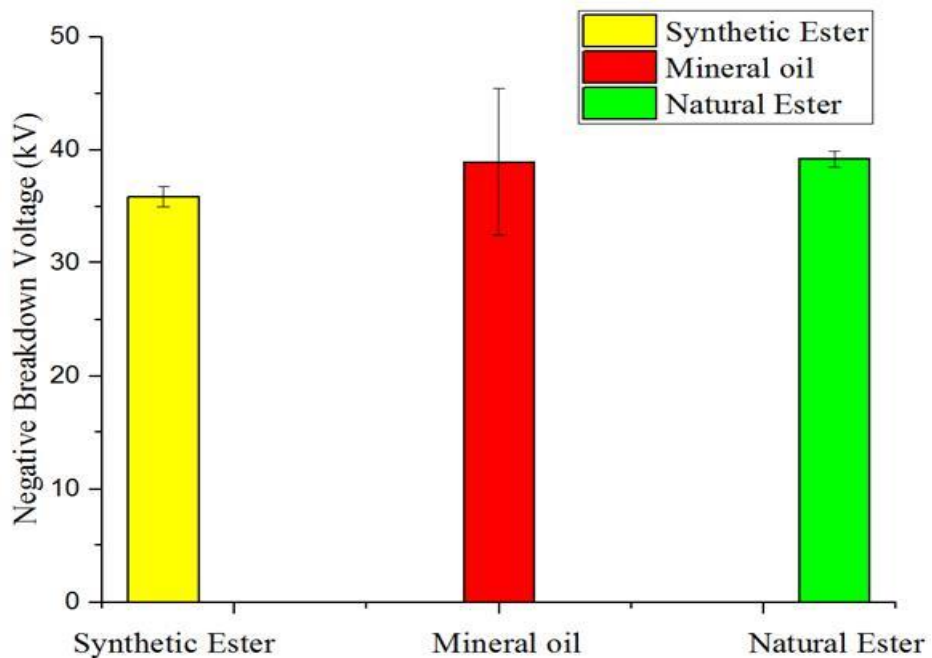


**Figure 7-2.** The negative DC breakdown voltage of mineral oil, synthetic ester, and natural ester. The mean value and standard deviation (error bars) were calculated using 10 independent breakdown events.

Figure 7-2 shows that the negative DC breakdown voltage of mineral oil ( $38.9 \pm 6.5$  kV) and natural ester liquids ( $39.2 \pm 0.7$  kV) were close to each other and were slightly higher than that of the synthetic ester ( $35.8 \pm 0.9$  kV).

**Table 7-1.** Positive and negative DC breakdown voltages of base mineral oil and synthetic and natural ester.

| <b>DC Breakdown Voltage ‘mean value <math>\pm</math> standard deviation’ (kV)</b> |                 |                 |
|---|-----------------|-----------------|
| <b>Liquid</b>   | <b>Positive</b> | <b>Negative</b> |
| Mineral Oil   | $22.3 \pm 1.9$  | $38.9 \pm 6.5$  |
| Synthetic Ester   | $21.3 \pm 1.2$  | $35.8 \pm 0.9$  |
| Natural Ester   | $23.7 \pm 1.1$  | $39.2 \pm 0.7$  |

Both positive and negative DC breakdown voltages and the standard deviations for mineral oil, synthetic ester, and natural ester are shown in Table 7-1. Under both positive and negative polarities, the synthetic ester showed a slightly lower breakdown voltage than the other liquids. Based on these results, considering the standard deviation, the maximum applied voltage of the pre-breakdown current measurement was selected to be +18 kV for positive energisation and -30 kV for negative energisation.

### **7.2.2 Pre-breakdown current measurement and mobility of charge carriers**

As discussed in Section 7.1, DC conductivity of liquids is an important parameter that can influence the design of HVDC systems and the management of insulating liquids stressed with DC voltage. Additionally, the mobility of charge carriers in the insulating fluids will affect the electrical field distribution in the HV equipment. In this section, the current-voltage (I-V) curves were obtained for Midel 7131, Diala S3, and rapeseed oil in a point-plane electrode topology. The mobilities of the charge carriers were obtained, and  $\sqrt{I(V)}$  curves were used for identification of different conductivity regimes, which will influence the distribution of the space-charge distribution between the electrodes. Three independent samples were measured for each type of liquid. The results are presented as the mean values of the three measurement results for each data point.

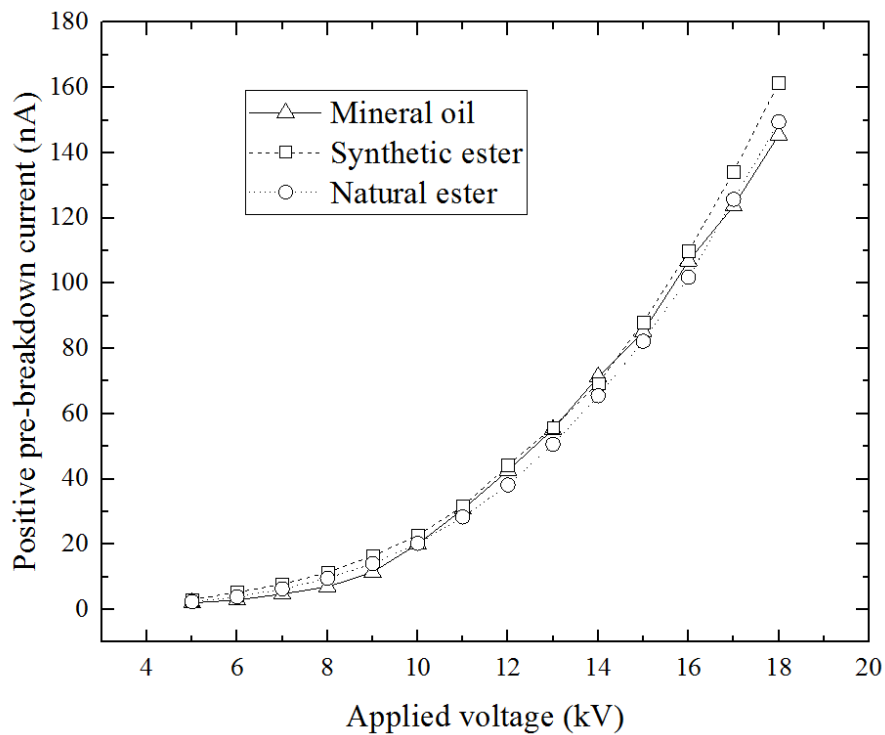


**Figure 7-3.** DC I-V plot for positive energisation. The solid line, dashed line, and dotted line are for visual guidance of the tendency for mineral oil, synthetic ester, and natural ester, respectively.

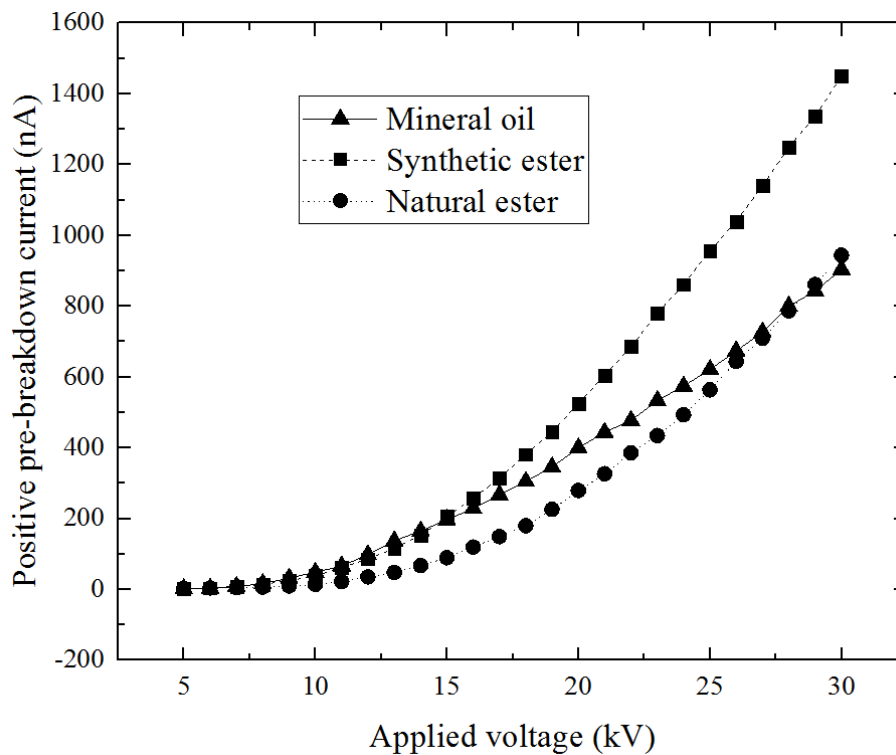


**Figure 7-4.** DC I-V plot for negative energisation. The solid line, dashed line, and dotted line are for visual guidance of the tendency for mineral oil, synthetic ester, and natural ester, respectively.

Figure 7-3 and Figure 7-4 show the I-V plot of mineral oil, synthetic ester, and natural ester under both positive and negative polarities. Synthetic ester provided a higher pre-breakdown current than the mineral oil and natural ester at the same voltage level. With an increase in the applied voltage, the pre-breakdown current rose rapidly. In [155], Butcher et al. indicated that, under the highly nonuniform field, there are three stages in the conduction process prior to the breakdown in liquid. In Stage 1, the resistive region, a resistive current exists at a low field, which will increase following the resistive characteristics with rising voltage. In Stage 2, the tunnelling region, with the applied field increasing, the effective barrier at the metal or dielectric interface is reduced and allows a ‘tunnelling’ mechanism to occur, which leads to the injection current rising rapidly. In Stage 3, the space-charge saturation region, the current reaches the space-charge saturation at high electrical field with the mobility of  $3 \times 10^3 \text{ cm}^2/\text{V}$  prior to breakdown. In Figure 7-3 and Figure 7-4, both positive and negative measurement results showed the Stage 1, resistive region, and Stage 2, tunnelling region. The theory proposed in [155] can explain the current increase behaviours under with the applied voltage increase.

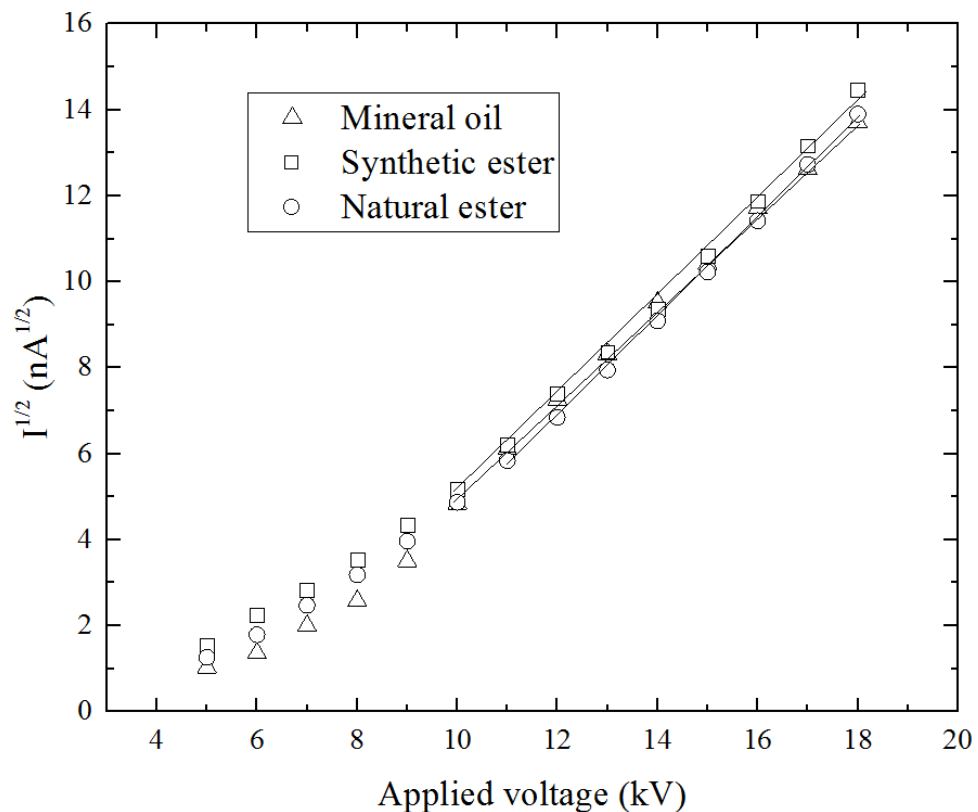


**Figure 7-5.** Plot of three oils, positive energisation.  $R^2$  coefficients: 0.9991 for mineral oil; 0.9987 for synthetic ester; 0.9995 for natural ester.

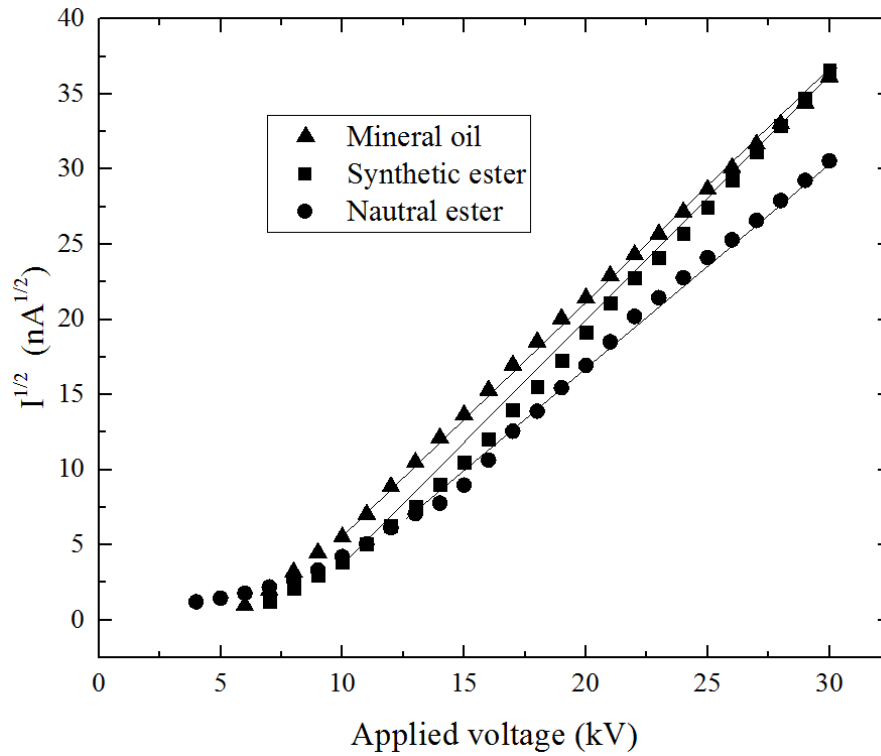


**Figure 7-6.** Plot of three oils, negative energisation.  $R^2$  coefficients: 0.9996 for mineral oil; 0.9990 for synthetic ester; 0.9988 for natural ester.

Figure 7-5 and Figure 7-6 show the square root of the conduction current for all three liquids for positive and negative energisation. The results showed that, at low voltages, the square root of the current behaves nonlinearly; however, with an increase in voltage,  $\sqrt{I(V)}$  becomes a linear function [231]. This linear behaviour indicates the space-charge saturation regime. The constant apparent mobility of the charge carriers,  $\mu$ , can be calculated using the  $\sqrt{I(V)}$  curve. The basis of this calculation method has been described in [231]. The straight lines in Figure 7-5 and Figure 7-6 were added to indicate the space-charge saturation range. In the region where the square root of the current has a linear relation with the applied voltage, the mobility,  $\mu$ , can be calculated using the following equations [232]:

$$y = Bx + A \text{ where } y = \sqrt{I(nA)}, x = V(kV) \quad (7.1)$$

$$B = \sqrt{\frac{2\mu\epsilon_o\epsilon_l}{d} \left[ \frac{nA^{1/2}}{kV} \right]}, \quad A = \sqrt{\frac{2\mu\epsilon_o\epsilon_l}{d} V_o} [nA^{1/2}] \quad (7.2)$$

$$\mu = \frac{B^2 10^{-15} d}{2\varepsilon_o \varepsilon_l} \left[ \text{cm}^2 \text{V}^{-1} \text{s}^{-1} \right], \quad (7.3)$$

where  $I$  is the current,  $V$  is the applied voltage,  $\varepsilon_o$  is the permittivity of free space,  $\varepsilon_l$  is the permittivity of the insulating liquid, and  $d$  is the gap distance between the HV point electrode and the grounded-plane electrode. The relative permittivity of the liquids are required in order to calculate the mobility. These values were taken from [232] and are  $\varepsilon_l = 2.2$  for mineral oil;  $\varepsilon_l = 3.2$  for synthetic ester;  $\varepsilon_l = 2.8$  for natural ester. The coefficient  $B$  and mobility,  $\mu$ , for each liquid are given in Table 7-2.

The calculation results showed that the apparent mobility of the charge carriers in mineral oil and synthetic ester liquids were slightly different compared with the values given in [177]. For negative energisation, the apparent mobility of the charge carriers in synthetic ester was slightly higher than the previously reported value ( $2.21 \cdot 10^{-3} \text{ cm}^2 \text{V}^{-1} \text{s}^{-1}$ ). The apparent mobility of the charge carriers in mineral oil was lower than the previously obtained value ( $3.44 \cdot 10^{-3} \text{ cm}^2 \text{V}^{-1} \text{s}^{-1}$ ), [232]. Natural ester had the lowest value of apparent mobility among all tested liquids.

For positive energisation, the apparent mobility of the charge carriers in mineral oil has the highest value,  $1.6 \cdot 10^{-3} \text{ (cm}^2 \text{V}^{-1} \text{s}^{-1})$ . The apparent charge mobility in the natural ester was slightly lower than mineral oil,  $1.4 \cdot 10^{-3} \text{ (cm}^2 \text{V}^{-1} \text{s}^{-1})$ . The apparent mobility of the charge carriers in synthetic ester was the lowest in this study. Different factors including pressure, temperature, and liquid kinematic parameters affected the apparent mobility of the charge carriers. It is known that the electrical field induces electro-hydrodynamic (EHD) motion in the liquid, which also contributes to the apparent mobility. A simple evaluation of the EHD mobility can be done by equating the kinetic energy of the moving liquid to the electrostatic energy in the liquid, [233], thus the EHD motilities is the square root of the relative permittivity of the liquid divided by its density. The EHD motilities evaluated for the three liquids used in the present work were similar in value ( $1.66 \cdot 10^{-3} \text{ (cm}^2 \text{V}^{-1} \text{s}^{-1})$  for mineral oil,  $1.71 \cdot 10^{-3} \text{ (cm}^2 \text{V}^{-1} \text{s}^{-1})$  for synthetic ester, and  $1.64 \cdot 10^{-3} \text{ (cm}^2 \text{V}^{-1} \text{s}^{-1})$  for natural ester) but lower than the measured apparent mobility shown in Table 7-2. Therefore, other factors such as an increase in the liquid velocity in nonuniform fields contributed to the apparent mobility obtained from the  $\sqrt{I(V)}$  curves, which were similar to the results in [155].

**Table 7-2.** Coefficient  $B$  and apparent mobility,  $\mu$ .

| Liquids         | Negative                 |                        | Positive                 |                        |
|-----------------|--------------------------|------------------------|--------------------------|------------------------|
|                 | $B, \frac{nA^{1/2}}{kV}$ | $\mu, \frac{cm^2}{Vs}$ | $B, \frac{nA^{1/2}}{kV}$ | $\mu, \frac{cm^2}{Vs}$ |
| Mineral Oil     | 1.50                     | 0.0029                 | 1.12                     | 0.0016                 |
| Synthetic Ester | 1.67                     | 0.0025                 | 1.15                     | 0.0012                 |
| Natural Ester   | 1.44                     | 0.0021                 | 1.16                     | 0.0014                 |

The results presented in Figure 7-5 and Figure 7-6 can be used for the identification of different conduction regimes in insulating liquids. For low voltage (low electrical field) regions, the conduction can be characterised by the Ohmic current (resistive regime region). In this case, the electrical field is governed by the Laplace equation and can be obtained using a standard electrostatic solver. With an increase in the applied voltage (higher electrical field), the space-charge saturation regime can be achieved. In this region, under HV stress, the current reaches its space-charge saturation limit [232], [155], which is described by Equation 7.1. In this case, a standard electrostatic solver was inadequate, and the Poisson equation should be used to obtain an accurate electrical field distribution in the dielectric liquid.

## 7.3 Space-charge Influenced Electrical Field

### 7.3.1 Field distribution without space charge

To investigate the electrical field distribution between the point-plane electrode topology, the space-charge effects should be considered. This was done by solving the Poisson and current continuity equations for the point-plane topology [234], [235]. The final equations for calculation of the space-charge dominated electrical field are given in this section.

In [234] and [235], the hyperbolic field expression was proposed and used to obtain the electrical field with no space charge (Laplacian field) in the point-plane electrode arrangement, Equation 7.4. The results of the Laplacian field calculations are shown in Figure 7-7, which represents an electrical field that follows the point-electrode centre axis with no space charge and is sometimes used as an approximation carried out in EHD analytical work.

$$E(x) = \frac{2aV_o}{\ln\left(\frac{4a}{r}\right)[x(2a-x) + (a-x)r]} \quad (7.4)$$

In this equation,  $V_o$  is the voltage potential,  $a$  is the distance between the tip radius centre and the plane surface,  $r$  is the tip radius, and  $x$  is the distance from the tip to the point of interest. For most cases, the tip radius  $r$  is much smaller than the distance between the tip radius centre and the plane surface  $a$ ; thus,  $a$  can be simply approximated as the axial distance between the tip and plane.

In the point-plane electrode topology, the point electrode (which is a sharp (gramophone) needle) is the HV electrode, and the plane electrode is the grounded electrode. Figure 7-7 shows the electrical field magnitude along the line from the centre of the HV point tip to the plane-electrode centre. The electrical field strength near the HV electrode (point) was high. As the distance from the HV electrode increased, the electrical field strength showed significant reduction in its magnitude. In the most of the inter-electrode gap, the electrical field was almost constant (close to its average value,  $V/d$ ).

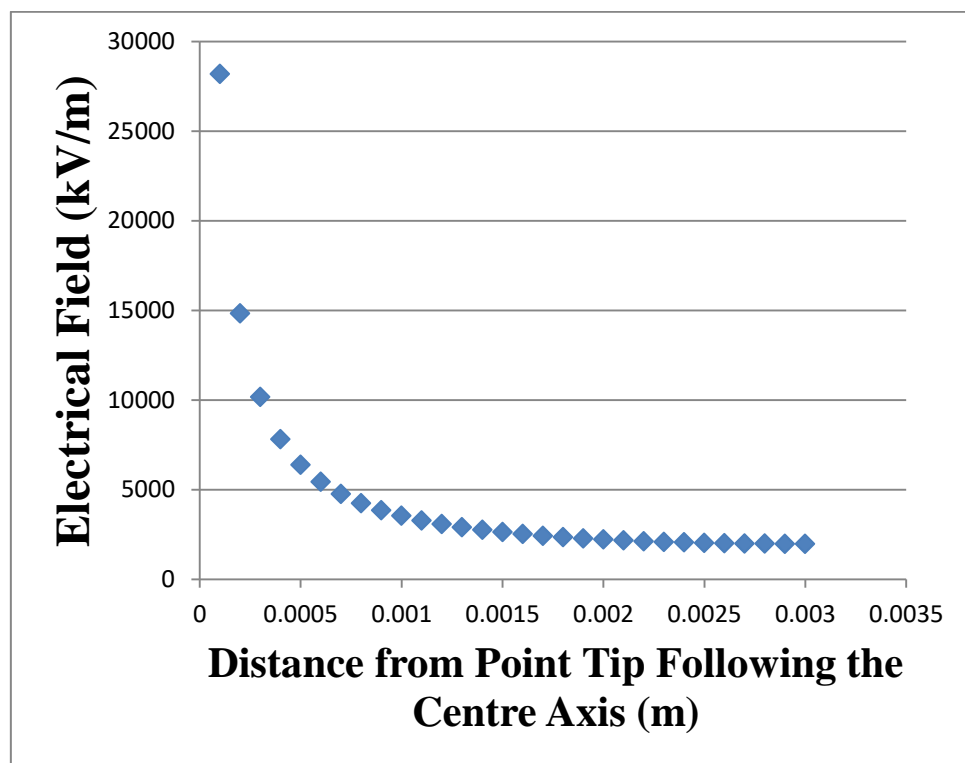


Figure 7-7. Electrical field with no space charge in the point-plane arrangement.

### 7.3.2 Field distribution with space charge

The mobility of the charge carriers in the liquid will be affected by the external electrical field (especially for high electrical fields). In this project, field calculations were used to analyse the field distribution under the positive and negative polarity. The applied voltages used in this project were

relatively low, and potentially will not affect the mobility significantly. To simplify the calculation process, the mobility was assumed to be constant.

In practical insulation liquids with non-zero conductivity, the space discharge in the inter-electrode gap results in a field distortion [234]. For the purpose of simulation of the practical space-charge-influenced electrical field that is governed by the charge carrier, created by the charge carriers with apparent mobility  $\mu$ , in [234], Coelho presented a mathematical expression to describe the field distribution with space discharge. In this case, the sign of the emitted charges is assumed to be that of the HV tip, their apparent mobility,  $\mu$ , is assumed to be independent of the field strength, and the diffusion current is assumed to be negligible with respect to the conduction current. The equations that describe the field distribution along the central line are as follows:

$$E(v) = \frac{\sqrt{\{\rho^2(2-\rho)^2 E_p^2 - Av[\rho(2-\rho) + (1-\rho)v - \frac{v^2}{3}]\}}}{(v+\rho)(2-v-\rho)} \quad (7.5)$$

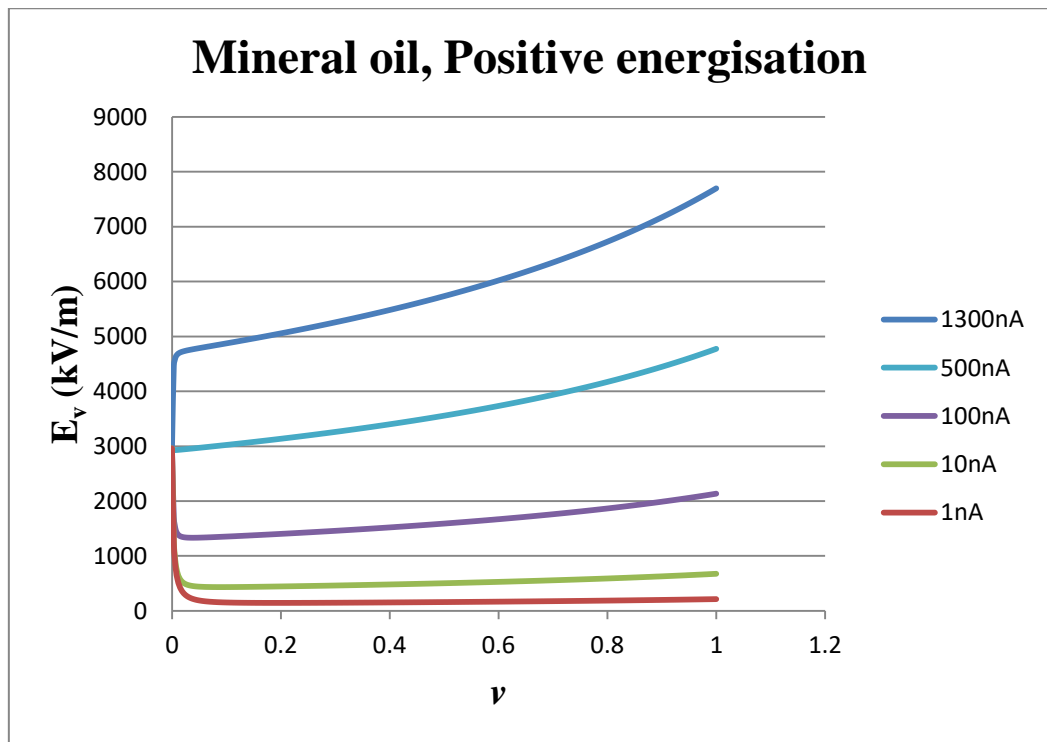
where

$$A = \frac{-2I}{\pi a \varepsilon_o \varepsilon_r \mu} \quad (7.6)$$

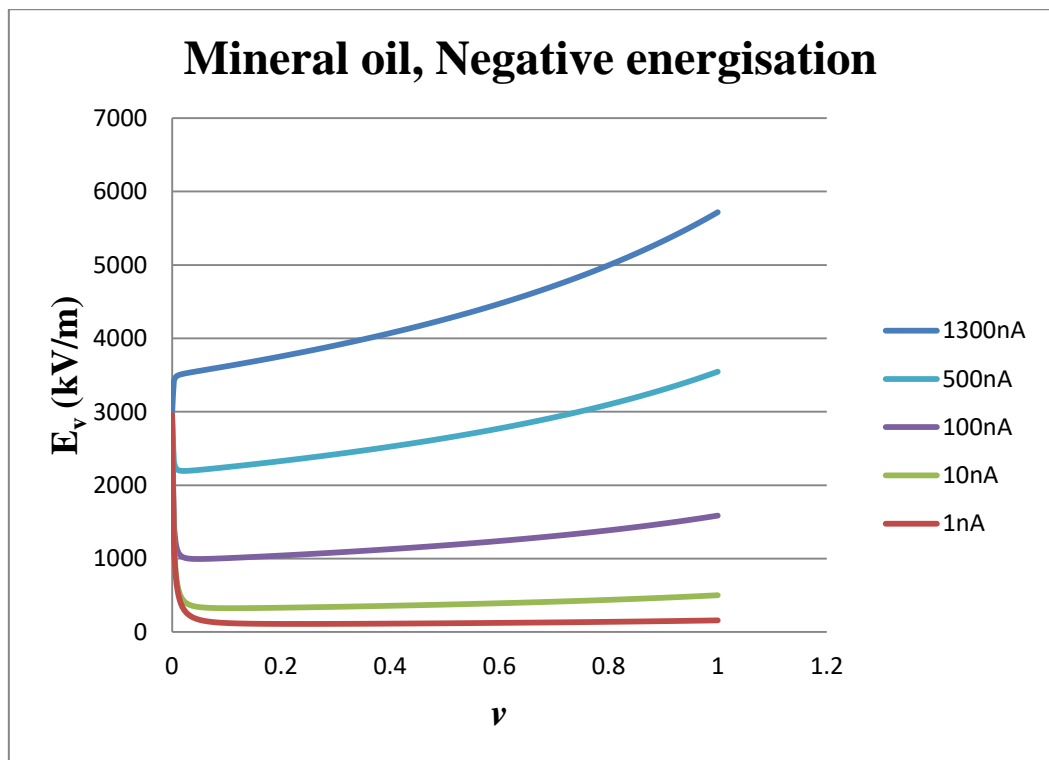
$$v = \frac{x}{a} \quad (7.7)$$

$$\rho = \frac{r}{2a} \quad (7.8)$$

In these equations,  $\varepsilon_o$  and  $\varepsilon_r$  are the vacuum permittivity and the liquid relative permittivity, respectively;  $a$  is the gap distance between the point-plane electrodes. Further,  $x$  is the distance from the tip to the point of interest, and  $v$  is the ratio of the distance from the tip to the point of interest and the gap distance, while  $E_p$  is the electrical field strength at the point of the tip. These equations have been used to investigate the field distribution of mineral oil, synthetic ester, and natural ester based on the mobility measurement results of the liquids presented in Section 7.2. The results of the calculation of the space-charge dominated field are presented in Figure 7-8 to Figure 7-10.

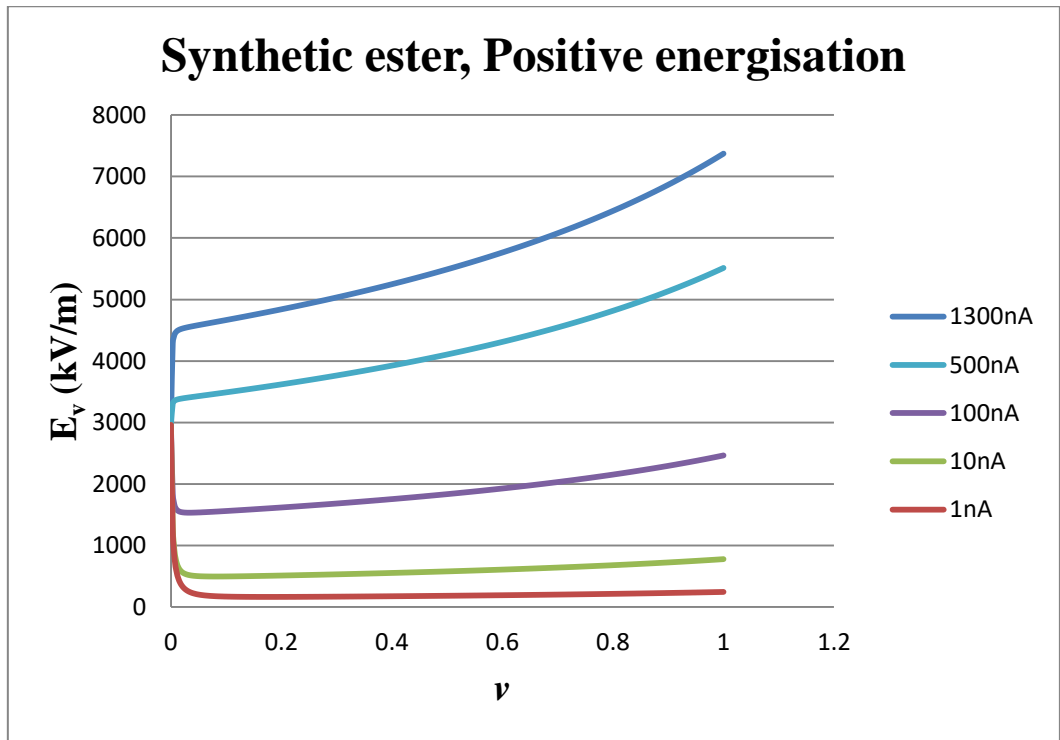


(a)

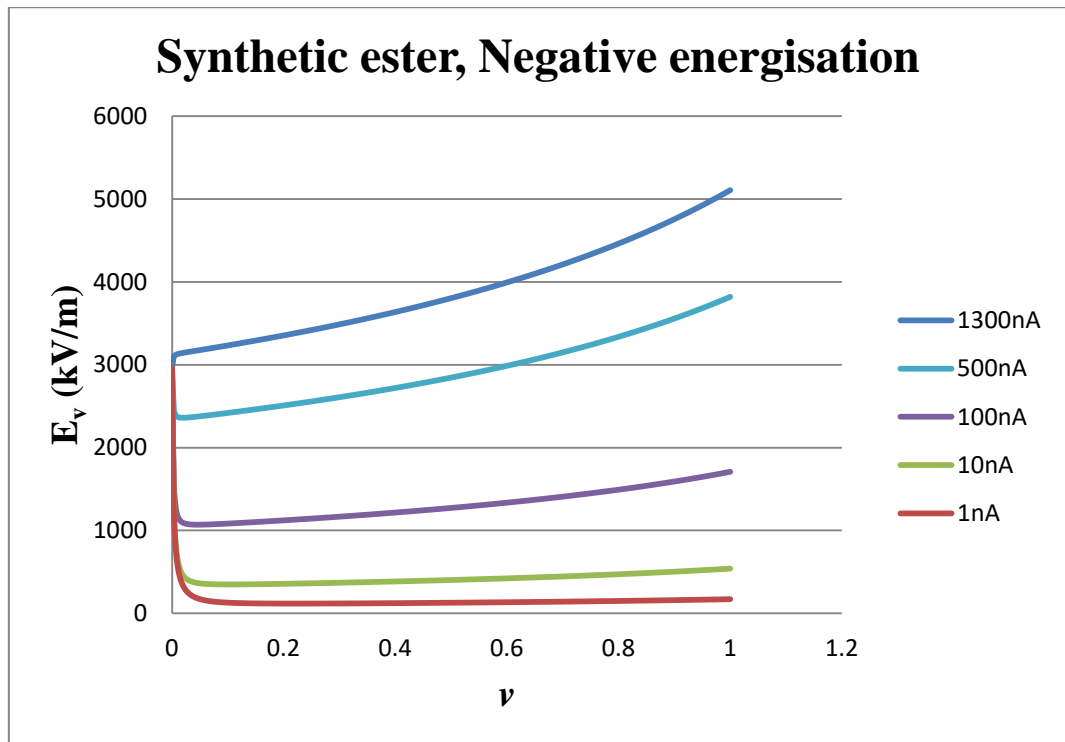


(b)

**Figure 7-8.** The electrical field  $E_v$  obtained by Equation 7.5 as a function of the normalised distance ( $x/d$ ) for mineral oil under positive (a) and negative energisations (b). Field distribution along the axis from the tip ( $\nu = 0$ ) to the plane ( $\nu = 1$ );  $a = 5$  mm,  $\mu = 0.016$  ( $\text{cm}^2/\text{Vs}$ ) (positive) and  $0.0029$  ( $\text{cm}^2/\text{Vs}$ ) (negative);  $\epsilon_r = 2.2$ .

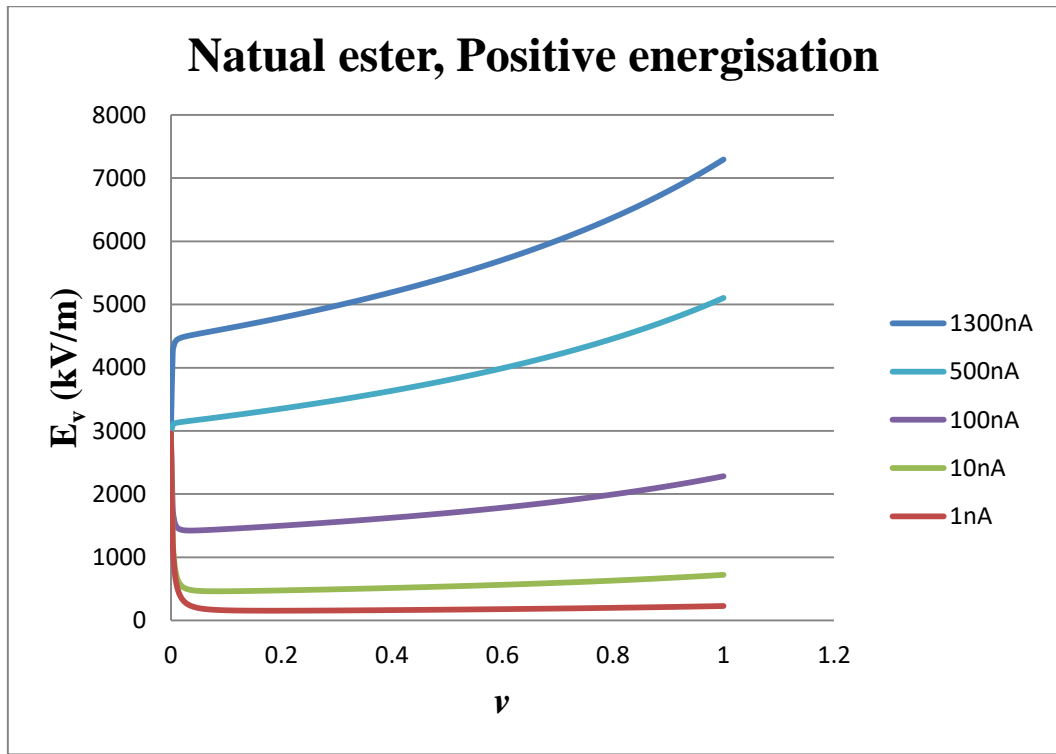


(a)

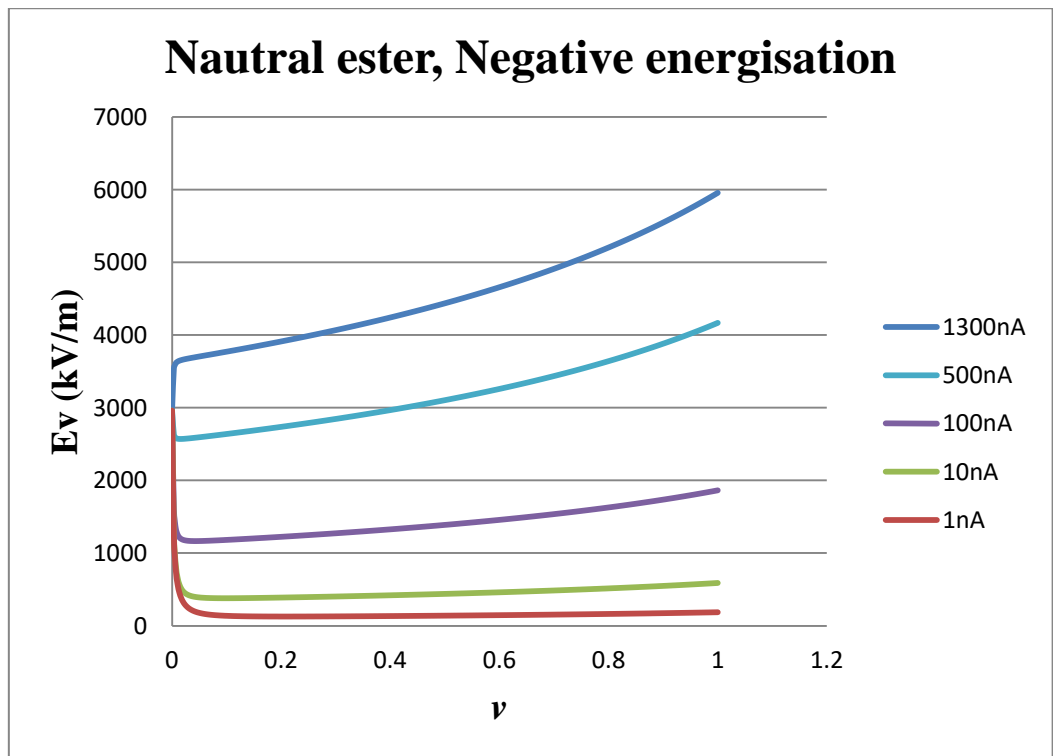


(b)

**Figure 7-9.** The electrical field  $E_v$  obtained by Equation 7.5 as a function of the normalised distance ( $x/d$ ) for synthetic ester under positive (a) and negative polarities (b). Field distribution along the axis from the tip ( $\nu = 0$ ) to the plane ( $\nu = 1$ );  $a = 5$  mm,  $\mu = 0.012$  ( $\text{cm}^2/\text{Vs}$ ) (positive) and  $0.0025$  ( $\text{cm}^2/\text{Vs}$ ) (negative);  $\epsilon_r = 3.2$ .



(a)



(b)

**Figure 7-10.** The electrical field  $E_v$ , obtained by Equation 7.5 as a function of the normalised distance ( $x/d$ ) for natural ester under positive (a) and negative polarities (b). Field distribution along the axis from the tip ( $v = 0$ ) to the plane ( $v = 1$ );  $a = 5$  mm,  $\mu = 0.014$  ( $\text{cm}^2/\text{Vs}$ ) (positive) and  $0.0021$  ( $\text{cm}^2/\text{Vs}$ ) (negative);  $\epsilon_r = 2.8$ .

Figure 7-8 to Figure 7-10 present the electrical field distribution with the space charge obtained by Equations 7.5-7.8 for different insulating liquids under both positive and negative energisations. In these calculations, the pre-breakdown currents were 1 nA, 10 nA, 100 nA, 500 nA, and 1300 nA, and the electrical field was calculated using these values of current in the liquid.

The results presented for the 1 nA current case showed that the electrical field distribution was similar to the situation in which no space charge was involved (similar to the Laplacian field). These results showed that, in the case of low currents through the dielectric liquid, there was insignificant space charge and the field distribution was almost the same as in the Laplacian case.

With the increase in the current (10 nA, 100 nA), the electrical field initially dropped rapidly with an increase in the distance from the HV electrode; however, the field strength started to increase closer to the plane electrode. In this case, the relatively large current means there were charge carriers in the inter-electrode gaps, and they changed the electrical field distribution. Under the influence of the field, these charges started to form the space charge and moved towards the electrode of the opposite polarity. Thus, the field distribution showed a clear distortion.

In the case of larger currents (500 nA, 1300 nA), the field distribution was completely different from the other cases. In this situation, the field strength near the tip was very low, and it increased slightly away from the HV tip. Then, the field strength steadily rose with the distance from the HV tip towards the ground electrode. These results showed that, when the higher current flowed in the gap between the electrodes, there was a large number of charge carriers, which disturbed the field distribution. An ionisation zone may exist near the HV electrode (if the field strength exceeded the ionisation threshold), and a significant number of charge carriers with a polarity opposite to the polarity of the HV electrode were gathered around the HV electrode and offset the high electrical field in this region. Thus, the field strength near the HV tip was low.

A streamer may be formed under the influence of these charges. The streamer is propagated away from the tip towards the plane electrode charge carriers behind the streamer head, forming the conductive channel and space charge, which distort the field. Ahead of the streamer head, neutral molecules form a resistive area, which results in a high field strength in this region. Thus, the electrical field distribution ahead of the streamer head can be calculated using Equation 7.5. The

results showed the difference in field distribution for the positive and negative energisations for all three liquids. The positive field strength was higher than the negative field strength in the same position along the central axis; thus, the positive streamer developed faster than the negative streamer. Therefore, this phenomenon can help to explain the lower breakdown voltage of the dielectric liquids stressed with positive HV compared with negative HV.

## **7.4 Potential Mechanisms of Nanoparticles on the Breakdown Strength of the Liquid**

The major objectives of this project include investigation of the AC and impulse breakdown voltages and pre-breakdown current characteristics of base mineral oil, synthetic ester, and natural ester and the same liquids with TiO<sub>2</sub> and BN nanoparticles (nanofluids). The experimental results indicated that the base ester liquids showed comparable dielectric properties with those of the traditional commercial mineral oil. Furthermore, the ester-based nanofluids provided comparable or even better dielectric performance compared with the nanofluid based on the mineral oil.

As described above, the charge carrier mobilities for three base insulating liquids were obtained. The electrical field distribution was also obtained using this apparent mobility for all three insulating liquids. However, the effect of nanoparticles on the dielectric properties of liquids is not fully understood yet. The traditional breakdown theory cannot explain the phenomenon of an increase in the breakdown strength with the addition of nanoparticles with specific concentrations to the insulating fluid. Instead, typically, it is expected that the breakdown strength decreases with an addition of contaminants to the dielectric liquid, especially with an increase in concentration of nanoparticles [114], [61]. Several potential mechanisms that could result in the enhancement of the dielectric properties of nanofluids have been proposed. In this section, a brief review of these potential mechanisms is presented. Understanding of these effects and mechanisms (effect of nanoparticles on the field distribution and propagation of streamers in dielectric liquids) is important for preparation of nanofluids that could be used in commercial power and pulsed power applications.

### **7.4.1 Polarisation of nanoparticles**

The breakdown characteristics of nanofluids under AC and impulse energisation can be explained from the point of view of streamer formation and propagation. In [17], [88], and [90], Segal et al.

reported that, in the electrical breakdown test, the AC breakdown voltage and positive lightning impulse breakdown voltages of magnetite nanofluids were significantly higher than those of base transformer oil. In [236] and [237], O'Sullivan et al. provided the electrodynamic analysis of mineral oil-based nanofluid with  $\text{Fe}_3\text{O}_4$ , and the results demonstrated that the conductive nanoparticles ( $\text{Fe}_3\text{O}_4$ ) acted as electron scavengers and converted the fast electrons to slow charged particles.

Hwang et al. [82], [83], [135] presented a model to explain the enhanced dielectric properties of transformer oils with  $\text{Fe}_3\text{O}_4$  nanoparticles [17], [98], [100]. The authors indicated that, because electrons move much faster than positive ions during the development of a streamer, nanoparticles can adsorb large numbers of electrons onto their surfaces. Meanwhile, the velocity of nanoparticles is much lower than the electron velocity; thus, the fast-moving electrons in the adsorption process are converted into slow-moving negative particles, which reduce the electrical field strength of the streamer head while further slowing the positive and negative ion movement velocity. Therefore, impulse voltage and time to breakdown of nanofluids are greater than that of the base oil [82], [83], [135].

In Figure 7-11, a dynamic polarisation model of a nanoparticle is presented. In the ideal conditions, a uniform  $z$ -directed electrical field is switched on at  $t = 0$ , and a uniform electron charge density along the  $z$ -axis is established due to ionisation and electron injection. Once a nanoparticle has relaxed electrically, the electrical field lines will be terminated by its bottom surface, which is the negatively charged surface and will be initiated from the top surface, which is the positively charged surface of the particle. The injected electrons follow the electrical field lines and approach the nanoparticle surface where the radial electrical field is positive,  $0 \leq \theta \leq \pi/2$ , as Figure 7-11 (a) shows.

These electrons will be deposited into the parts of nanoparticles where the charge is positive. Once the electrons are deposited on the nanoparticle, they redistribute themselves uniformly on the equipotential surface so that the total negative charge on the nanoparticle increases with time. This charging process modifies the electrical field outside the nanoparticle and continually reduces the area of the nanoparticle surface that has a positive radial electrical field component (the charging window on the particle surface), as Figure 7-11 (b) shows.

This charging process operates over time until the nanoparticle reaches the saturated charge condition, which indicates that there is no portion of the nanoparticle surface that has a positive radial electrical field component, as shown in Figure 7-11 (c). In this situation, the nanoparticle is said to be charge saturated, as no additional negative charge can flow onto the sphere.

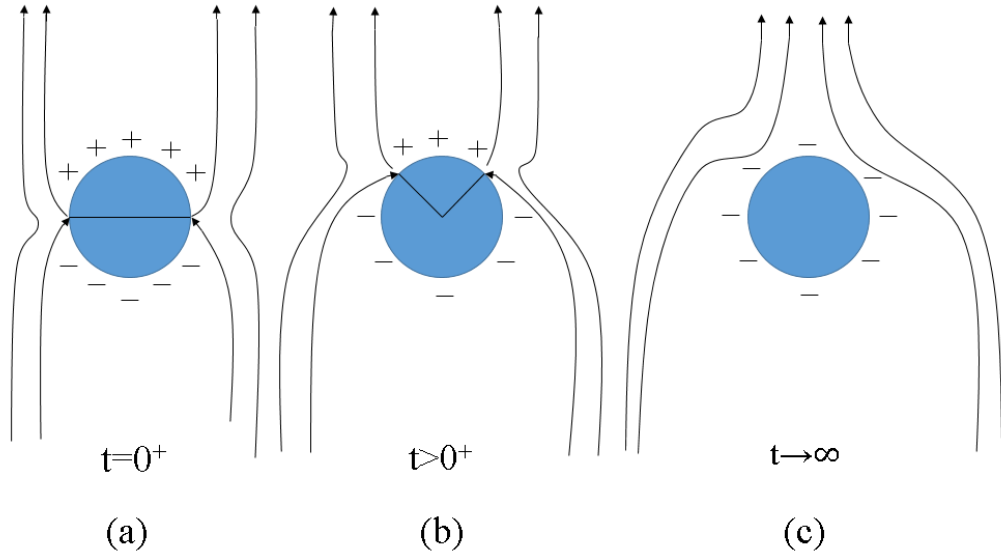


**Figure 7-11.** Model of nanoparticle polarisation. Figures plotted using data from [135].

In this model, for evaluation of the effect of different particles on the development of streamers in the transformer oil under the impulse voltage, Hwang introduced the charge relaxation time  $\tau_r$  which represents the rate at which the electrons are trapped on the surface of the nanoparticle and reflects the dynamic state of the adsorption process, in Equation 7.9:

$$\tau_r = \frac{2\varepsilon_1 + \varepsilon_2}{\sigma_1 + \sigma_2} \quad (7.9)$$

where  $\varepsilon_1$  is the relative permittivity of the fluid,  $\varepsilon_2$  is the relative permittivity of the nanoparticle,  $\sigma_1$  is the conductivity of the fluid, and  $\sigma_2$  is the conductivity of the nanoparticles.

In [135], Hwang indicated that the streamer formation and propagation were a timescale between nanoseconds to microseconds; thus, the conductive nanoparticle ( $\text{Fe}_3\text{O}_4$ ), which has a small relaxation time  $\tau_r$  ( $\tau_r = 7.47 \times 10^{-14}$ s), would be polarised very quickly and capture the free electron during the streamer. In the case in which the nanoparticle has a longer charge relaxation time  $\tau_r$ , such as that of

$\text{Al}_2\text{O}_3$  ( $\tau_r = 42.2\text{s}$ ), the influence of nanoparticles on the streamer development would not be so pronounced.

In [135], Hwang presented the model using the Gaussian law equation (7.10) and charge transport continuity equation (7.11–7.14) as the governing equations:

$$\nabla \cdot (\epsilon_1 \vec{E}) = \rho_p + \rho_n + \rho_e + \rho_{np} \quad (7.10)$$

$$\frac{\partial \rho_p}{\partial t} + \nabla \cdot (\rho_p \mu_p \vec{E}) = G_I + \frac{\rho_p \rho_e R_{pe}}{e} + \frac{\rho_p (\rho_n + \rho_{np}) R_{pn}}{e} \quad (7.11)$$

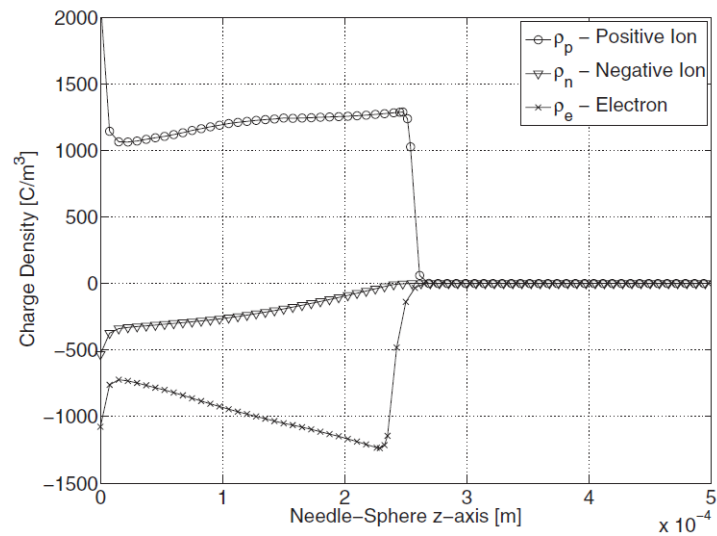
$$\frac{\partial \rho_n}{\partial t} - \nabla \cdot (\rho_n \mu_n \vec{E}) = \frac{\rho_e}{\tau_a} - \frac{\rho_p \rho_n R_{pn}}{e} \quad (7.12)$$

$$\frac{\partial \rho_e}{\partial t} - \nabla \cdot (\rho_e \mu_e \vec{E}) = -G_I - \frac{\rho_p \rho_e R_{pe}}{e} - \frac{\rho_e}{\tau_a} - \frac{\rho_e}{\tau_{np}} [1 - H(\rho_{np,sat} - \rho_{np})] \quad (7.13)$$

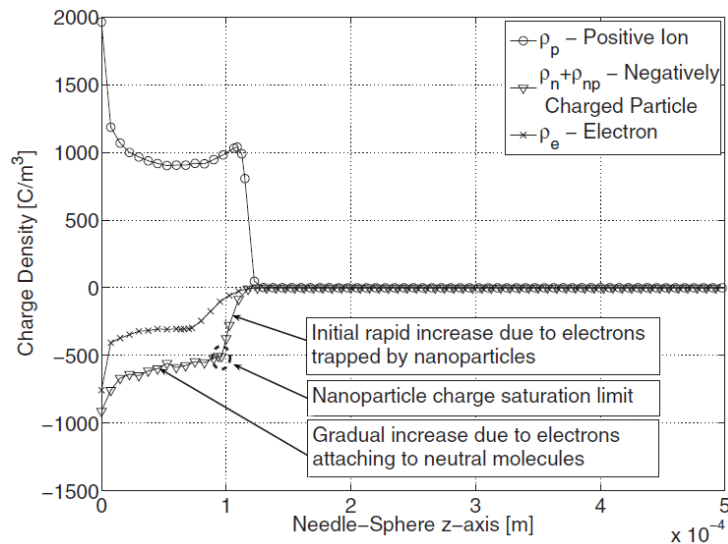
$$\frac{\partial \rho_{np}}{\partial t} - \nabla \cdot (\rho_{np} \mu_{np} \vec{E}) = \frac{\rho_e}{\tau_{np}} [1 - H(\rho_{np,sat} - \rho_{np})] - \frac{\rho_p \rho_{np} R_{pn}}{e} \quad (7.14)$$

In these equations,  $E$  is the electrical field intensity vector;  $\rho_p$ ,  $\rho_n$ ,  $\rho_e$ , and  $\rho_{np}$  are the densities of positive ion, negative ion, electron and charged nanoparticles, respectively, which are coupled to the Gaussian law equation. In addition,  $\mu_p$ ,  $\mu_n$ ,  $\mu_e$ , and  $\mu_{np}$  are the respective mobilities of the positive ion, negative ion, and electron and charged nanoparticles. The variables  $R_{pn}$  and  $R_{pe}$  are the Langevin recombination coefficients to describe the ion-ion and ion-electron recombination, respectively. Moreover,  $\tau_a$  is the attachment time constant of electrons combined with neutral molecules, and  $\tau_{np}$  is the attachment time constant of electrons combined with nanoparticles, while  $e$  is the electron charge. In Equations 7.13 and 7.14, the Heaviside function,  $H(\rho_{np,sat} - \rho_{np})$ , is used to model the nanoparticle charging limit, where  $\rho_{np,sat}$  is the nanoparticle saturation charging limit, and  $G_I$  is the field ionisation charge density rate source term.

The field simulation study [135] was performed using COMSOL software. Equations 7-10–7.14 have been solved in COMSOL. The results of the simulation in [135] are presented in Figure 7-12.



(a)



(b)

**Figure 7-12.** The simulation results of base transformer oil (a) and nanofluid (b) charge density distributions along the needle-sphere electrode axis at time  $t = 0.1 \mu\text{s}$ , given by the solution to the streamer model for transformer oil and transformer oil-based nanofluid with  $\rho_{np,sat} = -500 \text{ C/m}^3$  and  $\tau_{np} = 2 \text{ ns}$ . Positive ion charge density represented as cross symbols; negative ion charge density represented as circular symbols. Electron charge density represented as triangle symbols. Figure taken from [135].

The simulation of the charge particle density distribution in the nanofluid showed that the charge density of the negative charge particles initially increased rapidly due to the capture of free electrons by the nanoparticles. After the charge on the nanoparticles reached saturation, the density of negative

charge particles gradually increased because the free electrons attached to neutral molecules. The electron charge densities in the nanofluid were much lower than that in the base oil, which means the nanoparticles inhibited the streamer development.

This model explains the results presented in [17], [88], and [90], which provided the enhancement phenomenon of the dielectric performance of transformer oils with conductive nanoparticles (e.g.,  $\text{Fe}_3\text{O}_4$ ) that have a relaxation time constant of  $7.5 \times 10^{-14}$  s due to their high conductivity. However, this model cannot explain the change in the breakdown voltage of the transformer oil doped with SiC nanoparticles (less conductive nanoparticles with relaxation time constant of  $1.1 \times 10^{-12}$  s, and conductivity of  $1 \times 10^{-12}$  S/m) [20], [151]. Furthermore, this model cannot explain the change in the dielectric properties of mineral oils doped with the semi-conductive ( $\text{TiO}_2$ ) or insulated nanoparticles ( $\text{SiO}_2$ ), which have very low conductivity and thus long relaxation time constants at tens of seconds [114], [28], [29], [30], [31], [238], [239].

In summary, this dynamic charging model can only be used to explain the enhancement of the dielectric properties of nanofluids with nanoparticles that have microsecond-scale relaxation time constants. Thus, this model has some limitations and shortcomings.

#### **7.4.2 Model of trapping potential**

In 2008, Takada et al. introduced a trapping potential model to explain the enhancement of the dielectric properties of low-density polyethylene film (LDPE) containing a small amount of MgO nanoparticles (solid material) under high DC electrical stress (up to 250 kV/mm).

In [22], [134], [240], some researchers using this model tried to explain the enhancement of the dielectric properties of mineral oil-based [22], [240] and vegetable oil-based [134] nanofluids with various nanoparticles (AlN, ZnO,  $\text{SiO}_2$  [240], and  $\text{Fe}_3\text{O}_4$  [33]). The analysis results showed that this model can explain the results of nanofluids with  $\text{Fe}_3\text{O}_4$  and AlN nanoparticles but not the results of nanofluids with ZnO and  $\text{SiO}_2$ . More details and discussion about this model are presented below.

Meunier et al. in [241] and [242] and Teyssedre et al. in [243] indicated that, in the case of polymer insulators (solid material) under the external electrical field, the polarised molecules will form a dipole, which will become the charge carrier trap. The potential reason for this phenomenon is that there are chemical defects in the polymer molecule structure, such as 'C = O' and 'C = C'.

Based on the results and conclusions reported by Meunier et al. and Teysedre et al., Takada et al. [244] proposed a trapping potential model to explain the enhancement of dielectric properties of LDPE/MgO nanocomposite (solid material).

Figure 7-13 presents three cases of the dipole electrical charge and the electrical line distribution for low-density polyethylene (LDPE) (a), a spherical dielectric in LDPE (b), and a spherical conductor in LDPE (c). As Figure 7-13 presented, Takada et al. indicated that the difference between the relative permittivity of the nanoparticles and base liquids results in the distortion of the electrical field near the nanoparticles. Meanwhile the potential traps on the nanoparticle surfaces form the charge carrier trap. The difference between the traps of nanoparticles and the surrounding media determines the effect of the nanoparticles on the charge carriers under the external electrical field. If the depth of the nanoparticle traps is deeper than that of the surrounding media, the nanoparticles presented obvious enhancement on material dielectric properties. If the depth of the nanoparticle traps is shallower than that of the surrounding media, then the nanoparticle will not show a clear influence on the material dielectric properties.

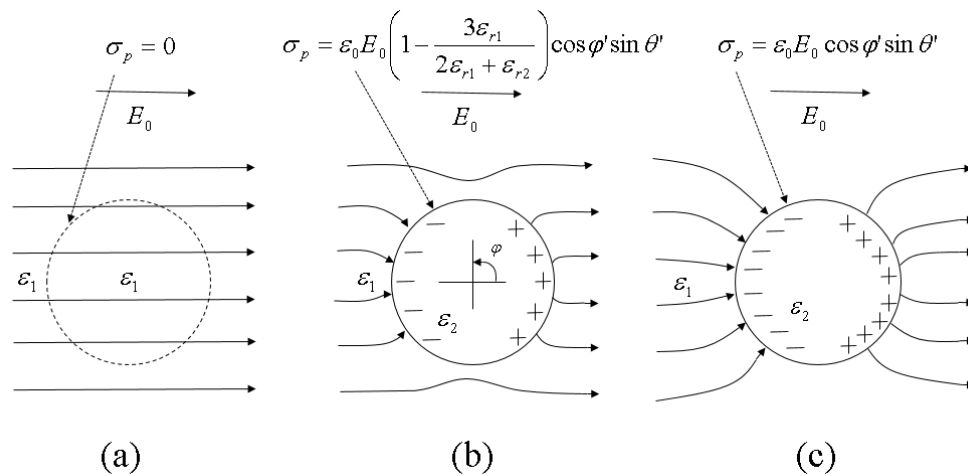


**Figure 7-13.** Dipole electric charge and electric line distribution for LDPE (a), a spherical dielectric in LDPE (b), and a spherical conductor in LDPE (c). Figures plotted using data from [244].

Takada et al. developed a mathematical expression to describe the surface charge density on the polarised nanoparticle (dipole), which depends on the external electrical field and the electrical potential distribution in [244]. The discussions below present the details of the model developed by Takada et al.

The dipole surface charge density  $\sigma_p$  is described by Equation 7.15. In this equation,  $\epsilon_{r1}$  is the relative permittivity of the nanoparticle,  $\epsilon_{r2}$  is the relative permittivity of the base liquid,  $E_0$  is the external field, and  $\sigma_p$  is the dipole surface charge density.

$$\sigma_p = \epsilon_0 E_0 \left( 1 - \frac{3\epsilon_{r1}}{2\epsilon_{r1} + \epsilon_{r2}} \right) \cos \varphi' \sin \theta'. \quad (7.15)$$

Using this mode, Zhou et al. in [22] calculated the nanoparticle trap depth at 0.5 eV, which is higher than that of the mineral oil (Karamay DB 25) 0.45 eV. Thus, this model is suitable to explain the enhancement of the dielectric properties (the breakdown voltage of AC, negative DC, and negative lightning impulse) of nanofluids.

In [134], Du et al. prepared vegetable oil-based nanofluids (FR3) with  $\text{Fe}_3\text{O}_4$  nanoparticles of various sizes (10 nm, 20 nm, and 30 nm). Using this mode, Du et al. calculated the nanoparticle maximum trap depth to be 5.86 eV, 11.73 eV, and 17.59 eV for 10 nm, 20 nm, and 30 nm nanoparticles, respectively. These results showed that the nanoparticle trap depth is much higher than that of the surrounding liquid (~0.45 eV), which can explain the enhancement of the dielectric properties (the breakdown voltage of AC, positive and negative lightning impulse) of nanofluids.

This model also can explain the change of AC breakdown voltage in mineral-oil-based AIN nanofluid (K125X) [240]. The dielectric strength of this nanofluid increases as the nanoparticle trap depth is 0.8 eV, which is higher than that of the mineral oil at 0.45 eV.

In [240], in the case of mineral-oil-based nanofluids (K125X) with ZnO and  $\text{SiO}_2$ , the AC breakdown strength of these nanofluids is higher than that for the base oil. However, the trap depth is 0.3eV for  $\text{SiO}_2$ , 0.35 eV for ZnO, which is shallower than that for mineral oil at 0.45 eV. In this situation, this model is not suitable.

In summary, this trapping potential model can explain some breakdown results of nanofluids based on the difference between the trap depth for nanoparticles, such as MgO [244] and AIN [240], and that of the host liquid; however, there are some limitations in the framework of this model, and it cannot be used universally for all kind of nanofluids.

### 7.4.3 Model of the electron shallow trap

In [245], Du et al. presented a model that is aimed at the explanation of the breakdown properties of mineral oil-based nanofluids with semi-conductive nanoparticles. The authors indicated that, in the case of suspension of semi-conductive nanoparticles, there is a large number of shallow traps at the nanoparticle surface and the interface between the nanoparticles and base liquid. These centres will trap and de-trap the high mobility electrons. In this trapping and de-trapping process, the electron kinetic energy will be dissipated and the electron velocity will be slowed. This phenomenon will lead to inhibition of the streamer development and will improve the dielectric strength of the transformer oil.

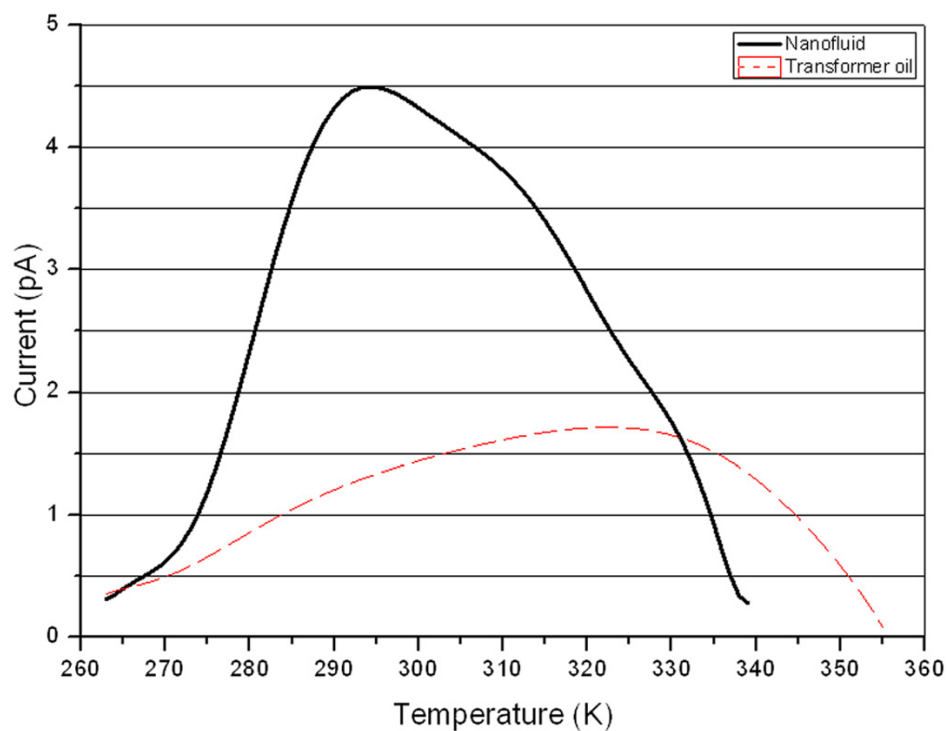


**Figure 7-14.** Results of thermally stimulated current (TSC) measurement, solid line is nanofluid current; red dashed line is base transformer oil [245].

In [245], thermally stimulated current (TSC) measurements were performed and the results are presented in Figure 7-14. In this test, the trap depths for the base oil and the nanofluid were 0.416 and 0.418 eV, respectively, which means that the traps of both these liquids were shallow traps. As Figure 7-14 shows, the TSC peak for the nanofluid was almost 2.5 times higher than that for the base oil, which means that there were high-density electron traps in the nanofluids. These high-density electrons traps reduced the electron mobility and the energy and hindered electrons passing through

the nanofluids. As a result, the ionisation of neutral molecules due to electron impact was weakened. Therefore, the field distortion and the streamer development due to neutral molecule ionisation was decreased, and the dielectric strength of nanofluid was enhanced [246].

In summary, this electron shallow trap model can explain the dielectric behaviour of the semi-conductive ( $\text{TiO}_2$ ) nanoparticle suspensions. However, there are no results that confirm that this model can explain the dielectric behaviour of the nanofluids with conductive and insulation nanoparticles. Thus, more research and experiments will be needed in the future to clarify these aspects and to develop a unified model.

## 7.5 Summary

In this chapter, the results of measurements of the DC breakdown strength of three liquids and the results of measurements the apparent mobility of the charge carriers in these fluids are presented and discussed. Based on these results, the space-charge-influenced electrical field distribution was obtained and analysed. The results showed that the space discharge significantly influences the electrical field distribution in the gap between electrodes. The apparent mobility of charge carriers is a key parameter to evaluate the liquid capability to carry the pre-breakdown current and to develop a significant space discharge. Furthermore, the space-charge-influenced field distribution provides a potential explanation for the higher breakdown voltage for the negative energisation compared with the positive energisation.

The discussion of the potential effects and mechanisms of influence of the dielectric behaviour of the nanofluids is presented and discussed in this chapter. In the case of the nanoparticle polarisation model, Hwang et al. introduced the field relaxation time constant order to evaluate the capability of nanoparticles to enhance the dielectric strength of liquids [82], [135], [83]. This model can explain the dielectric behaviour of the nanofluid with  $\text{Fe}_3\text{O}_4$  particles (which have a short relaxation time constant of  $7.5 \times 10^{-14}$  s). However, this model cannot be used for explanation of the experimental results (300 ns pulse non-destructive breakdown voltages, NDBD, per the ASTM standard) of nanofluids with SiC nanoparticles (which is a conductive nanoparticle; their relaxation time constant is  $1.1 \times 10^{-12}$  s, and their conductivity is  $1 \times 10^{-12}$  s) [20], [151]. Furthermore, this model cannot explain the dielectric behaviour of the nanofluids with semi-conductive or dielectric nanoparticles (with long relaxation

time in the range of tens of seconds) [28]–[31], [114], [238], [239]. Thus, this model can only be used to explain the enhancement of the dielectric properties of nanofluids with the nanoparticles that have microsecond-scale relaxation time constants. Thus, this model has some limitations and shortcomings.

Takada et al. proposed the trapping potential model in [244] to explain the enhanced dielectric behaviour of the solid nanocomposite (LDPE with MgO nanoparticle). Takada et al. calculated the surface charge density on the particle and the electrical potential around the nanoparticle.

In [22], [134], and [240], Shen et al., Zhou et al., and Du et al. used this model to try to explain the enhancement of the dielectric properties of mineral-oil-based [22], [240] and vegetable-oil-based [134] nanofluids with various nanoparticles (AlN, ZnO, SiO<sub>2</sub> [240], and Fe<sub>3</sub>O<sub>4</sub> [33]).

This model can explain the results of breakdown voltage enhancement of AC, negative DC, and negative lightning impulse of mineral-oil-based nanofluid (Karamay DB 25) [22]; the results of the breakdown voltage of AC, positive and negative lightning impulses of vegetable-oil-based nanofluids (FR3) with Fe<sub>3</sub>O<sub>4</sub> (10 nm, 20 nm, and 30 nm nanoparticle size) [134]; and the results of AC breakdown voltage enhancement of mineral-oil-based nanofluids (K125X) with AlN nanoparticles. The trap depths of the above nanoparticles were higher than those of the liquids; thus, the enhancement of the dielectric properties of nanofluids can be explained using this trapping potential model.

However, this model cannot explain the AC breakdown voltage enhancement of mineral-oil-based nanofluids (K125X) with ZnO and SiO<sub>2</sub> nanoparticles [240]. These results showed that the AC breakdown voltages of the nanofluids with ZnO and SiO<sub>2</sub> were higher than that of the base oil sample. However, the trap depths of ZnO and SiO<sub>2</sub> nanoparticles were shallower than that of the liquid. In this situation, this model is not suitable. Thus, this model still has some limitations for evaluating the capability of nanoparticle enhancement of dielectric liquid properties.

Du et al. developed the electron shallow trap model [245]. Du et al. indicated that the measurement results of the TSC in the nanofluid and in the base oil presented the difference in the shallow trap amount in the nanofluids and in the base oil. High TSC current means there is a large number of shallow traps that exist in the liquids and that trap and de-trap the fast electrons, resulting in reduction of their electron kinetic energy and moving velocity. Thus, ionisation due to the electron impact and

the streamer development will be inhibited. This model can explain the breakdown behaviour of the  $\text{TiO}_2$  semi-conductive nanoparticle suspensions.

However, there were no experiments using this method to investigate the nanofluids with conductive and insulation particles. It remains open for discussion whether this model is suitable for application to a wide range of nanoparticles and liquids. Further studies are required to answer this question.

# CHAPTER 8

## CONCLUSIONS AND FUTURE WORK

### 8.1 Brief review

This thesis is focused on the investigation of the breakdown performance of three insulating liquids (mineral oil, synthetic ester, and natural ester) and nanofluids based on these liquids (suspensions of TiO<sub>2</sub> and BN nanoparticles in Diala S3 mineral oil Midel 7131 synthetic ester, and food grade vegetable oil). The concentrations of nanoparticles which have been investigated were 0.0006%, 0.004%, 0.01%, 0.05%, and 0.1% (b/w). The main result of this thesis may be formulated as follows: it was established that semi-conductive nanoparticles affect the dielectric properties of nano-modified liquids; depending on the concentration of semi-conductive nanoparticles this change can be “positive” – an increase in the breakdown strength of the nanofluid or “negative” – nanoparticles result in lower breakdown strength of nanofluids. The optimal concentration of TiO<sub>2</sub> and BN nanoparticles in the tested liquids have been established, nanofluids with this concentration demonstrated the greatest improvement in the breakdown strength. During the course of this research project AC and impulsive breakdown voltages of base and nano-modified liquids have been investigated. AC breakdown voltage was obtained in accordance with the ASTM D1816 standard. Two categories of the impulsive breakdown test have been conducted: minimum breakdown voltage strength was obtained using the test procedure outlined in the ASTM D3300 and IEC 60897 international standard; in addition in order to satisfy requirements of the pulsed power industry the fixed impulsive breakdown voltage was obtained following the procedure outlined in [79], [80], [133].

Statistical difference analysis of the obtained results have been conducted using 95% confidence intervals in order to prove with a high degree of confidence that addition of nanoparticle results in the statistically significant change in the breakdown properties of the nanofluids. Also, the Weibull statistical analysis was applied to the obtained breakdown voltages and pre-breakdown times (in the case of impulsive breakdown), 3-parameters Weibull distribution allowed identification of the minimum breakdown voltage, shape and scale parameters for base and nano-modified fluids. Thus

breakdown properties of nanofluids with different concentrations of nanoparticles can be statistically characterized. Average streamer velocity has been obtained for all tested fluids in the case of the impulsive breakdowns.

The space charge influenced electric field distribution has been also obtained using I-V curves in base liquids, this field distribution and obtained charge carrier motilities help to explain the difference in the breakdown characteristics of the insulating liquids stressed with positive and negative impulses. The review of the theories which potentially describe the influence of nanoparticle on the breakdown characteristics of dielectric liquids has been conducted in this thesis.

## **8.2 Summary of results and major contributions**

### **8.2.1 Conclusion of AC breakdown test**

In the AC breakdown test, both TiO<sub>2</sub> and BN nano-modified samples were tested. The samples were prepared with mineral oil, synthetic ester, and natural ester. The results showed that both TiO<sub>2</sub> and BN nano-modified samples provided higher breakdown voltages than the base sample. The nanoparticle concentration showed that, with increased concentration, the breakdown voltage reached the crest and then started to decrease. The breakdown voltage of the BN nano-modified samples provided a rapid drop compared to that of the TiO<sub>2</sub> nano-modified samples with the concentration increase. For both TiO<sub>2</sub> and BN nano-modified samples, the optimal concentration occurred at the 0.0006% (b/w) concentration, which provided the highest breakdown voltage.

In the Weibull distribution analysis results, the breakdown voltages corresponding to the probabilities to breakdown of each test sample were presented. For the 5% breakdown voltage case, the base mineral oil sample showed the highest breakdown voltage (18.2 kV) (with synthetic ester at 15.6 kV and natural ester at 14.6 kV). For the 5% breakdown voltage case, at the 0.0006% (b/w) nano-modified sample, both TiO<sub>2</sub> and BN nanoparticles provided significant enhancement of the breakdown voltage. For the TiO<sub>2</sub> nano-modified sample, the breakdown voltage increased ~42.9% for the mineral oil, ~73.1% for synthetic ester, and ~31.5% for natural ester compare with that of base sample. For the BN nano-modified sample, the breakdown voltage increased ~39.6% for the mineral oil, ~70.5% for synthetic ester, and ~64.4% for natural ester compared with that of base sample. These results prove that nanoparticles not only improve the liquid average breakdown voltage but also

enhance the liquid breakdown voltage at a low breakdown probability. Considering the standard deviation effect, the results of statistical difference between the tested samples and CI calculation confirm the phenomenon of nanoparticle enhancement on the dielectric liquid breakdown voltage exists.

### **8.2.2 Conclusion of fixed-peak standard lightning impulse**

The results of the breakdown tests using fixed-peak standard lightning impulses showed that, at a specific nanoparticle concentration, both TiO<sub>2</sub> and BN nano-modified liquids provided longer pre-breakdown times than the base samples. For both TiO<sub>2</sub> and BN nano-modified samples, it was established that different concentrations of nanoparticles changed the pre-breakdown times in the case of positive and negative impulse stresses. It was found that the longest pre-breakdown time was demonstrated by the nano-modified samples with particle concentrations of 0.0006% (or in some cases of 0.004%). For the liquid samples in which the mass concentration of the nanoparticles exceeded 0.004%, the dielectric properties started to deteriorate, in which the pre-breakdown times started to become shorter. The pre-breakdown time of the optimal concentration samples provided significant improvement over that of the base liquids. For the TiO<sub>2</sub> nano-modified liquids, compared with the base liquids, the time to breakdown provided by the mineral oil exhibited a ~15% increase for the positive impulse and a ~17% for the negative impulse. The time to breakdown provided by the synthetic ester was a 15% increase for the positive impulse and a ~24% for the negative impulse. The time to breakdown provided by the natural ester was a ~10% increase for the positive impulse and a ~22% for the negative impulse. For the BN nano-modified samples, compared with the base sample, the time to breakdown provided by the mineral oil was a 9.6% increase for the positive impulse and an 18.9% for the negative impulse. The time to breakdown provided by the synthetic ester was a 121.4% increase for the positive impulse and a 14.1% for the negative impulse. The time to breakdown provided by the natural ester was a 24.5% increase for the positive impulse and a 29.2% for the negative impulse.

The average streamer propagation velocities in the nano-modified sample were calculated based on the measured pre-breakdown time. The results showed that the slowest streamer velocity was demonstrated by the nano-modified samples with particle concentrations of 0.0006% (or in some

cases of 0.004%). The TiO<sub>2</sub> nanoparticles provided a clear influence on the streamer propagation, which can transfer the streamer from a ‘quasi-fast streamer’ (third mode streamer in which the velocity is close to 10 km/s) to a ‘slow’ (second mode streamer in which the velocity is 1~2 km/s), such as the synthetic ester under the positive impulse. The BN nanoparticles also provided a slowing phenomenon on the streamer propagation but not as significantly as TiO<sub>2</sub> case.

The Weibull statistical analysis results of the time to breakdown showed that, in most cases, the nano-modified liquids not only provided longer average pre-breakdown times than the base sample but also provided longer pre-breakdown times at lower breakdown probabilities than the base sample.

Furthermore, the Weibull analysis of the breakdown results demonstrated that the shape parameters for nano-modified samples with the optimal concentration have similar values of the shape parameters as compared with the other concentration samples.

Thus, the optimal concentration samples provided the longest pre-breakdown times compared with the other concentration samples but their failure rate remains the same. These results showed that nano-modification of insulating liquids can enhance the liquid capability to inhibit streamer propagation. Statistical difference analysis calculated statistical difference between the mean values of the pre-breakdown times of nano-modified liquids and CIs confirm that the phenomenon of nanoparticle influence on the pre-breakdown time in nano-fluids is statistically significant.

### **8.2.3 Conclusion of the minimum-lightning impulse breakdown voltage test**

In the minimum-lightning impulse breakdown voltage series of tests, three liquid-based TiO<sub>2</sub> and BN semi-conductive suspensions were tested using the ASTM D3300 and IEC 60897 methods. Both the ASTM and IEC methods showed that most of the TiO<sub>2</sub> and BN nano-modified samples provided higher breakdown voltages than the base liquids. For liquids with the optimal concentration of nanoparticles, the TiO<sub>2</sub> nano-modified samples showed more obvious enhancement of the impulse breakdown voltage than the BN nano-modified samples. For example, using the ASTM method, the maximum enhancement of the impulse breakdown voltage was with the 0.0006% (b/w) concentration of TiO<sub>2</sub>, for example positive  $V_{bd}$  for the synthetic ester increased from 28.9 kV (base sample) to 43.9 kV, which corresponds to ~52% increase. The maximum enhancement in the impulse breakdown voltage for BN nano-modified liquids was with the 0.0006% (b/w) concentration of BN

nanoparticles, for synthetic ester positive  $V_{bd}$  increased from 28.9 kV (base sample) to 42.7 kV, which corresponds to ~47% increase.

The enhancement effect of the nano-particles (added to base liquids in optimal concentrations) on the impulse breakdown voltage of the ester liquids was greater compared to that of the impulse breakdown voltage of the nano-modified mineral oil. The positive impulse breakdown voltages of the all liquids were mostly lower than those of the negative polarity. However, the enhancement effect of the nanoparticles on the positive impulse breakdown voltages of the liquids was more obvious than the effect on the negative impulse breakdown voltages of the same liquids.

Under identical experimental conditions (same polarity, same base liquid, same nanoparticles, and the same concentration of nanoparticles), the breakdown voltages of the liquids measured using the ASTM method were lower than the breakdown voltages measured by the IEC method. The potential reason for this phenomenon is that, in the voltage raising procedure, the ASTM standard requires applying the same voltage three times before raising the voltage to the next step. In the case of the IEC method, the measurement procedure requires applying the voltage only one time before raising the voltage to the next step. Thus, for the ASTM method test, there is a higher probability of breakdown occurring at the same voltage, since there are more impulses applied at each voltage level than in the IEC method. Hence, the breakdown voltages measured using the ASTM method can be expected to be lower than the IEC method results.

The CI were calculated for the differences in the mean values of breakdown voltages of base and nano-modified liquids. The results confirm that, the enhancement phenomenon of nanoparticles (added in optimal concentration) on the breakdown voltage of nano-modified liquids is statistically significant.

#### **8.2.4 Conclusion of DC pre-breakdown current measurement, liquid mobility calculation, and further discussion**

In Chapter 7, the DC pre-breakdown current measurement results were presented. The apparent mobility of charge carriers was obtained for base liquids and the obtained results presented and discussed. The obtained results showed that mineral oil provided the lowest charge carrier mobility compared with ester liquid under both positive and negative polarities. These results indicated that

base mineral oil had a better capability to inhibit the streamer formation and propagation than ester liquid, hence explaining that, in most cases, base mineral oil provided better breakdown characteristics than ester liquids.

Using the obtained apparent charge carrier mobility, the field distribution analysis was performed. It was found that the space charge influenced electric field for positive and negative energisation is different. Thus these results can potentially explain the difference in the breakdown voltage which is under the positive polarity was typically lower than that under the negative polarity.

Several potential mechanisms of enhancement of the breakdown properties of liquids with nanoparticles were reviewed and discussed. Generally these mechanisms are developed based on the charge trapping theory. These mechanisms can only explain specific results but cannot be used to evaluate other published data. Thus, these models and theories still have some defects and limitations; hence, more experiments and theoretical model development are needed in future work. The discussion indicated that there is no uniform theory and model to explain most of the nanofluid breakdown experimental results yet.

### **8.2.5 Summary of major findings**

In summary, the project was focused on investigation of the breakdown and pre-breakdown performance of base insulating liquids and their nano-suspensions with different concentrations of  $\text{TiO}_2$  and BN nanoparticles.

The obtained results showed several important phenomena:

- Both  $\text{TiO}_2$  and BN nanoparticles as fillers in insulating liquids have significant influence on their breakdown properties.
- The concentration of nanoparticles has significant effects on the breakdown properties of nano-modified liquids. It was found that in most cases, the optimal concentration of both  $\text{TiO}_2$  and BN nanoparticles are between 0.0006% and 0.004% (b/w). Nano-modified liquids with such concentrations provided the highest breakdown strength under the AC and lightning impulse fields and the longest time to breakdown.

- Amongst three testes base liquids, the mineral oil provided better breakdown properties than both ester liquids. However, for nano-modified liquids, ester liquids provided comparable dielectric performance with the mineral oil.
- The food-grade rapeseed oil based nanofluid, provided comparable dielectric properties with commercial ester based nanofluids, which indicates that the food-grade natural ester can be considered a potential alternative to traditional insulation liquid for some practical applications.

### 8.2.6 Summary of major achievements and contributions

The major achievements and contributions are list as below:

- ❖ In this study, the comprehensive study of breakdown properties of food-grade natural ester and the comparison with those of commercial products (e.g., mineral oil and synthetic ester) are first time presented. The comprehensive study of breakdown properties of include the measure the breakdown voltage of liquids under AC, DC, and lightning impulse field; the measure pre-breakdown characteristic of liquids under DC and lightning impulse field (pre-breakdown time for lightning impulse experiment, pre-breakdown current for DC experiment)
- ❖ The nanofluid with TiO<sub>2</sub> nanoparticles act as a popular alternative to traditional insulating liquids, its breakdown properties have been investigate by a large number of researchers. Meanwhile, nanofluid with BN nanoparticles was found that it can provide higher thermal conductivity as compare with that of base insulating liquid. In this thesis, the comprehensive investigation of breakdown properties of nanofluid with BN nanoparticles and the comparison with those of nanofluid with TiO<sub>2</sub> nanoparticles are presented. The results indicate that the nanofluid with BN nanoparticles provide better breakdown properties as compare with those of base liquids but the enhancement on breakdown properties is not as significantly as that of nanofluid with TiO<sub>2</sub> nanoparticles.
- ❖ In this thesis, the comprehensive investigation of concentration influence on the breakdown properties of various liquids based nanofluid with TiO<sub>2</sub> and BN nanoparticles are first time presented. For the case of nanofluids with both TiO<sub>2</sub> and BN nanoparticles, the optimal concentration is found that between 0.0006% to 0.004% (b/w).

- ❖ The statistical difference between the breakdown properties of base liquids and nanofluids have been investigated to evaluate the statistical significance of the enhancement on the breakdown properties of nanofluid. The results prove in the 95% confidence level, the enhancements on the breakdown properties of nanofluids are statistically significant.
- ❖ The comparison studies of reliability of nanofluids are presented using Weibull statistical analysis. The comprehensive investigation of the effect factors on the reliability of nanofluids are first time presented in this thesis which include the various base liquids, different nanoparticles, various concentration of nanoparticles, stress AC and lightning impulse field.

### **8.3 Future Work**

To continue research work in the direction initiated in this research project, several areas can be identified as areas of potential future work.

- I. Investigation of ageing of nanofluids and partial discharge activity in nanofluids in addition to their breakdown and pre-breakdown performance. The partial discharge and ageing properties are very important for evaluation of performance of liquid dielectrics in high-power applications, as discussed in Section 2.4. The test results of the partial discharge and ageing properties can be combined with the results presented in this thesis and they can form a full picture of the breakdown behaviour of nano-modified mineral oils and esters.
- II. Another point is investigating the thermal conductivity of the base liquids and nanofluids. Since the insulation liquids in the transformer have two major functions, they are used as an insulation material and as a cooling material; the thermal conductivity of the insulation liquid is a very important parameter for power industry applications as discussed in Section 2.4. In practical applications, engineers and power apparatus designers not only have to consider the insulation material's dielectric properties but also must consider the insulation material's thermal conductivity. Thus, investigating the thermal conductivity of the base liquids and nanofluids based on mineral oil, synthetic ester, and food-grade natural ester will be worthwhile and necessary.

III. As discussed in Chapter 7, the enhancement mechanism of nanoparticles on the breakdown properties of nanofluids is not fully understood yet. To date, there is no a uniform theory or model that can explain most of the breakdown experimental results. Thus, investigating the operation mechanism of the nanoparticles' influence on the liquid dielectric properties is necessary since the breakdown phenomenon involves streamer formation and propagation. Investigating the streamer characteristics in nanofluids will be beneficial to understand the mechanism of influence of nanoparticles on the dielectric properties of the insulating liquids. . This investigation could include the pre-breakdown current measurement under the impulse and DC fields, the streamer shape and propagation velocity in liquids, and the simulation of the field distribution in nanofluid.

## REFERENCES

- [1] D. Peterchuck and A. Pahwa, "Sensitivity of transformer's hottest-spot and equivalent aging to selected parameters," *IEEE Trans. Power Deliv.*, vol. 17, no. 4, pp. 996–1001, 2002.
- [2] M. H. Ese, K. Liland, and L. Lundgaard, "Oxidation of paper insulation in transformers," *IEEE Trans. Dielectr. Electr. Insul.*, vol. 17, no. 3, pp. 939–946, 2010.
- [3] CIGRE Working Group A2.35, "Experiences in service with new insulating liquids," no. 436, pp. 1–95, 2010.
- [4] D. Martin, I. Khan, J. Dai, and Z. D. Wang, "An Overview of the Suitability of Vegetable Oil Dielectrics for Use in Large Power Transformers," *Euro TechCon*, pp. 4–23, 2006.
- [5] C. Perrier and A. Beroual, "Experimental Investigations on Liquids for Power Transformers: Mineral, Insulating Ester, and Silicone Oils," *Ieee Electr. Insul. Mag.*, vol. 25, pp. 6–13, 2009.
- [6] S. Tenbohlen and M. Koch, "Aging performance and moisture solubility of vegetable oils for power transformers," *IEEE Trans. Power Deliv.*, vol. 25, no. 2, pp. 825–830, 2010.

- [7] S. Arazoe, D. Saruhashi, Y. Sato, S. Yanabu, G. Ueta, and S. Okabe, "Electrical characteristics of natural and synthetic insulating fluids," *IEEE Trans. Dielectr. Electr. Insul.*, vol. 18, no. 2, pp. 506–512, 2011.
- [8] T. V. Oommen, "Vegetable oils for liquid-filled transformers," *IEEE Electr. Insul. Mag.*, vol. 18, pp. 6–11, 2002.
- [9] D. Martin and Z. D. Wang, "Statistical analysis of the AC breakdown voltages of ester based transformer oils," *IEEE Trans. Dielectr. Electr. Insul.*, vol. 15, no. 4, pp. 1044–1050, 2008.
- [10] X. Wang and Z. D. Wang, "Particle effect on breakdown voltage of mineral and ester based transformer oils," *Annu. Rep. - Conf. Electr. Insul. Dielectr. Phenomena, CEIDP*, pp. 598–602, 2008.
- [11] C. T. Duy, O. Lesaint, a. Denat, and N. Bonifaci, "Streamer propagation and breakdown in natural ester at high voltage," *IEEE Trans. Dielectr. Electr. Insul.*, vol. 16, no. 6, pp. 1582–1594, 2009.
- [12] R. Liu, C. Törnkvist, V. Chandramouli, O. Girlanda, and L. A. A. Pettersson, "Ester fluids as alternative for mineral oil: The difference in streamer velocity and LI breakdown voltage," *Annu. Rep. - Conf. Electr. Insul. Dielectr. Phenomena, CEIDP*, pp. 543–548, 2009.
- [13] C. P. McShane, J. L. Corkran, K. J. Rapp, and J. Luksich, "Aging of paper insulation retrofilled with natural ester dielectric fluid," *2003 Annu. Rep. Conf. Electr. Insul. Dielectr. Phenom.*, vol. 0, no. C, pp. 675–679, 2003.
- [14] C. P. McShane, K. J. Rapp, J. L. Corkran, G. a Gauger, and J. Luksich, "Aging of Kraft Paper in Natural Ester Dielectric Fluid," *Proc. 14th Int. Conf. Dielectr. Liq.*, pp. 173–177, 2002.
- [15] T. J. Lewis, "Nanometric Dielectrics," *IEEE Trans. Dielectr. Electr. Insul.*, vol. 1, no. 5, pp. 812–825, 1994.
- [16] Y. Cao, P. C. Irwin, and K. Younsi, "The future of nanodielectrics in the electrical power industry," *IEEE Trans. Dielectr. Electr. Insul.*, vol. 11, no. 5, pp. 797–807, 2004.

- [17] V. Segal, a. Hjortsberg, a. Rabinovich, D. Natrass, and K. Raj, "AC (60 Hz) and impulse breakdown strength of a colloidal fluidbased on transformer oil and magnetite nanoparticles," *Conf. Rec. 1998 IEEE Int. Symp. Electr. Insul. (Cat. No.98CH36239)*, vol. 2, pp. 619–622, 1998.
- [18] B. Du, J. Li, B. M. Wang, and Z. T. Zhang, "Preparation and breakdown strength of Fe<sub>3</sub>O<sub>4</sub> nanofluid based on transformer oil," *ICHVE 2012 - 2012 Int. Conf. High Volt. Eng. Appl.*, pp. 311–313, 2012.
- [19] W. Sima, X. Cao, Q. Yang, F. Yu, J. Shi, and H. Song, "Comparison and Analysis on the Impulse Breakdown Characteristics of Three Transformer Oil-based Nanofluids [in Chinese]," *High Volt. Eng.*, vol. 41, no. 2, pp. 374–381, 2015.
- [20] M. Chiesa and S. K. Das, "Experimental investigation of the dielectric and cooling performance of colloidal suspensions in insulating media," *Colloids Surfaces A Physicochem. Eng. Asp.*, vol. 335, no. 1–3, pp. 88–97, 2009.
- [21] T. S. Ramu, B. K. Keshavan, and K. N. Balasubramanya Murthy, "Application of a class of nano fluids to improve the loadability of power transformers," *Proc. IEEE Int. Conf. Prop. Appl. Dielectr. Mater.*, pp. 1–6, 2012.
- [22] Y. Zhou, Y. Wang, J. Tian, Y. Sha, X. Jiang, S. Gao, Q. Sun, and Q. Nie, "Breakdown Characteristics in Transformer Oil Modified by Nanoparticles," *High Volt. Eng.*, vol. 36, no. 5, pp. 1155–1159, 2010.
- [23] R. Liu, L. A. A. Pettersson, T. Auletta, and O. Hjortstam, "Fundamental research on the application of nano dielectrics to transformers," *Annu. Rep. - Conf. Electr. Insul. Dielectr. Phenomena, CEIDP*, pp. 423–427, 2011.
- [24] P. Kopčanský, K. Marton, and L. Tomco, "The Influence of Magnetic Nanoparticles on DC- and AC-Dielectric Breakdown in Transformer Oil-Based Magnetic Fluid," *Fundam. Appl. MHD, Conf.*, vol. c, pp. 329–332.
- [25] P. Kopčanský, L. Tomčo, K. Marton, M. Koneracká, M. Timko, and I. Potočová, "The DC dielectric breakdown strength of magnetic fluids based on transformer oil," *J. Magn. Magn. Mater.*, vol. 289, pp. 415–418, 2005.

- [26] P. Kopčanský, L. Tomčo, K. Marton, M. Koneracká, I. Potočová, and M. Timko, "The experimental study of the DC dielectric breakdown strength in magnetic fluids," *J. Magn. Magn. Mater.*, vol. 272, pp. 2377–2378, 2004.
- [27] P. P. C. Sartoratto, A. V. S. Neto, E. C. D. Lima, A. L. C. Rodrigues De S á and P. C. Morais, "Preparation and electrical properties of oil-based magnetic fluids," *J. Appl. Phys.*, vol. 97, no. 10, pp. 29–32, 2005.
- [28] Y. F. Du, Y. Z. Lv, F. C. Wang, X. X. Li, and C. R. Li, "Effect of TiO<sub>2</sub> nanoparticles on the breakdown strength of transformer oil," in *Electrical Insulation (ISEI), Conference Record of the 2010 IEEE International Symposium on.*, 2010, pp. 1–3.
- [29] Y. Du, Y. Lv, J. Zhou, X. Li, and C. Li, "Breakdown Properties of Transformer Oil-based TiO<sub>2</sub> Nanofluid," in *Electrical Insulation and Dielectric Phenomena (CEIDP), 2010 Annual Report Conference on*, 2010, pp. 1–4.
- [30] Y. Du, Y. Lv, C. Li, Y. Zhong, M. Chen, S. Zhang, Y. Zhou, and Z. Chen, "Effect of water adsorption at nanoparticle-oil interface on charge transport in high humidity transformer oil-based nanofluid," *Colloids Surfaces A Physicochem. Eng. Asp.*, vol. 415, pp. 153–158, 2012.
- [31] H. Jin, T. Andritsch, I. A. Tsekmes, R. Kochetov, P. H. F. Morshuis, and J. J. Smit, "Properties of mineral oil based silica nanofluids," *IEEE Trans. Dielectr. Electr. Insul.*, vol. 21, no. 3, pp. 1100–1108, 2014.
- [32] B. X. Du, X. L. Li, J. Li, and X. Y. Tao, "Effects of BN nanoparticles on thermal conductivity and breakdown strength of vegetable oil," *2015 IEEE 11th Int. Conf. Prop. Appl. Dielectr. Mater.*, pp. 476–479, 2015.
- [33] Y. Li, J. Zhou, Z. Luo, S. Tung, E. Schneider, J. Wu, and X. Li, "Investigation on two abnormal phenomena about thermal conductivity enhancement of BN/EG nanofluids," *Nanoscale Res. Lett.*, vol. 6, no. 1, pp. 1–7, 2011.
- [34] B. X. Du and X. L. Li, "High thermal conductivity transformer oil filled with BN nanoparticles," *IEEE Electr. Insul. Mag.*, vol. June 30, no. 2, pp. 1–4, 2014.

- [35] J. Taha-Tijerina, T. N. Narayanan, G. Gao, M. Rohde, D. A. Tsentalovich, M. Pasquali, and P. M. Ajayan, "Electrically insulating thermal nano-oils using 2D fillers," *ACS Nano*, vol. 6, no. 2, pp. 1214–1220, 2012.
- [36] I. Fofana and Y. Hadjadj, "Electrical-Based Diagnostic Techniques for Assessing Insulation Condition in Aged Transformers," *Energies*, vol. 9, no. 9, p. 679, 2016.
- [37] S. Safe, "Toxicology, structure-function relationship, and human and environmental health impacts of polychlorinated biphenyls: Progress and problems," *Environ. Health Perspect.*, vol. 100, pp. 259–268, 1992.
- [38] S. U. S. Choi and J. A. Eastman, "Enhancing thermal conductivity of fluids with nanoparticles," *ASME-Publications-Fed 231*, pp. 99–106, 1995.
- [39] M. Bakruteen, R. Karthik, and R. Madavan, "Investigation of critical parameters of insulating mineral oil using semiconductive nanoparticles," *Proc. IEEE Int. Conf. Circuit, Power Comput. Technol. ICCPCT 2013*, pp. 294–299, 2013.
- [40] Y. Zhong, Y. Lv, C. Li, Y. Du, M. Chen, S. Zhang, Y. Zhou, and L. Chen, "Insulating properties and charge characteristics of natural ester fluid modified by TiO<sub>2</sub> semiconductive nanoparticles," *IEEE Trans. Dielectr. Electr. Insul.*, vol. 20, no. 1, pp. 135–140, 2013.
- [41] A. H. Sharbaugh, J. C. Devins, and S. J. Rzed, "Progress in the Field of in Dielectric Electric Breakdown Liquids," *IEEE Trans. Electr. Insul.*, no. 4, pp. 249–276, 1978.
- [42] A. Beroual, "Electronic and gaseous processes in the prebreakdown phenomena of dielectric liquids," *J. Appl. Phys.*, vol. 73, no. 9, pp. 4528–4533, 1993.
- [43] J. F. Kolb, R. P. Joshi, S. Xiao, and K. H. Schoenbach, "Streamers in water and other dielectric liquids," *J. Phys. D. Appl. Phys.*, vol. 41, no. 23, p. 234007, 2008.
- [44] T. J. Gallagher, "Simple Dielectric Liquids-Mobility, Conduction, and Breakdown," in *Simple Dielectric Liquids-Mobility, Conduction, and Breakdown*, Bristol: J. W. Arrowsmith Ltd, 1975, pp. 70–112.

- [45] I. Adamzewski, "Ionization Conductivity and Breakdown in Dielectric Liquids," in *Ionization Conductivity and Breakdown in Dielectric Liquids*, London: Taylor & Francis Ltd, 1969, pp. 353–408.
- [46] T. J. Lewis, "A new model for the primary process of electrical breakdown in liquids," *IEEE Trans. Dielectr. Electr. Insul.*, vol. 5, no. 3, pp. 306–315, 1998.
- [47] F. M. J. McCluskey, F. Huynh, A. Denat, N. Bonifaci., and R. Kattan, "Bubble Formation in 'Simple' and Complex Liquids," in *IEEE International Symposium on Electrical Insulation*, 1994.
- [48] W. G. Chadband, "From bubbles to breakdown, or vice-versa," *Proc. 1993 IEEE 11th Int. Conf. Conduct. Break. Dielectr. Liq. (ICDL '93)*, pp. 184–193, 1993.
- [49] R. Kattan, A. Denat, and O. Lesaint, "Generation, growth, and collapse of vapor bubbles in hydrocarbon liquids under a high divergent electric field," *J. Appl. Phys.*, vol. 66, no. 9, pp. 4062–4066, 1989.
- [50] E. J. Murphy, "The generation of gases in the dielectric breakdown of oil," *J. Phys. D. Appl. Phys.*, vol. 3, no. 6, pp. 917–923, Jun. 1970.
- [51] R. Kattan, A. Denat, and N. Bonifaci, "Formation of vapor bubbles in non-polar liquids initiated by current pulses," *IEEE Trans. Electr. Insul.*, vol. 26, no. 4, pp. 656–662, 1991.
- [52] F. M. J. McCluskey and A. Denat, "The behavior of small bubbles generated by electrical current impulses over a wide range of applied pressures," *J. Appl. Phys.*, vol. 80, pp. 2049–2059, 1996.
- [53] O. Lesaint and G. Massala, "Positive streamer propagation in large oil gaps: experimental characterization of propagation modes," *IEEE Trans. Dielectr. Electr. Insul.*, vol. 5, no. 3, pp. 360–370, 1998.
- [54] P. Gournay and O. Lesaint, "On the gaseous nature of positive filamentary streamers in hydrocarbon liquids. II: Propagation, growth and collapse of gaseous filaments in pentane," *J. Phys. D. Appl. Phys.*, vol. 27, no. 10, pp. 2117–2127, 1994.

- [55] E. M. Hizal and S. Dincer, "Breakdown time lags and prebreakdown phenomena in transformer oil, effects of hydrostatic pressure," *J. Electrostat.*, vol. 12, pp. 333–343, 1982.
- [56] E. R. Bartnikas, *Engineering Dielectric Volume III: Electrical Insulating Liquids*. 1994.
- [57] J. C. Devins, S. J. Rzaad, and R. J. Schwabe, "Breakdown and prebreakdown phenomena in liquids," *J. Appl. Phys.*, vol. 52, no. 7, pp. 4531–4545, 1981.
- [58] A. Beroual and R. Tobazeon, "Prebreakdown Phenomena In Liquid Dielectrics," *IEEE Trans. Electr. Insul.*, no. 4, pp. 613–627, 1986.
- [59] D. Linhjell, L. Lundgaard, and G. Berg, "Streamer propagation under impulse voltage in long point-plane oil gaps," *IEEE Trans. Dielectr. Electr. Insul.*, vol. 1, no. 3, pp. 447–458, 1994.
- [60] R. E. Hebner, "Measurement of Electrical Breakdown in Liquids," in *The Liquid State and Its Electrical Properties*, E. E. Kunhardt, L. G. Christophorou, and L. H. Luessen, Eds. Boston, MA: Springer US, 1988, pp. 519–537.
- [61] M. Abdel-Salam, H. Anis, A. Ei-Morshedy, and R. Radwn, *High-Voltage Engineering: Theory and Practice*, 2nd ed. New York: Marcel Dekker Inc, 2000.
- [62] S. Mahmud, G. Chen, I. O. Golosnoy, G. Wilson, and P. Jarman, "Bridging in contaminated transformer oil under DC and AC electric field," *J. Phys. Conf. Ser.*, vol. 472, pp. 1–17, 2013.
- [63] S. Mahmud, G. Chen, I. O. Golosnoy, G. Wilson, and P. Jarman, "Bridging phenomenon in contaminated transformer oil," in *Proceedings of 2012 IEEE International Conference on Condition Monitoring and Diagnosis, CMD 2012*, 2012, pp. 180–183.
- [64] S. Mahmud, I. O. Golosnoy, G. Chen, G. Wilson, and P. Jarman, "Effect of different shapes of electrodes on bridging in contaminated transformer oil," *2014 IEEE Conf. Electr. Insul. Dielectr. Phenomena, CEIDP 2014*, pp. 114–117, 2014.
- [65] G. Chen and M. H. Zuber, "Pre-breakdown characteristics of contaminated power transformer oil," *Annu. Rep. - Conf. Electr. Insul. Dielectr. Phenomena, CEIDP*, pp. 659–662, 2007.

- [66] S. Mahmud, I. O. Golosnoy, G. Chen, G. Wilson, and P. Jarman, "Numerical simulations of bridging phenomena in contaminated transformer oil," *Annu. Rep. - Conf. Electr. Insul. Dielectr. Phenomena, CEIDP*, pp. 383–386, 2012.
- [67] Y. Zhou, M. Hao, G. Chen, G. Wilson, and P. Jarman, "Space charge polarization in insulating mineral oil," *Annu. Rep. - Conf. Electr. Insul. Dielectr. Phenomena, CEIDP*, no. 5, pp. 587–590, 2013.
- [68] M. Eklund, "Mineral insulating oils; functional requirements, specifications and production," *Conf. Rec. 2006 IEEE Int. Symp. Electr. Insul.*, pp. 68–72, 2006.
- [69] F. M. J. McCluskey, A. Denat, and O. Lesaint, "Breakdown and prebreakdown phenomena in liquids under positive impulse voltages," *IEEE Trans. Dielectr. Electr. Insul.*, vol. 1, no. 3, pp. 377–382, 1994.
- [70] "Midel 7131 Dielectric Insulating Fluid Overview," 2014.
- [71] Y. Zhou, "Electrical properties of mineral oil and oil/impregnated pressboard for HVDC converter transformers," Univeristy of Southampton, 2014.
- [72] Q. Liu, "Electrical Performance of Ester Liquids under Impulse Voltage for Application in Power Transformers," University of Manchester, 2011.
- [73] C. P. McShane, "New safety dielectric coolants for distribution and power transformers," *IEEE Ind. Appl. Mag.*, vol. 6, no. 3, pp. 24–32, 2000.
- [74] OECD, "INTRODUCTION TO THE OECD GUIDELINES FOR TESTING OF CHEMICALS SECTION 3 PART1: PRINCIPLES AND STRATEGIES RELATED TO THE TESTING OF DEGRADATION OF ORGANIC CHEMICALS," 2003.
- [75] "Midel 7131 Comparison to Alternative Technologies," 2014.
- [76] H. B. H. Sitorus, A. Beroual, R. Setiabudy, and S. Bismo, "Comparison of streamers characteristics in jatropha curcas methyl ester oil and mineral oil under lightning impulse voltage," in *IEEE International Conference on Liquid Dielectrics*, 2014, pp. 1–4.
- [77] C. T. Duy, O. Lesaint, N. Bonifaci, A. Denat, and Y. Bertrand, "High voltage breakdown and pre-breakdown properties in rape-seed insulating oil," in *2007 Annual Report-Conference on Electrical Insulation and Dielectric Phenomena (CEIDP)*, 2007, pp. 623–626.

- [78] C. T. Duy, O. Lesaint, A. Denat, and N. Bonifaci, "Streamer propagation and breakdown in natural ester at high voltage," in *2008 IEEE International Conference on Dielectric Liquids (ICDL)*, 2008, pp. 1–4.
- [79] ASTM D 1816 - 04, "Standard Test Method for Dielectric Breakdown Voltage of Insulating Oils of Petroleum Origin Using VDE Electrodes." 2004.
- [80] ASTM D 3300 - 00, "Standard Test Method for Dielectric Breakdown Voltage of Insulating Oils of Petroleum Origin Under Impulse Conditions." 2001.
- [81] L. R. Lewand, "Laboratory Testing of Natural Ester Dielectric Liquids," *Neta World*, pp. 1–4, 2004.
- [82] J. G. Hwang, F. O'Sullivan, M. Zahn, O. Hjortstam, L. a a Pettersson, and R. Liu, "Modeling of streamer propagation in transformer oil-based nanofluids," *Annu. Rep. - Conf. Electr. Insul. Dielectr. Phenomena, CEIDP*, pp. 361–366, 2008.
- [83] J. G. Hwang, S. Member, M. Zahn, F. M. O. Sullivan, L. A. A. Pettersson, O. Hjortstam, R. Liu, and S. Member, "Electron Scavenging by Conductive Nanoparticles in Oil Insulated Power Transformers," *Proc. Electrost. Jt. Conf.*, pp. 1–12, 2009.
- [84] X. Q. Wang and A. S. Mujumdar, "A review on nanofluids - Part I: Theoretical and numerical investigations," *Brazilian J. Chem. Eng.*, vol. 25, no. 4, pp. 613–630, 2008.
- [85] X. Q. Wang and A. S. Mujumdar, "A review on nanofluids - Part II: Experiments and applications," *Brazilian J. Chem. Eng.*, vol. 25, no. 4, pp. 631–648, 2008.
- [86] J. Philip and P. D. Shima, "Thermal properties of nanofluids," *Adv. Colloid Interface Sci.*, vol. 183–184, pp. 30–45, 2012.
- [87] Y. Hwang, J. K. Lee, C. H. Lee, Y. M. Jung, S. I. Cheong, C. G. Lee, B. C. Ku, and S. P. Jang, "Stability and thermal conductivity characteristics of nanofluids," *Thermochim. Acta*, vol. 455, no. 1–2, pp. 70–74, 2007.
- [88] V. A. Primo, B. García, and J. C. Burgos, "Applicability of Nanodielectric Fluids to the Improvement of Transformer Insulation Properties," 2016.
- [89] L. Blaney, "Magnetite (Fe<sub>3</sub>O<sub>4</sub>): Properties, synthesis, and applications," *Lehigh Rev.*, vol. 15, pp. 32–81, 2007.

- [90] S. Ito, Y. Yui, and J. Mizuguchi, "Electrical properties of semiconductive  $\alpha$ -Fe<sub>2</sub>O<sub>3</sub> and its use as the catalyst for decomposition of volatile organic compounds," *Mater. Trans.*, vol. 51, no. 6, pp. 1163–1167, 2010.
- [91] Neuberger.M, "Silicon Carbide Data Sheets," 1965.
- [92] M. Caglar, S. Ilican, Y. Caglar, and F. Yakuphanoglu, "Electrical conductivity and optical properties of ZnO nanostructured thin film," *Appl. Surf. Sci.*, vol. 255, no. 8, pp. 4491–4496, 2009.
- [93] AZO Materials, "Titanium Dioxide - Titania ( TiO<sub>2</sub>)," 2002.
- [94] F. M. Li, R. Waddingham, W. I. Milne, A. J. Flewitt, S. Speakman, J. Dutson, S. Wakeham, and M. Thwaites, "Low temperature (< 100°C) deposited P-type cuprous oxide thin films: Importance of controlled oxygen and deposition energy," *Thin Solid Films*, vol. 520, no. 4, pp. 1278–1284, 2011.
- [95] Accuratus ceramic corporation, "Boron Nitride Grade CA Material Properties."
- [96] AZoM, "Silica - Silicon Dioxide ( SiO<sub>2</sub> )," 2001.
- [97] Accuratus ceramic corporation, "94 % Alumina Material Properties," 2002.
- [98] V. Segal and K. Raj, "An investigation of power transformer cooling with magnetic fluids," *Indian J. Eng. Mater. Sci.*, vol. 5, no. 6, pp. 416–422, 1998.
- [99] V. Segal, D. Natrass, K. Raj, and D. Leonard, "Accelerated thermal aging of petroleum-based ferrofluids," *J. Magn. Magn. Mater.*, vol. 201, pp. 70–72, 1999.
- [100] V. Segal, A. Rabinovich, D. Natrass, K. Raj, and A. Nunes, "Experimental study of magnetic colloidal fluids behavior in power transformers," *J. Magn. Magn. Mater.*, vol. 215, pp. 513–515, 2000.
- [101] J. A. Mergos, M. D. Athanassopoulou, T. G. Argyropoulos, and C. T. Dervos, "Dielectric properties of nanopowder dispersions in paraffin oil," *IEEE Trans. Dielectr. Electr. Insul.*, vol. 19, no. 5, pp. 1502–1507, 2012.
- [102] J. Q. Zhou, Y. F. Du, M. T. Chen, C. R. Li, X. X. Li, and Y. Z. Lv, "AC and lightning breakdown strength of transformer oil modified by semiconducting nanoparticles," *Annu. Rep. - Conf. Electr. Insul. Dielectr. Phenomena, CEIDP*, pp. 652–654, 2011.

- [103] Y. Lv, X. Li, Y. Du, F. Wang, and C. Li, "Preparation and breakdown strength of TiO<sub>2</sub> fluids based on transformer oil," *2010 Annu. Rep. Conf. Electr. Insul. Dielectric Phenom.*, pp. 1–3, 2010.
- [104] Y. Du, Y. Lv, C. Li, M. Chen, Y. Zhong, J. Zhou, X. Li, and Y. Zhou, "Effect of semiconductive nanoparticles on insulating performances of transformer oil," *IEEE Trans. Dielectr. Electr. Insul.*, vol. 19, no. 3, pp. 770–776, 2012.
- [105] Y. F. Du, Y. Z. Lv, F. C. Wang, X. X. Li, and C. R. Li, "Effect of TiO<sub>2</sub> nanoparticles on the breakdown strength of transformer oil," *Conf. Rec. IEEE Int. Symp. Electr. Insul.*, vol. 2, pp. 1–3, 2010.
- [106] Y. Z. Lv, L. F. Wang, X. X. Li, Y. F. Du, J. Q. Zhou, and C. R. Li, "Experimental investigation of breakdown strength of mineral oil-based nanofluids," *Proc. - IEEE Int. Conf. Dielectr. Liq.*, pp. 1–3, 2011.
- [107] Y. Du, Y. Lv, J. Zhou, M. Chen, X. Li, and C. Li, "Effect of Ageing on Insulating Property of Mineral Oil-based TiO<sub>2</sub> Nanofluids," *IEEE Int. Conf. Dielectr. Liq.*, pp. 1–4, 2011.
- [108] C. Mu-tian, D. Yue-fan, L. Yu-zhen, Z. Jian-quan, L. Xiao-xin, L. Cheng-rong, and A. N. Preparation, "Effect of Nanoparticles on the Dielectric Strength of Aged Transformer Oil," pp. 664–667, 2011.
- [109] S. C. Pugazhendhi, "Experimental evaluation on dielectric and thermal characteristics of nano filler added transformer oil," *ICHVE 2012 - 2012 Int. Conf. High Volt. Eng. Appl.*, pp. 207–210, 2012.
- [110] D. E. A. Mansour, E. G. Atiya, R. M. Khattab, and A. M. Azmy, "Effect of titania nanoparticles on the dielectric properties of transformer oil-based nanofluids," *Annu. Rep. - Conf. Electr. Insul. Dielectr. Phenomena, CEIDP*, pp. 295–298, 2012.
- [111] H. Jin, P. H. F. Morshuis, A. R. Mor, and T. Andritsch, "An investigation into the dynamics of partial discharge propagation in mineral oil based nanofluids," *Proc. 2014 IEEE 18th Int. Conf. Dielectr. Liq. ICDL 2014*, pp. 1–4, 2014.

- [112] Y. Li, J. Zhou, S. Tung, E. Schneider, and S. Xi, "A review on development of nanofluid preparation and characterization," *Powder Technol.*, vol. 196, no. 2, pp. 89–101, 2009.
- [113] A. Hays, C. Marsh, J. Alvarado, and R. Franks, "The effect of nanoparticle agglomeration on enhanced nanofluidic thermal conductivity," *Int. Refrig. Air Cond. Conf. Purdue*, 2006.
- [114] Y. Z. Lv, Y. Zhou, C. R. Li, Q. Wang, and B. Qi, "Recent Progress in Nanofluids Based on Transformer Oil : Preparation and Electrical Insulation Properties," *IEEE Electr. Insul. Mag.*, vol. 30, no. 5, pp. 23–32, 2014.
- [115] C. T. Nguyen, F. Desgranges, N. Galanis, G. Roy, T. Mar??, S. Boucher, and H. Angue Mintsa, "Viscosity data for Al<sub>2</sub>O<sub>3</sub>-water nanofluid-hysteresis: is heat transfer enhancement using nanofluids reliable?," *Int. J. Therm. Sci.*, vol. 47, no. 2, pp. 103–111, 2008.
- [116] M. Kole and T. K. Dey, "Role of interfacial layer and clustering on the effective thermal conductivity of CuO-gear oil nanofluids," *Exp. Therm. Fluid Sci.*, vol. 35, no. 7, pp. 1490–1495, 2011.
- [117] P. K. Namburu, D. P. Kulkarni, A. Dandekar, and D. K. Das, "Experimental investigation of viscosity and specific heat of silicon dioxide nanofluids," *IET Micro Nano Lett.*, vol. 2, no. 3, pp. 67–71, 2007.
- [118] D. D. H. Fontes, G. Ribatski, E. B. Filho, and E. P. Bandarra Filho, "Experimental evaluation of thermal conductivity, viscosity and breakdown voltage AC of nanofluids of carbon nanotubes and diamond in transformer oil," *Diam. Relat. Mater.*, vol. 58, pp. 115–121, 2015.
- [119] K. B. Anoop, S. Kabelac, T. Sundararajan, and S. K. Das, "Rheological and flow characteristics of nanofluids: Influence of electroviscous effects and particle agglomeration," *J. Appl. Phys.*, vol. 106, no. 3, 2009.
- [120] N. Putra, W. Roetzel, and S. K. Das, "Natural convection of nano-fluids," *Heat Mass Transf. und Stoffuebertragung*, vol. 39, no. 8–9, pp. 775–784, 2003.

- [121] E. V. Timofeeva, J. L. Routbort, and D. Singh, "Particle shape effects on thermophysical properties of alumina nanofluids," *J. Appl. Phys.*, vol. 106, no. 1, 2009.
- [122] J. Chevalier, O. Tillement, and F. Ayela, "Rheological properties of nanofluids flowing through microchannels," *Appl. Phys. Lett.*, vol. 91, no. 23, 2007.
- [123] M. J. Pastoriza-Gallego, C. Casanova, J. L. Legido, and M. M. Piñeiro, "CuO in water nanofluid: Influence of particle size and polydispersity on volumetric behaviour and viscosity," *Fluid Phase Equilib.*, vol. 300, no. 1–2, pp. 188–196, 2011.
- [124] X. Wang, X. Xu, and S. U. S. Choi, "Thermal Conductivity of Nanoparticle - Fluid Mixture," *J. Thermophys. Heat Transf.*, vol. 13, no. 4, pp. 474–480, 1999.
- [125] A. Beheshti, M. Shanbedi, and S. Z. Heris, "Heat transfer and rheological properties of transformer oil-oxidized MWCNT nanofluid," *J. Therm. Anal. Calorim.*, vol. 118, no. 3, pp. 1451–1460, 2014.
- [126] H. Jin, T. Andritsch, P. H. F. Morshuis, and J. J. Smit, "AC breakdown voltage and viscosity of mineral oil based fullerene nanofluids," *Annu. Rep. - Conf. Electr. Insul. Dielectr. Phenomena, CEIDP*, pp. 703–706, 2013.
- [127] Y. Du, Y. Lv, C. Li, M. Chen, J. Zhou, X. Li, Y. Zhou, and Y. Tu, "Effect of electron shallow trap on breakdown performance of transformer oil-based nanofluids," *J. Appl. Phys.*, vol. 110, no. 10, 2011.
- [128] J. Liu, L. J. Zhou, G. N. Wu, Y. F. Zhao, P. Liu, and Q. Peng, "Dielectric frequency response of oil-paper composite insulation modified by nanoparticles," *Dielectr. Electr. Insul. IEEE Trans.*, vol. 19, pp. 510–520, 2012.
- [129] J. Li, Z. Zhang, P. Zou, S. Grzybowski, and M. Zahn, "Preparation of a vegetable oil-based nanofluid and investigation of its breakdown and dielectric properties," *IEEE Electr. Insul. Mag.*, vol. 28, no. 5, pp. 43–50, 2012.
- [130] M. Hanai, S. Hosomi, H. Kojima, N. Hayakawa, and H. Okubo, "Dependence of TiO<sub>2</sub> and ZnO nanoparticle concentration on electrical insulation characteristics of insulating oil," *Annu. Rep. - Conf. Electr. Insul. Dielectr. Phenomena, CEIDP*, pp. 780–783, 2013.

- [131] IEC 60156: 1995, “Insulating liquids - Determination of the breakdown voltage at power frequency - Test method,” 1995.
- [132] O. Koreh, K. Torkos, M. B. Mahara, J. Boressay, and V. Izvekov, “Study of water clusters in insulating oils by Fourier transform Infrared spectroscopy,” *IEEE Trans. Dielectr. Electr. Insul.*, vol. 5, no. 6, pp. 896–902, 1998.
- [133] IEC-60897, “Methods for the determination of the lightning impulse breakdown voltage of insulating liquids,” 1987.
- [134] B. Du, J. Li, F. Wang, W. Yao, and S. Yao, “Influence of Monodisperse Fe<sub>3</sub>O<sub>4</sub> Nanoparticle Size on Electrical Properties of Vegetable Oil-Based Nanofluids,” *J. Nanomater.*, vol. 2015, 2015.
- [135] J. G. Hwang, M. Zahn, F. M. O’Sullivan, L. A. A. Pettersson, O. Hjortstam, and R. Liu, “Effects of nanoparticle charging on streamer development in transformer oil-based nanofluids,” *J. Appl. Phys.*, vol. 107, no. 1, pp. 1–17, 2010.
- [136] Liquid and Gaseous Dielectrics Sectional Committee, “Indian Standard: GUIDE FOR DETERMINATION OF LIGHTNING IMPULSE ELECTRIC STRENGTH OF INSULATING LIQUIDS,” 1986.
- [137] Y. Lv, Y. Du, C. Li, B. Qi, Y. Zhong, and M. Chen, “TiO<sub>2</sub> nanoparticle induced space charge decay in thermal aged transformer oil,” *Appl. Phys. Lett.*, vol. 102, no. 13, pp. 1–3, 2013.
- [138] Z. Hu, K. Ma, W. WANG, R. Muhammad, Y. Zhou, W. Qi, Y. Du, C. Li, and Y. Lv, “Thermal Aging Properties of Transformer Oil-Based TiO<sub>2</sub> Nanofluids,” *Proc. - IEEE Int. Conf. Dielectr. Liq.*, pp. 1–4, 2014.
- [139] Y. Z. Lv, Y. F. Du, J. Q. Zhou, X. X. Li, M. T. Chen, C. R. Li, and G. L. Wang, “Nanoparticle Effect on Electrical Properties of Aged Mineral Oil Based Nanofluids,” *Proc. 7th Annu. Canada Conf. Power Syst. (CIGRE 12), Paris, Fr.*, pp. 1–7, 2012.
- [140] D. Li, W. Xie, and W. Fang, “Preparation and properties of copper-oil-based nanofluids,” *Nanoscale Res. Lett.*, vol. 6, no. 1, p. 373, 2011.

- [141] S. S. Botha, P. Ndungu, and B. J. Bladergroen, "Physicochemical properties of oil-based nanofluids containing hybrid structures of silver nanoparticles supported on silica," *Ind. Eng. Chem. Res.*, vol. 50, no. 6, pp. 3071–3077, 2011.
- [142] M. Singl and L. Kundan, "Experimental study on thermal conductivity of ethylene glycol based nanofluids containing Al<sub>2</sub>O<sub>3</sub> nanoparticles," *Int. J. Theor. Appl. Res. Mech. Eng.*, vol. 2, no. 3, pp. 125–130, 2013.
- [143] A. M. Gobin, M. H. Lee, N. J. Halas, W. D. James, R. A. Drezek, and J. L. West, "Near-infrared resonant nanoshells for combined optical imaging and photothermal cancer therapy," *Nano Lett.*, vol. 7, no. 7, pp. 1929–1934, 2007.
- [144] S. U. S. Choi, Z. G. Zhang, W. Yu, F. E. Lockwood, and E. A. Grulke, "Anomalous thermal conductivity enhancement in nanotube suspensions," *Appl. Phys. Lett.*, vol. 79, no. 14, pp. 2252–2254, 2001.
- [145] H. Jin, "Dielectric Strength and Thermal Conductivity of Mineral Oil based Nanofluids [Master Thesis]," Delft University of Technology, Delft, The Netherlands, 2015.
- [146] J. C. Maxwell, *A Treatise on electricity and magnetism*, Third Edit. New York, USA: Dover Publications INC, 1954.
- [147] Y. X. Zeng, X. W. Zhong, Z. Q. Liu, S. Chen, and N. Li, "Preparation and enhancement of thermal conductivity of heat transfer oil-based MoS<sub>2</sub> nanofluids," *J. Nanomater.*, vol. 2013, pp. 1–6, 2013.
- [148] H. E. Patel, T. Sundararajan, and S. K. Das, "An experimental investigation into the thermal conductivity enhancement in oxide and metallic nanofluids," *J. Nanoparticle Res.*, vol. 12, no. 3, pp. 1015–1031, 2010.
- [149] Y. Xuan, Q. Li, and W. Hu, "Aggregation structure and thermal conductivity of nanofluids," *AIChE J.*, vol. 49, no. 4, pp. 1038–1043, 2003.
- [150] E. Kuffel, W. S. Zaengl, and J. Kuffel, *High Voltage Engineering*. Oxford, UK: Pergamon Press, 1987.
- [151] M. H. Okba, M. H. Saied, M. Z. Mostafa, and T. M. Abdel-Moneim, "High voltage direct current transmission - A review, part I," in *2012 IEEE Energytech*, 2012, pp. 1–7.

- [152] N. M. Kirby, C. Horwill, and N. M. MacLeod, "Refurbishment strategies for HVDC projects," in *IEEE Power and Energy Society General Meeting*, 2012, pp. 1–6.
- [153] K. C. Koo and J. B. Higham, "The Effects of Hydrostatic Pressure, Temperature, and Voltage Duration on the Electric Strengths of Hydrocarbon Liquids," *J. Electrochem. Soc.*, vol. 108, no. 6, p. 522, 1961.
- [154] A. A. Zaky and R. Hawley, *Conduction and Breakdown in Mineral Oils*. Oxford: Pergamon Press, 1973.
- [155] M. Butcher, a. a. Neuber, M. D. Cevallos, J. C. Dickens, and H. Krompholz, "Conduction and breakdown mechanisms in transformer oil," *IEEE Trans. Plasma Sci.*, vol. 34, no. 2, pp. 467–475, 2006.
- [156] A. Nosseir, S. El-Debeiky, I. F. Hashad, and H. A-Bary, "Effect of temperature on the breakdown probability of liquid dielectrics," *IEEE Trans. Electr. Insul.*, no. 6, pp. 502–505, 1980.
- [157] R. Diabi, J. C. Filippini, C. Marteau, and R. Tobazeon, "On the role of temperature and impurities in the low field conduction of insulating liquids," *ICDL 12th Int. Conf. Conduct. Break. Dielectr. Liq.*, pp. 350–353, 1996.
- [158] I. Fofana, H. Borsi, and E. Gockenbach, "Moisture uptake of mineral oil at different air relative humidities and temperatures," *Annu. Rep. Conf. Electr. Insul. Dielectr. Phenom.*, pp. 276–279, 2000.
- [159] V. H. Dang, A. Beroual, and C. Perrier, "Comparative study of statistical breakdown in mineral, synthetic and natural ester oils under AC voltage," *Dielectr. Liq. (ICDL), IEEE Int. Conf.*, pp. 1–4, 2011.
- [160] J. M. Lehr, F. J. Agee, R. Copeland, and W. D. Prather, "Measurement of the Electric Breakdown Sub-nanosecond Regime," *IEEE Trans. Dielectr. Electr. Insul.*, vol. 5, no. 6, pp. 857–861, 1998.
- [161] D. Phenomena, "Inhibited rape-seed oil as substitute for mineral oils," pp. 268–271, 2002.

- [162] M. P. Wilson, I. V. Timoshkin, M. J. Given, S. J. MacGregor, T. Wang, M. Sinclair, K. J. Thomas, and J. M. Lehr, "Breakdown of mineral oil: Effect of electrode geometry and rate of voltage rise," *IEEE Trans. Dielectr. Electr. Insul.*, vol. 19, no. 5, pp. 1657–1664, 2012.
- [163] I. L. Hosier, A. Guushaa, E. W. Westenbrink, C. Rogers, A. S. Vaughan, and S. G. Swingler, "Aging of biodegradable oils and assessment of their suitability for high voltage applications," *IEEE Trans. Dielectr. Electr. Insul.*, vol. 18, no. 3, pp. 728–738, 2011.
- [164] Y. Du, A. V. Mamishev, B. C. Lesieutre, M. Zahn, and S. H. Kang, "Moisture solubility for differently conditioned transformer oils," *IEEE Trans. Dielectr. Electr. Insul.*, vol. 8, no. 5, pp. 805–811, 2001.
- [165] M. Koch, "Improved Determination of Moisture in Oil-Paper-Insulations by Specialised Moisture Equilibrium Charts," *XIVth Int. Symp. High Volt. Eng.*, pp. 508–513, 2005.
- [166] "Shell Diala S3 ZX-IG Dried Technical Data Sheet," 2009.
- [167] R. Badent, K. Kist, and A. J. Schwab, "Rape-Seed Oil- a Substitute for Mineral Oils?," *High Volt. Eng. 1999. Elev. Int. Symp. Conf.*, vol. 3, no. 467, pp. 140–143, 1999.
- [168] R. Badent, M. Hemmer, and A. J. Schwab, "Inhibited rape-seed oil as substitute for mineral oils," *Electr. Insul. Dielectr. Phenom.*, pp. 268–271, 2002.
- [169] V. H. Dang, A. Beroual, and C. Perrier, "Comparative study of statistical breakdown in mineral, synthetic and natural ester oils under AC voltage," *IEEE Trans. Dielectr. Electr. Insul.*, vol. 19, no. 5, pp. 1508–1513, 2012.
- [170] Q. Liu, Z. D. Wang, and F. Perrot, "Impulse breakdown voltages of ester-based transformer oils determined by using different test methods," *Annu. Rep. - Conf. Electr. Insul. Dielectr. Phenomena, CEIDP*, no. 1, pp. 608–612, 2009.
- [171] A. Ciuriuc, P. V. Notingher, M. Jovalekic, and S. Tenbohlen, "Experimental study on vegetable and mineral transformer oils properties," *2014 Int. Conf. Optim. Electr. Electron. Equipment, OPTIM 2014*, pp. 169–174, 2014.
- [172] W. M. L. B. Naranpanawe, M. A. R. M. Fernando, J. R. S. S. Kumara, E. M. S. N. Naramapanawa, and C. S. Kalpage, "Performance analysis of natural esters as transformer

liquid insulation - Coconut, castor and sesame oils,” *2013 IEEE 8th Int. Conf. Ind. Inf. Syst. ICIIIS 2013 - Conf. Proc.*, pp. 105–109, 2013.

[173] D. Vukovi and S. Tenbohlen, “Comparative Evaluation of Breakdown Strength of Natural Esters and Mineral oil,” *16 th Int. Symp. High Volt. Equip.*, pp. 1–11, 2009.

[174] M. Hemmer, R. Badent, and a. J. Schwab, “Electrical properties of rape-seed oil,” *Annu. Rep. Conf. Electr. Insul. Dielectr. Phenom.*, no. 1, pp. 83–86, 2002.

[175] C. Kocatepe, E. Taslak, C. F. Kumru, and O. Arıkan, “An Investigation on Vegetable Oils as Potential Insulating Liquid,” *Int. J. Electr. Comput. Energ. Electron. Commun. Eng.*, vol. 9, no. 8, pp. 739–742, 2015.

[176] M. A. G. Martins and A. R. Gomes, “Comparative Study of the Thermal Degradation of Synthetic and Natural Type in the Thermal Degradation,” *IEEE Electr. Insul. Mag.*, vol. 28, no. 2, pp. 22–28, 2012.

[177] C. P. McShane, J. Corkran, K. Rapp, and J. Luksich, “Natural Ester Dielectric Fluid Development,” *Transm. Distrib. Conf. Exhib. 2005/2006 IEEE PES*, pp. 18–22, 2006.

[178] P. Z. Wang, “Use of Ester based Insulating Fluids in Power Transformers,” no. November, 2009.

[179] I. Cotton, “Dissolved Gas Analysis of Alternative Fluids for Power Transformers,” *IEEE Electr. Insul. Mag.*, vol. 23, no. 5, pp. 5–14, 2007.

[180] B. S. H. M. S. Y. Matharage, M. A. R. M. Fernando, M. A. A. P. Bandara, G. A. Jayantha, and C. S. Kalpage, “Performance of coconut oil as an alternative transformer liquid insulation,” *IEEE Trans. Dielectr. Electr. Insul.*, vol. 20, no. 3, pp. 887–898, 2013.

[181] H. M. Wilhelm, M. B. C. Stocco, L. Tulio, W. Uhren, and S. G. Batista, “Edible natural ester oils as potential insulating fluids,” *IEEE Trans. Dielectr. Electr. Insul.*, vol. 20, no. 4, pp. 1395–1401, 2013.

[182] J.-C. Lee, W.-H. Lee, S.-H. Lee, and S. Lee, “Positive and negative effects of dielectric breakdown in transformer oil based magnetic fluids,” *Mater. Res. Bull.*, vol. 47, no. 10, pp. 2984–2987, 2012.

- [183] W. Sima, J. Shi, Q. Yang, S. Huang, and X. Cao, "Effects of conductivity and permittivity of nanoparticle on transformer oil insulation performance: Experiment and theory," *IEEE Trans. Dielectr. Electr. Insul.*, vol. 22, no. 1, pp. 380–390, 2015.
- [184] P. Kopčanský, K. Marton, and L. Tomco, "The Influence of Magnetic Nanoparticles on DC- and AC-Dielectric Breakdown in Transformer Oil-Based Magnetic Fluid," *Fundam. Appl. MHD, Conf.*, pp. 329–332, 2005.
- [185] P. Kopcanský, L. Tomco, K. Marton, M. Koneracka, I. Potocova, and M. Timko, "The experimental study of the DC dielectric breakdown strength in magnetic fluids," *J. Magn. Magn. Mater.*, vol. 272, pp. 2377–2378, 2004.
- [186] A. Wypych, I. Bobowska, M. Tracz, A. Opasinska, S. Kadlubowski, A. Krzywania-Kaliszewska, J. Grobelny, and P. Wojciechowski, "Dielectric properties and characterisation of titanium dioxide obtained by different chemistry methods," *J. Nanomater.*, vol. 2014, 2014.
- [187] AEROXIDE, "TiO<sub>2</sub> P 25 Hydrophilic fumed titanium dioxide Characteristic physico-chemical data," 2014.
- [188] T. Zhang, M.-Q. Wu, S.-R. Zhang, J. Xiong, J.-M. Wang, D.-H. Zhang, F.-M. He, and Z.-P. Li, "Permittivity and its temperature dependence in hexagonal structure BN dominated by the local electric field," *Chinese Phys. B*, vol. 21, no. 7, p. 77701, 2012.
- [189] LOWER FRICTION, "Hexagonal Boron Nitride (hBN) Powder."
- [190] X. Q. Wang and A. S. Mujumdar, "Heat transfer characteristics of nanofluids: a review," *Int. J. Therm. Sci.*, vol. 46, no. 1, pp. 1–19, 2007.
- [191] W. Yu and H. Xie, "A Review on Nanofluids: Preparation, Stability Mechanisms, and Applications," *J. Nanomater.*, vol. 1, pp. 1–17, 2012.
- [192] R. Saidur, K. Y. Leong, and H. A. Mohammad, "A review on applications and challenges of nanofluids," *Renew. Sustain. Energy Rev.*, vol. 15, no. 3, pp. 1646–1668, 2011.
- [193] C. A. Yeckel and R. D. Curry, "Electrostatic Field Simulation Study of Nanoparticles Suspended in Synthetic Insulating Oil," *IEEE Trans. Plasma Sci.*, vol. 38, no. 10, pp. 2514–2519, 2010.

- [194] W. R. Viali, G. B. Alcantara, P. P. C. Sartoratto, M. A. G. Soler, E. Mosiniewicz-Szablewska, B. Andrzejewski, and P. C. Morais, "Investigation of the molecular surface coating on the stability of insulating magnetic oils," *J. Phys. Chem. C*, vol. 114, no. 1, pp. 179–188, 2010.
- [195] C. Choi, H. S. Yoo, and J. M. Oh, "Preparation and heat transfer properties of nanoparticle-in-transformer oil dispersions as advanced energy-efficient coolants," *Curr. Appl. Phys.*, vol. 8, no. 6, pp. 710–712, 2008.
- [196] L. Xuedong and Z. Zhen, "Development and Application of Mechanochemical Surface Modification of Powers [In Chinese]," *J. Jiangsu Institue Petrochemical Technol.*, vol. 14, no. 4, pp. 32–35, 2002.
- [197] Y. Jiang and J. Cheng, *Powder engineering [Chinese Edition]*. Hefei: Hefei University Press, 2006.
- [198] Malvern instruments, "Zetasizer Nano Series User Manual," 2004.
- [199] R. J. Kisch, "Using Refractive Index to Monitor Oil Quality in High Voltage Transformers," 2008.
- [200] Malvern, "Selecting an appropriate particle absorption for laser diffraction particle size calculations," 2014.
- [201] Y. Yamada, H. Uyama, S. Watanabe, and H. Nozoye, "Deposition at low substrate temperatures of high-quality TiO<sub>2</sub> films by radical beam-assisted evaporation.," *Appl. Opt.*, vol. 38, no. 31, pp. 6638–6641, 1999.
- [202] J. R. Devore, "Refractive Indices of Rutile and Sphalerite," *J. Opt. Soc. Am.*, vol. 41, no. 6, p. 416, 1951.
- [203] T. Takahashi, H. Itoh, and M. Kuroda, "Structure and properties of CVD-BN thick film prepared on carbon steel substrate," *Journal of Crystal Growth*, vol. 53, no. 2, pp. 418–422, 1981.
- [204] J.-X. Deng, X.-K. Zhang, Y. Qian, X.-Y. Wang, G.-H. Chen, and D.-Y. He, "Optical properties of hexagonal boron nitride thin films deposited by radio frequency bias magnetron sputtering," *Chinese Phys. B*, vol. 18, no. 9, pp. 4013–4018, 2009.

- [205] J. J. Pouch, S. A. Alterovitz, K. Miyoshi, and J. D. Warner, "Boron Nitride: Composition, Optical Properties, and Mechanical Behavior," 1987.
- [206] M. P. Wilson, "Impulse Breakdown of Liquid-Solid Interfaces," University of Strathclyde, 2011.
- [207] International Electrotechnical Commission, "International Standard IEC 60060-1; High-voltage test techniques – Part 1: General definitions and test requirements," 2010.
- [208] National Grid PLC, "Innovation Funding Incentive, Electricity Transmission R&D Programme Detailed Reports," 2010.
- [209] Q. Liu and Z. Wang, "AC and Lightning Breakdown Strength of Mineral Oil Nytro Gemini X and 10Gbn," in *International Electrical Insulation Conference*, 2009, pp. 14–19.
- [210] M. J. Gardner and D. G. Altman, "Confidence intervals rather than P values : estimation rather than hypothesis testing," *Stat. Med.*, vol. 292, pp. 746–750, 1986.
- [211] R. Ichiki, S. Kanazawa, K. Tomokiyo, S. Akamine, M. Kocik, and J. Mizeraczyk, "Investigation of three-dimensional characteristics of underwater streamer discharges," *Jpn. J. Appl. Phys.*, vol. 51, no. 10, 2012.
- [212] W. Weibull, "Statistical distribution function of wide applicability," *J. Appl. Mech.*, vol. 18, pp. 293–297, 1951.
- [213] J. P. Klein and M. L. Moeschberger, *Survival Analysis: Techniques for Censored and Truncated Data*, Second., vol. 19, no. 5. Springer-Verlag New York, Inc., 2003.
- [214] NCSS Statistical Software, "Distribution ( Weibull ) Fitting."
- [215] D. Martin and Z. D. Wang, "Statistical analysis of the AC breakdown voltages of ester based transformer oils," *IEEE Trans. Dielectr. Electr. Insul.*, vol. 15, pp. 1044–1050, 2008.
- [216] Y. Du, Y. Lu, C. Li, M. Chen, J. Zhou, X. Li, and T. Liu, "Insulating property and mechanism of semiconducting nanoparticles modified transformer oils," *Proc. Chinese Soc. Electr. Eng.*, vol. 32, no. 10, pp. 177–182, 2012.

- [217] H. Jin, P. H. F. Morshuis, J. J. Smit, and T. Andritsch, "The effect of surface treatment of silica nanoparticles on the breakdown strength of mineral oil," in *IEEE 18th International Conference on Dielectric Liquids (ICDL)*, 2014, pp. 1–4.
- [218] D. Vuković, S. Tenbohlen, J. Harthun, C. Perrier, and H. Fink, "Breakdown strength of vegetable-based oils under AC and lightning impulse voltages," *Proc. - IEEE Int. Conf. Dielectr. Liq.*, 2011.
- [219] M. D. Judd, L. Yang, and I. B. B. Hunter, "Partial discharge monitoring for power transformers using UHF sensors part 2 : field experience," *IEEE Electr. Insul. Mag.*, vol. 21, no. 3, pp. 5–13, 2005.
- [220] T. J. Gallagher, "Simple Dielectric Liquids-Mobility, Conduction, and Breakdown," in *Simple Dielectric Liquids-Mobility, Conduction, and Breakdown*, London: J. W. Arrowsmith Ltd, 1975, pp. 94–100.
- [221] J. A. Kok and M. M. G. Corbey, "Breakdown of liquid insulating and dielectric material," *Appl. Sci. Res.*, vol. B, no. 6, pp. 197–206, 1957.
- [222] L. Yuzhen, W. Wang, M. Kaibo, S. Zhang, Y. Zhou, C. Li, and Q. Wang, "Nanoparticle Effect on Dielectric Breakdown Strength of Transformer Oil-Based Nanofluids," *Annu. Rep. - Conf. Electr. Insul. Dielectr. Phenomena, CEIDP*, pp. 680–682, 2013.
- [223] A. Fallah-Shojaie, A. Tavakoli, M. Ghomashpasand, and S. Hoseinzadeh, "Experimental evaluation on the dielectric breakdown voltage of fresh and used transformer oil mixed with titanium dioxide nanoparticles in the Gilan electrical distribution company," *2013 21st Iran. Conf. Electr. Eng. ICEE 2013*, vol. c, pp. 13–16, 2013.
- [224] G. Massala and O. Lesaint, "Positive streamer propagation in large oil gaps: Electrical properties of streamers," *IEEE Trans. Dielectr. Electr. Insul.*, vol. 5, no. 3, pp. 371–380, 1998.
- [225] J. G. Hwang and M. Zahn, "Mechanisms Behind Positive Streamers and Their Distinct Propagation Modes in Transformer Oil," *IEEE Trans. Dielectr. Electr. Insul.*, vol. 19, no. 1, pp. 162–174, 2012.

- [226] A. Denat, O. Lesaint, and F. M. Cluskey, "Streamer and Breakdown Phenomena Under Step and Lightning Impulses in Various Hydrocarbon Liquids," pp. 142–145, 2014.
- [227] Y. Li, M. X. Zhu, H. B. Mu, J. B. Deng, G. J. Zhang, J. Jadidian, M. Zahn, W. Z. Zhang, and Z. M. Li, "Transformer Oil Breakdown Dynamics Stressed by Fast Impulse Voltages : Experimental and Modeling Investigation," *IEEE Trans. Plasma Sci.*, vol. 42, no. 10, pp. 3004–3013, 2014.
- [228] W. Choo, G. Chen, and S. G. Swingler, "Electric field in polymeric cable due to space charge accumulation under DC and temperature gradient," *IEEE Trans. Dielectr. Electr. Insul.*, vol. 18, no. 2, pp. 596–606, 2011.
- [229] U. Gafvert, A. Jaksts, C. Tornkvist, and L. Walfridsson, "Electrical field distribution in transformer oil," *Electr. Insul. IEEE Trans.*, vol. 27, no. 3, pp. 647–660, 1992.
- [230] R. Coelho and J. Debeau, "Properties of the tip-plane configuration," *J. Phys. D. Appl. Phys.*, vol. 4, no. 9, pp. 1266–1280, Sep. 1971.
- [231] S. D. Smith, "Design and test experience with natural ester fluid for power transformers," *Proc. IEEE Power Eng. Soc. Transm. Distrib. Conf.*, pp. 35–36, 2006.
- [232] I. V. Timoshkin, M. J. Given, R. A. Fouracre, S. J. MacGregor, and J. M. Lehr, "Charge injection energy barriers and charge mobilities in insulating liquids," *Annu. Rep. - Conf. Electr. Insul. Dielectr. Phenomena, CEIDP*, pp. 613–616, 2009.
- [233] O. M. Stuetzer, "Magnetohydrodynamics and Electrohydrodynamics," *Phys. Fluids*, vol. 5, no. 5, p. 534, 1962.
- [234] R. Coelho and J. Debeau, "Properties of the tip-plane configuration," *J. Phys. D. Appl. Phys.*, vol. 4, no. 9, pp. 1266–1280, 1971.
- [235] J. Shrimpton, *Charge Injection Systems- Physical Principles, Experimental and Theoretical Work*. Berlin: Springer-Verlag, 2009.
- [236] F. M. O'Sullivan, "A model for the initiation and propagation of electrical streamers in transformer oil and transformer oil based nanofluids," *Thesis (Ph. D.)--Massachusetts Inst. Technol. Dept. Electr. Eng. Comput. Sci. 2007.*, 2007.

- [237] F. O'Sullivan, J. G. Hwang, M. Zahn, O. Hjortstam, L. Pettersson, R. Liu, and P. Biller, "A model for the initiation and propagation of positive streamers in transformer oil," *Conf. Rec. IEEE Int. Symp. Electr. Insul.*, no. 1, pp. 210–214, 2008.
- [238] M. Rafiq, Y. Lv, and C. Li, "A Review on Properties , Opportunities , and Challenges of Transformer Oil-Based Nanofluids," vol. 2016, 2016.
- [239] Y. Du, Y. Lu, C. Li, M. Chen, J. Zhou, X. Li, and T. Liu, "Insulating property and mechanism of semiconducting nanoparticles modified transformer oils," *Zhongguo Dianji Gongcheng Xuebao (Proceedings Chinese Soc. Electr. Eng.*, vol. 32, no. 10, pp. 177–182, 2012.
- [240] L. Shen, "Research on the Nano-modified Transformer Oil's Preparation and Characterization [Ph.D Thesis] [in chinese]," Huazhong Univerisity of Science and Technology, 2012.
- [241] M. Meunier and N. Quirke, "Molecular modeling of electron trapping in polymer insulators," *J. Chem. Phys.*, vol. 113, no. 1, pp. 369–376, 2000.
- [242] M. Meunier, N. Quirke, and A. Aslanides, "Molecular modeling of electron traps in polymer insulators: Chemical defects and impurities," *J. Chem. Phys.*, vol. 115, no. 6, pp. 2876–2881, 2001.
- [243] G. Teyssevre and C. Laurent, "Charge transport modeling in insulating polymers: From molecular to macroscopic scale," *IEEE Trans. Dielectr. Electr. Insul.*, vol. 12, no. 5, pp. 857–874, 2005.
- [244] T. Takada, Y. Hayase, Y. Tanaka, and T. Okamoto, "Space charge trapping in electrical potential well caused by permanent and induced dipoles," *IEEE Trans. Dielectr. Electr. Insul.*, vol. 15, no. 1, pp. 152–160, 2008.
- [245] Y. Du, Y. Lv, C. Li, M. Chen, J. Zhou, X. Li, Y. Zhou, and Y. Tu, "Effect of electron shallow trap on breakdown performance of transformer oil-based nanofluids," *J. Appl. Phys.*, vol. 110, no. 10, pp. 20–24, 2011.

[246] Y. Du, "The Influence of TiO<sub>2</sub> Nanoparticles on Insulation Properties and Charge Transport in Transformer oil [Ph.D Thesis] [in chinese]," North China Electric Power University, 2013.

# APPENDIX: PUBLISHED JOURNAL PAPER

Yi Jing, Igor V. Timoshkin, Mark P. Wilson, Martin J. Given, Scott J. MacGregor, Tao Wang, and Jane M. Lehr. 'Dielectric properties of natural ester, synthetic ester Midel 7131 and mineral oil Diala D'. *IEEE Transactions on Dielectrics and Electrical Insulation* 21.2 (2014): pp. 644–652.

## Dielectric Properties of Natural Ester, Synthetic Ester Midel 7131 and Mineral Oil Diala D

Yi Jing, Igor V. Timoshkin, Mark P. Wilson, Martin J. Given, Scott J. MacGregor, Tao Wang

Department of Electronic and Electrical Engineering  
University of Strathclyde, 204 George Street, Glasgow, G1 1XW, UK

and Jane M. Lehr

Sandia National Laboratories, PO Box 5800, MS 1193, Albuquerque, NM 87185-1193, USA

### ABSTRACT

The insulating liquids used in industrial applications are typically mineral oils. In recent years however, significant attention has been paid to alternative insulating fluids, including synthetic and natural ester liquids. In order to expand their practical applications, it is important to have detailed information on their dielectric properties. In this present paper, the dielectric properties of synthetic ester, Midel 7131; mineral oil, Shell Diala D; and vegetable (rapeseed) oil have been investigated. It has been shown that Midel 7131 has a higher ac breakdown voltage (27.6 kV) as compared with Diala D oil (26.4 kV) and rapeseed oil (24.6 kV). However, the breakdown voltage of the Diala D oil has the smallest standard deviation (7%) amongst the tested liquids (13% for Midel 7131 and 11% for rapeseed oil). Statistical analysis of the breakdown voltages has been conducted and it has been shown that the ac breakdown voltages can be described by a normal distribution. dc  $I$ - $V$  characteristics have been measured and the space charge saturation regime has been observed for all three liquids starting from  $\sim 9$  kV for positive energisation and  $\sim 10$  kV for negative energisation in the point-plane topology. Apparent mobilities of the charge carriers in the tested liquids have been obtained using  $I^{1/2}$ - $V$  curves; these mobilities can be used for calculation of the space charge influenced distribution of the electric field in liquid insulators stressed with dc voltage. Such analysis can be important for design and exploitation of HVDC power systems.

Index terms - Liquid dielectrics, breakdown, conduction.

### 1 INTRODUCTION

**DIELECTRIC** liquids are used to provide insulation protection in high-voltage (HV) systems. These liquids also facilitate thermal stability of HV equipment due to their thermo-conduction properties. The insulating liquids typically employed in power systems are naphthenic mineral oils. However, stringent environmental protection regulations encourage operators and manufacturers of HV equipment to use bio-degradable liquids with low toxicity. Reduction of the footprint of modern high-voltage and pulsed-power equipment results in demand for insulating liquids with improved dielectric properties, due to the resultant higher levels of electrical stress. In response to this demand, manufacturers of dielectric liquids are actively investing in the development of new products, such as natural and synthetic esters, for applications in the power and pulsed-power industries.

Natural, organic oils and synthetic esters are considered as potential substitutes for traditional naphthenic mineral oils. However, their dielectric properties are not yet fully known, especially in the case of dc energisation. Recent advances and investments in HVDC systems require detailed information about the dielectric behavior of insulating fluids under ac and dc electric stresses [1]. HVDC techniques are suitable for transmission of electrical power over long distances, and with the development of renewable sources this approach has attracted the attention of the power industry for transmission of electrical power generated by offshore wind farms. In HVDC systems, for example in HVDC converter transformers, the insulation is stressed with both ac and dc voltages. Therefore, it is important to investigate the dielectric properties of insulating liquids, and to understand their behavior under both types of energisation. As indicated in a report by National Grid [1], "DC transformers cost in the region of £5M per phase and failures have significant outage cost". Also, it is known that the HVDC transformer failure rate exceeds the failure rate of conventional transmission-based units by 5-10 times [1].

*Manuscript received on 19 January 2013, in final form 11 September 2013, accepted 24 October 2013.*

Under ac conditions the field distribution is dominated by the permittivity of the dielectric and the conductivity is regarded as only being significant in its contribution to losses in the system. However, the formation of bubbles as a result of Joule heating which is dependent on the conductivity has been proposed as a mechanism for liquid breakdown [2]. In addition, under dc conditions, it has been shown in solid insulation systems that conductivity and the resulting space charge distribution dominates the field distribution rather than the permittivity [3]. For a liquid, due to the higher mobilities of charge carriers, it is likely that the effect of space charge distributions will be more significant. The presence of this space charge implies that field calculations based on solutions to the Laplace equation will be inadequate and approaches based on the Poisson and current continuity equations are required [4]. To perform such analyses of the field distributions, information on the effective mobility of the charge carriers in the liquids is required. At present, measurement of the dc conductivity of oil is not routine, [1], and it is not possible to derive effective mobilities for the charge carriers from the data sheets provided by manufacturers. Information on the dc dielectric behavior of insulating liquids will potentially influence design of HVDC systems and will help to manage these liquids.

This paper reports experimental data on the dielectric characteristics of three insulating liquids: Diala D; a synthetic ester fluid, Midel 7131 and a food-grade rapeseed oil. The ac breakdown voltage of the dielectric fluids has been measured using a test cell manufactured according to the ASTM D1816-04 standard and the mean breakdown voltage has been calculated. Statistical analysis using the Microsoft Office Excel 2003 and OriginPro v.8.6 software packages has shown that the data is normally distributed allowing calculation of the standard deviation of the breakdown voltage and this has been used to estimate the 1, 10, 50 and 90% breakdown probability for each liquid. This data is relevant to the design of power and pulse power equipment, [5-11], as it affects safety-margin design requirements for liquid-insulated, high-voltage equipment. Values of the effective mobility of the charge carriers in the liquids were obtained from pre-breakdown  $I-V$  characteristics, measured in a point-plane electrode topology, following the procedure reported in [12].

## 2 AC BREAKDOWN VOLTAGE TESTS

### 2.1 EXPERIMENTAL ARRANGEMENT

AC breakdown voltages of the liquids under investigation were measured in an electrode configuration which satisfies the ASTM D1816-04 standard, [13]. The tests were conducted at atmospheric pressure and room temperature. From the data presented in [14] the expected increase in the breakdown strength of mineral oil is ~5% when the ambient pressure is increased from 0 to 1 atm. It is known that temperature affects the conduction and breakdown properties of the insulating liquids, [15, 16]. However, a change in temperature of 20 °C to 80°C only resulted in a ~7% decrease in the ac breakdown voltage for mineral oil, [17]. From data in [18] changes of  $\pm 5^\circ\text{C}$  about a temperature of 20 °C leads to

a ~5% change in measured conductivity. Therefore, it is assumed that the small shifts in ambient temperature and pressure that occurred in the course of the measurements will have had negligible effects on the results obtained.

The oil samples were used "as received" with no pretreatment before measurements. It is known that contaminants and moisture in dielectric fluids affect their breakdown properties, [15]. For example, a ~34% decrease in the ac breakdown strength for mineral oil with 43% relative humidity as compared with dry oil has been reported in [19]. Many different pretreatment protocols have been described in the literature aimed at reducing moisture, dissolved gases and contaminants from liquid samples: samples have been degassed and dried but not filtered, [11]; filtered using a relatively large filter (10-16  $\mu\text{m}$ ) but not degassed or dried, [20], or only filtered using a 5  $\mu\text{m}$  filter, [21]. The results of dielectric studies in which "as received" insulating fluids were used without any additional filtration, de-gassing or de-humidification are reported in the literature, [22, 23]. In the work reported on aged biodegradable oils, [24], no details of pre-treatment of the liquids prior to or post-ageing is reported. Given this wide range of possible pre-treatments the authors felt that using the oils as received provided the starting point for assessing the relative properties of the three liquids. This approach has the advantage that the obtained results help to understand the dielectric behavior of commercially-available insulating liquids used in practical engineering applications without additional processing. The results obtained in the present paper are compared with the studies in which pre-treated dielectric liquids have been used.

Figure 1 show the electrode topology used in the present tests. A pair of spherically-capped, polished, brass electrodes was incorporated into a ceramic container; the electrode profile is shown in Figure 1. The gap between the two electrodes is 0.5 mm. AC breakdown voltages were measured using a Tektronix TDS220 digital storage oscilloscope and a Tektronix P6015A HV probe.

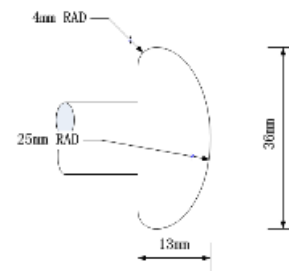


Figure 1. Cross section of spherically-capped electrode.

A Foster breakdown test apparatus was used as the power source. This apparatus produces a 50 Hz ac voltage across the test cell, filled with the liquid under test. AC voltage was applied across the electrodes of the test cell with a rate-of-rise of 1 kV/s. 70 breakdown events were registered for each liquid sample. Average breakdown voltages were calculated using breakdown data obtained in three independent tests (fresh samples were used for each test) for each type of liquid.

The samples were kept under vacuum for 1.5 hours at room temperature to remove gas bubbles introduced into the liquid samples during pouring procedure. The electrodes were polished after each series of tests to remove damage produced by breakdowns, and the test cell and electrodes were cleaned with alcohol and then washed with distilled water. The test cell and electrodes were then dried in an oven for 2 hours with 40°C to remove water prior to the next test.

The relative water content of the liquids used in the present study has been examined using "Omniport 20" moisture in oil probe (E+E Elektronik GmbH). This can be converted into an absolute water content using the linear relationship between these two values, [25]. The water solubility values for Diala D (~77 ppm), Midel 7131 (~2600 ppm) and rapeseed (~772 ppm) oils required for this analysis have been taken from papers [26, 27], and [28], respectively. The evaluated absolute water content for Diala D is ~39 ppm, Midel 7131 is ~1352 ppm and for rapeseed oils is ~417 ppm. These values are not exact and given here for evaluation purpose only, such high values of the absolute water content can be explained by the fact that the liquid samples were kept in ambient laboratory conditions, [19].

## 2.2 EXPERIMENTAL RESULTS

Figure 2 shows ac breakdown voltages for Midel 7131 synthetic ester fluid, Diala D mineral oil and rape-seed oil. Each point in this graph shows the average breakdown voltage of three individual tests. This figure shows that the breakdown voltages for all three liquids display considerable spread. Potential conditioning in the breakdown behavior of liquids (slightly lower breakdown voltages for shots 5-20) may be observed in Figure 2, however this conditioning is not well pronounced. Therefore, statistical analysis of breakdown data was conducted using the full data set of 70 data points.

Figure 2 shows a dependence of the breakdown voltage,  $V_{br}$ , of the three tested fluids on the breakdown number,  $N$ , which demonstrates a slight increase in  $V_{br}$  with  $N$ . This tendency has also been noted in [29] and in [11] for mineral oil and natural ester liquid, and can potentially be explained by removal of gas bubbles and impurities in the liquid and "conditioning" of the electrodes (removal of sharp micro-asperities on the electrode's surface) by spark discharges. The inter-electrode gap in the ac breakdown study reported in [11] was 1 mm. The authors of [20] observed that the breakdown voltage values "are scattered around a mean value" and noted that in their tests the higher values of the ac breakdown voltage were usually observed at the beginning of the breakdown tests. The inter-electrode gap used in [20] was 2.5 mm. No noticeable conditioning can be observed in the breakdown series for mineral oils and ester fluids presented in paper [20]. However, in [30] the authors reported a pronounced increase in the ac breakdown voltage for the mineral oil which stabilizes after ~10 breakdown events. The electrode conditioning effect is discussed in [15], where it is shown that the breakdown strength of degassed *n*-hexane in a sub-mm gap increases significantly during the first 50 breakdown events (from 300 to 750 kV/cm), then decreases and stabilizes.

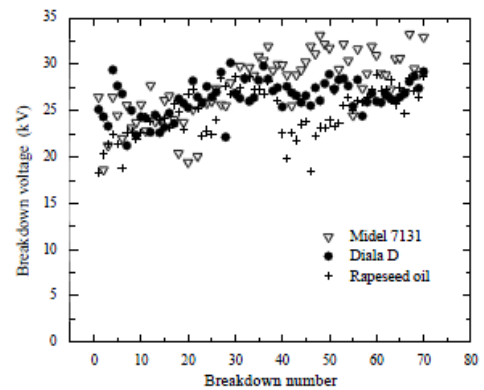


Figure 2. Distribution of breakdown voltage of tested liquids.

Figure 3 shows frequency histograms of breakdown voltages for each of the tested liquids.

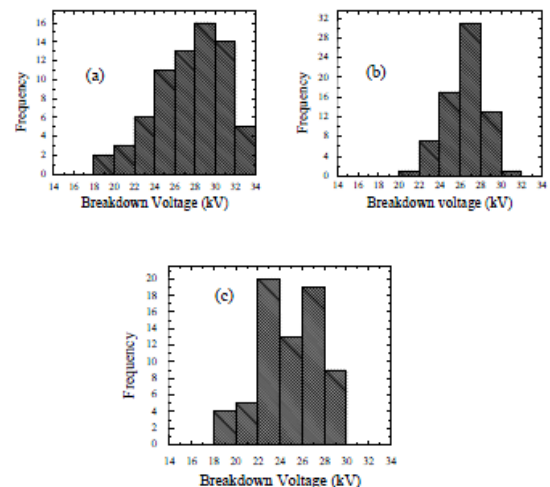


Figure 3. Histogram of average breakdown voltage for Midel 7131, (a); Diala D, (b); and rapeseed oil, (c).

The breakdown voltage values of Diala D concentrate in the region of 25-29 kV, indicating a relatively narrow variation in breakdown voltage. The breakdown voltages for Midel 7131 are mostly concentrated in the region of 23-33 kV; this spread in the breakdown voltages is larger than that for Diala D oil. The majority of the breakdown voltages for the rapeseed oil are located in the region of 21-29 kV. The results of the statistical analysis of the breakdown voltage data for these liquids (average breakdown voltage and standard deviation) are shown in Table 1.

As can be seen from Table 1, Midel 7131 has the highest average ac breakdown voltage, 27.6 kV, however the standard deviation is also high, 3.5 kV. Diala D demonstrated the minimum standard deviation, 1.9 kV with an average breakdown voltage of 26.4 kV.

Table 1. The mean breakdown voltage and its standard deviation.

|              | Mean (kV) | Standard deviation (kV and %) |
|--------------|-----------|-------------------------------|
| Midel 7131   | 27.6      | 3.5 (13%)                     |
| Diala D      | 26.4      | 1.9 (7%)                      |
| Rapeseed oil | 24.8      | 2.7 (11%)                     |

The rapeseed oil has the lowest average breakdown voltage, 24.8 kV (~ 6% lower than that of Diala D), however its standard deviation value (11%) is between those for Midel 7131 (13%) and Diala D (7%). These values are close to the standard deviation values obtained in [11] for mineral oil (Nytro 10 GB, 9.5%), synthetic ester (Midel 7131, 13%) and natural ester (FR3, 13%). The liquids used in [11] were cleaned (filtered, dehydrated and de-gassed) before the tests. These data show that the insulating liquids "as received" have similar spread in their breakdown voltages as compared with the cleaned insulating liquids, and the ac breakdown voltages of the food-grade rapeseed oil are close to the ac breakdown voltages of the commercially-available insulating liquids. Therefore, such natural ester fluids can potentially be used in some practical applications which require an inexpensive, environmentally-friendly liquid dielectric, with good breakdown stability.

Although the particle content in the tested fluids have not been examined, it is interesting to note that impurities in dielectric liquids can not only decrease, but in some cases increase their dielectric strength. For example, paper [31] reported on the ac and impulsive breakdown voltages of the pure, commercially available transformer oil, Univolt-60 (oil A), and the same oil doped with 0.3% anthracene (oil B). This paper shows that the dielectric strength of oil B can be higher or lower than that of oil A, depending on the inter-electrode distance and the field non-uniformity factor (the ratio between the maximum and average fields in the gap). The authors concluded that anthracene "inhibits the 60 Hz breakdown initiation process in quasi-uniform fields" and "increases ability of streamers to propagate across the gap" in the case of highly divergent electric fields, [31]. An apparent increase in the dielectric breakdown strength of the insulating oils seeded with magnetite nano-particles has been reported in number of papers, [32-34]. However, the detailed discussion of this interesting effect and its potential practical applications is beyond the scope of the present paper.

The statistical analysis of the ac breakdown results (70 average breakdown voltages for each liquid) performed in the present paper is based on the normal distribution. It has been shown that this type of distribution can be used in the analysis of the ac breakdown voltages of mineral oils, natural and synthetic esters, [11, 20]. If the data are distributed normally, the standard deviations for each of these three liquids can be established. Reliable standard deviation in breakdown voltage is important for comparison of the dielectric performance of insulating liquids; it is desirable to use a liquid with minimum spread in its breakdown voltage. This will provide a higher degree of predictability in the dielectric performance, which can affect the design and maintenance of the high-voltage systems. The mean and standard deviation values obtained for the normally-distributed breakdown voltages can be used in the design of power systems for prediction of the dielectric performance of insulating liquids. The mean voltage,  $U_{50\%}$  and the withstand voltage,  $U_{1\%}$  are used in the insulation design of high-voltage equipment, [30, 35].

In order to determine the distribution of the breakdown voltage for each liquid, the Kolmogorov-Smirnov test of normality was used and  $p$ -values were calculated (the significance level was set to 0.05). If the  $p$ -value is higher than this level, the hypothesis that the breakdown voltage values can be described by the normal distribution is accepted. Table 2 shows the results of the normality test. As can be seen from Table 2, all three populations of the breakdown voltages for Midel 7131, Diala D and rapeseed oil potentially belong to the normal distribution.

Table 2. Hypothesis test results of three tested samples.

|              | $p$ - value | Conformity to normal distribution |
|--------------|-------------|-----------------------------------|
| Midel 7131   | 0.32035     | Accepted                          |
| Diala D      | 0.10015     | Accepted                          |
| Rapeseed oil | 0.10468     | Accepted                          |

Figures 4-6 show cumulative probability plots of the breakdown voltages of these liquids, and the data predicted by the normal distribution (solid reference lines). These figure show that the experimental breakdown data (open circles) deviate from the predicted cumulative distribution functions (solid straight lines in these figures) for probabilities below ~10% and above ~90%. The experimental data show that the actual breakdown voltage is lower than the voltage predicted by the cumulative normal distribution. This information can be important for manufacturers of power systems, and should be taken into account in the design of such systems.

The predicted breakdown voltages with probabilities of 1%, 10%, 50% and 90%,  $V_{1\%}$ ,  $V_{10\%}$ ,  $V_{50\%}$  and  $V_{90\%}$ , have been calculated assuming that the data are distributed normally, and these voltage are given in Table 3.  $V_{1\%}$ ,  $V_{10\%}$ ,  $V_{50\%}$  and  $V_{90\%}$  voltages can be compared with the actual breakdown voltages in order to evaluate the risk levels associated with insulation design based on statistical analysis.

Table 3.  $V_{1\%}$ ,  $V_{10\%}$ ,  $V_{50\%}$ ,  $V_{90\%}$  values for the tested liquids.

|              | $V_{1\%}$ | $V_{10\%}$ | $V_{50\%}$ | $V_{90\%}$ |
|--------------|-----------|------------|------------|------------|
| Midel 7131   | 18.6      | 22.9       | 28.9       | 31.9       |
| Diala D      | 21.2      | 23.5       | 26.5       | 28.7       |
| Rapeseed oil | 18.3      | 21.6       | 24.8       | 28.5       |

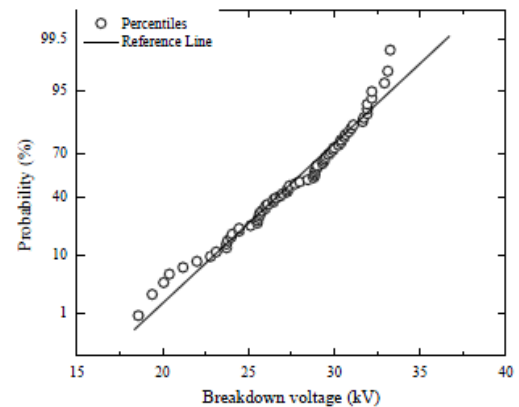


Figure 4. Normal probability plot of Midel 7131.

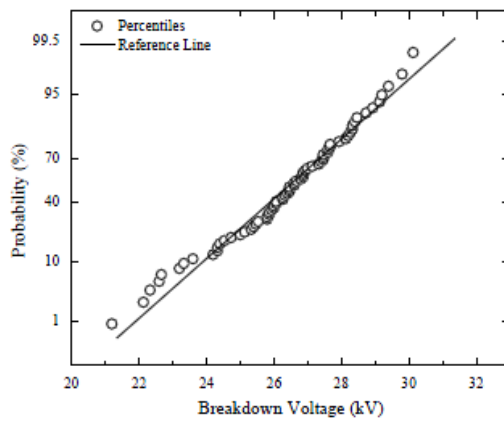


Figure 5. Normal probability plot of Diala D.

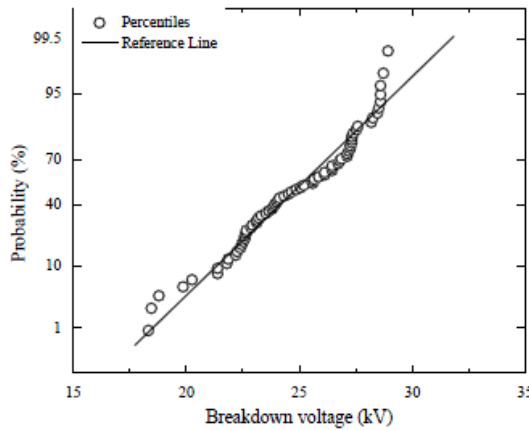


Figure 6. Normal probability plot of rapeseed oil.

### 3 DC PRE-BREAKDOWN CURRENT

#### 3.1 EXPERIMENTAL ARRANGEMENT

As it was discussed in the Introduction, the dc conductivity is important parameter which can influence design of the HVDC systems and management of the insulating liquids stressed with dc voltage. Also, the mobility of charge carriers in the insulating fluids will affect the electric field distribution in the high voltage equipment. In the present work,  $I$ - $V$  curves were obtained for Midel 7131, Diala D and rapeseed oil in a point-plane electrode topology. The mobility of the charge carriers has been obtained and  $\sqrt{I(V)}$  curves are used for identification of different conductivity regimes which will influence the space charge distribution between the electrodes. The gap between the electrodes was 5 mm, and the radius of the needle tip was  $\sim 14 \mu\text{m}$ . Both positive and negative dc voltages were applied to the point electrode. The conduction current in the oil samples was measured using a custom-built, current-sensing

amplifier, with a  $1 \text{ k}\Omega$  current-viewing resistor. The voltage output from the amplifier was monitored using a Tektronix TDS2024 digital storage oscilloscope, and the applied voltage was monitored using a TESTEC HVP-40 HV probe.

#### 3.2 TEST PROTOCOL

The point-plane electrode topology described in Section 3.1 was stressed with dc voltage; the voltage was increased from 0 to the maximum value that could be applied without inducing breakdown (positive: +18 kV; negative: -30 kV) in 1 kV steps. The conduction current values were recorded for each voltage step. Three independent current tests were conducted per fluid, using a fresh liquid sample for each test. As in the case of ac breakdown tests, the test cell and electrodes were cleaned with alcohol, washed with distilled water, and dried in an oven after each set of three measurements.

#### 3.3 RESULTS: MOBILITY OF CHARGE CARRIERS

Figures 7-8 show the square root of the conduction current for all three liquids for negative and positive energisation. The results show that at low voltages the square root of current behaves non-linearly; however with an increase in voltage  $\sqrt{I(V)}$  becomes a linear function, [36]. This linear behavior indicates the space-charge saturation regime. The constant apparent mobility of the charge carriers,  $\mu$ , can be calculated using the  $\sqrt{I(V)}$  curve. The basis of this calculation method has been described in [36]. The straight lines in Figures 7-8 were added to indicate the space charge saturation range. In the region where the square root of current has a linear relation with the applied voltage, the mobility,  $\mu$ , can be calculated using the following equations:

$$y=Bx+A,$$

$$\text{where } y=\sqrt{I} \text{ (nA)}, x=V \text{ (kV)} \quad (1)$$

and

$$B = \sqrt{\frac{2\mu\epsilon_0\epsilon_r}{d} \left[ \frac{nA^{1/2}}{kV} \right]}, \quad A = \sqrt{\frac{2\mu\epsilon_0\epsilon_r V_0}{d} \left[ nA^{1/2} \right]} \quad (2)$$

$$\mu = \frac{B^2 10^{-15} d}{2\epsilon_0\epsilon_r} \left[ \text{cm}^2 \text{V}^{-1} \text{s}^{-1} \right]$$

where  $I$  is current,  $V$  is applied voltage,  $\epsilon_0$  is permittivity of free space, and  $\epsilon_r$  is relative permittivity of the insulating liquid,  $d$  in the gap distance between the point high voltage electrode and the grounded plane electrode.

The relative permittivities of the liquids are required in order to calculate the mobility, these values have been taken from [37] and they are:  $\epsilon_r = 2.5$  for rapeseed oil;  $\epsilon_r = 2.8$  for Diala D oil;  $\epsilon_r = 3.2$  for Midel 7131 liquid. The coefficient  $B$  and mobility,  $\mu$ , for each liquid are given in Table 4.

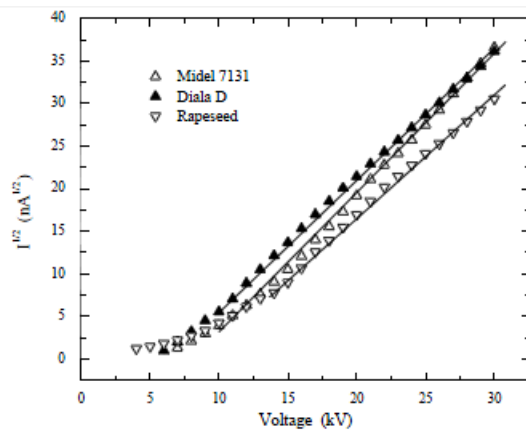


Figure 7.  $\sqrt{I(V)}$  plot of three oils, negative energisation.  $R^2$  coefficients: 0.9990 for Midel 7131; 0.9996 for Diala D; 0.9988 for rapeseed oil.

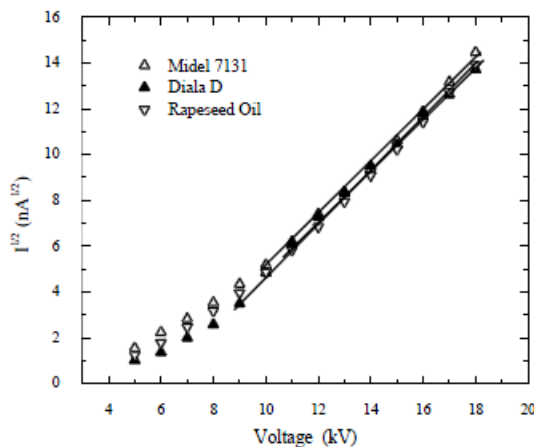


Figure 8.  $\sqrt{I(V)}$  plot of three oils, positive energisation.  $R^2$  coefficients: 0.9987 for Midel 7131; 0.9991 for Diala D; 0.9995 for rapeseed oil.

The calculation results show that the apparent mobility of the charge carriers in Midel 7131 and Diala D liquids are slightly different as compared with the values given in [37]. For negative energisation, the apparent mobility of the charge carriers in Midel 7131 is slightly higher than the previously reported value ( $2.21 \times 10^{-3} \text{ cm}^2 \text{ V}^{-1} \text{ s}^{-1}$ ). The apparent mobility of the charge carriers in Diala D oil is lower than the previously obtained value ( $3.44 \times 10^{-3} \text{ cm}^2 \text{ V}^{-1} \text{ s}^{-1}$ ), [37]. Rapeseed oil has the lowest value of apparent mobility of the tested liquids.

For positive energization, the apparent mobility of the charge carriers in Diala D has the highest value,  $1.6 \times 10^{-3} \text{ cm}^2 \text{ V}^{-1} \text{ s}^{-1}$ . The apparent charge mobility in the rapeseed oil is slightly lower than Diala D,  $1.4 \times 10^{-3} \text{ cm}^2 \text{ V}^{-1} \text{ s}^{-1}$ . The apparent mobility of the charge carriers in Midel 7131 is the lowest in this study. Different factors including pressure, temperature, and liquid kinematic parameters affect the apparent mobility of the charge carriers.

It is known that the electric field induces electrohydrodynamic (EHD) motion in the liquid, which also makes a contribution to the apparent mobility. A simple evaluation of the EHD mobility can be done by equating the kinetic energy of the moving liquid to the electrostatic energy in the liquid, [38], thus the EHD mobility is the square-root of the relative permittivity of the liquid divided by its density. The EHD mobilities evaluated for the three liquids used in the present work are similar in value ( $1.71 \times 10^{-3} \text{ cm}^2 \text{ V}^{-1} \text{ s}^{-1}$  for Midel 7131,  $1.66 \times 10^{-3} \text{ cm}^2 \text{ V}^{-1} \text{ s}^{-1}$  for Diala D oil and  $1.64 \times 10^{-3} \text{ cm}^2 \text{ V}^{-1} \text{ s}^{-1}$  for rapeseed oil) but lower than the measured negative apparent mobilities shown in Table 4. Therefore, other factors such as an increase in the liquid velocity in non-uniform fields contribute to the apparent mobilities obtained from the  $\sqrt{I(V)}$  curves, which are similar to the results obtained in [36].

Table 4. Coefficient  $B$  and apparent mobility,  $\mu$ .

|              | Negative                 |                        | Positive                 |                        |
|--------------|--------------------------|------------------------|--------------------------|------------------------|
|              | $B, \frac{nA^{1/2}}{kV}$ | $\mu, \frac{cm^2}{Vs}$ | $B, \frac{nA^{1/2}}{kV}$ | $\mu, \frac{cm^2}{Vs}$ |
| Midel 7131   | 1.67                     | 0.0025                 | 1.15                     | 0.0012                 |
| Diala D      | 1.50                     | 0.0029                 | 1.12                     | 0.0016                 |
| Rapeseed oil | 1.44                     | 0.0021                 | 1.16                     | 0.0014                 |

The results presented in Figures 7-8 can be used for the identification of different conduction regimes in the insulating liquids. In low voltages (low electric field), the conduction can be characterized by the Ohmic current (resistive regime region). In this case, the electric field is governed by the Laplace equation and can be obtained using a standard electrostatic solver. With an increase in the applied voltage (higher electric field), the space charge saturation regime can be achieved. In this region, under high-voltage stress, the current reaches its space-charge saturation limit, [36], [37], which is described by Equations 1 and 2. In this case a standard electrostatic solver is inadequate and the Poisson equation should be used in order to obtain an accurate electric field distribution in the dielectric liquid.

#### 4 CONCLUSIONS

The ac breakdown voltages of Midel 7131 liquid, Diala D mineral oil and natural vegetable oil have been obtained using the ASTM D1816-04 standard test geometry and short inter-electrode gap, 0.5 mm. The fresh liquids used in the present study were tested "as received", and no special measures were taken in order to clean or remove water from these liquids.

Midel 7131 (synthetic ester) has a higher ac breakdown voltage as compared with Diala D mineral oil and rapeseed oil. The breakdown voltage of the Diala D oil has the smallest standard deviation (7%) amongst the tested liquids (13% for Midel 7131 and 11% for rapeseed oil). These results – the higher ac breakdown voltage of Midel 7131 than for the mineral oil, and the high standard deviation in the breakdown voltage for Midel 7131 than that for the mineral oil – are similar to the results obtained for degassed and dehydrated liquids in [11]. The breakdown ac electric field values obtained for the synthetic ester (Midel 7131) and mineral oil

(Diala D) in the present study (552 kV/cm and 496 kV/cm respectively) are slightly higher than the breakdown field values obtained in [11] for Midel 7131 (470 kV/cm) and the mineral oil, Nytro 10GN (390 kV/cm). This can be explained by the shorter inter-electrode distance used in the present work (0.5 mm) as compared with 1 mm distance in [11]. It is known that the breakdown field is a non-linear function of the inter-electrode gap, and higher breakdown field can be achieved in shorter gaps stressed with impulsive and ac voltages (this can potentially be explained by smaller number of impurities in shorter gaps). Previous work, [39], reports  $E_{br} \sim 1/d^{0.25}$  dependency of the breakdown strength,  $E_{br}$ , on the short, sub-mm, inter-electrode gap distance,  $d$ , for *n*-hexane stressed with impulsive voltage. Using this dependency, the breakdown field for the Midel 7131 obtained in the present paper for 0.5 mm can be extrapolated into 1 mm gap, and this extrapolated value of 464 kV/cm is very close to 470 kV/cm obtained in [11]. Another study, [40], shows that the breakdown voltage is a non-linear function of the distance for 50 Hz ac energisation, which means that the breakdown field decreases with an increase in the inter-electrode distance. It is shown in [15] that the breakdown voltage increases non-linearly with the inter-electrode gap spacing for sub-mm distances.

The food-grade rapeseed oil (natural ester) used in the present work has the lowest average breakdown voltage and the standard deviation which is between those for synthetic ester and mineral oil,  $24.8 \pm 2.7$  kV. However, the breakdown voltage level is only ~6% lower than the breakdown voltage of the mineral oil tested in the present work. The breakdown voltage of the rapeseed oil decreases with its relative humidity. The authors of [35] reported a ~25% decrease in the ac breakdown voltage for rapeseed oil which was in contact with ambient air for 10 days as compared with dry rapeseed oil. The authors concluded that in order to use the rapeseed oil as industrial insulating fluid, this oil should be dried and isolated from air in order to minimize moisture uptake, [11]. Reference [41] shows that natural ester with a relative water content of 50% has ac breakdown voltage more than two times lower than the dry ester liquid. The breakdown field values reported in [42], 214-226 kV/cm for dry oil and 169 kV/cm for oil which was in contact with ambient air, are relatively low. The same research group reported breakdown strength of 325 kV/cm for the rapeseed oil in [22]. The authors of [11] reported a higher breakdown field for the natural ester fluid, FR3 (410 kV/cm), than the breakdown field for the mineral oil, Nytro 10 GBN (390 kV/cm), which demonstrates that potentially, the breakdown voltage of the natural ester fluid can be as high the breakdown voltage of the synthetic ester (see also [20]). The breakdown field for the rapeseed oil found in the present paper is higher than those reported in [22] and [42], which can potentially be attributed (amongst other possible factors which are not considered here) to the shorter inter-electrode gap of 0.5 mm used in the present study, as compared with 2 mm in [22] and 2.5 mm in [42]. Again, assuming that the  $E_{br} \sim 1/d^{0.25}$  dependency is valid, the extrapolation of the rapeseed oil breakdown field obtained in the present work for 0.5 mm gap (496 kV/cm) into 1 mm gap gives a value of 416 kV/cm which is very close to the

breakdown field reported in [11] for the natural ester fluid, 410 kV/cm. Reference [43] also demonstrates that the ac breakdown strength of insulating liquids including food-grade vegetable oil reduces substantially (by more than two times) with an increase in the gap from 0.3 to 3.0 mm.

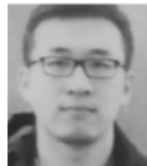
Statistical analyses of the obtained breakdown voltages show that these voltages can be described by the normal distribution for all three liquids. The actual breakdown voltages demonstrate noticeable deviation from the perfect normal distribution for voltages below  $V_{10\%}$  and for voltages above  $V_{90\%}$ . These results can be important for design and management of the high-voltage systems.

*I-V* characteristics for Midel 7131, Diala D and natural vegetable oil have been measured using both negative and positive high-voltage dc energisation. The electrode system used in these tests was a point-plane topology. The obtained *I-V* characteristics were used to determine the apparent mobility of the charge carriers in these liquids. The apparent mobilities obtained in the present work for Midel 7131 and Diala D liquids are similar to the values reported in [37]. The apparent mobility of the charge carriers in the rapeseed oil is also similar to the mobility values of charges in the mineral oil and Midel 7131 ester fluid (the difference is up to ~20%). The  $\sqrt{I(V)}$  curves show that the space charge saturation regime is observed for all three liquids starting from ~9 kV for positive energisation and ~10 kV for negative energisation. These voltage levels indicate the threshold in the dc electric stress above which the Laplacian equation is not valid and the Poisson equation should be solved in order to obtain the accurate values of the electric field in the insulating liquids.

## 5 REFERENCES

- [1] "Innovation funding incentive. Electricity transmission R&D Program detailed reports", Annual Report, National Grid Plc, London, UK, 2011/2012.
- [2] V. M. Atrazhev, V. S. Vorob'ev, I. V. Timoshkin, M. J. Given and S. J. MacGregor, "Mechanisms of Impulse Breakdown in Liquid: The Role of Joule Heating and Formation of Gas Cavities", *IEEE Trans. Plasma Sci.*, Vol. 38, pp. 2644 – 2651, 2010.
- [3] W. Choo, G. Chen and S. G. Swingler, "Electric field in polymeric cable due to space charge accumulation under DC and temperature gradient", *IEEE Trans. Dielectr. Electr. Insul.*, Vol. 18, pp. 596 – 606, 2011.
- [4] U. Gafvert, A. Jaksts and G. Tornkvist, "Electrical Field Distribution in Transformer Oil", *IEEE Trans. Electr. Insul.*, Vol. 27, No. 3, pp.647-660, 1992.
- [5] D. Martin, I. Khan, J. Dai and Z. D. Wang, "An Overview of the Suitability of Vegetable Oil Dielectrics for use in Large Power Transformers", *The Annual Euro TechCon Conf.*, Chester, UK, pp 1-20, 2006.
- [6] MIDEL 7131 Power Transformer 135MVA/238kV, <http://www.midel.com/library>, accessed on 25 October 2013.
- [7] P. Hopkinson, "Progress Report on Natural Ester for Distribution and Power Transformers", Panel discussion overview presented at the IEEE Power Eng.Soc. Transmission and Distribution Conf., USA, pp. 15-17, 2006.
- [8] C. P. Meshane, J. Corkran, K. Rapp and J. Luksich, "Natural Ester Dielectric Fluid Development", *IEEE Power Eng. Soc. Transmission and Distribution Conf.*, pp. 18-22, 2006.
- [9] S. D. Smith, "Design and Test Experience with Natural Ester Fluid for Power Transformers", *IEEE Power Eng. Soc. Transmission and Distribution Conf.*, pp. 35-36, 2006.
- [10] S. P. Moore, "Some Considerations for New and Retrofill Applications of Natural Ester Dielectric Fluids in Medium and

- Large Power Transformers”, IEEE Power Eng. Soc. Transmission and Distribution Conf., pp. 25-29, 2006.
- [11] D. Martin and Z. Wang, “Statistical analysis of the AC breakdown voltages of ester based transformer oils IEEE Trans. Dielectr. Electr. Insul., Vol. 15, No.4, pp.1044-1050, 2008.
- [12] T. J. Gallagher, *Simple Dielectric Liquids-Mobility, Conduction, and Breakdown*, pp. 1-42, Oxford University Press, London, 1975.
- [13] ASTM D1816-04, Standard test method for dielectric breakdown voltage of insulating oils of petroleum origin using VDE electrodes.
- [14] K. C. Kao and J. B. Higham, “The Effects of Hydrostatic Pressure, Temperature, and Voltage Duration on the Electric Strengths of Hydrocarbon Liquids”, *J. Electrochemical Soc.*, pp.552-528, 1961.
- [15] A. A. Zaky, R. Hawley, *Conduction and Breakdown in Mineral Oils*, Pergamon Press, Oxford, 1973.
- [16] M. Butcher, A. Neuber, M. Cevallos, J. Dickens and H. Krompholz, “Conduction and breakdown mechanisms in transformer oil”, *IEEE Trans. Plasma Sci.*, Vol. 34, No.2, pp. 467-475, 2006.
- [17] A. Nousseir, S. El-Debeiky, I. F. Hashad, H. A-Bary, “Effect of temperature on the breakdown probability of liquid dielectrics”, *IEEE Trans. Electr. Insul.*, Vol. 15, No. 6, pp. 502-505, 1980.
- [18] R. Diabi, J. C. Filippini, C. Marteau and R. Tobazeon, “On the role of temperature and impurities in the low field conduction of insulating liquids”, *IEEE 12th Int'l. Conf. Conduction Breakdown Dielectric Liquids (ICDL)*, pp 350 – 353, 1996.
- [19] I. Fofana, H. Borsi and E. Gockenbach, “Moisture uptake of mineral oil at different air relative humidities and temperatures”, *IEEE Conf Electr. Insul. Dielectr. Phenomena*, pp.276-279, 2000.
- [20] V.-H. Dang, A. Beroual and C. Perrier, “Comparative study of statistical breakdown in mineral, synthetic and natural ester oils under AC voltage”, *IEEE Int'l. Conf. Dielectr. Liquid*, pp.1-4, 2011.
- [21] J. M. Lehr, F. J. Agee, R. Copeland and W. D. Prather “Measurement of the Electric Breakdown Strength of Transformer Oil in the Sub-nanosecond Regime”, *IEEE Trans. Dielectr. Electr. Insul.*, Vol. 5, No. 6, pp.857-861, 1998.
- [22] R. Badent, M. Hemmer and A. J. Schwab, “Inhibited rapeseed oil as substitute for mineral oils”, *IEEE Conf. Electr. Insul. Dielectr. Phenomena*, pp. 268-271, 2002.
- [23] M. P. Wilson, I.V Timoshkin, M. J. Given, S. J. MacGregor, T. Wang, M. A. Sinclair, K. J. Thomas and J. M. Lehr, “Breakdown in mineral oil: Effect of electrode geometry and rate of Voltage Rise”, *IEEE Trans. Dielectr. Electr. Insul.*, Vol. 19, No. 5, pp.1657-1664, 2012.
- [24] I. L. Hosier, A. Guu-shaa, E. W. Westenbrink, C. Rogers, A. S. Vaughan and S. G. Swingler, “Aging of biodegradable oils and assessment of their suitability for high voltage applications”, *IEEE Trans. Dielectr. Electr. Insul.*, Vol. 18, pp.728–738, 2011.
- [25] Y. Du, A. V. Mamishev, B. C. Lesieutre, M. Zhan and S. H. Kang, “Moisture solubility for differently conditioned transformer oils”, *IEEE Trans. Dielectr. Electr. Insul.*, Vol. 8, No.5, pp. 805-811, 2001.
- [26] M. Koch, “Improved determination of moisture in oil-paper-insulations by specialised moisture equilibrium charts”, *XIV Int'l. Conf. High Voltage Eng.*, p.508, 2005.
- [27] S. Tenbohlen, M. Koch, “Aging performance and moisture solubility of vegetable oils for power transformers”, *IEEE Trans. Power Delivery*, Vol.25, No.2, pp. 825-830, 2010.
- [28] M. Hemmer, *Rapeseed Oil as Insulation and Cooling in Transformers*, PhD thesis, University of Karlsruhe, Germany, 2004.
- [29] I. Adamczewski, *Ionization, Conductivity and Breakdown in Dielectric Liquids*, Taylor & Francis Ltd, London, 1969.
- [30] D. Vukovic, S. Tenbohlen, J. Harthum, C. Perrier and H. Fink, “Breakdown strength of vegetable-based oils under ac and lightning impulse voltages”, *IEEE Int'l. Conf. Dielectric Liquids*, pp.1-4, 2011
- [31] C. Hosticka “Dependence of Uniform/Nonuniform Field Transformer Oil Breakdown on Oil Composition” *IEEE Trans. Electrical Insulation*, Vol. 14, No. 1, pp. 43-50, 1979.
- [32] V. Segal, A. Hjortsberg, A. Rabinovich, D. Natrass and K. Raj, “AC (60 Hz) and impulse breakdown strength of a colloidal fluid based on transformer oil and magnetite nanoparticles”, *IEEE Int'l. Sympos. Electr. Insul.*, pp. 619-622, 1998.
- [33] G. Hwang, Markus Zahn, F. O'Sullivan, L. Pettersson, O. Hjortstam and R. Liu “Effects of nanoparticle charging on streamer development in transformer oil-based nanofluids”, *J. Appl. Phys.*, Vol. 107, pp.014310-1-17, 2010.
- [34] M. J. Given, M. P. Wilson, P. McGlone, I. V. Timoshkin, T. Wang and S. J. MacGregor, “The Influence of Magnetite Nano Particles on the Behaviour of Insulating Oils for Pulse Power Applications”, *IEEE Conf. Electr. Insul. Dielectr. Phenomena*, pp. 40-43, 2011.
- [35] G. Tinh, C. Vincent and J. Regis, “Statistical dielectric degradation of large volume oil-insulation”, *IEEE Trans. Power App. Syst.*, Vol. 101, pp. 3712-3721, 1982.
- [36] M. Butcher, A. Neuber, M. Cevallos, J. Dickens and H. Krompholz, “Conduction and breakdown mechanisms in transformer oil”, *IEEE Trans. Plasma Sci.*, Vol. 34, No. 2, pp. 467-475, 2006.
- [37] I.V. Timoshkin, M. J. Given, R.A. Fouracre, S. J. MacGregor and J. M. Lehr, “Charge injection energy barriers and charge mobilities in insulating liquids”, *IEEE Conf. Electr. Insul. Dielectr. Phenomena*, pp. 613-616, 2009.
- [38] O. M. Stuetzer, “Magnetohydrodynamics and Electrohydrodynamics”, *Phys Fluids*, Vol. 5, No. 5, pp.534-544, 1962.
- [39] V. Y. Ushakov, V. F. Klimkin, S. M. Korobeynikov, *Impulse Breakdown of Liquids*, Springer-Verlag Berlin Heidelberg, 2007.
- [40] <http://cas.web.cern.ch/cas/Belgium-2009/Lectures/PDFs/Tommasini.pdf>, accessed 10 September 2013.
- [41] CIGRE Report 436 “Experiences in service with new insulating liquids”, Working Group A2.35, 2010.
- [42] R. Badent, K. Kist, B. Ruggemeier, W. Zierhut and A.J. Schwab, “Dielectric Characteristics of Rape-Seed Oil”, *IEEE Conf. Electr. Insul. Dielectr. Phenomena*, Vol. 2, pp. 456-459, 1998.
- [43] M. Marci and I. Kolcunova, “Electric breakdown strength measurement in liquid dielectrics”, *9th Int'l. Conf. Environment and Electr. Eng.*, pp. 427 – 430, 2010.



Yi Jing was born in Shanxi Province, China in 1987. He received the B.Eng. and M.Sc. degrees in electronic and electrical engineering from the University of Strathclyde, Glasgow, UK, in 2010 and 2011, respectively. He is presently studying for the Ph.D. Degree at the University of Strathclyde, working on a project to analyze the dielectric properties of insulating liquids.



Igor V. Timoshkin (M'07) received a degree in physics from the Moscow State University (Russia) in 1992, and the Diploma and the Ph.D. degree from the Imperial College of Science, Technology and Medicine, (London, UK) in 2001. After graduation from MSU he worked as a Researcher at Moscow State Agro-Engineering University, and then at the Institute for High Temperatures of Russian Academy of Sciences before moving to ICSTM in 1997. He joined the University of Strathclyde (Glasgow, UK) in 2001, where he became a Senior Lecturer in 2011.

His research interests include properties of solid and liquid dielectric materials, electronics of plasma discharges in condensed media, practical applications of electro-hydraulic and high-power ultrasound pulses, bio-dielectrics and effects of electromagnetic fields on biological objects.



Martin J. Given (M'99) is currently a Senior Lecturer in the Department of Electronic and Electrical Engineering at the University of Strathclyde. He received the B.Sc. degree in physics from the University of Sussex in 1981 and the Ph.D. degree in electronic and electrical engineering from the University of Strathclyde in 1996. His research interests include, ageing processes and condition monitoring in solid and liquid insulation systems, high speed switching and pulse power applications.



Mark P. Wilson (M'10) was born in Stranraer, Scotland, in 1982. He received the B.Eng. (with honours), M.Phil., and Ph.D. degrees in electronic and electrical engineering from the University of Strathclyde, Glasgow, U.K., in 2004, 2007, and 2011, respectively. He is presently working as a Teaching Associate at the University of Strathclyde, where he continues to investigate surface flashover of solids immersed in insulating oil. Mark is a member of the IEEE Nuclear and Plasma Sciences Society, from

whom he received a Graduate Scholarship Award in 2011, the IEEE Dielectrics and Electrical Insulation Society, and the IET.



Scott J. MacGregor (M'95) received the B.Sc. and Ph.D. degrees from the University of Strathclyde, Glasgow, U.K., in 1982 and 1986, respectively. He became a Pulsed Power Research Fellow in 1986 and a Lecturer in pulsed-power technology in 1989. In 1994, he became a Senior Lecturer, with a promotion to Reader and Professor of High Voltage Engineering, in 1999 and 2001, respectively. From January 2010 he became a Dean of Engineering Faculty of the University of Strathclyde. His research interests include high-

voltage pulse generation, high-frequency diagnostics, high-power repetitive switching, high-speed switching, electronic methods for food pasteurization and sterilization, generation of high-power ultrasound (HPU), plasma channel drilling, pulsed-plasma cleaning of pipes, and stimulation of oil wells with HPU.



Tao Wang received the B.Eng and M.Sc. degrees from Northeast China Dianli University (China) in 1993 and 1996, respectively, and the Ph.D. degree from the University of Strathclyde (Glasgow, UK) in 2005. He then joined the Newland Entech as a research fellow developing high efficiency industrial ozone generator. He joined the Department of Electronic and Electrical Engineering of University of Strathclyde as a lecturer in 2010. His research interests include non-thermal gas discharges and their

applications in gas synthesis, water disinfection and advanced oxidation process in water



Jane Lehr (S'91-M'96-SM'02-F'08) received the B.Eng. degree from the Stevens Institute of Technology, Hoboken, NJ, and the Ph.D. degree in electro physics from Polytechnic University, New York, NY. Since 2002, she has been a Member of the Technical Staff with the Exploratory Pulsed Power Technologies Branch, Sandia National Laboratories, Albuquerque, NM, USA. Prior to joining Sandia National Laboratories, she was with the Directed Energy Directorate, Air Force Research Laboratory, USA. Dr. Lehr is a Past President of the IEEE Nuclear and Plasma Sciences Society.